

ADA 269058

REPORT DOCUMENTATION PAGE

Form Approved

OMB No. 0704-0188

Public reporting burden for this collection of information is estimated to average 1 hour per response, including the time for reviewing instructions, searching existing data sources, gathering and maintaining the data needed, and completing and reviewing the collection of information. Send comments regarding this burden estimate or any other aspect of this collection of information, including suggestions for reducing this burden, to Washington Headquarters Services, Directorate for Information Operations and Reports, 1215 Jefferson Davis Highway, Suite 1204, Arlington, VA 22202-4302, and to the Office of Management and Budget, Paperwork Reduction Project (0704-0188), Washington, DC 20503.

1. AGENCY USE ONLY (Leave blank)		2. REPORT DATE		3. REPORT TYPE AND DATES COVERED Final Report 15 Feb 93 - 14 Jan 94	
4. TITLE AND SUBTITLE Advanced Solid State Lasers/Compact Blue-Green Lasers Organization of the 1993 Photonics Science topical Meetings				5. FUNDING NUMBERS F49620-93-1-0181	
6. AUTHOR(S) Dr Jarus W Quinn				8. PERFORMING ORGANIZATION REPORT NUMBER AFOSR-TR- 93 0645	
7. PERFORMING ORGANIZATION NAME(S) AND ADDRESS(ES) Optical Society of America 2010 Massachusetts Avenue NW Washington DC 20036				10. SPONSORING/MONITORING AGENCY REPORT NUMBER 2301/DS	
9. SPONSORING/MONITORING AGENCY NAME(S) AND ADDRESS(ES) AFOSR/NE 110 Duncan Avenue Suite B115 Bolling AFB DC 20332-0001				11. SUPPLEMENTARY NOTES	
12a. DISTRIBUTION/AVAILABILITY STATEMENT This document has been approved for public release and sale; its distribution is unlimited.				12b. DISTRIBUTION CODE UNLIMITED	
13. ABSTRACT (Maximum 200 words) The following symposium was held Advanced Solid State Lasers Compact Blue-Green Lasers Integrated Photonics Research Nonlinear Guide-Wave Optics Optical Amplifiers & Their Applications Optical Design for Photonics Photonics in Switching Quantum Optoelectronics Shortwavelength: Physics With Intense Laser Pulses Soft X-Ray Protection Lithography Ultrafast Electronics & Optoelectronics Optical Computing Spatial Light Modulators					
14. SUBJECT TERMS 93 8 31 094				15. NUMBER OF PAGES 15. PRICE CODE	
17. SECURITY CLASSIFICATION OF REPORT UNCLASS		18. SECURITY CLASSIFICATION OF THIS PAGE UNCLASS		19. SECURITY CLASSIFICATION OF ABSTRACT UNCLASS	
				20. LIMITATION OF ABSTRACT UL	

DTIC
ELECTE
SEP 02 1993
S A D

93-20374
93-20374

**Best
Available
Copy**



Advanced Solid-State Lasers

*Summaries of papers presented
at the Advanced Solid-State
Lasers Topical Meeting*

February 1-3, 1993
New Orleans, Louisiana

TECHNICAL DIGEST
CONFERENCE EDITION

Sponsored by
Optical Society of America

Technical Cosponsor
IEEE/Lasers and Electro-Optics
Society

Partially Supported by
Air Force Office of Scientific
Research
Defense Advanced Research
Projects Agency
Night Vision & Electro-Optics
Directorate
Office of Naval Research

Compact Blue-Green Lasers

*Summaries of papers presented
at the Compact Blue-Green
Lasers Topical Meeting*

February 2-4, 1993
New Orleans, Louisiana

1993 Technical Digest Series
Volume 2

CONFERENCE EDITION

Sponsored by
Optical Society of America

In Cooperation with
IEEE/Lasers and Electro-Optics
Society

Partially Supported by
Air Force Office of Scientific
Research
National Science Foundation

Optical Society of America
2010 Massachusetts Avenue, NW
Washington, DC 20036-1023

Articles in this publication may be cited in other publications. In order to facilitate access to the original publication source, the following form for the citation is suggested:

Name of Author(s), "Title of Paper," in Advanced Solid-State Lasers and Compact Blue-Green Lasers Technical Digest, 1993 (Optical Society of America, Washington, D.C., 1993), Vol. 2, pp. xx-xx.

ISBN Number

Conference Edition	1-55752-277-4
Postconference Edition	1-55752-278-2 (Compact Blue-Green Lasers only)
(Note: Postconference Edition includes postdeadline papers for Compact Blue-Green Lasers only.)	
1993 Technical Digest Series	1-55752-317-7

Library of Congress Catalog Card Number

Conference Edition	92-62709
Postconference Edition	92-62710 (Compact Blue-Green Lasers only)

Copyright © 1993, Optical Society of America

Individual readers of this digest and libraries acting for them are permitted to make fair use of the material in it, such as to copy an article for use in teaching or research, without payment of fee, provided that such copies are not sold. Copying for sale is subject to payment of copying fees. The code 1-55752-317-7/93/\$2.00 gives the per-article copying fee for each copy of the article made beyond the free copying permitted under Sections 107 and 108 of the U.S. Copyright Law. The fee should be paid through the *Copyright Clearance Center, Inc.*, 21 Congress Street, Salem, MA 01970.

Permission is granted to quote excerpts from articles in this digest in scientific works with the customary acknowledgment of the source, including the author's name and the name of the digest, page, year, and name of the Society. Reproduction of figures and tables is likewise permitted in other articles and books provided that the same information is printed with them and notification is given to the Optical Society of America. Republication or systematic or multiple reproduction of any material in this digest is permitted only under license from the Optical Society of America; in addition, the Optical Society may require that permission also be obtained from one of the authors. Address inquiries and notices to Director of Publications, Optical Society of America, 2010 Massachusetts Avenue, NW, Washington, DC 20036-1023. In the case of articles whose authors are employees of the United States Government or its contractors or grantees, the Optical Society of America recognizes the right of the United States Government to retain a nonexclusive, royalty-free license to use the author's copyrighted article for United States Government purposes.

This work relates to a Department of the Navy Task issued by the Office of Naval Research. The U.S. Government has a royalty license through the world in all copyrightable material contained herein.

This material is based upon work supported by the National Science Foundation. Any opinions, findings, and conclusions or recommendations expressed in this publication are those of the author(s) and do not necessarily reflect the views of the National Science Foundation.

The views and conclusions contained in this document are those of the author(s) and should not be interpreted as necessarily representing the official policies or endorsements, either expressed or implied, of the Air Force Office of Scientific Research or the U.S. Government.

Printed in U.S.A.

CONTENTS

Agenda of Sessions.....	v
AMA High Power Diode-Pumped 1 μ m Lasers.....	1
AMB Diode-Pumped 1 μ m Nd Lasers Poster Session.....	17
AMC Nd Lasers.....	51
AMD Novel Laser Technology.....	71
AME Nonlinear Frequency Conversion 1 Poster Session.....	91
AMF Nonlinear Frequency Conversion 2.....	127
ATuA Novel Laser Materials 1.....	145
ATuB Novel Optical Materials Poster Session.....	163
ATuC Novel Laser Materials 2.....	199
ATuD Transition-Metal-Ion Lasers 1.....	217
ATuE Transition-Metal-Ion Lasers 2 Poster Session.....	237
ATuF LiSAF Lasers.....	269
CTuA Applications of Compact Blue-Green Lasers 1.....	289
CTuB Applications of Compact Blue-Green Lasers 2.....	297
CTuC Blue-Green Semiconductor Lasers.....	305
AWA Mid-IR Lasers 1.....	321
AWB Mid-IR Lasers 2 Poster Session.....	341
CWA Organic Nonlinear Materials.....	377
JWA Joint Session on Inorganic Nonlinear Materials.....	387
JWB Joint Session on Frequency Upconversion in Bulk Devices 1.....	399
JWC Joint Poster Session.....	409
JWD Joint Session on Frequency Upconversion in Bulk Devices 2.....	441
JWE Joint Session on Upconversion Lasers.....	453
CThA Frequency Upconversion in Waveguide Devices 1.....	467
CThB Frequency Upconversion in Waveguide Devices 2.....	483
CThC Poster Session.....	495
Key to Authors and Presiders.....	507

ADVANCED SOLID-STATE LASERS TECHNICAL PROGRAM COMMITTEE

Albert Pinto, *Chair, US Army Night Vision and Electro-Optics Directorate*
Tso Yee Fan, *Program Chair, MIT Lincoln Laboratory*
Thomas Baer, *Technical Council Representative, Spectra-Physics Laser Diode Systems*
James C. Barnes, *NASA*
Ralph L. Burnham, *Fibertek, Inc.*
Bruce H. Chal, *University of Central Florida/CREOL*
David C. Hanna, *University of Southampton, U.K.*
Charles L. Marquardt, *U.S. Naval Research Laboratory*
Stephen Payne, *Lawrence Livermore National Laboratory*
Richard C. Powell, *University of Arizona*
William R. Rapoport, *Allied-Signal, Inc.*
Francois Salin, *University of Paris, France*
Donald J. Smith, *U.S. Air Force*
Evgenii V. Zharikov, *Academy of Sciences of Russia*

COMPACT BLUE-GREEN LASERS TECHNICAL PROGRAM COMMITTEE

William P. Risk, *General Chair, IBM Almaden Research Center*
John D. Bierlein, *Program Chair, E. I. DuPont de Nemours Company*
James M. DePuydt, *Program Chair, 3M Company*
Mark W. Dowley, *Program Chair, Liconix*
William J. Kozlovsky, *Program Chair, IBM Almaden Research Center*
Gunnar Arvidsson, *Institute of Optical Research*
Thomas M. Baer, *Spectra-Physics Laser Diode Systems*
Peter F. Bordul, *Crystal Tech., Inc.*
Bruce H. Chal, *University of Central Florida, CREOL*
Lap-Tak Cheng, *E. I. DuPont de Nemours Company*
Jeff Dixon, *University of Central Florida, CREOL*
Martin M. Fejer, *Stanford University*
Daniel Guillot, *Uniphase Corporation*
David C. Hanna, *University of Southampton, UK*
Hiroshi Kukimoto, *Tokyo Institute of Technology, Japan*
Tsuneo Mitsuya, *Matsushita Electric Industrial Co., Ltd., Japan*
Michio Oka, *Sony Corporation, Japan*
Takatomo Sasaki, *Osaka University, Japan*
Kimio Tatsuno, *Hitachi Ltd., Japan*
Shinsuke Umegaki, *Keio University, Japan*

MONDAY, FEBRUARY 1, 1993

Advanced Solid-State Lasers

LA SALLE BALLROOM B&C

7:50 am-8:00 am

OPENING REMARKS

Albert Pinto, *US Army Night Vision & Electro-Optics Directorate, Presider*

8:00 am-9:30 am

AMA, HIGH POWER DIODE-PUMPED 1 μ m LASERS

Rudolf G. Buser, *US Army Night Vision & Electro-Optics Directorate, Presider*

8:00 am (Invited)

AMA1 One J/pulse, 100-W, diode-pumped, near diffraction limited, phase-conjugated, Nd:YAG master oscillator power amplifier, Randall J. St. Pierre, Hagop Injeyan, Rodger C. Hilyard, Mark E. Weber, Jacqueline G. Berg, Michael G. Wickham, Carolyn S. Heofer, Jason P. Machan, *TRW Space and Technology Group*. We have assembled and tested a diode-pumped, phase-conjugated Nd:YAG master oscillator power amplifier (PC MOPA). One J/pulse has been extracted at a repetition rate of 100 Hz with a beam quality of $1.1 \times$ D.L. from a zig-zag slab amplifier. This combination of average power and beam quality makes this the brightest solid-state laser reported to date. (p. 2)

8:30 am

AMA2 Conductively cooled diode-pumped phase conjugate Nd:YLF laser with 0.5 J, 100 Hz at 547 nm output, E. Gregor, S. Matthews, R. Muir, O. Kahan, T. Chen, J. Source, M. Polumbo, C. Kalina, K. Nielson, J. Ortiz, *Hughes Aircraft Co.* Conductive cooling techniques using heat pipes were demonstrated in a diode-pumped phase-conjugate Nd:YLF laser at 100 Hz with 0.5 J output at 547 nm. (p. 5).

8:45 am

AMA3 High-power diode-pumped solid-state industrial laser, R. Burnham, P. Bournes, J. Kasinski, K. Le, D. DiBiase, *Fibertek, Inc.* A new generation of high-power diode-pumped solid-state laser modules has been developed for industrial applications. In initial experiments 200 W output has been obtained with Nd:YAG at 12-% duty cycle. (p. 8)

9:00 am

AMA4 High-power single-mode diode-pumped graded-reflectivity-mirror-stable oscillator, Jeff Kasinski, Pat Bournes, Ralph Burnham, *Fibertek, Inc.* A Q-switched diode-pumped oscillator utilizing a GRM in a stable resonator is presented with output near 100 mJ at $\leq 1.5 \times$ diffraction-limited and 5% electrical efficiency. Performance is demonstrated up to 100 Hz; scalability to higher repetition, energy, and efficiency is illustrated. (p. 11)

9:15 am

AMA5 Efficient diode-pumped cw Nd:YAG laser with 60-W near-diffraction-limited output, S. C. Tidwell, J. F. Seamans, M. S. Bowers, *STI Optronics, Inc.* A novel diode-pumped Nd:YAG laser is discussed which produces a cw output of 60-W TEM₀₀ and 92-W multimode with optical efficiencies of 26% and 44%, respectively. (p. 14)

LA SALLE BALLROOM A

9:30 am-10:30 am

AMB, DIODE-PUMPED 1 μ m Nd LASERS POSTER SESSION/COFFEE BREAK

AMB1 High repetition rate, high average power, pulsed diode-pumped Nd:YAG oscillators, C. E. Hamilton, C. I. Miyake, F. D. Braun, *STI Optronics, Inc.* A 200-Hz, 3-W Q-switched Nd:YAG oscillator is end-pumped by four quasi-cw diode arrays. Operation that is insensitive to the diode wavelength and fifth harmonic generation are described. (p. 18)

AMB2 2.4-ns pulse generation in a solid-state passively Q-switched, laser-diode-pumped Nd:YAG laser, Y. Isyanova, D. Welford, *Schwartz Electro-Optics Inc.* We report generation of 5-mJ, 2.4-ns Q-switched pulses from a single-frequency, TEM₀₀-mode, laser-diode-pumped Nd:YAG laser using F₂ color centers in LiF. (p. 21)

AMB3 Flashlamp-pumped Nd:BaY₂F₈

Norman P. Barnes, Keith E. Murray, *NASA Langley Research Center*; Alette Cassanho, Kenneth M. Dinndorf, Hans P. Jenssen, *Massachusetts Institute of Technology*. Flashlamp-pumped laser performance of Nd:BaY₂F₈ has been achieved both at 1.0488 and 1.3176 μ m using a laser rod only 48 mm long. Because of the short length, an unusual pulse-forming network was required. Laser performance will be reported and compared with Nd:YAG under the same conditions. (p. 24)

AMB4 Efficient, Q-switched Nd:YAG laser end-pumped by a high-power diode laser array

Ti Chuang, Horacio R. Verdun, *Fibertek, Inc.* We report an efficient, Q-switched Nd:YAG laser end-pumped by a three-bar high power diode array. The laser delivered 2.2 mJ/pulse with pulse width of 19.6 ns. (p. 26)

AMB5 Diode-pumped Nd:YAG laser with parabolic pump cavity

H. Zbinden, R. Weber, *Institute of Applied Physics, Switzerland*. A simple, scalable transverse pump design for diode-pumped Nd:YAG lasers is presented. The diode light is focused by a parabolic reflector onto the laser rod. (p. 29)

AMB6 Spectroscopy of Nd:KYF₄

Y. Yamaguchi, H. P. Jenssen, A. Cassanho, *Massachusetts Institute of Technology*. A single crystal of Nd:KYF₄ was grown by the top seeded solution growth technique. The absorption and emission spectra show that there are more than two neodymium sites in this crystal. (p. 32)

AMB7 High repetition rate, diode-end-pumped Nd:YLF laser

A. J. W. Brown, Roy Mead, Walter R. Bosenberg, *STI Optronics, Inc.* We have developed a diode-end-pumped Nd:YLF laser with Q-switched outputs > 5 mJ at repetition rates up to 500 Hz. Frequency conversion to the ultraviolet with nonlinear crystals and to the visible and infrared with an OPO is discussed. (p. 35)

DTIC QUALITY INSPECTED 1

Accession For	
NTIS	CRA&I
DTIC	YAB
Unannounced	
Justification	
By	
Distribution /	
Availability Codes	
Dist	Avail and/or Special
A-1	

ASSL (Cont.)

AMB8 Laterally diode-pumped, c-axis Nd:YLF laser, Newton Sims, Jr., *Science and Technology Corp.*; Norman P. Barnes, *NASA Langley Research Center*. Lateral diode pumping of c-axis Nd:YLF rather than the more conventional a-axis Nd:YLF has proven to be highly efficient. Total optical to optical conversion efficiency of 0.38 was obtained at 1.053- μ m with a 5 mm diameter rod. A 4mm diameter rod demonstrated optical conversion efficiencies of 0.335 and 0.015 on the 1.053- μ m and the 1.313- μ m transitions respectively. (p. 38)

AMB9 Simple model of the Mars Observer laser altimeter laser transmitter, Robert S. Afzal, *NASA Goddard Space Flight Center*. The Mars Observer laser altimeter utilizes a space-qualified diode-laser-pumped Q-switched Nd:YAG laser transmitter. We present a simple numerical model of the laser energetics predicting the pulse energy, pulse width and temperature dependence. (p. 41)

AMB10 Q-switched diode-pumped Nd:YAG lasers, Judith M. Dawes, Peter Dekker, Ying Cai, David S. Knowles, Stuart Jackson, James A. Piper, *Macquarie Univ., Australia*. Power scaling and thermal issues in a diode-pumped Nd:YAG laser using a nonfocussing solid collector geometry are presented. This laser yields Q-switched pulses of 10.9 mJ and 75 ns, from an absorbed pump energy of 50 mJ. (p. 44)

AMB11 Comparison of Nd³⁺ in GdLiF₄ and YLiF₄ by Fourier spectroscopy, H. Weidner, R. E. Peale, X. X. Zhang, M. Bass, B. H. T. Chai, *Univ. Central Florida*. Fourier spectra (500 to 22,000 cm⁻¹ at 1 cm⁻¹ resolution) of Nd³⁺ in GdLiF₄ and YLiF₄ demonstrate that these laser crystals are isostructural. (p. 47)

LA SALLE BALLROOM B&C

10:30 am–12:00 m

AMC, Nd LASERS

Ralph L. Burnham, *Fibertek Inc., President*

10:30 am (Invited)

AMC1 Nd:GdVO₄ crystal—a new material for diode-pumped solid-state lasers, V. G. Ostroumov, I. A. Shcherbakov, A. I. Zagumennyi, *Russian Academy of Sciences, Russia*; G. Huber, T. Jensen, J. P. Meyn, *Univ. Hamburg, Germany*. Nd:GdVO₄ crystals were grown by the Czochralski technique. Neodymium lifetime is 94 μ s and absorption coefficient at 808 nm is more than 70 cm⁻¹. Lasing was obtained at ⁴F_{3/2}→⁴F_{13/2}, ⁴I_{11/2} transition slope efficiency for 1.06 μ m was 54%. (p. 52)

10:45 am

AMC2 Laser performance of a new laser crystal—Nd:GdLiF₄, X. X. Zhang, M. Bass, J. Lefaucheur, A. Pham, A. B. Villaverde, B. H. T. Chai, *Univ. Central Florida*. Laser action of a new crystal—Nd:GdLiF₄ has been demonstrated for the first time in both pulsed and cw laser-pumped operation. In pulsed operation a slope efficiency of 58% was obtained from the first sample studied. (p. 55)

11:00 am

AMC3 Frequency-shifted feedback Nd:YLF laser, M. W. Phillips, G. Y. Liang, J. R. M. Barr, *Southampton Univ., U.K.* We report the free-running and injection-seeded operation of a Nd:YLF laser incorporating frequency-shifted feedback to generate either broadband or discrete multifrequency spectra with bandwidths up to 140 GHz (fwhm). (p. 58)

11:15 am

AMC4 Determination of the effective lower-level lifetime for Nd:YLF and Nd:YAG through experimental measurement and computer modeling, Stephen J. Sheldrake, Steven C. Matthews, Katherine V. Palombo, David Capps, *Hughes Aircraft Co.* We report Nd:YLF and Nd:YAG lower-level lifetimes, determined by experimentally measuring amplifier gain recovery and extraction efficiency and comparing with rate equation model predictions. (p. 61)

11:30 am

AMC5 Direct measurements of the terminal-level lifetime for Nd³⁺-doped laser materials, C. Bibeau, S. A. Payne, H. T. Powell, *Lawrence Livermore National Laboratory*. We have directly measured the terminal-level lifetime of Nd³⁺ in several glass and crystalline media using a pump (2.41 μ m) and probe (1.06 μ m) experimental technique. (p. 64)

11:45 am

AMC6 Efficient surface-emitting laser-diode matrices side-pumped Nd:YAG slab, C. Larat, M. Schwarz, G. Feugnet, J. P. Pocholle, *Thomson-CSF, France*. New high-power monolithic surface-emitting laser diodes are used to pump Nd:YAG slab in QCW mode. The laser delivers 6.5 mJ in the free running mode. (p. 67)

12:00 m–1:30 pm

LUNCH

LA SALLE BALLROOM B&C

1:30 pm–3:00 pm

AMD, NOVEL LASER TECHNOLOGY

Evgenii V. Zharikov, *Russian Academy of Science, Russia, President*

1:30 pm

AMD1 Modeling of high-power, end-pumped solid-state lasers, Thomas M. Baer, Mark S. Keirstead, *Spectra-Physics Laser Diode Systems, Inc.* We present the results of a numerical model of high-power, end-pumped, solid-state lasers. The model provides accurate predictions of eigenmode properties (beam-size, divergence, amplitude profile, M²) in laser cavities with large phase aberrations due to pump-induced thermal gradients. (p. 72)

1:45 pm

AMD2 Propagation effects in variable reflectivity resonators, E. Mottay, E. Durand, E. Audouard, *B. M. Industries, France*. A numerical and experimental study of propagation effects in variable-reflectivity resonators shows that the beam profile is extremely sensitive to residual diffraction in the resonator. (p. 75)

MONDAY, FEBRUARY 1, 1993—Continued

ASSL (Cont.)

2:00 pm

AMD3 Power scaling and wavelength conversion of cw diode-pumped lasers, Larry R. Marshall, Alex Kaz, Horatio R. Verdun, *Fibertek, Inc.* TEM₀₀ cw-diode-pumped lasers generate 3.3 W (end-pumped) and 6 W (side-pumped), at 7% electrical efficiency. Nonlinear conversion gives 3.1 W at 523 nm, and 1.7 W at 1540 nm, at 15 kHz. (p. 78)

2:15 pm

AMD4 Application of four-wave mixing by gain saturation for the control of solid-state laser systems, M. J. Damzen, G. J. Crofts, R. P. M. Green, *Imperial College, U.K.* A high-reflectivity (x2500) Nd:YAG four-wave mixing device is developed into a phase conjugate laser resonator demonstrating gain gratings as a potential nonlinear optical technology for laser control. (p. 81)

2:30 pm

AMD5 Ultrahigh sensitivity measurement of Doppler shift with a microchip solid-state laser, Kenju Otsuka, *NTT Basic Research Laboratories, Japan*. Intensity modulation of a LiNdP₄O₁₂ microchip solid-state laser by extremely weak (e.g., < -100 dB) Doppler-shifted light injection and application to an ultrahigh sensitivity velocity meter are demonstrated. (p. 84)

2:45 pm

AMD6 High duty-cycle diode-pumped Nd:YLF slab laser, A. D. Hays, R. Burdham, *Fibertek, Inc.* We have obtained 10-W average power and 6.5-W in the fundamental mode from a Nd:YLF slab laser pumped by four 20% duty-cycle laser diode arrays. (p. 87)

LA SALLE BALLROOM A

3:00 pm–4:00 pm

AME, NONLINEAR FREQUENCY CONVERSION 1 POSTER SESSION/ REFRESHMENT BREAK

AME1 Q-switching of a Nd:YAG phase conjugate laser using externally stimulated Brillouin scattering, R. A. Lamb, *Defence Research Agency, U.K.*; M. J. Damzen, *Imperial College of Science and Technology, U.K.* A Q-switched Nd:YAG phase conjugate laser has been demonstrated. The passive Q-switch was in the form of a phase conjugate mirror using stimulated Brillouin scattering as the nonlinearity. (p. 92)

AME2 2.95- μ m intracavity difference-frequency laser, F. J. Effenberger, G. J. Dixon, *Univ. Central Florida*. Cw radiation at 2.95 μ m has been generated by intracavity difference-frequency mixing. Noncritical phase matching in a y-cut KTP crystal was used to mix the 1.064- μ m intracavity field of a diode-pumped Nd:YAG laser with an external input at 0.78 μ m. (p. 95)

AME3 Hot images from obscurations, J. T. Hunt, K. R. Manes, P. A. Renard, *Lawrence Livermore National Laboratory*. Certain damage observed on the optics in NOVA is consistent with nonlinear holographic imaging. Our analysis shows how to circumvent this problem and leads to an explanation for a twenty year old puzzle. (p. 99)

AME4 Stimulated Brillouin scattering and phase conjugation of a 2.1- μ m Cr,Tm,Ho:YAG laser, W. T. Whitney, *U.S. Naval Research Laboratory*; A. M. Scott, *Defence Research Agency, U.K.* We have narrowed the linewidth of a 2.12- μ m Cr,Tm,Ho:YAG laser and have obtained stimulated Brillouin scattering in CS₂ with high efficiency. (p. 102)

AME5 AgGaSe₂ OPO pumped by a LiNbO₃ OPO, Jean Raffy, Thierry Debuisschert, Jean-Paul Pocholle, Michel Papuchon, *Thomson-C.S.F., France*. We describe an AgGaSe₂ OPO pumped by a LiNbO₃ OPO itself pumped by a Q-switched Nd:YAG laser. (p. 105)

AME6 Tunable red solid state laser, Ian Lee, *McDonnell Douglas*. A Nd:YAG-pumped KTP OPO provided 1.57 μ m and 1064 nm beams for efficient sum frequency mixing in KTP to 634 nm. The output is tunable in the visible. (p. 108)

AME7 Diffractive analysis of an external resonant ring for quadrupling Nd lasers, M. S. Bowers, S. C. Tidwell, J. F. Seamans, D. D. Lowenthal, *STI Optonics, Inc.* Effects of diffraction, depletion, and ring propagation are modelled for an external resonant ring containing two nonlinear crystals. Results show that the process is stable and can efficiently convert infrared to ultraviolet. (p. 112)

AME8 Harmonic generation of tunable lasers without any adjustment, Harry Rieger, *Naval Command Control and Ocean Surveillance Center*. Harmonic generation (over 100 nm) of tunable lasers that requires no adjustments for phase matching was accomplished using wavelength dispersive optics and a BBO doubler. Such a setup also provides efficient broadband harmonic generation. (p. 115)

AME9 Numerical simulation and realization of a KTP optical parametric oscillator, J. M. Breteau, C. Jourdain, T. Lepine, F. Simon, *Thomson-TRT Defense, France*. We have developed a numerical simulation of a KTP OPO in the dynamic regime. Predictions are in good agreement with experimental results. (p. 118)

AME10 Wavelength diversity and agility by polarization tuning of stimulated Raman conversion, K. V. Palombo, D. W. Mordaunt, E. Gregor, *Hughes Aircraft Co.* Polarization tuning of stimulated rotational and vibrational Raman conversion of a frequency-doubled Nd:YAG laser is used to demonstrate both wavelength diversity and agility. (p. 121)

AME11 Injection-seeded tuning of a pulsed optical parametric oscillator: applications and performance, M. J. Johnson, J. G. Haub, B. J. Orr, *Macquarie Univ., Australia*. A tunable β -barium borate optical parametric oscillator is useful for spectroscopy and nonlinear optics. Its performance, with and without injection seeding, is characterized and modeled. (p. 124)

MONDAY, FEBRUARY 1, 1993—Continued

ASSL (Cont.)

LA SALLE BALLROOM B&C

4:00 pm–5:30 pm

AMF, NONLINEAR FREQUENCY CONVERSION 2

Charles L. Marquardt, *U.S. Naval Research Laboratory, Presider*

4:00 pm (Invited)

AMF1 Novel resonant ring for converting the output of a mode-locked infrared laser into ultraviolet light with high efficiency, S. C. Tidwell, J. F. Seamans, D. D. Lowenthal, *STI Optronics, Inc.*; G. Matone, G. Girodano, *Laboratori Nazionali di Frascati, Italy*. A resonant ring produces over 5 W of 263-nm light with a slope efficiency of 39% from an infrared mode-locked Nd:YLF laser input. (p. 128)

4:15 pm (Invited)

AMF2 Recent advances in ZnGeP₂ mid-infrared optical parametric oscillators, P. G. Schunemann, P. A. Budni, M. G. Knights, T. M. Pollak, E. P. Chicklis, *Lockheed Sanders*; C. L. Marquardt, *U.S. Naval Research Laboratory*. We report 37% slope (26% overall) conversion efficiency from a 2- μ m pumped OPO using ZnGeP₂ at ambient temperature, and sustained operation at 1.2 J/cm². By cooling lossy (~ 0.38 cm⁻¹) crystals we also achieved 27% slope (24% overall) conversion efficiency. (p. 131)

4:30 pm

AMF3 Optical parametric frequency conversion properties of KTiOAsO₄ (KTA), W. R. Bosenberg, *STI Optronics, Inc.*; L. K. Cheng, J. D. Bierlein, *Science and Engineering Laboratory*. Tuning curves and oscillation thresholds for optical parametric frequency generation in KTiOAsO₄ (KTA) are presented along with Sellmeier equations that predict its phase-matching behavior. (p. 134)

4:45 pm

AMF4 Noncritically phase-matched cw mode-locked optical parametric oscillator in KTP, A. Nebel, C. Fallnich, R. Beigang, *Univ. Kaiserslautern, Germany*. We report efficient operation of noncritically phase-matched optical parametric oscillators pumped by cw mode-locked Ti:sapphire lasers generating ps and fs pulses in the near infrared spectral region. Power efficiencies up to 40% were obtained with stable transform limited pulses. (p. 136)

5:00 pm

AMF5 External frequency conversion of tunable femtosecond pulses, C. Fallnich, A. Nebel, R. Beigang, *Univ. Kaiserslautern, Germany*. We report efficient frequency conversion of cw mode-locked femtosecond Ti:sapphire laser radiation down to 190 nm. Nearly transform limited pulses with a pulse length of 150 fs and average powers of 420 mW and 195 mW were obtained for the second and third harmonic, respectively. (p. 139)

5:15 pm

AMF6 Stimulated Raman scattering of picosecond pulses in barium nitrate crystals, Petr G. Zverev, Tasoltan T. Basiev, *General Physics Institute, Russia*; James T. Murray, Richard C. Powell, Roger J. Reeves, *Oklahoma State Univ.* Frequency shifting of picosecond pulses by stimulated Raman scattering was investigated in Ba(NO₃)₂ crystals. First Stokes conversion efficiencies were measured to be up to 25%. (p. 142)

LA SALLE BALLROOM B&C

6:30 pm–8:00 pm

AMG, POSTDEADLINE PAPER SESSION

Francois Salin, *University of Paris, Presider*

TUESDAY, FEBRUARY 2, 1993

Advanced Solid-State Lasers

LA SALLE BALLROOM B&C

8:15 am-9:45 am

ATuA, NOVEL LASER MATERIALS 1

Richard C. Powell, *University of Arizona, President*

8:15 am

ATuA1 Incongruent melting fluoride crystals as new laser hosts, A. Pham, J. Lefaucheur, J. Nicholls, G. Lutts, B. Chai, *CREOL*. We report here our effort to grow three new laser host crystals from peritectic melts. We grow these crystals with the same equipment and technique that we normally use for congruent melting compounds. This approach opens new opportunities to search for better laser hosts. (p. 146)

8:30 am

ATuA2 Crystal growth and spectroscopic characterization of Tm-doped oxyapatites and orthosilicates, Gregg H. Rosenblatt, *SFA, Inc.*; Gregory J. Quarles, Leon Esterowitz, *U.S. Naval Research Laboratory*; Mark H. Randles, John E. Creamer, *Litton Airtron Synoptics*; Roger F. Belt, *Litton Airtron*. We have studied the spectroscopic features of Tm³⁺ in three different hosts; CaY₄(SiO₄)₃O, CaLa₄(SiO₄)₃O, and Y₂SiO₅. Compared with Tm:YAG the absorption lines in the near infrared are considerably stronger, with similar linewidths. The lifetimes of the ³F₄ → ³H₆ transition for these hosts at 2 μm are typically 0.6 ms to 1.5 ms as compared to 10 ms in Tm:YAG. (p. 147)

8:45 am

ATuA3 Physics of Yb-doped laser crystals with the apatite structure, L. D. DeLoach, S. A. Payne, W. F. Krupke, L. K. Smith, W. L. Kway, J. B. Tassano, *Lawrence Livermore National Laboratory*. We report our spectroscopic studies and assessment of the favorable crystal field environments produced for Yb³⁺ in apatite-structure crystals. (p. 150)

9:00 am

ATuA4 High-power ytterbium-doped fiber laser operating around 1.11-μm, C. J. Mackechnie, W. L. Barnes, D. C. Hanna, J. E. Townsend, *Univ. Southampton, U.K.* Using a pump source of 1.064 μm, greater than 500 mW of power at 1.115 μm has been obtained from a ytterbium-doped silica fiber laser. (p. 153)

9:15 am

ATuA5 Excited state absorption in Nd³⁺-doped laser crystals, Y. Guyot, R. Moncorge, *Univ. Lyon I, France*. Detailed excited-state absorption spectra have been recorded in the wavelength regions of pumping and of stimulated emissions of the Nd³⁺-doped Y₃Al₅O₁₂, YLiF₄ and LaMgAl₁₁O₁₉ laser crystals. (p. 156)

9:30 am

ATuA6 Active medium for all-solid-state tunable ultraviolet laser, Mark A. Dubinskii, Vadim V. Semashko, Alexander K. Naumov, Ravil Yu. Abdulsabirov, Stella L. Korableva, *Kazan State Univ., Russia*. The results of spectroscopic studies, tunable gain and lasing features of Ce³⁺-activated colquirite crystals are reported. This is the first all-solid-state ultraviolet laser, based on rare-earth ion d-f transitions. (p. 159)

LA SALLE BALLROOM A

9:45 am-10:45 am

ATuB, NOVEL OPTICAL MATERIALS POSTER SESSION/COFFEE BREAK

ATuB1 Cw-lasing of Pr:YAlO₃ at room temperature, A. Bleckmann, F. Heine, J. P. Meyn, K. Petermann, G. Huber, *Univ. Hamburg, Germany*. We describe for the first time cw oscillation of a Pr³⁺-doped YAlO₃ crystal at room temperature. The oscillation wavelengths realized so far are 613.9 nm, 621.6 nm, 662.4 nm, 719.5 nm, 746.9 nm, 753.7 nm and 996.0 nm. (p. 164)

ATuB2 Relative upconversion rates in Tm-Ho-doped crystals, K. M. Dinndorf, A. Cassanho, Y. Yamaguchi, H. P. Jenssen, *Massachusetts Institute of Technology*; M. Tonelli, *Univ. Pisa, Italy*. Cross-relaxation and relative upconversion rates are obtained. A simple model is developed and the role of cross-relaxation in reducing loss due to upconversion is discussed. (p. 167)

ATuB3 Tunable erbium-doped fiber ring laser using fiber-birefringence tuning technique, Paul D. Humphrey, John E. Bowers, *UC-Santa Barbara*. A simple new method of controlled tuning of fiber lasers is presented. Tuning is monotonic with the angular position of a single coil of fiber. (p. 170)

ATuB4 Modified dye-doped polymer active media with advanced laser damage resistance and photochemical stability, V. N. Serova, A. A. Vasilev, E. L. Koryagina, *Kazan Chemical-Technology Institute, Russia*; M. A. Dubinskii, A. K. Naumov, V. V. Semashko, *Kazan State Univ., Russia*. Laser studies of new dye-doped metacrylic copolymers have been performed. Significant improvement of laser damage resistance, photochemical stability, and efficiency was obtained using new versions of modificatory additives. (p. 173)

ATuB5 Broad-band thin film plate polarizer for high-power femtosecond solid-state lasers, Donny Mal A. Aminou, *Alpine Research Optics Corp.*; Jeff Squier, *Center for Ultrafast Optics*. We discuss plate polarizers that dramatically improve the tunability to femtosecond regenerative amplifiers of high-power solid-state lasers. (p. 176)

ATuB6 Electrooptically fast tunable miniature diode-laser-pumped Nd:YAG ring oscillator, I. Freitag, I. Kropke, H. Welling, *Laser Zentrum Hannover e.V., Germany*. We present a novel structure of a miniature diode-pumped single-frequency ring laser. Fast frequency tuning is achieved using an integrated electrooptical modulator. (p. 179)

ATuB7 Multisite optical spectra and energy levels of trivalent thulium-doped yttrium scandium gallium garnet, Michael D. Seltzer, John B. Gruber, Marian E. Hills, *Naval Air Warfare Center*; Gregory J. Quarles, *U.S. Naval Research Laboratory*; Clyde A. Morrison, *U.S. Army Adelphi Laboratory Center*. Site-selective laser excitation spectra of thulium-doped yttrium scandium gallium garnet (Tm³⁺:YSGG) reveal the presence of thulium ions in multiple sites which exist as a consequence of intrinsic crystal disorder in YSGG. (p. 182)

ATuB8 Comparison of proton and gamma-irradiated Nd-doped materials longitudinally pumped at 0.8 μm, T. S. Rose, R. A. Fields, *The Aerospace Corp.* The effect of space environment proton damage on laser performance is examined for Nd:YAG, Nd:YLF, and Nd:Cr:GSGG. The nature of the damage and its annealing properties suggest some relevant laser design criteria. (p. 185)

ASSL (Cont.)

ATuB9 Determination of laser efficiencies for Yb-doped apatite-structure hosts. L. K. Smith, S. A. Payne, W. F. Krupke, L. D. DeLoach, W. L. Kway, Lawrence Livermore National Laboratory; B. H. T. Chai, CREOL. We have measured the laser efficiency of three types of Yb-doped crystals, all of which possess the apatite structure. Details of the laser experiments and properties are discussed. (p. 188)

ATuB10 Energy transfer calculations using a quantum mechanical model. Norman P. Barnes, NASA Langley Research Center; Elizabeth D. Filer, Lockheed Engineering and Science Company; Clyde A. Morrison, Harry Diamond Laboratories. Energy transfer processes in sensitized laser materials were analyzed by using a quantum mechanical model to predict energy levels and branching ratios and summing over these energy levels, polarizations, and sites at different distances and orientations. Significant differences exist between this approach and the commonly used Dexter model. (p. 191)

ATuB11 High-peak power, Q-switched Nd:YLF laser end-pumped by a diode laser bar. B. Frei, T. Graf, J. E. Balmer, Univ. Berne, Switzerland. We report on a high-peak power, Q-switched Nd:YLF laser oscillator end-pumped by a fiber-optically coupled, 50-W, quasi-cw diode laser bar. Both pulse-transmission mode (PTM) and the more conventional pulse-reflection mode (PRM) Q-switching techniques have been realized. (p. 193)

ATuB12 Thermal properties of erbium glass lasers. A. McInnes, J. Richards, Defence Science and Technology Organisation, Australia. The relative influence of thermal loading on gain, lensing, birefringence and rod deformation has been studied in a flashlamp-pumped Er glass laser. (p. 196)

LA SALLE BALLROOM B&C

10:45 am–12:00 m

ATuC, NOVEL LASER MATERIALS 2
Stephen Payne, Lawrence Livermore National Laboratory, Presider

10:45 am

ATuC1 Subpicosecond pulse generation from a laser-diode-pumped, self-starting additive-pulse mode-locked Nd:LMA laser. D. W. Hughes, A. A. Majidabadi, J. R. M. Barr, D. C. Hanna, Southampton Univ. U.K. We report the generation of 750-fsec pulses from an additive-pulse mode-locked $\text{La}_{0.9}\text{Nd}_{0.1}\text{NgAl}_{11}\text{O}_{19}$ laser-pumped by a 3-W laser diode. (p. 200)

11:00 am

ATuC2 Cw passive mode-locking of a new $\text{Nd}^{3+}:\text{GdVO}_4$ crystal laser. E. Sorokin, I. Sorokina, E. Wintner, Technische Univ. Wien, Austria; A. I. Zagumennyi, I. A. Shcherbakov, General Physics Institute, Russia. We report the first demonstration of efficient passively mode-locked laser based on new $\text{Nd}^{3+}:\text{GdVO}_4$ crystal. Pulses of 2.4-ps duration with 330 mW of output power are observed. (p. 203)

11:15 am

ATuC3 $\text{Nd}^{3+}:\text{Ca}_2\text{Al}_2\text{SiO}_7$ —a new solid state laser material for diode pumping. B. Viana, D. Saber, A. M. Lejus, D. Vivien, Laboratoire de Chimie Appliquée de L'Etat Solide, France; R. Romero, C. Wyon, Division Optique L.E.T.I.-C.E.N.G. France. $\text{Nd}^{3+}:\text{Ca}_2\text{Al}_2\text{SiO}_7$ laser material presents interesting optical properties: broad and strong red absorption and near infrared emission as well as very promising first laser characteristics. (p. 206)

11:30 am

ATuC4 Spectroscopic and sensitization analysis of Er, Yb, and Cr ions in calcium fluorophosphate. Thomas H. Allik, Science Applications International Corp.; John B. Gruber, San Jose State Univ.; Michael D. Seltzer, Marian E. Hills, Naval Air Warfare Center; Clyde A. Morrison, U.S. Army Adelphi Laboratory Center; Bruce H. T. Chai, CREOL; J. Andrew Hutchinson, Larry D. Merkle, U.S.A. Night Vision and Electro-Optics Directorate. Analysis of absorption, fluorescence, and site-selective excitation spectra of Er, Er-Yb, and Er-Cr in $\text{Ca}_5(\text{PO}_4)_3\text{F}$ suggest that this system has favorable spectral characteristics for producing eye-safe stimulated emission. (p. 209)

11:45 am

ATuC5 Next laser glasses for nuclear fusion. T. Izumitani, Hoya Corp. New laser glasses are obtained from Nd:Yb aluminate glass and Yb:Er phosphate glass, which satisfy Naito's requirement for nuclear fusion laser material: (1) saturation fluence of 10 J/cm², (2) thermal shock resistance 3 W/cm, (3) nonlinear refractive index $< 3 \times 10^{-13}$ esu, (4) fluorescence lifetime > 4 ms. (p. 212)

12:00 m–1:30 pm

LUNCH

1:30 pm–3:00 pm

ATuD, TRANSITION-METAL-ION LASERS 1

William R. Rapoport, Allied-Signal, Inc., Presider

1:30 pm

ATuD1 150-fs, 1.5-TW, 10-Hz $\text{Ti}:\text{Al}_2\text{O}_3$ laser system. P. H. Chiu, Art Magana, Koichi Yamakawa, John Davis, Continuum; J. D. Kmetec, Lightwave Electronics. Described is a 1.5-TW, 150-fs $\text{Ti}:\text{Sapphire}$ ($\text{Ti}:\text{Al}_2\text{O}_3$) laser system operating at 10-Hz repetition rate. The system design was based on regenerative/multipass amplifiers and the technique of chirped-pulse amplification. (p. 218)

TUESDAY, FEBRUARY 2, 1993—Continued

ASSL (Cont.)

1:45 pm

ATuD2 High-power, gain-guided Ti:Al₂O₃ laser: theory and experiment, F. Salin, F. Estable, E. Mottay, L. Brunel, B. M. Industries, France. We report on the use of gain guiding in a Ti:Al₂O₃ rod to produce 150-mJ, diffraction-limited, tunable pulses from a flat-flat resonator. (p. 221)

2:00 pm

ATuD3 Ti:chrysoberyl as a high-saturation-fluence amplification medium for Ti:sapphire lasers, Nobuhiko Sarukura, Yusaburo Segawa, *The Institute of Physical and Chemical Research (RIKEN)*, Japan; Kiyoshi Yamagishi, *Mitsui Mining and Smelting Co.*, Japan. Ti:chrysoberyl is shown to be a high-saturation-fluence amplification material for Ti:sapphire lasers. A 52-dB gain is demonstrated using a confocal 6-pass configuration. (p. 224)

2:15 pm

ATuD4 Femtosecond pulses generated from a synchronously pumped chromium-doped forsterite laser, A. Seas, V. Petricevic, R. R. Alfano, *CUNY, Stable, transforme.J, limited*, tunable femtosecond pulses were generated from a synchronously pumped forsterite laser. Pulses with duration of 105 fs FWHM were produced between 1240 and 1270 nm. (p. 227)

2:30 pm

ATuD5 A cw mode-locked Cr⁴⁺:YAG laser, P. M. W. French, N. H. Rizvi, J. R. Taylor, *Imperial College, U.K.*; A. V. Shestakov, *IRE-POLUS, Russia*. A cw wave, room-temperature Cr⁴⁺:YAG laser, tuning from 1.37 to 1.51 μ m, is described. Mode locking of this novel laser is reported for the first time. (p. 230)

2:45 pm

ATuD6 Spectroscopy and laser operation of Mn⁵⁺-doped vanadates, Larry D. Merkle, *Night Vision and Electro-Optics Directorate*; Horacio R. Verdun, Bruce McIntosh, *Fibertek, Inc.* Mn⁵⁺-doped orthovanadate crystals, grown by Czochralski method, exhibit strong absorption at diode wavelengths, long fluorescence lifetime and room temperature laser output near 1200 nm. (p. 233)

LA SALLE BALLROOM A

3:00 pm–4:00 pm

ATuE, TRANSITION-METAL-ION LASERS 2 POSTER SESSION/ REFRESHMENT BREAK

ATuE1 Cr:Mg₂GeO₄ and Cr:CaMgSiO₄: new potential tunable solid-state laser crystals, V. Petricevic, A. Seas, R. R. Alfano, *CUNY*; M. R. Kokta, *Union Carbide Corp.*; M. H. Randles, *Litton-Airtron, Synoptics*. Basic spectroscopic properties of Cr:Mg₂GeO₄ and Cr:CaMgSiO₄ were studied in order to evaluate their potential for tunable laser operation in the 1150–1450-nm range. (p. 238)

ATuE2 Absorption and emission properties of the new laser-active center Mn⁵⁺ in several crystalline hosts, Horacio R. Verdun, *Fibertek, Inc.* Results for Ca₅(PO₄)₃F, Sr₅(PO₄)₃F, and Y₂(SiO₄)O will be presented and compared with those obtained for Sr₃(VO₄)₂ and Ba₃(VO₄)₂. (p. 241)

ATuE3 Picosecond spectroscopy of excited states in transition-metal-ion doped new laser materials, V. P. Mikhailov, N. V. Kuleshov, *Belorussian State Univ. Belarus*. Saturation of absorption and excited-state dynamics are investigated in a number of laser crystals doped with tetrahedrally coordinated Cr⁴⁺, V³⁺ and Co²⁺ ions using picosecond pump-and-probe experimental technique. (p. 244)

ATuE4 Cr⁴⁺:YSGG-passive Q-switched for multipikes Nd lasers, I. V. Klimov, I. A. Shcherbakov, V. B. Tsvetkov, *Russian Academy of Sciences, Russia*. The passive multipikes Q-switch mode of three types of flashlamp-pumped Nd lasers, such as Nd:YAG, Cr,Nd:YSGG, Cr,Nd:GSAG, using water-cooled Cr⁴⁺:YSGG modulator was experimentally investigated. (p. 246)

ATuE5 All solid-state pulsed-mode Cr:forsterite laser, Ti Chuang, Horacio R. Verdun, *Fibertek, Inc.* The Cr:forsterite laser is pumped by a diode-pumped, Q-switched Nd:YAG laser. The design and laser performance are presented. (p. 249)

ATuE6 Spectroscopic and laser studies of Cr⁴⁺-doped garnets and Y₂SiO₅, S. Kuck, K. Petermann, U. Pohlmann, G. Huber, *Univ. Hamburg, Germany*; T. Schonherr, *Univ. Dusseldorf, Germany*. The temperature-dependent absorption, emission, and lifetime data of Cr⁴⁺-doped garnet crystals and of Cr⁴⁺:Y₂SiO₅ are presented. The unusual laser behavior of Cr⁴⁺:YAG is explained by polarized excited-state absorption measurements. (p. 252)

ATuE7 Photoionization and excited state absorption in YAlO₃:Ti crystals, S. A. Basun, S. P. Feofilov, A. A. Kaplyanskii, A. F. Ioffe, *Physico-Technical Institute, Russia*; G. Huber, K. Petermann, *Univ. Hamburg, Germany*. Visible excitation of YAlO₃:Ti³⁺ at T = 77 K results in a photocurrent, which depends quadratically on the pumping power. This indicates that the photoionization of Ti³⁺ occurs as a two-step process via the intermediate ²E-state. (p. 255)

ATuE8 Luminescence properties of Cr-doped LiNbGeO₅ laser crystal, H. Manaa, R. Moncorge, *Univ. Lyon I, France*; A. V. Butashin, B. Mill, A. A. Kaminskii, *Russian Academy of Science, Russia*. Cr-doped LiNbGeO₅ single crystals have been grown and lased in the near infrared around 1.3–1.4 μ m. We report on detailed spectroscopic measurements and compare to other Cr(4+) doped crystalline materials. (p. 258)

TUESDAY, FEBRUARY 2, 1993—Continued

ASSL (Cont.)

ATuE9 Gain measurements and average power limitations in Cr³⁺:LiSrAlF₆, F. Hanson, C. Bendall, *NCCOSC/RDTE*. Gain for flashlamp-pumped Cr:LiSAF and Cr:LiSCAF from 790–1000 nm and roll-off with flashlamp repetition rate up to thermal fracture are reported. (p. 261)

ATuE10 Narrow linewidth flashlamp-pumped Ti:Al₂O₃ laser, H. Takada, F. Kannari, M. Obara, *Keio Univ., Japan*. A flashlamp-pumped narrow linewidth Ti:Al₂O₃ laser using a grazing incident grating cavity at a relatively small incident angle is described. (p. 264)

ATuE11 Mode-locking of near infrared lasers with V³⁺:YAG crystal as a saturable absorber, V. P. Mikhailov, N. I. Zhavoronkov, N. V. Kuleshov, V. A. Sandulenko, K. V. Yumashev, P. V. Prokoshin, *Univ. Belarus*. The use of vanadium-doped YAG crystal as a solid-state saturable absorber for near infrared lasers is reported. Mode-locked and Q-switched operations are realized for Ti:Al₂O₃, Pr:YAlO₃, Nd:YAG and Nd:YALO₃ laser systems. (p. 266)

LA SALLE BALLROOM B&C

4:00 pm–5:30 pm

ATuF, LISAF LASERS

James C. Barnes, *NASA, Presider*

4:00 pm

ATuF1 TW Cr:LiSrAlF₆ laser system, T. Ditmire, H. Nguyen, M. D. Perry, *Lawrence Livermore National Laboratory*. We have developed a Cr:LiSrAlF₆ laser system capable of producing peak powers in excess of 1 TW. Chirped pulse amplification in a Cr:LiSAF regenerative amplifier produces 5 mJ at 5-Hz repetition rate. Further amplification in Cr:LiSAF yields recompressed pulse energies of 150 mJ and pulse duration under 135 fsec at a 1-Hz repetition rate. (p. 270)

4:15 pm

ATuF2 Generation of tunable pulses as short as 33 fs from Cr:LiSrAlF₆ lasers, N. H. Rizvi, P. M. W. French, J. R. Taylor, *Imperial College, U.K.* A cw, argon-ion pumped, Cr³⁺:LiSrAlF₆ laser is reported for the first time which, passively mode-locked using a saturable absorber, generates 33 fs pulses. (p. 273)

4:30 pm

ATuF3 High repetition rate cw-pumped Cr:LiSAF femtosecond regenerative amplifier, Francois Balembois, Patrick Georges, Francois Salin, Gerard Roger, Alain Brun, *Univ. Paris-Sud, France*; Jean Luc Tapié, *Domaine Technologique de Saclay, France*. We have developed a cw krypton ion-pumped Cr:LiSAF regenerative amplifier for femtosecond pulses producing 11-μJ pulses at 830 nm and at a 5-kHz repetition rate. (p. 276)

4:45 pm

ATuF4 Upconversion in Cr:LiSGaF and Cr:LiSAF, M. A. Noginov, H. P. Jenssen, A. Cassanho, *Massachusetts Institute of Technology*. Upconversion was quantitatively investigated as a function of Cr concentration, pumping density and temperature. The application range of the simplest law "αn²" was found. (p. 279)

5:00 pm

ATuF5 Optical and physical properties of the LiSrAlF₆:Cr laser crystal, S. A. Payne, W. F. Krupke, L. D. DeLoach, L. K. Smith, J. B. Tassano, W. L. Kway, *Lawrence Livermore National Laboratory*. Measurements of several properties important to the laser operation of Cr:LiSAF are reported including the thermomechanical properties, durability, and Auger upconversion rates. (p. 282)

5:15 pm

ATuF6 Higher average power operation of Cr:LiSAF and Cr:LiSGaF pumped by alexandrite, W. R. Rapoport, *Allied-Signal, Inc.* The alexandrite pump laser was used to test the relative thermal failure points of several samples for different heat exchanging geometries. In addition, a Q-switched alexandrite pump laser and a cw Ti:sapphire laser were used to measure the relative gain/loss for Cr:LiSAF and Cr:LiSGaF. (p. 285)

TUESDAY, FEBRUARY 2, 1993—Continued

Compact Blue-Green Lasers

PELICAN BALLROOM

10:20 am–10:30 am

OPENING REMARKS

William P. Risk, *Program Chair*

10:30 am–12:00 pm

CTuA, APPLICATIONS OF COMPACT BLUE-GREEN LASERS 1

Mark W. Dowley, *Liconix, Presider*

10:30 am (Invited)

CTuA1 Compact blue-green lasers for future optical disk systems, Shigeo Kubota, Michio Oka, Hisashi Masuda, *Sony Corp, Japan*. We describe an aberration-free, low-noise SHG green laser for 6 time areal bit density optical disk and direct modulation in efficient KTiOPO₄ sum frequency mixing. (p. 290)

11:00 am (Invited)

CTuA2 Displays, high-definition television, and lasers, William E. Glenn, *Florida Atlantic Univ*. The technical limitations on the development of high-definition television is an adequate display. Solid state laser technology combined with light valve technology can satisfy this need. (p. 293)

11:30 am (Invited)

CTuA3 Imaging and analysis of semiconductor surfaces with a blue-green laser scanning system, Bruce Worster, *Ultrapointe Corp*. A system to provide 3-D images of submicron surface structure, composition, and defects on semiconductor wafer surfaces using a multiwavelength blue-green laser is described. (p. 296)

12:00 pm–1:30 pm

LUNCH

PELICAN BALLROOM

1:30 pm–2:45 pm

CTuB, APPLICATIONS OF COMPACT BLUE-GREEN LASERS 2

Daniel Guillot, *Uniphase Corp., Presider*

1:30 pm (Invited)

CTuB1 Use of air-cooled argon ion lasers in automated genetic analysis, Mel N. Dronick, *Applied Biosystems, Inc*. Automated analysis of genetic material using laser-based fluorescence excitation is reviewed. Lower cost laser sources would dramatically expand the market for this technology. (p. 298)

2:00 pm (Invited)

CTuB2 Short wavelength gas lasers—future and applications, William T. Silfvast, *Univ. Central Florida*. An overview of short wavelength gas lasers will be presented including a summary of their characteristics, new developments in the field, and existing and potential future applications. (p. 300)

2:30 pm

CTuB3 Laser-induced fluorescence detection in capillary electrophoresis with a blue frequency doubled light source, Fredrik Laurell, *Institute of Optical Research, Sweden*; Mårten Jansson, Johan Roeraade, *Royal Institute of Technology, Sweden*. Frequency-doubled blue light generated in a KTP QPM waveguide has been used for laser-induced fluorescence detection of fluorophore-marked amino acids in capillary electrophoresis. (p. 301)

2:45 pm–3:15 pm

REFRESHMENT BREAK

PELICAN BALLROOM

3:15 pm–4:45 pm

CTuC, BLUE-GREEN SEMICONDUCTOR LASERS

James M. DePuydt, *3M Company, Presider*

3:15 pm (Invited)

CTuC1 Growth of ZnMgSSe and fabrication of blue laser diodes, K. Akimoto, H. Okuyama, T. Miyajima, Y. Morinaga, F. Hiei, M. Ozawa, *Sony Corp*. We report on material properties of ZnMgSSe, and successful cw operation at 77 K of ZnSe/ZnMgSSe double heterostructure and multi-quantum-well laser diodes. (p. 306)

3:45 pm (Invited)

CTuC2 Advances in II-VI blue-green laser diodes, C. T. Walker, J. M. DePuydt, M. A. Haase, J. Qiu, H. Cheng, *3M Company*. Some recent advances in II-VI laser diodes include the development of electrical contacts to p-type ZnSe with lower contact resistances, the growth of high quality lattice matched ternaries and the realization of increased efficiencies in CD₂Zn_{1-x}Se quantum wells grown by atomic layer epitaxy. To gain some perspective of the status of II-VI diode laser, we compared the performance of these devices with the minimum requirements that must be met by a laser in optical recording systems. (p. 309)

4:15 pm

CTuC3 Thermal characterization of a II-VI blue semiconductor laser, R. R. Drenten, T. Marshall, J. Gaines, J. Petruzzello, *Philips Laboratories*. The temperature behavior of the active region of a blue laser is studied, using the temperature dependence of the wavelength spectrum. (p. 313)

CTuC4 Paper withdrawn.

4:30 pm

CTuC5 Digital alloy quantum wells of CdSe/ZnSe: new structures for blue-green lasers, H. Luo, S. Short, N. Samarth, A. Yin, A. Pareek, M. Dobrowolska, J. K. Furdyna, *Univ. Notre Dame*; P. Ahrenkiel, M. Al-Jassim, *National Renewable Energy Laboratory*; F. C. Peiris, J. R. Buschert, *Goshen College*. We report the study of digital alloy quantum wells of CdSe/ZnSe, which show excellent optical characteristics compared to ZnCdSe/ZnSe quantum wells. (p. 317)

WEDNESDAY, FEBRUARY 3, 1993—Continued

Advanced Solid-State Lasers

LA SALLE BALLROOM B&C

8:00 am–9:30 am

AWA, MID-IR LASERS 1

Donald J. Smith, *U.S. Air Force, Presider*

8:00 am

AWA1 Pulsed gain measurements and 3- μ m cw laser operation in Er³⁺-doped crystals, B. J. Dinerman, P. F. Moulton, D. M. Rines, *Schwartz Electro-Optics*. We report results of pulsed gain measurements and cw laser action near 3 μ m in Er:YSGG, GGG, YAG, BYF, and YLF. Large gains and high efficiencies are observed. (p. 322)

8:15 am

AWA2 Cw-cascade laser operation in Er:YLF and Er:KYF at room temperature, B. Schmaul, G. Huber, R. Clausen, *Univ. Hamburg, Germany*; B. Chai, *Univ. Central Florida*. Cw cascade lasing was demonstrated in 1% and 0.5% Er-doped yttrium lithium fluoride (YLF) at 1620 nm and 2810 nm, in 1% Er-doped potassium yttrium fluoride (KYF) at 1612 nm and 2804 nm at room temperature for the first time. (p. 325)

8:30 am

AWA3 All-optical modulation of a 2.7- μ m erbium-doped fluorozirconate fiber laser, Ch. Frerichs, *Technical Univ. Braunschweig, Germany*. A 2.7- μ m Er³⁺-doped fluorozirconate fiber laser, diode pumped at 800 nm, has been modulated by diode pumping the lower laser level at 1550 nm at kHz-rates. (p. 328)

8:45 am

AWA4 Diode-pumped single-frequency Ho:Tm:YLF, John P. Deyst, Grady J. Koch, Mark E. Storm, *Hughes/STX Corp.* Single-frequency lasing in a monolithic crystal of Ho:Tm:YLF is reported. Maximum single-frequency output power of 6 mW at a wavelength of 2.050 μ m is demonstrated. Frequency tuning is also described. (p. 331)

9:00 am

AWA5 Design and performance of a high-power, diode-pumped 2.1- μ m Tm,Ho:YAG laser, G. J. Quarles, S. R. Bowman, J. G. Lynn, C. L. Marquardt, S. K. Searles, B. J. Feldman, *U.S. Naval Research Laboratory*. We describe the design and performance of a transverse diode-pumped, Tm, Ho:YAG laser which produces 9 W average power. Multi-burst Q-switched, 60-ns, 25 mJ/pulses and frequency conversion to 4–5 μ m have been demonstrated. (p. 334)

9:15 am

AWA6 Self-mode-locking properties of Tm:YAG-lasers, Frank Heine, Ernst Heumann, Gunter Huber, *Institut für Laser-Physik, Germany*. Self-mode-locking of a cw-pumped Tm:YAG-laser was observed for the first time. Pulse formation process was strongly influenced by thermal lensing effects. (p. 337)

9:30 am–9:35 am

Advanced Solid-State Lasers

CLOSING REMARKS

T. Y. Fan, *Program Chair*

LA SALLE BALLROOM A

9:35 am–10:30 am

AWB, MID-IR LASERS 2 POSTER SESSION/COFFEE BREAK

AWB1 Single-longitudinal-mode and Q-switched diode-pumped Tm, Ho:YLF oscillators, Charley P. Hale, Sammy W. Henderson, Paul J. M. Suni, *Coherent Technologies, Inc.* We report on laser developments exploiting Tm,Ho:YLF pumped at 792 nm using 3-W diode lasers. Tunable cw and Q-switched laser results at various temperatures are described. (p. 342)

AWB2 Spectroscopy and lasing in Ho:Tm:Lu₃Al₅O₁₂, Elizabeth D. Filer, *Lockheed Engineering and Science Co.*; Norman P. Barnes, *NASA Langley Research Center*; Felipe E. Naranjo, *Science and Technology Corp.*; Milan R. Kokta, *Union Carbide Corp.* Crystal growth and spectroscopy has been accomplished and lasing has been demonstrated in what the authors believe is a new laser material, Ho:Tm:Lu₃Al₅O₁₂. Using a Ti:Al₂O₃ laser pump, lasing was observed at 2.10 μ m, a wavelength previously predicted to have a low threshold for lasing. Other spectroscopic features correspond well with predictions. (p. 345)

AWB3 Comparative study of diode-pumped two-micron laser materials, S. R. Bowman, G. J. Quarles, J. G. Lynn, B. J. Feldman, *U.S. Naval Research Laboratory*. We have studied the characteristics of Tm and Ho/Tm YAG lasers using high-power laser-diode pumping. Measurements of laser performance have been combined with spectroscopic measurements and compared to our rate equation models for these materials. (p. 347)

AWB4 Room temperature 2- μ laser action of Ho³⁺-doped YSGG, GSAG, YSAG and YAG crystals, I. V. Klimov, I. A. Shcherbakov, V. B. Tsvetkov, *Russian Academy of Sciences, Russia*. We investigate the energy output and thermolens parameters of Cr,Tm,Ho-doped active rods at different repetition rates. (p. 349)

AWB5 Long pulselength two-micron lasers for LAWS application, Mahendra G. Jani, *Science and Technology Corp.*; Norman P. Barnes, Keith E. Murray, *NASA Langley Research Center*. Efficient operation of both Ho:Tm:Cr:YAG and Ho:Tm:Er:YLF has been demonstrated using microsecond-long pulselengths. Q-switched operations in both standing wave and unidirectional ring resonators are compared. (p. 352)

AWB6 Alexandrite laser-pumped Ho:Tm:YLF laser performance, Chang J. Lee, Gooywan Han, *Hampton Univ.*; Clayton H. Bair, Norman P. Barnes, Philip Brockman, Robert V. Hess, *NASA Langley Research Center*. Experimental and theoretical results for a Ho:Tm:YLF laser in which the crystal length, Ho concentration, output coupler, and pump pulselength were varied are presented. (p. 355)

WEDNESDAY, FEBRUARY 3, 1993—Continued

ASSL (Cont.)

AWB7 Pump saturation for the 2- μ m Tm laser, Christian Hauglie-Hanssen, N. Djeu, *Univ. South Florida*. We have obtained a pump saturation formula for the 2- μ m Tm³⁺ laser and applied it to the analysis of data taken on Tm:YVO₄. (p. 358)

AWB8 Dependence of Ho upconversion rate constants in YAG on dopant concentration, L. B. Shaw, X. B. Jiang, R. S. F. Chang, N. Djeu, *Univ. South Florida*. Upconversion rate constants from ⁵I₇ to ⁵I₆ and ⁵I₆ in Ho:YAG have been determined for dopant concentrations between 1% and 10%. (p. 361)

AWB9 Tm, Ho doped alumino-zirco-fluoride glass sensitized with Yb ions, T. Izumitani, B. Peng, X. Zou, *Hoya Corp., Japan*. Tm³⁺, Ho³⁺ doped glasses and crystals have been investigated for upconversion laser (blue, green, red) and eye-safe laser. We developed 1.88 μ , 2.0, 2.84 and 0.8 μ new laser glasses using Tm³⁺, Ho³⁺ ions together with sensitizer Yb ions in alumino-zirco-fluoride glass. (p. 364)

AWB10 On the optical center in Cr³⁺-doped YAG, Hergen Eilers, Uwe Hommerich, Stuart M. Jacobsen, William M. Yen, *Univ. Georgia*. The optical spectra of Cr³⁺-doped YAG is shown to be due to more than one center. (p. 367)

AWB11 Spectroscopic investigations of the near infrared center in Cr-doped Y₂SiO₅, U. Hommerich, H. Eilers, S. M. Jacobsen, W. M. Yen, *Univ. Georgia*; W. Jia, Y. Wang, *Univ. Puerto Rico*. High-resolution measurements on Cr:Y₂SiO₅ have been carried out. Piezo spectroscopic studies show the sensitivity of the zero phonon lines toward the crystal field. (p. 370)

AWB12 Upconversion studies in laser-diode-pumped Tm,Ho:YLiF₄, G. Hansson, A. Callenas, C. Nilsson, *National Defense Research Establishment, Sweden*. The temperature dependence of the upconversion rate constant for the Ho ⁵I₇ level has been calculated from spectral measurements on a laser-diode-pumped Tm,Ho:YLiF₄ crystal. (p. 373)

Compact Blue-Green Lasers

PELICAN BALLROOM

8:45 am–9:30 am

CWA, ORGANIC NONLINEAR MATERIALS

Shinsuke Umegaki, *Keio Univ., President*

8:45 am (Invited)

CWA1 Enhanced SHG with a periodically poled nonlinear organic copolymer, Heihachi Sato, Yuji Azumai, Iwao Seo, *Mitsubishi Petrochemical Co., Japan*. Introducing a periodic corrugation of nonlinear optical susceptibility into an organic copolymer, second-harmonic power has been extremely enhanced by taking both inter-mode quasi-phase-matching and Cerenkov-radiative phase-matching. (p. 378)

9:15 am

CWA2 Organic crystal 3,5-dimethyl-1-(4-nitrophenyl)pyrazole for compact visible light sources, H. Hyuga, C. Goto, Y. Okazaki, A. Harada, S. Mitsumoto, K. Kamiyama, *Fuji Photo Film Co., Ltd., Japan*; S. Umegaki, *Keio Univ., Japan*. An organic DMNP is used in generating RGB light-waves simultaneously by a crystal-cored fiber and a blue light-wave noncritically by an intracavity configuration. (p. 382)

9:30 am–10:30 am

COFFEE BREAK

WEDNESDAY, FEBRUARY 3, 1993—Continued

Joint ASSL and CBGL Sessions

LA SALLE BALLROOM B&C

**10:30 am–11:30 am
JWA, JOINT SESSION ON INORGANIC
NONLINEAR MATERIALS**

Peter F. Bordui, *Crystal Technology, Inc.,
President*

10:30 am (Invited)

JWA1 Periodic domain-inverted non-linear optics, Hiromasa Ito, Choichi Takyu, Motoki Ohashi, *Tohoku Univ., Japan*. An e-beam method is developed for the fabrication of domain-reversed volume grating in LiNbO₃. Blue SHG experiment was performed to demonstrate efficient nonlinear interactions. Periodic domain-inverted structure has potential for the various nonlinear optical interactions. (p. 388)

11:00 am

JWA2 Comparative experimental study of KTA and KTP for the SHG at 1.32 μ m and 1.064 μ m, B. Boulanger, G. Marnier, J. P. Fève, B. Ménaert, X. Cabirol, *Univ. de Nancy I, France*; C. Bonnin, P. Villeval, *Cristal Laser S.A., France*. We compare phase-matching conditions and nonlinear optical coefficients $\chi^{(2)}$ of flux-grown KTA and KTP crystals for the SHG at 1.32 μ m and 1.064 μ m. (p. 391)

11:15 am

JWA3 Second-order optical nonlinear properties of corona-poled glass films, A. Okada, K. Mito, K. Sasaki, *Keio Univ., Japan*. The mechanism responsible for the induced $\chi^{(2)}$ in the corona-poled glass films is discussed on the basis of their second-order nonlinear properties. (p. 395)

**11:30 am–12:30 pm
LUNCH**

LA SALLE BALLROOM B&C

**12:30 pm–2:00 pm
JWB, JOINT SESSION ON
FREQUENCY UPCONVERSION IN
BULK DEVICES 1**

David C. Hanna, *Southampton Univ.,
President*

12:30 pm (Invited)

JWB1 Overview of bulk SHG activities in Japan, Takatomo Sasaki, *Osaka Univ., Japan*. The present status of the bulk type SHG device development in Japan using internal cavity resonant method for high density optical memories is presented. (p. 400)

1:00 pm (Invited)

JWB2 Diode laser upconversion in bulk nonlinear resonators—an overview of recent progress, G. J. Dixon, *Univ. Central Florida*. Recent progress in the field's resonant sum frequency generation and external resonant diode doubling is discussed. The possibilities for watt-level visible devices and the issues separating bulk nonlinear devices from the commercial marketplace are detailed. (p. 401)

1:30 pm

JWB3 Stable and efficient generation of green light by intracavity frequency doubling of Nd:YVO₄ lasers, Y. Kitaoka, S. Ohmori, K. Yamamoto, M. Kato, *Matsushita Electric Industrial Co., Ltd., Japan*; T. Sasaki, *Osaka Univ., Japan*. Stable and efficient green light in frequency doubling of Nd:YVO₄ pumped by laser diode with grating feedback optics has been demonstrated. (p. 402)

1:45 pm

JWB4 Characterization for the single-mode-operation of diode-pumped Nd:YVO₄ lasers for intracavity doubling, K. Tatsuno, S. Helmfrid, T. Andou, *Hitachi, Ltd., Japan*; T. Miyai, *Hitachi Metals, Japan*. Single axial- and polarization-mode perturbations in cavity parameters were characterized for the intracavity-doubled Nd:YVO₄ lasers to avoid fluctuations in the green output power due to the nonlinear coupling between the modes. (p. 405)

**2:00 pm–2:30 pm
BREAK**

LA SALLE BALLROOM A

**2:00 pm–4:15 pm
JWC, JOINT POSTER SESSION**

JWC1 Comparative Fourier spectroscopy of Ho³⁺ and Yb³⁺ in KYF₄, BaY₂F₈, and YLiF₄, R. E. Peale, X. X. Zhang, M. Bass, B. H. T. Chai, *Univ. Central Florida*. Fourier spectroscopy (500 to 22,000 cm⁻¹ at 1 cm⁻¹ resolution) gives accurate Ho³⁺, Yb³⁺ levels in KYF₄, BaY₂F₈ and LiYF₄ for upconversion energy transfer comparisons. (p. 410)

JWC2 Pairwise visible to UV up-conversion in Ho³⁺ and Tm³⁺ doped CaMgCl₂, Ali Gharavi, Gary L. McPherson, *Tulane Univ.* Up-conversion is observed at 11 K when ¹G₄(D) state of Tm³⁺ and ⁵F₅(D), ⁵F₄(E), ⁵F₃(F), ⁵F₂(G) and ³K₆(H) state of Ho³⁺ are pumped. These states absorb between 655 and 450 nm. The dynamics and pathways are studied which reveal a pairwise energy transfer between distinct pairs of Ho³⁺ or Tm³⁺ in crystals. (p. 413)

JWC3 Ho concentration dependence of Yb, Ho upconversion energy transfer in KYF₄, X. X. Zhang, M. Bass, B. H. T. Chai, *CREOL*. The dependence of Yb, Ho up-conversion energy transfer efficiency on the Ho concentration in KYF₄ is reported. The energy transfer mechanism is discussed. (p. 414)

JWC4 Blue, green and red, Tm³⁺, Ho³⁺ doped upconversion laser glasses, sensitized by Yb³⁺ and Er³⁺, T. Izumitani, *Hoya Corp.* Blue light emission from Yb³⁺–Tm³⁺, green light emission from Yb³⁺–Ho³⁺ and red light emission from Er³⁺–Tm³⁺ doped glasses were obtained. Emission mechanism is discussed. (p. 417)

JWC5 Nonuniformity of the phase-matching angle in flux grown KTP crystal, Takatomo Sasaki, Akio Miyamoto, Sadao Nakai, Atsushi Yokotani, *Research Development Corporation of Japan*. The phase-matching angle (PMA) in a flux grown KTP crystal was measured. It was found that the PMA changed up to 0.38 degrees corresponding to the change of n_z . (p. 420)

WEDNESDAY, FEBRUARY 3, 1993—Continued

Joint Sessions (Cont.)

JWC6 Radiative transition probabilities of trivalent rare-earth ions in LiYF_4 . C. Li, Y. Guyot, C. Linares, R. Moncorgé, M. F. Joubert, *Univ. Claude Bernard Lyon 1, France*. The radiative transition probabilities within the Nd^{3+} , Er^{3+} , Ho^{3+} and Tm^{3+} $4f$ manifolds in LiYF_4 are calculated using the Judd-Ofelt theory. The results are compared to the experimental data. (p. 423)

JWC7 Power and spatial characteristics of electron-beam-pumped semiconductor laser emitters made by different technologies. A. L. Gurskii, S. V. Davydov, E. V. Lutsenko, I. I. Kulak, A. I. Mitcovets, G. P. Yablonskii, *Academy of Science of Belarus*. The output power dependences from pump intensity for semiconductor electron-beam-pumped laser emitters based on II-VI crystals and their spatial parameters have been studied. (p. 426)

JWC8 Generation of 369.4-nm radiation by efficient doubling of a diode laser. A. Williams, D. J. Seidel, L. Maleki, *Jet Propulsion Laboratory*. We report on the generation of 369.4-nm radiation using a 738.8-nm diode laser and a lithium triborate doubling crystal in a buildup ring cavity. (p. 429)

JWC9 Self-frequency-doubling laser crystal $\text{Nd}:\beta\text{-BaB}_2\text{O}_4$. T. Ebihara, Y. Matsuka, H. Toratani, *HOYA Corp., Japan*; Liu Lin, *Chinese Academy of Science, China*. We report crystal growth conditions, second order nonlinear optical efficiency and spectroscopic properties of a new self-frequency-doubling crystal, $\text{Nd}:\beta\text{-BaB}_2\text{O}_4$. (p. 431)

JWC10 Tunable blue light source by intracavity frequency doubling of a Cr-doped LISAF laser. Francois Balembois, Patrick Georges, Francois Salin, Gerard Roger, Alain Brun, *Univ. Paris-Sud, France*. A Q-switched $\text{Cr}:\text{LiSrAlF}_6$ laser was intracavity frequency doubled by using a LiIO_3 crystal in order to produce tunable blue pulses (395–435 nm) with 7 mW average power at 407 nm. (p. 434)

JWC11 Comparison of Yb, Ho up-conversion energy transfer in different fluoride crystals. X. X. Zhang, M. Bass, B. H. T. Chai, R. E. Peale, *Univ. Central Florida*. Detailed spectroscopic comparison study of the Yb, Ho upconversion energy transfer in BaY_2F_8 , KYF_4 , and LiYF_4 is presented. Yb,Ho:KYF₄ may have promise as a green upconversion laser. (p. 437)

LA SALLE BALLROOM B&C

**2:30 pm–3:45 pm
JWD, JOINT SESSION ON
FREQUENCY UPCONVERSION IN
BULK DEVICES 2**

Thomas M. Baer, *Spectra-Physics Laser Diode Systems, Presider*

**2:30 pm (Invited)
JWD1 Controlling chaos in an intracavity-doubled Nd:YAG laser.** Rajarshi Roy, *Georgia Institute of Technology*. Theoretical analysis and experimental results on the control of chaotic fluctuations in an intracavity-doubled Nd:YAG laser are described. (p. 442)

**3:00 pm
JWD2 Fundamental walk-off compensation in KTP.** J. L. Nightingale, *Coherent Laser Group*. An oblique angle of incidence can provide walk-off compensation in Type II phase-matching. Using this technique, 264 mW of 532-nm radiation was generated with 22% conversion efficiency in a laser-diode-pumped, intracavity-doubled laser. (p. 443)

**3:15 pm
JWD3 SHG of a high-power coherent laser diode.** Robert Waarts, Ross Parke, Derek Nam, David Welch, David Mehuys, Amos Hardy, Robert Lang, Steve O'Brien, Don Scifres, *Spectra Diode Labs*. In this paper we describe frequency-doubled operation of a monolithic, high-power, GaAs master oscillator power amplifier, which radiates in a single spatial and spectral mode. (p. 446)

**3:30 pm
JWD4 Low threshold quasi-three-level 946 nm laser operation of an epitaxially grown Nd:YAG waveguide.** D. C. Hanna, A. C. Large, D. P. Shepherd, A. C. Tropper, *Univ. Southampton, U.K.*; I. Chartier, B. Ferland, D. Pelenc, *Commissariat a l'Energie Atomique, France*. We report the use of an epitaxially grown waveguide to achieve low threshold quasi-three-level laser operation of Nd:YAG at 946 nm. (p. 449)

**3:45 pm–4:15 pm
REFRESHMENT BREAK**

LA SALLE BALLROOM B&C

**4:15 pm–5:30 pm
JWE, JOINT SESSION ON
UPCONVERSION LASERS**
Bruce Chai, *Univ. of Central Florida, Presider*

**4:15 pm (Invited)
JWE1 Upconversion fiber lasers.** S. G. Grubb, *AT&T Bell Laboratories*. Over the past two years, 11 different CW, room-temperature visible upconversion fiber lasers have been demonstrated with output powers of up to 200 mW. Several of these laser and fiber material systems are reviewed with emphasis on the 3-photon Tm blue upconversion fiber laser. (p. 454)

**4:45 pm
JWE2 Ho-Yb fluoride glass fiber for green lasers.** A. Shikida, H. Yanagita, H. Toratani, *HOYA Corp., Japan*. Dependence of Yb³⁺ sensitizer and host glass composition on Ho³⁺ green emission and population inversion thresholds of various fibers are reported. (p. 457)

**5:00 pm
JWE3 Cooperative energy transfer in a Yb-Pr-doped ZBLAN fiber.** A. Remillieux, B. Jacquier, *Univ. Lyon I, France*; H. Poignant, *C.N.E.T., France*. We report the observation of cooperative energy transfer in a co-doped Yb-Pr fluoride fiber. Pulsed laser excitation induces intense blue and red fluorescences of Pr³⁺ ions. (p. 461)

**5:15 pm
JWE4 Near infrared pumped ZnSe and ZnSSe blue lasers.** X. H. Yang, W. Shan, J. M. Hays, J. J. Song, *Oklahoma State Univ.* Near-infrared pumped blue laser emission of ZnSe and $\text{ZnS}_{0.05}\text{Se}_{0.95}$ single crystal samples has been observed at the temperature ranging from 10 to 200 K. (p. 464)

THURSDAY, FEBRUARY 4, 1993

Compact Blue-Green Lasers

PELICAN BALLROOM

8:30 am–10:15 am

CThA, FREQUENCY UPCONVERSION IN WAVEGUIDE DEVICES 1

Martin M. Fejer, *Stanford Univ.*, *Presider*

8:30 am (Invited)

CThA1 Quasi-phases-matched waveguides periodically poled by applying an external field for efficient SHG, M. Yamada, N. Nada, M. Saitoh, K. Watanabe, *Sony Corp.*, *Japan*. We present current results about our efficient QPM-SHG devices in lithium niobate fabricated by applying the external electric field method. (p. 468)

9:00 am (Invited)

CThA2 Linear and nonlinear optical properties of annealed proton exchanged LiNbO₃ waveguides, M. L. Bortz, L. A. Eyres, M. M. Fejer, *Stanford Univ.* We discuss the characterization of the linear and nonlinear optical properties of annealed proton exchanged LiNbO₃ necessary for the optimization of guided wave frequency conversion devices. (p. 470)

9:30 am

CThA3 Phase-matched and Cerenkov-type second-harmonic blue light generation in ion-implanted KNbO₃ waveguides, D. Fluck, P. Günter, *Swiss Federal Institute of Technology, Switzerland*; M. Fleuster, Ch. Buchal, *Institut für Schicht- und Ionentechnik, Germany*. We present results on the fabrication and tailoring of slab and channel waveguides in KNbO₃ by He ion implantation. We report phase-matched as well as Cerenkov-type SHG at wavelengths of ~430 nm with normalized conversion efficiencies of up to 41%/W cm. (p. 473)

9:45 am

CThA4 Fabrication of periodically inverted domain structures in LiTaO₃ using proton exchange, Satoshi Makio, Fumio Nitanda, Kohei Ito, Masayoshi Sato, *Hitachi Metals, Ltd.*, *Japan*. Using proton exchange with one-directional heating, deeply inverted periodic domains were fabricated in LiTaO₃. Blue light SHG was emitted from the waveguide devices. (p. 476)

10:00 am

CThA5 Frequency doubling of laser diode using periodically domain-inverted LiTaO₃, K. Yamamoto, K. Mizuuchi, Y. Kitaoka, M. Kato, *Matsushita Electric Industrial Co., Ltd.*, *Japan*. Locking the lasing wavelength of laser diode by grating feed-back technique, 3.1 mW of stable blue SHG has been demonstrated by a periodically domain-inverted LiTaO₃ waveguide. (p. 480)

10:15 am–10:45 am

COFFEE BREAK

PELICAN BALLROOM

10:45 am–12:00 m

CThB, FREQUENCY UPCONVERSION IN WAVEGUIDE DEVICES 2

John D. Bierlein, *E. I. DuPont de Nemours Co.*, *Presider*

10:45 am (Invited)

CThB1 Quasi-phase-matching (QPM) in the channel Rb:KTP waveguides, Eugene A. Shcherbakov, Vladislav A. Maslov, *Russian Academy of Science, Russia*. The periodic domain-inverted gratings induced by dielectric film cladding was demonstrated in KTP crystal. It was shown that in Rb:KTP channel waveguides, the third-order QPM resulted in the SHG ($\lambda = 400$ nm) efficiency of 29% W⁻¹cm⁻². (p. 484)

11:15 am

CThB2 KTP segmented waveguides as concurrent Bragg reflectors and SHG, M. G. Roelofs, W. Bindloss, A. Suna, J. D. Lee, J. D. Bierlein, *E. I. du Pont de Nemours & Co.* We discuss the design of segmented waveguides satisfying simultaneously the Bragg condition (feedback for diode stabilization) and the quasi-phases-matching condition for SHG. (p. 485)

11:30 am

CThB3 Generation of 425-nm light by waveguide frequency doubling of a GaAlAs laser diode in an extended-cavity configuration, W. P. Risk, W. J. Kozlovsky, W. Lenth, S. D. Lau, *Almaden Research Center*; G. L. Bona, H. Jaekel, D. J. Webb, *Zurich Research Laboratory, Switzerland*. A periodically poled KTP waveguide was used for efficient frequency doubling of a GaAlAs laser diode operated in an extended-cavity configuration. A blue power of 0.21 mW was generated at 425 nm from 22 mW of 850-nm power. (p. 489)

11:45 am

CThB4 Characteristics of KTiOPO₄ waveguides up to high-power densities, P. A. Morris, J. B. Brown, J. D. Bierlein, *E. I. du Pont de Nemours & Co.* Changes in the propagation characteristics of KTiOPO₄ waveguides exposed to 458, 514, and 790 nm cw radiation at power levels of 5 kW/cm²–1 MW/cm² are discussed. (p. 492)

12:00 m–1:30 pm

LUNCH

LA SALLE BALLROOM A

1:30 pm–3:00 pm

CThC, POSTER/POSTDEADLINE PRESENTATION

CThC1 Cerenkov-type SHG in lossy slab waveguides, T. Kinoshita, K. Sasaki, *Keio Univ.*, *Japan*; Y. Yokoh, H. Ashtaka, *Ube Industries, Ltd.*, *Japan*; N. Ogata, *Sophia Univ.*, *Japan*. A remarkable reduction of undesirable loss influence for the efficient Cerenkov-type SHG is theoretically analyzed and experimentally demonstrated. (p. 496)

CThC2 Compact Raman shifter, D. E. Gakhovich, A. S. Grabchikov, V. A. Orlovich, *Belarus Academy of Sciences, Belarus*; S. S. Dvornikov, *STC Solar, Belarus*. We discuss the results of the experimental investigation of the stimulated Raman scattering under conditions of tightly focusing with the pumping by third and second harmonics of YAG:Nd lasers. (p. 498)

CThC3 GaN for short wavelength devices: growth kinetics and techniques, Jennifer Ross, Nathan Newman, Mike Rubin, *Lawrence Berkeley Laboratory*. We present the thermodynamic and kinetic processes involved in GaN thin film growth and the limiting factors for nitrogen incorporation. Using this information, we produce GaN films with n-type concentrations as low as 8×10^{14} cm⁻³. (p. 500)

3:00 pm–3:30 pm

REFRESHMENT BREAK

PELICAN BALLROOM

3:30 pm–5:20 pm

ROUNDTABLE DISCUSSION

5:20 pm–5:30 pm

Compact Blue-Green Lasers

CLOSING REMARKS

John D. Bierlein, *Program Cochair*

Monday, February 4, 1993

High Power Diode-Pumped 1 μm Lasers

AMA 8:00am–9:30am
La Salle Ballroom B&C

Rudolf G. Buser, *Presider*
U.S. Army Night Vision & Electro-Optics Directorate

One Joule Per Pulse, 100 Watt, Diode-Pumped,
Near Diffraction Limited, Phase Conjugated, Nd:YAG
Master Oscillator Power Amplifier

Randall J. St. Pierre, Hagop Injeyan*, Rodger C. Hilyard, Mark E. Weber,
Jacqueline G. Berg, Michael G. Wickham, Carolyn S. Hoefer, and Jason P. Machan

TRW Space and Technology Group
One Space Park R1/1184, Redondo Beach, CA 90278
(310) 812-0085

Summary

A 100 W average power, diode-pumped, phase conjugated Nd:YAG master oscillator power amplifier (PC MOPA) has been assembled and characterized. The laser uses a small diode-pumped master oscillator to drive a diode-pumped, zig-zag slab amplifier in a folded, 2-pass configuration to provide efficient extraction. SBS phase conjugation in freon is used to correct the aberrations in the amplifier and obtain a near diffraction limited beam. 1 J has been extracted at a repetition rate of 100 Hz with a beam quality of $1.1 \times D. L.$ The pulse duration is 7 ns with excellent spatial uniformity making it ideal for doubling and parametric conversion. The optical efficiency of the laser is 22% and using an average diode array efficiency of 43%, the overall efficiency is 9.3% (not including the power supply and cooling system).

Figure 1 shows the schematic layout of the laser. A beam from the master oscillator propagates through a Faraday isolator, is beam expanded and clipped by a reference aperture to provide a spatially uniform beam. The beam then propagates through a polarizer and is image relayed into the amplifier. The beam propagates through the upper half of the amplifier, is image relayed onto a prism which translates the beam vertically and returns to the lower half of the amplifier. Following two amplification passes the beam is again image relayed onto the SBS cell and retraces its path towards the polarizer. A quarter-wave plate placed in front of the SBS cell rotates the beam polarization and the amplified beam is extracted by the polarizer. Image relaying is used throughout the optical train to minimize the effects of diffraction, maintain beam uniformity and optimize coupling efficiency between various apertures.

The master oscillator uses a 3 mm diameter and 8 cm long rod. It is side pumped by 6 SDL 3-bar stacks. The diodes are close coupled to the rod which is AR coated at 808 nm on one side and HR coated on the opposite side for optimum pump absorption. The Q-switched cavity uses an unstable resonator with a gaussian reflectivity outcoupler. 10 mJ pulses with a pulse duration of 9 ns are obtained with excellent pulse to pulse amplitude ($\leq 0.3\%$) and directional ($\leq 1\%$) stability. The overall efficiency of the master oscillator was approximately 4% but because it represents only 1% of the total extracted energy, it was not a factor in the overall efficiency. The 3 mm diameter output beam is expanded by a factor of 5 and clipped by a 9×7.5 mm aperture to provide a 4.5 mJ spatially uniform rectangular beam at the amplifier.

The amplifier consists of a water cooled $0.6 \times 2.7 \times 12$ cm zig-zag slab fabricated by Litton-Airtron. The slab ends are cut for near normal incidence at 50° relative to the horizontal making the internal zig-zag angle approximately 40° . A 1 mm channel of water flow on each side provides uniform and symmetric cooling of the slab. The slab is side pumped by a 2×5 cm array of SDL diodes on each side for a total of 20 cm^2 . Each

1 cm² module consists of a 25-bar stack operating at a peak power of 1500 W for a duration of 150 μ s. Small signal gain measurements have indicated a stored energy of 1.8 J for a storage efficiency of 41%. Average small signal gains of 2.9 were measured across the slab aperture when using a 150 μ s diode pulse duration (Figure 2) at which point parasitic oscillations began to appear. OPD measurements at 100 Hz repetition rate using a HeNe laser Mach-Zehnder interferometer have shown a residual OPD, after tilt subtraction, of approximately 0.6 waves. OPD levels an order of magnitude larger have been corrected with good fidelity using SBS in similar PC MOPA configurations¹.

The SBS medium consisted of Freon 113. Freon 113 is a liquid at room temperature and has shown excellent SBS properties in previous experiments using 1 μ m lasers². Energies > 1.5 J have been injected in Freon using simple focus geometry without encountering breakdown or competing processes. Threshold energies on the order of 2-3 mJ, slope efficiencies near unity and a demonstrated dynamic range in excess of 500:1, make this material an ideal choice for phase conjugated solid state laser applications.

Figure 3 shows the optical layout used for the extraction experiments. Diagnostic wedges were used throughout the layout to measure the energy at key positions. An energy-in-a-bucket diagnostic was used to measure beam quality at the output. Energy measurements included the energy injected into the amplifier, the energy injected into the SBS cell, the energy returned from the SBS cell, the output energy and the energy outcoupled by the Faraday isolator which measures energy lost to birefringence. Figure 4 shows the extracted energy and the beam quality as a function of the input MO energy with a 7.5 x 9 mm aperture. 1 J was extracted with a beam quality of 1.1 x D.L. at the maximum MO energy of 4.5 mJ in the amplifier. The corresponding net extraction efficiency is 55% (62% within the sampled aperture). The system optical efficiency was 22% and the overall efficiency was 9.3% including the master oscillator but not counting the power supply and cooling systems. These numbers represent record performance for Q-switched, Joule class lasers and the combination of average power and beam quality makes this the brightest laser reported to date (Brightness = Ave. Power/4 λ^2 BQ²). The pulse duration was 7 ns FWHM showing a small amount of compression of the 9 ns near gaussian MO pulse. Figure 5 shows the near field and far-field intensity distribution of the extracted beam. The excellent near field uniformity is ideal for frequency doubling and parametric conversion and is attributed to the zig-zag amplifier and image relaying. The far field spot showed no measurable angular jitter. Figure 6 shows the energy out vs. energy into the SBS cell; the slope efficiency of 85% includes the round trip losses from the lens and the uncoated input window of the SBS cell (2% for the lens, 8% for the air/window interface and 1% from the liquid/window interface). This makes the intrinsic slope efficiency of the SBS medium 95%. Near perfect linearity at average power levels of 30 W highlights the absence of competing processes. The average power of 30 W in the SBS cell also is the highest reported for a short pulse system.

References

1. R. St. Pierre, H. Injeyan, M. Wickham and C. Hoefer, paper CThD4, Technical Digest, CLEO 91, May 12-17, Baltimore MD.
2. R. St. Pierre, H. Injeyan, and J. Berg, paper CTuN3, Technical Digest, CLEO 92, May 10-15, Anaheim CA.

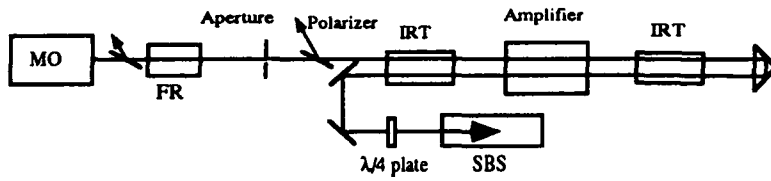


Figure 1. Schematic layout of LARRE (laser for risk reduction experiments)

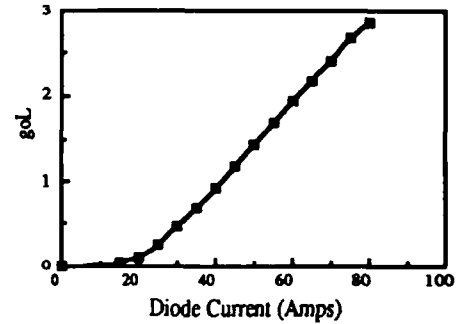


Figure 2. Amplifier small signal gain as a function of diode current

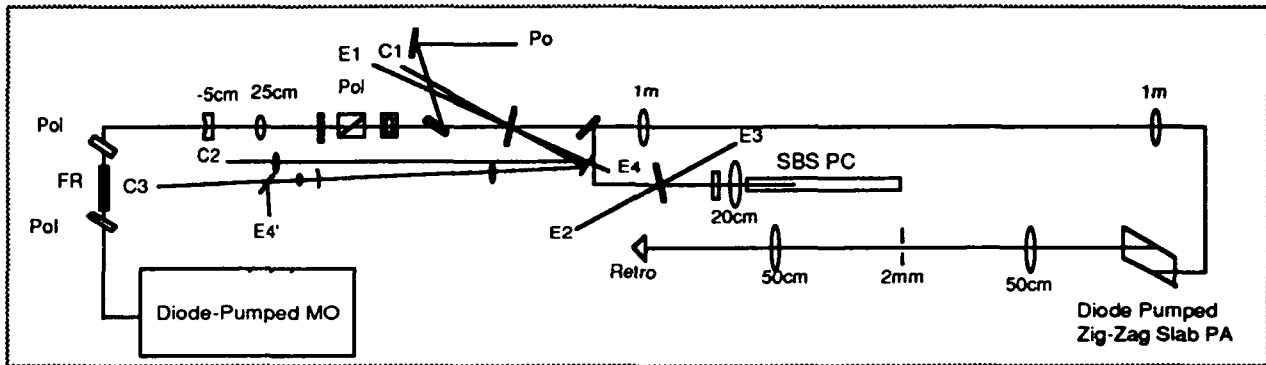


Figure 3. Detailed optical layout of the LARRE phase conjugated MOPA

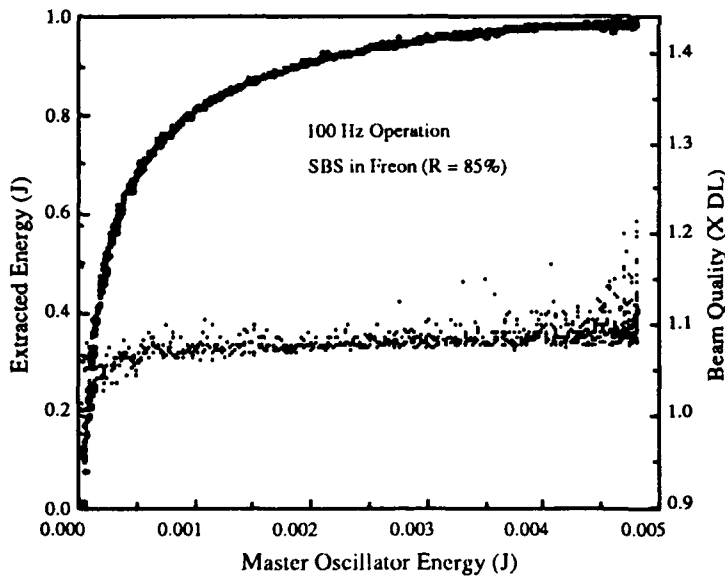


Figure 4. Extracted energy and beam quality as a function of master oscillator energy.

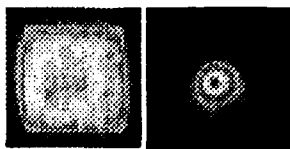


Figure 5. Near-field and far-field intensity distributions of the extracted beam

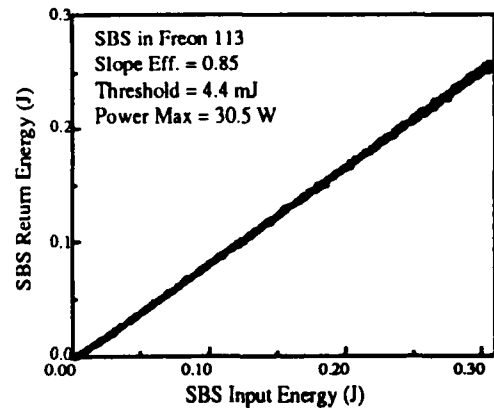


Figure 6. SBS reflectivity in Freon 113

**A CONDUCTIVELY COOLED DIODE PUMPED PHASE CONJUGATE Nd:YLF
LASER WITH 0.5 JOULE ,100 Hz AT 547nm. OUTPUT.**

BY

**E. Gregor, S. Matthews, R. Muir, O. Kahan, T. Chen, J. Source,
M. Polumbo, C. Kalina, K. Nielson and J. Ortize.**

**Electro Optical Systems
Hughes Aircraft Company
El Segundo,CA 90245
310/616-3955**

The development of efficient laser diodes at ~800 nm to be used as the pump source for solid state laser materials has revitalized the solid state laser technology. The overall efficiencies have been extended from 1% to 10 %. The improved efficiencies and, reduced by a factor of 3, heating of the laser crystals have opened the door for passive cooling technologies to be applied to medium energy lasers at pulse rates at the 100 Hz level. Passive cooling, without the use of flowing liquids are preferred when the laser is taken out of the laboratory into severe environments including space.

We are presenting here the results obtained from the brassboard hardware. The design of the unique conductively cooled diode pumped heads was developed on Hughes IR&D funds in 1989 and is described in Figure 1. (US Patent #4969155). These passively cooled laser heads were combined with the unique properties of Nd:YLF and a double-pass master oscillator power amplifier (MOPA) architecture using a phase conjugate mirror, depicted in Figure 2. This MOPA architecture, the phase conjugate mirror and the low thermal lensing properties of Nd:YLF were selected to reduce the thermal effects which limit performance at 100 Hz operation.

The second harmonic generation (SHG) crystals were located in the phase conjugated part of the MOPA where compensation is provided to thermally induced distortion. This phase conjugate MOPA laser architecture has been used at Hughes for several years with flash lamp pumped lasers at the 1 Joule 30 Hz level. (1),(2).

Heat removal from the pump diodes was accomplished by conduction from the diode aluminum heat sink through heat pipes to an external heat sink. The laser rod was also conductively cooled to the aluminum heat sink and then heat pipes removed the heat to an external heat sink. The heat pipes used are sealed containers which transport the heat internally very efficiently through a phase change process and are commonly used in space applications.

The brassboard laser system was demonstrated to the following performance parameters:

WAVELENGTH	524 nm
OUTPUT ENERGY	500 mJ/pulse
REPETITION FREQ	100 Hz
PULSE WIDTH (FWHM)	<15 nsec
COHERENCE	<1cm
BEAM QUALITY	<2x diff.lim.

This work was conducted under contract F33615-90-C-1504 for the Air Force Wright Laboratory Electro-Optical Sources Branch with F. R. Kile as technical manager.

References:

- (1) E. Gregor, D. W. Mordaunt, S. C. Matthews, O. Kahan, A. R. Muir, and M. Palombo, SPIE Vol.1627 Solid State Lasers III, 1992, pp.65-73.
- (2) D. A. Rockwell, IEEE J. Quantum Electron., 24, 1124, 1988.



Figure 1. The conductively cooled diode pumped laser head features passive cooling of the pump diode arrays and the laser rod.

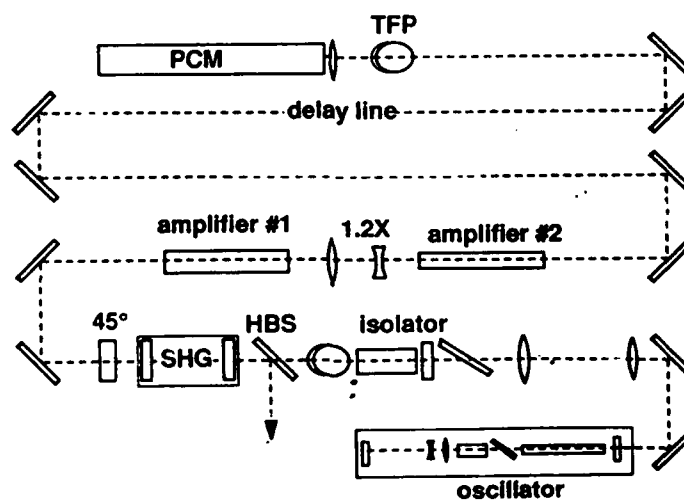


Figure 2. The optical diagram identifies the major components of a MOPA featuring phase conjugation and oscillator isolation.

High-Power Diode-Pumped Solid-State Industrial Laser

R. Burnham, P. Bournes, J. Kasinski, K. Le and D. DiBiase
Fibertek, Inc.
510-A Herndon Parkway
Herndon, VA 22070
(703) 471-7671

Diode-pumped solid-state lasers continue to make advances in terms of average and peak power, efficiency and reliability. The most recent advances have been made in the average power capabilities of diode pump arrays which in turn allows the output power of diode-pumped lasers to be scaled in an economically advantageous way. As an example, quasi-cw pulsed arrays have now been operated at duty cycles up to 40% with peak powers of over 50 W per one-cm diode bar. Bars can be stacked at densities of $\approx 10/\text{cm}$ to produce average pump fluxes of over $200 \text{ W}/\text{cm}^2$. With these advances, it becomes the task of solid-state laser designers to use this power effectively for the development of high-brightness diode-pumped lasers.

In this paper we describe results obtained with a compact diode-pumped rod laser module with an output power capability of up to 500 W. To date this module has been operated with Nd:YAG as gain medium pumped by 80 1-cm diode bars arranged in 16-bar stacks on 4-cm long impingement-cooled mounts. A diagram of the laser pump module is shown in Figure 1. The diode arrays are arranged around the rod in 5-fold symmetry. Each 1 cm segment of the rod is pumped by 20 diode bars which produce a peak power output of $1000 \text{ W}/\text{cm}$. The active length of the module is 4 cm so that the total peak optical input power to the module is 4000 W. The module was operated at duty cycles up to 12% which was limited by the diode array electrical driver. The maximum input to the laser rod was therefore 480 W. The diode pump arrays are cooled in parallel. At a flow rate of $\approx 1 \text{ gpm}$ the temperature rise at the diode array junction is approximately 1 C per % duty cycle. The diode arrays are connected in series electrically and operated at 150 V with currents up to 70 amps. The electrical efficiency of the diode pump arrays was approximately 45%.

The pump module used a 1% doped, Nd:YAG laser rod with a diameter of 1 cm and a length of 6.5 cm. The output power vs. pulse repetition rate for the diode pumped module operating multimode are shown in Figure 2. The maximum output power obtained was 196 W at 400 pps with a $300 \mu\text{s}$ pump pulse. Varying the pulse length had a minimal effect on the average power. This indicates that diode array frequency chirp during the pulse is not a problem in the laser. There is also no noticeable change in the energy/pulse as the duty cycle is increased to 12%. This implies that there is no large shift in the average pump wavelength of the pump arrays as the duty cycle increases.

At the maximum 12% duty cycle at which the laser was operated, the power input from the DC power supply to the diode arrays was 1100 W. The electrical efficiency of the laser was therefore 17.8%. The optical conversion efficiency based on the diode array output at 808 nm was 41%.

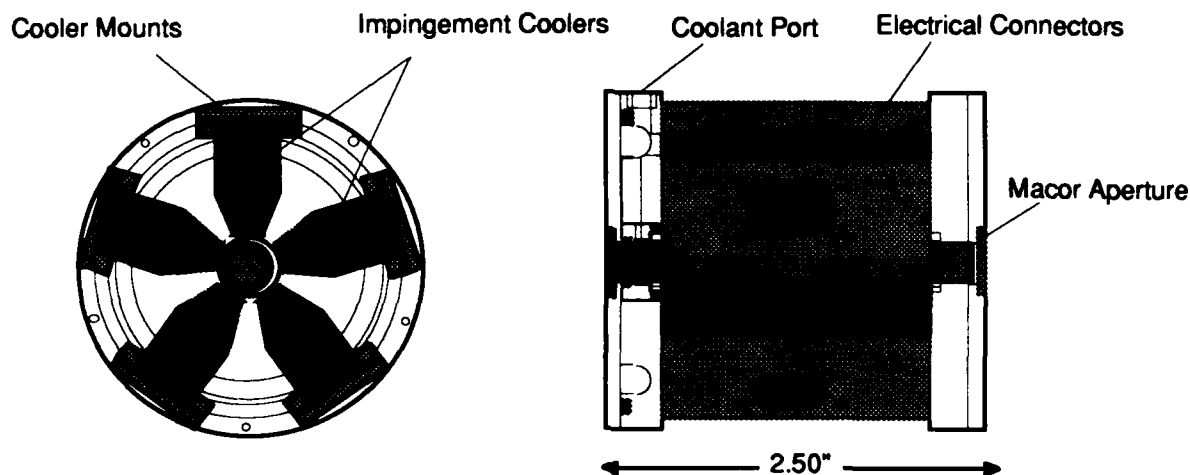


Figure 1. Schematic diagram of high power diode pumped solid-state laser module.

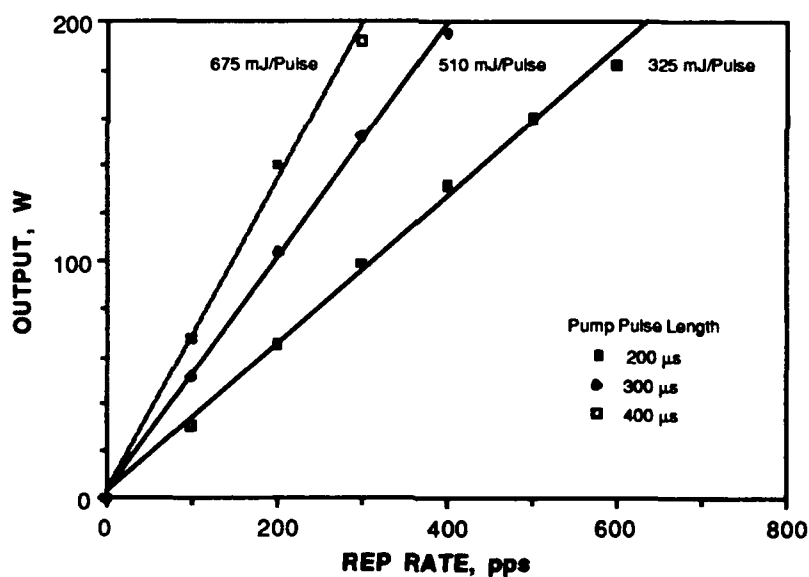


Figure 2. Nd:YAG laser output vs repetition rate for various pump pulse lengths. The maximum duty cycle in each case is 12%.

An important consideration for high-power solid-state lasers is the thermo-optical properties of the laser rod. We have measured the thermal lensing and thermal stress-induced birefringence in the present laser as a function of power input to the laser rod. Both lensing and birefringence were measured using a 6 mm diameter collimated HeNe beam at 633 nm as a probe. The measured thermal reciprocal focal length was found to be linearly dependent on pump power input with a

slope of 0.10 diopter per percent duty cycle. For the present laser this lensing corresponds to 0.0025 D / W incident on the laser rod.

Stress induced birefringence was also measured using the HeNe probe beam. Depolarization loss is plotted as a function of duty-cycle in Figure 3. The loss has a Lorentzian dependence on pump power as expected for a Gaussian probe beam. The measured thermal lensing and birefringence are in good agreement with a thermo-optical model of the Nd:YAG laser rod pumped in our configuration. Both were measured without laser flux in the rod and therefore represent an upper limit on the thermal aberration expected in an operating laser. Data taken at 633 nm has been adjusted to give the expected depolarization at 1.06 μm .

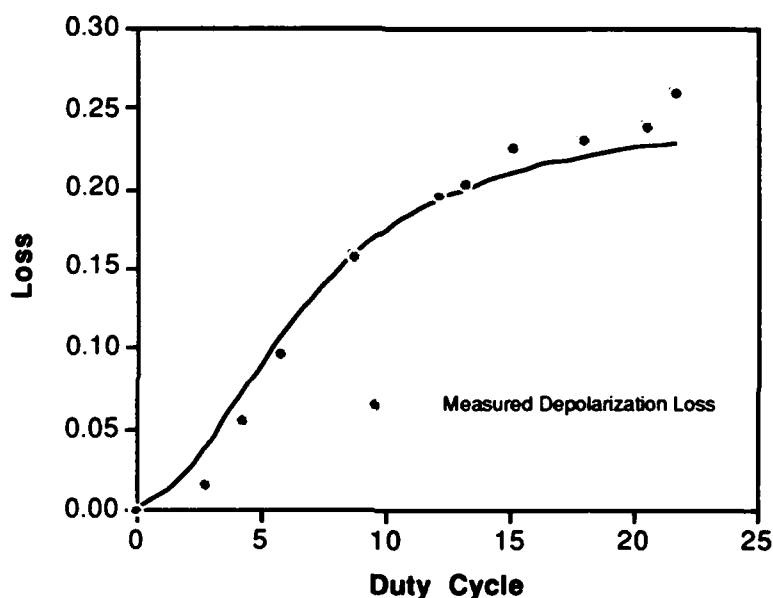


Figure 3. Thermal stress birefringence measured for the high-power diode-pumped Nd:YAG laser module.

The high-power laser pump module is intended for application in a range of industrial lasers with power output from 100 W to 1 kW. One module will provide up to 500 W average power when used at the maximum output of the diode pump arrays (60W/bar at 25 % duty cycle). In order to increase the output, two pump modules will be used in tandem. This configuration allows for correction of the thermal effects using correction optics (lenses and waveplates) located between the modules.

For most applications high beam quality is also required. To address this requirement we are developing unstable resonators with graded reflectivity output mirrors to provide single transverse mode output. The fact that the thermo-optical effects in the diode-pumped laser are relatively mild, and that the excitation density in our design is centrally peaked and circularly symmetric implies that extremely high beam quality will be obtained. The results of high-brightness resonator experiments will be reported.

High-Power Single-Mode Diode-Pumped Graded-Reflectivity-Mirror/Stable Oscillator

Jeff Kasinski, Pat Bournes, and Ralph Burnham
Fibertek, Inc., 510 Herndon Pkwy, Herndon, VA 22070, (703)-471-7671

1. Introduction

Diode-pumping of solid-state media has been demonstrated to have significantly enhanced solid-state laser performance in terms of higher efficiency and greater average power at higher repetition rates in a smaller, more robust package. With the new vistas for more demanding applications that this approach has opened, there is a greater challenge to improve many laser output parameters without sacrificing performance in any others. In particular, many applications that use high energy densities (e. g., radar, welding, cutting), require simultaneous optimization of beam quality and overall efficiency with high pulse energy at high repetition rates.

In this paper, a Nd:YAG diode-pumped oscillator is demonstrated which operates Q-switched at the 100 mJ level in a near diffraction-limited beam at 10% absolute optical efficiency at repetition rates up to 100 Hz. The novel resonator design incorporates a graded reflectivity mirror (GRM) in a normally stable cavity. This oscillator is of high enough energy to be used for efficient, high-beam-quality amplification to better than 1 J.¹ This oscillator is designed as the front end to a diode-pumped MOPA which will produce 50 W at 532 nm at 100 Hz with a wallplug efficiency of 5%. Higher energy and repetition rate scaling of the oscillator is also illustrated.

2. Experimental

Various resonators were investigated based on the design of Figure 1. The gain medium was a Nd:YAG rod (5 mm or 6.3 mm diameter), side-pumped by 80, 60W Spectra Diode Array laser diode bars (5 bar stacks) arranged in 8-fold circular symmetry;¹ the laser was operated with either one or two of these units. The laser diodes were run at 60W/bar at a pump pulse width of 150 μ sec at repetition rates up to 125 Hz. The laser was Q-switched with Solgel coated KD*P (Cleveland Crystals).

The cavity end mirrors were restricted to a concave/convex configuration; the curvatures and cavity length were adjusted to investigate both stable and unstable resonators. The output coupler was a GRM (National Optics Institute of Canada)² with a reflectivity profile given by

$$R(r) = R_0 \exp(-(r/a)^2) \quad (1)$$

where R_0 is the peak reflectivity and a is the intensity reflectivity Gaussian radius; R_0 was kept to 50% (the highest available for good damage threshold) while a ranged from 0.7 mm to 2.0 mm.

3. Results

High beam quality, high pulse energy output has recently been accomplished in flashlamp Nd:YAG lasers with the use of a GRM in normally unstable confocal resonators.^{2,3} However, for high efficiency performance with a diode-pumped laser, this approach must be modified. The operational difference in a diode-pumped laser is a lower gain — for an equal output, achieving higher efficiency requires a lower stored energy (or gain) for a given output. Since lower gain necessitates a lower output coupling, an unstable/GRM resonator, which has very high output coupling, is a poor match for this situation.

A design to maintain both high efficiency and high beam quality in a diode-pumped oscillator was to use a GRM in a normally stable resonator (Figure 1B). A concave/convex cavity somewhat near the stability boundary ($g_1 g_2 = 0.9$) was chosen to maintain a large spot size throughout the resonator for a higher extraction efficiency. The GRM acts as a soft aperture to discriminate against higher order modes. It was

found that the mode quality of any GRM resonator is determined primarily by the Fresnel number of the GRM, which is given by

$$\frac{2a^2}{\lambda L} \quad (2)$$

where L is the cavity length. This is illustrated in Figure 2., in which the diffraction-limitedness of the beam was measured as a function of various GRM spot sizes; this relationship holds for both stable and unstable resonators, as both of these are represented in the data of Figure 2. For Fresnel numbers of about ≤ 2 , the output is essentially diffraction limited; both the near and far field beam profiles are Gaussian.

The output energy of the beam is illustrated in Figure 3 for the optimized stable/GRM resonator (80 bars, HR = +3 m, GRM = -4 m, $a = 1.0$ mm). The QS energy is 70 mJ with an optical slope efficiency of 17%, corresponding to absolute optical and electrical efficiencies of 10% and 5%. This output was $1.5\times$ diffraction-limited. The output energy is a factor of 2 greater than what could be obtained by using a uniform output coupler with a hard aperture to restrict the cavity to single mode. The output was also a factor of 1.6 greater than what could be obtained in an optimized unstable resonator with $M=1.25$; further, with an unstable resonator of such low magnification, the stable/GRM had an order of magnitude better pointing stability.

The energy and mode quality was maintained up to 70 Hz; above this, thermal birefringence of the head was enough to distort the mode. The beam quality was regained above 70 Hz when the birefringence was compensated with a porro prism (Figure 1A.); in this configuration, the laser could be run up to the 100 Hz limit of the diodes. In this porro prism cavity, output was 53 mJ and was limited to $2.2\times$ diffraction-limited by the porro knife edge. This can be eventually improved by removing the porro and using a phase rotator between two identical heads to compensate the thermal birefringence. This resonator should be scaleable in average power to repetition rates well above 100 Hz; work is ongoing in this area. Preliminary investigations into energy scaleability with two heads (144 bars) in an unstable resonator demonstrate 115 mJ diffraction-limited output with 10% optical efficiency; a higher slope efficiency but high threshold value indicates that even higher gain is necessary for higher efficiency in the unstable approach.

4. Conclusions

A novel diode-pumped stable/GRM oscillator was demonstrated to maintain simultaneously high energy, repetition rate, and beam quality with output of 70 mJ at $\leq 1.5\times$ diffraction-limited at $1.06\ \mu\text{m}$ with an electrical efficiency of 5% at repetition rates up to 70 Hz; output at 100 Hz of 53 mJ and near $2\times$ diffraction-limited can be improved even further with a phase-rotator-compensated two head design. This oscillator is currently being implemented into a spaced-based diode-pumped MOPA for a projected performance of near-diffraction-limited 500 mJ at 532 nm at 100 Hz and 5% wallplug (including cooling and all overhead) efficiency.

Acknowledgements

This work was supported by the U. S. Airforce Wright Research and Development Center (WRDC/ELOS), contract #F33615-90-C-1503.

References

1. J. Kasinski, W. Hughes, D. DiBiase, P. Bournes, and R. Burnham, *IEEE J. Quant. Elect.*, **28**, (1992), 977.
2. K. Snell, N. McCarthy, M. Piché, and P. Lavigne, *Opt. Comm.*, **65**, (1988), 377.
3. S. De Silvestri, V. Magni, O. Svelto, and G. Valentini, *IEEE J. Quant. Elect.*, **26**, (1990), 1500.

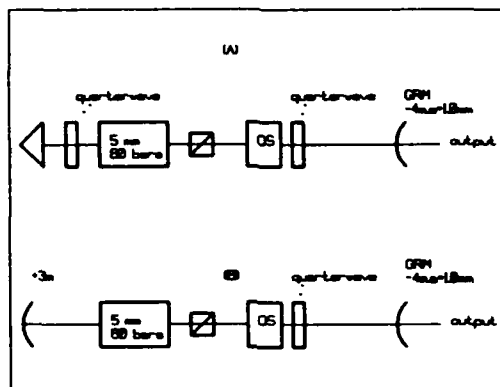


Figure 1: Oscillator Schematic. (1A) = birefringence compensation with porro prism; head = 80 bars or 144 bars circularly symmetric side-pumping, 5 mm or 6.3 mm diameter Nd:YAG rod, effective lens of +3 m at 100 Hz. (1B) stable/GRM resonator; head as in 1A; output = 70 mJ at $\leq 1.5\times$ diffraction-limited with 5% electrical efficiency.

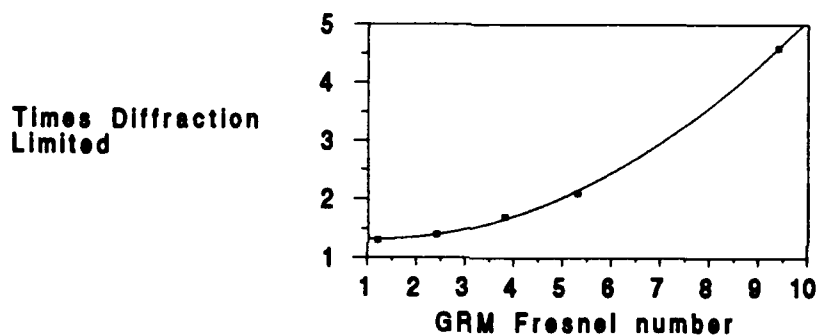


Figure 2: Beam quality versus GRM reflectivity spot size. Data represents both stable and unstable resonators. Output is essentially diffraction limited for Fresnel number ≤ 2 .

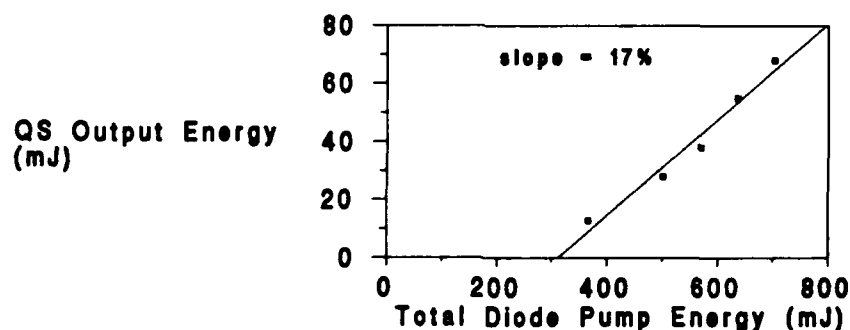


Figure 3: Output of stable/GRM oscillator. Energy = 70 mJ, $\leq 1.5\times$ diffraction-limited up to 70 Hz with optical slope efficiency of 17%. For 70 Hz - 100 Hz, high beam quality output of 53 mJ is obtained with porro prism compensation of thermal birefringence.

Efficient Diode-Pumped cw Nd:YAG Laser

With 60 W Near-Diffraction-Limited Output

S. C. Tidwell, J. F. Seamans, and M. S. Bowers

STI Optronics, Inc.

2755 Northup Way, Bellevue, Washington 98004-1495

(206) 827-0460

We have previously reported on a scalable end-pumped laser architecture which used four 10-W cw laser diode bars to pump a laser that produced a multimode output power of 15 W[1]. This approach has the economic advantages of utilizing diode bars, which are the least expensive source of diode power in terms of cost per watt[2], and operating with very high wall-plug efficiencies. In the present work, we have used the same power scaling approach[3] to extend the multimode output power of cw diode-pumped lasers to 92 W. In addition, thermal distortion and stress-induced birefringence have been corrected in this laser to produce a TEM₀₀ output power of 60 W with an optical-to-optical efficiency of 26%. This is the first demonstration that the effects of higher-order thermal non-uniformities, which are inherent to end-pumped lasers, can be overcome.

We use an angularly-multiplexed pump geometry to deliver the diode power to the rod end. Four 15-W laser diode bars (SDL-3450-S) are arrayed around both ends of each rod as shown in Fig. 1. The two sets of diodes on each rod are clocked 45° with respect to one another to produce a circular gain distribution. The efficiency with which pump light is transferred from the diode and absorbed in the rod is over 80%. Thus, of the available 60-W pump power per rod end approximately 50 W is absorbed. The primary advantage of end-pumping for cw lasers is that the pump power is concentrated in the central portion of the rod, as shown in Fig. 2, where it produces high gain and can be

extracted efficiently by the fundamental mode.

A resonator having a symmetry plane between the two rods, as illustrated in Fig. 3, was designed for high beam quality extraction tests. The symmetry assures the mode sizes are nominally the same in both rods. The resonator uses flat end mirrors separated from the rods by 65 cm and a rod separation of 20 cm. A -16-cm focal length lens located at the symmetry plane compensates for most of the thermal lensing in the rods. The birefringence is corrected by placing a quartz polarization rotator between the two rods[4]. If the thermally-induced stresses and ray paths are identical in the two rods then the depolarization and bifocusing can be cancelled by rotating the polarization of all rays by 90° between rods.

The thermally-induced spherical aberration is corrected by an aspheric surface on the lens at the symmetry plane. The proper asphere shape is simply that which reverses the phase at the symmetry plane, effectively making the asphere a phase conjugator. The asphere used in our experiments was diamond-machined in a CaF₂ substrate and post-polished to reduce scatter losses. The asphere has an effective diameter of 5.58 mm over which the transmitted wavefront deviates from an ideal -16 cm sphere by 15.2 waves. A stable output power of 60 W and beam quality of 1.3 times diffraction-limited was obtained with the flat/flat resonator and a total diode power of 235 W.

In summary, we have demonstrated a diode-end-pumped cw Nd:YAG laser which produces an output power of 92 W in a multimode beam and 60 W in a near-diffraction-limited beam. The laser uses a total of sixteen 15-W laser diode bars pumping two short rods in an angularly-multiplexed pump geometry. A diamond-machined asphere and a quartz polarization rotator are used in a symmetric resonator to correct thermal distortion and the stress-induced birefringence for TEM₀₀ extraction. The optical-to-optical efficiencies are 44% and 26% for multimode and TEM₀₀ operation, respectively. The high efficiency of the end-pumped oscillator and the use of laser diode bars as pump sources provides significant economic advantage for this design.

REFERENCES

1. S. C. Tidwell, J. F. Seamans, C. E. Hamilton, C. H. Muller, and D. D. Lowenthal, *Opt. Lett.* **16**, 584 (1991).
2. For a cost comparison, the price of a 15-W laser diode bar is less than twice that of a 0.5-W fiber-coupled laser diode (Spectra Diode Labs, Inc., private communication).
3. S. C. Tidwell, J. F. Seamans, M. S. Bowers, and A. K. Cousins, *IEEE J. Quantum Electron.* **28**, 997 (1992).
4. W. C. Scott and M. de Wit, *Appl. Phys. Lett.* **18**, 3 (1971).

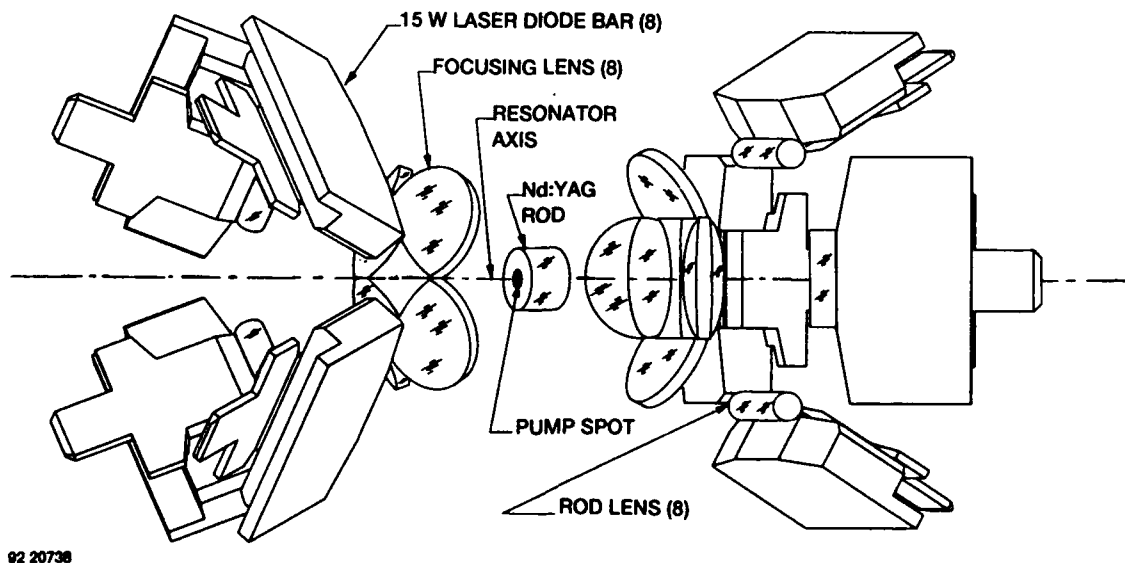
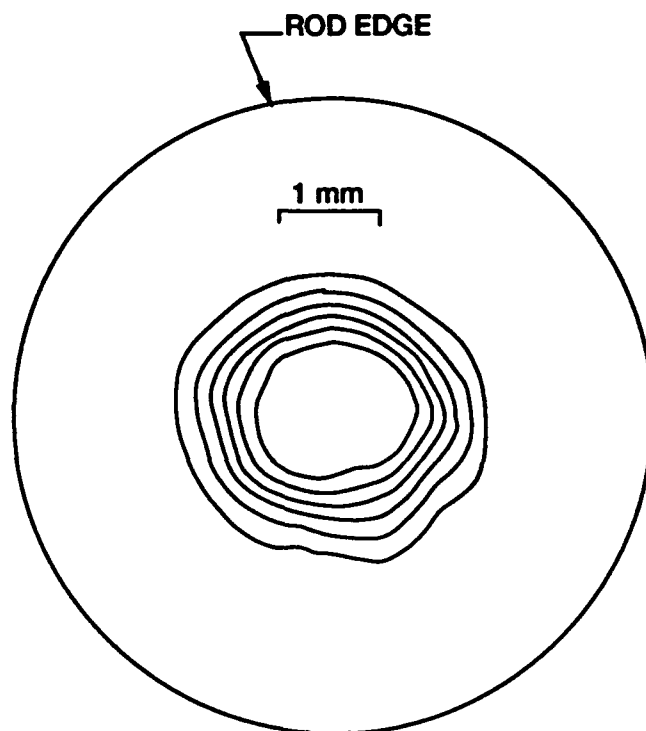
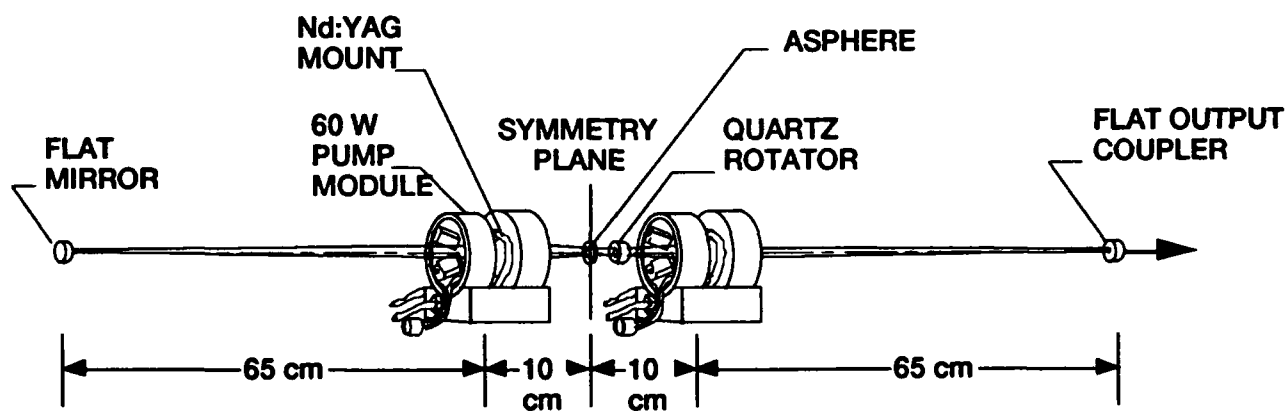


Figure 1. Angularly-multiplexed pump geometry is used to focus the power of eight 15-W laser diode bars (60 W per end) into a small volume in each laser rod.



92 20752

Figure 2. Fluorescence profile of a 6.35-mm diameter end-pumped Nd:YAG rod. A total of approximately 100 W of pump power is absorbed in the rod. 70 W is encircled within the 2.4-mm mode diameter.



92 20737

Figure 3. Symmetrical resonator used in TEM_{00} extraction experiments. Symmetry between the two laser rods allows straightforward correction of the thermal distortion and stress-induced birefringence.

Monday, February 1, 1993

**Diode-Pumped
1 μm Nd Lasers
Poster Session**

AMB 9:30am–10:30am
La Salle Ballroom A

High-Repetition-Rate, High-Average-Power, Pulsed Diode-Pumped Nd:YAG Oscillators

C.E. Hamilton, C.I. Miyake, and F.D. Braun

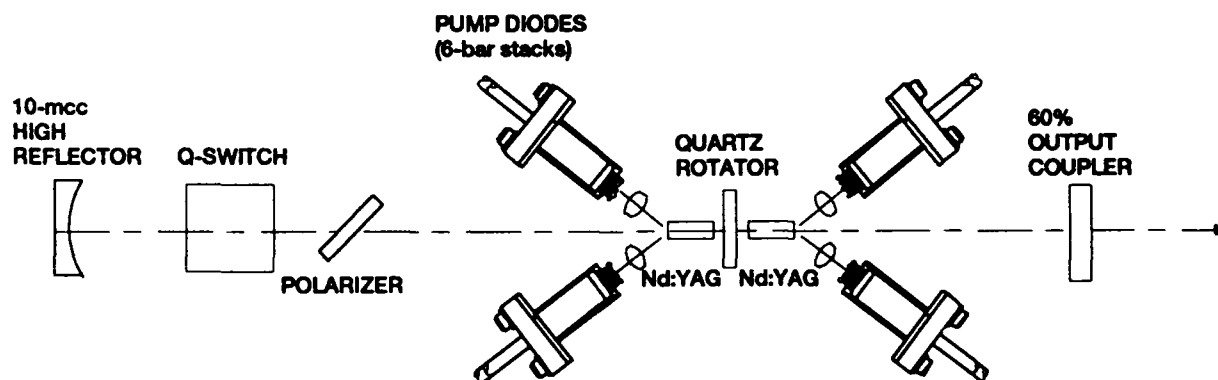
STI Optronics, Inc.

2755 Northup Way, Bellevue, Washington 98004-1495

(206) 827-0460

Development of high-repetition-rate, high-average-power diode-pumped Nd³⁺ lasers is of great interest, especially with high-duty-factor quasi-cw diodes becoming readily available. Most of the effort to date has centered on side-pumped lasers,[1-5] using both rod and slab geometries, although end-pumped lasers are being pursued as well.[6] In this paper, we report on a diode-end-pumped, Q-switched Nd:YAG laser in which either a single Nd:YAG rod or a pair of Nd:YAG rods are pumped by four quasi-cw laser diode arrays. This, to our knowledge, is the first system that utilizes multiple laser diode arrays in an end-pumping configuration. Two versions of the oscillator are described. One is designed to be insensitive to the diode emission wavelength. Such an oscillator is suitable for applications where the operating temperature, and hence the diode emission wavelength, will likely vary. The second oscillator that we describe does require tuning of the laser diodes to the Nd³⁺ absorption at 808 nm. Our emphasis here is to develop a high-repetition-rate, Q-switched oscillator that generates a beam with sufficiently high beam quality for efficient harmonic generation. As part of this effort, the second through the fifth harmonics are generated using this laser.

Insensitivity of the first oscillator to the pump wavelength is brought about by end pumping 3.0-cm-long, 3-mm-diameter Nd:YAG rods. Due to the long absorption length, the diode emission is effectively absorbed as long as the emission is between 803 and 822 nm. The diode-pumped Nd:YAG oscillator, illustrated in Figure 1, is a two-rod oscillator configured as a plano-concave resonator with a cavity length of 40 cm. The output coupler is 60 percent reflective, and the high reflector has a 10-m radius of curvature. The oscillator is birefringence compensated by a quartz polarization rotator between the Nd:YAG rods, and Q-switching is accomplished with a standard arrangement of a thin film polarizer and KD*P Pockels cell. Due to availability, one Nd:YAG rod is doped to 0.8 percent and the other rod is doped to 1.1 percent. Each Nd:YAG rod is end pumped through one face by two quasi-cw laser diode arrays (Spectra Diode Labs SDL-3230-ZLE). Each diode array, made up of six diode bars that are separated by 800 μ m, is capable of producing 200- μ s, 72-mJ pulses at a duty factor of 6 percent. In this work, the laser diode arrays are operated at a reduced pulse energy of 58 mJ. The diode emissions are angularly multiplexed into the rods at a multiplexing angle of 30° off of



92 20828

Figure 1. Q-switched Nd:YAG oscillator. The oscillator is configured to generate pulses that are insensitive to the diode emission wavelength, and hence the diode temperature. This done by end pumping two 3.0-cm-long, 3-mm-diameter rod with four quasi-cw laser diode arrays.

the normal to the rod face. The optics for coupling the diode emission into the Nd:YAG rods are similar to those used in recently developed 15-W and 80-W diode-pumped Nd:YAG oscillators.[7,8] For each diode array, a rod lens array consisting of six 800- μm -diameter quartz rods collimates the fast axes of the separate diode bar outputs. Due to a slight mismatch in the rod lens and diode bar spacings, the collimated outputs angularly separate by as much as 38° (full angle across the array). The outputs are regrouped with either a 13-mm or 19-mm focal length cylindrical lens immediately following the rod lens array. A 14-mm focal length, $f/1$ spherical lens then focuses the near-collimated diode emission onto the face of the Nd:YAG rod. The resulting small signal gain, g_0 , averaged over the aperture of the rod pair is 0.94 at a diode coolant temperature of 15°C , and monotonically decreases to 0.79 at 45°C .

The temperature dependence of the output pulse energy from the Q-switched oscillator is illustrated in Figure 2. At repetition rates below 50 Hz, the pulse energy decreases by only 25 percent as the diode coolant temperature is raised from 15°C to 45°C . The reduction in the pulse energy is 35 percent at 200 Hz. The observed reductions are largely attributable to a 10-percent reduction in the diode pulse energy over the 15 - 45°C temperature increase. When the diodes are operated at constant pulse energy over the 15 - 45°C range, the oscillator pulse energy at 200 Hz drops by only 16 percent. Measurement of the temporal shape at constant diode drive current reveals that the duration changes from 14-ns FWHM at 15°C to 18-ns

FWHM at 45°C . Furthermore, the near-field spatial shape remains near-Gaussian throughout the temperature range.

The second oscillator that we will discuss is similar to the wavelength-insensitive device. The only difference is that the quartz rotator and the pair of 3-cm-long rods have been replaced by a single 7.5-mm-long, 6-mm-diameter Nd:YAG rod that is doped to 1.1 percent. The larger diameter allows for more efficient coupling of the diode emission into the rod, plus it removes any hard aperture from the cavity. A gain-switched version of the oscillator, in which the Q-switch and the polarizer have been removed as well, produces 53-mJ pulses at 300 Hz (average power = 16 Watts). For initial work on harmonic generation, the Q-switched oscillator is operated at only 30 Hz. The Q-switched oscillator produces 29-mJ pulses that have a FWHM duration of 15 ns. The near-field spatial shape of the beam is best described as an elliptical Gaussian with an aspect ratio of 1.5. An M^2 measurement, where a second moment analysis is carried out on the acquired spatial profiles,[9] indicates that the beam is 1.1 times diffraction limited along the minor axis of the ellipse (polarization direction), and 1.6 times diffraction limited along the major axis. With this beam, the second through the fifth harmonics have been generated. Our emphasis is on efficiently producing the fifth harmonic ($\lambda = 213 \text{ nm}$) using an optically simple, single-beam-line arrangement of nonlinear crystals. Both the $1\omega+4\omega$ and $2\omega+3\omega$ mixing techniques for fifth harmonic generation[10] are investigated. Initial results on harmonic generation are given in Table 1.

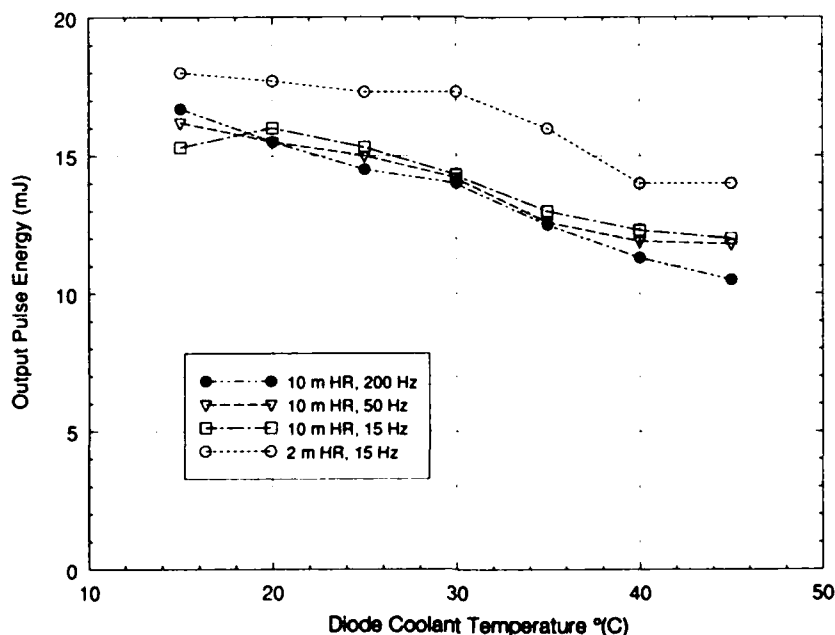


Figure 2. Dependence of the output pulse energy from the Q-switched oscillator on the diode coolant temperature. All of the results except those with the open circles pertain to the oscillator with the 10-m radius high reflector. The open circle results are for an oscillator with a 2-m radius high reflector.

Table 1. Harmonic Generation Summary

Harmonic	Crystal	Phase Matching	Phase Matching Angle (deg)	Crystal Length (mm)	Pulse Energy (mm)
1.064 μm	---	---	---	---	28 (1 GW cm^{-2})
532 nm	LBO	Type I	$\theta = 90^\circ, \phi = 12^\circ$	15	16
355 nm	LBO	Type II	$\theta = 40^\circ, \phi = 90^\circ$	15	8
266 nm	KD*P	Type I	$\theta = 86^\circ$	8	5
213 nm	BBO	Type I ($1\omega+4\omega$)	$\theta = 52^\circ$	10	1.1
213 nm	BBO	Type I ($2\omega+3\omega$)	$\theta = 69^\circ$	5	0.5

To summarize, we have described two diode-pumped Nd:YAG oscillators, both of which use multiple laser diode arrays in an end-pumping configuration. One oscillator, designed to be insensitive to the diode emission wavelength, produces pulses in which the energy, duration, and spatial shape vary slowly with the diode coolant temperature. The second oscillator utilizes a single large-diameter rod for production of pulses with high beam quality. Efficient generation of the second through fifth harmonics has been demonstrated at low repetition rates. Future work will involve extending Q-switched operation of the second oscillator to 300 Hz, with the eventual goal being to generate the harmonics efficiently at this high repetition rate.

REFERENCES

1. J.J. Kasinski, W. Hughes, D. DiBiase, P. Bournes, and R. Burnham, *IEEE J. Quantum Electron.* **28**, 977 (1992).
2. L.E. Holder, C. Kennedy, L. Long, and G. Dube, *IEEE J. Quantum Electron.* **28**, 986 (1992).
3. L.R. Marshall, A. Kaz, and R.L. Burnham, *Opt. Lett.* **17**, 186 (1992).
4. B.J. Comaskey, R. Beach, G. Albrecht, W.J. Benett, B.L. Freitas, C. Petty, D. VanLue, D. Munding and R.W. Solarz, *IEEE J. Quantum Electron.* **28**, 992 (1992).
5. R. Beach, J. Davin, S. Mitchell, W. Benett, B. Freitas, R. Solarz and P. Avizonis, *Opt. Lett.* **17**, 124 (1992).
6. H.R. Verdun and T. Chuang, *Opt. Lett.* **17**, 1000 (1992).
7. S.C. Tidwell, J.F. Seamans, C.E. Hamilton, C.H. Muller, and D.D. Lowenthal, *Opt. Lett.* **16**, 584 (1991).
8. S.C. Tidwell, J.F. Seamans, M.S. Bowers, and A.K. Cousins, *IEEE J. Quantum Electron.* **28**, 997 (1992).
9. A.E. Siegman, "New Developments in Laser Resonators," *SPIE Volume 1224, Optical Resonators*, ps. 2 (1990).
10. D. Eimerl, L. Davis, S. Velsko, E.K. Graham, and A. Zalkin, *J. Appl. Phys.* **62**, 1968 (1987).

2.4-ns Pulse Generation in a Solid-State Passively Q-Switched, Laser-Diode-Pumped Nd:YAG Laser

Y.D. Isyanova and D. Weiford

Schwartz Electro-Optics Inc., 45 Winthrop Street
Concord, MA 01742. (508) 371 2299

In the present work, we report for the first time passive Q-switching of a laser-diode-pumped solid-state laser using a solid-state saturable absorber. The saturable absorber material of choice for 1064-nm operation is gamma-irradiated (5.5×10^8 rads total dose) F_2^+ :LiF in which the active absorber site is the F_2^+ color center [1]. The only addition to a conventional two-mirror linear resonator is the insertion of a window-like piece of AR-coated F_2^+ :LiF material. The simplicity and small size of such a Q-switch is ideally suited for use in compact laser-diode-pumped laser designs. The use of a short resonator, high output coupling, and low unsaturated absorber transmission leads to short pulse generation and increased longitudinal mode selection.

The resonator used in this work is shown in Figure 1. TEM_{00} -mode operation was obtained by the use of a novel side-pumping geometry, described earlier [2], that achieves near-Gaussian pump energy deposition in the laser rods. A pair of opposing Brewster-angled, 12-mm long, semicircular-cross-section (3-mm diameter) Nd:YAG laser rods were each side-pumped by a 5-bar stack of quasi-cw laser diodes (SDL 3230 devices). The resonator TEM_{00} -mode size matches that of the deposited energy in the laser rods, thereby ensuring efficient TEM_{00} -mode operation (see Figure 2).

The laser was operated at 20 Hz pulse-repetition-rate with 200- μ s duration pump pulses. In normal-mode operation, the laser generated pulses of up to 19.5 mJ energy with 16% conversion efficiency and 22.6% slope efficiency. In Q-switched operation, 2.4-ns duration pulses were obtained at 5 mJ energies with 5.2% conversion efficiency. The reduction in efficiency in the Q-switched mode can be accounted for by the energy required to bleach the saturable absorber.

Table 1 summarizes the Q-switched performance obtained with different lengths of F_2^+ :LiF, which are characterized by their unsaturated single-pass transmissions. The laser-diode-pump energy was equal to the threshold energy for single-pulse generation in each case. Further increasing the pump energy leads to multiple-pulse generation with the same energy in each pulse. Note, the data for the 12% transmission F_2^+ :LiF material showed improved pulse durations of 2 ns. However, the pulse energies were reduced to 4 mJ by the onset of damage to one of the Nd:YAG laser rods. Prior to this damage, the laser had generated 2.4-ns duration, 5 mJ pulse for a period of tens of minutes.

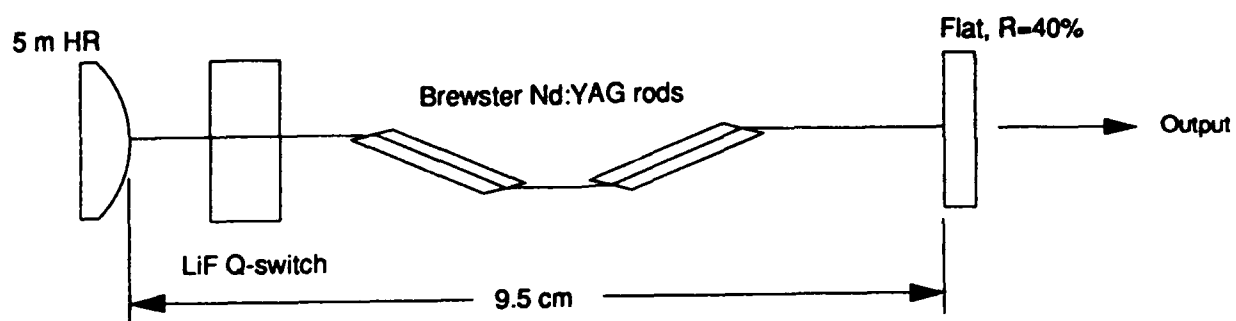


Figure 1. Passive Q-switched laser resonator.

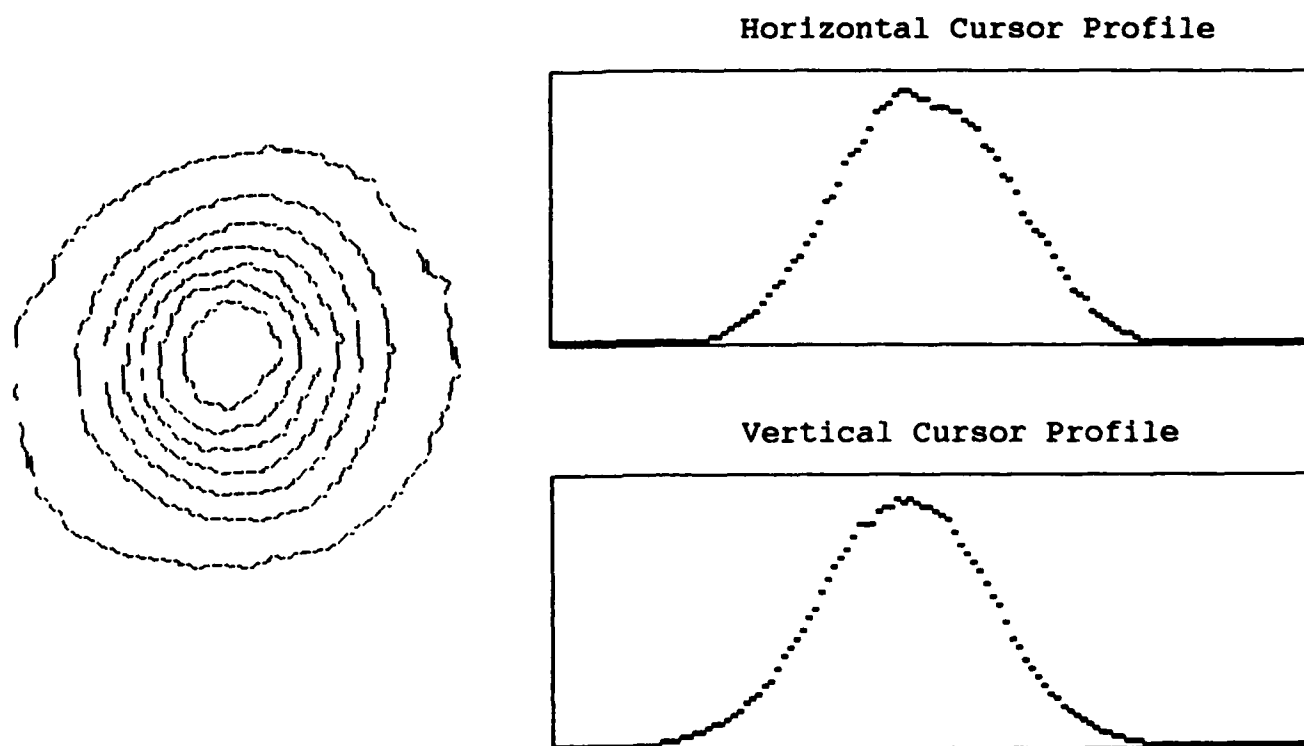


Figure 2. TEM₀₀-mode beam profile.

Table 1. Passive Q-switched laser performance.

F_2 :LiF Trans' (%)	E_{pump} (mJ)	E_{out} (mJ)	τ (ns)
55	58	1.3	5.9
46	73	2.5	3.6
35	83	3.8	2.8
27	97	5.0	2.4
12	121	4.0	2.0

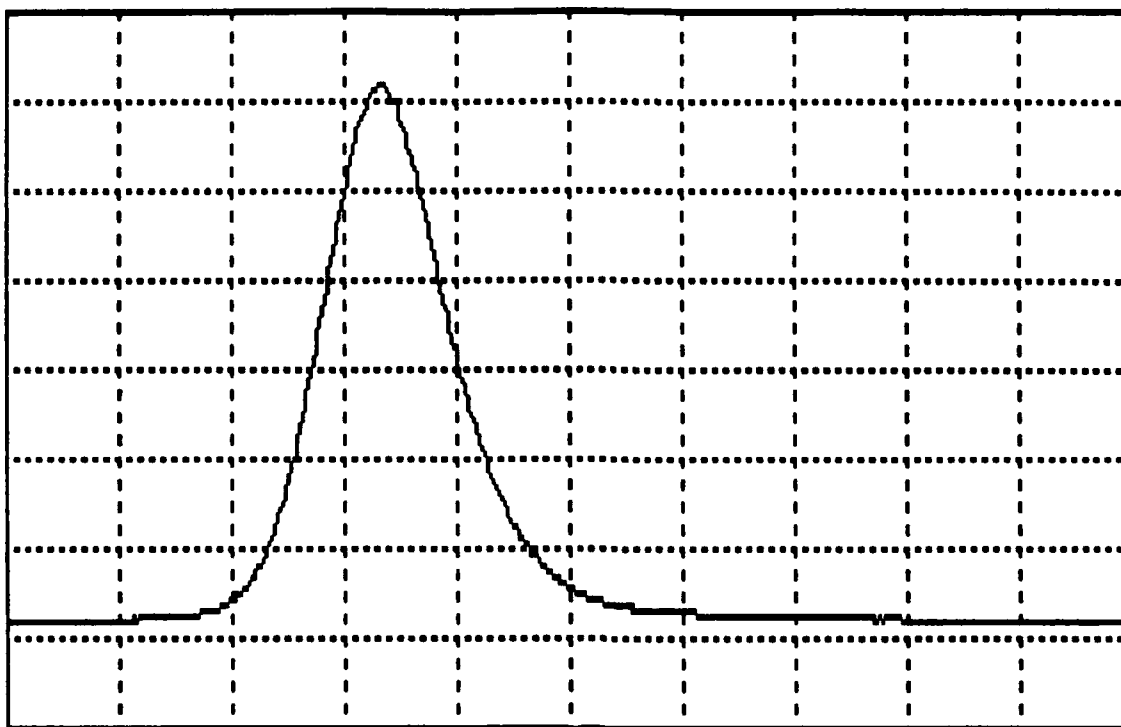


Figure 3. 2.4-ns duration passive Q-switched laser pulse. (2 ns/div timescale).

A 2.4-ns duration pulse is shown in Figure 3. The lack of longitudinal mode-beating is a characteristic of single-frequency operation. This was obtained by using the F_2^+LiF material as an intracavity etalon to suppress other longitudinal modes.

In summary, we have demonstrated for the first time an all solid-state passively Q-switched laser that generates 5-mJ, 2-ns, single-frequency pulses with a TEM_{00} beam profile. The major advantages for this approach compared to electro-optic Q-switch technology are the elimination of drive electronics and simplified resonator configurations.

This research was supported by NASA Goddard Space Flight Center under Small Business Innovative Research program contract #NAS5-30882.

References.

- [1] Y. Isyanova, A.L. Levit, B.D. Lobanov, N.T. Maksimova, V.M. Ovchinnikov, Y.A. Pirogov, B.A. Simin, and P.A. Tsurulnik, "New developments in solid-state lasers," *Bulletin of the Academy of Sciences of the USSR, Physical Science Series*, **48**, 97, 1984.
- [2] D. Welford, D.M. Rines, and B.J. Dinerman, "Efficient TEM_{00} -mode operation of a laser-diode side-pumped Nd:YAG laser," *Optics, Letts.*, **23**, 1850, 1991.

FLASHLAMP PUMPED Nd:BaY₂F₈

Norman P. Barnes
Keith E. Murray
NASA Langley Research Center
Hampton, VA 23681

Arlette Cassanho
Kenneth M. Dinndorf
Hans P. Jenssen
Massachusetts Institute of Technology
Cambridge, MA 02139

Summary

Nd:BaY₂F₈ has been operated under flashlamp pumping conditions at both 1.0488 and 1.3176 μm . To the best of the authors knowledge, operation on the 1.32 μm transition has not been reported before. Nd:BaY₂F₈ is an attractive material both from the point of view of the long upper laser level lifetime and the birefringent nature of this laser material. By utilizing a birefringent laser material, a polarized output is usually obtained and the stimulated emission cross section can be varied for the particular application. By utilizing these properties, the efficiency of this laser can be enhanced.

Even with the difficulties of crystal growth of this laser material, a laser rod 5.0 by 48 mm in length was produced. Growth of this material is hampered by the large induced strain to which the boule is subjected upon cooling. While large boules can be grown, they often shatter upon cooling or upon cutting.

Both absorption and emission spectra were recorded as a function of polarization for this material. Spectra are complicated since this material is biaxial and the axes corresponding to the index of refraction ellipsoid do not correspond to the crystallographic axes. Lifetime of the upper laser level was measured to be 456 ± 10 microseconds. With the long upper laser level lifetime, this laser material appears attractive for laser diode pumping applications.

Both normal mode and Q-switched operation was achieved at 1.05 μm . Normal mode operation with a variety of output mirror reflectivities has been recorded. Because of the short length of laser rod and concomitant short flashlamp, low electrical energies near threshold could not be delivered due to power supply limitations. Using laser output energy versus electrical energy data well above threshold, linearly extrapolated thresholds are less than 1.0 J of electrical energy. Thresholds increase as the negative logarithm of the output mirror reflectivity. Highest slope efficiency, 0.0082, was achieved with a 0.60 reflecting mirror.

Q-switched operation at $1.05\text{ }\mu\text{m}$ produced efficiencies comparable to the normal mode performance and pulselengths approaching 20 nsec at the higher laser output energies.

Normal mode and Q-switched operation were also obtained on the $1.32\text{ }\mu\text{m}$ transition. In this case, the thresholds were considerably higher while the slope efficiency is considerably lower. As an example, with a 0.80 reflecting output mirror, the linearly extrapolated threshold was 7.0 J. Maximum slope efficiency for normal mode operation was 0.0016.

Although the threshold for the $\text{Nd:BaY}_2\text{F}_8$ laser was quite low, the slope efficiency was not as high as expected. To determine the influence of the pulse forming network on these observations, a Nd:YAG laser rod was evaluated under similar circumstances. A Nd:YAG laser rod with the same diameter, 5.0 mm, but with a somewhat longer length, 60.0 mm, was used with the same pulse forming network. While thresholds were lower for Nd:YAG , the slope efficiency was higher for $\text{Nd:BaY}_2\text{F}_8$. Consequently, even through the optical quality of the latter laser material was lower than that of the former, $\text{Nd:BaY}_2\text{F}_8$ was able to produce more energy under these circumstances.

Efficient, Q-Switched Nd:YAG Laser End-Pumped by a High Power Diode Laser Array

Ti Chuang and Horacio R. Verdún

Fibertek, Inc.

510 Herndon Parkway, Herndon, VA 22070

Tel: (703) 471-7671 / Fax: (703) 471-5806

The end-pumped configuration of diode-pumped solid-state lasers has undergone extensive development since the first such configuration was reported.¹ The main advantage of the end-pumping configuration has been its high coupling efficiency between the pump energy and the laser output energy. Here we present the performance of an efficient, Q-switched Nd:YAG laser end-pumped by a three-bar high power diode laser array.

This laser is based upon our earlier work on this type of pumping configuration.² The structure of this laser is depicted in Figure 1, where OC is the output coupler (a convex OC is drawn here); QS is a KD*P Q-switch; POL is a set of folded thin film polarizers; YAG is an Nd:YAG crystal and DL represents a pumping module which contains a diode laser array and a beam shaping optics. The diode laser array is a SDL-3230-TB model manufactured by Spectra Diode Labs. It consists of three 1 - cm bars in a stack with a spacing of 0.3 mm between bars. The emission wavelength of the diode array is temperature-tuned to around 808 nm. The diode array is mounted on a water-cooled heat sink to maintain the optimal operating temperature. The key component of this laser is a well-designed beam shaping optics that transfers the widely divergent diode array output into a pumping volume of the YAG crystal that matches the laser resonator mode volume. The energy transfer efficiency of this optics is $\sim 88\%$. The detailed description of this beam shaping optics is given in Reference 3. The Nd:YAG crystal has a nominal Nd concentration of 1 at. %. One end of this crystal is flat and AR coated at 1.06 μm , the other end has a radius of curvature of 25 cm and is coated HT at 808 nm and HR at 1.06 μm . This curved end and the output coupler form the laser resonator. The YAG crystal is 10 mm in length and 6.25 mm in diameter. The crystal rod was wrapped with one layer of indium wire before it was inserted into an aluminum housing. The indium was then compressed by a flange having a ring shaped insert. This technique helps to achieve low thermal impedance and to reduce the mounting stresses. The aluminum housing was cooled by convection. Two types of the output coupler (OC) were used in this work: a flat one and a $r = 5$ cm convex one.

The pumping diode array operated in a pulsed mode. The pulse duration was 200 μs and the repetition rate was 50 Hz. The diode array delivered 27 mJ/pulse at 86 A of diode current. A simple calculation revealed that, given the radius of curvature on one end of the YAG rod, the convex OC would perform better in terms of mode matching and resonator stability. We set out to check this by employing a plain resonator without POL and QS but with a flat or a convex OC, both have the same reflectivities of 95% at 1.06 μm . The resonator length was ~ 14.3 cm. The result is shown in Figure 2. This result is consistent with the prediction. For the curved OC the slope efficiency, obtained by a least-squares fit, is 44.3% while that for the flat OC is 38.2%. The optical to optical conversion efficiency is 26.7% for the curved OC and is 24.5% for the flat OC. The laser beam profile for either case was nearly TEM_{00} , although better beam profiles could be obtained by sacrificing the output energies.

For the Q-switched operation of this laser, we chose the convex OC of $r = 5$ cm and 85% reflection at $1.06 \mu\text{m}$ and a KD*P Q-switch. The operational structure of this Q-switched version is shown in Figure 1. The polarizer set shown there was used in the reflection mode to achieve the polarization required for the Q-switch operation while eliminating the astigmatism that can be caused by using the polarizer in the transmission mode. The resonator length (geometrical) for this case was about 13.2 cm. With the pumping energy of 27 mJ, we achieved the output energy of 2.2 mJ/pulse with pulse width of 19.6 ns. This energy translates into a peak power of more than 110 kW. This value is quite significant considering the size of this laser. An oscilloscope trace of this output pulse is given in Figure 3, where the horizontal scale is 20 ns/div. The beam divergence of the laser output is approximately two times of the diffraction limit.

There is still room to improve this Q-switched laser. We found that the Q-switch used in this work had quite a lot insertion loss. By using a Q-switch with lower loss, the performance can be improved. Also the folded polarizer set introduced a significant amount of loss to the resonator. For example, the measured slope efficiency of this laser, when using the flat OC of 95% reflection and the POL set while removing the QS, is 29.2% (This value is to be compared with 38.2% cited above.). To overcome this loss, we designed a resonator using an intracavity anamorphic prism at the Brewster angle positioned between a concave OC and a YAG rod, whose two ends are flat. This prism serves two purposes: 1) it is a polarizing element and 2) it expands the resonator mode diameter. The consequence of this is that the prism increases the mode volume at the pumping site for better mode matching and decreases the intensity at the QS site. The later is important because a LiNbO_3 can be then used as a Q-switch to reduce the insertion loss, for LiNbO_3 is known to have lower insertion loss than KD*P but also lower damage threshold than KD*P. We have tested this design. The improvement is very promising. Using a 2 m concave output coupler coated at 95% reflection at $1.06 \mu\text{m}$ and a flat-flat YAG rod having AR coating at one end and HR/HT coating at the other, we achieved the slope efficiency of 38.5% with the polarized output. The beam profile was also nearly TEM_{00} . The further improvement and the Q-switching operation of the design has been under way.

This Q-Switched laser has been successfully employed to pump an all solid-state Cr:Forsterite laser.³ The frequency doubling and quadrupling of this laser have also been undertaken. These results will be reported. This miniaturized, Q-switched Nd:YAG laser will find its applications where compactness and high efficiency of an Nd:YAG laser are major requirements.

This work was supported by Fibertek, Inc. through its IR&D program.

REFERENCES

1. D. L. Sipes, Appl. Phys. Lett. **47**, 74 (1985)
2. Horacio R. Verdún and Ti Chuang, Opt. Lett. **17**, 1000 (1992)
3. Ti Chuang and Horacio R. Verdún, paper submitted to Advanced Solid-State Lasers, Eighth Topical Meeting, New Orleans, Louisiana, Feb. 1- 3, 1993

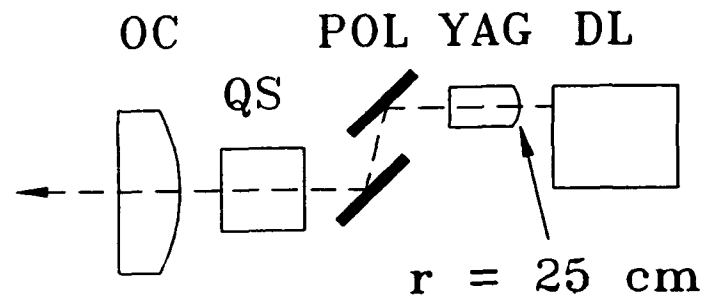


Fig.1. The structure of the laser. See text for explanations of symbols.

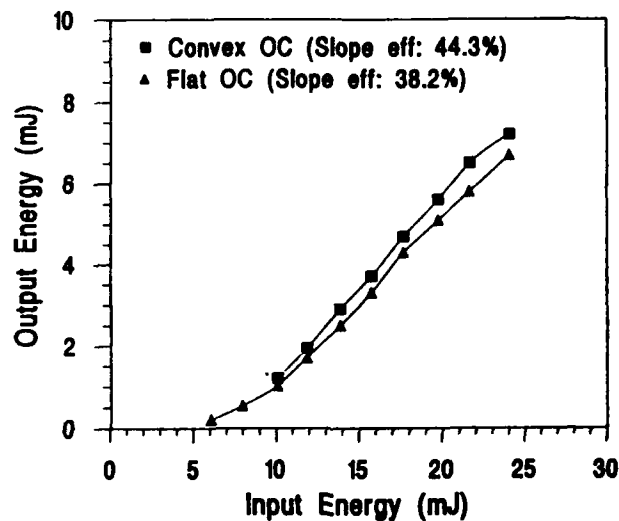


Fig.2. The performances of the laser without QS and polarizer set. A convex OC and a flat OC were used in this experiment. Both OCs have 95% reflectivities at $1.06 \mu\text{m}$.

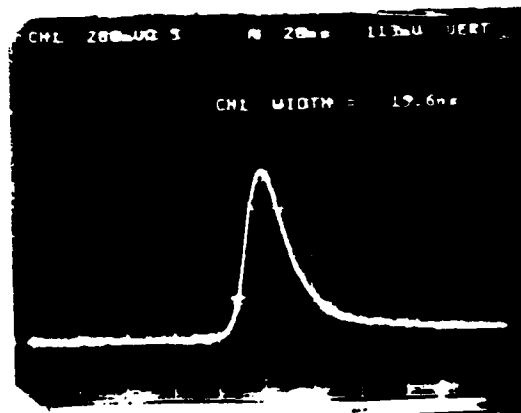


Fig.3. The temporal profile of the output Q-switched pulse of the laser, taken from a digital oscilloscope (Texttronix 2440) trace. The pulse width is 19.6 ns.

Diode Pumped Nd:YAG Laser with Parabolic Pump Cavity

H. Zbinden and R. Weber

Institute of Applied Physics, Sidlerstr.5, 3012 Bern, Switzerland

Tel: +41 31 65 89 37 Fax: +41 31 65 37 65

Diode pumping of solid state lasers has developed into a promising technique even for high power lasers. Basically there are two possible pumping schemes: Longitudinal pumping provides high efficiencies and good beam quality but demands complicated and expensive optics [1] or fiber-optics [2] and sophisticated setups for scaling to high powers, such as multiple facet pumped systems with folded resonators [3,4,5] or multiple gain elements [6]. Transverse pumping is easily scalable to higher powers, but lacks high efficiency in fundamental mode operation [7]. Considering that diode laser power is decreasing in price we focused our work not on maximum efficiency but on a simple scalable setup that provides optimal transversal pumping and efficient cooling of the laser rod, without expensive optics and complicated adjusting. We present a novel transverse pump design for diode pumped Nd:YAG lasers using a parabolic reflector.

The experimental setup is shown in Fig. 1, the plane of the drawing is perpendicular to the rod axis. The laser can be pumped by an array of 2x4 5 W

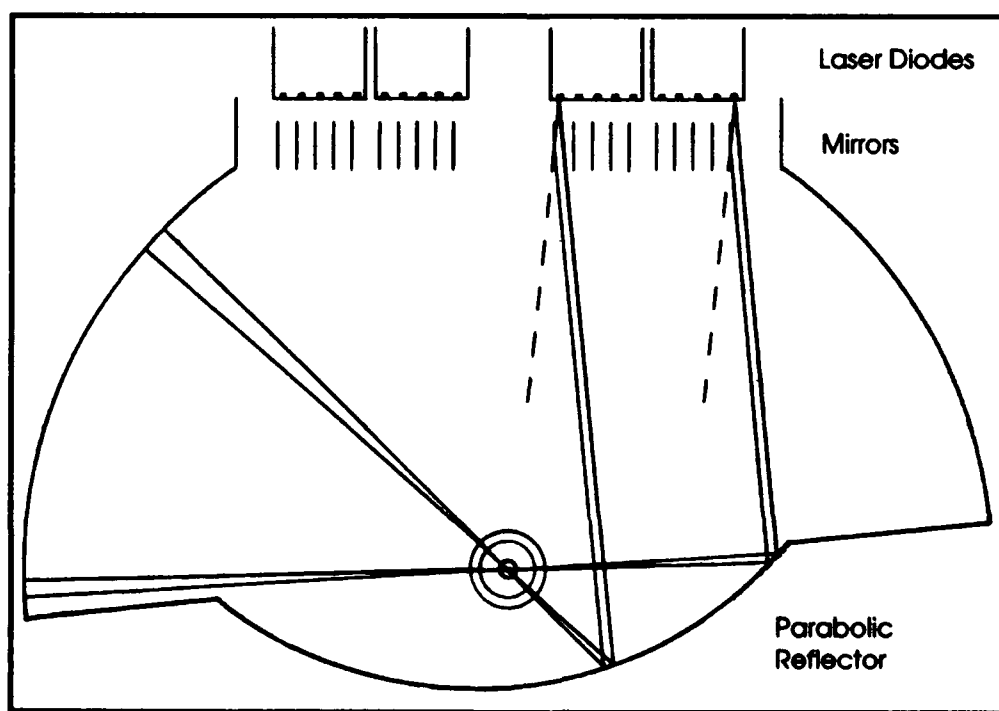


Fig. 1

Siemens Laser diode bars, each 1 cm broad with five 400 μm wide light emitting zones on 2 mm centers. The typical dual lobed emission of the laser diodes has a divergence of about 40 degrees in the direction perpendicular to the junction. In the direction parallel to the junction the angle between the two lobes is 6 degrees, but the divergence of one lobe is about 1.5 degree (FWHM). Putting an array of small mirrors (gold plated microscope cover-glasses) perpendicularly in front of the diodes (one beside each emitting zone) one lobe is reflected in the direction of the other. Therefore the divergence is reduced by a factor 4 to 1.5 degree. Taking benefit of this relative small divergence, the diode light is focused by a parabolic reflector (electro-gilded aluminium) onto a laser rod with a diameter of 2 mm. In the other (high divergence) direction two parallel 9 mm spaced electro-gilded aluminium plates confine the diode radiation within the length of the laser rod of 15 mm. The light not absorbed in a first pass through the rod is reflected at spherical mirrors for a second pass. There is sufficient space to cool the laser rod with a conventional water sleeve. The diodes are cooled (and wavelength tuned) by temperature controlled water.

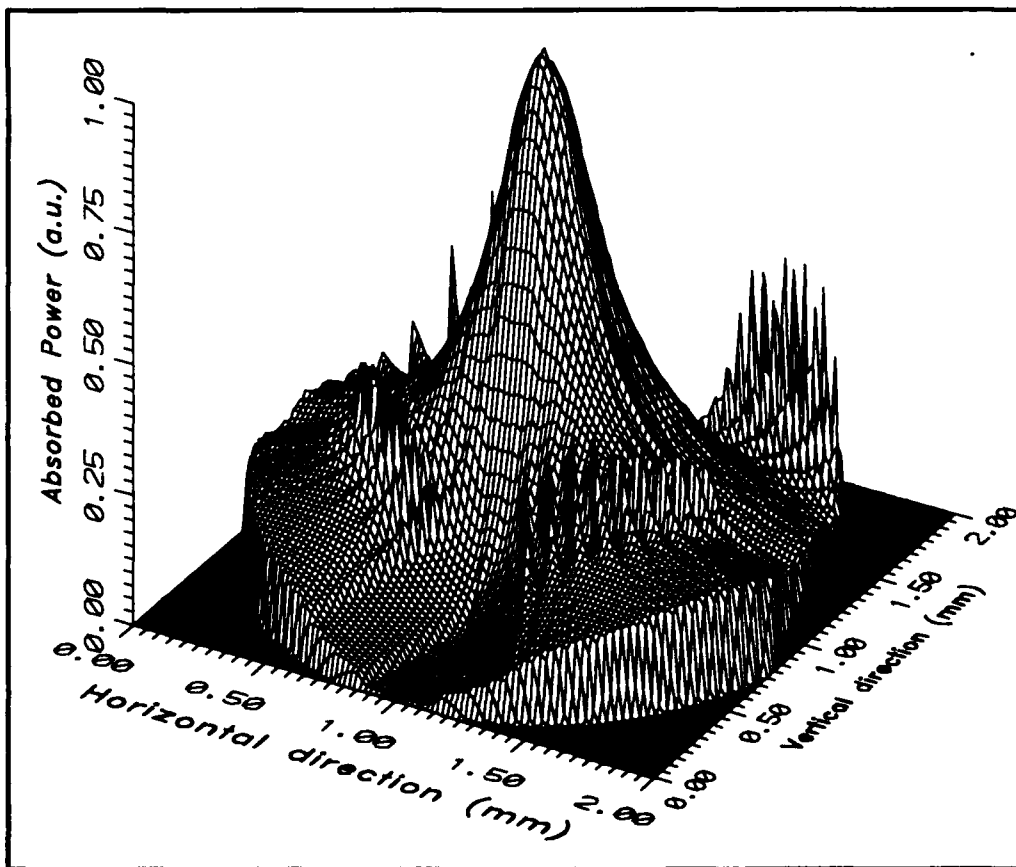


Fig. 2

We have carried out detailed ray tracing calculations. Fig. 2 gives the radial distribution of the absorbed power in the laser rod for an absorption coefficient of 4.2 cm^{-1} . With this parameter 67% of the pump power is absorbed.

First measurements performed with two diodes showed that the main criterion of our setup is fulfilled: The laser system is absolutely not sensitive on small variations of the relative positions of the laser diodes, mirror array, laser rod and parabolic reflector. The smallest tolerance of approx. 50-100 μm is given for a lateral displacement of the mirrors relative to the diodes. The whole laser can be easily assembled without any alignment, except for the mirrors of the resonator. The obtained TEM_{00} 1.06 μm output power from the 2x15 mm rod did not exceed 300 mW. The laser diodes at our disposition were composed of five discrete 400 μm emitters with large spectral variation ($\pm 3 \text{ nm}$) therefore only a part (the exact value could not be measured) of the diode power was actually absorbed. The estimated threshold was 3 W absorbed power, for a 30 cm long plano-convex resonator with 2% output coupling. Measurements with adequate (monolithic 5x400 μm structure) laser diodes will be presented at the conference.

References:

- [1] S.C. Tidwell, J.F. Seamans, C.E. Hamilton, C.H. Muller, and D.D. Lowenthal
Efficient, 15 W output power, diode-end-pumped Nd:YAG laser
Opt. Lett. **16**, 584 (1991)
- [2] H. Zbinden, and J.E. Balmer
Q-switched Nd:YLF laser end pumped by a diode laser bar
Opt. Lett. **15**, 1014 (1990)
- [3] T.M. Baer, D.F. Head, P. Gooding, G.J. Kintz, and S. Hutchison
Performance of Diode-Pumped Nd:YAG and Nd:YLF Lasers in a Tightly Folded Resonator Configuration
IEEE J. Quantum Electron. **28**, 1131 (1992)
- [4] S. Watanabe, S. Kudo, T. Yamane, and K. Washio
Efficient and high power Nd:YAG laser multiple facet end pumped by laser diodes.
in Tech. Dig. CLEO, Baltimore, MD, 1989, paper PD 8
- [5] C. Pfistner, P. Albers, H.P. Weber
Efficient Nd:YAG slab longitudinally pumped by diode lasers
IEEE J. Quantum Electron. **26**, 827 (1990)
- [6] J. Frauchiger, P. Albers, and H.P. Weber
Scalable laser configuration for laser diode pumped Nd:YAG
in Digest of Conference on Tunable Solid-State lasers (OSA, Washington, D.C. 1990),
p. 284
- [7] R. Burnham and A.D. Hays
High-power diode-array-pumped frequency-doubled cw Nd:YAG laser
Opt. Lett. **14**, 27 (1989)

Spectroscopy of Nd:KYF₄

Y. Yamaguchi, H. P. Jenssen and A. Cassanho
Center for Materials Science and Engineering
Massachusetts Institute of Technology
Cambridge Ma 02139
Tel.: (617) 253-6878

KYF₄ has similar structure to NaYF₄, which has been shown by Knowles et al.¹ to be a potential candidate for diode pumped solid state lasers. Both structures are basically transformed from the CaF₂ structure². Dubinskii et al.³ recently reported an emission spectrum of Nd:KYF₄. However, they did not identify more than one site in this crystal. More recently Sytsma⁴ reported several luminescent sites for Gd³⁺ in KYF₄. In this paper, we report spectroscopic result of multisites in Nd:KYF₄.

The crystal structure of KErF₄, isostructural to KYF₄, has been reported by Aleonard et al.². This crystal has a non-centrosymmetric trigonal structure and the space symmetry is P3₁12. The lattice parameters are $a=14.08\text{\AA}$, $c=10.12\text{\AA}$. They reported that there are three cation sites in the unit cell, the first site is occupied by erbium, the second and third sites are occupied randomly by erbium and potassium. The site symmetries for all the sites are low-2. The lattice parameters of KYF₄ are $a=14.083\text{\AA}$, $c=10.117\text{\AA}$, that have been reported by Ardashnikova et. al.⁵.

Both NaYF₄ and KYF₄ crystals have to be grown from a non-stoichiometric composition by a top seeded solution growth technique. However, contrary to NaYF₄, KYF₄ crystals can be grown as large boules, at relatively fast pulling rates as demonstrated by Chai⁶

A single crystal of KYF₄ doped with neodymium was pulled from a melt of composition of 43% YF₃ and 57% KF in argon gas atmosphere. The crystallization temperature was approximately 810°C. Oriented single crystal spectroscopic samples were cut from the grown crystal. The crystal was identified as KYF₄ by a X-ray powder diffraction measurement.

Absorption spectra were obtained by using a Perkin Elmer Lambda 9 spectrophotometer. The emission spectra were taken using a McPherson 1m monochromator using either a S1 type photo-multiplier tube or a liquid nitrogen cooled InSb detector in combination with a lock-in amplifier. The pumping source was either a

Ti-sapphire laser, with the wavelength monitored by a wave meter, or an argon laser. The pumping power in the crystal was about 60 mw.

Low temperature (4K) spectra reveal that there are multiple sites in this crystal. These sites can be broadly classified as two classes of sites. This is illustrated in figure 1. In the emission spectra, further identification of sites was possible by tuning the pump laser for selective excitation. A portion of the $^4F_{3/2}$ to $^4I_{9/2}$ spectrum for several pump wavelengths is shown in figure 2. Based on these spectra we have identified a total of 6 sites. Figure 3 shows the energy levels of one site of each class for the $^4F_{3/2}$, $^4I_{11/2}$ and $^4I_{9/2}$ manifolds. It is interesting to note that for the class 1 sites only one level in the $^4I_{11/2}$ manifold could be identified.

The fluorescence lifetime was similarly measured using a tunable, pulsed laser for excitation. All the sites had lifetimes in the range 750-850 μ s at 4K. In Ref.3 the room temperature life time was reported to be \approx 650 μ s.

-
- 1 D.Knowles, A.Cassanho and H.P.Jenssen, OSA Proceedings on Tunable Solid State Lasers, 1989, vol5, 139-145
 - 2 S.Aleonard, Y.Le Fur, L.Pontonier, M.F.Gorius and M.Th.Roux, Ann. Chim. Fr., 3, 417-427 (1978)
 - 3 M.A.Dubinskii, N.M.Khaidukov, I.G.Garipov, L.N.Dem'yanets, A.K.Naumov, V.V.Semashko and V.A.Malyusov, J.Modern Optics, 37, 1355-1360 (1990)
 - 4 J. Sytsma, S J Kroes, G. Blasse and N.M. Khaiukov., J. Phys: Condens. Matter 3 (1991) 8959-8966
 - 5 E.I.Andashnikova, M.P.Borzenkova and A.V.Novoselova, Russ. Inorg. Chem., 25, 833-836 (1980)
 - 6 B. Chai, Private communication

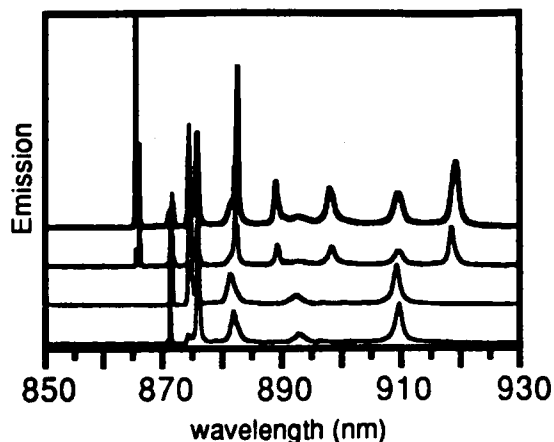


Fig 1a $^4F_{3/2}$ to $^4I_{9/2}$ emission at 4K in Nd:KYF₄. The two upper traces belong to class 1 sites and the two lower to class 2 sites. The sites were selectively excited by a tunable laser.

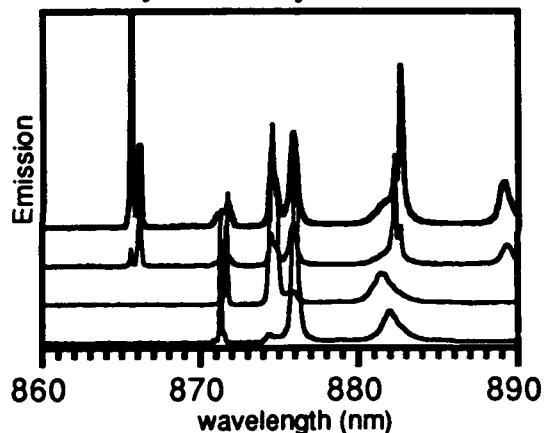


Fig 1b Same as 1a with the wavelength scale expanded to show differences within the two classes of sites.

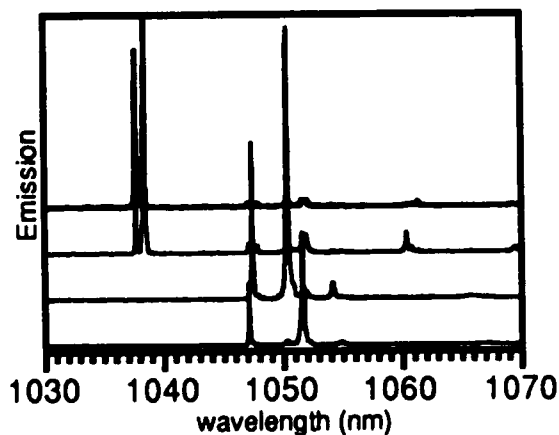


Fig 1c $^4F_{3/2}$ to $^4I_{11/2}$ emission at 4K showing the two classes of sites.

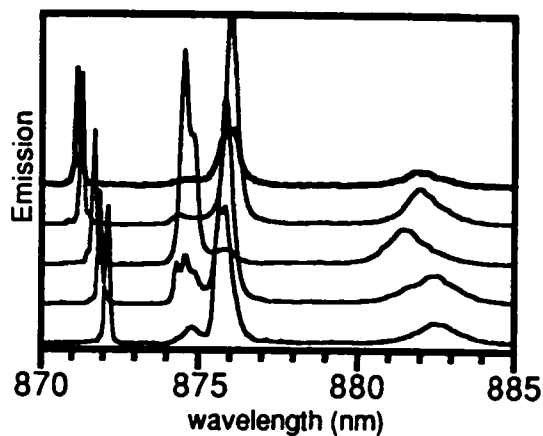


Fig. 2 A portion of the $^4F_{3/2}$ to $^4I_{9/2}$ spectrum of class 2 sites. The wavelength scale is expanded to show four different sites.

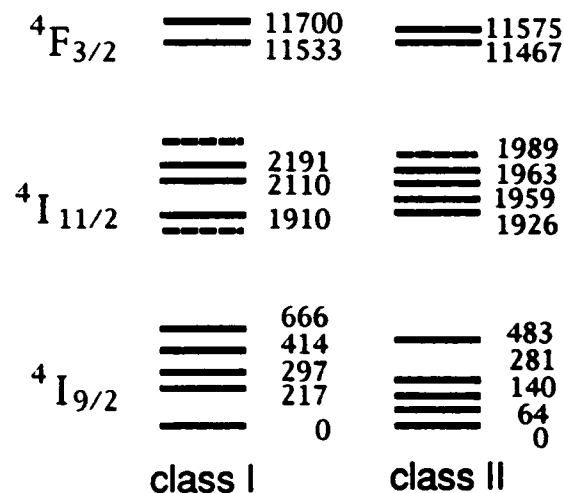


Fig. 3 Energy levels of one site of each class for the $^4F_{3/2}$, $^4I_{11/2}$ and $^4I_{9/2}$ manifolds.

High-Repetition-Rate, Diode-End-Pumped Nd:YLF Laser

A.J.W. Brown, Roy Mead, and Walter R. Bosenberg
STI Optronics, Inc.
2755 Northup Way
Bellevue, Washington 98004-1495
(206) 827-0460

Diode-pumped lasers have been the focus of much attention in recent years in an effort to exploit the potential of higher efficiencies, greater reliability, longer lifetimes, lower cost and compact designs offered as compared to their flashlamp-pumped counterparts. A large variety of laser materials pumped by cw and quasi-cw laser bars have been reported in the literature. Many potential applications of these devices, especially those involving nonlinear frequency conversion, require high peak powers, good beam quality and high repetition rates. Q-switching of cw-pumped lasers such as Nd:YAG results in high repetition rate operation but low peak powers which can limit the efficiency in nonlinear frequency conversion processes.[1] Q-switching of lasers pumped by quasi-cw diodes results in higher peak powers but lower repetition rates. The recent development of 20% duty cycle quasi-cw diode bars has allowed high repetition rates whilst maintaining high peak powers.

We report here on the development of a diode-end-pumped Nd:YLF laser pumped by two quasi-cw diode laser bars. The end-pumping technique offers the ability to overlap the gain region with the fundamental laser resonator mode resulting in higher efficiency operation as compared to side-pumped geometries. The laser produces Q-switched pulses up to 6 mJ with a temporal duration of 18 ns (FWHM) at repetition rates up to 500 Hz. These high-peak-power pulses have been efficiently converted into the green and ultra-violet using standard nonlinear crystals. Further, the output from the laser has been used to pump an OPO resulting in tunable radiation in the red and near-infrared.

Figure 1 shows a schematic of the laser. Each end of a 1% Nd doped YLF rod is pumped by a quasi-cw diode laser bar (SDL Model 3230-S). These bars produce 60 W peak pump power and are designed for operation at 20%

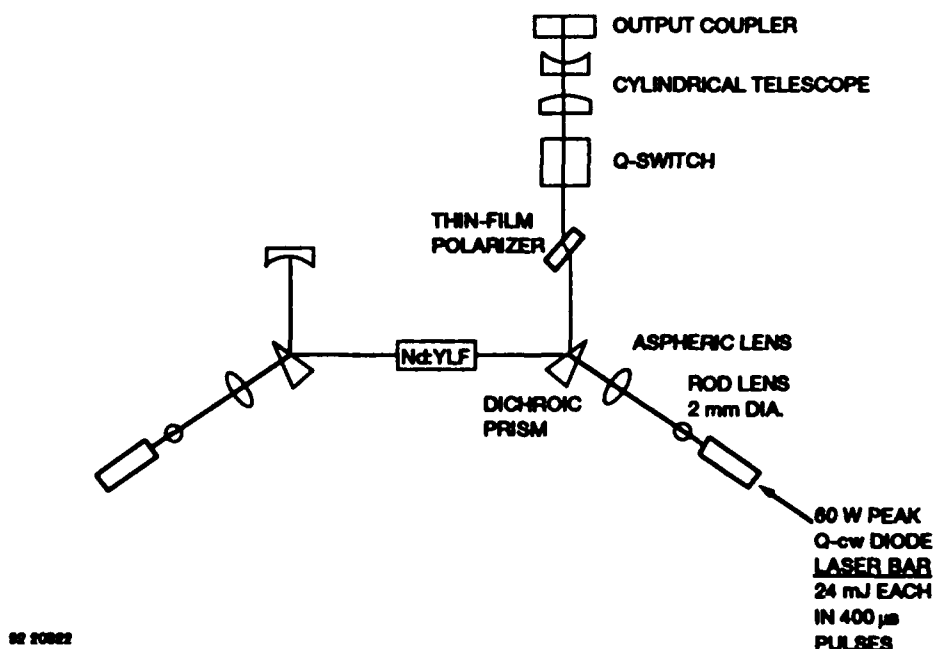


Figure 1. Schematic diagram of the diode-end-pumped Q-switched Nd:YLF laser.

duty factor, allowing repetition rates of 500 Hz to be achieved with 400 μ s pump pulses. An AR-coated rod lens is used to collect and nearly collimate the light emitted from the fast axis of the diode and a short focal length asphere focuses the output onto the YLF rod through a dichroic prism. The prisms are coated for maximum transmission of the pump light and maximum reflectance at the laser wavelength. The resulting pump spot in the Nd:YLF rod is strongly elliptical, measuring 1.6 mm x 0.3 mm (FWHM). To efficiently extract the energy from such an elliptical gain distribution in a TEM₀₀ mode an intracavity cylindrical telescope of magnification 4 is used. The laser resonator mirrors consist of a 1.2 m radius of curvature maximum reflector and a flat, 70% reflectivity output coupler. A thin film polarizer and KD*P electro-optic Pockels cell are used to provide Q-switched operation.

Under long-pulse conditions, without intra-cavity elements, this laser has produced up to 15 mJ of linearly-polarized output at 1.047 μ m with a pulse duration close to the diode pump pulse. With the added intra-cavity elements the long pulse output drops, to <10 mJ and in Q-switched operation typical outputs of 5-6 mJ in pulses of 18 ns (FWHM) duration are achieved. Figure 2 shows the temporal profile of a Q-switched pulse. Evident in this figure are the temporal modulations caused by beating of longitudinal cavity modes. At repetition rates above 100 Hz a slight decrease in pulse energy has been observed. This is attributed in part to an observed decrease in diode output power at higher repetition rates. Some thermal effects in the Q-switch have also been observed and are presently being investigated.

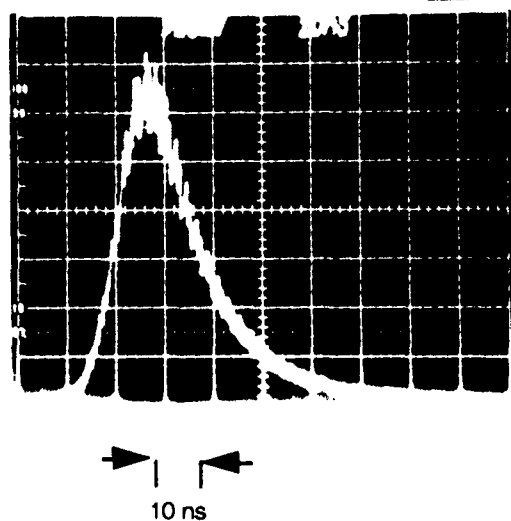


Figure 2. Temporal profile of a Q-switched pulse.

Figure 3 shows an image taken with a CCD camera and beam profiler of the output beam at a distance of 45 cm from the output coupler. At this point the beam is round and the profile Gaussian in both axes. Because of the intracavity cylindrical telescope the divergence of the beam in the two axes is different resulting in an elliptical beam on either side of this position but still with excellent Gaussian profile in both axes. A measurement of the beam quality for both axes resulted in a value of $M^2 < 1.1$, confirming the exceptionally high beam quality from this laser.

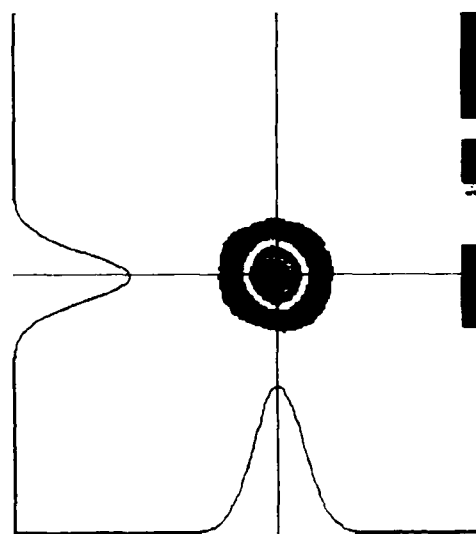


Figure 3. Spatial profile of beam 45 cm from output coupler, showing Gaussian profile in both axes.

Frequency doubling the output of this laser has been investigated using KTP, LBO and BBO. The simplest and most efficient arrangement uses a 3 x 3 x 10 mm KTP crystal angle cut for type II phase matching at 1.047 μ m, placed near the output coupler, directly after a half-wave plate. Typical conversion efficiencies of 55-60% have been realized resulting in a 523-nm output of ~3 mJ. In the case of LBO and BBO the output beam was focussed into the crystal but the resulting conversion efficiencies were somewhat lower than obtained with KTP. The high peak powers from this laser also allow efficient tripling and quadrupling of the output into the ultraviolet. Using a combination of KTP and BBO crystals to triple the output, energies approaching 0.75 mJ have been obtained at 349 nm. In quadrupling experiments a 2.5-cm long noncritically phase matched KDP crystal has resulted in output energies approaching 0.5 mJ at 262 nm.

The frequency-doubled output from this laser has also been used to pump a KTP OPO providing tunable radiation in the red and near-infrared. The OPO consisted of two, x-cut, 15-mm long KTP crystals in a 4-cm long flat-flat cavity. The pump beam was double-passed through the crystals by reflection off the output coupler which was appropriately coated for maximum reflection at the pump wavelength and ~90% transmission at the signal and idler wavelengths. The second cavity optic was coated for maximum transmission of the pump light and maximum reflectance of the signal. Using appropriate mirrors and crystals the OPO has been tuned over the range 0.64 μm - 2.9 μm . The efficiency varied over this range due to the change in effective nonlinear coefficient. The highest efficiency was observed at a signal wavelength of 0.991 μm corresponding to an idler wavelength of 1.11 μm . In this region the OPO threshold was 0.36 mJ (20 MW/cm²). Running at 8 times above threshold, 54% conversion of the incident pump photons was achieved.

In summary we will report on the development of a diode-end-pumped Nd:YLF laser capable of operation at high repetition rate. The device produces Q-switched outputs in excess of 5 mJ per pulse. Frequency conversion to the green and ultraviolet will be discussed and results obtained using this source to pump an OPO producing tunable red and infrared light will be presented.

REFERENCES

1. T.M. Baer, D.F. Head and P. Gooding, "High peak power Q-switched Nd:YLF laser using a tightly folding resonator," presented at CLEO, May 21, 1990, Anaheim, CA, paper CMF2.
2. D.C. Shannon and R.W. Wallace, "High-power Nd:YAG laser end pumped by a cw, 10 mm x 1 μm aperture laser-diode bar," *Opt. Lett.* **16**, 318, 1991.

Laterally Diode Pumped , c-axis Nd:YLF Laser

Newton Sims, Jr.
Mahendra G. Jani
Science and Technology Corporation
Hampton, Virginia 23666

Norman P. Barnes
NASA Langley Research Center
Hampton, Virginia 23665-5225

Lateral diode pumping of Nd:YLF has demonstrated a high efficiency when operated in a c-axis orientation rather than the conventional a-axis orientation. diode pumped laser efficiency can be approximated as a product of several efficiency factors including the absorption efficiency, the storage efficiency and the extraction efficiency [1]. Nd:YLF has been recognized as an attractive laser material for laser diode pumping applications since the upper laser level lifetime of 500 μ sec is twice that of Nd:YAG. Having selected Nd:YLF on this basis, the performance can be further optimized by selecting the orientation of the laser rod with respect to the crystal axes. With the conventional orientation of the a-axis along the cylindrical axis of the laser rod, both the high 1.047 μ m and the somewhat lower gain 1.053 μ m transitions are available. However, in this configuration lateral diode pumping will primarily utilize the a-axis absorption features. On the other hand, with the c-axis aligned along the rod axis, the stronger c-axis absorption features can be utilized. In the c-axis orientation, only the lower gain 1.053 μ m transition is available. Using calculated values for the absorption and extraction efficiencies, it was determined that the total efficiency would be greater in the c-axis orientation. Experiments performed with c-axis Nd:YLF laser rods support this prediction.

Laser diode arrays were selected particularly for Nd:YLF and then temperature tuned for optimized c-axis absorption. While diode pumping of Nd:YLF has been demonstrated previously, it was often achieved with laser diode arrays which were selected for pumping of Nd:YAG. It has been shown that laser diode pumping of Nd:YLF can be optimized by selecting the pump wavelength to be significantly shorter, as shown in Figure 1. It may be noted that optimization of the pump wavelength for c-axis operation occurs at 792 nm while optimization for a-axis operation occurs at 797 nm, and diodes for pumping Nd:YAG have spectral emissions centered near 808 nm.

Normal mode, pulsed, c-axis Nd:YLF laser experiments employing a symmetrical arrangement of three high power laser diode arrays were performed with three different rod diameters. Highest efficiencies were obtained with a 4 mm diameter rod. The maximum pulse energy obtained at 1.053 μ m was 112 mJ. 502 mJ were obtained at 1.313 μ m. The conversion efficiency of the total optical output of the diodes to the 1.053 μ m laser output was 0.335, and the slope efficiency was 0.373. The conversion efficiency for the 1.313 μ m laser was 0.150, while the slope efficiency was 0.178. Plots of these laser performances

ABSORPTION SPECTRA OF Nd:YLF

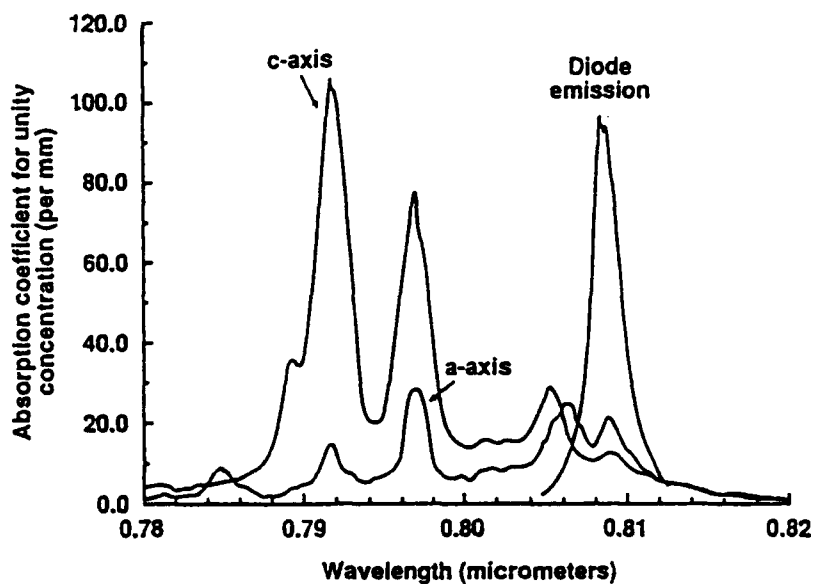


Figure 1. Absorption features of both a-axis and c-axis Nd:YLF in the GaAlAs diode spectral emission range along with a measured diode spectra intended for pumping Nd:YAG.

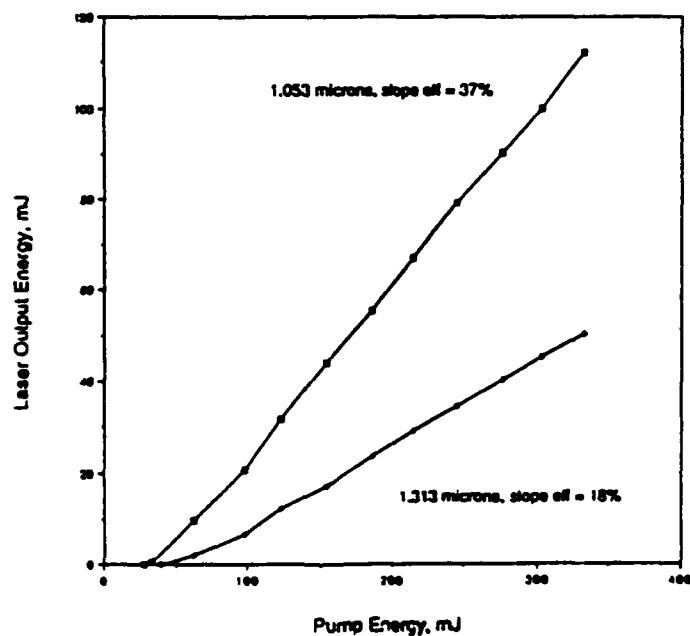


Figure 2. Laser performance curves for diode pumped c-axis Nd:YLF.

are shown in Figure 2. Resonator losses calculated from the threshold pump energies and the output mirror reflectivities were 0.0087 indicating high optical quality for the c-axis rods. Advantage was taken of the low heat load experienced in efficient diode pumping. The only cooling employed in the pump head was conductive cooling to metal heatsinks, and no negative effects were observed in going from 2 Hz pulse repetition rate to 10 Hz.

References

- [1] N. P. Barnes, M. E. Storm, P. L. Cross, and M. W. Skolaut, "Efficiency of Nd Laser Materials with Laser Diode Pumping," IEEE J. Quant. Elect. QE-26, pp. 558-569, (1990).

A Simple Model of the Mars Observer Laser Altimeter Laser Transmitter

Robert S. Afzal

Code 924, NASA Goddard Space Flight Center, Greenbelt, MD 20771 (301) 286-5669

The Mars Observer Laser Altimeter^{1,2} (MOLA) incorporates a diode laser pumped Nd:YAG laser transmitter. To our knowledge MOLA will utilize the first diode laser pumped solid state laser to operate in space. The laser transmitter (LT) was designed to survive launch and the journey to Mars with the following specifications:

	<u>Weight</u>	<u>Avail. Power</u>	<u>Energy</u>	<u>Pulse width</u>	<u>Rep. Rate</u>	<u>Lifetime</u>
Specs.	6.25 Kg	14 W	40 mJ	10 nS	10 Hz	6×10^8 shots
Actual	5.38 Kg	13.7	41 mJ	7.6 nS	10 Hz	TBD

The laser is still required to deliver 35 mJ pulses after 0.6 billion shots. Further constraints, perhaps even more demanding, were those of cost and delivery time. This paper describes the MOLA laser and presents a simple model predicting the operational behavior of the laser based on the available test results.

Description of the laser

The MOLA laser transmitter was designed² and built by McDonnell-Douglas Electronic Systems Co. in St. Louis, MO. At the heart of which is a diode laser pumped slab of Cr:Nd:YAG within a Q-switched crossed Porro resonator. Figure 1 shows a schematic of the laser. A nine bounce zig-zag slab of 1% doped Nd:YAG was codoped with 0.05% Cr for purposes of radiation hardening. The Brewster cut slab had a 3.4 x 3.4 mm cross section. Thermal and gain inhomogeneities within the slab are compensated for by image inversion off of each bounce inside the slab. 4 stacks of 11 diode laser bars side pump the slab and the opposite slab face is aluminium coated to reflect the unabsorbed pump light back into the crystal. The diode stacks are pulsed at 10 Hz for a duration of 150 μ s with a peak output power of 1760 watts at room temperature.

The slab is placed within a crossed Porro "z" resonator with the LiNbO₃ Q-switch in one arm of the "z" and the gain medium in the other. A 0.57λ waveplate compensates for depolarization in the Q-switch arm Porro prism. The waveplate prism pair rotate the polarization 90° in a double pass creating a low Q resonator. $1/4 \lambda$ voltage applied on the Q-switch then creates the high Q condition. Output coupling is achieved by rotating a $1/4 \lambda$ plate in the gain arm of the "z" and coupling out the orthogonal polarization through one of the polarizing cubes. The lasers' optimal output coupling can then be empirically determined simply by rotating the $1/4 \lambda$ plate and maximizing the output power.

Description of the numerical model

We began with the standard coupled ordinary differential equations describing the operation of a Q-switched laser^{3,4}. The Q-switch is modeled as a decaying exponential term in the dissipative cavity losses. The equations to be numerically integrated are:

$$(1) \quad \frac{dN}{dt} = -\gamma_{sc} N \phi \quad (2) \quad \frac{d\phi}{dt} = \frac{2\sigma I N \phi}{t_r} - \frac{\phi}{t_c}$$

where N is the inversion density and ϕ is the cavity photon density.

All the work however in making this model correspond to measured experimental data lies in an accurate determination of the initial conditions and a proper choice of the equation constants. The initial photon density is chosen to be 1 for simplicity. The initial inversion density was determined by considering the total number of photons emitted from the diodes and absorbed by the slab that yielded a Nd ion in the excited state. The initial inversion was given by:

$$(3) \quad N_0 = \frac{P t_p \alpha \xi \chi \eta}{V h \nu}$$

where $P = 1700$ W is the peak diode pump power emitted by the stacks, $t_p = 150$ μ s the square pulse pump duration, $\alpha = 0.9$ (typically) the double pass absorbed fraction, $\chi = 0.9$ for a pump coupling efficiency, $\xi = 0.965$ for the quantum efficiency of the radiationless transfer from the pump level to the $^4F_{3/2}$ upper laser manifold⁵, $h \nu = 2.44 \times 10^{-19}$ J for the photon energy and $V = 0.59$ cm³ the slab volume. Reduction of the initial inversion density by spontaneous emission is accounted for by the factor $\eta = 0.737$. We therefore started our equations with an initial inversion of $\approx 10^{18}$ cm⁻³.

Other equation constants used were as follows. t_r is the cavity optical round trip time which for a 37 cm long cavity is 2.47 ns. The nonuseful losses (nonoutput coupling) in the cavity were $L = 0.35$. The Q-switch is then incorporated into the differential equations as an explicit time dependent loss term given by:

$$(4) \quad L(t) = L(1 + e^{-\frac{t}{\tau}})$$

$\tau = 30$ ns is the characteristic rise time of the Q-switch. The cavity decay time is then given by $t_c = t_r / (L(t) - \ln(R))$ where R is the effective output coupler reflectivity.

Careful attention must be given to the value of the cross section because this number effects both the output energy and pulsewidth predictions. There have been many values for the stimulated emission cross section σ published in the literature over the years. Based on two recent high quality determinations of the cross section^{5,6} the value of 2.8×10^{-19} cm² was used. Since our pulsewidths are $\approx 10^{-8}$ s $\gg 10^{-11}$ s the intramanifold Stark level thermalization time⁷, we consider the 1.064 μ m transition occurring from the $^4F_{3/2} \rightarrow ^4I_{11/2}$ manifold not the $R_2 \rightarrow Y_3$ sublevels. Even though the sublevel cross section is 6.5×10^{-19} cm², in the long pulse regime the sublevels are in thermal equilibrium so we use the manifold to manifold value which is 2.8×10^{-19} cm². In this regime the values given in ref.5,6 agree. The value used for the 'inversion reduction factor'³ $\gamma = 1.2$. Due to the rapid thermalization time, the $^4F_{3/2}$ doublet can be considered a single level. The equilibrium Boltzman distribution of the $^4I_{11/2}$ manifold places $\approx 20\%$ of the atoms in the Y_3 sublevel. Therefore for every excited atom there is only a reduction of ≈ 1.2 in the inversion. Given these parameters the equations can be solved numerically obtain the output pulse energy and width.

Temperature Dependence

The temperature dependence of the LT is solely incorporated into the temperature dependence of the pump diodes. The first correction is a slight linear dependence on the output power with temperature given by $P = 1756 - 4.4T$ where T is in $^{\circ}$ C and P is in watts. The second and more important effect of temperature is on the diode wavelength. Our model assumes a 1 nm shift in wavelength for every 3.125 $^{\circ}$ C change in temperature.

The 44 diode bars are spread out in wavelength over 6 nm. The percent absorption of each bar was determined by considering the overlap of the bar's wavelength and the Nd:YAG absorption spectra. An ensemble absorbed fraction of the total power was calculated by summing over the 44 bars. That fraction of total absorbed power is then calculated for every 3.125 $^{\circ}$ C change in temperature from 9 $^{\circ}$ to 38 $^{\circ}$ C. An eighth order polynomial fit to the data provides a continuous dependence of the total fraction of absorbed pump energy on temperature over the region 9 $^{\circ}$ to 38 $^{\circ}$. That fraction is then used in equation (3) for α . Therefore the temperature dependence is incorporated directly into the initial conditions of the system. Figure 2 compares the predicted and measured temperature behavior of the LT. The operational temperature range can then be directly

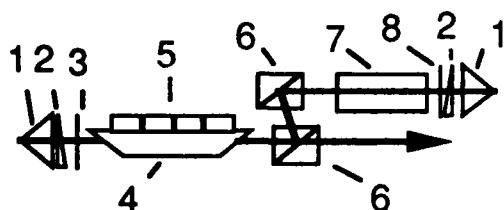
tailored to operate over different temperature regions expected to be experienced by the instrument by choosing various diode bar wavelength combinations.

Conclusions

We have presented a simple numerical model of the MOLA LT that predicts the output energy, pulsewidth and temperature dependence to better than 10% of the available data. As with most laser models the largest sources of error come from experimental determination of the input parameters such as pump power and pump absorption. The equation constants pose another problem. Even with a well studied material as Nd:YAG, there are uncertainties in the material parameters. Careful consideration must be given to the regime of application, due to this much better than 10% accuracy should not be expected at this level of treatment. However, it is interesting to note that the essential physics of this laser seems to have been captured by our model without the need for a more detailed approach. This will now provide us with a powerful tool to develop of future diode laser pumped solid-state lasers.

References

- 1) M.T. Zuber, D.E. Smith, S.C. Solomon, D.O. Muhlman, J.W. Head, J.B. Garvin, J.B. Abshire, and J.L. Bufton; J. Geophys. Res., Vol. 97, No. E5, p 7781, (1992).
- 2) G. Gaither et al.; CLEO '91, Baltimore MD, Technical Digest, CFI2, p 520
- 3) J.J. Degnan; IEEE J. Quantum Electron., Vol. 25, No. 2, p 214, (Feb. 1989).
- 4) W. Koechner, Solid State Laser Engineering, New York: Springer-Verlag, 1976, ch. 8.
- 5) E.B. Treacy and Z. Lu, "Negative Lens Laser", SBIR Phase I final report, Candela Laser Corp., Wayland MA, Office of Naval Research Contract # N 00014-90-C-0187, Arlington VA.
- 6) W.F. Krupke, M.D. Shinn, J.E. Marion, J.A. Caird, and S.E. Stokowski; J. Opt. Soc. Am. B, Vol. 3, No. 1, pp 102-113, (January 1986).
- 7) L.A. Riseberg and H.W. Moos; Phys. Rev., Vol. 174, No. 2, p 429, (Oct. 10, 1968) and W.M. Yen, W.C. Scott and A.L. Schawlow; Phys. Rev., Vol. 136, No. 1A, p A271, (Oct. 5, 1964).



- 1- Porro Prism
- 2- Risley Wedge
- 3- $\frac{1}{4} \lambda$ Plate
- 4 - Cr:Nd:YAG Slab
- 5 - Diode Laser Stacks
- 6- Polarizers
- 7 - Lithium Niobate Q-switch
- 8- 0.57λ plate

Figure 1

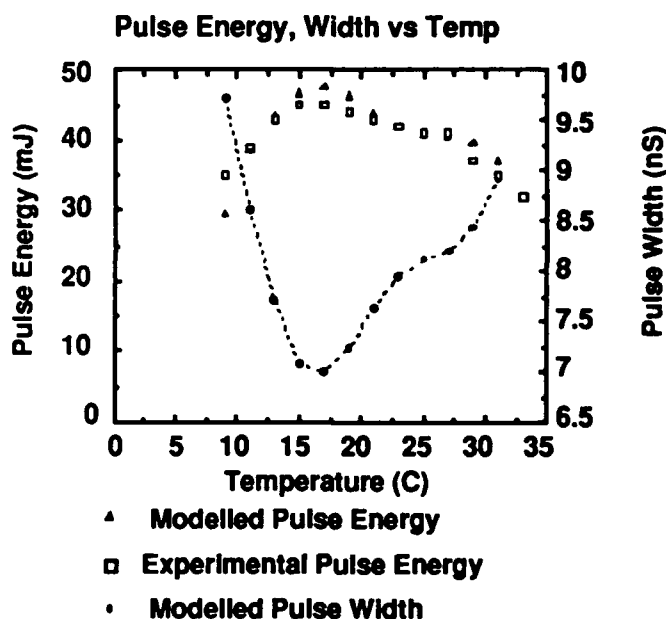


Figure 2

Q-switched diode-pumped Nd:YAG lasers

Judith M. Dawes, Peter Dekker, Ying Cai, David S. Knowles, Stuart Jackson and
James A. Piper
Macquarie University,
Center for Lasers and Applications,
Sydney, 2109. Australia.

Diode-pumped Nd:YAG lasers offer advantages of simplicity, efficiency and compactness in a range of applications. As powerful diode arrays become more readily available, moderate power sources for laser ranging can be developed. A transversely pumped nonfocussing solid collector geometry, which is insensitive to misalignment, was described previously (1). In this paper are presented results for its power scale-up and improved Q-switching operation, and also aspects of its thermal behaviour.

Since the design uses a prism containing a Nd:YAG rod cemented into position, the collector assembly is mechanically robust and simple to align. The gain is distributed uniformly across the rod profile by total internal reflection of the diode light from the sides of the prism, as shown in figure 1A. It is possible to scale up the power to the Nd:YAG rod by placing an extra one or two diode arrays at the sides of the prism, to simulate 4-way pumping by a larger single array. This also allows studies of thermal effects in the laser material. Measurements of the birefringence of the rod, incorporating effects of temperature and stress allow comparison of different prism and glue materials. At higher pump power, the hold-off efficiency of the acousto-optic Q-switch decreases, and electro-optic Q-switching is preferred. However, problems due to birefringence in the laser medium may arise. The Q-switch crystal used, Li NbO_3 , is also vulnerable to surface damage at high intracavity fluences.

The prism collector geometry yields a uniform gain profile, and consequently it is insensitive to misalignment at the partial expense of pump efficiency. For a diode array of about 120 W peak power, the absorbed power is estimated to be 70 W. Medium to high power lasers require multiple or larger pump sources. Placing two pumped Nd:YAG rods in the same laser cavity is considerably less efficient than using two diode arrays to pump the same rod, due to losses in the rods and AR coatings. The second array is placed to supplement the 4-way pumping, as in figure 1B, or in a variation of the arrangement, as in figure 1C. (The advantage of the scheme in figure 1C is that the assembly may be suitably heat sunk through the hypotenuse of the prism. Further, the prism material could be sapphire, to enhance the heat transfer efficiency.) The pumping efficiency for these arrangements is estimated to be around 50 %, which could be improved with the use of AR coatings on the prism surfaces. The gain profile is less uniform than in the single diode pumped case. The maximum pumping power was achieved with three diode arrays disposed at each of the prism facets, as shown in figure 1D. This system was not optimised with respect to coatings, and allowed an efficiency of 45 % absorbed pump energy.

Two issues were addressed with these systems; thermal effects in the Nd:YAG rod as a result of mounting in the solid collector, and Q-switch efficiency. In seeking a suitable bonding agent for the gap between the rod and the prism, we found that Dow Corning silicone 93-500 and Epotek epoxy 301-2 were best in terms of optical properties and setting quality. However at high average pump power, the epoxy bonded prism cracked at the side where the laser rod was closest to the diode. The silicone, which is more flexible, is thus the preferred material for mechanical reasons. However it is found that at higher pump powers, the silicone causes more birefringence than does epoxy. The measurements of birefringence contrasting the two materials are shown in figure 2. A steady state model of the temperature behaviour of the pumped rod suggests that the epoxy contributes mechanical stress which partly compensates the temperature induced birefringence. The heat conductivities of the silicone and epoxy were measured by an AC calorimetry technique to be; epoxy 301-2 $0.171 \text{ Wm}^{-1}\text{K}^{-1}$ and silicone 93-500 $0.153 \text{ Wm}^{-1}\text{K}^{-1}$ (2).

Electro-optic and acousto-optic Q-switching were compared. At lower pump powers, either method yielded short pulses of moderate energy (8 ns, 1-3 mJ). With more than a total of 240 W pump power, we found that the acousto-optic Q-switch, Gooch and Housego model QS-080, which had a diffraction efficiency of 18 % at 1.06 μm , allowed prepulses containing up to 50 % of the pulse energy. Electro-optic Q-switching allowed better hold-off, despite the losses due to birefringence in the Nd:YAG. While we used a birefringence compensating cavity (1) for some measurements, it was harder to align as its displacement (2.7 mm) was slightly less than the rod diameter. Thus a standard polariser (either a Ward polariser or thin film dielectric) was used. The acceptance angle of the polariser is typically very narrow, and in our hemispherical cavity the beam divergence contributed some loss. At higher pump powers, a flat-flat cavity was stable due to thermal lensing in the YAG rod, and while emitting a multimode beam, its output divergence was within the polariser acceptance angle.

The Q-switch itself contributes some loss as the pulse builds up in the cavity. Ideally the Q-switch has a step function voltage, from approximately 1400 V to 0 V. In practice, with either a krytron based switch or avalanche transistors, we measure a negative going pulse of a few hundred volts, which gradually relaxes to 0 over a time of microseconds. Since our laser pulse is emitted about 60 ns after the voltage is switched, the pulse is building up with a considerable loss (about 7 % per pass) in the Q-switch at this time. The output coupler for the cavity is 30 %. This Q-switch loss can be measured by observing the energy rejected from the polariser as a fraction of the output energy. (This rejected energy also contains a loss due to birefringence in the YAG rod, and represents up to 70 % of the output.) The addition of a quarter wave plate to the cavity, tuned for optimum output pulse, appears to reduce this problem considerably and compensates for the dynamic loss of the Q-switch, and the birefringence of the Nd:YAG. (The rejected energy drops to 10 % of the output pulse energy.) Using this scheme, we have measured optimum Q-switched pulses of 10.9 mJ, and 7.5 ns pulsewidth at a repetition rate of 10 Hz, with a total diode input of 120 mJ of which we estimate 50 mJ was absorbed.

Table 1 shows results for repetition rate scaling, recorded at somewhat lower pulse energies. The QS pulse delay shows the delay between the voltage switch and

the output pulse. As the cavity is 12 cm long, this represents about 75 round trips. Note that in this arrangement, all the diodes are held at the same temperature. If a single larger diode array were used, and appropriately temperature tuned, better efficiency is expected.

In conclusion, we have shown that the solid collector geometry has potential for moderate power scale-up, and when Q-switched, yields pulses of 10.9 mJ and 7.5 ns from an absorbed pump power of 50 mJ.

Table 1. Results for Q-switching at a range of conditions

Repetition rate	QS pulse energy	QS pulse width	QS pulse delay	QS average power
10 Hz	6.7 mJ	10 ns	68 ns	67 mW
25 Hz	7.0 mJ	10 ns	62 ns	174 mW
50 Hz	6.4 mJ	12 ns	70 ns	321 mW

References

- (1) J.M. Dawes, S. Jackson, Y. Cai, P. Dekker and J. A. Piper, Advanced Solid State Lasers, paper TuB3, 1992.
- (2) The measurements were performed by Mr Norman Booth of University of Technology, Sydney.

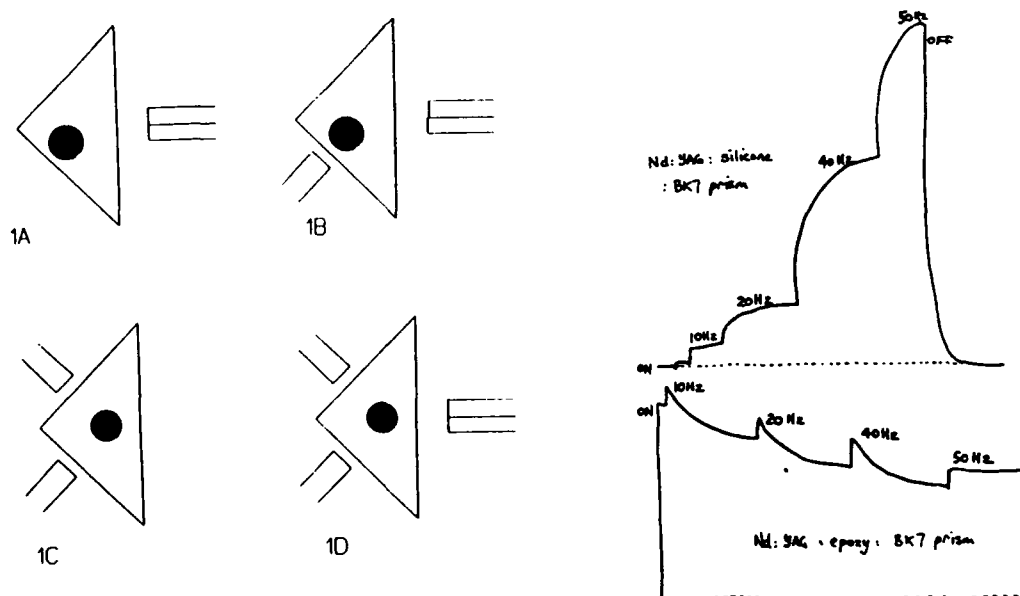


Figure 1; Geometries for solid collectors with 1, 2 or 3 pump sources.

Figure 2; Birefringence of Nd:YAG rod side pumped by a 240 W diode with varying pulse repetition rate.

Comparison of Nd³⁺ in GdLiF₄ and YLiF₄ by Fourier spectroscopy

H. Weidner¹, R. E. Peale¹, X. X. Zhang², M. Bass^{1,2,3}, and B. H. T. Chai^{2,4}

¹Department of Physics, ²Center for Electro-Optics and Lasers, ³Department of Electrical Engineering, ⁴Department of Mechanical Engineering, University of Central Florida, Orlando, FL 32816 Tel. (407) 823-5206

Laser action of a new crystal Nd:GdLiF₄ (Nd:GLF) is being reported for the first time by Zhang et al. at this conference[1]. Both pulsed and CW laser pumped action are observed. A slope efficiency of 58% percent was observed in pulsed mode with no attempt to optimize. One advantage of this material over YLiF₄ (YLF) is that much higher Nd concentrations can be realized.

Low resolution, room temperature absorption spectra[1] reveal essentially no difference in peak positions with Nd:YLF. Here we present a high resolution low temperature study in order to accurately determine the energy levels of Nd:GLF and to compare these with Nd:YLF levels determined by us using the same technique. Our spectra indicate that GLF and YLF are isostructural and that linewidths are unaffected by the high Nd concentrations.

We have measured polarized, temperature dependent, transmission spectra of from 500 to 22,000 cm⁻¹ at a resolution of 1 cm⁻¹ using a Bomem DA8 Fourier spectrometer. One advantage of the Fourier technique for characterization of laser materials is its high frequency accuracy, being 0.004 cm⁻¹ at 2000 cm⁻¹ for the Bomem.

The high optical quality single crystal of Nd:GLF was grown by the modified Czochralski pulling technique. It was nominally doped with 5 at. % Nd. The actual Nd³⁺ concentration in the crystal is estimated to be about 4 at. %[1]. The Nd concentration of our YLF sample was nominally 3% but is estimated to be 1.1 at. %.

Figure 1 shows the ⁴I_{9/2} → ⁴F_{5/2}, ²H_{9/2} transitions at a sample temperature of 80 K.. The two groups of strong bands at the center of the spectra are used for diode pumping of lasers. The lower trace, taken at a resolution of 4 cm⁻¹, gives the spectrum of Nd:GLF; the upper trace (2 cm⁻¹ resolution) gives the Nd:YLF spectrum. The very close similarity in both the number, spacing and relative strength of lines in each of the two materials is strong evidence that they are isostructural.

Figure 2 presents the ⁴I_{9/2} → ⁴F_{3/2} bands. The ⁴F_{3/2} levels are the initial states for 1 μm laser operation. The lower GLF spectrum was taken at a resolution of 4 cm⁻¹; the upper YLF spectrum at 0.5 cm⁻¹ resolution. The two spectra appear nearly identical. The strongest line and the weak line just to its left in each spectrum are transitions from the ground level to each of the two ⁴F_{3/2} Stark components. The other weak lines on the low frequency side are transitions originating in thermally populated Stark components of the ground ⁴I_{9/2} multiplet. The weak lines on the high frequency side may be pair lines. It is important that the linewidths in the two materials are nearly the same, despite their different doping levels.

The final levels of the 1 μm laser transitions are determined from the ⁴I_{9/2} → ⁴I_{11/2} spectrum plotted in Figure 3. Both spectra were collected at 1 cm⁻¹ resolution, which was necessary to resolve the majority of lines. Again the close similarity of the spectra for each of the two materials is evident.

Table I gives those energy levels determined from these data which are relevant to diode-pumped lasing. Nd:YLF has never been measured by the Fourier technique, so we present our determination of its levels. These values differ from measurements made

previously by grating spectroscopy[2] by significantly more than the linewidths.

In conclusion, we have measured the transmission spectrum of Nd^{3+} in a single crystal of GdLiF_4 , a newly demonstrated laser material. The spectra are nearly identical to those of Nd:YLiF_4 , strongly indicating that the two crystals are isostructural. The high dopant concentration in the GLF sample appears to affect the transitions of interest insignificantly. In addition, we will present a comparison of the Fourier luminescence spectra for the two laser crystals, and also a comparison of low and high concentration GLF samples.

Table I. Levels determined from thermal replica patterns in the 80 K transmission spectra.

Nd:YLF

$^4I_{9/2}$	0, 132, 182 cm^{-1}
$^4I_{11/2}$	1997.1, 2040.1, 2042.4, 2077.0, 2226.8, 2261.9
$^4F_{3/2}$	11535.7, 11594.5
$^4F_{5/2}, ^2H_{9/2}$	12535.3, 12544.9, 12625.7, 12641.8, 12663.0, 12729.5, 12803.7, 12829.4

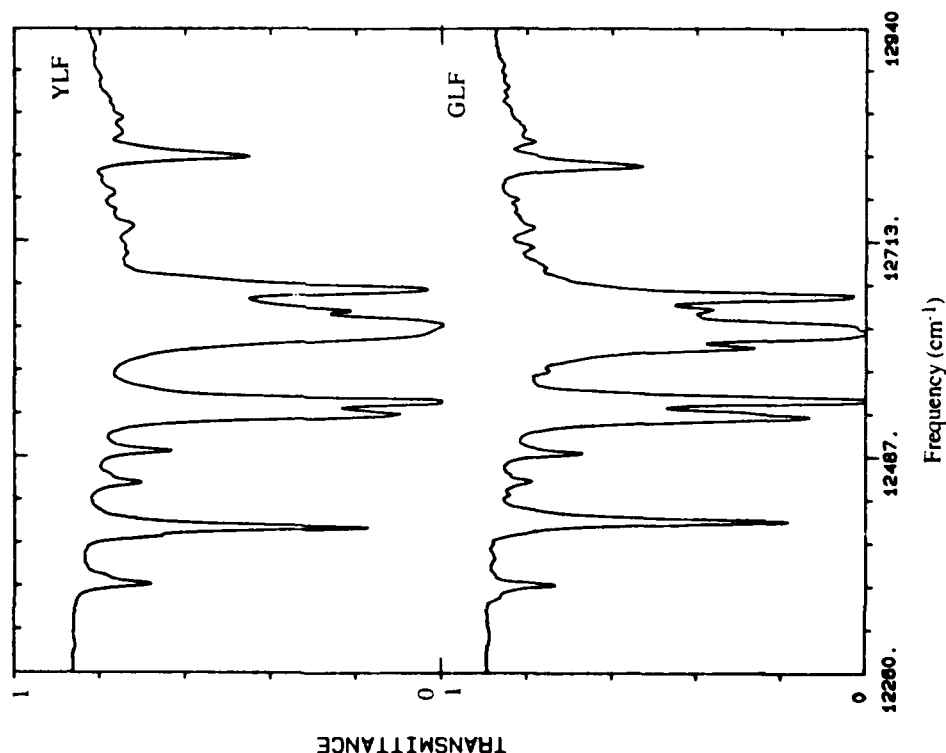
Nd:GLF

$^4I_{9/2}$	0, 128, 182
$^4I_{11/2}$	1992.6, 2036.4, ---, 2071.6, 2210.6, ---
$^4F_{3/2}$	11530.9, 11588.7
$^4F_{5/2}, ^2H_{9/2}$	12528.9, 12545, 12617.9, 12641, 12657.2, ---, 12792.7, ---

References

- [1]. X. X. Zhang, M. Bass, J. Lefaucheur, A. Pham, A. B. Villaverde, and B. H. T. Chai, proceedings of this conference.
- [2]. A. A. S. da Gama, G. F. de Sá, P. Porcher, and P. Caro, J. Chem. Phys. **75**, 2583, (1981).

Figure 1. $^4I_{9/2} \rightarrow ^4F_{5/2}, ^2H_{9/2}$ transitions. These are the diode-pumping bands at 80 K.



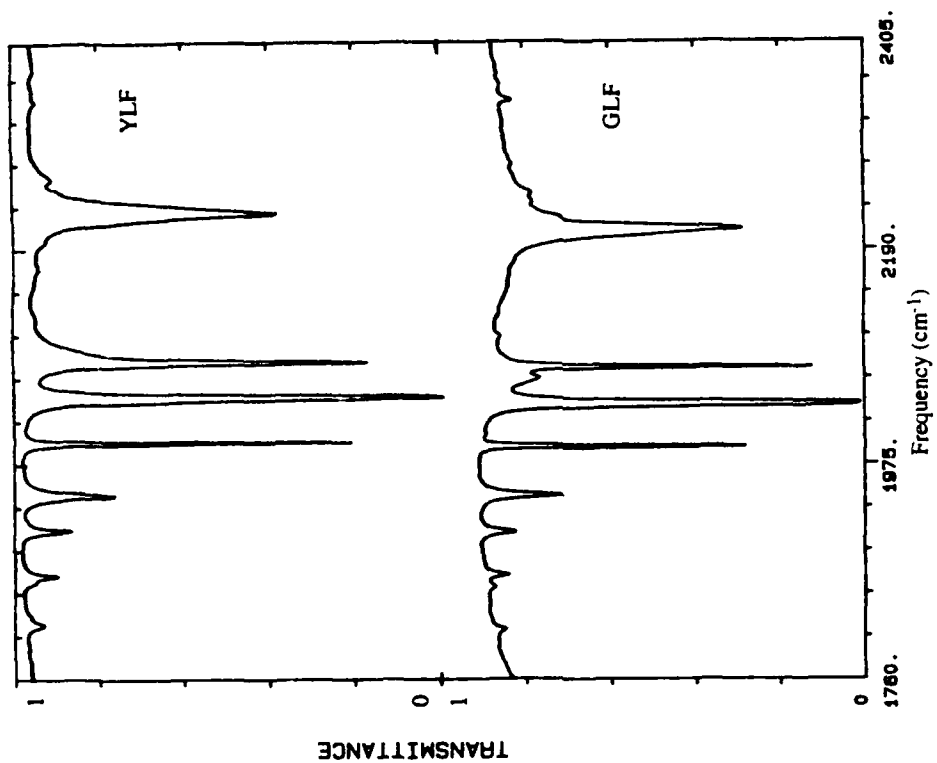


Figure 3. $4I_{9/2} \rightarrow 4I_{11/2}$ transitions at 80 K.

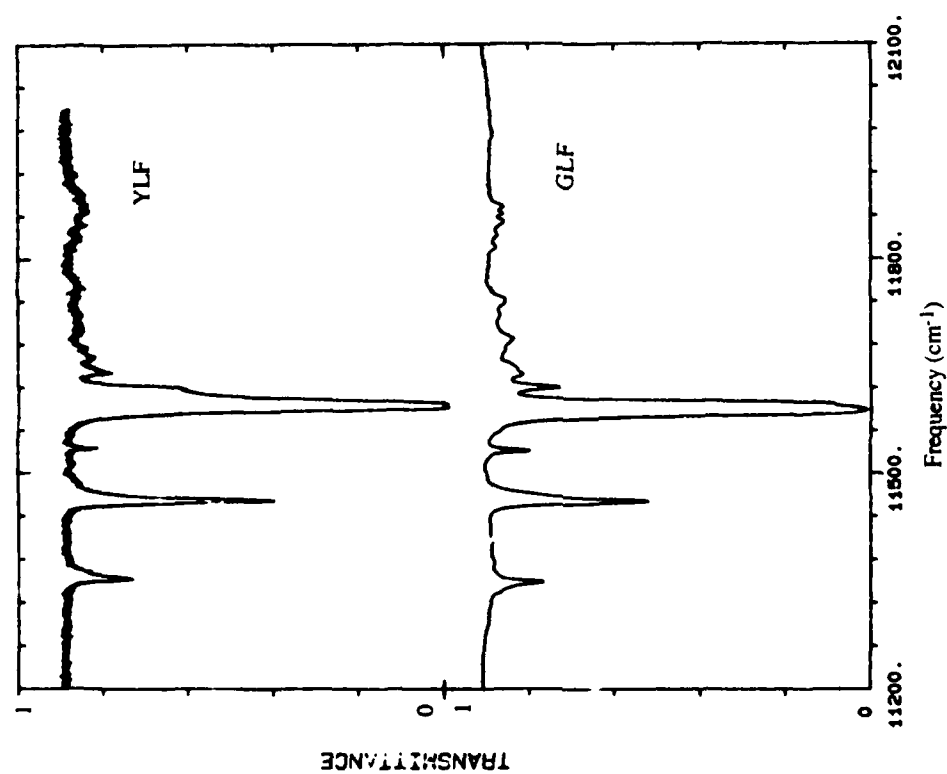


Figure 2. $4I_{9/2} \rightarrow 4F_{3/2}$ transitions at 80 K.

Monday, February 1, 1993

Nd Lasers

AMC 10:30am-12:00m
La Salle Ballroom B&C

Ralph L. Burnham, *Presider*
Fibertek, Inc.

Nd:GdVO₄ Crystal - a New Material for Diode-Pumped Solid-State Lasers

V.G.Ostroumov, I.A.Shcherbakov, A.I.Zagumennyi

General Physics Institute of Russian Academy of Sciences

117942 Moscow, Vavilov str., 38, Russia, Fax: (095)135-02-70

G.Huber, T.Jensen, J.P.Meyen

Institute of Laser Physics University of Hamburg

Jungiusstrasse 11, 2000 Hamburg 36, Germany

One of the most promising candidates for diode pumped solid-state lasers is Nd:YVO₄. However, the crystals grown of Nd:YVO₄ of high optical quality meets a lot of difficulties, which prevent wide use of this material. In this paper we report about the growing and laser operation of new media Nd:GdVO₄. From technological point of view this material has a number of advantages, which open the possibility of obtaining high optical quality samples.

In RVO₄ structure (where R = Sc, Y or rare-earth ions) vanadium ions are surrounded by four oxygen atoms, which form a slightly pressed tetrahedron. The rare-earth ions are placed in distorted oxygen dodecahedron, that causes very strong dependence of spectroscopic properties on the orientation of the crystal.

We assumed that the spectroscopic and laser properties of Nd:GdVO₄ crystals might be similar to those ones of Nd:YVO₄. That follows from the relationship of lattice parameters of YVO₄ ($a = 7.123$ Å, $c = 6.291$ Å, $c/a = 0.8832$) and GdVO₄ ($a = 7.211$ Å, $c = 6.350$ Å, $c/a = 0.8806$). Replacing of Y³⁺ ions by larger Gd³⁺ ions increases the distances between dodecahedral lattice sites and decreases the ion-ion interactions between the neighbor Nd³⁺ ions and also makes segregation coefficient closer to the unity.

Nd:GdVO₄ crystals were grown by the Czochralskii technique in a radiofrequency-heated iridium crucible. The orientation of growth was $\langle 100 \rangle$ or $\langle 101 \rangle$. The Nd³⁺ concentration varied from 0.9 at.% up to 6 at.%. The temperature of melting was 1780°C.

The pump absorption coefficients at 808 nm are $\alpha = 74 \text{ cm}^{-1}$ ($E \parallel C$) 10 cm^{-1} ($E \perp C$) (Fig.1), the neodymium lifetime is equal to 94 ns for the concentration of neodymium 0.9 at.%. We estimated emission cross-section of Nd:GdVO₄ (refraction index for 1.06 and 1.32 nm was taken as 2) the following: $\sigma_{1.06}^{\parallel} = 6 \cdot 10^{-19} \text{ cm}^2$, $\sigma_{1.06}^{\perp} = 3 \cdot 10^{-19} \text{ cm}^2$, $\sigma_{1.34}^{\parallel} = 1.5 \cdot 10^{-19} \text{ cm}^2$, $\sigma_{1.34}^{\perp} = 0.8 \cdot 10^{-19} \text{ cm}^2$.

The upper index indicates the orientation between E vector and c-axes of the crystal, the lower index indicated the wavelength.

Nd:GdVO₄ were tested both under Ar (514 nm) and diode pumping (808 nm) in the end-pump configuration. In case of Ar pumping we got lasing at 1.06 nm (${}^4F_{3/2} \rightarrow {}^4I_{11/2}$) and 1.34 nm (${}^4F_{3/2} \rightarrow {}^4I_{13/2}$). The resonator was formed by two mirrors with the radius of curvature 5 cm and the reflectivities of the output mirrors are 95% for 1.06 nm and 98% for 1.34 nm. The slope efficiency of Nd:GdVO₄ at 1.06 nm and 1.34 nm was 53% and 14%, respectively.

In case of diode end-pumping the resonator was formed by high reflector with the radius of curvature 5 cm and output mirror with reflectivity of 95% or 90%. The slope efficiencies in both cases were about the same as 54% that is due to high gain (Fig.2), but the threshold was lower for 95% output coupler. We estimated the losses as about 1% at 1.06 nm that is much higher than for YAG:Nd.

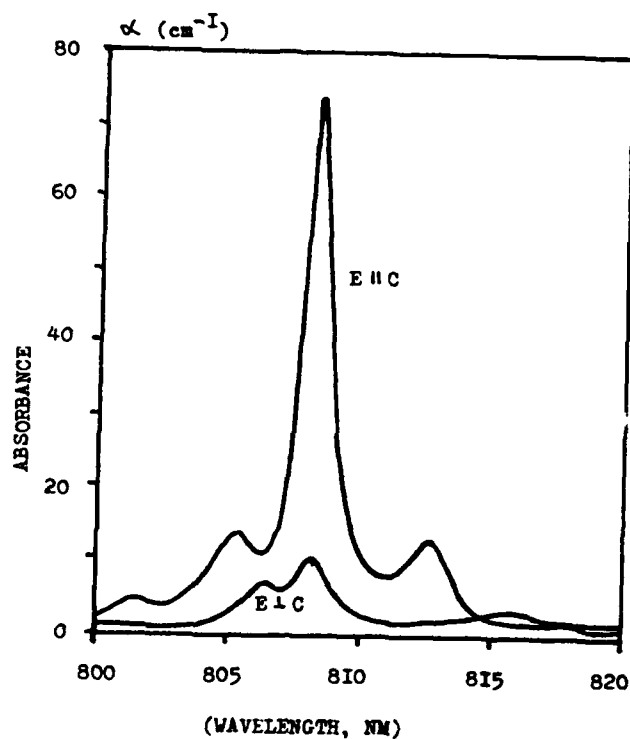


Fig.1. Absorption spectra of Nd:GdVO₄ crystal

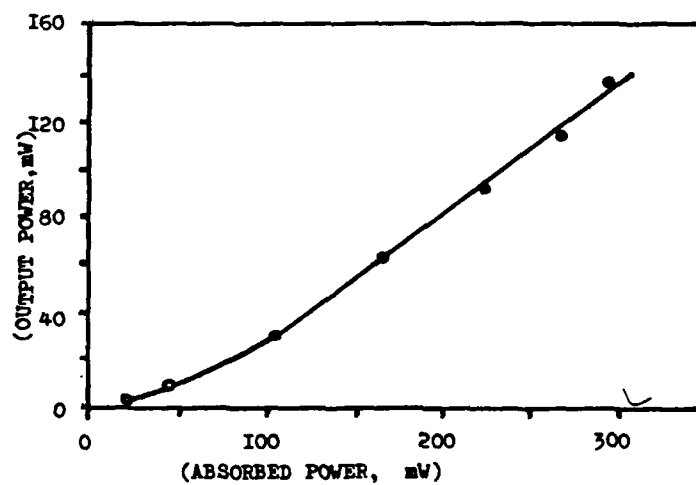


Fig.2. Input-output curve for diode-pumped Nd:GdVO₄ laser at 1.06 μm.
Reflectivity of output mirror is 95%

Laser Performance of a New Laser Crystal - Nd:GdLiF₄

X.X. Zhang, M. Bass, J. Lefaucheur, A. Pham, A.B. Villaverde*, and B.H.T. Chai

Center for Research in Electro-optics and Lasers

University of Central Florida

12424 Research Parkway, Orlando, FL 32826

Tel. (407) 658-6800

*on leave from Universidade Estadual De Campinas, Campinas, SP, Brazil

We report in this paper the efficient lasing performance of a new crystal, Nd³⁺ doped GdLiF₄ (GLF). This material was studied as part of an effort to find new laser hosts for efficient diode pumping. So far Nd:YLiF₄ (YLF) and Nd:Y₃Al₅O₁₂ (YAG) are the only commercially available crystals used in diode pumped lasers. Even though YAG and YLF are both good hosts, they can not be doped with more than 1 at. % Nd³⁺ and retain high optical quality. Such a limitation restricts the developments of practical, compact, high power diode-pumped solid state lasers.

The limit on the Nd doping concentration in both YLF and YAG results from the size mismatch of the Nd³⁺ ion and the Y³⁺ ion in both crystals. To avoid this we choose GdLiF₄ as a substitute host since the ionic radius of the Gd³⁺ ion is 1.06 Å [1] and a much better match to Nd³⁺ (1.12 Å [1]) than Y³⁺ (1.015 Å [1]). High optical quality single crystals of Nd:GLF were grown by the modified Czochralski pulling technique.

The room temperature polarized absorption spectra of a Nd:GLF sample are shown in Fig. 1. For comparison, the absorption spectra of a 1.2 at. % Nd:YLF sample are also given in Fig. 1. The absorption spectra of both samples are almost identical except for the following facts: 1) the absorption coefficient of Nd:GLF is more than three times higher than that of Nd:YLF due, in large part, to the higher Nd³⁺ concentration in GLF and 2) the existence of the absorption features in the region from 250 to 320 nm in the Nd:GLF spectra originating from absorption by the Gd³⁺ (⁸S_{7/2} → ⁶P_{3/2-7/2}, ⁶I_{7/2-11/2}) of the host material. The similarity of the absorption spectra is not surprising since GLF is isostructural with YLF. The actual Nd³⁺ concentration in the GLF crystal is estimated to be about 4 at. % from the absorption data.

The polarized emission spectra in the 1 μm region of Nd:GLF at room temperature are shown in Fig. 2 and are very similar to those of Nd:YLF. The main peak is centered at 1.047 μm for π-polarization (E//C) and at 1.053 μm for σ-

polarization ($E \perp C$). The fluorescent decay of the $^4F_{3/2}$ level of the 4 at. % Nd: GLF is non-exponential with a $1/e$ decay time about 248 μ s, whereas the decay of a 1 at. % Nd:GLF is given by a single, pure exponential function with a decay time of 495 μ s.

A 1 mm thick, flat / flat (C-axis in plane), 4 at. % Nd:GLF sample was used to demonstrate lasing. The initial test employed a concave ($R = 50$ cm) high reflector (HR@1.05 μ m, 90 % T @ ~ 800 nm) and a flat partial reflector (98.8% R @ 1.05 μ m) to form the laser cavity. Pulsed excitation was achieved with a long pulse LiSAF laser tuned to 793 nm and focused with a 20 cm focal length lens. CW excitation employed a Ti:sapphire laser at 797 nm focused with a 5 cm focal length lens. The cavity lengths were 5 and 7 cm for the pulsed and CW tests, respectively. For comparison, a commercial 1.2 at. % Nd:YLF crystal from Lightning Optics, Inc. (3 mm diameter x 6 mm long) was also tested in the same cavities.

The laser output as a function of the absorbed energy or power is given for pulsed operation in Fig. 3(a) and CW operation in Fig. 3(b). The threshold is 180 μ J and 85 mW for GLF, 40 μ J and 29 mW for YLF for pulsed and CW operation respectively. The slope efficiency in pulsed operation is about the same, 58%, for GLF and YLF. In CW operation the slope efficiency is 23% for GLF and 30% for YLF. Lasing from Nd:GLF is linear polarized along the C-axis (π -polarization) and occurs at 1.047 μ m, the same wavelength as that of Nd:YLF. It is not surprising that the threshold of 4 at. % Nd:GLF is higher than that of 1.2 at. % Nd:YLF, since the decay time of the former is only 248 μ s compared to 500 μ s of the latter. The relatively low slope efficiency for CW operation is most probably due to the mismatch of the pump size and the cavity mode size. Improvements in the quality of the Nd:GLF and progress towards optimizing the concentration is expected to result in improved laser performance. Results obtained for more optimized crystals and resonator will be reported.

In summary, we have identified a new laser host, Nd:GdLiF₄, and for the first time demonstrated the laser action with both pulsed and CW pumping. Our results show that the spectroscopic and laser properties of Nd:GLF are very similar to those of Nd:YLF, but Nd:GLF offers the possibility of accommodating higher concentration of Nd³⁺ ions. As a result, this new material is very promising.

References:

1. D.R. Lide, ed., CRC Handbook of Chemistry and Physics, CRC Press, Inc., 71th edition, 4-126, 1990-91

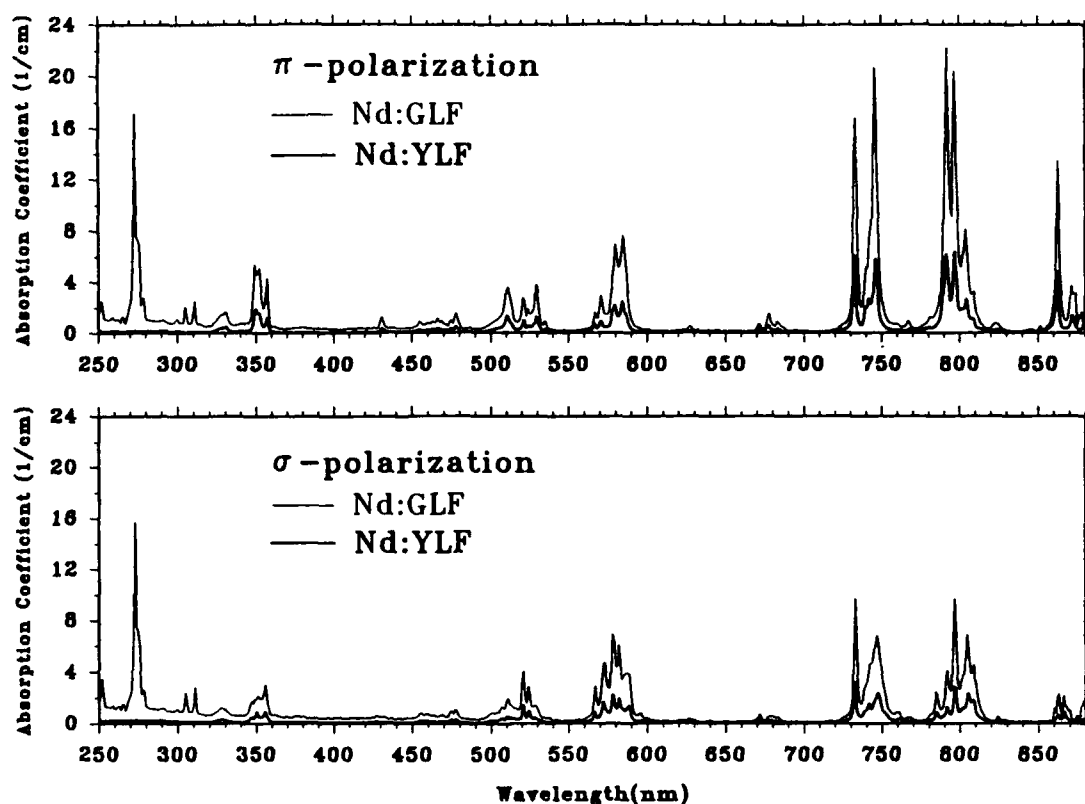


Fig. 1. Polarized absorption spectra of Nd:GdLiF₄ and Nd:YLiF₄ in the optical region at room temperature

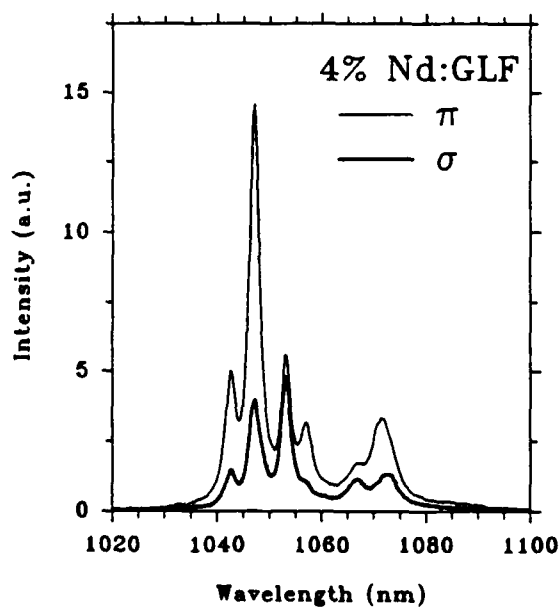


Fig. 2. Polarized emission spectra of Nd:GdLiF₄ in the 1 μ m region at room temperature

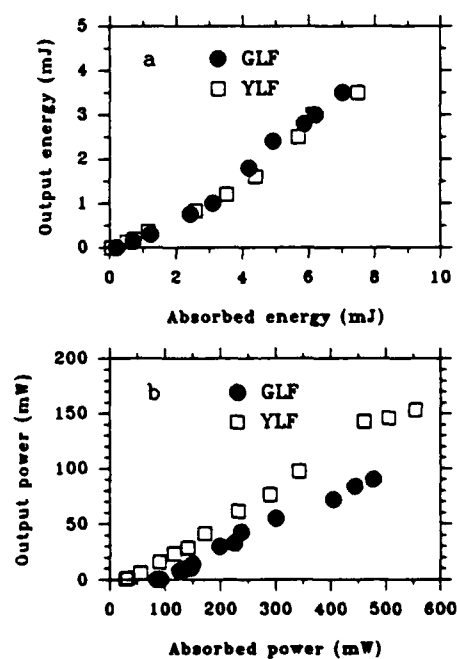


Fig. 3. Laser output as a function of the absorbed energy or power for Nd:GdLiF₄ and Nd:YLiF₄ lasers: a) pulse pumped and b) CW pumped

A frequency-shifted feedback Nd:YLF laser

M.W. Phillips, G.Y. Liang and J.R.M. Barr

Optoelectronics Research Centre, Southampton University, SO9 5NH, U.K.
Tel +44 703 595000

The use of frequency-shifted feedback (FSF) in a laser cavity to obtain cw oscillation with a broadband, modeless frequency spectrum has been investigated in a number of laser materials, including DCM dye [1] and semiconductor diodes [2]. In this scheme, an acousto-optic modulator (AOM) imposes a discrete frequency shift on the intracavity field of the laser on each transit of the cavity. This prevents the evolution of axial modes in the laser spectrum which arise through the constructive interference between light of the same phase and frequency after successive cavity transits. Furthermore, by satisfying a resonant condition between the frequency shift and the cavity roundtrip frequency, pulses have been observed in an FSF Rh6G dye laser [3], with a repetition rate equal to the modulator frequency. It should be emphasised, however, that the pulsed behaviour is not the result of "mode-locking", and the resonant condition for stable pulsing in the FSF laser is much more relaxed than in conventional mode-locked lasers.

The broadband nature of the FSF laser arises from the accumulative effect of regenerative amplification and frequency shifting of broadband spontaneous noise across the gain bandwidth of the laser [4]. If instead, the laser is seeded with a monochromatic source of sufficient power at an appropriate frequency offset from the peak of the effective gain profile, then the seed, rather than the spontaneous noise, will experience regenerative amplification and repeated frequency shifting. This results in the generation of a comb of discrete frequency components in the laser spectrum, the spacing of which is determined purely by the modulator frequency and not the length of the laser cavity. Such seeding has been demonstrated successfully in an FSF DCM dye laser [5], generating multi-frequency emission over a 30 GHz bandwidth.

In this paper, we describe the performance of a Nd:YLF laser incorporating frequency-shifted feedback. To the best of the authors' knowledge, this is the first report characterising the temporal and spectral behaviour of a rare earth doped FSF laser. Since the dynamic behaviour of the FSF laser results from the interplay between gain saturation and active frequency shifting, the relatively long upper state lifetime of the excited Nd ion of 430 μsec (in comparison to a few nanoseconds typically in dye lasers), leads to oscillatory behaviour that has not previously been reported.

The cavity configuration is depicted in Fig. 1. The gain medium was a plane-Brewster Nd:YLF rod cut for 1.047 μm oscillation. This was end-pumped with a cw Ti:sapphire laser operating at 802 nm. The modulator was a Q-switch (Isle Optics model no. QS080) with a broad rf resonance response centred at $\nu_m = 80$ MHz. This was oriented at Bragg angle to frequency upshift the intracavity field. FSF operation was achieved by retroreflecting the first order diffraction beam from the modulator, causing a roundtrip frequency shift of $2\nu_m$. The zeroth order beam provided the main output coupling of the laser, the power in which was optimised for a diffraction efficiency of 55%. The cavity length was 1.87 m, satisfying the cavity resonance condition for an applied rf frequency of $\nu_m = 80$ MHz.

The power performance of the free-running laser is illustrated in Fig. 2. This was obtained for 1.6 W of rf power applied to the AOM at a frequency of 80 MHz. The laser threshold was just 250 mW and the power slope efficiency was 25%. These values are quite respectable for the Nd:YLF laser, despite the poorer power performance predicted for FSF lasers in reference 4. Indeed, the performance of the laser was considerably better than that reported previously in FSF dye lasers and it would be well suited to optical pumping by moderately low power AlGaAs diode lasers.

The temporal output of the free-running laser consisted of a driven relaxation oscillation of varying amplitude depending on the pump power and cavity alignment. By sampling frequency components across the laser spectrum we have observed a delay in the buildup of intensity between the high and low wings of the spectrum during the oscillation spike. This suggests the oscillation was driven by the frequency sweeping action of the modulator across the gain profile. Pulsed output at the cavity roundtrip frequency was also noted when satisfying the cavity resonance condition. However, pulsing was unstable with a typical pulse duration of 2 nsec.

The free-running bandwidth of the laser was 140 GHz. To ascertain the broadband nature of the spectrum, the FSF laser was heterodyned with a single frequency Nd:YLF laser tuned to the centre of the FSF laser spectrum. The resulting rf spectrum showed a broadband background with spikes corresponding to amplitude fluctuations in the FSF laser periodic in the cavity roundtrip time. The broad background component was indicative of modeless operation of the FSF laser.

The single frequency laser was also used to seed the FSF laser. Initially, the FSF laser bandwidth was restricted to 1.9 GHz using an intracavity etalon. The optical spectrum could then be monitored with a 3 GHz scanning confocal interferometer with a resolution of 30 MHz. Fig. 3(a) shows the optical spectrum in the absence of a seed signal for a pump power of 2 W. The broadband nature of the spectrum is clearly observed. On applying 5 μ W of seed signal at a frequency offset of -5 GHz from the laser centre frequency (the modulator being set for frequency upshifting), the broadband spectrum was replaced by a discrete multi-frequency spectrum as shown in Fig. 3(b), indicating successful seeding over this laser bandwidth. By removing the intracavity etalon and monitoring the output through a hierarchy of external etalons, seeding over the entire 140 GHz bandwidth could be observed for a seed signal in excess of 20 μ W.

Seeding the laser also has the benefit of stabilising the laser against relaxation oscillations. As a result, on matching the cavity resonance condition, stable pulsing was observed at twice the modulator drive frequency (160 MHz). The duration of these pulses is determined by the coherence across the frequency comb and hence by the stability of the single frequency seed source. An autocorrelation of these pulses is presently being carried out and the results of this measurement will be discussed at the meeting.

The free-running laser has applications wherever a broadband spectrum is required, for example as a source for optical gyroscopes, or perhaps for the optical cooling of atoms. The frequency comb generated by the injection-seeded laser provides a convenient source for high resolution spectroscopic measurements. Since comb generation in the FSF laser is non-resonant, the frequency spacing is independent of the length of the resonator and may be tuned over the entire resonance bandwidth of the modulator (typically a few tens of megahertz). This is in contrast to the more familiar frequency comb generation in frequency-modulated (FM) lasers, where the resonant nature of the process restricts frequency tuning to just a few tens of kilohertz [6]. A brief description of some of these applications will be presented.

References

1. I.C.M. Littler, S. Balle and K. Bergmann, *J.Opt.Soc.Am.B*, **8**, 1412 (July 1991).
2. P.I. Richter and T.W. Hansch, *Opt.Comm.*, **85**, 414 (October 1991).
3. F.V. Kowalski, S.J. Sattil and P.D. Hale, *Appl.Phys.Lett.*, **53**, 734 (August 1988).
4. I.C.M. Littler and J.H. Eschner, *Opt.Comm.*, **87**, 44 (January 1992).
5. I.C.M. Littler and K. Bergmann, *Opt.Comm.*, **88**, 523 (April 1992).
6. D.W. Hughes, J.R.M. Barr and D.C. Hanna, *Opt.Lett.*, **16**, 147 (February 1991).

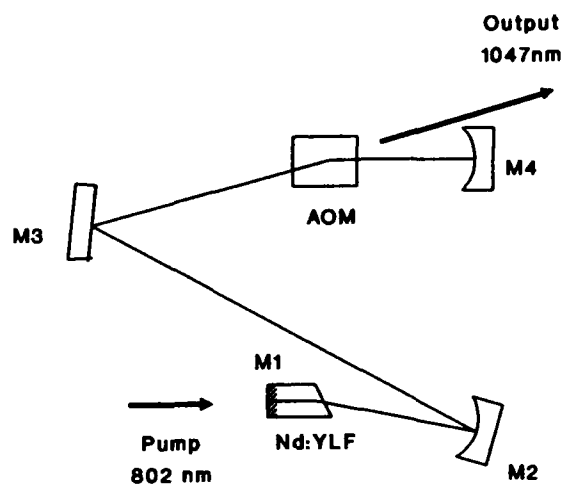


Fig. 1. FSF cavity configuration. M1-M4 are high reflectivity mirrors, AOM is an acousto-optic Q-switch.

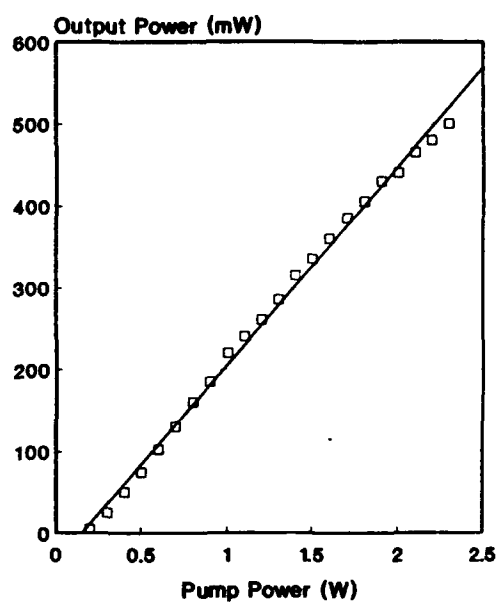
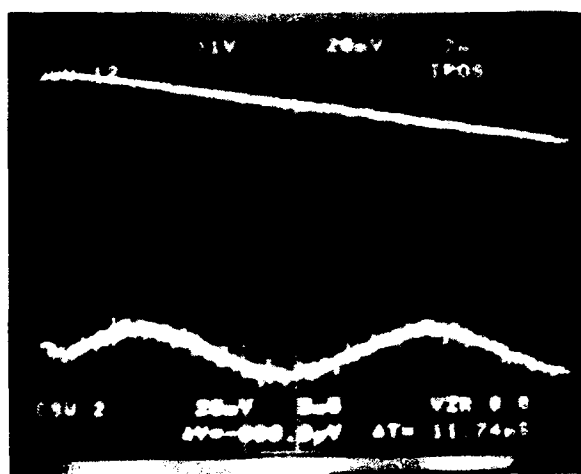
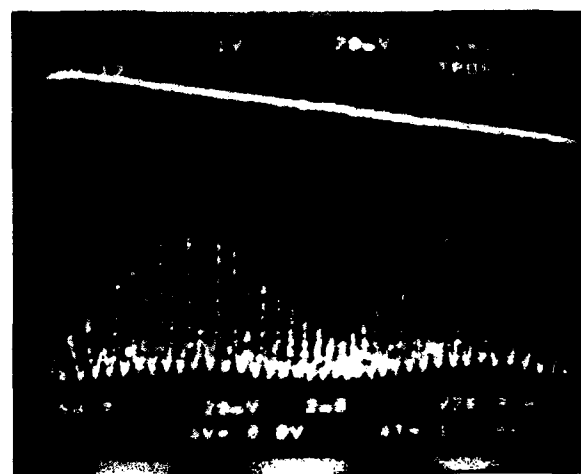


Fig. 2. Power characteristic of the FSF laser.



(a)



(b)

Fig. 3. Optical spectrum of the bandwidth-restricted FSF laser. (a) Free-running operation. (b) Seeded operation. The envelope separation corresponds to the 3 GHz free spectral range of the interferometer.

Determination of the Effective Lower Level Lifetime for Nd:YLF and Nd:YAG Through Experimental Measurement and Computer Modeling

K. Palombo, S. Matthews, S. Sheldrake, D. Capps

*Hughes Aircraft Company, Building E1, Mail Stop B118, P.O. Box 902
El Segundo, California 90245*

Introduction

A lower level lifetime on the order of, or greater than, the extracting laser pulsewidth acts as a bottleneck limiting the maximum extraction efficiency. We have modeled these effects for Nd:YAG and Nd:YLF using a 2 dimensional, phase conjugated double pass amplifier code (DPAC). The amplifier module of this code determines the temporal and spatial inversion or gain based upon a full four level rate equation model. We have also performed experiments which determine the extraction efficiency versus input fluence, and gain recovery versus time, for these two materials and correlated these results with the DPAC model for various effective lower level lifetimes and material parameters. We report values for the effective lower level lifetime of Nd:YLF and Nd:YAG based upon this work.

Measurement of the lower level lifetime is difficult directly because the necessary direct excitation wavelength is infrared and is highly absorbed and the level relaxes nonradiatively. Indirect methods measure the gain recovery time following Q-switching in an oscillator using a weak CW probe laser and correlate these results with a full four level oscillator code (1,2,3) or in an amplifier by similarly measuring the gain recovery following a short saturating pulse with similar correlation to a full four level amplifier code (3,4). A third method is luminescence dumping where a sample is excited in the visible, and a short pulse laser dumps the upper level rapidly. Again by comparison with a model the degree of luminescence dumping is related to the material laser parameters.

Our results differ basically in that our DPAC model incorporates temporal and spatial profiles of the saturating pulse, and distributed spatial gain and loss. Additionally, they differ in that the probe laser is also a short pulse (as opposed to CW laser) spectrally matched to the probed amplifier. We compare two laser materials under near identical experimental conditions and procedures.

The DPAC model used in the work was developed to determine the performance of advanced solid-state lasers. It is used iteratively with a wave optics code to incorporate diffractive effects. It provides for full four level rate equation modelling of laser media including Stark level splitting and occupancy factors of the sublevels, cross relaxation between levels and sublevels and lower level relaxation. Spatial and temporal characteristics of the input and output, as well as spatial characteristics of the gain, are incorporated. Losses can be distributed or lumped.

Gain recovery versus time for Nd:YLF and Nd:YAG was measured in a single pass amplifier configuration. The gain recovery time was investigated by probing the small signal gain remaining in a test amplifier at various times following the traversal of a saturating pulse through the amplifier. A small probe pulse was passed through the test amplifier following the saturating pulse, and its peak amplitude was used to measure the remaining small signal gain in the test amplifier. A comparison of the probe pulse amplitude with the test amplifier on and off provided the measurement of remaining small signal gain in the test amplifier. Extraction efficiency versus input fluence was measured in both materials in the single pass amplifier configuration. Energy stored in the amplifier was determined by a measurement of the small signal gain (g_0). This value was then used in the relationship:

$$E_{\text{stored}} = \ln(g_0) * \text{area} * E_{\text{sat}}$$

where E_{sat} is the material effective saturation parameter. Energy extracted from the amplifier was then measured for various input energies.

Experimental Results

The test setup is shown in Figure 1. For measurement of gain recovery versus time the saturating pulse was provided by a phase-conjugated MOPA, and a second oscillator provided the pulse used to probe the remaining small signal gain in the test amplifier. The probe pulse was directed through the test amplifier at a small angle with respect to the saturating pulse. These two beams could then be spatially separated, allowing the amplitude of the probe pulse to be measured at a high speed photodiode without being swamped by the saturating pulse. Scatter from the saturating pulse reaching the photodiode provided a time reference between the saturating and probe pulses. Q-switching control between the MOPA oscillator and the probe oscillator allowed small signal gain to be probed at the desired times (from 15 to 100 nsec). For measurement of the extraction efficiency versus input fluence a calorimeter was placed behind the test amplifier to measure both input energy and extracted energy.

For correlation with experiments the DPAC model was implemented as a single pass amplifier using the relevant measured experimental parameters (stored energy, effective area, distributed/end losses, gain and pulsewidth). A long-pulse effective saturation fluence (at ambient) of 0.82 J/cm^2 for Nd:YLF and 0.58 J/cm^2 for Nd:YAG was assumed. Input temporal pulse shapes, intensity profiles and stored energy profiles closely matching experimental conditions were used. The time history of the laser rod gain is determined by the DPAC model. These results, along with experimentally determined points, are presented in Figure 2 for Nd:YLF and in Figure 3 for Nd:YAG.

The extraction efficiency versus input fluence was determined using DPAC for various values of effective lower level lifetime. The results are shown for Nd:YLF and Nd:YAG in Figures 4 and 5 respectively, along with corresponding experimental data. For Nd:YLF a 20 nsec lower-level lifetime provides a best match between boht gain recovery and energy extraction efficiency modeling and the experimental data. For Nd:YAG the best match is found at a 5 nsec lower level lifetime.

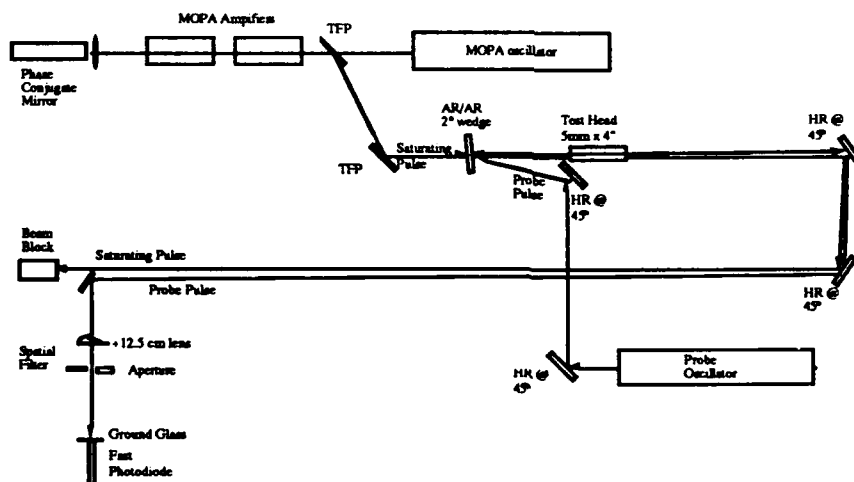


Figure 1. Test setup for measurements in the single pass amplifier configuration.

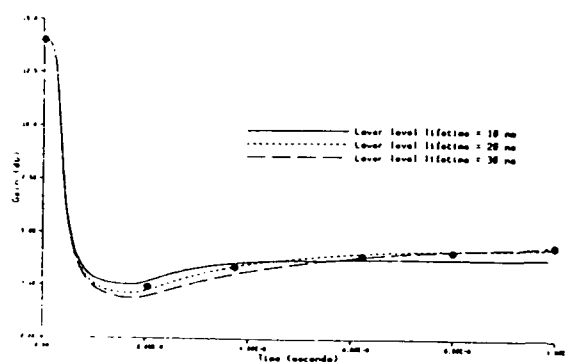


Figure 2 Modeled Nd:YLF gain recovery and experimental results

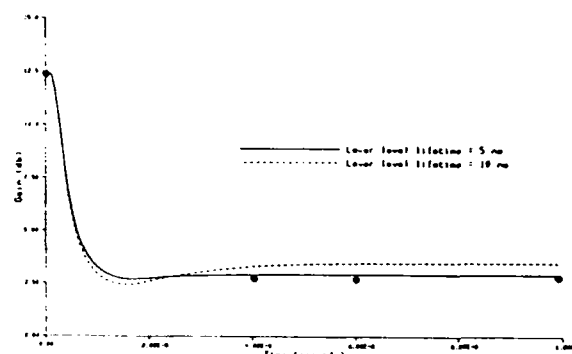


Figure 3. The same information as in previous figure, for Nd:YAG.

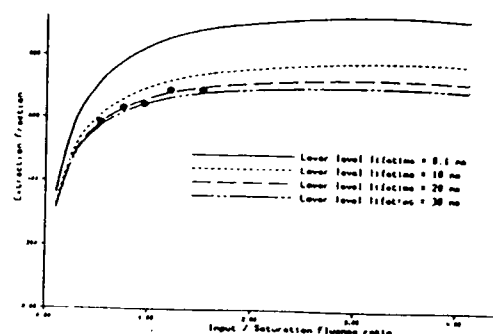


Figure 4 Modeled extraction efficiency versus input fluence for various lifetimes, with experimental results, for Nd:YLF.

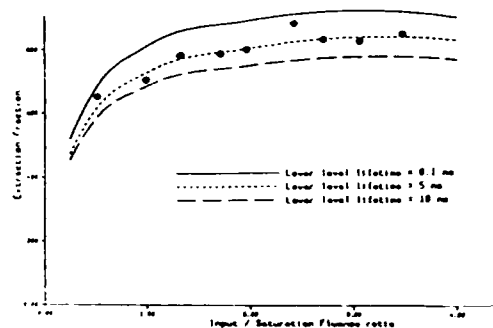


Figure 5. The same information as in previous figure, for Nd:YAG.

Summary

In conclusion, we have determined effective lower level lifetimes of approximately 20 nsec for Nd:YLF and less than or equal to 5 nsec for Nd:YAG using experimental data and computer modeling. In a single pass amplifier configuration comparison of DPAC computer modeling results with experimental data for small signal gain recovery and extraction efficiency indicated these values.

References

1. F.E. Hoxis, M. Stuff, C.J. Kennedy; B. Vivian, "Low-Level Relaxation of Nd:YAG"
2. T. Fan, "Effect of Finite Lower Level Lifetime on Q-switched Lasers", IEEE J. of QE, Vol. 24, No. 12, pages 2345-2349, Dec. 1988.
3. R. Utano, G. Perresini, Private Communication.
4. V. Inanov, Y. Senatskii, G. Sklizko, "Influence of Nonradiative Relaxation of the Levels of an Active Transition of Nd³⁺ Ions in Glass on the Amplification of High Power Nanosecond Pulses.", Sov. J. of QE, Vol. 16, No. 3, pages 422-424, March 1986.
5. V. Inanov, Y. Senatskii, G. Sklizko, "Numerical Modulation of the Dynamics of Inversion Dumping and of Amplification of Nanosecond Pulses in Neodymium Glass", Sov. J of QE, Vol. 17, No.2, pages 184-190, Feb, 1987.

Direct Measurements of the Terminal-Level Lifetime
for Nd³⁺-Doped Laser Materials

C. Bibeau, S. A. Payne, and H. T. Powell
University of California
Lawrence Livermore National Laboratory
P.O. Box 5508
Livermore, CA 94550
510-422-7798

Numerous investigations of nonradiative transitions in neodymium-doped laser glass and crystalline media have been made over the last three decades. A direct determination of the terminal-level lifetime for the $^4I_{11/2} \rightarrow ^4I_{9/2}$ transition has been particularly arduous due to the difficulty in generating the infrared wavelengths and short pulse lengths necessary to probe the lower levels. The Nd terminal-level lifetime is nevertheless an important optical parameter for the design and performance specifications of many pulsed laser systems. The value of the terminal lifetime relative to the laser pulsewidth determines whether the laser will operate as a three or four level system. For the condition of the terminal lifetime being greater than that of the pulsewidth, the metastable neodymium population will be bottlenecked, and the saturation fluence, and thus extraction efficiency, will be lower than expected. In this abstract we describe a method to directly measure the $^4I_{11/2}$ lifetime for neodymium in a variety of host media.

The pump and probe technique is shown in Figure 1. A 2.41 μm beam will pump population from the $^4I_{9/2}$ ground state to the $^4I_{13/2}$ level. A weak 1.06 μm beam, delayed with respect to the pump beam, will then probe the population at the $^4I_{11/2}$ level by exciting a fraction of those ions to the $^4F_{3/2}$ level. The excited ions will subsequently emit radiation at 0.88 μm with a signal strength that is proportional to the population residing at the terminal level. So, as the population at the $^4I_{11/2}$ terminal level drains into the ground state, the 0.88 μm emission should decrease and a temporal history of the terminal-level population will evolve. As also shown in Figure 1, for some materials there exists the possibility of a second resonance condition that would add an additional contribution to the temporal profile. The resulting profile would then be an overlap of the $^4I_{13/2}$ and $^4I_{11/2}$ lifetimes. Through theoretical calculations, the overlap can be unfolded and the terminal-level lifetime resolved.

The experimental scheme is shown in Figure 2. A high pressure Raman cell filled with diatomic hydrogen gas is used to generate the 1.91 μm (Stokes shifted) light. The 1.91 μm light and the 1.06 μm amplified output of a Nd:YAG oscillator is combined in a

mixing crystal to produce $2.41\text{ }\mu\text{m}$ (4155 cm^{-1}) radiation. The sample is then pumped with the $2.41\text{ }\mu\text{m}$ pulse and probed with the $1.06\text{ }\mu\text{m}$ pulse while the $0.88\text{ }\mu\text{m}$ emission is recorded as a function of the time delay between pulses. The pulse lengths are approximately 100 ps at the FWHM.

The data for a phosphate glass sample with 1% neodymium doping is shown in Figure 3. We measured the terminal lifetime to be $\sim 500\text{ ps}$ with an error of 300 ps. Further modeling and improved experimental conditions are expected to enhance the accuracy of this result in the near future. We find that this is in agreement with two independent theoretical calculations. One calculation, in which the reduced saturation fluence is fitted to several extraction efficiency data, predicts a terminal-level lifetime of $\sim 674\text{ ps}$.¹ An independent formulation which describes the exponential dependence of the transition rate on energy gap to the next lowest level predicts a lifetime of $\sim 1\text{ ns}$ for a $\sim 1700\text{ cm}^{-1}$ energy gap.² We have also made measurements for LG-660, a silicate glass with results that yield a lifetime of $>1.5 \pm .6\text{ ns}$. These experiments will be extended to include numerous hosts such as oxide, fluoride and vanadate crystals, and phosphate, silicate and fluoride glasses.

In summary, we have made direct measurements of the population decrease in the $^4\text{I}_{13/2}$ and $^4\text{I}_{11/2}$ levels of several neodymium doped hosts.

References

1. J. B. Trenholme, private communication
2. C. B. Layne, W. H. Lowdermilk, M. J. Weber, IEEE J. Quantum Electron. **11**, 798 (1975).

This work was performed under the auspices of the U.S. Department of Energy, Office of Basic Energy Sciences, Division of Materials Sciences, by Lawrence Livermore National Laboratory under Contract No. W-7405-ENG-48.

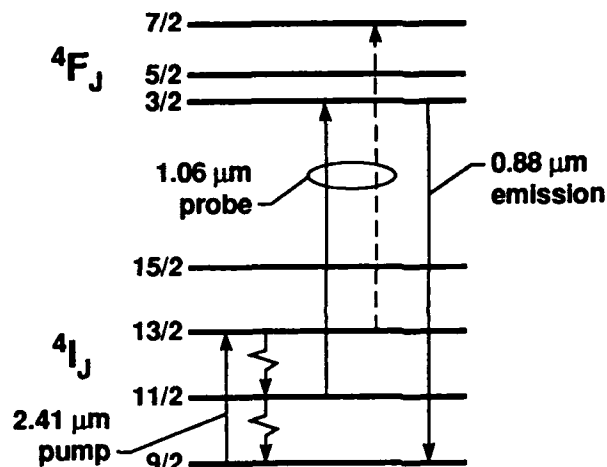


Figure 1. Nd^{3+} energy levels along with pump, probe, and emission transitions.

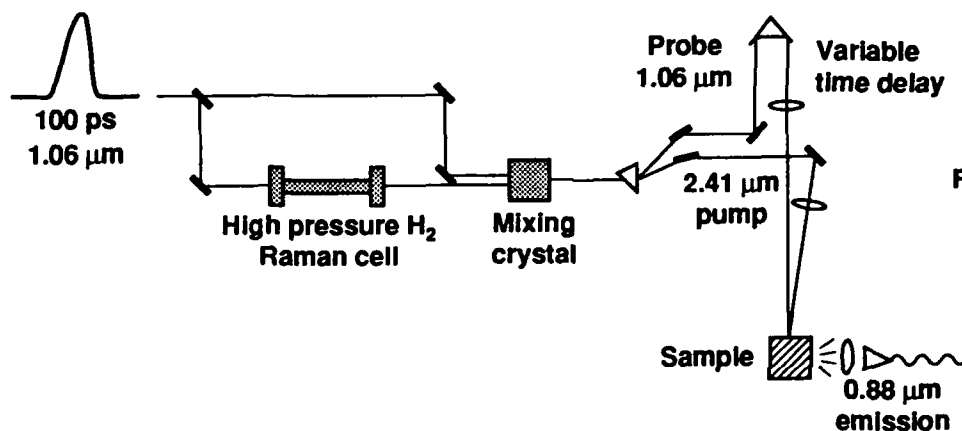


Figure 2. Experimental scheme.

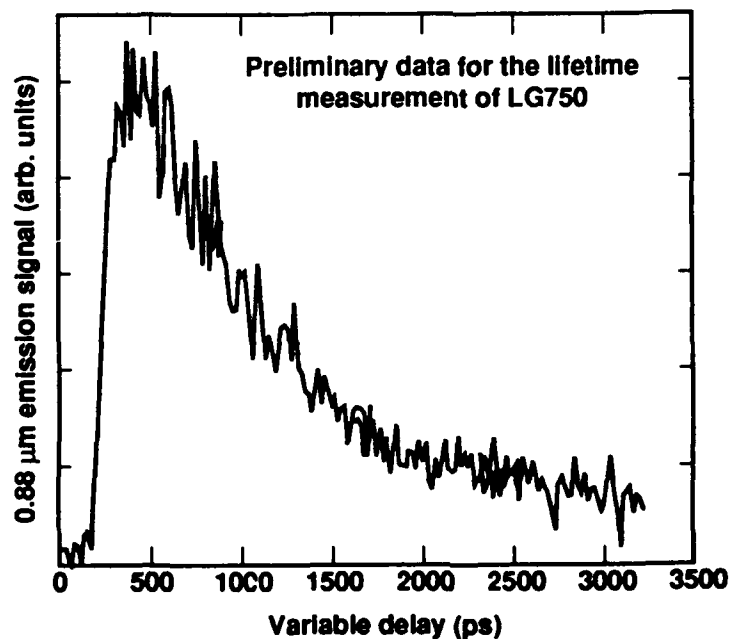


Figure 3. $0.88 \mu\text{m}$ emission as a function of time delay between the pump and probe pulse.

EFFICIENT SURFACE EMITTING LASER DIODES MATRICES SIDE-PUMPED Nd:YAG SLAB

C. LARAT, M. SCHWARZ, G. FEUGNET, J.P. POCHOLLE
Thomson-CSF, Laboratoire Central de Recherche, Domaine de Corbeville,
F-91404 ORSAY, FRANCE.
Tel. : 33 1 60197000 ; Fax : 33 1 60197416.

Optical pumping of Nd:YAG by laser diodes (single laser diode, arrays or bar-stacks) has already been demonstrated in various experiments. We report the use of new high power Surface Emitting Laser Diodes (SELDs) matrices to achieve Nd:YAG slab optical pumping [1]. The SELD is a promising monolithic alternative to the stacking of diode arrays in order to get high pump power density [2,3].

The SELD's basic structure uses cleaved laser facets and 45° angle etched mirrors to reflect the output laser beam normally to the epitaxial plane. A duplication of this basic structure in the two directions of this plane result in a monolithic 2D laser diode matrix. Four $3.0 \times 3.4 \text{ mm}^2$ SELDs (120 laser diodes each) were used in our experiments. The 808 nm emission wavelength is achieved with a 25°C temperature operation and the spectral width is about 4.5 nm. With an 100 A current control and a repetition rate of 100 Hz, one SELD delivers 7 mJ energy per pulse (35 W peak power, 200 μs long). The optical divergence of the beam is about 20° (full width at half maximum) in each direction. A small concavity of the integrated reflecting mirrors induces the reduction of the usually observed large divergence (50°) in the direction perpendicular to the epitaxial plane. A more complete technical description of the SELD and up-to-date results shall be found in reference [4].

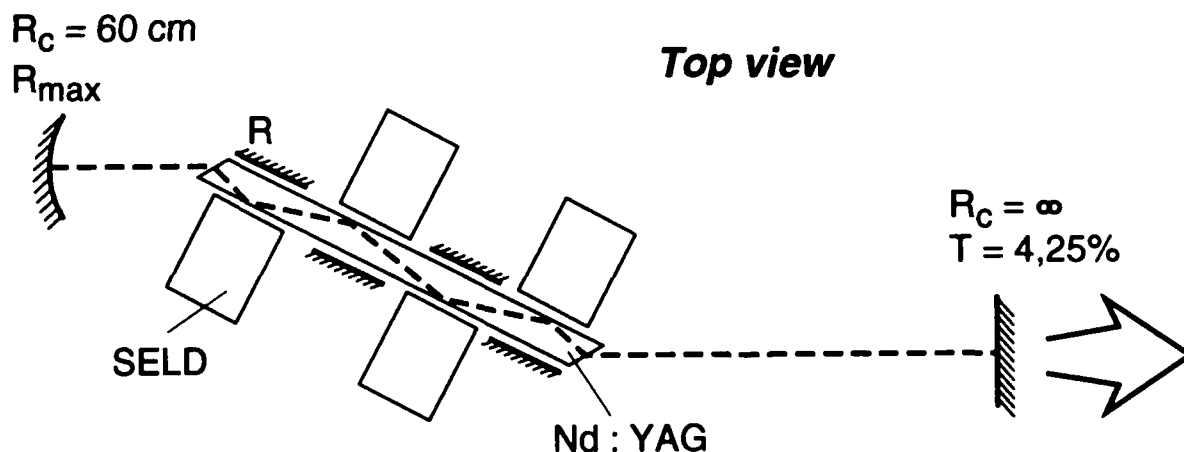
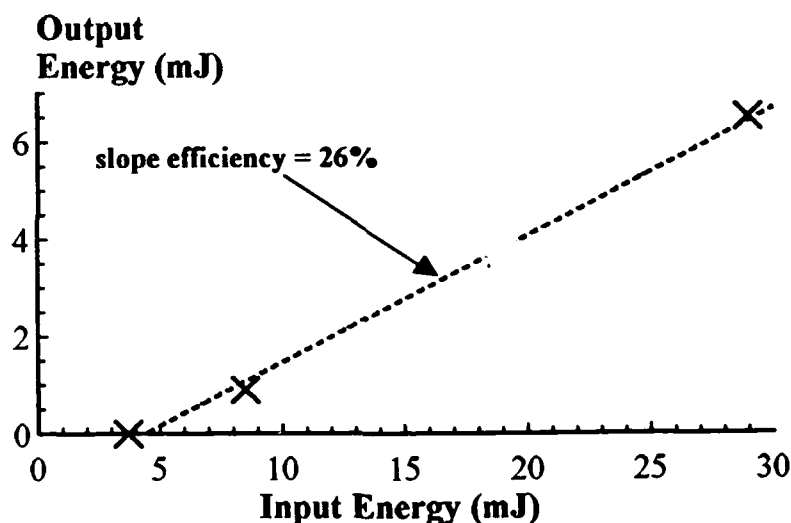


Figure 1: Laser cavity layout (not to scale).

Figure 1 shows the cavity lay out. The gain medium is a Brewster cut Nd:YAG zigzag slab (2 mm thick). The SELD are located in front of each total internal reflection in the slab. No additional optical coupling element is used. The SELD to slab distance is as short as possible (about 1.5 mm). The single pass absorption of the pumping beam is about 40%, corrections from the 8% Fresnel reflection on each face included. The unabsorbed pump power of each SELD is re injected in the Nd:YAG by reflectors (R) placed on the opposite side of the pumped surface.

The optical cavity is a stable planoconcave resonator. Total intracavity losses of 5% are estimated by the determination of the laser threshold for various output coupler. Free running results are reported in figure 2. The repetition rate is 30 Hz and the output pulse width is 150 μ s long. As the repetition rate increases up to 100 Hz, the output energy level decreases of about 5%. This reduction is mainly due to both a little decrease of the pumping energy level and a broadening of its spectral width.



*Figure 2: Output energy versus incident energy in free running mode.
Output coupler : $T = 4.25\%$. ROC = 60 cm. Cavity length = 14 cm.*

The best results in Q-switch mode are obtained with a double pass cavity (figure 3) which reduces the width of the highly multimode transverse emission in the vertical direction. In that configuration, the laser delivers 3 mJ in the free running mode (acousto-optic cell included) and 60 kW peak power in Q-switch mode (figure 4).

We have demonstrated the laser action of Nd:YAG zigzag slab pumped by a high power monolithic Surface Emitting Laser diodes. Laser performances were explored both in free running mode and in Q-switch mode. These results might be improved by matching the SELD emitting area geometry and the laser mode.

The authors wish to thank C. Carrière, B. Groussin and A. Parent from Thomson Hybrides for providing the SELDs. The development of the SELD was supported by the DRET (Direction des Recherches, Etudes et Techniques), the MRE (Ministère de la Recherche et de l'Espace) and the Thomson-CSF group.

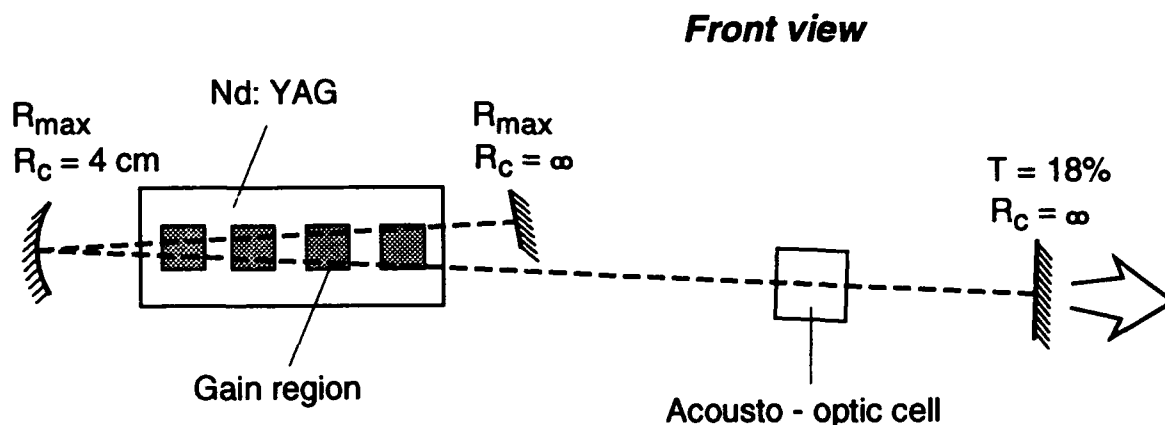


Figure 3 : laser cavity layout for *Q*-switch operation (not to scale).

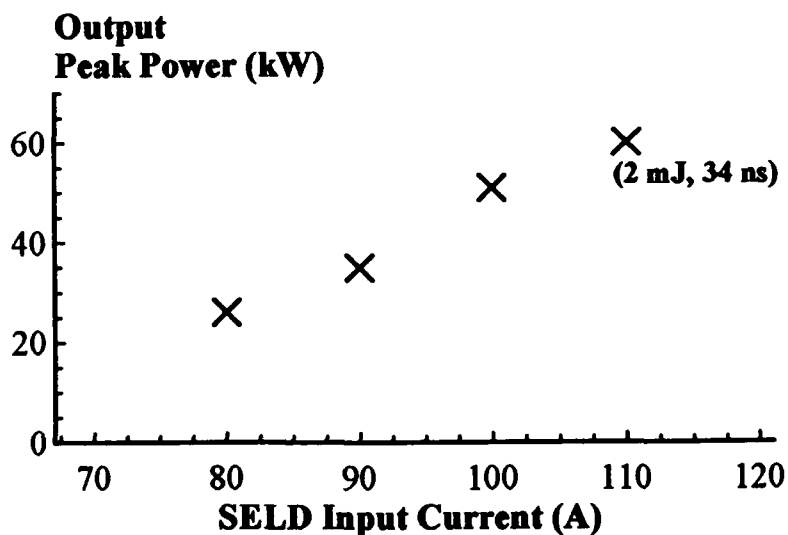


Figure 4 : Peak power versus SELD input current in a *Q*-switch mode.

Output coupler : $T = 18\%$. $ROC = 4\text{ m}$. Total cavity length = 30 cm.

- [1] C. Larat, M. Schwarz, J. P. Pocholle, "High power surface emitting laser diode pumping of Nd:YAG slab", *Electron. Lett.* (1992) 28 pp. 1630-1631.
- [2] Z. L. Liau, J. N. Walpole, "Surface-emitting GaInAsP/InP laser with low threshold current and high efficiency", *Appl. Phys. Lett.* (1985) 46 pp. 115-117.
- [3] S. S. Ou, M. Jansen, J. J. Yang, L. J. Mawst, T. J. Roth, "High power CW operation of InGaAs/GaAs surface-emitting lasers with 45° intracavity micro-mirrors", *Appl. Phys. Lett.* (1991) 59 pp. 2085-2087.
- [4] B. Groussin, C. Carrière, A. Parent, ... to be published in *Electronics Letters*.

Monday, February 1, 1993

Novel Laser Technology

AMD 1:30pm–3:00pm
La Salle Ballroom B&C

Evgenii V. Zharikov, *Presider*
Russian Academy of Science, Russian Federation

Modeling of High Power End-pumped Solid-State Lasers.

Thomas M. Baer and Mark S. Keirstead
 Spectra-Physics Laser Diode Systems, Inc.
 1250 Charleston Rd.
 Mountain View, CA 94043
 (415) 961 9100

Longitudinally pumped geometries have proven to be the optimal design for low to medium power (0.01 W to 1 W) TEM₀₀, diode-pumped, solid-state lasers. Scaling to higher pump levels is thought to be hindered by the presence of significant thermal gradients in the active medium giving rise to phase aberration of the resonator eigenmode. Initial experimental results appeared to support this conclusion in diode-pumped Nd:YAG lasers. [1,2] In this paper we describe experimental results and theoretical models of high power, end-pumped, Nd:YLF and Nd:YVO₄ lasers which include the effects of thermally induced aberrations of the eigenmode. The model is in good agreement with experiment, predicting highly efficient fundamental mode operation with close to diffraction limited performance ($M^2 < 1.1$).

In order to calculate the eigenmode of a resonator including phase aberrating elements a numerical approach is necessary since analytical solutions for these types of resonators do not currently exist. We have chosen to use a full two dimensional diffraction algorithm employing Fast Fourier Transform propagation techniques. The laser mode is represented as a two dimensional complex field which is propagated through multiple round trips within the resonator. The effects of mirrors, apertures, mode-matched gain and saturation, and thermally induced phase aberrations are all included as amplitude or phase operators acting on the field matrix at appropriate positions within the laser resonator. After propagating the field matrix 50 to 100 round trips through the laser resonator the spatial structure and energy no longer changes and the field matrix becomes an accurate approximation to the eigenmode of the resonator.

The accuracy of a numerical solution for the eigenmode depends critically on the model describing the pump induced aberration. Several analytical models for the aberrations have been discussed previously. [2,3] In contrast, we have chosen to measure the aberration directly using interferometric techniques. The active medium is placed in one arm of an interferometer and is end-pumped just as it would be in the laser system. A HeNe probe beam double passes through the pumped region of the active medium and experiences the same phase aberrations as the laser eigenmode. An unaberrated portion of the probe interferes with the aberrated beam and creates a fringe pattern on a vidicon camera. The resulting fringe pattern is analyzed using standard fringe capture and analysis techniques and the phase front of the aberrated probe beam is computed. The measured phase front is least squares fit to a 15 term Zernicke polynomial. The Zernicke series includes terms representing the focusing power, spherical aberration, astigmatism, coma and higher order phase terms contained in the thermal aberration. The phase aberration effecting the laser eigenmode is

calculated by multiplying the Zernicke polynomial coefficients by an appropriate wavelength scaling factor. The resulting phase operator is a radially dependent phase multiplier that operates on the field matrix once per resonator round trip, thus modeling the effect of the thermal aberration.

In general there are two components to the measured thermal phase aberrations: distortions in the surface of the active medium and index variation due to temperature gradients. Using the interferometer described above we can measure directly the distortion of the surface of the active medium and separate these effects. In transversely pumped systems the surface distortion effects are usually small enough to be ignored. However, in end-pumped Nd:YLF and Nd:YVO₄ we measure these effects to be roughly the same size as the temperature-gradient-induced index of refraction variations! (The analytical models in references 2 and 3 do not include these surface effects and are more appropriate for Nd:YAG systems where the surface distortion is negligible.) We want to stress that our approach, actually measuring the phase aberrations, includes both surface and index aberrations, since the interferometer measures the total phase change on the probe beam.

Figures 1 and 2 contain plots of the equiphase surfaces of the interferometer probe beam for both Nd:YVO₄ and Nd:YLF pumped at approximately 9 W of incident power from a diode bar coupled to a fiber bundle. [4] The diameter of the pump volume in the active medium is approximately 0.6 mm. The thermal aberration in Nd:YVO₄ is an order of magnitude greater than Nd:YLF. The thermal aberrations in both media cannot be represented accurately by a simple lens or even a spherically aberrated lens. Mode-matched pumping causes significant radial variations in temperature of the active medium creating high order radial phase aberrations which require including at least 15 terms in a Zernicke series or, in other words, phase variations varying up to the sixth power in radius.

Figure 3 contains a plot of the mode radius versus position for the Nd:YLF and Nd:YVO₄ lasers and a comparison with the results of the numerical calculation described above. The theory is in very good agreement with the experiment. The theoretical model predicts an M^2 of less than 1.1 for both of these laser systems and this is confirmed by our experimental results. The TEM₀₀ slope efficiency for these lasers systems at high pump levels is 45%, close to that observed at low pump powers, indicating that thermal aberrations do not appear to limit TEM₀₀ power extraction. In both cases the numerical results accurately predict the measured mode parameters. In spite of the presence of a large thermal aberration in Nd:YVO₄ (which includes significant spherical aberration and higher order aberration terms) the fundamental mode has a smooth Gaussian profile and an excellent M^2 .

The results of the model and the supporting experiments indicate that phase aberrations induced by mode-matched pumping do not appear to limit the TEM₀₀ power. The ultimate limit to scaling these end-pumped systems appears to be determined by either the stability range of the resonator (which can be limited by the added focusing power of the thermal aberration) or the fracture limit of the active medium.

References:

1. S. C. Tidwell, Jonathan F. Seamans, and Dennis D. Lowenthal, High-Average-Power End-Pumped Nd:YAG Laser Development, OSA Proceedings on Advanced Solid-State Lasers, Lloyd L. Chase and Albert A. Pinto, eds. (Optical Society of America, Washington, D.C. 1992), Vol 13, pp 178-181.
2. J. Frauchiger, P. Albers, and H.P. Weber, Modeling of Thermal Lensing and Higher Order Ring Mode Oscillation in End-Pumped Solid-State Lasers, IEEE J. Quantum Electron., vol QE-28, p. 1046 (1992).
3. A.K. Cousins, Temperature and Thermal Stress in Finite-Length, End-pumped Laser Rods, IEEE J. Quantum Electron., vol QE-28, p. 1057 (1992).
4. Thomas M. Baer and Mark S. Keirstead, 10 W TEM₀₀ output from a diode-pumped, solid-state laser, in Conference on Lasers and Electro-optics, 1991 (Optical Society of America, Washington, D.C.) p. 490.

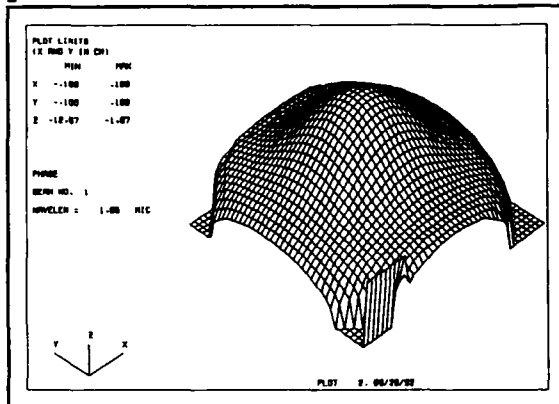


Figure 1. Phase aberration in Nd:YVO₄ due to index and surface variations. Note that the peak to valley phase variation is about 12 rad.

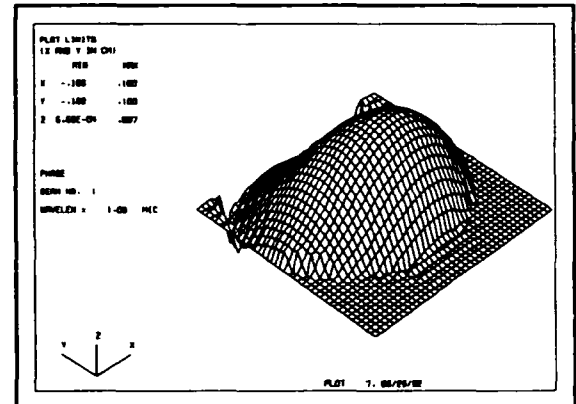


Figure 2. Phase aberration in Nd:YLF. Note that the peak to valley variation in phase is less than 0.7 rad, an order of magnitude smaller than Nd:YVO₄.

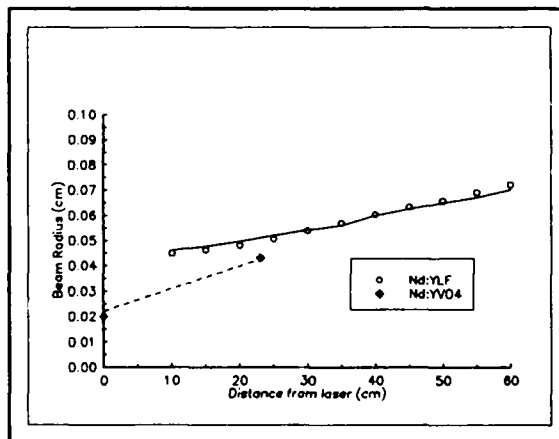


Figure 3. Mode radius versus distance from the laser. Solid and dotted lines are results of numerical model.

PROPAGATION EFFECTS IN VARIABLE REFLECTIVITY RESONATORS

E. Mottay, E. Durand and E. Audouard

B.M. Industries
7 rue du Bois Chaland
CE 2901 LISSES
91029 EVRY Cedex - FRANCE

The generation of high energy, diffraction limited laser beams from solid-state laser is of primary interest to the scientific community. Such lasers are suitable for injection seeding, therefore offering single transverse and longitudinal mode emission. They are for instance particularly adapted to the pumping of Optical Parametric Oscillators. An early approach for achieving this goal was the use of unstable resonators, which provided high energy, diffraction limited laser emission. However, the hard-edged output couplers traditionally used strongly affects the spatial intensity profile of the laser beam. The development of output couplers with a variable reflectivity profile has greatly improved the spatial repartition of the beam, since they avoid shadowing and diffraction caused by the hard-edged output coupler. However, residual diffraction effects can still lead to serious intensity modulations during propagation. Diffraction of the laser beam through the active medium (usually crystalline rod) is especially important on this regard.

We have developed a numerical model based on the Beam Propagation Method. This model takes into account diffraction effects, thermal lensing in the active medium, gain saturation and depletion of the stored energy. It is used to predict the actual size and profile of the emitted beam at different distances of propagation. We applied this model to three resonators, using different variable reflectivity output couplers.

The configuration of each resonator is described in figure 1. It consists of a high reflectivity concave mirror M1, a variable reflectivity output coupler M2 (National Optics Institute, Québec). The pumping head PH (model TY-714 from B.M. Industries) consists of a YAG rod, diameter 7 mm and length 100 mm, pumped by one linear flashlamp in a diffuse cavity. The electrical pump energy is 20 J, and the repetition rate is 10 Hz. The oscillator is Q-switched by an electro-optic Q-switch, consisting of a Pockels cell PC, a quarter-wave plate WP and a Glan-Taylor polarizer GP. The resonator length is 50 cm. The reflectivity profile of the output coupler is defined by :

$$R(r) = R_0 \exp\left(-\frac{2r^2}{\omega_m^2}\right)$$

The output beam profile depends on three parameters, which are summed up in the following table. They are the peak reflectivity R_0 of the variable reflectivity output coupler, the order n of the reflectivity profile and the filling ratio f , defined as the ratio between the beam size in the Nd:YAG rod and the rod diameter :

$$f = \frac{2\omega_0}{d} = \frac{\omega_m}{d} \sqrt{M^2 - 1}$$

where M is the geometrical magnification of the resonator.

Resonator	R_0	f	n
resonator # 1	0.11	0.28	3
resonator # 2	0.23	0.45	3
resonator # 3	0.20	0.45	2

The beam intensity profiles are measured with a CCD camera coupled to a beam analysing system (Excitech model PROF256). In order to realize a true near-field measurement, the output of the laser is imaged onto the surface of the camera with a magnification of 1/2. Intermediate field measurement are realized after a converging lens, and far field measurement are realized at the focus of a converging lens, with a 4 meter focal length. In order to provide data for the computer model, the small signal gain of the pumping head has been determined by probing the pumped YAG rod with the low intensity beam from a CW diode-pumped laser. The thermal lensing has been measured by sending an expanded collimated HeNe beam into the YAG rod with different thermal loads, and extrapolating the data to the low average power where the oscillator is operated. Figure 2 shows the calculated and measured near-field profiles for the three different output couplers. The agreement with the numerical model is very good, qualitatively and quantitatively. The dip at the center of the profiles associated to resonator #2 and resonator #3 is due to the high value of the reflexion coefficient. Figure 3 shows the calculated and measured far-field profiles. Here again, the agreement with the numerical model is very good. These results demonstrate the high beam quality achievable with variable reflectivity resonators. The beam divergence is close to 0.35 mrad (full energy, full angle) which indicates quasi-diffraction limited beams.

A important feature of variable reflectivity resonators is the beam profile in the intermediate field, i.e. after a the beam has propagated for a few meters in the free space. This analysis has generally been overlooked, although it points out critical parameters for the design of variable reflectivity resonators. Figure 4 shows the intermediate field beam profiles for the three different resonators compared here. These profiles have been recorded after a converging lens, in order to simulate propagation at different distances. The results presented here correspond to a free space propagation of about three meters. They are in good agreement with the numerical simulations. These profiles underline the importance of residual diffraction effects in variable reflectivity resonators. The crystalline cylindrical Nd:YAG rod is the primary source for these residual diffraction effects. Even a small truncature of the intra-cavity gaussian beam by the rod edges can cause intensity modulations in the intermediate field. Two important effects are noticeable in the results presented in figure 4. The first intensity profile exhibits no high frequency modulations; this profile corresponds to the resonator with the smallest filling ratio, defined as the ratio between the beam size in the near field and the Nd:YAG rod diameter. Secondly, one can see that the intensity profile associated to the gaussian mirror (resonator #3) is far more modulated than the profile associated to the supergaussian mirror (resonator #2). This is due to the fact that a gaussian profile has a longer "tail" than a supergaussian profile, and therefore diffraction effects in the YAG rod are more pronounced. The previous results points out the fact that a smooth profile in the near and far fields is fairly easy to achieve. However, for intermediate field profiles, which are the most commonly used in practical situation, there is a trade-off in the design of the resonator between the output energy, which requires large mode volume to be maximized, and smoothness of the beam profile, which requires small mode volume to avoid diffraction sharp in the YAG rod. On this regard, supergaussian profiles are to be preferred, because of their sharp drop in reflectivity.

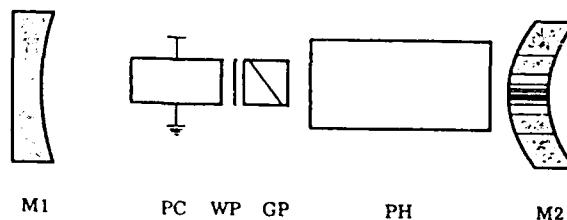


Fig. 1. Variable-reflectivity resonator layout

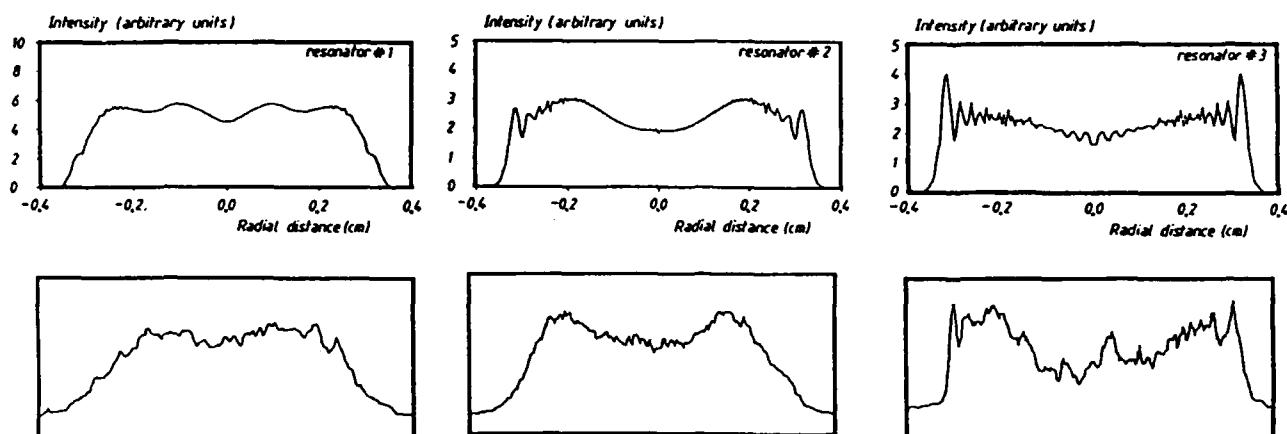


Fig. 2. Near-field calculated (upper graphs) and measured (lower graphs) intensity profiles.

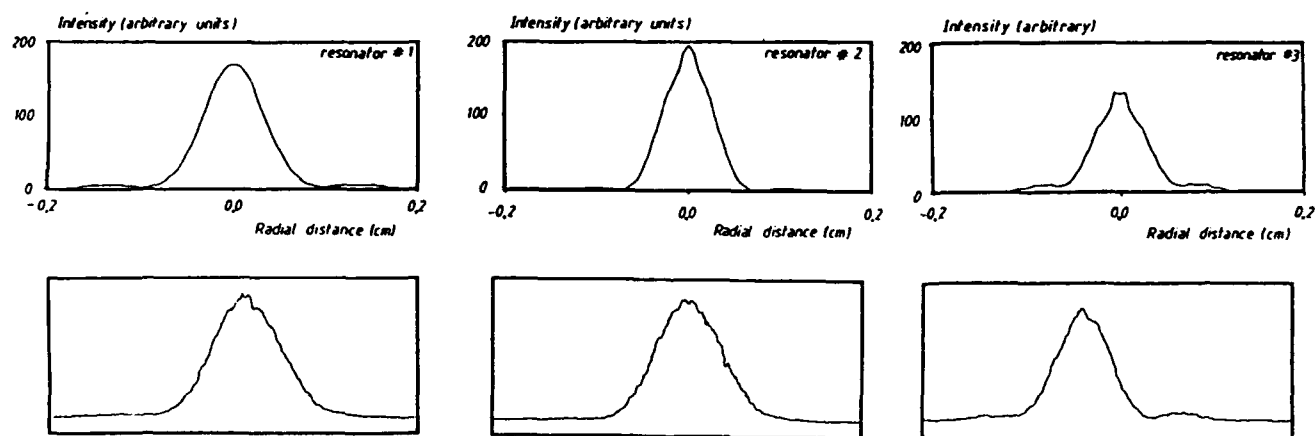


Fig. 3. Far-field calculated (upper graphs) and measured (lower graphs) intensity profiles.

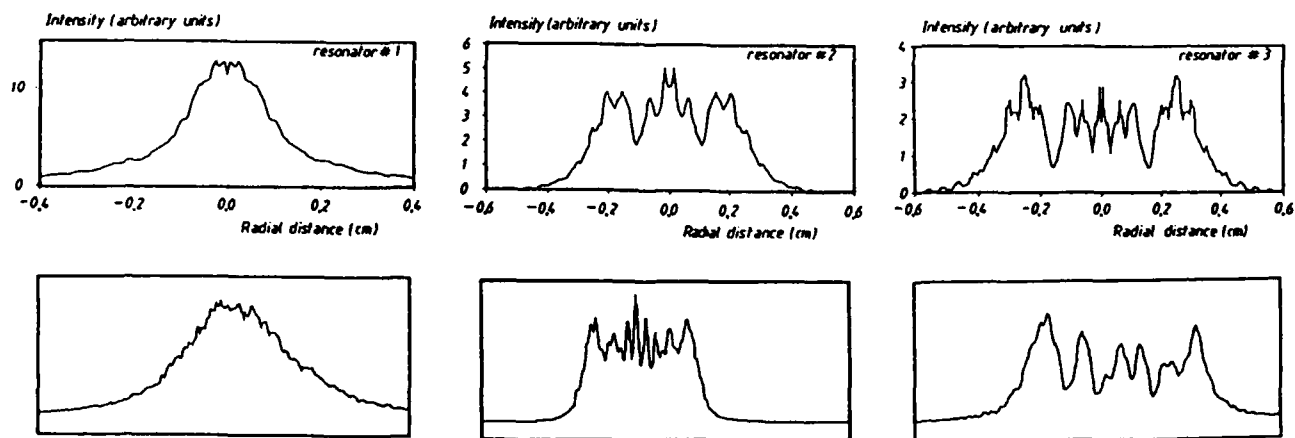


Fig. 4. Intermediate-field calculated (upper graphs) and measured (lower graphs) intensity profiles.

Power Scaling and Wavelength Conversion of CW Diode-Pumped Lasers

Larry R. Marshall, Alex Kaz, and Horatio R. Verdun
Fibertek, Inc. 510 Herndon Pky., Herndon VA, 22070.

End pumping has long been regarded the most efficient means of pumping solid state lasers. High gain is essential for efficient CW and Q-switched laser operation, and this is achieved in end pumping by tightly focusing the diode pump light. Power scaling of end pumped devices is limited by two factors. Firstly, higher-wattage pump powers can only be obtained from distributed diode sources such as fibre-coupled or linear arrays. This necessarily enlarges the minimum spot size to which the output of the array can be focused and reduces the confocal length; thus decreasing gain. Secondly, thermal stresses induce lensing and birefringence which reduce beam quality (and even destroy the crystal). At high pump power densities, we have found that upconversion (where the population is depleted from the upper laser level) poses a third limitation, by reducing the gain. Side pumping, on the other hand, can be scaled without the latter limitations because the pump energy can be distributed over a larger volume for the same mode size, but at the cost of reduced efficiency. The goal of this work was to simultaneously achieve efficient TEM₀₀ power scaling, high gain, and short-pulse Q-switched operation; thus bringing CW lasers into the same arena as pulsed lasers, for pumping non-linear optical processes for wavelength conversion.

We report here, novel end-pumping configurations producing up to 3.3 W of linearly polarised TEM₀₀ output, with an electrical efficiency of 7.3 %. In contrast, new side-pumping geometries produce up to 6 W of linearly polarised TEM₀₀ output, with an electrical efficiency of 6.8 %; only slightly lower than for end pumping. We are currently scaling the side-pumped device, by the addition of a second gain module which should raise the TEM₀₀ power above the 10 W level.

The end-pumped laser configuration is shown in figure 1. The gain medium is a trapezoid of Nd:YLF, with the focused diode output passing through its back surface. The gain medium acts as an intracavity mirror, so that the laser beam is reflected off its back surface, thus matching the cavity mode to the gain volume.

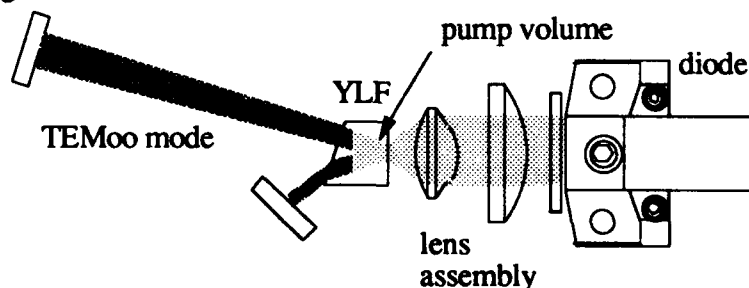


Figure 1 : End pumped laser configuration.

Various crystal-axis orientations were investigated, to maximise gain and minimise thermal

lensing. In the optimum orientation, the laser produced 4.1 W of multimode output and 3.3 W of TEM₀₀ output, at 1047 nm, for 16.2 W of pump power. Although the TEM₀₀ output was elliptical, the axes diverged at 1.05 ± 0.05 (major) and 1.1 ± 0.05 (minor) times the diffraction limit. At this pump power, the thermal lensing was astigmatic, with focal lengths of - 0.8 m in the c-plane and + 2.15 m in the a-plane (for c-polarised light). This astigmatism in lensing is a serious limitation to power scaling of end-pumped, TEM₀₀, Nd:YLF lasers (and explains the ellipticity). Furthermore, the large spot size needed to match the focused diode output gives a rather low single-pass gain, of 7 %. Upconversion effects became noticeable at pump powers exceeding 5 W, and for the maximum pump power of 16.2 W, caused severe thermal distortion and gain reduction. Upconversion losses scale with excited-state population, and so are especially degrading to repetitive Q-switching, where they deplete the population inversion stored during the Q-spoiled cycle. We observed up to 50% reduction in Q-switched power, as a result of this effect.

The side-pumped laser configuration is shown in figure 2. When pumped at 16.5 W, this device produced 4.5 W of multimode output and 3.1 W of TEM₀₀ output. Thermal lensing was also astigmatic for this pump geometry, with focal lengths of - 1.6 m (c-plane) and + 2.5 m (a-plane), which is significantly less than was observed for end pumping. The electrical efficiency for TEM₀₀ operation was 6.8 %. When the pump power was increased to 28 W by multiplexing two diode outputs, 8.5 W of multimode and 6 W of TEM₀₀ output were obtained at 1047 nm in linear polarisation. The divergence of the TEM₀₀ output was 1.1 ± 0.05 times the diffraction limit. We also demonstrated 6 W of polarised TEM₀₀ output, by placing a second 15 mm length of Nd:YLF in the cavity and pumping it with a separate 15 W diode array. Thus power scaling is relatively simple for this pump geometry, using a combination of diode multiplexing and additional gain elements. We are currently scaling the system by the addition of a second gain element and pair of multiplexed diodes, which should give over 10 W of TEM₀₀ output.

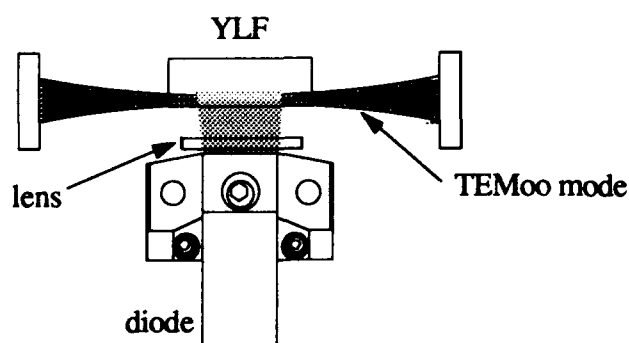


Figure 2 : Side Pumped Laser.

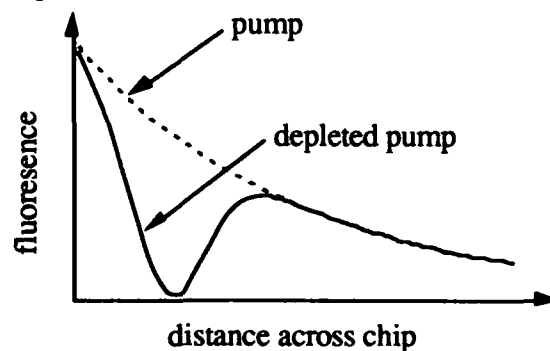


Figure 3 : Absorbed power & TEM₀₀ overlap.

The key to the efficient TEM₀₀ performance of the side pumped laser is illustrated in figure 3, which shows the pump absorption in the crystal, and its depletion by TEM₀₀ mode operation. By maximising the absorption near the surface of the Nd:YLF crystal, we obtained a high degree of

overlap between the TEM₀₀ mode and gain volume. The edge of the crystal acts as the limiting aperture for TEM₀₀ mode size, and has lower diffraction loss than a conventional circular aperture, thus allowing the mode to lase closer to the edge of the gain medium where the gain is highest. The single pass gain of this device, when pumped at 16 W, was 25 %. Thus gains as high as those for end-pumped systems are obtained, but at pump-power densities an order-of-magnitude lower than for end pumping. This lower pump-power density reduces the thermal effects described above, and also eliminates the upconversion problems seen in the end-pumped laser. This leads to the key result of this work; namely, that CW diode pumped lasers can be efficiently scaled in power, to produce high beam quality Q-switched output, suitable for pumping non-linear optical processes.

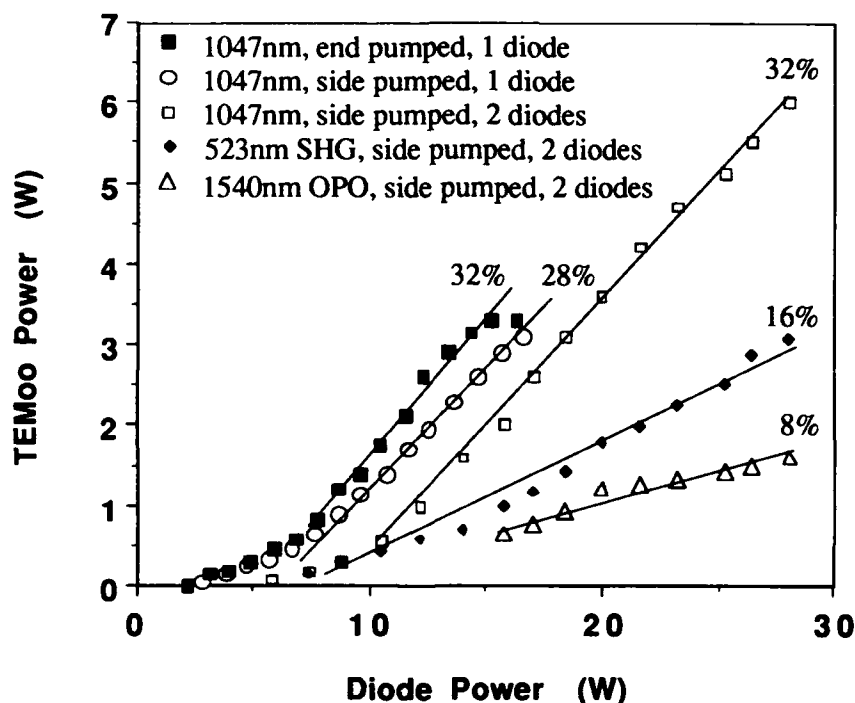


Figure 4 : Summary of output powers obtained from the various laser configurations investigated. The linear fits are labeled with optical slope efficiencies.

In Q-switched operation, the high gain produced by the side pumped laser gave pulses as short as 30-40 ns, at repetition rates of 10-20 kHz and output power of 5.1-5.5 W. In this configuration, we obtain 3.1 W of second harmonic output using a 10 mm length of KTP cut for SHG at 1047 nm. Also, we have demonstrated 1.5 W of output at 1.54 μm at 15 kHz, using a non-critically phase matched KTP optical parametric oscillators. The conversion efficiency of these devices was 30 % to the signal alone, which is quite comparable to the 35 % efficiencies typically observed with pulse DPLs, in our earlier work. We will report detailed measurements of thermal lensing, and the upconversion phenomena, previously thought to be insignificant in Nd:YLF. As well as further power-scaling results. We will also detail the new non-linear wavelength-conversion techniques developed for this device.

**The Application of Four-Wave Mixing by Gain Saturation
for the Control of Solid-State Laser Systems**

M.J.Damzen, G.J.Crofts and R.P.M.Green
Laser Optics Section, The Blackett Laboratory, Imperial College,
London SW7 2BZ, U.K.
Tele.No.: 071 589 5111

Summary

Gain saturation is a nonlinear optical process in which the gain coefficient of the medium ($\alpha(\text{cm}^{-1})$) has the intensity-dependent form $\alpha = \alpha_0/(1-I/I_s)$, under steady-state conditions, where I is the laser intensity, I_s is the saturation intensity of the medium and α_0 is the small-signal gain coefficient. When two or more coherent beams are incident on the gain medium their interference induces gain gratings that can result in efficient beam diffraction. Such nonlinear gain gratings can produce strong beam interaction effects and in particular we show in this work that high-efficiency four-wave mixing can be achieved in solid-state gain media. We show that such dynamic gain gratings are a potential technology for the nonlinear optical control of solid-state laser systems.

An early attempt to demonstrate phase conjugation by gain saturation in a solid-state gain medium (Nd:YAG) by Tomita¹ achieved only poor efficiency (reflectivity of 0.1% and 1 μ J of conjugate energy). In recent experiments we have however demonstrated the ability to perform high-efficiency four-wave mixing in Nd:YAG (reflectivity of 2500 - (250000%) - and conjugate energy of 50mJ). We have also utilised this technique to form a novel phase conjugate Nd:YAG laser system in which a single Nd:YAG rod acts simultaneously as both the gain medium and phase conjugator.

Using a conventional four-wave-mixing geometry in a flashlamp-pumped Nd:YAG rod (diameter 9.5mm, length 78mm) with counterpropagating pump beams (E_1 and E_2) from a Q-switched Nd:YAG laser with pulse duration 16nsec, conjugate reflectivity of ~10% is achieved. However, by using two-pass and four-pass schemes (see Figure 1) conjugate reflectivity is enhanced to ~200% and ~250000%, respectively². A significant feature of the four-pass geometry is that the energy in the conjugate beam (50mJ) can be greater than the input four-wave mixing pump beam energy. Figure 2 shows

the energy of the conjugate beam as a function of the input energy of the signal beam.

As well as operation with short pulses (16nsec), four-wave mixing is also achieved when the pump beams are operated in a long-pulse mode ($\sim 100\mu\text{sec}$ relaxation oscillation period). Conjugate energy reflectivity of ~ 30 is achieved for the long-pulse mode in the four-pass geometry.

We have also used the four-wave mixing gain device as an amplifying phase conjugate mirror which together with a conventional mirror ($R=50\%$) angled in the probe beam direction (the probe input beam was blocked in this arrangement) formed a phase conjugate Nd:YAG laser resonator³. This is the first operation, to our knowledge, in which a solid-state gain medium is simultaneously the gain and the phase conjugator in the laser system. Operation of this laser system in both the Q-switched and long-pulse four-wave mixing pump beam modes has been achieved and its operational characteristics will be presented, including the production of diffraction-limited TEM_{00} operation.

We conclude by noting that saturable gain four-wave mixing in Nd:YAG can be very efficient and is shown to be competitive with other phase conjugation techniques. Phase conjugate laser resonators based on this technology may have a role to play in spatial control of laser systems, especially for scaling to high average powers. The writing of dynamic gain gratings may also have potential applications for the coherent coupling of laser beams and laser cavities in both flashlamp-pumped and diode-pumped laser systems.

1. A.Tomita, Appl.Phys Lett., **34**, 463 (1979)
2. G.J.Crofts, R.P.M.Green, M.J.Damzen, "An investigation of multipass geometries for efficient DFWM in Nd:YAG", Opt.Lett., **17**, 920 (1992)
3. M.J.Damzen, R.P.M.Green and G.J.Crofts, "High-efficiency four-wave mixing by gain saturation of nanosecond and microsecond radiation in Nd:YAG", Opt.Lett., to be published 1st Oct., vol.17 (1992)

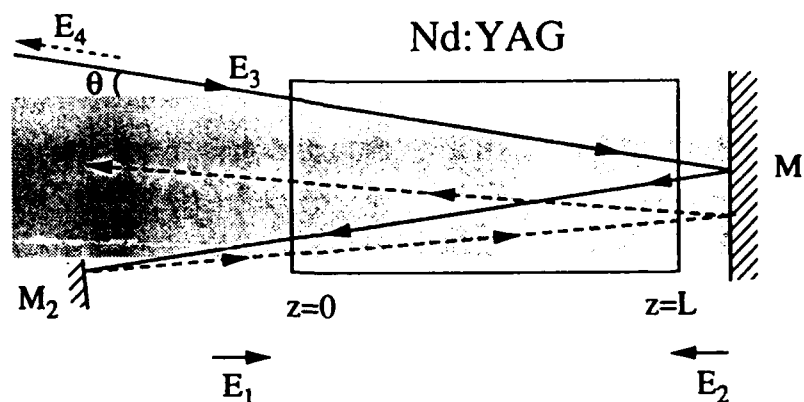


Figure 1. Two-pass (without mirror M2) and four-pass (with mirror M2) four-wave-mixing schemes. The shaded area represents the region filled by the counterpropagating pump beams (E_1 and E_2).

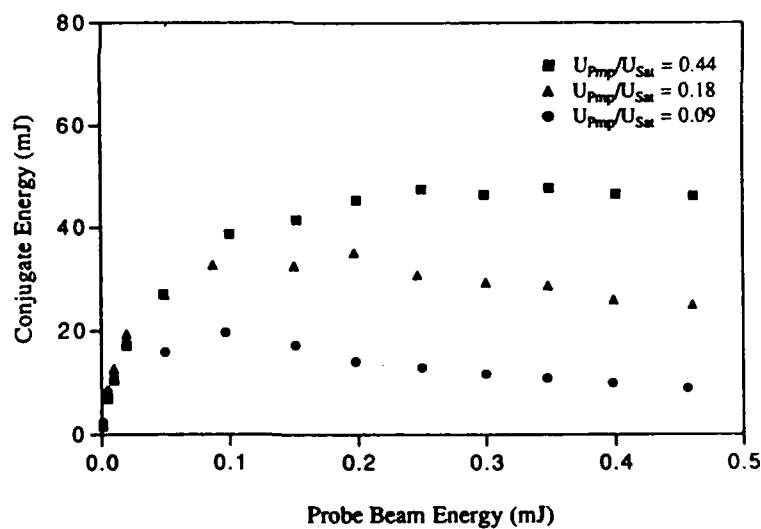


Figure 2. Energy of the conjugate beam as a function of the probe energy for different values of the pump beam energy fluence (U_{pmp}) normalised to the saturation fluence (U_{sat}) of Nd:YAG.

Ultra-High Sensitivity Measurement of Doppler-Shift with a Microchip Solid-State Laser

Kenji Otsuka

NTT Basic Research Laboratories, Musashino-shi, Tokyo, 180 JAPAN

Telephone +81 422 59 3367

Light-injection-induced phenomena in lasers, such as injection locking¹⁾ and return-light-induced instabilities,²⁾ are of profound interest because of the basic properties of laser dynamics as well as their practical importance. Microchip lasers with low external Q cavity manifest the effect of external light. In an early experiment using Nd stoichiometric lasers, the author found the resonant excitation of relaxation oscillations, resulting from Doppler-shifted light injection from a moving light-scattering object.³⁾ In this paper, the application of this phenomenon to ultra-high sensitivity Doppler-shift measurements in wide velocity regions is demonstrated experimentally. A theoretical model that includes multimode effects and successfully explains experimental results is given.

The experimental arrangement is shown in Fig. 1. The LiNdP₄O₁₂ (LNP) crystal was 1 mm thick and both ends of the crystal were coated with dielectric mirrors (transmission at 1.32 μ m of 0.1 and 1 percent). An argon laser served as a pump. The oscillation threshold was 130 mW and the slope efficiency was 13 percent. The LNP laser radiation was linearly polarized along the pseudorhombic c axis. Two-longitudinal-mode oscillation was obtained above $w = P/P_{th} = 1.09$ (P : threshold pump power), three-longitudinal-mode oscillation was observed above $w = 1.7$ and so on. Part of the output light was used for monitoring output waveforms and power spectra with an InGaAs photodiode having a 120 MHz bandwidth. The main beam was focused on a rotating circular paper sheet stuck to a metal plate which was attached to the rotating arm. The laser power impinging on the paper sheet was changed by a variable attenuator. The following injection-induced modulation was clearly observed even if the impinging light was attenuated by greater than -30 dB. On the basis of the measured intensity of scattering light along the strongest direction, the intensity of scattered light injected back into the LNP laser is estimated to be < -100 dB weaker than the lasing intensity!

Figure 2 show power spectra as a function of the angular velocity v when $w = 1.43$ and the impinging light was attenuated by -7 dB. The spectral peaks f_D in power spectra were found to coincide exactly with the Doppler-shift frequency $f_D = v \cos \theta_s / \lambda$ (λ : oscillation wavelength), where θ_s is the angle between the laser axis and the velocity vector. Output waveforms are shown in Fig. 3, where $w = 1.64$ and the impinging light power was attenuated by -30 dB. This implies that the spectral peaks in the power spectra are not simple "beat notes" between lasing field and Doppler-shifted scattered light field.

The observed phenomenon can be understood in terms of injection-induced intensity modulation resulting from interference between oscillating field \tilde{E}_i and Doppler-shifted field $\tilde{E}_{i,s}$ injected into the laser cavity, where i denotes the modal index. The light-injection model equations for rotating-wave approximation fields in spatially-hole-burned lasers like LNP are given as follows:

$$dN_0/dt = P - N_0/\tau - \sum_{k=1}^N B_k S_k (N_0 - N_k/2), \quad (1)$$

$$dN_i/dt = -N_i/\tau + B_i N_0 S_i - N_i \sum_{k=1}^N B_k S_k, \quad (2)$$

$$dE_i/dt = [B_i (N_0 - N_i/2) - 1/\tau_p] (E_i/2) + (\kappa/\tau_t) E_{i,s} \cos(\Psi_i(t) + \phi_{i,s}(t)), \quad (3)$$

$$d\Psi_i/dt = \omega_i - \omega_{i,s} - (\kappa/\tau_t) (E_{i,s}/E_i) \sin(\Psi_i(t) + \phi_{i,s}(t)), \quad i = 1, 2, \dots, N \quad (4)$$

where N_0 is the space average of population inversion density, N_i is the first spatial Fourier component of population inversion for the i -th mode, P is the pump power, $S_i = E_i^2$, $E_{i,s}(t) \propto E_i(t - t_d)$ (t_d : delay time), τ is the population lifetime, τ_p is the photon lifetime, κ is the effective amplitude transmission coefficient of the output mirror, τ_l is the roundtrip time in the cavity, Ψ_i is the phase difference between the two fields and $\phi_{i,s}$ expresses phase fluctuations of scattered light, whose frequency spectrum has a Gaussian frequency dependence.⁴⁾ The summation terms express the cross-saturation of population inversion among oscillating modes. The sinusoidal functions in the equations express the interference effect of the lasing field \vec{E}_i and the corresponding scattered field $\vec{E}_{i,s}$. Eqs. (1)-(4) imply that individual modes are modulated by injected light at Doppler-shift frequency $\omega_D = |\omega_i - \omega_{i,s}|$ independently of N and this local interaction affects the whole system dynamics through the cross-saturation.

The intensity modulations were completely suppressed when the polarization direction of the return-beam was rotated 90 degrees by a Faraday rotator and an analyzer inserted between the laser and the scattering object, and the interference between the two beams was suppressed. This provides clear evidence that the interference between the two fields is essential for the observed intensity modulations.

The crucial point for intensity modulation is the external Q factor $\propto \tau_l$. An equivalent parameter is $K = \tau/\tau_p$ since τ_p is proportional to τ_l . In the present microchip LNP laser, $\tau = 120\mu s$ and K is extremely large, on the order of $10^5 - 10^6$. In general, the sensitivity of lasers to external light injection increases with decreasing the size of lasers, i.e., increasing K value.⁵⁾ Therefore, the effective modulation index becomes very large even if the scattered light intensity is extremely small. In usual solid state lasers, $K = 10^3$. The key for sensitive detection of the Doppler-shift resulting from injected scattered-light-induced intensity modulation is a large K number in the microchip laser. Intensity modulations at the Doppler-shift frequency f_D like those in Fig. 3 were reproduced quite well by numerical simulations in wide velocity regions, assuming an extremely small $\eta = E_{i,s}/E_i (< 10^{-5})$. The corresponding intensity of scattered light injected back into the laser is ~ 100 dB weaker than lasing intensity. The modulation depth of the output decreases as the rotation speed increases, reflecting the frequency response characteristics of the laser.

These observations indicate the possible application of this phenomenon to ultra-high sensitivity velocity meters. In the experiments, a Doppler-shift was clearly detected in the region of $30 \text{ kHz} < f_D < 30 \text{ MHz}$ (e.g., velocity along the laser axis = $3.9 \text{ cm/s} - 39 \text{ m/s}$) at $w = 1.05$ with ~ 30 dB attenuation. The dynamic range of velocity measurements can be increased by increasing w , since the modulation bandwidth increases with w .⁶⁾ (In this particular experiment, the upper velocity limit was imposed by the rotation speed of the rotating arm). The present scheme enables us to measure different velocities simultaneously. An example of simultaneous measurements is shown in Fig. 4, where the main beam was divided into three beams and they were impinged on different positions of the rotating paper sheet with different θ_s , where the main beam intensity was attenuated by ~ 25 dB. From this power spectrum peaks $f_{D,1}$, $f_{D,2}$ and $f_{D,3}$, we can determine velocities along the laser axis simultaneously. In the proposed system, the laser itself acts as a highly-sensitive "detector" of beat signals resulting from the large lifetime ratio K , and has an intensity modulated output corresponding to the velocity of the light-scattering object, yielding an easy measurement of Doppler shift. In conventional laser Doppler velocity meters, on the other hand, the beat signal between a laser light field and a weak Doppler-shifted scattered field is detected as a basic quantity. This requires sophisticated optics and highly-sensitive electronics. The present phenomenon, which is expected in general micro-cavity lasers, could be also applied to measure diffusive motion of Brownian particles⁴⁾ and scattering spectroscopy.

References

- 1) C. J. Buczek, R. J. Freiberg, and M. L. Skolnick: *Proc. IEEE* **61** (1973) 1411.
- 2) For a review, see K. Otsuka: *SPIE Nonlinear Optics and Materials*, **1497** (1991) 432 and references therein.

- 3) K. Otsuka: IEEE J. Quantum Electron. **QE-15** (1979) 655.
- 4) F. T. Arecchi: in *Quantum Optics*, ed. R. J. Glauber (Academic Press, New York and London, 1969), p. 57.
- 5) K. Otsuka: IEEE J. Quantum Electron. **QE-12** (1976) 438.
- 6) D. E. McCumber: Phys. Rev. **141** (1966) 306.

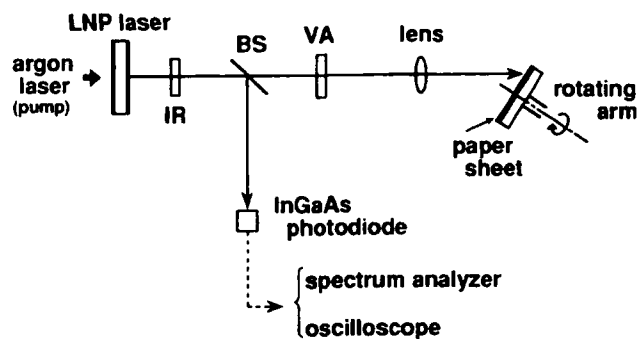
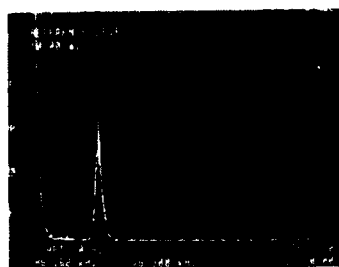
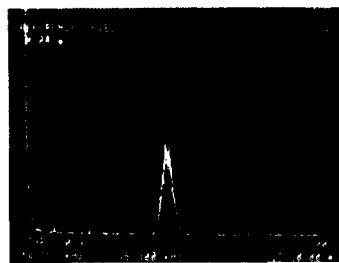


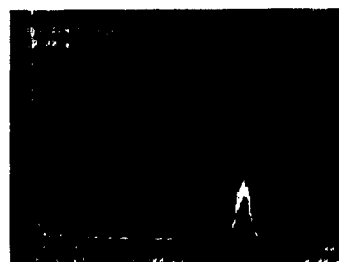
Fig. 1. Experimental arrangement. IR: infrared transmission filter, BS: beam splitter, VA: variable attenuator.



(a)



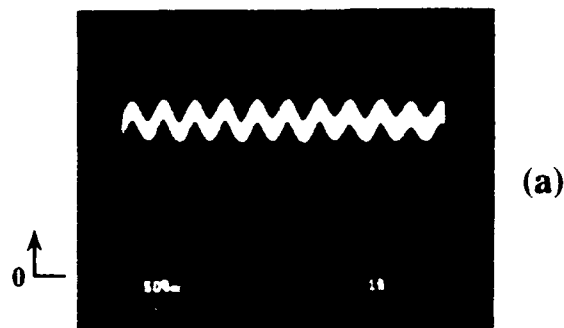
(b)



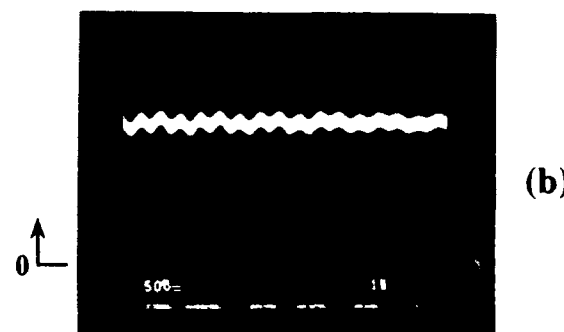
(c)

↑ zero frequency ↑ f_D 1.5MHz/div

Fig. 2. Power spectra for different velocities, where $w = 1.43$, $\theta_s = 45^\circ$. (a) $v = 5.9$ m/s, (b) 12.3 m/s, (c) 17.8 m/s. 1.5 MHz/div.



(a)



(b)

1μs/div

Fig. 3. Output waveforms for different velocities, where $w = 1.64$, $\theta_s = 45^\circ$. (a) $v = 2$ m/s, (b) 3 m/s.

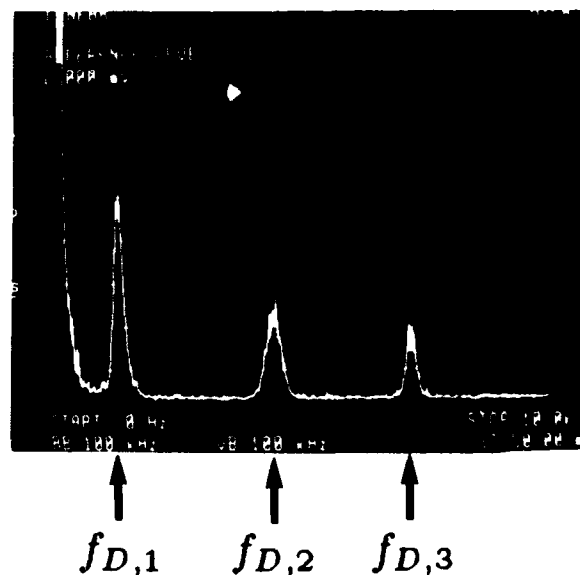


Fig. 4. Simultaneous measurement of different velocities, where $w = 1.14$. 1 MHz/div.

High Duty-Cycle Diode-Pumped Nd:YLF Slab Laser

A.D.Hays and R. Burnham
Fibertek, Inc.
ph. (703) 471-7671

We have demonstrated 10 W multimode and 6.5 W TEM₀₀ average power from a side-pumped Nd:YLF solid state laser operated at 1 kHz repetition rate. The laser slab was transversely pumped using four 1 cm long by GaAlAs linear arrays. The optical path of the laser beam was straight through the crystal.

Pump arrays used for this experiment were manufactured by Spectra Diode Laboratories and mounted on impingement coolers for efficient heat transfer. The quasi-cw laser diode were driven with pulse lengths of 200 μ sec for a duty-cycle of 20%. None of the diode arrays showed any signs of degradation due to the high duty-cycle operation. Center wavelength of the diodes was 806 nm with a FWHM linewidth of ≈ 4 nm at 80 A drive current. The laser slab utilized in our experiment had a 3 x 4 cross section and was 50 mm long. The crystal was a-axis with its c-axis parallel to the pump direction. The crystal face opposite the pump face was HR coated to provide two-pass absorption in the gain medium. This arrangement allowed for approximately 74% absorption over the 8 mm path length. A high index glass rod lens was used to collimate the pump light and produce a thin gain stripe in the crystal. To improve mode overlap for TEM₀₀ operation two pair of anamorphic prisms were employed to ellipsize the gaussian mode inside the laser crystal.

Thermal lensing within the laser slab was highly astigmatic for π -polarization with focal lengths of 150 cm and -50 cm for lensing parallel ($f_{\pi_{\parallel}}$) and perpendicular ($f_{\pi_{\perp}}$) respectively to the c-axis. Thermal lensing for σ -polarization was considerably less than for π -polarization and measure to be 400 cm and less than -750 cm for $f_{\sigma_{\parallel}}$ and $f_{\sigma_{\perp}}$. These focal lengths are not consistent with results reported^{1,2} for uniform pumping which indicates the importance of pump geometry and heat removal when using laser diodes as a pump source. The temperature gradients, due to the narrow pump volume within the slab, produced a greater dn/dt along the c-axis than for uniform pump distributions. We attribute the difference in thermal lensing observed here, compared to those of previous investigators, to our pump geometry. Thermal lensing for π -polarization was strong enough, that when placed within a near-hemispherical cavity without polarizing elements, the laser was unstable at 1.047 μ m

and operated on the lower gain $1.053\ \mu\text{m}$ line. When used with a polarizer to control transition selection in the multimode configuration both transitions produced similar output energies. Results given here are for $1.053\ \mu\text{m}$ operation. Laser performance for both multimode and TEM_{00} operation is shown in figure 1.

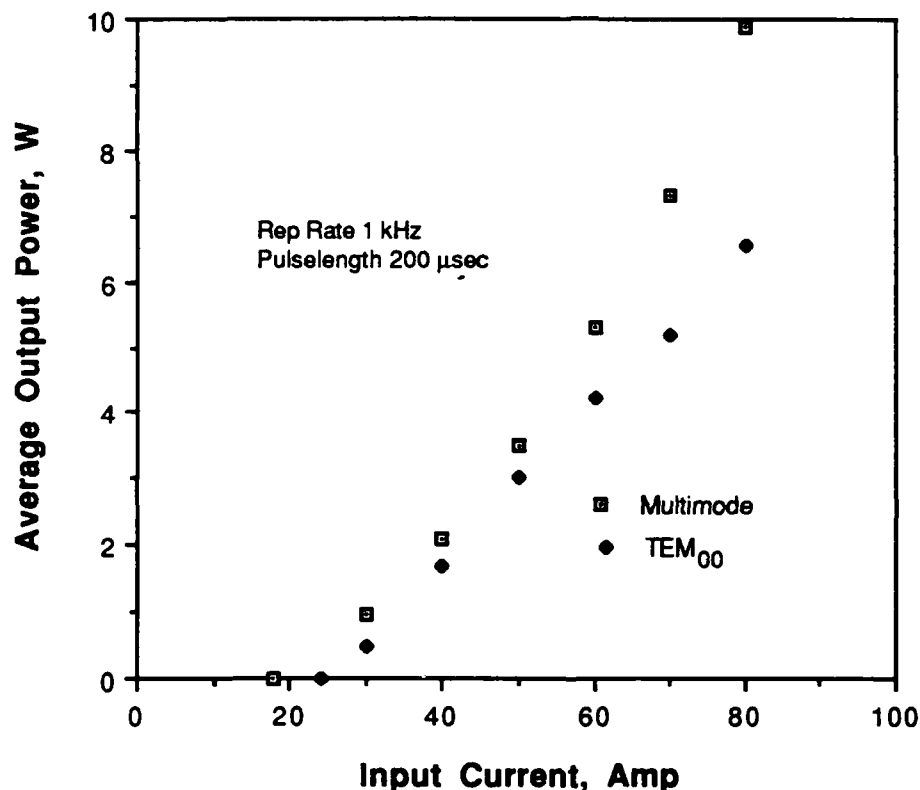


Fig. 1 Output of Nd:YLF slab laser verses laser diode input current.

Currently the system is being tested by Intelligent Surgical Lasers, Inc. in a regenerative amplifier for ophthalmic surgery. As a regenerative amplifier the system was reduced to a drive current of 65 ampere for an output energy of 1 mJ when seeded by a 45 psec diode-pumped mode-locked Nd:YLF laser. The laser module is under development as an alternative to a 4000 W arc-lamp system currently employed. The diode-pumped laser module requires only 200 W of electrical power with significant lifetime improvements over arc-lamp systems.

References:

- 1) Herman Vanherzeele, "Thermal lensing measurement and compensation in a continuous-wave modelocked Nd:YLF laser," Optics Letters. vol 13, 369 (1988)
- 2) Thomas M. Pollak, W.F. Wing, Robert J. Grasso, E.P. Chicklis, and Hans P. Jenssen, "CW Laser Operation of Nd:YLF," IEEE J. Quantum Electron. QE-18, 404 (1982)

Monday, February 1, 1993

Nonlinear Frequency Conversion 1

Poster Session

AME 3:00pm–4:00pm
La Salle Ballroom A

Q-Switching of a Nd:YAG Phase Conjugate Laser Using External Stimulated Brillouin Scattering.

R.A. Lamb Defence Research Agency, Fort Halstead,
Sevenoaks, Kent. TN14 7BP. UK.

M.J. Damzen The Blackett Laboratory, Imperial College
of Science and Technology, Prince Consort
Road, London. SW7 2BZ. UK.

Phase conjugate laser resonators using stimulated Brillouin scattering (SBS) have been the subject of numerous investigations. The approach usually adopted is to include the SBS medium inside a laser cavity with a conventional back mirror initiating laser oscillations and triggering SBS [1]. Although workers employing this type of resonator have reported some success the high intra-cavity intensities experienced by the SBS medium will limit the average power, peak power and repetition rate of the output.

Recently Pashinin et al [2] have reported an alternative cavity configuration in which the SBS medium resides outside the conventional cavity. Pashinin et al used a Li:F^{2+} colour-centre saturable absorber to Q-switch the cavity and provide the high peak power required to initiate Brillouin scattering. The output beam was found to have a TEM_{00} mode and efficient energy extraction at high repetition rates using high purity SBS media.

We have investigated a similar resonator configuration with a view to further simplify the cavity design. In this investigation we have found it possible to obtain reliable lasing action without the necessity for intra-cavity Q-switching.

Experiment.

The laser cavity is as shown in figure 1. The two plane mirrors $R_1=30\%$ and $R_2=20\%$, the Nd:YAG rod with a diameter of 9.5mm, and a small-signal single pass gain of 10, define a conventional laser cavity whose optical length was 0.94m. This cavity length gives an axial mode spacing equal to the frequency shift of C_2F_6 which was taken to be $\nu_B=160\text{MHz}$ [3].

$$L_{\text{cavity}} = \frac{c}{2\nu_B}$$

The beam quality was controlled by the use of a weak negative lens of focal length -4m positioned 5cm from R_2 , which forces the cavity to operate in an unstable regime and helps discriminate against higher transverse modes. Also the increase in the TEM_{00} mode volume increases the energy extraction efficiency from the rod.

A gas cell containing the SBS medium C_2F_6 at a pressure of 30 atmospheres was positioned 10cm from the mirror R_2 . This cell acts as both a phase conjugate mirror and as a Q-switch. When SBS is triggered the cavity losses are reduced because of the higher reflectivity and reduced diffraction

losses of the phase conjugate oscillations. The mirror R_1 becomes the output coupler. The repetition rate was variable between 1 to 10 Hz with most of the data taken at 2Hz.

With the SBS cell blocked the output through R_2 consisted of a series of relaxation oscillations with a typical duration of 400ns FWHM, and separated by about 2.5 μ s. The total output lasted for a duration of about 80 μ s. The energy transmitted through R_2 was 620mJ and the output through R_1 was 340mJ. From these measurements the average power of a single relaxation spike transmitted through R_2 , and incident on the SBS cell was calculated to be about 56kW. A simple calculation using Gaussian beam optics yields a value of about 6kW for the SBS threshold.

Hence the average power of a relaxation spike is about 10 times threshold, and SBS should be readily achieved. This is what is observed with Q-switched outputs in excess of 230mJ and of duration 40ns- see figure 2. Temporal modulation of the pulse with a period equal to the round trip time of the conventional cavity is also evident.

A bandwidth of 1GHz was measured for the SBS Q-switched resonator, and for the conventional resonator with the SBS cell removed. Hence, the presence of the SBS cell does not reduce the bandwidth of the output. With a mode spacing of 160MHz, the number of axial cavity modes was about 7.

We also observed a double Q-switched output due to gain recovery in the Nd:YAG rod. This occurred about 45-55 μ s after the first Q-switch, and had an energy comparable to that of the first. By angle tuning one of the cavity mirrors the relaxation oscillation could be delayed resulting in a single powerful Q-switched pulse.

The far field spatial beam pattern had the appearance of a central lobe with a surrounding ring structure as expected from a unstable resonator -figure 3. The full angular beam divergence was measured to be 1.8mrads -less than two times the diffraction limit.

Another version of the laser has been investigated in which the mirror R_2 is replaced by a curved Gaussian profiled mirror, and with the negative lens removed. Q-switched outputs in excess of 500mJ have been obtained to date. Further investigations aimed at improving the beam quality and reducing the temporal modulation are continuing.

References

- 1 H. Meng and H. J. Eichler: Nd:YAG laser with a phase-conjugating mirror based on stimulated Brillouin scattering in SF₆ gas; Op Lett, vol 16, No 8, page 5, (April) 1991
- 2 P. P. Pashinin, E. I. Shklovsky, and V. S. Sidorin: Characteristics of a SBS Self-Injection Locked Laser; Laser Physics, Vol 1, No 2, page 160, 1991.
- 3 M. J. Damzen, M. H. R. Hutchinson, and W. A. Schroeder: Direct measurement of the acoustic decay times of hypersonic waves generated by SBS; IEEE J. Quantum Electron, Vol QE-23, No 3, p 328, 1987.

Figure 1: Experimental Layout.

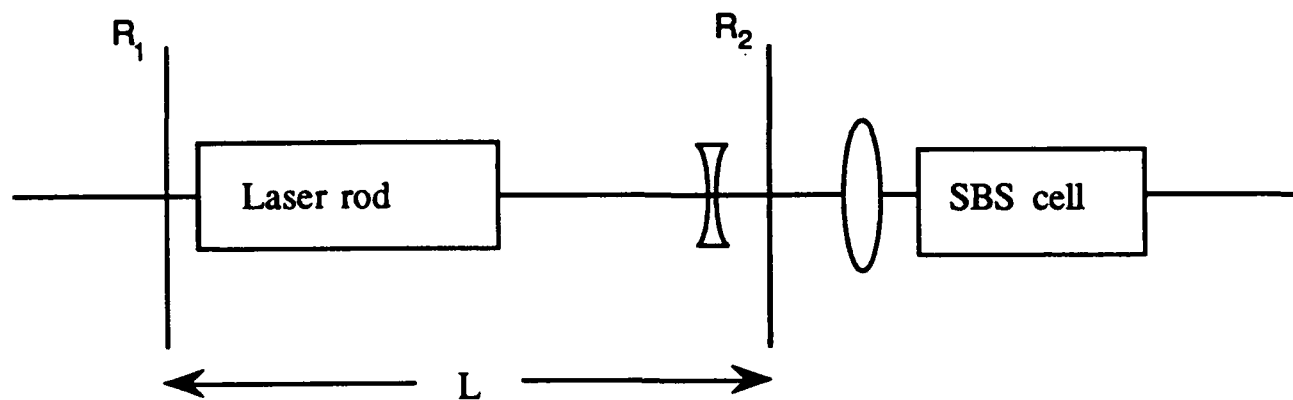


Figure 2: Q-switched output.

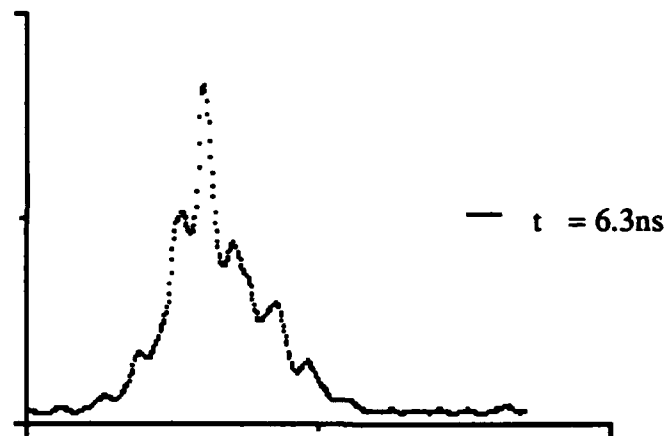
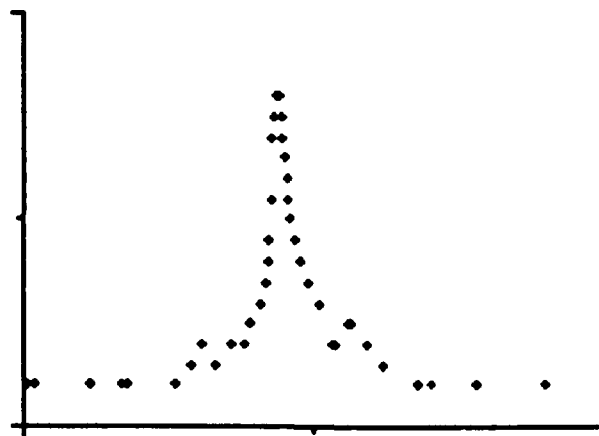


Figure 3: Far field beam profile for a Q-switched output.



2.95 μm Intracavity Difference-frequency Laser

F. J. Effenberger
and
G. J. Dixon

Center for Research on Electro-Optics and Lasers
and Department of Electrical Engineering
University of Central Florida
Orlando, FL 32826

Compact, tunable, CW laser sources operating in the spectral region between 2.5 μm and 3.5 μm are needed for spectroscopy, remote sensing, pollution analysis, and medicine. While Pb-salt diodes are capable of generating output over a broad spectral region, they are quite expensive and the tuning range of any particular diode is limited. Nonlinear difference frequency generation is an alternative method of generating output in this spectral region. In this paper we describe the results of initial experiments in which a 0.78 μm input beam was mixed with the intracavity field of a diode-laser-pumped 1.06- μm laser to generate difference frequency output at 2.9 μm .

All-solid-state blue sources, based on intracavity sum frequency generation between the intracavity field of a 1.064 μm Nd:YAG laser and an 0.810- μm input beam have been described by a number of authors^{1,2}. In these devices, noncritical, Type II phase matching in y-axis KTP was used to generate the sum frequency. Although the output efficiencies of early devices were quite low, resonant enhancement of the signal input inside the laser cavity has recently led to substantial increases in output efficiency.³

Y-axis KTP can also be used to generate the 2.9 μm difference frequency between an intracavity 1.064- μm field and a 0.780- μm input. The z-polarized difference frequency output is generated when both input fields are polarized along the x-axis of the crystal. Shorter wavelengths can be generated by changing the angle of the KTP and the wavelength of the input. Figure 1 shows the output wavelength and phase matching angle in the y-z plane as a function of input wavelength, computed from the Sellmeier equations for KTP⁴. Of particular interest is the fact that output wavelengths spanning the range between 2.5 μm and 2.9 μm can be generated with a 0.030 μm variation in input wavelength.

Most of this range could be swept out by heating and cooling a 0.770 μm GaAlAs diode laser.

The cavity configuration used for our experiment is shown schematically in Figure 2. The 1.064 μm laser is pumped by a 1-watt broad-area diode that is imaged into a 5mm-long Nd:YAG crystal with a GRIN lens. The 0.78 μm input from a Ti:sapphire laser was focused into the cavity through the curved mirror and mixed with the intracavity field in a 5-mm long, y-cut KTP crystal positioned near the flat, CaF_2 output mirror. A Faraday isolator placed between the Ti:sapphire laser and the 1.064 μm cavity eliminated feedback-induced instabilities in the Ti:sapphire laser.

By changing the polarization and wavelength of the input source it was possible to generate either 0.459 μm or 2.9 μm . With the input polarized along the z axis and the input tuned to 0.809 μm , approximately 1.3 mW of 0.459 μm output was produced at an input power of 500 mW. When the input was polarized along the x axis and tuned to 0.78 μm , approximately 25 μW of 2.95 μm output was generated at the same input power. The theoretical conversion efficiency ratio for the two cases is proportional to the inverse ratio of the two output wavelengths⁵ and is equal to 41. The measured ratio of 52 is somewhat lower due to absorption in the KTP crystal that begins to increase at 2.8 μm .

Recent work with signal-resonant sum frequency lasers⁶ indicates that resonantly enhancing a 0.78 μm input from a 50 mW diode laser inside the laser resonator should yield CW output powers exceeding 250 μW .

REFERENCES:

1. D.W. Anthon, G.J. Dixon, M.G. Ressler, and T.J. Pier, SPIE Proc. **898**, 68 (1988).
2. J.C. Baumert, F.M. Schellenberg, W. Lenth, W.P. Risk, and G.C. Bjorklund, Appl. Phys. Lett. **51**, 2192 (1987).
3. P.N. Kean and G.J. Dixon, Opt. Lett. **17**, 127 (1992)
4. K. Kato, IEEE J. of Quantum Electron., **27**, 1137 (1991)
5. A. Yariv, Quantum Electronics, 3rd Ed. (John Wiley & Sons, New York, 1989), 427
6. Peter Kean, Personal communication, Sept. 15, 1992

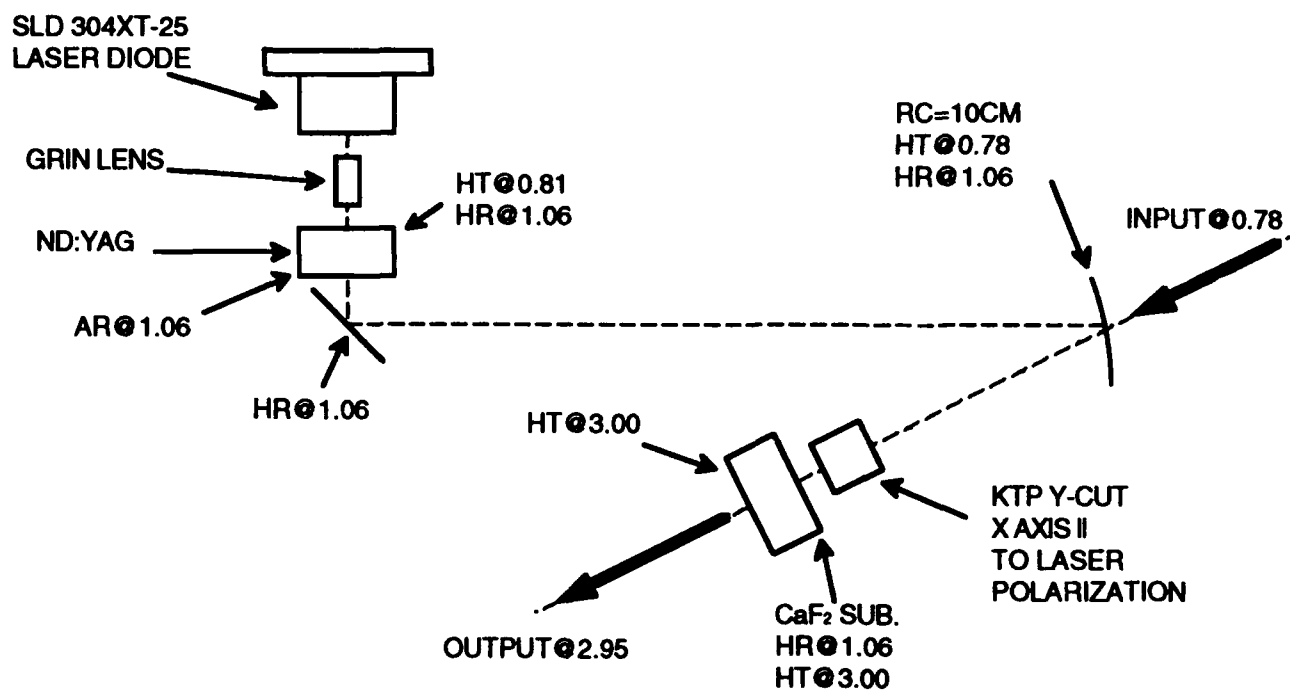


Figure 2- Optical schematic of intracavity difference frequency mixer.

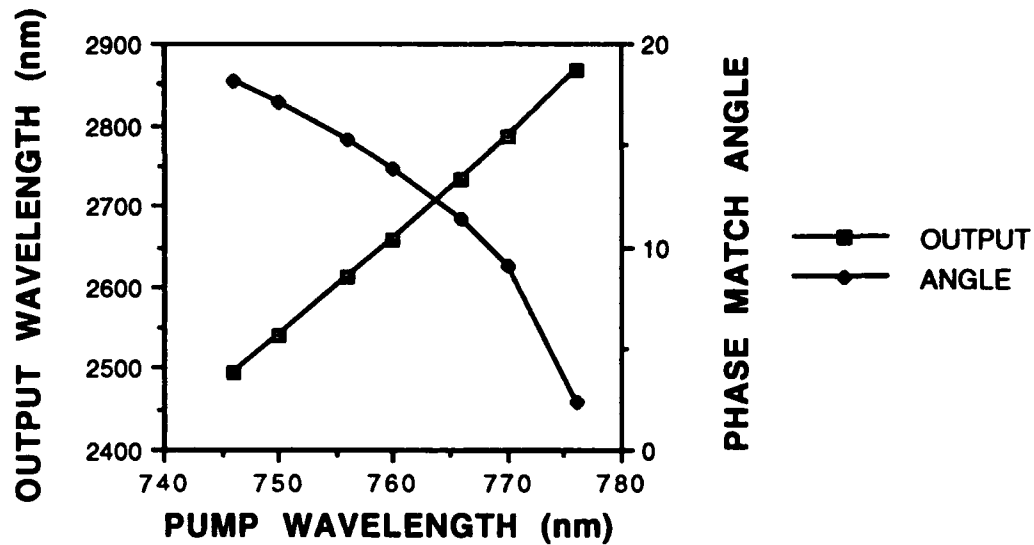


Figure 1 - Phase matching curves for difference frequency generation in KTP between a variable wavelength input and $1.064 \mu\text{m}$. Output wavelength and phase matching angle are shown as a function of input pump wavelength. The input and the $1.06 \mu\text{m}$ beams are polarized along the x axis while the output is polarized in the y-z plane. The angle shown in the figure is between the direction of propagation and the y axis in the y-z plane.

Hot images from obscurations

J. T. Hunt, K. R. Manes and P. A. Renard

Lawrence Livermore National Laboratory, University of California

P.O.Box 808

Livermore, California 94551-9900

510-4221100

For almost two decades unexplained optical damage has limited the performance of high power solid state laser systems. The syndrome is characterized by damaged components in the highest flux regions of laser systems during shots for which the anticipated average irradiances experienced by these damaged optics should have been several times lower than typical damage thresholds. The observed damage has generally been associated with small-scale self-focusing, but the prevailing wisdom has not, until now, provided a specific mechanism. Occasionally, damaged components have displayed a curious pattern: damage sites appear on alternating optics in periodic trains such as are common in solid-state lasers made up of numerous Brewster-angled glass disk amplifiers. It is hard to imagine a mechanism by which contamination could skip every other optic. The damage has all the earmarks of small-scale self-focusing—it is only apparent on the highest power laser shots, it often leaves enough damage to force the replacement of several expensive optics, and it effectively erases its own tracks making the original causes difficult to diagnose.

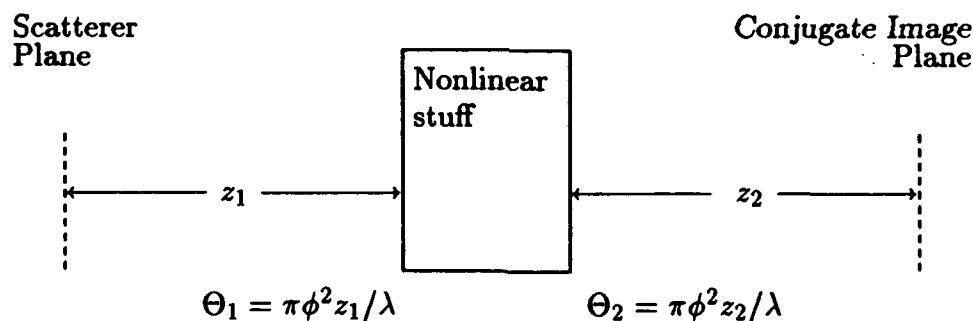


Figure 1. Propagating left to right, first through a vacuum following an obscuration, then through some nonlinear stuff, then through another vacuum region.

A simple example, sketched in Figure 1, illustrates our explanation for this type of phenomenon. The interaction of a wave scattered from an obscuration with a strong background wave in a nonlinear medium will produce a volume phase hologram that, like a Fresnel zone phase lens, focuses some of the strong background wave downstream. In a thin slab of homogeneous material—thickness d , refractive index n , and nonlinear index n_2 —light of wavelength λ and initial irradiance I_0 will experience a constant phase push-back provided by

$$B = kdI_0 \frac{n_2}{n} = \frac{2\pi d I_0 n_2}{\lambda n} \quad (1)$$

which we call the B -integral accumulated in this slab. For an opaque scatterer giving rise to a pure-real scattered field, the on-axis intensity in the conjugate plane at $z_2 = z_1$

following such a slab is given by

$$\frac{I}{I_0} = 1 + B^2; \quad (2)$$

For a translucent or transmitting scatterer which provides some phase to the scattered field, we find the on-axis, conjugate-image intensity

$$\frac{I}{I_0} = (1 + B)^2; \quad (3)$$

Since it is often the case that high power laser systems are designed for $B \approx 2$, there is potential for five- to nine-times the background irradiance in planes which satisfy the conditions represented in Figure 1. Even an ideal hard edged circular block can not produce a Poisson bright spot more than four times as intense as the background wave. Such a nonlinear mechanism can cause optical damage well downstream from an obscuration.

Under suitable assumptions that lead to a linearized diffraction theory¹, the Fourier decomposition of the scalar field for a scattered wave in the wake of an obscuration, $\psi_s = I_0 \sum a_j(z) e_j(x, y)$, can be obtained within any medium of uniform refractive index from a compact matrix procedure that recovers the Fourier coefficients from initial conditions:

$$a = \begin{pmatrix} u(z) \\ v(z) \end{pmatrix} = \begin{pmatrix} \cosh \Theta S & -\sinh \Theta S / S \\ -S \sinh \Theta S & \cosh \Theta S \end{pmatrix} \begin{pmatrix} u(0) \\ v(0) \end{pmatrix} = M \begin{pmatrix} u(0) \\ v(0) \end{pmatrix}, \quad (4)$$

where the various quantities used are:

$$\Theta = \frac{k\phi^2 z}{2} = \frac{\pi\phi^2 z}{\lambda}; \quad S = \sqrt{\frac{2B}{\Theta} - 1}. \quad (5)$$

If the "nonlinear stuff" in Figure 1 is some arbitrary collection of slabs and vacuum regions, we simply multiply individual matrix representations to obtain an overall transformation for the Fourier coefficients from scatterer plane to conjugate image plane. With the help of the following vacuum translation matrix,

$$T(\Theta) = \begin{pmatrix} \cos \Theta & -\sin \Theta \\ \sin \Theta & \cos \Theta \end{pmatrix}, \quad (6)$$

the overall transformation can be written in operator notation as:

$$\begin{aligned} \mathcal{T} &= T(\Theta_2) M T(\Theta_1) \\ &= \left(M - \frac{1}{2} \left[T\left(\frac{\pi}{2}\right), M \right] T\left(\frac{\pi}{2}\right) \right) T(\Theta_1 + \Theta_2) + \frac{1}{2} \left[T\left(\frac{\pi}{2}\right), M \right] T\left(\frac{\pi}{2}\right) T(\Theta_1 - \Theta_2), \end{aligned} \quad (7)$$

which can be compactly expressed as the sum of two waves:

$$\mathcal{T} = \underbrace{(M - W) T(\Theta_1 + \Theta_2)}_{\text{Diverging Wave}} + \underbrace{W T(\Theta_1 - \Theta_2)}_{\text{Converging Wave}}, \quad (8)$$

where

$$W = \frac{1}{2} \left[T\left(\frac{\pi}{2}\right), M \right] T\left(\frac{\pi}{2}\right).$$

It is safe to ignore the diverging wave arising from the scatterer because of the usual amplitude decrease provided by the diffractive term $T(\Theta_1 + \Theta_2)$. But the converging, or conjugate, wave will add coherently in the plane $\Theta_2 = \Theta_1$ with an amplitude determined by W . In that plane, for a slab of arbitrary thickness,

$$W = -\frac{1}{2} \left[\frac{\sinh \Theta S}{S} + S \sinh \Theta S \right] \begin{pmatrix} 0 & -1 \\ -1 & 0 \end{pmatrix} \quad (9)$$

which leads to a power gain for a scattered wave which may be written

$$G = 1 + \frac{B^2 \sinh^2 \sqrt{2B\Theta - \Theta^2}}{2B\Theta - \Theta^2}. \quad (10)$$

If the slab is thin, the result in Equation (2) is obtained. In a periodic train of slabs, alternate slabs following an obscuration experience high fields. For combinations of slabs, numerical results are easily generated for certain classic obscuration shapes. Figure 2 shows the expected peak-to-background on-axis intensity for a series of 10 evenly spaced, thin, slabs, when the initial obscuration is a circular opaque scatterer.

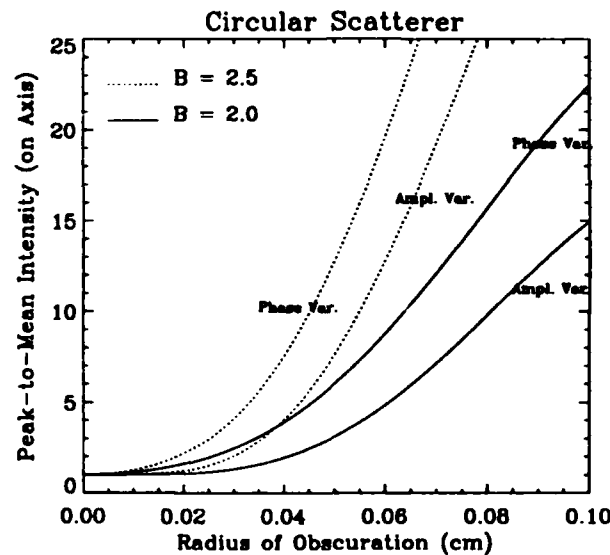


Figure 2. For 10 equally spaced slabs, expected peak variation of axial intensity in conjugate plane of a scatterer.

The results in this figure have been confirmed by experimental evidence. Since computation of the transform represented in Equation (7) is quite simple for arbitrary arrangements of slabs representing optical elements in a laser chain, this formalism is helpful for staging considerations where high peak irradiances and insufficient spatial filtering conspire to produce hot spots far upstream of any obscuration.

REFERENCES:

- [1] We follow J. B. Trenholme's perturbation analysis outlined in the 1975 *Laser Annual Report*, UCRL-50021-75, Lawrence Livermore National Laboratory, pp237-242.

Stimulated Brillouin scattering and phase conjugation of a 2.1 μm Cr,Tm,Ho:YAG laser

W. T. Whitney
Laser Physics Branch
Naval Research Laboratory
Washington, DC 20375

A. M. Scott
Defence Research Agency
Malvern, Worcestershire WR14 3PS, UK.

The 2- μm holmium laser is an exciting candidate for many applications including coherent laser radar. It is efficient, relatively eyesafe, and has good atmospheric transmission. However, at moderate to high average power, the material exhibits strong thermal lensing,¹ which adversely affects laser efficiency and beam quality. It is expected that stimulated Brillouin scattering (SBS) phase conjugation techniques can be used to correct the detrimental effects of thermal lensing.

At last year's meeting we reported² SBS with the holmium laser in CCl_4 using a ring threshold reduction technique.³ However, the results showed poor reflection efficiency and were not easily reproducible. Subsequent Fabry-Perot (F-P) measurements showed that the bandwidth of the laser was quite broad ~ 100 GHz, so that the short laser coherence length (~ 3 mm) not only severely restricted the effective SBS interaction length, but also made correct adjustment of the ring optical path extremely critical.

The laser used in the current experiments was Q-switched, room-temperature, flashlamp-pumped Cr,Tm,Ho:YAG⁴ tuned to 2.1207 μm with a birefringent filter. This wavelength was chosen because it gave the narrowest linewidth ~ 30 GHz. The linewidth was narrowed to ~ 600 MHz by the addition of 2 low-loss intracavity etalons. This assured that the coherence length ~ 50 cm would not limit the SBS interaction length. The temporal profile of the laser showed significant modulation due to axial mode beating. Fast Fourier transforms of temporal profiles indicated 4 to 6 axial modes separated by $c/(2L) = 167$ MHz consistent with the F-P measurements. The laser produced up to ~ 25 mJ in a ~ 200 -ns pulse fwhm and was restricted by an intracavity iris to a TEM_{00} mode as determined with a linear pyroelectric array. The pulse repetition rate was 1 Hz.

With this frequency narrowed laser it was straightforward to obtain consistent single-focus SBS in liquid CS₂. The threshold energy required for SBS was ~11 mJ. This is the first SBS demonstration to our knowledge with Ho laser radiation using a simple single-focus geometry. By use of a second focus in the same medium the energy threshold was reduced to ~8.5 mJ. The threshold was further reduced to ~5 mJ by use of two foci plus a loop⁵ which fed back the beam passing through the SBS cell and refocused it to overlap the input beam at an angle. The feedback beam allows a four wave mixing interaction in addition to the normal Brillouin interaction and thus provides a degree of positive feedback which lets the conjugate beam build up to high intensity. With the loop scheme, the SBS energy efficiency was >60% with a slope efficiency >80%.

We have also investigated the phase conjugation fidelity of the scattered light. With the loop the reflected light nearly reproduced the input beam in both the near and the far fields indicating excellent fidelity. However, the reflected light from single-focus SBS showed that both near and far-field beam diameters increased to ~125% those of the input beam indicating less than perfect conjugation. This may be due to lack of speckle structure in the input beam, the fact that the SBS was very close to threshold,⁶ or possibly competing effects such as thermal heating or self-focusing in the SBS medium.

When a phase aberrator plate was placed in the input beam increasing the divergence by a factor ~5, it was found that ~80% of the loop SBS energy was in a Gaussian beam profile only slightly larger than the original. The results indicated that the fidelity was ~65%. The distortions due to the aberrator prevented single-focus SBS.

In future experiments, we will investigate ring threshold reduction and a master oscillator power amplifier configuration.

We thank Michael T. Duignan of Potomac Photonics, Inc. for assistance with this work and Steven Bowman for useful discussions and use of equipment.

References

- ¹ S. R. Bowman, M. J. Winings, R. C. Y. Auyeung, J. E. Tucker, S. K. Searles, and B. J. Feldman, "Laser and spectral properties of Cr,Tm,Ho:YAG at 2.1 μ m," IEEE J. Quantum Electron. **27**, 2142-2149 (1991).

- ² W. T. Whitney, M. T. Duignan, B. J. Feldman, and S. R. Bowman, "Stimulated Brillouin scattering of a Cr,Tm,Ho:YAG laser at 2.1 μm " Advanced Solid-State Lasers Topical Meeting, Santa Fe, Feb 17-19, 1992, paper ME3.
- ³ V. I. Odintsov and L. F. Rogacheva, "Efficient phase conjugation under parametric-feedback conditions," JETP Lett. **36**, 344-347 (1983); S. Pfeifer, R. Johnson, and W. Carrion, "Experimental investigation of threshold reduction techniques in stimulated Brillouin scattering," Paper CMG3, Conference on Lasers and Electro-Optics, Technical Digest Series 10, (Optical Society of America, Washington, D. C., 1991) p. 50.
- ⁴ S. R. Bowman, M. J. Winings, S. Searles, and B. J. Feldman, "Short-pulsed 2.1 μm laser performance of Cr, Tm, Ho:YAG" IEEE J. Quantum Electron. **27**, 1129-1131, (1991).
- ⁵ G. K. N. Wong and M. J. Damzen, "Investigations of optical feedback used to enhance stimulated scattering," IEEE J. Quantum Electron. **26**, 139-148 (1990).
- ⁶ C. B. Dane, W. A. Neuman, and L. A. Hackel, "Pulse-shape dependence of stimulated-Brillouin-scattering phase-conjugation fidelity for high input energies," Opt. Lett. **18**, 1271-1273 (1992).

AgGaSe₂ OPO PUMPED BY A LiNbO₃ OPO

J. Raffy, T. Debuisschert, J.-P. Pocholle and M. Papuchon

Laboratoire Central de Recherches, THOMSON-C.S.F.,
 Domaine de Corbeville
 91404 Orsay Cedex, France
 tel: 60-19-79-46
 fax: 60-19-74-16

Many important applications like LIDAR or remote sensing rely on the availability of I.R. tunable laser sources in the transparency range of the atmosphere. To produce the adequate wavelength, a solution is to use an Optical Parametric Oscillator (O.P.O.) . The main advantages of O.P.O.'s are to provide a widely tunable output wavelength and to use solid state technology. An adequate non-linear crystal is AgGaSe₂¹. Unfortunately, phase-matching can not be obtained using a pump wavelength of 1.064 μm emitted by the widely used Nd:YAG laser. We have thus used a pump wavelength at about 2 μm produced by an other O.P.O.² based on a LiNbO₃ crystal³ itself pumped by a Nd:YAG laser (figure 1).

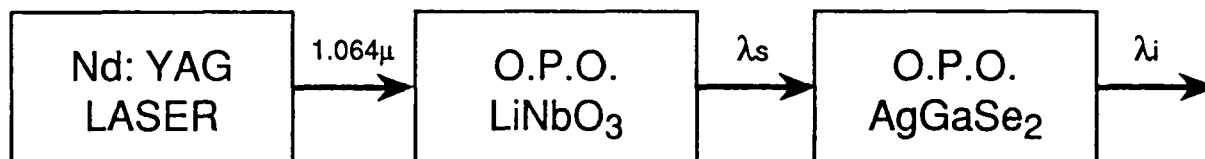


Figure 1: Synoptic scheme of the experiment
 λ_s is the signal beam of the first OPO
 λ_i is the idler beam of the second OPO

The Nd:YAG source is a Q-Switch laser producing pulses with a FWHM of 20 ns at a repetition rate of 50 Hz. The laser oscillates in a single spatial mode with a beam waist of 1.6 mm. The first O.P.O. uses a 5 cm long LiNbO₃ crystal. It is cut to be phase-matched at degeneracy ($\theta = 47^\circ$), i.e. to produce 2.12 μm beams. The threshold measured experimentally is 8 mJ, what is in good agreement with theory⁴.

The maximum pump energy per pulse is 40 mJ. At this pumping level, a depletion of 54 % is measured (figure 2). The maximum available energy in the signal is then 10 mJ.

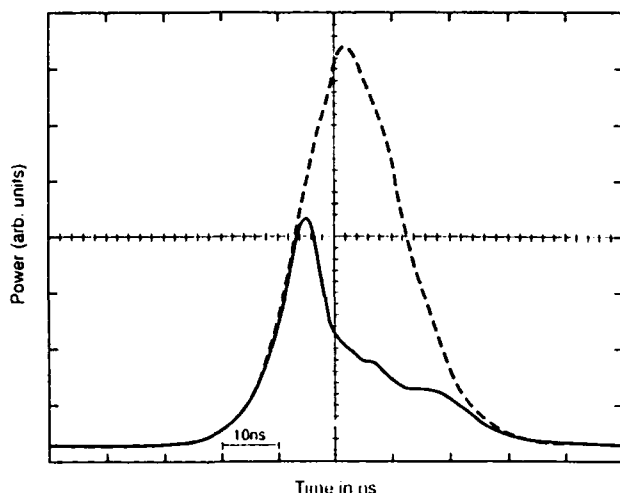


Figure 2: Depletion of the pump through the first O.P.O.

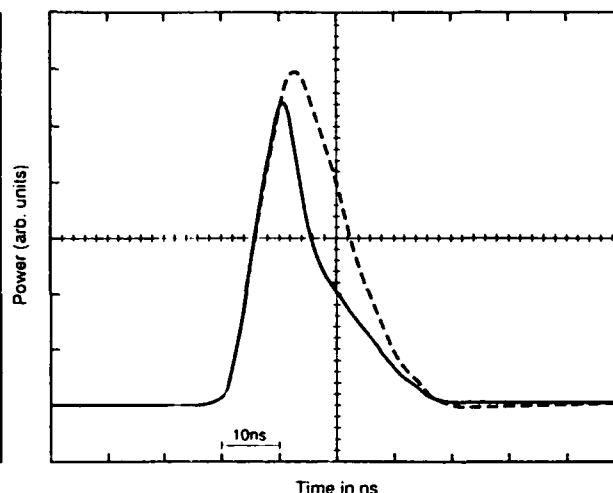


Figure 3: Depletion of the pump through the second O.P.O.

A tunability has been observed between 1.44 and 4.1 μm . The limitation comes from the lack of transparency of the crystal for wavelengths exceeding 4.1 μm . The spectrum of the signal has a FWHM of 2.7 nm. The time duration of the outcoming pulse is 15 ns.

The AgGaSe_2 crystal used in the second O.P.O. has a length of 25 mm. One major advantage of pumping with an O.P.O. is that the wavelength of the pump can be tuned to optimize the efficiency conversion at the desired wavelength. This optimum pump wavelength has been found to be 1.82 μm .

The maximum energy obtained from the second O.P.O. is 600 μJ (signal and idler) at $\lambda_s=2.6 \mu\text{m}$ and $\lambda_i=6 \mu\text{m}$ for a pump energy of 10 mJ at 1.82 μm . This corresponds to a conversion efficiency of 6%. The pump depletion (figure 3) is found to be 27%. The energy in the Nd:YAG pulse is 40 mJ giving an overall efficiency of 1.5%.

One possible development of this device is to make it single-mode using injection techniques for example. A single-mode, tunable laser source could find important applications in spectroscopy. Another improvement is to replace the standard Nd:YAG laser we have used by a diode pumped Nd:YAG laser since these latter can now produce high energy pulses [5],[6].

References:

- [1] R.C. Eckardt, Y.X. Fan, R.L. Byer, C.L. Marquardt, M.E. Storm and L. Esterowitz Appl. Phys. Lett. **49**, 608 (1986).
- [2] D. Guyer, C. Hamilton, F. Braun, D. Lowenthal and J. Ewing, in *Conference on Lasers and Electro-Optics*, Vol. 10 of 1991 OSA Technical Digest Series (Optical Society of America, Washington, D.C., 1991), paper CPDP6.
- [3] R.L. Herbst, R.N. Fleming and R.L. Byer Appl. Phys. Lett. **25**, 520 (1974).
- [4] S.J. Brosnan and R.L. Byer IEEE J. Quantum Electron. **QE-15**, 415 (1979).
- [5] L.R. Marshall, A. Kaz and R.L. Burnham Opt. Lett. **17**, 186 (1992).
- [6] L.R. Marshall, A. Kaz and R.L. Burnham, in *Conference on Lasers and Electro-Optics*, Vol. 12 of 1992 OSA Technical Digest Series (Optical Society of America, Washington, D.C., 1992), paper CWQ2.

Tunable Red Solid State Laser

Author: Ian Lee
 McDonnell Douglas Electronic Systems Co
 Mailcode 111 1151
 P.O. Box 516
 St. Louis Mo 63166
 Tel: 314 232 3702

We have produced a tunable red laser emission using SFM to combine the output of an OPO with the residual Nd:YAG pump beam.

The KTP OPO is pumped by an electro-optically Q switched multimode diode array pumped NdYAG oscillator. The pump laser operated at 2Hz with an output energy up to 110mJ. The output pulse had a FWHM duration of 13ns and a divergence of 2mR in a 5x5 mm beam. The beam area was reduced using a x2 reduction scope to increase the intensity to the $+100\text{MWcm}^{-2}$ level.

The KTP OPO was an x-axis cut, $\theta = 90^\circ$, $\phi = 0^\circ$ which we'll call an xz cut (θ , ϕ is angle to z and x axis respectively). The xz cut crystal provided a NonCritical Phasematch (NCPM) condition with broad angular and thermal acceptance bandwidths for the device. This cut also has a high effective nonlinear coefficient (d_{eff}) providing a low threshold energy, in our case 48mJ. We achieved 25mJ output at $1.57\mu\text{m}$ with 105 mJ input at 120MWcm^{-2} , which is 24% conversion efficiency. The OPO output had a pulse width of 10ns FWHM. The output shot to shot stability was $\pm 10\%$ at these pump levels. The line width was $\sim 3\text{nm}$ FWHM.

The output from the OPO consisted of both $1.57\mu\text{m}$ and $1.064\mu\text{m}$ energy in the same polarization state. Waveplates were used to make these polarizations orthogonal before pumping the SFM crystal. We had predicted a type II phase match condition in KTP at $\theta = 63^\circ$, $\phi = 0^\circ$ which provides a d_{eff} comparable with Type II SHG for 1.064nm . The crystal was 14.5 mm in length and uncoated leading to high Fresnel losses. We have calculated an optimum length of 5mm to minimize phase effects with our pump beam conditions. The d_{eff} is high enough that efficient conversion can still be obtained with this length of crystal. The other factor that determines the efficiency of the process is the photon ratio between the 1.57 and $1.064\mu\text{m}$ beams, ideally we want a photon ratio of 1:1. However as these photons are of different frequencies we require more energy in the $1.064\mu\text{m}$ beam. We have calculated that a 65% to 35% energy ratio for the 1.064 and $1.57\mu\text{m}$ beams respectively gives a good photon

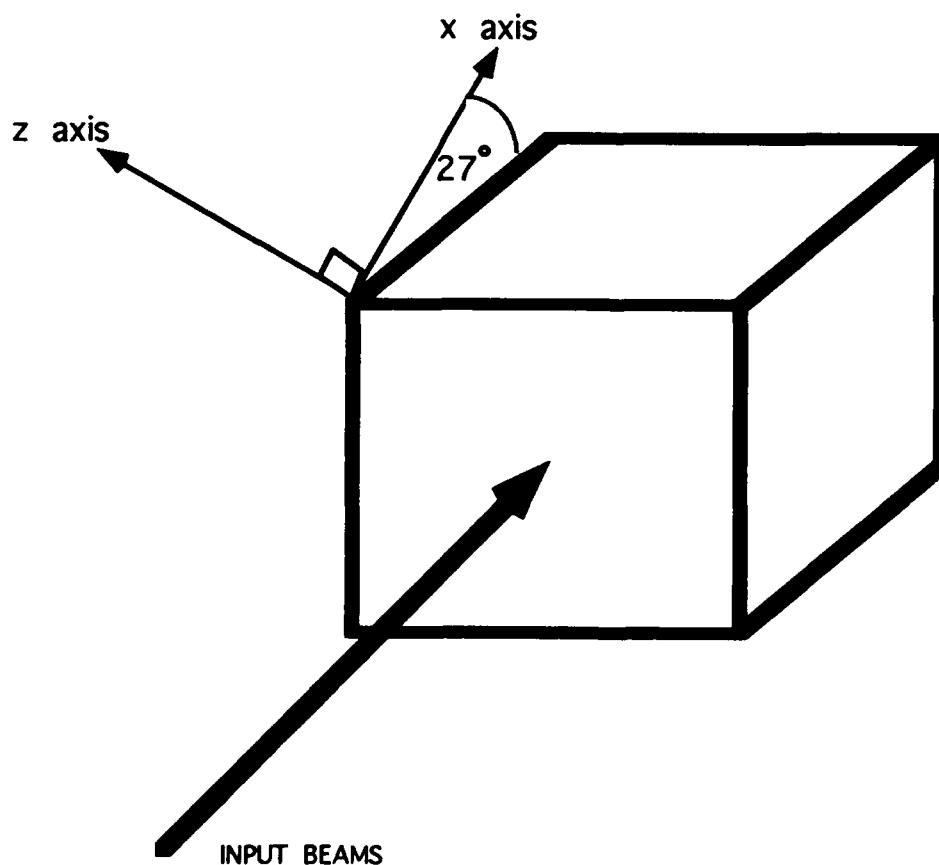
ratio. We have demonstrated 31% conversion efficiency in our 1.57 μm monolithic OPO which approaches the ideal photon ratio.

In our initial experiment we have only a 24% conversion efficiency in the OPO leading to a large photon imbalance. Due to our input divergence of 4mR we also had a crystal which is longer than its' coherence length. Under these conditions we observed an output energy of 9.6 mJ from an initial 1.064 μm energy of 105mJ. After accounting for Fresnel losses we had an internal conversion efficiency of 11.2%. The output was temporally stable with a FWHM pulse width of 10ns.

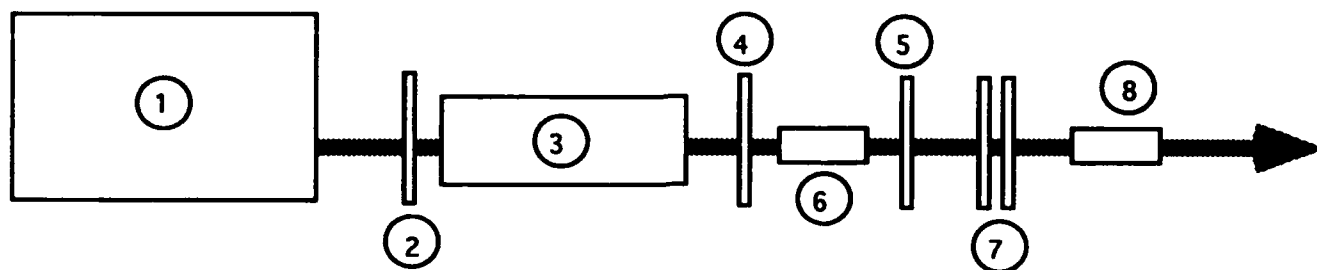
We have calculated that with a low photon imbalance and our current beam divergence that with a 5 or 6mm long crystal pumped at 150 MWcm^{-2} conversion efficiencies of 40% can be expected.

The OPO output is tunable and we can tune the output from the Sum Frequency Mixer in the red, the tuning range will be small, around 10nm, but this may be useful for certain applications.

Diagram of KTP SFM crystal



SCHEMATIC OF LAYOUT FOR SUM FREQUENCY MIXING IN KTP



1/ NdYAG LASER (PUMP LASER) @ 1064nm

2/ 1064nm 1/2 WAVEPLATE

3/ BEAM REDUCTION TELESCOPE OR FOCUSING OPTICS

4/ HR1.54-1.57um AR 1064nm MIRROR

5/ ~50%R 1.54-1.57um AR 1064nm MIRROR

6/ KTP OPO CRYSTAL CUT FOR 1.57 OR 1.54um OPERATION

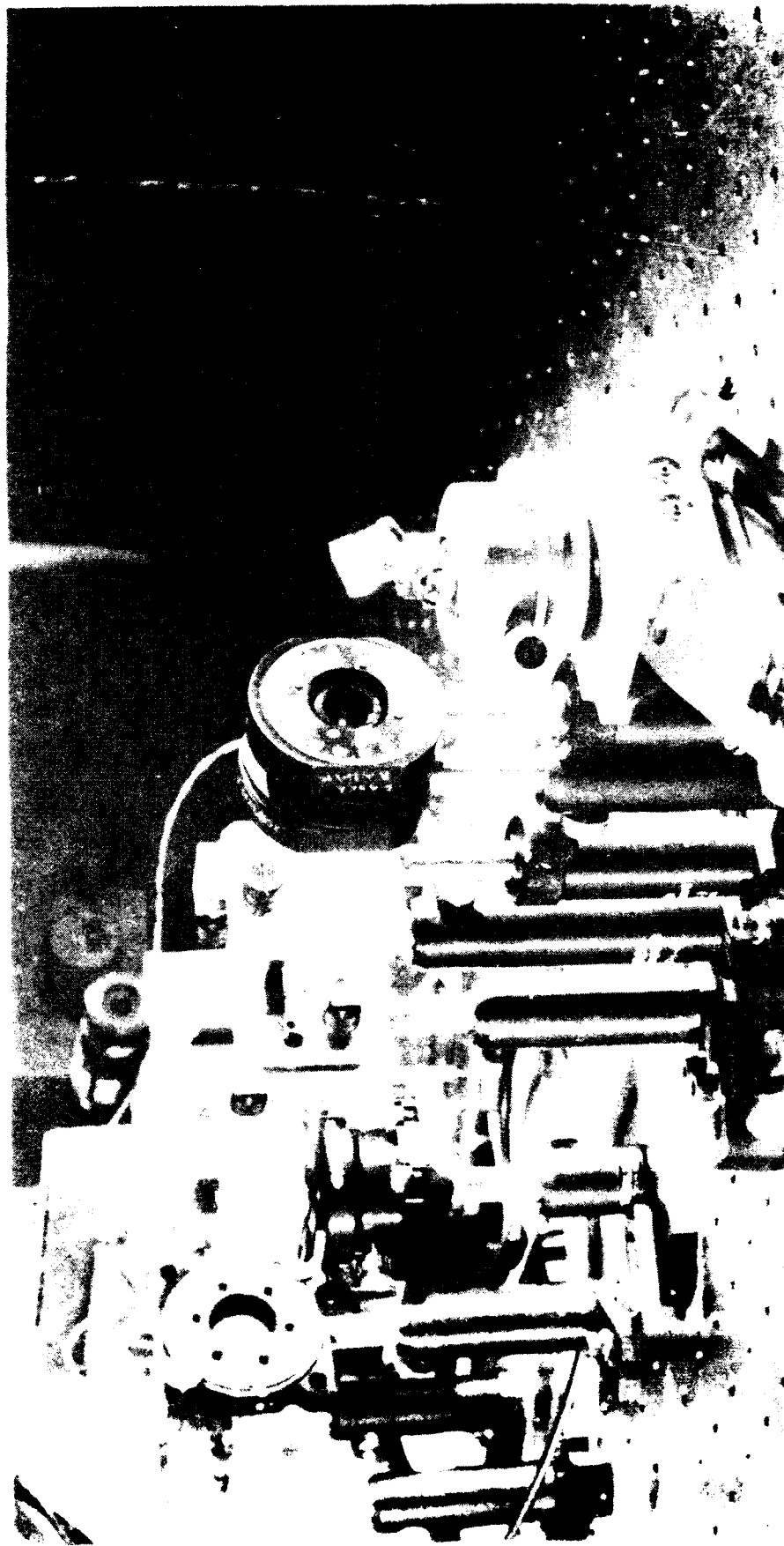
7/ WAVPLATES 1/2 WAVE@ 1.54&1.57um 1/4 WAVE @ 1064nm

8/ KTP CRYSTAL CUT PHI=0 THETA = 63 DEGREES

634nm SFM Laser

192753

MDESC-L&ES



All Solid state approach to wavelength diversity which provides pulsed laser output at 634nm. The system uses a standard diode pumped Nd:YAG oscillator to produce 1064nm output. This output is converted to 1570nm using an Optical Parametric Oscillator (OPO). The OPO output, along with the residual 1064nm beam, is converted to 634nm using Sum Frequency Mixing in a second crystal. Anticipated conversion efficiency of the 1064nm to 634nm is 40%

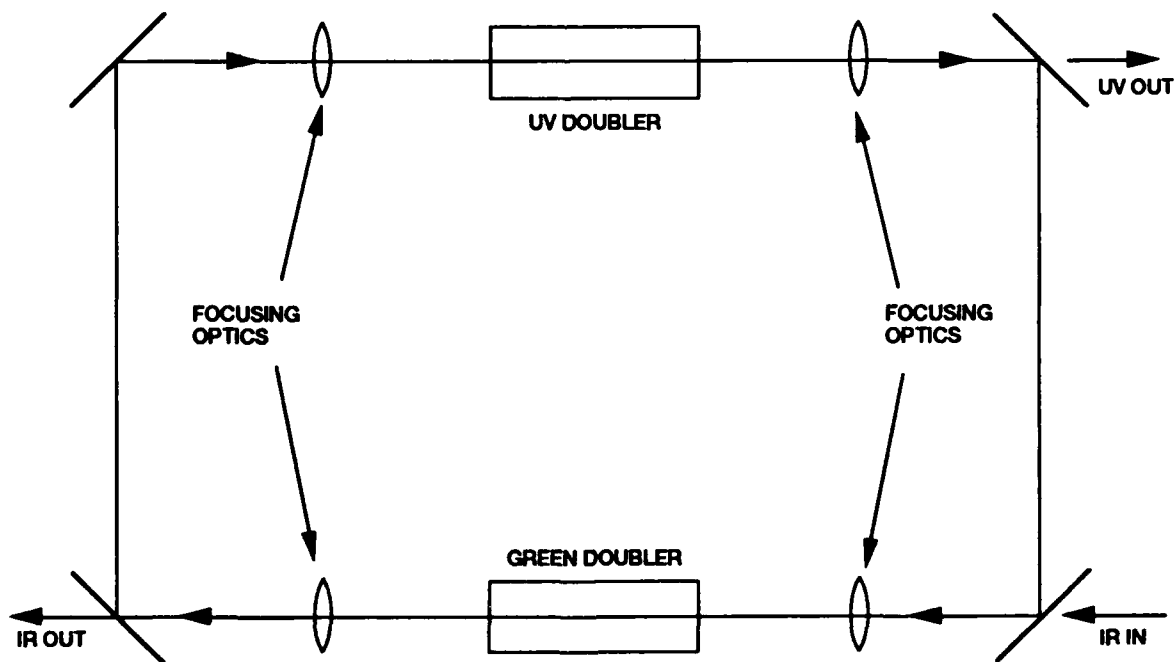
McDonnell Douglas Electronic Systems Company

Diffractive Analysis of an External Resonant Ring for Quadrupling Nd Lasers

M. S. Bowers, S. C. Tidwell, J. F. Seamans, and D. D. Lowenthal
STI Optronics, Inc.
2755 Northup Way, Bellevue, Washington 98004-1495
(206) 827-0460

A new technique for generating high-power ultraviolet radiation from a cw mode-locked Nd laser was proposed¹ and recently demonstrated in our laboratory for the first time. In this scheme, the infrared radiation is frequency doubled in a nonlinear crystal placed in a ring cavity that resonantly enhances the generated green light (see Fig. 1). Within the ring, a second nonlinear doubling crystal converts some of the green light into the UV. The remaining green light continues to propagate around the ring where it enhances IR to green conversion provided that the ring length is adjusted to allow the waves to add coherently. This technique promises to provide much higher UV power levels than have previously been available in commercial cw lasers and may have a far-reaching impact on many applications including basic research, photolithography, and material processing.

Previous analysis¹ of the performance of this scheme has shown that by circulating high power levels of green light in the ring, UV radiation can be generated with high efficiency. This analysis assumed that the laser beams are flat in space and time so that the efficiency of the process can be calculated by following single rays. However, in reality the beams must be tightly focussed into the nonlinear crystals, and therefore, one would expect that diffraction in the second harmonic generation process and ring propagation effects are important in determining the buildup of the green light in the ring and the sensitivity of the ring to various parameters, such as IR spot size versus the green cavity mode size, cavity length, and UV doubling crystal nonlinear drive.



92 20828

Figure 1. Schematic of the resonant ring for converting IR light into the UV. The green light generated internal to the ring is resonated.

In this paper, we describe a model for the external resonant ring which includes diffraction and depletion in the SHG process, and the effects of propagating around the ring. The calculations start with a Gaussian IR beam introduced into the doubler, and the generated green beam is computed taking into account diffraction and depletion. The generated green is then propagated to the UV generating crystal using knowledge of the $ABCD$ matrix elements for the propagation. The doubling of the green to UV is then computed, again with full diffraction and depletion, and the residual green is then propagated around back to the green doubling crystal. The green beam is then adjusted for passive cavity losses and multiplied by a phase shift (e^{-ikL}) for propagating through the ring length L . This green beam is then combined with the next IR pulse in the green doubling crystal and new green is generated. If the phases of the IR and green which enter the doubling crystal are properly matched, this process will generate more green light which is again propagated to the UV crystal. This process of propagating the green light around the ring is iterated to simulate the buildup of the green beam in the ring.

Sample results from the computer simulation are shown in Figs. 2 and 3. In Fig. 2, the IR depletion efficiency

is shown as a function of the number of round trips in the ring for different values of the ratio of the IR input beam spot size to the green beam bare cavity mode size. The cavity length for each case was adjusted for maximum efficiency and a 10% passive loss per round trip was assumed. The UV crystal was detuned so that no UV was being generated. For all three IR beam sizes, the ring came to a steady state, which means that the resonated green beam settled into a single transverse mode which reproduced itself on successive round trips. The highest IR depletion is obtained when the IR spot size is matched to the green cavity mode size. When the IR spot size is increased or decreased by a factor of 2, the IR depletion is much lower. Examination of the resultant steady-state green beam shows that it is nearly Gaussian in all cases with a spot size nearly the same as the bare cavity mode of the ring. This is because the fundamental Gaussian mode of the ring resonator is more closely phasematched to the input IR beam which is also Gaussian. Thus, the SHG process discriminates extremely well against higher-order transverse modes of the ring cavity.

The recirculating green wavefront must have the correct phase relationship with the IR beam to maximize the green enhancement. If the two wavefronts are out of

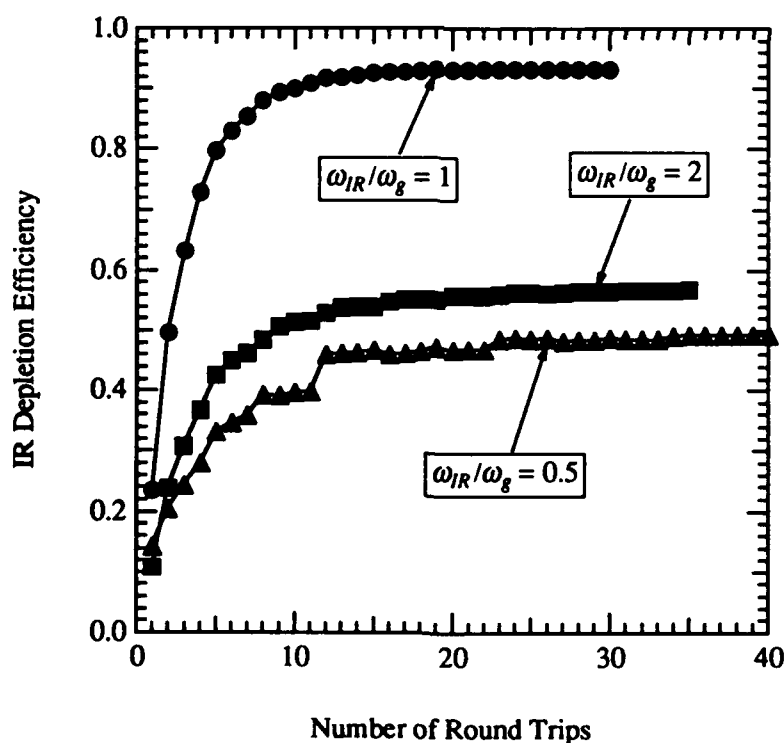


Figure 2. IR depletion efficiency for different ratios of the IR beam size to the green cavity mode size (ω_{IR}/ω_g). The ring parameters and crystal lengths are kept fixed.

phase from the optimum, back conversion of the green to the IR will occur in the SHG process. The amount of tolerable dephasing of the cavity length for different values of the single-pass ring loss is shown in Fig. 3. Even with 20% cavity loss, the length of the ring must be controlled to within a few hundredths of the green wavelength, which will require some active feedback stabilization. Assuming the proper phase relationships are maintained, the model predicts that IR to UV efficiencies as high as 75% can be achieved with 3% passive ring losses and 15% single-pass conversion of the green to UV. For this case, the circulating green power is quite large (~75 W), and since the single-pass conversion into the UV can be low short (i.e. 1-2 mm) UV generating crystals can be employed. The use of short crystals should reduce UV absorption and heating difficulties.

In conclusion, a model for an external resonant ring for quadrupling Nd laser radiation, which includes diffraction, depletion, and ring propagation effects, has been developed. The model shows that the process is stable and can lead to extremely high IR to UV conversion efficiencies, even with short UV crystals.

References

1. G. Giordano and G. Matone, *Nuovo Cimento* **12**, 927 (1990).

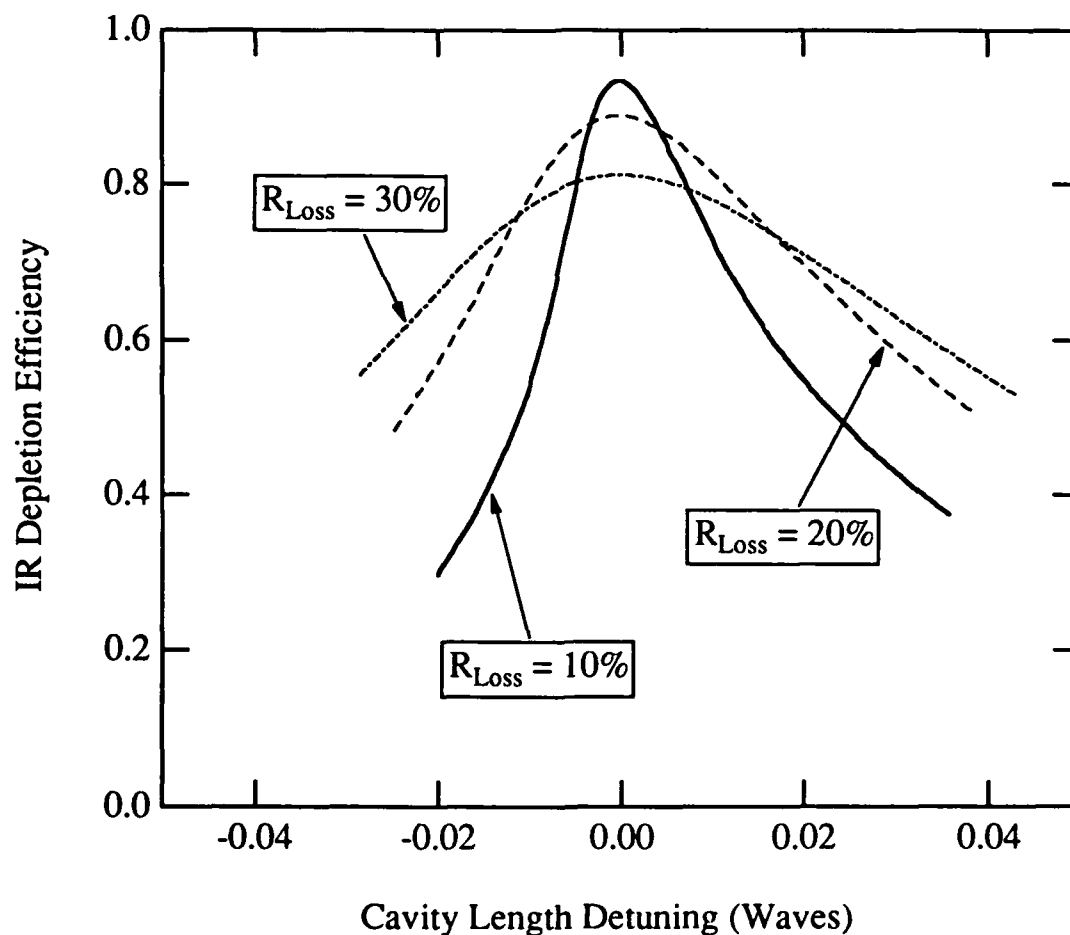


Figure 3. IR depletion is extremely sensitive to small changes in the cavity length.

Harmonic Generation of Tunable Lasers

Without any Adjustment

Harry Rieger*

Naval Command Control and Ocean Surveillance Center RDT&E Division (NRaD)

* on site contractor to NRaD by W. J. Schafer Associates Inc.
17127 Pomerado Way
San Diego, CA. 92128
Tel.: (619) 553-6244

Tunable solid state laser technology is making rapid progress. Development of tunable solid state materials such as Ti:sapphire and Cr:LiSAF/LiCAF combined with new broad band nonlinear materials such as BBO and LBO enable wavelength tunability from the UV to the IR.

Tuning a tunable laser from one wavelength to another requires adjustment of an intracavity filter either by electronics or mechanical means. In order to obtain the higher harmonics output, the nonlinear crystal requires proper adjustment of angle, temperature, or electrical field to meet the phase match conditions. Such adjustment require an operator or a sophisticated control system.

We have demonstrated a concept that provides harmonic generation without the need for any adjustment.

The concept for harmonic generation of wide band tunable lasers is based on the fact that the laser beam wavelength changes. By utilizing wavelength dispersing elements, the different wavelengths will have different angles, and since phase matching in nonlinear crystals can be done by angle tuning, all we have to do is match the wavelength dispersion of the dispersive optics to the angular wavelength dependence of the nonlinear crystal.

As an example, the angular tuning of a BBO type I doubler for phase matching between 900-1000nm is 2.2 deg. in the crystal; dispersive optics that provide such angular dispersion between 900 and 1000nm would eliminate the need for adjustment.

The angular dispersive element can be prisms or diffraction gratings. Gratings are relatively inefficient and may not have the required threshold damage for some laser beams, unless the beam was expanded. Prisms on the other hand can have very high damage threshold and high throughput especially at Brewster angle.

Different optical substrates have different indices of refraction dependence on wavelength. Most commercially available isosceles Brewster prisms would not provide sufficient angular dispersion. The options are: 1) using nonconventional materials with high index of refraction dependence on wavelength such as rutile $\text{TiO}_2^{(1)}$, 2) using sufficient number of prisms in series, or 3) magnifying the angular dispersion of commercially available prisms.

Figure 1 shows the optical set up that accomplishes proper angular magnification so that no adjustment is required for harmonic generation of a tunable pulsed Ti:S laser.

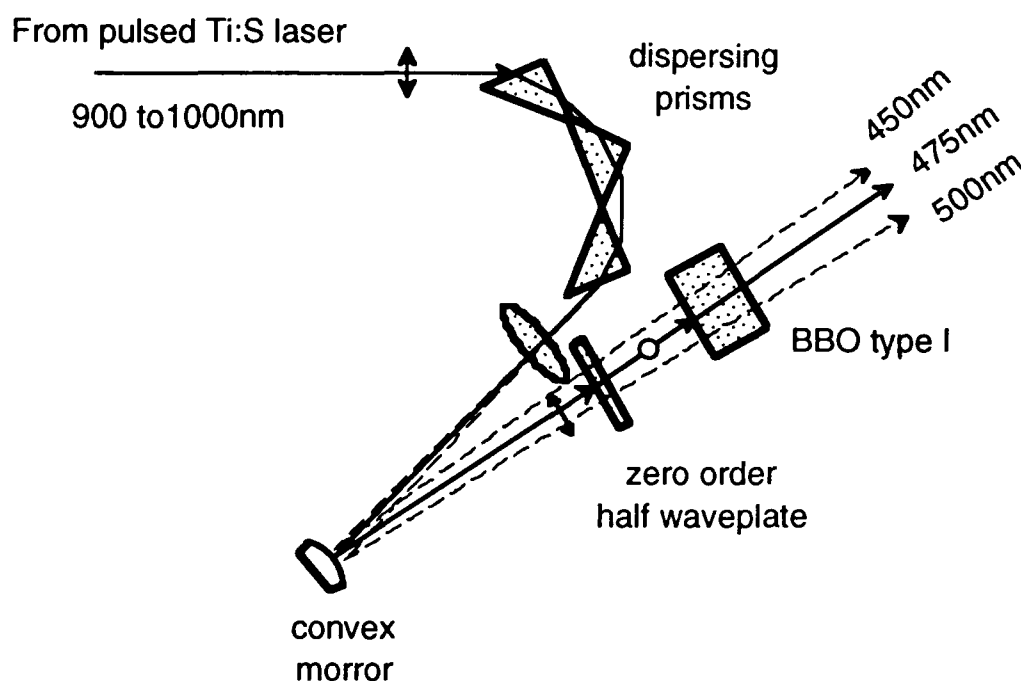


Figure 1 - Experimental set-up for tunable SHG without any adjustments

Three fused silica isosceles Brewster prisms in series provide only ~ 0.5 deg. dispersion between 900 and 1000 nm, compared to the ~ 3 deg. required for the BBO crystal (including the air interface). An angular magnification of ~ 6 is required to eliminate any adjustments. The angular magnification is accomplished by the convex mirror. The laser beam will hit a different point on the mirror at different wavelengths. A flat mirror will give a magnification of 1 at any distance from the prisms, larger magnification is obtained by smaller radius of curvature and/or larger distance from the

prisms. The fine adjustment of the magnification is made by adjusting the distance between the convex mirror and the prisms set. The convex mirror will also diverge the laser beam. The focusing lens will compensate for the divergence by the convex mirror to produce a collimated beam going into the BBO crystal. To minimize losses in the prisms, the beam polarization should be in the plane of the prisms, but in order to project the proper angle in the BBO type I crystal a zero-order (broad band) half waveplate is required to rotate the polarization by 90 deg.. One more issue must be considered; the aperture of the BBO must be sufficient to accommodate for the range of wavelengths (a practical system will require only few millimeters of aperture).

The pointing of the harmonic beam will vary with wavelength. For those applications that require pointing accuracy, a reverse process can be implemented to eliminate any angular variation with wavelength.

Efficient harmonic generation requires very well collimated and near diffraction limited beam, in addition to narrow linewidth. The above described set up can obtain efficient harmonics generation even for broad band beam since the spectrum angular divergence in the nonlinear crystal will meet the phase matching conditions of the entire beam bandwidth⁽²⁾.

References

- (1) J. Krasinski and A. Sieradzan, "An improved automatically tunable second harmonic generation of dye laser," Opt. Comm. 26, pp. 389-390, 1978
- (2) M. Skeldon, R. Craxton, T. Kessler, W. Seka, R. Short, S. Skupsky, and J. Soures, "Efficient harmonic generation with a broad-band laser," IEEE J. of Q.E. Vol. 28. No. 5. pp. 1389-1399, 1992

NUMERICAL SIMULATION AND REALISATION OF A KTP OPTICAL PARAMETRIC OSCILLATOR

J. M. BRETEAU, C. JOURDAIN, T. LEPINE, and F. SIMON

THOMSON-TRT DEFENSE/Optronics Division

rue Guynemer, BP 55, 78283 GUYANCOURT Cédex/FRANCE

Phone number : (33-1) 30 96 71 03

INTRODUCTION :

Since its first demonstration [1], the Optical Parametric Oscillator (OPO) has proved to be a very attractive tunable infrared source. Using Potassium Titanyl Phosphate (KTP) as nonlinear crystal, the Nd:YAG laser operating at $1.064 \mu\text{m}$ can be frequency shifted to eye safe wavelengths near $1.55 \mu\text{m}$.

The operation of the OPO is described by a set of three nonlinear, coupled differential equations [2]. These equations cannot be literally solved except for the threshold and the efficiency [3-5].

We have numerically solved coupled equations for a KTP OPO in the dynamic regime. Theoretical predictions are in very good agreement with experimental results.

SIMULATION :

In order to simplify the problem, we have assumed that :

- the pump, signal and idler beams are spectrally single mode,
- the intensity profile of the pump beam is uniform,
- the phase matching condition $\Delta k = 0$ is satisfied.

As initial conditions for the signal and idler beams, we have used the quantum fluctuations of the electric field in the vacuum [6]. For an OPO using a single crystal of KTP, $4 \times 4 \times 16 \text{ mm}^3$ in size and X cut for non critical type II phase-matching, inside a resonator consisting of two plane parallel mirrors, we have calculated the mirrors reflectivities at the three wavelengths of interest in order to optimize the output energy of the signal.

EXPERIMENTAL RESULTS :

We have used a flashlamp pumped Q-switch Nd:YAG laser as a pump source, supplied by BMI. This laser delivers $12.5 \text{ ns} - 50 \text{ mJ}$ pulses at a repetition rate of 50 Hz , in a quasi gaussian beam. The input mirror is AR at $1.064 \mu\text{m}$, HR at $1.579 \mu\text{m}$, and 50% reflective at $3.262 \mu\text{m}$. The output mirror is HR at $1.064 \mu\text{m}$, 83% reflective at $1.579 \mu\text{m}$, and 60% reflective at $3.262 \mu\text{m}$. Such values are close to the calculated reflectivities. For a pump power of 40 mJ , the OPO delivers more than 10 mJ at $1.579 \mu\text{m}$, which corresponds to an efficiency greater than 25% and a slope greater than 33% . The threshold is close to 10 mJ .

DISCUSSION :

The parameters which appeared to be very critical are :

- the KTP absorption at the three wavelengths of interest, which needed to be carefully measured for each crystal,

- the effective nonlinear coefficient d_{eff} . Theoretical and experimental investigations [7] have led to a value of 1.52 pm/V.

It should be noted that this simulation works without any adjustment parameter.

In figure 1, signal energy has been plotted versus pump energy, both for theoretical and experimental results. In figure 2 (resp.3), the pump and the transmitted pump (resp. the transmitted pump and the signal) are superimposed both for theoretical and experimental results. It can be seen that theoretical predictions are very close to experimental results.

CONCLUSION :

A numerical simulation of a KTP OPO has been developed. Predictions are in very good agreement with experimental results. It allows us :

- to predict the performances of the OPO in the dynamic regime (ie the temporal profiles and energies for signal and idler waves). This is the first time to our knowledge.
- to optimize the main parameters of the OPO.

We will report further results of these calculations, together with more experimental data.

REFERENCES :

- [1] J. A. Giordmaine and R. C. Miller, Phys.rev.lett, 14, june 1965.
- [2] Y. R. Shen, "The principles of nonlinear optics", Wiley InterScience.
- [3] S. J. Brosnan and R. L. Byer, IEEE J. Quantum Electronics, QE 15, n° 6, june 1979.
- [4] S. E. Harris, Proceedings of the IEEE, 57, dec 1969.
- [5] Laser handbook, edited by F. T. Arrechi and E. O. Schulz-DuBois, 1972.
- [6] C. Cohen-Tannoudji et al, "Photons et atomes", InterEditions/Editions du CNRS, 1987.
- [7] B. Boulanger et al, OEC'92, PD 7, July 1992, Tokyo.

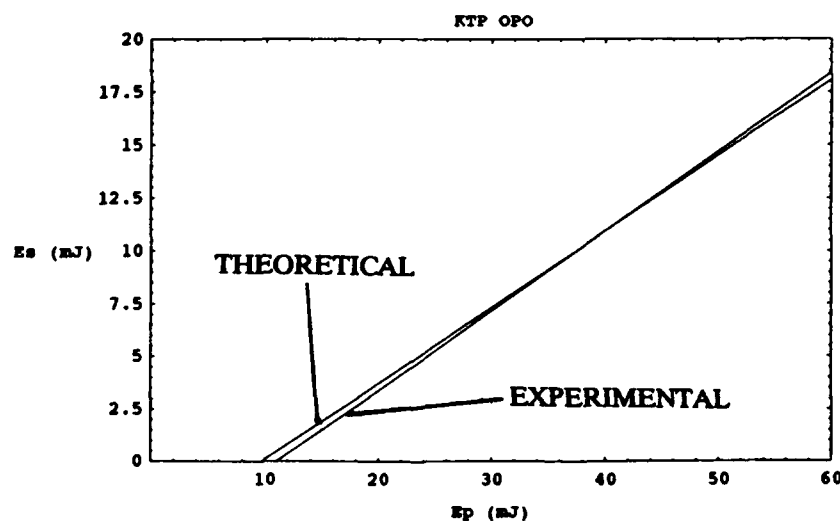


Figure 1 : signal energy vs. pump energy.

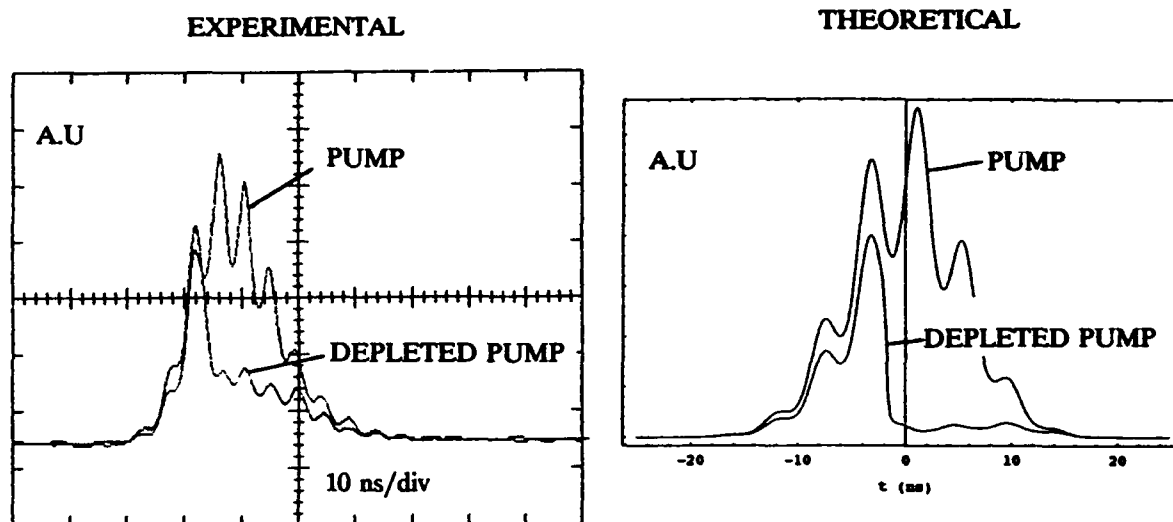


Figure 2 : the pump and the depleted pump
(the depleted pump is represented on an expanded scale)

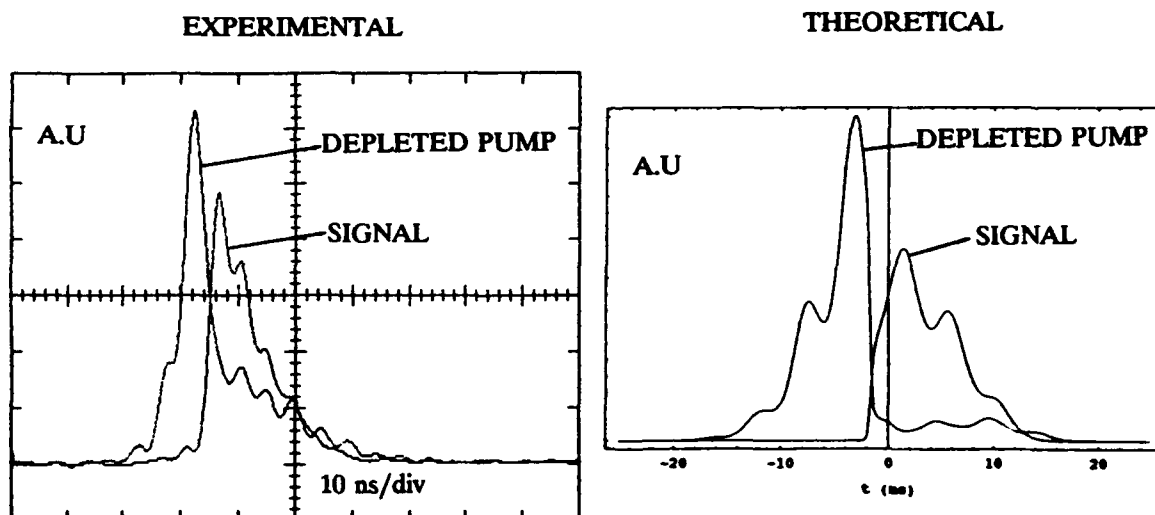


Figure 3 : the depleted pump and the signal
(the depleted pump is represented on an expanded scale)

Wavelength Diversity and Agility by Polarization Tuning of Stimulated Raman Conversion

K. V. Palombo, D. W. Mordaunt and E. Gregor
Hughes Aircraft Company, M.S. E1/B118
P. O. Box 902
El Segundo, CA 90245
310-616-5422

A number of requirements have been observed in recent years which require a laser source that exhibits either wavelength diversity or wavelength agility. Wavelength diversity may be defined as a multiple wavelength output derived from a single laser source. Wavelength agility, on the other hand, is the ability of a single wavelength source to change its output wavelength by a significant amount. Both of these features are suitable for diverse applications such as spectroscopy, remote sensing, speckle suppression, and laser countermeasures. We have previously used stimulated rotational Raman conversion of a frequency doubled Nd:YAG laser to demonstrate a broad wavelength output ranging from the green to the red portions of the visible spectrum.¹⁻³ This paper reports a patented technique⁴ which demonstrates both wavelength diversity and agility in a single device, using stimulated Raman conversion of a 532 nm frequency doubled Nd:YAG laser.

The basis for the device utilizes the polarization dependence of the rotational Raman gain. For a gaseous Raman medium such as hydrogen, at relatively low pressures of a few atmospheres, the stimulated rotational Raman gain is higher for circularly polarized pump light than for linearly polarized pumps. By optimizing the gas pressure and pump intensity, the pump polarization can be used to determine whether stimulated rotational or vibrational Raman will dominate the conversion process. With the appropriate choice of pump conditions, circularly polarized pump light will cause rotational Raman to dominate, while linearly polarized pump light will result in vibrational Raman scattering. Using a double pass Raman configuration provides higher efficiency of conversion and more flexibility in the choice of wavelengths produced. By adjusting the input pump polarization in the first pass, either rotational or vibrational Raman will occur. The polarization can then be changed between the first and second passes through the Raman medium. This allows the choice of producing only rotational Raman in both passes, only vibrational Raman in both passes or producing rotational scattering in one pass and vibrational scattering in the other.

The experimental set-up is shown in Figure 1. Two Raman cells filled with low pressure hydrogen (H₂) gas were used in tandem. A rotatable waveplate prior to each cell controlled the polarization within that cell. The high intensities required to achieve Raman conversion within the cells were achieved by focussing the energy within each cell. The linearly polarized 532 nm pump radiation was first passed through a rotatable $\lambda/4$ plate, and focussed into the first Raman cell with a spherical lens. The energy was then re-collimated with an identical lens. It then passed through a second rotatable $\lambda/4$ plate, and was focussed into the second Raman cell. After passing through this cell the beam was re-collimated again prior to being analyzed. Analysis of the wavelengths produced was performed with an Optical Multichannel Analyzer (OMA) consisting of a diffraction grating spectrograph which is used to illuminate a linear detector array.

The pump laser used in this work was a Nd:YAG phase-conjugated, master oscillator power amplifier (MOPA). The output of this laser is TEM₀₀ and is multi-longitudinal mode (consisting of approximately 5 modes). The 1064 nm output was frequency doubled to provide approximately 350 mJ at 532 nm with a 25 nsec FWHM pulse and approximately 1.5 times diffraction limited beam divergence.

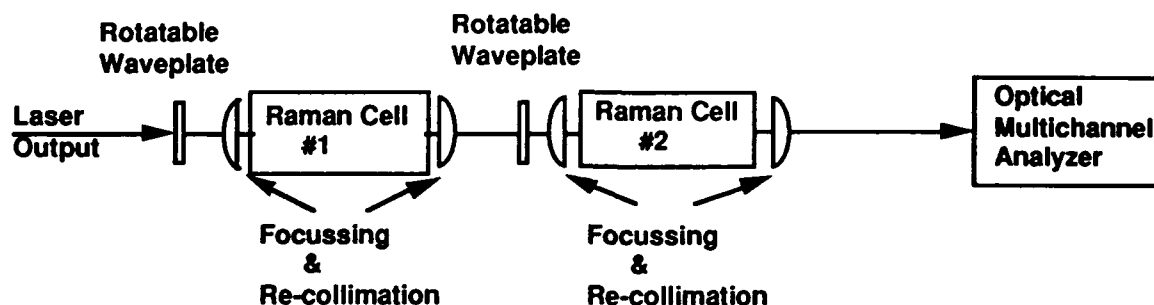


Figure 1. A continuously variable wavelength distribution was achieved by individually varying the polarization of the input to two Raman cells in a tandem configuration.

Pressure of the H₂ gas within the two Raman cells was optimized to produce the desired wavelength ranges. To achieve rotational Raman conversion the pressure in the Raman cells must be low, less than several atmospheres. At higher pressures, some vibrational Raman conversion occurs even with a circularly polarized input. To achieve purely rotational Raman conversion, the pressure in both cells was optimized such that it was as high as possible (for maximum gain), without creating significant vibrational Raman conversion for a circularly polarized pump. In this manner purely rotational conversion could be achieved with circular polarization, and good vibrational conversion could be achieved with linear polarization. The F# of the focussing lenses was optimized for high conversion efficiency and to avoid optical breakdown within the cells.

A continuously variable wavelength distribution was achieved by rotating the $\lambda/4$ plates prior to each cell, generating variable polarization conditions within the cells. Differing amounts of rotational and vibrational Raman conversion occurred for each polarization condition, thus generating the variable wavelength distribution. Table 1 shows the percentage of energy (in terms of % of input pump energy) present in each of the Raman lines. RS_x represents the "x"th rotational Stokes line, VS_y the "y"th vibrational line, and VS_y+RS_x the "x"th rotational shift of the "y" vibrational Stokes line. In each case the total equals approximately 85% of the input pump energy, since 15% of the energy is lost due to heating of the Raman medium and large angle scattering. In the first row of each column the polarization present in the first and then the second cell is indicated. The distributions in Table 1 are representative of what can be achieved with this method. By using various degrees of ellipticity of polarization, many more such distributions can be achieved. Figure 2 shows an example of the wavelength distribution for linear polarization in the first cell and circular polarization in the second cell. Figure 3 shows a distribution for elliptical polarization in the first cell and linear polarization in the second cell.

With circular polarization in the first cell, the output of that cell is primarily first, second and third rotational Stokes lines with some residual pump energy, although small amounts of higher order rotational lines are present. When the polarization in the second cell is also circular, further rotational conversion of these lines occurs, seeded by the small amounts of higher order lines. This allows greater conversion to higher orders, and a more uniform distribution over a broad wavelength range. When linear polarization is present in the first cell, the output of that cell consists of residual pump and first vibrational Stokes. Linear polarization in the second cell generates significant second vibrational Stokes, while circular polarization in the second cell allows some rotational conversion of the residual pump and first vibrational Stokes.

References

1. Greater than 90% Conversion Efficiency by Stimulated Rotational Raman Scattering in Hydrogen (H₂), E. Gregor, D. W. Mordaunt, and K. V. Strahm, Technical Digest for the Topical Meeting on Nonlinear Optics: Materials, Phenomena and Devices, Paper TP1, pages 90-91, IEEE Lasers and Electro-Optics Society, New York, 1990.

2. Rotational Raman Conversion into Five Wavelengths of Equal Intensity, E. Gregor, D. W. Mordaunt, and K. V. Strahm, in OSA Proceedings on Advanced Solid-State Lasers, Volume 6, ed. by H. P. Jenssen and G. Dube, pp. 342-349, 1991.

3. Efficient Rotational Raman Conversion in Hydrogen, Deuterium and Hydrogen/ Deuterium Mixes using a Phase Conjugated Pump Laser, E. Gregor, O. Kahan and D. W. Mordaunt, Technical Digest for the 1989 Conference on Lasers and Electro-Optics (CLEO), paper FD3, Optical Society of America, Washington D. C. (1989).

4. U. S. Patent Number 5,099,147, Raman Converter with Variable Wavelength Distribution, E. Gregor, D. W. Mordaunt and K. V. Strahm, issued March 24, 1992.

Table 1. Wavelength distributions achieved for several polarizations conditions. Energy is expressed as a percentage of the input pump energy. The first row of each column indicates the respective polarization conditions in the first and second cells which achieved the distribution shown.

Raman Line	Wavelength (nm)	% of pump Circular Circular	% of pump Circular Linear	% of pump Linear Circular	% of pump Linear Linear	% of pump Elliptical Linear
AS1	516	0	0	0	0	1.8
Pump	532	9.9	13	18.6	22.5	16.0
RS1	549	19	17.3	19.8	0	21.4
RS2	567	16.2	14.9	2.4	0	7.7
RS3	587	13.7	13.4	0	0	2.0
RS4	608	12.1	10.6	0	0	0.5
RS5	630	6.8	5.3	0	0	0.3
RS6	655	1.3	1.4	0	0	1.5
VS1	683	0.5	1.0	20.4	50	9.0
VS1+RS1	711	1.3	1.4	22.7	0	17.8
VS1+RS2	743	1.8	2.9	1.2	0	6.5
VS1+RS3	776	2.5	3.8	0	0	
VS1+RS4	813	0	0	0	0	
VS2	954	0	0	0	12.5	

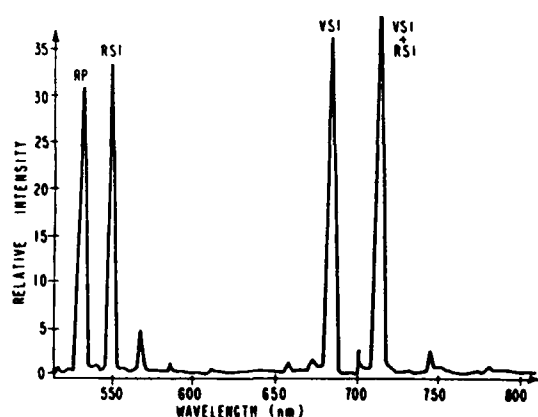


Figure 2. Wavelength distribution achieved with linear polarization in the first cell and circular polarization in the second cell.

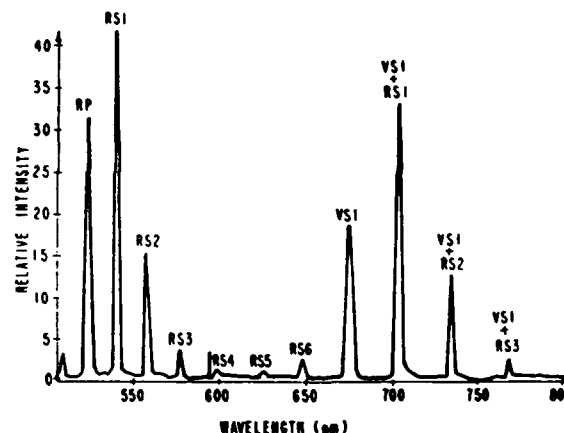


Figure 3. The wavelength distribution with elliptical polarization in the first cell and linear polarization in the second cell.

Injection-seeded tuning of a pulsed optical parametric oscillator: applications and performance

M. J. Johnson, J. G. Haub, and B. J. Orr

*School of Chemistry and Centre for Lasers & Applications,
Macquarie University, Sydney 2109, Australia*

Phone: 61-2-805-8289 / -8275; Fax: 61-2-805-8313

Optical parametric oscillator (OPO) devices, pumped by ns-pulsed lasers and based on gain media such as β -barium borate (BBO), enable coherent wavelength generation with high efficiency over a broad spectral range. This is demonstrated in Fig. 1, which shows the fundamental tuning range (0.41 – 2.6 μm) of a BBO OPO pumped by 355-nm pulsed laser radiation. Also shown in Fig. 1 is the extended ultraviolet tuning range ($\sim 0.2 - 0.4 \mu\text{m}$) attainable¹ by nonlinear-optical second-harmonic generation (SHG) or sum-frequency generation (SFG) in BBO, KDP, or KD*P. Difference-frequency generation (DFG) experiments in LiIO_3 are also in progress, aiming to extend the infrared tuning range out to $\sim 5 \mu\text{m}$.

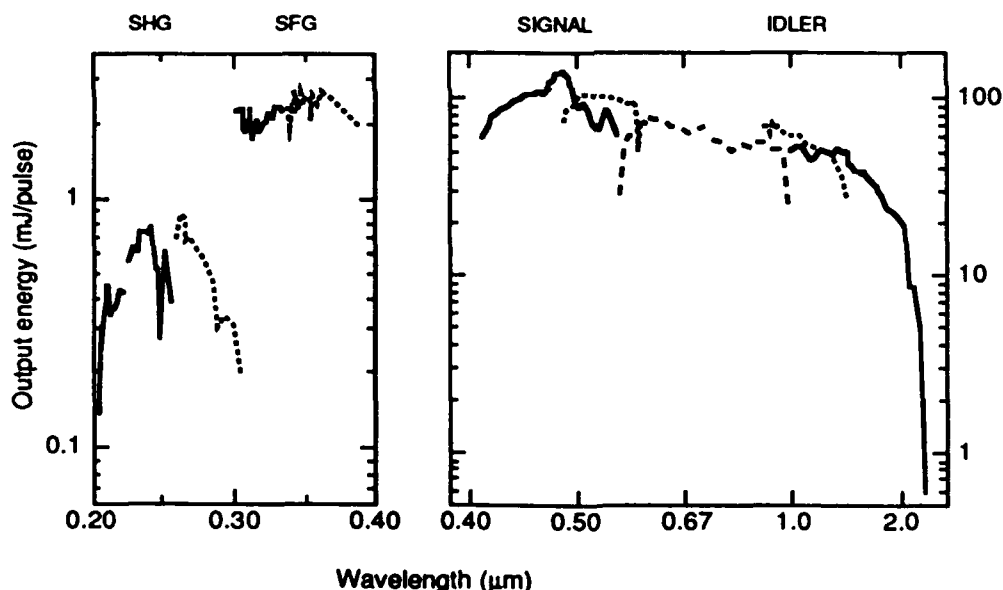


Figure 1: Tuning curves of a BBO OPO, with observed output energies displayed on logarithmic scales. The OPO signal and idler outputs are shown in the right-hand section, obtained with 355-nm, ≤ 315 -mJ, 5-ns pulsed pump radiation and yielding tens of mJ of OPO output for the fundamental tuning range (0.41 – 2.6 μm); these results were recorded in collaboration with A. Fix, T. Schröder, and R. Wallenstein of Universität Kaiserslautern, Germany. The left-hand section shows ultraviolet wavelength extension (0.2 – 0.4 μm) by SHG or SFG, with output energies in the mJ range obtained with an OPO signal pulse energy of ~ 10 mJ.

Many potential OPO applications require continuous narrowband tunability, which is typically achieved by a combination of active wavelength selection and cavity control. A straightforward alternative entails injection seeding of a singly-resonant OPO cavity, at either the signal or idler wavelength, with narrowband radiation from a low-intensity tunable laser, such as a dye laser² or a diode laser. The possibility that injection seeding might enable continuous narrowband tuning of the OPO signal and idler wavelengths has long been anticipated,³ but only recently realised.² This approach provides narrowband ($\sim 0.1 \text{ cm}^{-1}$) signal and idler outputs which can be scanned continuously in photoacoustic-absorption² and coherent-Raman⁴ spectroscopic experiments, without relying on intracavity etalons or gratings. An OPO-based apparatus for coherent anti-Stokes Raman spectroscopy (CARS) is shown schematically in Fig. 2. This can be used⁴ either for scanned CARS experiments, employing the injection-seeding method of OPO wavelength control, or for multiplex CARS experiments, relying on the intrinsically broad bandwidth of signal radiation from a free-running OPO.

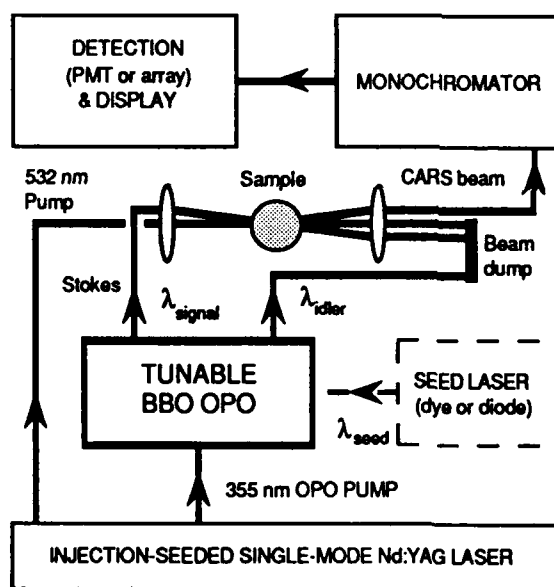


Figure 2: Schematic of a spectroscopic system for CARS measurements, using a tunable BBO OPO. A single-mode Nd:YAG laser generates both 355-nm OPO pump radiation and 532-nm Raman pump radiation. Visible OPO signal radiation (wavelength λ_{signal}) is the Raman Stokes beam, combined with the 532-nm Raman pump beam and focused into the sample zone, while the accompanying OPO idler radiation (λ_{idler}) is rejected. The anti-Stokes beam generated by the CARS process is detected by a monochromator and a photomultiplier (for scanned CARS) or a photodiode array (for multiplex CARS). In scanned CARS, the BBO output wavelengths are controlled (see dashed portion) by injection seeding at either the signal or idler wavelength, with narrowband radiation (λ_{seed}) from a tunable seed laser.

Detailed theoretical and experimental investigations of the mode of operation of an injection-seeded BBO OPO are also underway. Computer simulation of a pulsed, injection-seeded OPO, based on an earlier CW model,⁵ reproduces much of the observed performance of our BBO OPO. The model numerically solves a set of coupled first-order rate equations depicting the time evolution of all fields (single-mode pump, multimode signal and idler) in the OPO cavity. It satisfactorily simulates phenomena such as pump depletion, OPO output pulse

shapes and seed-induced spectral narrowing. As anticipated,³ injection seeding lowers the threshold for OPO operation and reduces the output pulse build-up time, causing the OPO wavelength to favor the cavity mode(s) closest to the seed wavelength. As illustrated in Fig. 3, the model indicates how the OPO signal or idler wavelength follows that of a continuously scanned seed source, with minimal adjustment of BBO crystal angle. It also guides optimisation of injection-seeding parameters, such as choice of seed power and temporal overlap of the seed pulse with the pump pulse, and allows examination of the interesting intermediate regime between strong seeding and free-running OPO operation.

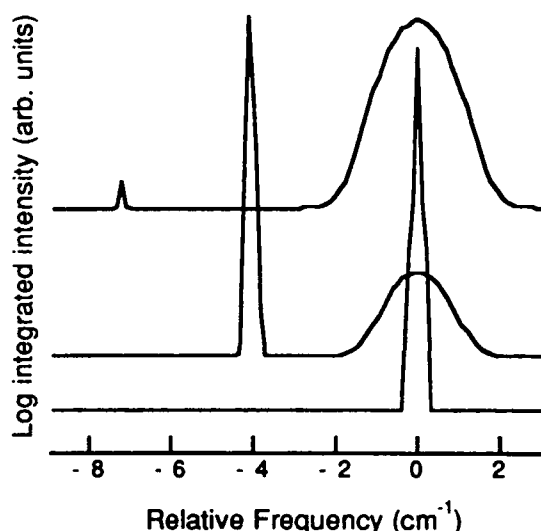


Figure 3: Model-based tuning curves for an injection-seeded OPO, showing output intensity (on a logarithmic scale) as seed wavelength is scanned. Pump and seed pulses have 6-ns-FWHM gaussian time-profiles and peak intensities 4.0 and 0.035 times the OPO threshold, respectively. Bandwidths of the seed radiation and the OPO gain profile are 0.20 and 2.5 cm^{-1} FWHM, respectively; the OPO cavity has a longitudinal mode spacing of 0.12 cm^{-1} and plane-waves are assumed. When the seed is tuned to the centre of the OPO gain profile, as in the bottom trace, strong seeding results and 100% of the OPO output is narrowband. Tuning the seed 4.0 cm^{-1} away from gain centre, as in the middle trace, causes 10% of the OPO output to be broadband. With a frequency separation of 7.2 cm^{-1} , as in the top trace, 99.8% of the OPO output is broadband. These results are sensitive to various operating parameters, and effectively emulate the performance of our BBO OPO.

References

1. J. G. Haub, M. J. Johnson, H.-D. Barth, and B. J. Orr, "Tunability of an optical parametric oscillator by injection seeding: nonlinear-optical and spectroscopic applications," in *Nonlinear Optics: Materials, Fundamentals, and Applications Technical Digest, 1992* (Optical Society of America, Washington, D.C., 1992), Vol. 18, pp. 427 - 429.
2. J. G. Haub, M. J. Johnson, B. J. Orr, and R. Wallenstein, *Appl. Phys. Lett.* **58**, 1718 (1991).
3. J. E. Bjorkholm and H. G. Danielmeyer, *Appl. Phys. Lett.* **15**, 171 (1969); Y. X. Fan, R. C. Eckardt, R. L. Byer, J. Nolting, and R. Wallenstein, *Appl. Phys. Lett.* **53**, 2014 (1988).
4. M. J. Johnson, J. G. Haub, H.-D. Barth, and B. J. Orr, "OPO CARS: rotationally resolved coherent anti-Stokes Raman spectroscopy using a tunable optical parametric oscillator," submitted to *Opt. Lett.* (August 1992).
5. E. S. Cassedy and M. Jain, *IEEE J. Quant. Electron.* **15**, 1290 (1979).

Monday, February 1, 1993

Nonlinear Frequency Conversion 2

AMF 4:00pm–5:30pm
La Salle Ballroom B&C

Charles L. Marquardt, *Presider*
U.S. Naval Research Laboratory

Novel Resonant Ring for Converting the Output of a Mode-Locked IR Laser into UV Light With High Efficiency

S. C. Tidwell, J. F. Seamans, and D. D. Lowenthal

STI Optronics, Inc., 2755 Northup Way
Bellevue, Washington 98004-1495 (206) 827-0460

G. Matone and G. Giordano

Istituto Nazionale Di Fisica Nucleare
Laboratori Nazionali di Frascati
Rome, Italy

There are a number of applications, including photolithography, materials processing, and basic research, which would benefit from the development of a reliable high-power UV source. The objective of the current work is to develop an efficient all-solid-state UV source which produces over 5 W using a commercial Nd:host drive laser.

Previous workers have used two external cavities in series to obtain the fourth-harmonic of high-power cw [1] and mode-locked Nd lasers [2]. Although very high efficiencies have been obtained in the first SHG cavity overall IR to UV conversion efficiencies have been less than 1% due to losses between cavities and in the UV conversion cavity.

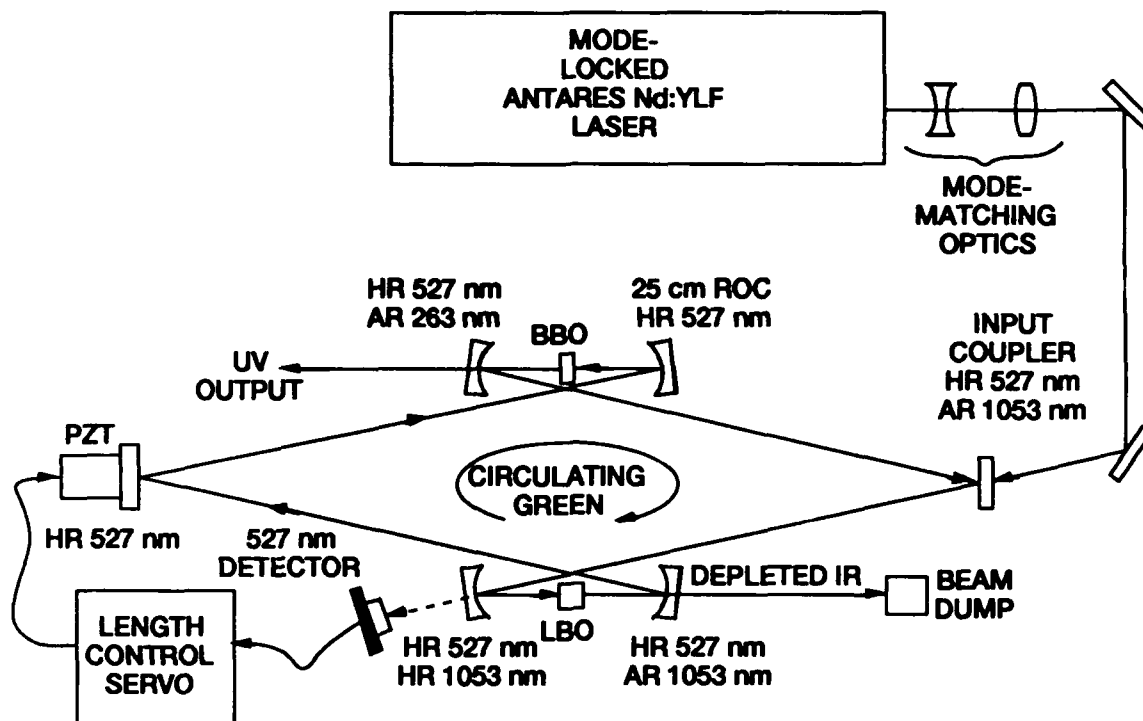
A new approach was recently proposed for generating forth-harmonic light which uses two nonlinear crystals in a single-resonant cavity [3]. A mode-locked IR laser is used to produce the second-harmonic light in a single pass through the first doubling crystal. The green light is then resonated in the external cavity and the residual IR light is discarded. The length of the resonant ring is such that the resonated pulse overlaps the next IR pulse in the mode-locked train. The presence of circulating green light which is in phase with the IR drive pulse greatly enhances the conversion of IR to green. In our experiments, the SHG efficiency increases from approximately 17% to greater than 70% when the green power is resonant. The forth-harmonic is then generated in a second crystal in the cavity and immediately coupled out.

The experimental setup we use is shown schematically in Figure 1. The drive laser is a mode-locked Antares Nd:YLF laser which produces 15 W with a wavelength of 1.053 μm , a repetition frequency of 76 MHz, and a pulse length of 50 ps. Mode-matching optics are used to spatially overlap the IR beam with the cavity mode in the LBO crystal. The IR beam is injected into the ring through

a mirror which transmits 84% of the IR beam and reflects greater than 99.7% of the circulating green beam. Within the 3.95-m ring the doubling and quadrupling crystals are both located between pairs of 25-cm ROC mirrors. The waist sizes for the IR and green beams in the LBO crystal and the green beam in the UV crystal are all 40 μm . The LBO crystal is 15 mm in length and cut for type I noncritical phase matching at 166°C. Experiments have been done with AR-coated and Brewster's angle KDP and BBO crystals for generating the UV light. The results reported here were obtained with an AR-coated BBO crystal 2 mm thick. The UV light is transmitted through a dichroic mirror ($T_{\text{uv}} > 90\%$) and the green light is reflected back to the input coupler to combine with the next IR input pulse. Round-trip cavity losses are approximately 3% for the green light.

Initial attempts to lock the length of the external ring to the Antares resonator using an amplitude modulation technique have been unsuccessful due to the high bandwidth (approx. 10 kHz) required for the servo. We believe that this ring can be successfully locked using the Pound-Drever method although interesting differences result from the fact that we do not resonate the injected light. Our data has been acquired during free-running operation, when the two cavities are drifting in and out of phase with respect to one another at random. Figure 2 shows signals from detectors monitoring the depleted IR, circulating green, and output UV powers as the cavities drifts through resonance. It is evident that the cavity reaches steady state because the pulses have flat tops and also because the duration of the flat region (approx. 600 μs) is much longer than the cavity buildup time (approx. 300 ns).

The efficiency of converting the IR to UV is the product of the IR input efficiency, the IR depletion, and the



92 20827

Figure 1. Schematic of fourth-harmonic generating resonant ring.

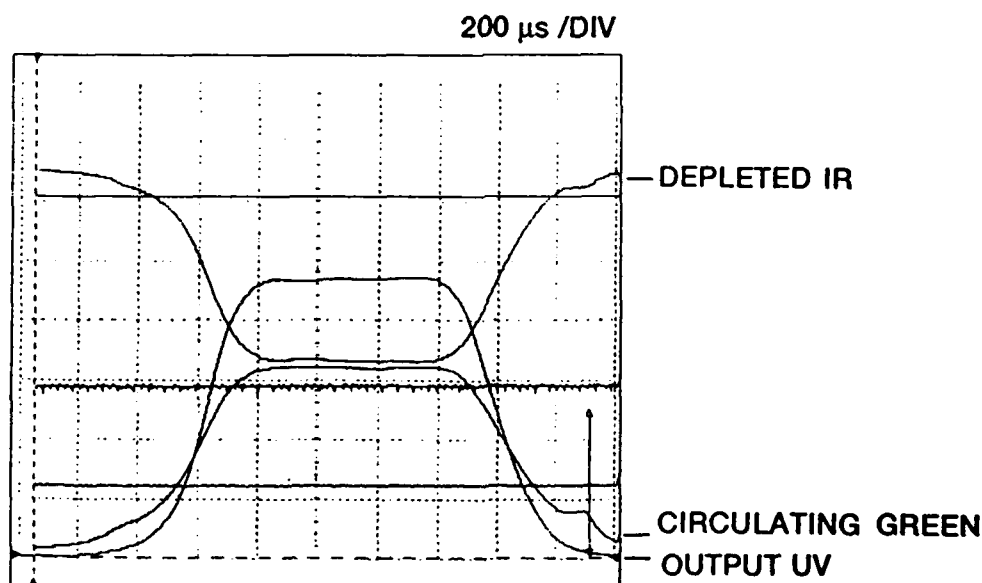


Figure 2. Detector signals show how power in the three wavelengths change as resonators drift through resonance.

UV output efficiency. The efficiency with which the IR light is transmitted to the LBO crystal is 79%. With circulating powers between 60 W and 93 W we measure IR depletions between 70% and 75%. Finally, with 3% fixed loss and a 2-mm thick AR-coated BBO crystal cut for type

I doubling to 263 nm, the UV output efficiency is greater than 60% for the circulating powers given above. Thus, at an IR drive power of 15 W the overall conversion efficiency to UV power is approximately 30% and, as shown in Figure 3, the slope efficiency is 39%.

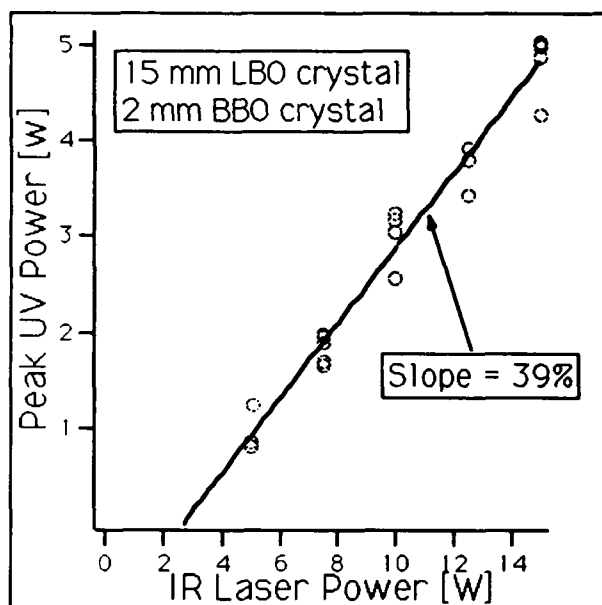


Figure 3. UV output powers greater than 5 W have been produced with a 15-W IR input for an overall conversion efficiency greater than 30% and a slope efficiency of 39%.

References

1. Christopher C. Pohalski, private communication.
2. G. P. A. Malcolm, M. A. Persaud, and A. I. Fergusson, *Opt. Lett.* **16**, 983 (1991).
3. G. Giordano, and G. Matone, *Il Nuovo Cimento* **12**, 927 (1990).

Recent Advances in ZnGeP₂ Mid-IR Optical Parametric Oscillators

P.G.Schunemann, P.A. Budni, M.G. Knights, T.M. Pollak
and E.P. Chicklis
Lockheed Sanders, MER15-1813, P.O.B. 868, Nashua NH 03061-0868
(603) 885-3010

C.L. Marquardt
Naval Research Laboratory, Code 6550, Washington DC 20375
(202) 404-8611

INTRODUCTION

ZnGeP₂ is currently one of the most promising nonlinear optical materials for efficient frequency conversion into the mid-IR spectral region¹. Because of its exceptionally high thermal conductivity² and virtual absence of thermal lensing³, ZnGeP₂ is a viable material choice for many applications requiring high average powers and high pulse repetition frequencies. In the past, applications involving 2- μ m pumping have been hampered by the presence of a large stoichiometry-related absorption near the band edge. Recently however, an intensive effort in ZnGeP₂ crystal growth has produced large, crack-free crystals with sufficiently low 2- μ m absorption ($\sim 0.25 \text{ cm}^{-1}$) to allow efficient operation as a 2- μ m pumped OPO at uncontrolled ambient temperature.¹ The present experiments demonstrate higher slope (37%) and overall (26%) conversion efficiencies using a low loss crystal at ambient temperature. We also show that by cooling, comparable efficiencies can be achieved in crystals having substantially higher near band edge absorptions.

EXPERIMENTAL RESULTS

The two ZnGeP₂ crystals used in these experiments were grown at Lockheed Sanders¹; cut to $6 \times 6 \times 11 \text{ mm}^3$ and $4.5 \times 4.5 \times 14.6 \text{ mm}^3$, oriented at $\theta = 55^\circ$ for Type I phasematching near degeneracy with 2.05 μ m pumping. After the final anneal, the 2.05 μ m absorption coefficients as determined by polarized spectrophotometry were: ($\alpha_o = 0.26$; $\alpha_e = 0.58$) cm^{-1} and ($\alpha_o = 0.38$; $\alpha_e = 0.77$) cm^{-1} , respectively. (Note that since ZnGeP₂ is a positive uniaxial crystal the 2.05 μ m pump beam for a Type I OPO is o-polarized.) Both crystals were commercially polished and coated (AR @ 2.05 μ m and 3.5-5.0 μ m); no laser damage was observed for pump fluences as high as $\sim 1.2 \text{ J/cm}^2$ (the maximum fluence used in our experiments).

The pump laser was a diode-pumped A/O Q-switched Tm:Ho:YLF oscillator operated at 77K. Its output characteristics for all the experiments were: wavelength = 2.05 μ m, TEM₀₀ mode, linearly polarized, Q-switched pulse width = $18 \pm 1 \text{ nsec}$ (FWHM), pulse repetition frequency = 1500 Hz, total output power = 3.0 watts. Prior to entering the OPO, the pump beam was passed through optics which permitted control and monitoring of the power and polarization of the pump radiation incident on the OPO crystal, and then through a focusing lens which produced a beam waist having a $1/e^2$ diameter of 0.57 mm at the center of the crystal, with a

confocal region extending over about 15 cm. Using this arrangement, with the laser output power held constant at 3.0 watts, the pump power incident on the OPO could be varied continuously up to a maximum of 2.3 watts.

The OPO was collinearly pumped and doubly resonant, with a 5 meter high reflector and a flat output coupler. The two output couplers we used had transmissions of 20% and 40% between 3.6 μm and 4.7 μm . All optics were AR coated at 2.05 μm .

The ambient temperature (RT) OPO performance of both crystals was evaluated with a 20 mm long cavity; the crystals were mounted on a 1/2" stainless steel post without temperature control. For evaluation at cryogenic temperature (77 K; LNT) the higher loss crystal was attached to the cold finger of a small dewar, and enclosed by AR coated ZnSe windows. This configuration necessitated the use of a longer OPO resonator (37mm).

Figure 1 illustrates the OPO efficiencies obtained in the RT (curves A and B) and LNT experiments (curve C). Curve A shows data for the low loss (0.26 cm^{-1}) crystal using a 40% transmissive output coupler. We achieved total power conversion efficiency of 26% (679 mW threshold, 37% slope). The maximum sustained power output was 585 mW, at a pump fluence $\sim 1.2 \text{ J/cm}^2$. The OPO output beam appeared as a single circular spot when viewed on fluorescent cards. Curve B shows similar data for the higher loss (0.38 cm^{-1}) crystal at RT using a 20% transmissive output coupler. The threshold was 520 mW, and the slope was $\sim 6\%$. Insertion of this crystal into the dewar raised the RT threshold to ~ 1 watt, but had little effect on the slope efficiency.

Introduction of liquid nitrogen into the coolant reservoir lowered the threshold to ~ 400 mW and raised the slope efficiency to $\sim 25\%$, with no adjustments having been made to the cavity alignment. The LNT data shown in curve C were taken after making minor alignment corrections to compensate for mechanical movement which occurs during cool down. With this optimized alignment the OPO threshold at LNT was 295 mW, and the slope efficiency was 27%. Pumping with 2.3 watts we obtained 552 mW of OPO output, an absolute power conversion efficiency of 24%. The mechanism by which the enhancement of the efficiency occurs appears to be partially, but not totally, explained by the dependence of the pump wave absorption on temperature.

In addition to the OPO experiments we also determined the absorption coefficients for the pump radiation at RT and LNT, and the spectral composition of the OPO outputs. The e-wave and o-wave absorption coefficients at 2.05 μm were determined from the pump beam transmission of the crystal mounted in the cryostat before and after cooling. We found that at RT, $\alpha_o(2.05 \text{ } \mu\text{m}) = 0.36 \pm 0.01 \text{ cm}^{-1}$ and $\alpha_e(2.05 \text{ } \mu\text{m}) = 0.78 \pm 0.01 \text{ cm}^{-1}$, in agreement with spectrophotometric data. At LNT we found that $\alpha_o(2.05 \text{ } \mu\text{m}) = 0.17 \pm 0.01 \text{ cm}^{-1}$, reduced by a factor of 2 from its RT value; but $\alpha_e(2.05 \text{ } \mu\text{m}) = 0.77 \pm 0.01 \text{ cm}^{-1}$, essentially the same as the RT value.

OPO output wavelengths were measured using a 0.5 m monochromator. At RT the OPO operated around degeneracy, emitting throughout the region between 3.9-4.3 μm . At LNT the signal and idler peak wavelengths were found to be 3.62 μm and 4.72 μm respectively. The corresponding signal and idler bandwidths were

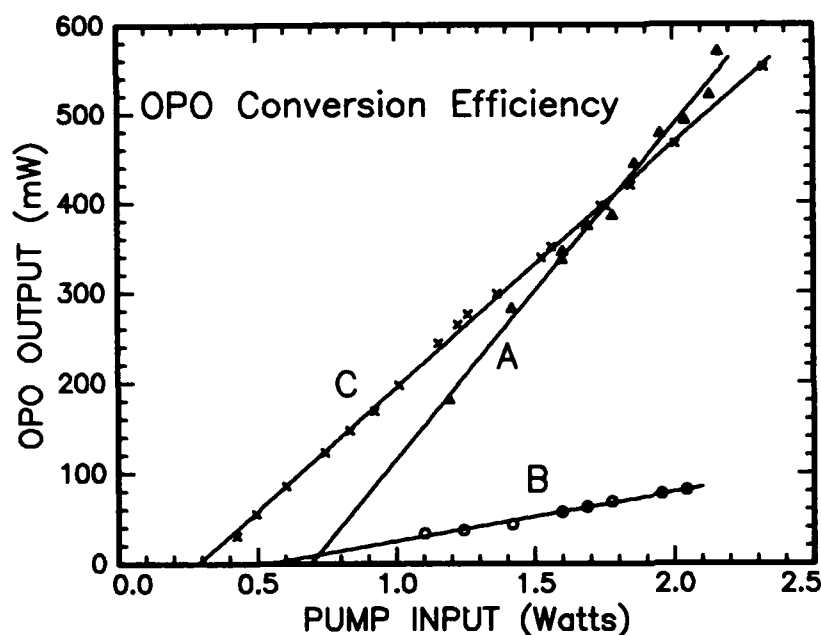


Fig.1 Efficiency of a $2\ \mu\text{m}$ pumped ZnGeP_2 OPO. Curves A and B show room temperature data for crystals having pump absorptions of 0.26 and $0.38\ \text{cm}^{-1}$, respectively. Curve C shows similar data for the higher loss crystal when it was cooled to 77°K .

approximately $0.12\ \mu\text{m}$ and $0.18\ \mu\text{m}$ (FWHM). The observed spectral shift is well outside the range of small angular deviations which could occur upon cooling, and it is qualitatively consistent with phase matching calculations for ZnGeP_2 at low temperatures.

SUMMARY AND CONCLUSIONS

We have demonstrated 37% slope (26% overall) conversion efficiency from a $2\ \mu\text{m}$ pumped room temperature ZnGeP_2 OPO with sustained output power of 585 mW at a pump fluence $\sim 1.2\ \text{J}/\text{cm}^2$. By cooling a higher loss ($\alpha_0 = 0.38\ \text{cm}^{-1}$) ZnGeP_2 crystal we have achieved OPO operation comparable to that obtained with a low loss crystal. Our results suggest that low temperature OPO operation in ZnGeP_2 may provide an additional approach to mid-IR frequency conversion, particularly if adequate efficiencies can be achieved using TE coolers.

REFERENCES

1. P.A. Budni, P.G. Schunemann, M.G. Knights, T.M. Pollak and E.P. Chicklis, Proc. ASSL (OSA, 1992) Vol.13, pp. 380-383.
2. From recent measurements on Sanders material by D. Beasley and G. Catella (Cleveland Crystals) $K = 0.31\ \text{W cm}^{-1} \text{ } ^\circ\text{K}^{-1}$.
3. C.L. Marquardt, D.G. Cooper, P.A. Budni, M.G. Knights, K.L. Schepler, R. DeDomenico and G.C. Catella, paper TuWW5, presented at OSA/ILS-VIII, Albuquerque, NM, Sept. 1992.

Optical Parametric Frequency Conversion Properties of KTiOAsO_4 (KTA)

W. R. Bosenberg
STI Optronics, Inc.
2755 Northup Way
Bellevue, WA 98004
(206) 827-0460

L. K. Cheng and J. D. Bierlein
Science and Engineering Laboratory
Experimental Station
Wilmington, DE 19880-0306

Optical parametric oscillators (OPO) have established themselves as efficient, reliable, solid-state sources of tunable radiation that can operate in many regions of the spectrum where no viable laser sources exist. One such region, 3 - 5 μm , is particularly interesting for many spectroscopic and remote sensing applications. Using other established nonlinear optical materials such as BBO, KTP, LBO, lithium niobate, AgGaS_2 , AgGaSe_2 , and ZnGeP_2 to obtain light in this spectral region has proven impractical due to their lack of transmission and/or their low optical damage thresholds. Recently, large single domain crystals of potassium titanyl arsenate (KTiOAsO_4 , KTA) have been grown.^[1] This material is similar in many ways to its isomorph, the more well-known material, KTP, but has better transmission at infrared wavelengths (IR cutoff is $\sim 5 \mu\text{m}$). Here, experimental results are presented demonstrating the utility of KTA for generating tunable radiation in the infrared.

Inclusion-free KTA crystal boules of up to 35 x 31 x 58 mm^3 were grown by flux techniques using either the tungstate or pure arsenate flux similar to what has been previously reported.^[2] To promote the formation of single domain crystal, a trivalent oxide of In (dopant level ~ 0.2 wt. %) was added into the melt and the crystal growth was carried out below the Curie temperature of KTA ($t_c \sim 880^\circ\text{C}$). From these boules three single domain KTA crystals were fabricated suitable for optical parametric frequency conversion. Crystal 1 was cut at $\theta = 49^\circ$, $\phi = 0^\circ$ (x-z plane) and was 4.8 x 3 x 8.3 mm^3 (x-z, y, length) in size. Crystals 2 and 3 were both cut at $\theta = 90^\circ$, $\phi = 0^\circ$ (x-axis). Crystal 2 was 4 x 3 x 10 mm^3 (y, z, length), while Crystal 3 was 5.9 x 6.8 x 10.7 mm^3 (y, z, length). Crystal 2 was grown using a $\text{K}_5\text{As}_3\text{O}_{10}$ flux while Crystals 1 and 3 were grown from the tungstate flux.^[2] To varying degrees, refractive index striations were observed in all three crystals.

The OPO tuning curves for KTA pumped at 1.064 μm and 532 nm were measured by observing sum frequency generation in the KTA of the signal and idler waves from the output of a KTP OPO pumped at the above two wavelengths. The KTP signal wavelength was measured with a monochromator, and the KTA was angle tuned on a calibrated rotation mount to give the largest sum frequency output. The results are shown in Figures 1 and 2. A single smooth phase matching peak was observed for each of the data points in Figures 1 and 2 indicating no evidence of multi-domaining in the KTA crystals. The solid lines in the figures are the calculated tuning curves based on the following Sellmeier equations:

$$\begin{aligned} &(\lambda \text{ in microns}) \\ n_x^2 &= 2.1106 + 1.0318/[1 - (0.2109/\lambda)^2] - 0.0090 \lambda^2 \\ n_y^2 &= 2.3889 + 0.7790/[1 - (0.2378/\lambda)^2] - 0.0105 \lambda^2 \\ n_z^2 &= 2.3472 + 1.1011/[1 - (0.2402/\lambda)^2] - 0.0141 \lambda^2 \end{aligned}$$

These Sellmeier equations are obtained from a best fit of the refractive index data measured with undoped KTA in the spectral region of 0.45 - 1.5 μm .^[1] The infrared coefficient (the coefficient of the last term in each equation) was then adjusted to best fit the OPO tuning curve data from this study.

Crystals 2 and 3 were also used in an OPO configuration to measure oscillation thresholds relative to KTP when pumped by 1.064 μm radiation. The OPO configuration was the standard two mirror flat-flat cavity. The input coupler was highly reflecting ($R > 98\%$) at the signal wavelength and highly transmitting ($R \sim 10\%$) at both the pump and idler wavelengths. The output coupler had reflectivities of $R = 98\%$ at the pump wavelength, $R = 10\%$ at the signal wavelength and $R \sim 10\%$ at the idler wavelength. The KTP crystal used as a comparison is cut the same ($\theta = 90^\circ$, $\phi = 0^\circ$) but is 15 mm in length. These results

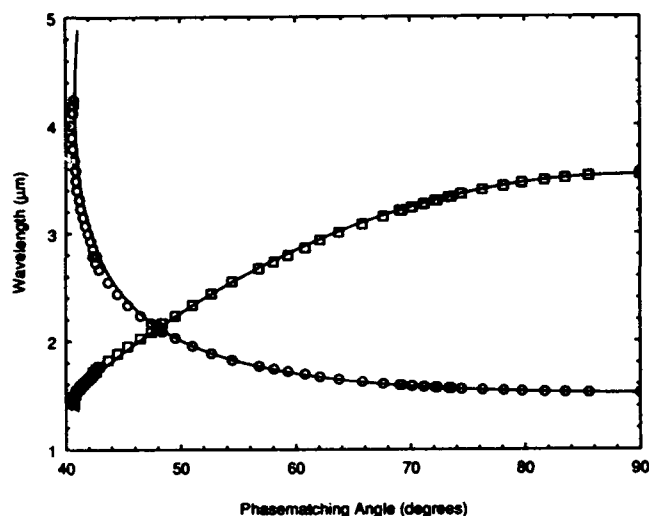


Figure 1. Experimentally measured optical parametric tuning curves for KTA pumped by 1.064 μm radiation for angle tuning in the x-z plane ($\phi = 0^\circ$). Solid lines are calculated tuning curves obtained from Sellmeier equations given in the text.

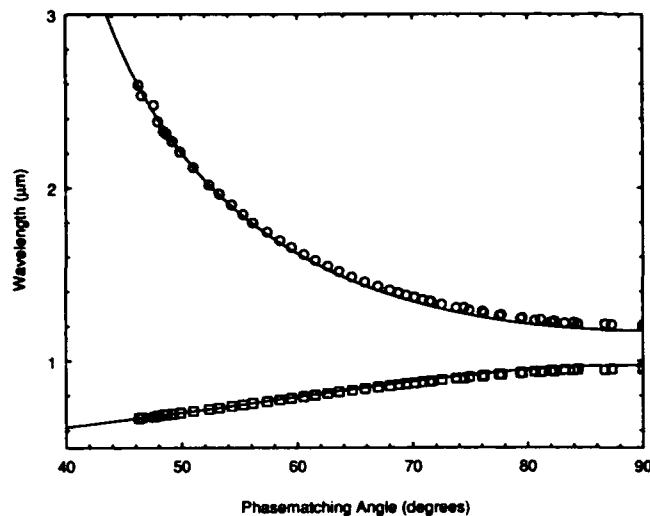


Figure 2. Same as Fig. 1 except that the pump wavelength is 532 nm.

are summarized in Table 1. Although the KTP has a lower threshold energy and intensity, this is mainly due to the longer length of the KTP crystal as all crystals have similar threshold nonlinear drives. The KTA #2 crystal was pumped up to 2.6 times above threshold obtaining a total conversion efficiency (signal + idler) of ~20%. Pumping was limited by damage to the input coupler. This OPO was not optimized in any way; it only shows that KTA operates similarly to KTP as an OPO material.

KTP. KTA is a very promising material for optical parametric frequency generation in the important 3 - 5 μm region of the spectrum.

REFERENCES

1. L.K. Cheng, L.T. Cheng, J.D. Bierlein, F.Z. Zumsteg, and A.A. Ballman, submitted for publication in Appl. Phys. Lett., Sept. 1992.

Table 1. OPO Parameters for noncritical phase matching along the x-axis for KTA and KTP.

	KTA #2	KTA #3	KTP
Crystal Length (mm)	10	10.7	15
Wavelength (μm)			
signal	1.520	1.524	1.572
idler	3.547	3.525	3.292
Threshold Energy (mJ)	21	23	10
Threshold Intensity (MW/cm ²)	210	230	100
Nonlinear Drive (C ² L ² I) @ threshold	2.4	3.0	2.5
Slope Efficiency (%)	38	40	53

In summary, the optical parametric phase matching behavior of the new material KTA has been experimentally measured for pump wavelengths of 532 nm and 1.064 μm . Some OPO oscillation threshold and conversion efficiency data has been obtained for comparison of this material to

2. L.K. Cheng, J.D. Bierlein, and A.A. Ballman, J. Crystal Growth 110, 697 (1991).

Noncritically phasematched cw mode locked optical parametric oscillator in KTP

A. Nebel, C. Fallnich, and R. Beigang

Fachbereich Physik
Universität Kaiserslautern
Erwin Schrödinger Str. 46
6751 Kaiserslautern
Tel.: (049) 631 205 2180
Fax.: (049) 631 205 3300

Cw mode locked optical parametric oscillators (OPO) are very efficient tunable light sources for the generation of pico- and femtosecond pulses in the near infrared spectral region. KTP (KTiPO_4) has turned out to be an extremely efficient material for the realisation of OPOs in this spectral range. Using an x-z-plane crystal cut for critical phase matching ps and fs pulses were generated around $1.3 \mu\text{m}$ [1,2,3].

In this contribution we report on a noncritically phase matched KTP OPO pumped by a Ti:Sapphire laser. The KTP crystal was cut for type II phase matching in the xy-plane ($e - e + o$) so that for the pump wave length used *noncritical phase matching* becomes possible ($\phi = 0^\circ$, $\theta = 90^\circ$).

The noncritical phase matching arrangement offers some important advantages compared to a critically phasematched OPO:

- no beam walk off between pump, idler and signal wave
- highest possible effective nonlinear coefficient
- easy tuning by tuning the pump wavelength (no realignment required)
- crystal length limited only by the difference in group velocity between pump, idler and signal wave
- easy alignment of the OPO cavity

A comparison between a x-y-cut and a x-z-cut OPO pumped by a Ti:Sapphire laser is given in table I. The tuning range of a x-z-cut critically phase matched OPO is larger compared to a x-y-cut OPO. In particular, there is no gap between $1.6 \mu\text{m}$ and $2.2 \mu\text{m}$.

For the operation of the OPO the KTP crystal ($3 \times 3 \times 6 \text{ mm}^3$) is placed in the waist of a 4-mirror ring cavity. The pump beam is focussed collinearly through one of the spherical mirrors with lenses of different focal length ($75 \text{ mm} < f < 150 \text{ mm}$). The cavity length was matched to the length of the pump laser as required for synchronous pumping. The accuracy of the OPO cavity length depends on the pump pulse length. In the case of ps pump pulses ($\Delta t \approx 1.5 \text{ ps}$) stable operation with constant pulse length and small peak-to-peak amplitude fluctuations ($< 10\%$) was obtained within a resonator length intervall of approximately $5 \mu\text{m}$. This behavior is in contrast to synchronously pumped lasers. Owing to the lifetime in the upper laser level the gain medium provides gain also for a finite cavity mismatch between pump and laser pulses resulting in a distorted pulse shape. In the

	x-y-plane	x-z-plane
d_{eff} (pm/V)	7.6	max. 6.4
FOM ((pm/V) ²)	10.6	max. 7.4
Phase match angle ϕ θ	0° 90°	0° 45°
Walk off angle	0°	2.5°
Tuning range signal (μm) (μm)	1.03 - 1.64 2.16 - 3.34	0.83 - 2.2 2.2 - 4.5

Table I: Comparison between x-y-cut and x-z-cut KTP crystal. The figure of merit (FOM) is defined as $\text{FOM} = (d_{\text{eff}})^2 / n_p n_s n_i$. The tuning range corresponds to a pump wavelength range from 700 nm to 1100 nm.

case of an OPO there will be no oscillation outside a small length intervall given, in principle, by the pump pulse length. For precision adjustment of the cavity length the plane high reflector was mounted on an piezoelectric transducer and a precision translation stage. Even with such stringent requirements for the accuracy of the resonator length no active stabilisation of the OPO resonator length was necessary to guarantee stable OPO operation.

For fs pump pulses ($\Delta t \approx 130$ fs) OPO operation was obtained over a similar cavity mismatch range, however, stable operation with short pulses was achieved only within ± 1 μm. Therefore for fs-OPO-operation a cavity length stabilisation is of advantage.

The crystal length of 6 mm was optimized for ps pulses by calculating the differences in group velocity for pump, signal and idler wave. For longer crystals the overlap between pump signal and idler wave will considerably decrease after a few round trips in the resonator.

Tuning was accomplished, both for the ps- and fs-OPO, by tuning the pump wavelength. Due to the noncritical phase match arrangement no realignment during tuning is required except for the wings of the tuning range caused by the change of index of refraction. With the Ti:Sapphire laser used in these experiments a tuning range from 1.052 μm to 1.214 μm and from 2.286 μm to 2.871 μm was achieved for the signal and idler wave, respectively, for the ps-OPO. The fs-OPO was tuned from 1.05 μm to 1.15 μm (signal wave) and from 2.24 μm to 2.7 μm (idler wave). Both tuning ranges were only limited by the tuning ranges of the pump lasers. A typical tuning curve for the ps-OPO is shown in figure 1. Maximum signal wave output powers of 510 mW were obtained around 1.14 μm corresponding to a total power efficiency as defined by $\eta = (P_s + P_i) / P_p$ of 40 %. The maximum average power of the fs-OPO was 300 mW for the signal wave at 1.1 μm.

The pulse width was determined with an intensity autocorrelation measurement. Assuming a sech^2 pulse shape the pulse length was 1.15 ps at the center of the tuning range of the ps-OPO. The

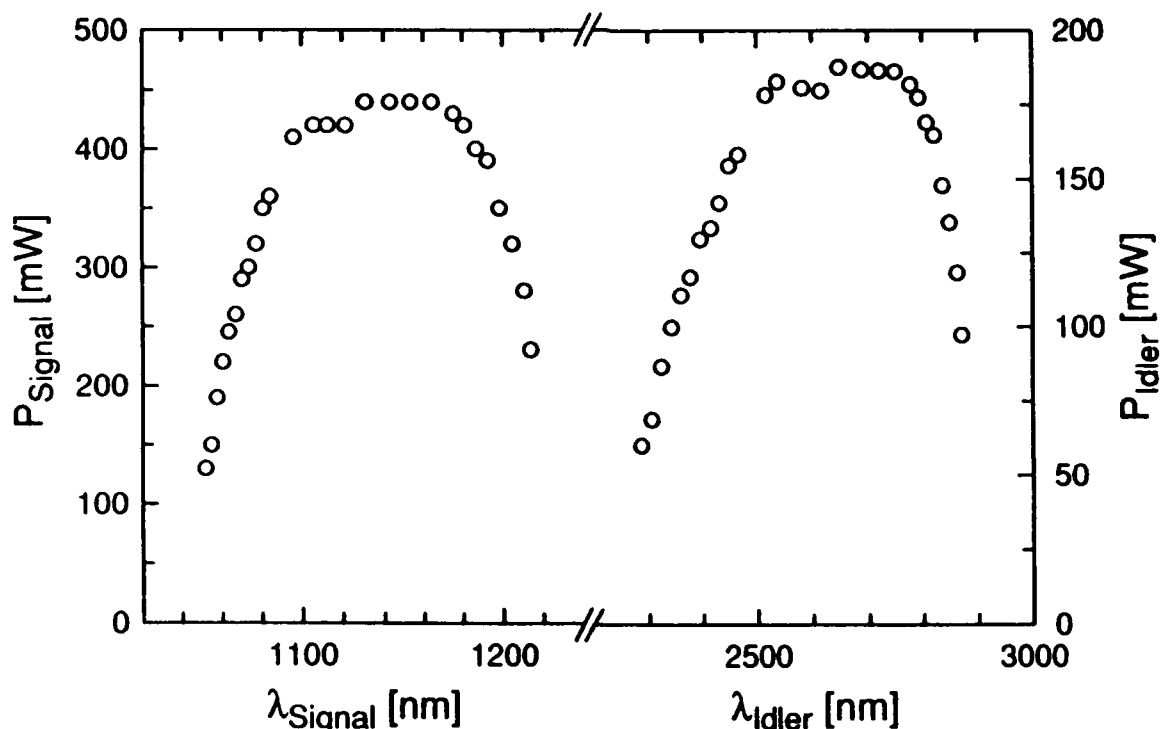


Fig. 1: Ps-OPO tuning curve for idler and signal wave.

spectral bandwidth of 303 GHz as measured with a monochromator resulted in a time-bandwidth product $\Delta\nu \Delta t = 0.35$ clearly indicating transform limited pulses. An interferometric autocorrelation measurement supported this assumption.

In the case of the fs-OPO, however, the pulse length was increased to 386 fs compared to the 130 fs pump pulses. In addition, the pulses were strongly chirped with a total bandwidth of approximately 20 nm. No compensation of the group velocity dispersion in the OPO resonator was applied yet.

References

1. D. C. Edelstein, E. S. Wachmann, and C. L. Tang, *Appl. Phys. Lett.* **54**, 1728 (1988)
E. S. Wachmann, D. C. Edelstein, and C. L. Tang, *Opt. Lett.* **15**, 136 (1990)
E. S. Wachmann, D. C. Edelstein, and C. L. Tang, *J. Appl. Phys.* **70**, 1893 (1991)
2. Q. Fu, G. Mak, and H. M. van Driel, *Opt. Lett.* **17**, 1006 (1992)
G. Mak, Q. Fu, and H. M. van Driel, *Appl. Phys. Lett.* **60**, 542 (1992)
3. W. S. Pelouch, P. E. Powers, and C. L. Tang, *Opt. Lett.* **17**, 1070 (1992)

External frequency conversion of tunable femtosecond pulses

C. Fallnich, A. Nebel, and R. Beigang

Fachbereich Physik
Universität Kaiserslautern
Erwin Schrödinger Str. 46
6751 Kaiserslautern
Tel.: (049) 631 205 2180
Fax.: (049) 631 205 3300

External frequency conversion of cw mode locked Ti:Sapphire radiation in β -Barium Borate (BBO) and Lithium-Triborate (LBO) crystals has turned out to be a very efficient method to generate bandwidth limited picosecond pulses in the wavelength range from 190 nm to 520 nm [1, 2]. For pulse lengths down to 1.3 ps and crystal lengths up to 8 mm no pulse lengthening was observed and power efficiencies up to 38 % have been obtained. In the case of femtosecond pulses (150 fs), however, such crystal length will lead to a substantial increase in pulse length and much shorter crystals have to be used to maintain the original pulse length of the fundamental radiation.

In this contribution we report on a detailed investigation of the generation of second, third and fourth harmonic of fs cw mode locked Ti:Sapphire radiation. In particular, the influence of different crystal lengths of two nonlinear materials, LBO and BBO, on the pulse length, the time-bandwidth product and a possible frequency chirp of the harmonic pulses was investigated.

The experimental set up is shown in Fig. 1. The Ti:Al₂O₃ laser used in these experiments produced a maximum average power (repetition rate 76 MHz) of 1.45 W at 785 nm, the tuning range extended from 710 nm to 805 nm and the pulse length was between 120 fs and 150 fs. Assuming a sech^2 pulse shape the time-bandwidth product of $\Delta\nu \Delta t \approx 0.5$ indicates almost transform limited pulses. After frequency doubling radiation at frequency ω and 2ω is separated, the polarization of ω is rotated by 90° for type I phase matching to generate 3ω , and the temporal delay between ω and 2ω induced in the doubling crystals as a result of the different group velocities is compensated in an optical delay line for ω . The third harmonic is tunable from 236 nm to 268 nm limited by the tuning range of our Ti:Al₂O₃ laser. The generated radiation at 3ω is then separated from the fundamental, polarization and temporal delay between ω and 3ω are adjusted, and both beams at ω and 3ω are focussed into a BBO crystal for sum frequency generation. Fundamental and fourth harmonic are separated by a quartz prism.

A characterization of the generated pulses was obtained by means of an intensity auto- or crosscorrelation and a measurement of the spectral bandwidth at ω , 2ω , and 3ω . In particular, the pulse width of the third harmonic was obtained by a crosscorrelation measurement between ω and 3ω in a 2 mm long BBO crystal where the difference frequency was generated. Typical data are shown in table I for different crystal lengths and crystal combinations to generate 2ω , 3ω , and 4ω . All tripling experiments were performed with a 1 mm long BBO crystal.

It is obvious from this table that for bandwidth limited pulses at pulse lengths of around 150 fs crystal lengths of approximately 1 mm have to be chosen. With a 1 mm LBO crystal for frequency doubling we have obtained 420 mW average power at 2ω corresponding to an efficiency of 30 %. Subsequent frequency tripling in a 1 mm BBO crystal resulted in 195 mW average power at 3ω

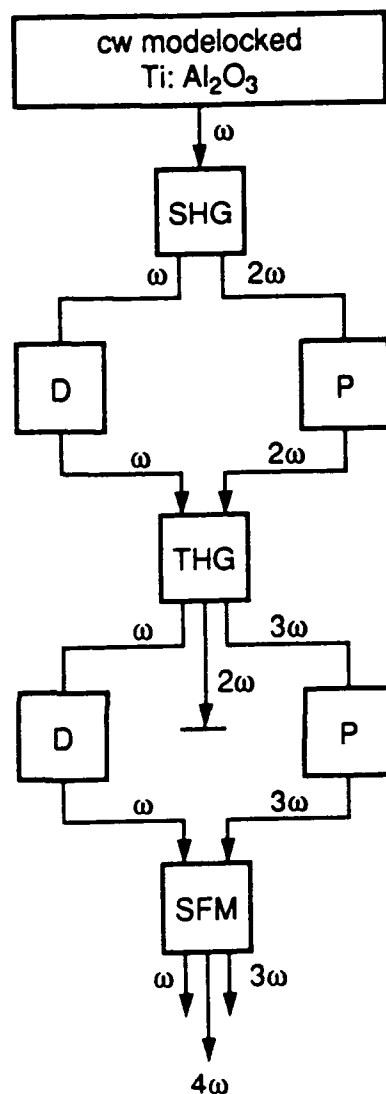


Figure I: Experimental set up

with a pulsewidth of 180 fs and a time bandwidth product of 0.75, comparable to the original pulses.

Although the conversion efficiency for frequency doubling in BBO is higher compared to LBO ($P_{av}(2\omega) = 780$ mW) the poor beam profile at 2ω caused by the larger walk off angle did not allow for higher conversion efficiencies at 3ω . In addition the pulse length at 2ω was increased resulting in a time bandwidth product of 1.16. Therefore for bandwidth limited pulses and for further frequency conversion processes LBO has to be used as the doubling crystal.

The fourth harmonic was generated in a BBO crystal which is the only crystal to allow phase matched sum frequency generation between ω and 3ω . The only crystal available was 6.85 mm long which is not well suited for the sum frequency generation of fs pulses. In first experiments we did observe the fourth harmonic around 195 nm, but the output power was less than 1 mW. Improved

results with shorter crystals will be presented at the conference.

		LBO (1 mm)	LBO (8 mm)	BBO (2 mm)
ω	P(W)	1.45	1.45	1.45
	Δt (fs)	142	132	140
	$\Delta t \Delta \nu$	0.5	0.5	0.5
2ω	P(mW)	400	670	780
	η	27.6 %	46.2 %	54 %
	Δt (fs)	150	380	280
	$\Delta t \Delta \nu$	0.62	1.12	1.16
3ω	P(mW)	195	110	80
	η	36.4 %	21.4 %	14.5 %
	Δt (fs)	180	-	-
	$\Delta t \Delta \nu$	0.75	-	-
4ω	P(mW)	< 1	-	-
	η	-	-	-

Table I: Typical data for the generation of 2ω , 3ω and 4ω for different crystal lengths. The third harmonic was generated in a 1 mm long BBO crystal, the fourth harmonic in a 6.85 mm long BBO crystal.

All these results are in reasonable agreement with calculations of the pulse lengths of 2ω , 3ω and 4ω considering the difference in group velocity between the various harmonics. In LBO the difference is in general smaller, so that longer crystals can be used. For the third and fourth harmonic, however, only BBO allows for phase matching over the total tuning range of the Ti:Sapphire laser. Owing to the high peak power of the fs fundamental pulses the conversion efficiencies are still comparable to or even larger compared to ps frequency conversion where longer crystals can be used.

In summary we have shown that external frequency conversion in LBO and BBO crystals is an efficient method to generate tunable femtosecond pulses down into the deep ultraviolet spectral region. Nearly transform limited pulses with pulse lengths of 150 fs and average powers of 420 mW and 195 mW were obtained at 390 nm and 260 nm, respectively. With longer crystals the efficiencies can be increased at the expense of the pulse length. Sum frequency generation between ω and 3ω allows for the generation of femtosecond pulses down to 190 nm. The whole possible tuning range of the Ti:Sapphire laser can, in principle, be utilized to generate femtosecond pulses from 190 nm to 520 nm.

References:

1. A. Nebel and R. Beigang, Opt. Lett. **16**, 1729 (1991)
2. A. Nebel and R. Beigang, Opt. Commun. accepted for publication (1992)

Stimulated Raman Scattering of Picosecond Pulses
in Barium Nitrate Crystals

Petr G. Zverev and Tasoltan T. Basiev

General Physics Institute

Vavilov str., 38, Moscow, 117942, Russia

Phone: (095) 135-03-18

and

James T. Murray, Richard C. Powell, and Roger J. Reeves

Center for Laser Research, Oklahoma State University

Stillwater, OK, 74078, U.S.A.

Phone: (405) 744-6575

The use of solid state materials for stimulated Raman scattering (SRS) can result in high gain, reliable, small dimension devices for shifting laser output frequencies. However, few crystals have been identified that possess narrow, isolated intensive Raman active vibronic modes necessary to produce efficient scattering [1]. Normally, these intense modes can be attributed to strong internal symmetrical vibrations within covalent ion complexes, such as $(\text{CO}_3)^{-1}$, $(\text{NO}_3)^{-1}$ and $(\text{WO}_4)^{-1}$. It was suggested earlier by Eckhardt [1] that molecular crystals containing these complexes should exhibit strong SRS.

SRS in $\text{Ba}(\text{NO}_3)_2$ crystals has been demonstrated previously using nanosecond excitation pulses [2,3]. The SRS gain at 532 nm was measured by Karpukhin et al. [2] to be 47 ± 5 cm/GW. $\text{Ba}(\text{NO}_3)_2$ crystals were also used to shift the radiation of a tunable LiF:F_2^- color center laser ($\lambda = 1.1\text{--}1.25 \mu\text{m}$) to near IR spectral region of 1.2 to $1.6 \mu\text{m}$ [3]. The maximum SRS efficiencies of the first and second Stokes components in this configuration were quoted as being 60% and 18%, respectively.

In this paper we present the first demonstration of SRS with picosecond pulses in $\text{Ba}(\text{NO}_3)_2$ crystals. The transverse relaxation time T_2 of the $\nu_1(A_1')$ Raman active vibronic mode was estimated to be 25 ps [3]. The excitation pulses in our experiments were measured to be 22 ± 2 ps. Therefore, the experiments discussed were performed in the transient SRS regime.

The theory of SRS has been extensively developed previously [4,5]. In the approximation of a plane, nondepleted pump wave the intensity of the first Stokes component is defined by

$$I_s(L) = I_s(0) \exp\{G\}. \quad (1)$$

In the steady state region the gain exponent is defined as

$$G = g_{ss} I_p L \quad (2)$$

where g_{ss} is the steady state Raman gain, I_p is the pump intensity and L is the length of the nonlinear Raman media.

In the transient case, where $T_p < T_2$, the transient growth of the molecular vibration wave must be considered. Carman et al. [5] performed a detailed numerical analysis of the transient SRS. Following ref. [6], the main result that we want to extract from this analysis is the factor F . This is the factor by which the pump intensity under transient conditions must be increased as compared to steady state to reach the threshold for SRS. In our experiment we have the ratio $T_2/T_p \approx 1.1$. For a Gaussian shaped pump pulse under threshold conditions, the analysis of ref. [5,6] yields the factor $F \approx 10$. Thus the threshold conditions for SRS in our experimental case should be obtained when the gain exponent $G_{tr}^{(thresh)}$ is ten times greater than $G_{ss}^{(thresh)}$.

In the experimental setup used for this work, the second harmonic output of a mode locked Nd-YAG laser was used as a pump source. The output energy and pulse duration of this laser was measured to be 2 mJ/pulse and 22 ± 2 ps, respectively. We used two methods to measure the parameters of the scattered light. One was composed of a monochromator, photomultiplier tube and digital oscilloscope. This system was used to measure SRS efficiency from a single laser pulse. The other system was composed of a 60° glass prism, aperture and energy meter. This system was used to measure the absolute SRS efficiency.

The barium nitrate samples were cut along the [110] crystallographic axis. These samples were 50 and 40 mm long with the apertures 9×9 and 12×15 mm, respectively. $Ba(NO_3)_2$ crystals are transparent in the wide spectral region from 340 to 1800 nm.

In the forward scattered radiation direction, the first (563 nm), second (599 nm) and third (639 nm) Stokes, and first antistokes (504 nm) components of the illuminating 532 nm pump beam were present. Figure 1(a) shows the dependence of the forward scattered (inside 1.5° cone) first Stokes efficiency on the input pump intensity for crystals of lengths 50 mm and 40 mm. The threshold intensities were measured to be 1.1 and 1.45 GW/cm², respectively. These are in good agreement with the exponential dependence of the SRS intensities on the crystal length as predicted by Eqs. (1) and (2).

The threshold gain obtained from our experimental data and steady state Raman gain g_{ss} , gives us $G_{tr}^{(thresh)} = 260 \pm 30$. As predicted this value is a factor of 10 larger than $G_{ss}^{(thresh)}$, that is commonly defined to be 25.

Figure 1(b) shows the overall efficiency of the first and second Stokes SRS in the 50 mm long $Ba(NO_3)_2$ crystal. It can be seen that a first Stokes efficiency of 25% and second Stokes efficiency of 5% can be obtained at the input pump intensity of 2 GW/cm². A further increase of the pump intensity leads to saturation of the SRS efficiencies.

The angular dependences of the SRS radiation for different pump intensities were also investigated. The divergence of the first Stokes radiation increases with the input pump intensity from 1° to 4° . This blooming of the first Stokes radiation can be attributed to the onset of the threshold for off-axis SRS. That is, as the pump intensity increases it becomes possible for off-axis spontaneously scattered first Stokes radiation to be

amplified. Likewise, the second Stokes radiation, created by cascading SRS of the first Stokes component, displays an analogous distribution at small angles. We observed an absorption cone in the first Stokes radiation and intense cones of both second and third Stokes components, at angles 1.9° , 3.6° and 5.5° , respectively. The appearance of this cones is ascribed to the four photon mixing processes [7].

In summary, we have demonstrated that $\text{Ba}(\text{NO}_3)_2$ crystals can be used as a high gain Raman media with picosecond pulses. The results obtained in these experiments are in agreement with the theoretical predictions for transient SRS. The results show the feasibility of using solid state Raman shifters for producing frequency shifts in the output of picosecond pulse lasers.

REFERENCES

1. G.Eckhardt IEEE J. Quantum Electron., QE-2 (1966) 1.
2. S.N.Karpukhin, A.I.Stepanov Sov. J. Quantum Electron., 16 (1986) 1027.
3. T.T.Basiev et al. Sov. J. Quantum Electron. 17 (1987) 1560.
4. W.Kaiser, M.Maier: In "Laser Handbook", 2 (N.-Holland, Amsterdam 1972), Chap. E2, 1077.
5. R.L.Carman et al. Phys. Rev. A 2 (1970) 60.
6. D.C.Hanna et al. IEEE J. Quantum Electron. QE-22 (1986) 332.
7. R.Chiao and B.P.Stoicheff Phys. Rev. Lett. 12 (1964) 290.

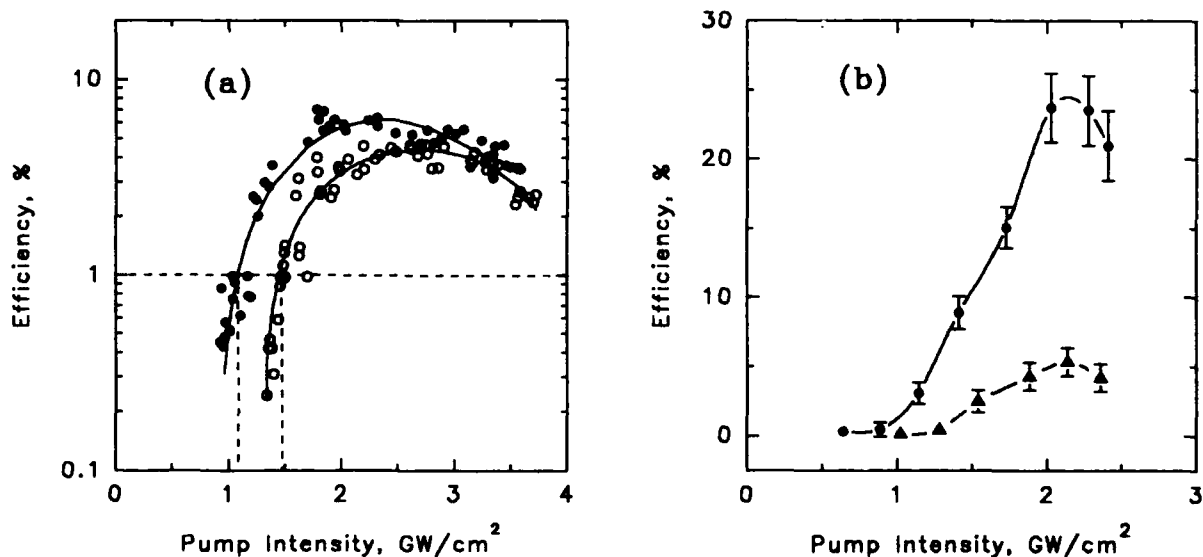


Fig.1(a). First Stokes SRS efficiencies in $\text{Ba}(\text{NO}_3)_2$ crystals of different length. Filled circles correspond to 50 mm and hollow - 40 mm crystal length.

Fig.1(b). First (circles) and second (triangles) Stokes efficiencies versus input pump intensity.

Tuesday, February 2, 1993

Novel Laser Materials 1

ATuA 8:15am–9:45am
La Salle Ballroom B&C

Richard C. Powell, *Presider*
University of Arizona

Incongruent Melting Fluoride Crystals as New Laser Hosts

A. Pham, J. Lefaucheur, J. Nicholls, G. Lutts, and B. Chai
CREOL, University of Central Florida,
12424 Research Parkway, Orlando, Florida 32826

Ever since the discovery of solid state lasers, host material selection has been confined to congruent melting compounds. This is because the Czochralski pulling is the only technique capable to produce large size high quality single crystals with reasonable amount of time. The conventional lamp pumped system requires large size single crystal rods as lasing medium.

The availability of high power laser diodes changes the whole thinking of solid state laser design. Not only we do not need large rods as lasing medium, the tolerance of thermal mechanical strength of the host materials is also somewhat relaxed. Moreover, because of the intrinsic low peak power of these laser diodes, it is desirable to select material with long fluorescence lifetime and low non-radiative losses. Fluoride compounds, in general, fit these criteria well.

So far all the known fluoride laser hosts either melt congruently or are very close to it. These include MgF_2 , ZnF_2 , CaF_2 , SrF_2 , LaF_3 , LiYF_4 , BaY_2F_8 , KY_3F_{10} , KMgF_3 , KZnF_3 , SrAlF_5 , $\text{Na}_3\text{Ga}_2\text{Li}_3\text{F}_{12}$, and more recently LiCaAlF_6 , LiSrAlF_6 . Among them, only four (LaF_3 , LiYF_4 , BaY_2F_8 , KY_3F_{10}) are capable for rare earth doping and LiYF_4 is the only compound that has been extensively studied.

Clearly, in order to optimize lasing properties, we should consider the structural criteria first rather than congruent melting as basis for material selection. This means that in case we find a desirable structure but incongruent melting, we must be able to overcome the problem. This is indeed the case. We report here our effort to grow three new laser host crystals from peritectic melts. They are KYF_4 , LiGdF_4 and KLiYF_5 . We are able to grow these crystals using the same equipment and technique that we normally do for congruent melting compounds. Although the pull rate is slower around 0.3 to 0.5 mm per hour, it is significantly faster than normal flux growth method. The key of this success is the high sensitivity of an improved computer controlled weight feed back system.

In all cases, we have to either construct our own phase diagram or correct the existing ones based on our growth data. Among them, KYF_4 was most extensively investigated. The peritectic composition is located at 43% YF_3 + 57% KF . The crystal is hexagonal and the preferred growth direction is c-axis. We are able to grow high quality crystals using the entire peritectic region until reaching the eutectic point. LiGdF_4 has the largest shift of peritectic point away from the stoichiometric composition and is, thus, most difficult to grow. The peritectic composition is located at 29% YF_3 + 71% LiF . The growth rate is down to 0.3 mm per hour and the yield is low. We can only use a small portion of the peritectic curve before the constitutional supercool overwhelms. The peritectic point of KLiYF_5 is near 43% YF_3 + 57% KF + 57% LiF . It has the lowest growth temperature around 600°C. The crystal is monoclinic and has an excellent (010) cleavage plane. Although the growth is not difficult, the crystal does cleave and crack badly during cooling. Moreover, the crystal also contains a lot of inclusions. We have not yet fully optimize the growth condition yet.

We have demonstrated here that the current weight-feed-back controlled Czochralski puller can be used to pull high quality crystals from an incongruent, peritectic melt. The growth rate is slower but still quite adequate. This approach opens new opportunities to search for better laser hosts.

Crystal Growth and Spectroscopic Characterization of Tm-doped Oxyapatites and Orthosilicates

Gregg H. Rosenblatt
SFA, Inc. Landover, MD 20875
Phone (202) 404-7283

Gregory J. Quarles and Leon Esterowitz
Code 6551, Naval Research Laboratory
Washington, DC 20375-5320
Phone (202) 404-8609

Mark H. Randles and John E. Creamer
Litton Airtron SYNOPTICS, PO Box 410168, Charlotte, NC 28241
Phone (704) 588-2340

Roger F. Belt
Litton Airtron, 200 East Hanover Ave, Morris Plains, NJ 07950
Phone (201) 539-5500

SUMMARY

The interest in diode pumped solid state lasers in the 2 μm region in recent years has been well documented. The need for compact, highly efficient sources has led to the increased study of new laser hosts which may improve upon the current state of the art. We have grown and analyzed the spectroscopic properties of two Tm^{3+} -doped silicate oxyapatite hosts and one orthosilicate. These hosts are $\text{CaY}_4(\text{SiO}_4)_3\text{O}$ [CaYSOAP], $\text{CaLa}_4(\text{SiO}_4)_3\text{O}$ [CaLaSOAP], and Y_2SiO_5 [YOS]. We shall compare the spectroscopic properties of these new hosts with those of Tm^{3+} -doped YAG, and show that these new hosts may offer improvements to Tm^{3+} :YAG in minimizing upconversion, increasing tunability in the 2 μm region, and improving laser performance for the 2.3 μm transition.

All crystals examined in this paper were grown by the Czochralski technique. CaYSOAP and CaLaSOAP are uniaxial crystals in which Tm^{3+} is directly substituted for either Y or La without need for charge compensation. As seen in Steinbruegge, et al.,¹ these hosts readily accept trivalent rare earths, with distribution coefficients near unity. YOS is a biaxial crystal, making polarized absorption measurements quite difficult.

SPECTROSCOPY

The focus of the spectroscopic measurements centered around the absorption of Tm^{3+} in the near infrared region for eventual pumping with GaAlAs diodes. All absorption spectra were measured with Glan-Thompson polarizers and a Perkin-Elmer Lambda 9 Spectrophotometer at room temperature. Lifetime measurements were also taken at the appropriate wavelengths by using a Nd:YAG pulsed dye laser pump source (8 ns pulsewidth). Lifetimes of the 2 μm

transition were measured with an InSb detector, and a S1 response photomultiplier tube detected near infrared lifetimes. All lifetime measurements were taken at room temperature.

A complete set of spectroscopic results can be seen in Table 1. This data shows that both $\text{Tm}^{3+}:\text{CaY SOAP}$ and $\text{Tm}^{3+}:\text{CaLa SOAP}$ have significantly stronger absorption coefficients at the 790 nm diode pumping region when compared to a $\text{Tm}^{3+}:\text{YAG}$ sample of equal concentration. The $^3\text{H}_4$ absorption peak for 6% $\text{Tm}:\text{CaY SOAP}$ is 5 to 6 times stronger than that for 6% $\text{Tm}:\text{YAG}$. Also of interest is the shift in absorption strength from the $^3\text{F}_3$ transition to the $^3\text{H}_4$ transition. At 680 nm the absorption in $\text{Tm}:\text{YAG}$ is 3 times stronger than the 785 nm absorption, whereas in $\text{Tm}:\text{CaY SOAP}$ the reverse is true. The comparative absorption spectra of $\text{Tm}:\text{CaY SOAP}$ and $\text{Tm}:\text{YAG}$ can be seen in figure 1.

From the spectroscopic data, $\text{Tm}:\text{CaLa SOAP}$ and especially $\text{Tm}:\text{CaY SOAP}$ appear to be excellent candidates for improved 2 μm solid state lasers. Increased absorption at 790 nm can allow for a reduction in Tm^{3+} dopant concentration, which would help decrease the amount of detrimental ground state absorption in the 2 μm lasing region, as well as minimize the upconversion processes which lower the efficiency of higher concentration Tm^{3+} lasers. A reduction in ground state absorption could create a broader tuning range in the shorter wavelength region. The increased 790 nm absorption would also allow for very short laser crystal lengths, promoting better mode matching possibilities for diode pumped lasers. Another Tm^{3+} laser transition, the $^3\text{H}_4$ to $^3\text{H}_5$ 2.3 μm laser, may be better suited for a Tm^{3+} -doped silicate oxyapatite because a very low concentration Tm crystal is needed to eliminate the 2 for 1 process of the 2 μm transition. Concerning the lifetime data, the shortening of the $^3\text{F}_4$ 2 μm transition from 10 ms in $\text{Tm}:\text{YAG}$ to 1.6 ms in $\text{Tm}:\text{CaLa SOAP}$ and 0.59 ms in $\text{Tm}:\text{CaY SOAP}$ should not affect quasi-cw diode pumped operation, since the diode pulses are on the order of 1 ms.

In summary, Tm^{3+} -doped oxyapatites appear to be excellent candidates for diode pumped 2 μm lasers: they are not difficult to grow, and they offer stronger absorption linewidths in the near infrared wavelength region.

REFERENCES

1. K.B.Steinbruegge, T.Henningsen, R.H.Hopkins, R.Mazelsky, N.T.Melamed, E.P.Riedel, and G.W.Roland, Appl. Opt. 11, 999 (1972).

Nominal Crystal	Ion Density (#/cm ³)	³ H ₄ Abs. peak & FWHM (nm)	³ H ₄ Abs. coeff. (cm ⁻¹)	³ F ₃ Abs. peak & FWHM (nm)	³ F ₃ Abs. coeff. (cm ⁻¹)	$\tau_{^3H_4}$	$\tau_{^3F_4}$
6% Tm:CaY SOAP	9.4×10^{20}	E // C 790 nm (3.2 nm)	33.5	E // C 682.2 nm (10 nm)	6	15 μ s	585 μ s
6% Tm:CaLa SOAP	8.4×10^{20}	E // C 791 nm (5 nm)	6.9	E // C 682.6 nm (10 nm)	2.9	70.5 μ s	1.63 ms
6% Tm:YOS	1.1×10^{21}	790.7 nm (2.1 nm)	7.6	679.2 nm (~ 4 nm)	9.8	8.5 μ s	1.72 ms
				675.7 nm (~2 nm)	10.1		
6% Tm:YAG	8.3×10^{20}	785.4 nm (3 nm)	5.74	681 nm (3 nm)	15.1	20 μ s	10 ms

Table 1. All measurements taken at room temperature. Polarized absorption data is indicated.

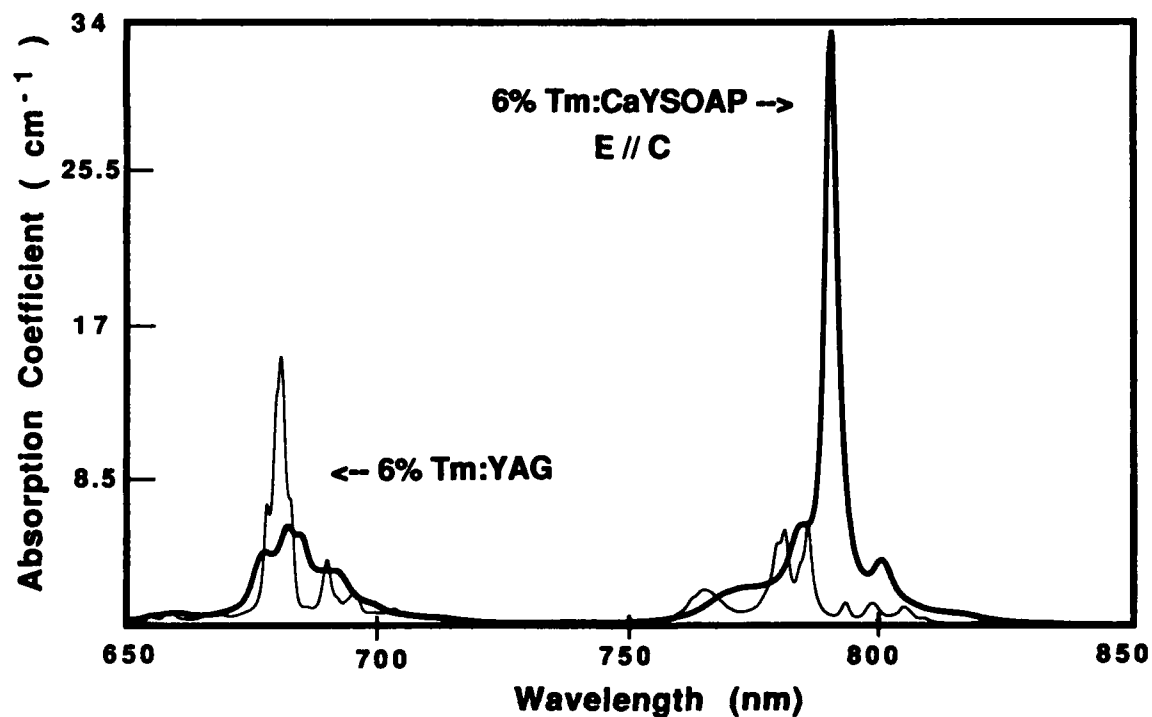


Figure 1. Room temperature absorption spectra of 6% Tm:YAG vs. 6% Tm:CaY SOAP

Physics of Yb-Doped Laser Crystals
with the Apatite Structure

L. D. DeLoach, S. A. Payne, W. F. Krupke, L. K. Smith
W. L. Kway, and J. B. Tassano

Lawrence Livermore National Laboratory
P.O. Box 5508
Livermore, CA 94550
510-423-8241

Solid state lasers based on Yb-doped media can be efficiently pumped by strained-layer InGaAs diodes.¹ For several reasons, such a system offers an attractive alternative to the AlGaAs diode-pumped Nd³⁺-laser widely employed in science and industry. First, recent data suggest that the InGaAs diode lasers may provide advantages of longer operating lifetimes and lower degradation rates as compared with the AlGaAs diode lasers.^{2,3} Second, the Yb³⁺ ion has three to four times longer energy storage lifetime than does Nd³⁺ for the same host. In this paper we report our investigations of Yb-doped crystals with the apatite structure as a promising class for InGaAs diode-pumpable media.

A study of several Yb-doped crystalline media identified fluorapatite, Ca₅(PO₄)₃F, or FAP, to possess a more favorable crystal field environment for Yb than many oxide and fluoride hosts.⁴ Strongly polarized absorption and emission features give rise to a large pump cross section at 905 nm and a large extraction cross section at 1043 nm with a lifetime comparable to those found in oxide crystals ($\tau_{em} = 1.1$ msec). Moreover, the laser performance of a Ti:sapphire pumped Yb:FAP crystal was investigated and slope efficiencies as high as 79% were measured.⁵

The fluorapatite structure is well-known for its diverse crystal chemistry such that an efficient Yb:FAP laser readily suggest the investigation of chemical analogs for similar applications. Such an investigation is twofold in its potential benefits: 1) a superior or complementary Yb-laser may be identified, and 2) an understanding may be gained of the physics producing the favorable spectroscopic properties. To this intent, we have grown and characterized Yb-doped crystals of Sr₅(PO₄)₃F, Ba₅(PO₄)₃F and Ca₅(PO₄)₃Cl to compare with Ca₅(PO₄)₃F properties.

Our studies of the FAP analogs reveal similar physical and optical properties. Most important, the Yb spectroscopy reveals the same anisotropic features which dominate the absorption and emission spectra in FAP, and the measured Yb³⁺ lifetimes are all within $\pm 20\%$. Among these crystals, the most promising new laser candidate is Sr₅(PO₄)₃F, or S-FAP, which yields the longest Yb³⁺ lifetime among the apatites studied, $\tau_{em} = 1.26$ msec, and the highest extraction cross section observed for Yb, $\sigma_{em} = 7.3 \times 10^{-20}$ cm². Consequently, Yb:S-FAP has been investigated as a laser pumped by a Ti:sapphire laser operating at 899 nm. Figure 1 shows measured slope efficiencies as high as 71% for the Yb:S-FAP data shown. The favorable spectroscopic properties for Yb in S-FAP and the overall laser performance suggest Yb:S-FAP should, like Yb:FAP, serve usefully as an InGaAs diode-pumpable medium.

Although the other analogs are not observed to have any significant advantages as laser media, they contribute to our overall understanding of the Yb spectroscopy in these materials. To this end, we have measured unpolarized low temperature (~ 20 K) emission spectra of Yb in the various apatite crystals and observe both electronic and vibrational lines. Figure 2 is a plot of low temperature emission for the different apatite hosts. The x-axis is in wavenumbers where 0 cm⁻¹ is defined to be the "zero-line" energy. Arrows mark where we observe the four electronic levels (e) which are expected for the Yb³⁺ ion and additional levels arising from (PO₄) group vibrations (ν_p) and lattice vibrations (ν_l).⁶ It is evident in the region of the laser line for these materials, 500-700 cm⁻¹, significant interactions of electronic and phosphate vibrational energies are occurring. In fact, the level of electronic-vibrational coupling increases as the divalent metal cation changes from Ca < Sr < Ba and as the halogen ion changes from Cl < F. The significance of the Ca₅(PO₄)₃Cl sample is the conspicuous absence of the phosphate vibrational levels in the vicinity of the local electronic state. Where the phosphate vibration energies are sufficiently close to

the electronic energy, a resonant enhancement of the vibronic level leads to increased transition strength to the vibrational level. Interestingly, it is this resonant electronic-vibrational interaction between Yb^{3+} and the (PO_4) groups which give rise to the laser line of the Yb:FAP and Yb:S-FAP lasers.

This work was performed under the auspices of the U.S. Department of Energy by Lawrence Livermore National Laboratory under contract no. W-7405-Eng-48.

References

1. P. Lacovara, H. K. Choi, C. A. Wang, R. L. Aggarwal, and T. Y. Fan, *Opt. Lett.* **16**, 1089-1091 (1991).
2. R. M. Kolbas, N. G. Anderson, W. D. Laidig, Y. Sin, Y. C. Lo, K. Y. Hsieh, and Y. J. Yang, *IEEE J. Quantum Electron.* **24**, 1605-1613 (1988).
3. D. P. Bour, D. B. Gilbert, K. B. Fabian, J. P. Bednarz, and M. Ettenberg, *IEEE Photon. Technol. Lett.* **2**, 173-174 (1990).
4. L. D. DeLoach, S. A. Payne, L. K. Smith, W. L. Kway, L. L. Chase, and W. F. Krupke, *OSA Proc., Advanced Solid-State Lasers*, L. L. Chase and A. A. Pinto, Eds., vol. 13, pp. 293-295 (1992).
5. S. A. Payne, W. F. Krupke, L. K. Smith, L. D. DeLoach, and W. L. Kway, *OSA Proc., Advanced Solid-State Lasers*, L. L. Chase and A. A. Pinto, Eds., vol. 13, pp. 222-229 (1992).
6. W. E. Klee and G. Engel, *J. Inorg. Nucl. Chem.* **32**, 1837-1843 (1970).

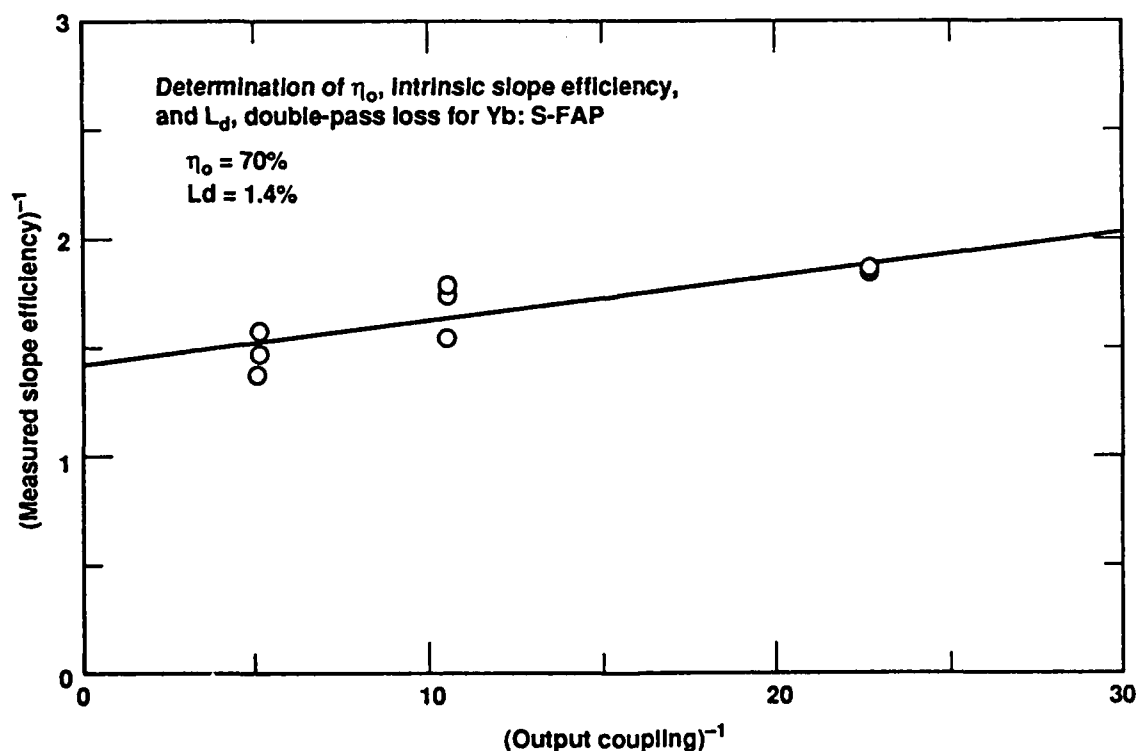


Fig. 1. Efficiency data acquired for the Yb:S-FAP laser crystal. Measurements were made for the three output couplers (O.C.) indicated.

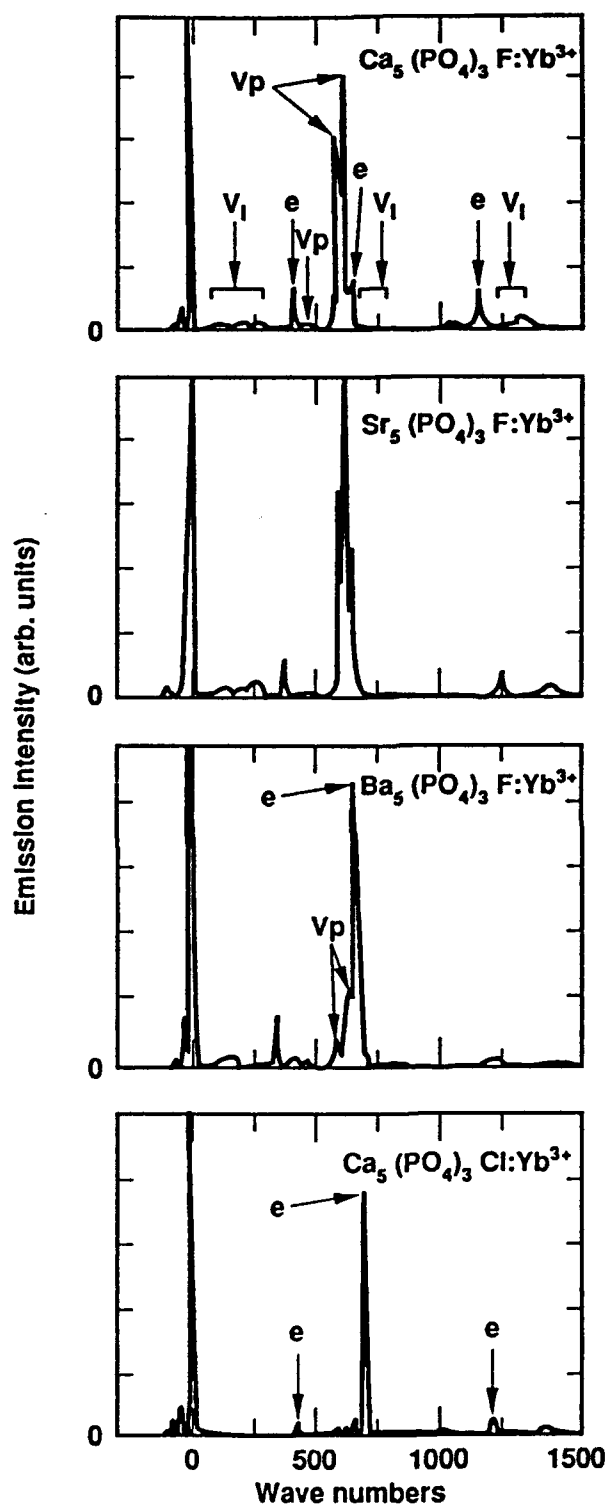


Fig. 2. Low temperature (~ 20 K) emission spectra for the Yb-doped apatite hosts. The abscissa is in wavenumbers where 0 cm^{-1} is the "zero-line" energy. Energy levels are marked by an arrow and "e" for electronic, "vp" for phosphate vibration, and "vl" for lattice vibration.

High Power Ytterbium-doped Fibre Laser operating around 1.11 μ m

C. J. Mackechnie, W. L. Barnes, D. C. Hanna, J. E. Townsend

Optoelectronics Research Centre,

University of Southampton,

Southampton,

SO9 5NH,

United Kingdom.

TEL: +44 703 593145

FAX: +44 703 593142

Trivalent Ytterbium in glass fibres is well known for having a very broad emission band in the 1 μ m region, and in various glass hosts stimulated emission has been achieved from 974nm to 1170nm[1],[2]. So far, the powers reported for the long wavelength end of this range, above 1100nm, have been rather low. We can now report greater than 500mW of CW output power at 1115nm. This is achieved by pumping an Yb³⁺ doped silica fibre at a much longer wavelength than is normally used. Whereas in previous reports pump wavelengths have centred around 850nm, we have used both a Nd:YLF TFR laser operating at 1.047 μ m and a Nd:YAG, at 1.064 μ m to excite the system. Thus the potential problems of ASE at 974nm and lasing operation in the middle peak of the emission band at 1.040 μ m are automatically excluded since net gain is only available at longer wavelengths than the

pump. Lasing operation can then occur in the tail of the emission spectrum at around 1115nm. At this wavelength, using 100m of Yb^{3+} doped silica, (concentration: 700ppm, radius: $6\mu\text{m}$, NA: 0.17) we have measured 600mW of CW output, where feedback was provided by the 4% reflection from the bare fibre output end and a high reflector at the launch end of the fibre. With an estimated launch efficiency of 45% this implies a slope efficiency with respect to absorbed power of 62%. The gain in this system was actually high enough that with only the two cleaved ends lasing emission was still observed in this case at $1.106\mu\text{m}$. The longest wavelength reached, with a high reflector butted to each end of the fibre, was 1134nm, but our calculations indicate that by using appropriate mirrors or by using fibre gratings it should be possible to achieve significant output powers at even longer wavelengths.

The achievement of high powers at these wavelengths fills a gap in the spectrum of available lasers. The Yb^{3+} fibre source also has the possibility of being tuned over a range of some 50nm above 1100nm, making it a very flexible and convenient alternative to present sources in this region such as a Nd:YAG operating at 1123nm. This is of particular relevance in view of recent results reported by Grubb et al.[3], who used a Nd:YAG laser operating at 1123nm to produce the first-single-wavelength pumped, CW, room temperature, blue up-conversion laser. In fact we have now used the Yb^{3+} fibre described here, operating at $1.114\mu\text{m}$, to pump a Tm^{3+} doped ZBLAN fibre and have obtained lasing emission at 480nm.

Thus the Yb^{3+} doped silica fibre laser pumped by a Nd:YAG or Nd:YLF laser offers a simple and convenient route to efficient CW operation in the infra-red region beyond $\sim 1.08\mu\text{m}$ where few convenient sources are available. Performance achieved to date has been with unoptimised fibres. Efforts are now directed at optimised operation and longer wavelength operation and results of these efforts will be reported.

- [1] 'Yb-doped monomode fibre laser: Broadly tunable operation from 1.010 μ m to 1.162 μ m and 3-level operation at 974nm.' D.C.Hanna, R.M.Percival, I.R.Perry, R.G.Smart, P.J.Suni, and A.C.Tropper, *J. Modern Optics*, 37, pp329-331 1987
- [2] 'Laser Diode pumped Yb-doped single mode tunable fibre laser.' V.P.Gapontsev and I.E.Samartsev, A.A.Zayats and R.R.Loryan, WC1-1, *Advanced Solid State Lasers*, Hilton Head, March 1991.
- [3] 'CW room-temperature blue upconversion fibre laser' S.G.Grubb, K.W.Bennett, R.S.Cannon and W.F.Humer, *Electronic Lett.* 28, 13, June 1992

EXCITED STATE ABSORPTION IN Nd^{3+} DOPED LASER CRYSTALS

Y. GUYOT, R. MONCORGE

Université de Lyon I, URA 442 CNRS, 69622 Villeurbanne, France

Different causes were invoked recently^{1,2,3} to account for the laser performance of Nd^{3+} doped laser crystals such as $\text{Y}_3\text{Al}_5\text{O}_{12}$ (YAG), YLiF_4 (YLF), or $\text{LaMgAl}_{11}\text{O}_{19}$ (LMA).

CW laser measurements showed, for example, in case of diode pumping around 800 nm, laser slope efficiencies above threshold well below the quantum defect-limited value (≈ 75 percent), and it was demonstrated then³ that a more or less adequate overlap of the pump beam and cavity waists within the laser crystal and/or the possibility of having inhomogeneously broadened emission lines could be responsible for that.

Other authors^{1,4,5,6} also invoked pumping of "dead sites", energy transfer of pump radiation to "poison centers" and/or excited-state absorption (ESA) both in the pumping and in the laser emission wavelength domains, but these conclusions, especially in the case of ESA, were often speculative, if plausible, and not backed up by definitive and clear spectroscopic measurements.

Thus, to clarify the situation and, more particularly, to estimate the real contribution of ESA, we report here direct measurements of excited-state excitation (ESE) spectra and of ESA cross sections. These measurements were made in Nd:YAG, Nd:YLF and Nd:LMA (LNA) in their laser emission domains around 1.06 and 1.32 μm and in various pumping regions of interest for flash-lamp and diode laser excitations as well, in the visible and in the near infrared.

The ESA data in the emission domains were collected with the aid of two-beam experiments, one laser beam to populate the Nd^{3+} emitting level $^4\text{F}_{3/2}$ and another beam to probe ESA.

As an example, we show in Figs 1 and 2 the ESE spectra recorded around

1.06 and 1.32 μm in the case of Nd:YAG. This original results are very important since they show definitively that in Nd:YAG, no ESA is predicted -from the energy level scale of Nd^{3+} in this material- and is actually observed at the laser wavelengths of 1.06415 and 1.3187 μm .

The situation in Nd:YLF and in Nd:LMA is more complex since the spectra are strongly polarized. It is found for example that prediction of ESA in Nd:LMA was not so straightforward as expected before ¹.

In the end our presentation on that matter will be completed by an analysis of the possible effect of ESA on the thermooptical (thermal lensing, birefringence) properties of these Nd doped laser materials and, more particularly, in a flash-lamp pumped Nd:YAG laser rod, since big changes were observed when such a rod was lasing or not.

More details will be presented at the conference. A discussion will be developed too concerning the use of the Judd-Ofelt formalism to derive theoretically the ESA cross-sections obtained in the pump-probe experiments.

Acknowledgements:

Thanks are expressed to Mr. Ch. Wyon (LETI/CEA) and Mr. J.P. Denis (CRISMATEC) who provided us with some of the crystals, Mrs G. Brassard and E. Mottay (B.M.Industries) who provided us with the flash-lamp pump chamber and Prof. P. Laporte and Mr. X. Banti (Université de St Etienne) for their aid in collecting some of the data.

References:

1. T.Y. Fan and M.R. Kokta, IEEE J. Quant. Elect. QE 25, 1845 (1989).
2. T.Y. Fan and R.L. Byer, IEEE J. Quant. Elect. QE 24, 895 (1988).
3. N. Mermillod, R. Romero, I. Chartier, C. Garapon and R. Moncorgé, IEEE J. Quant. Elect. QE 28, 1179 (1992).
4. D.P. Devor and L.G. Deshazer, Opt. Comm. 46, 97 (1983).
5. D.P. Devor, L.G. Deshazer and R.C. Pastor, IEEE J. Quant. Elect. QE 25(8), 1863 (1989).
6. M.L. Kliever and R.C. Powell, IEEE J. Quant. Elect. QE 25, 1850 (1989)

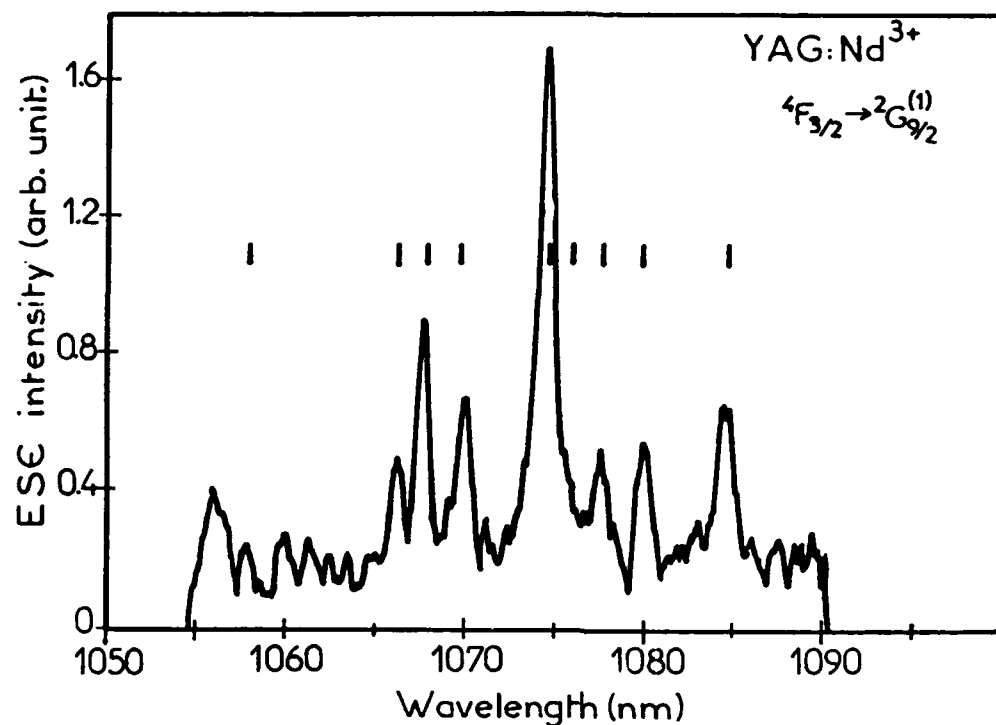


Fig.1: Room temperature excited-state excitation spectrum ($^4G_{7/2}$ emission monitored) of Nd:YAG around 1.06 μm .

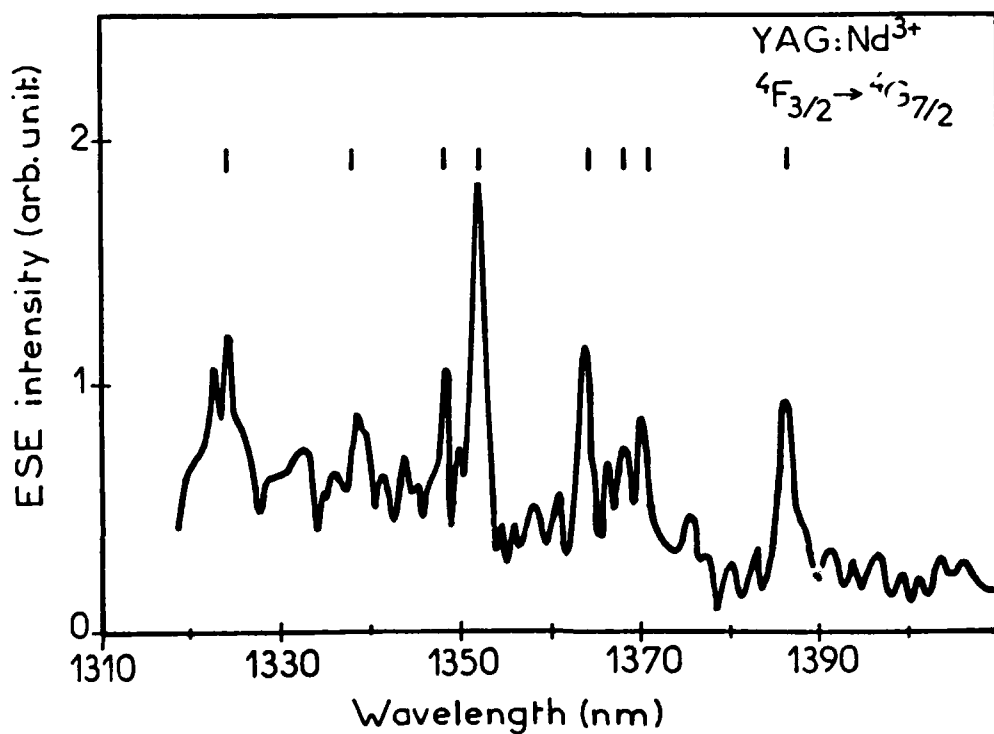


Fig.2: Room temperature excited-state excitation spectrum ($^4G_{7/2}$ emission monitored) of Nd:YAG around 1.32 μm .

ACTIVE MEDIUM FOR ALL-SOLID-STATE TUNABLE UV LASER

Mark A. Dubinskii, Vadim V. Semashko, Alexander K. Naumov,

Ravil' Yu. Abdulsabirov, Stella L. Korableva.

Kazan State University; 18 Lenin Str., 420008 Kazan, Russia

Since 1979 /1/, Ce^{3+} -activated dielectric crystals are the most attractive candidates for the application as an UV tunable solid-state laser active media. However, only three laser media of such kind have been discovered ($\text{YLF}:\text{Ce}^{3+}$ /1/, $\text{LaF}_3:\text{Ce}^{3+}$ /2/, and $\text{LiLuF}_4:\text{Ce}^{3+}$ /3/) despite the large amount of other Ce^{3+} -activated crystals-candidates studied so far (e.g., /4, 5/). So, the search for new Ce-activated media is of great importance. And the most attractive would be the medium suitable for pumping by the UV harmonics of commercially available solid-state lasers, in contrast to known excimer-pumped media /1-3/, to realize the all-solid-state tunable laser source.

Here we report the results of spectroscopic studies, tunable gain features and lasing from the first medium of such kind - Ce^{3+} -activated LiCaAlF_6 single crystal pumped by the quadrupled output of a Q-switched Nd-YAG laser at 266 nm.

$\text{LiCaAlF}_6:\text{Ce}^{3+}$ ($\text{LiCAF}:\text{Ce}$) fluorescence spectra obtained display nearly double-humped shape characteristic of Ce^{3+} ion in most of the hosts /1-3,5/. The main peak positions are about 287 and 309 nm. The spectra also give an indication of multisite character of the Ce^{3+} activation which is concentrational-

ly dependent. The fluorescence lifetime was found to be of 50 ± 5 ns, the quantum yield - about 90%. The pump-probe experiments with the 266 nm pumping gave the evidence of significant tunable single-pass gain. The gain vs wavelength dependence is shown in Fig. 1. The gain curve shape follows the fluorescence spect-

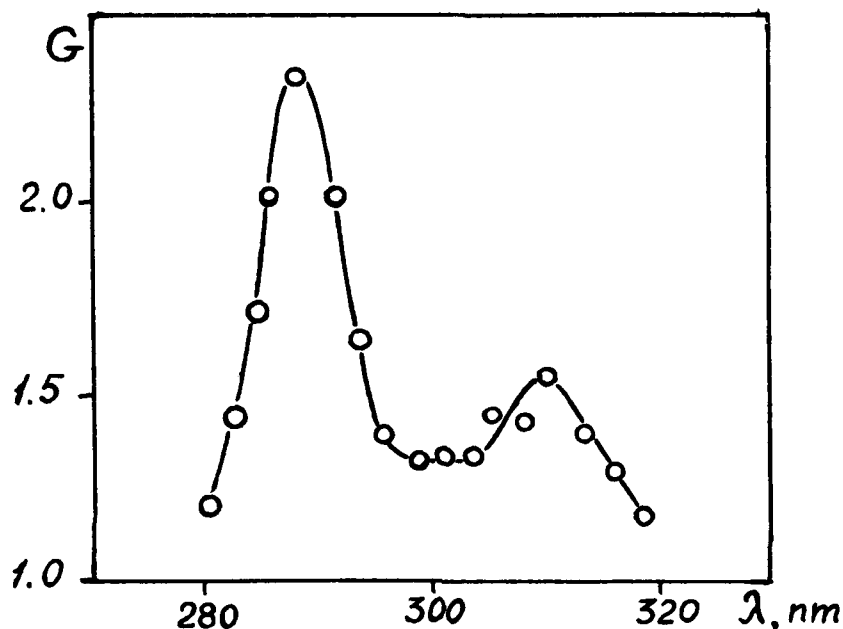


Figure 1. LiCAF:Ce gain spectrum.

rum, which means qualitatively the absence of significant ESA in the gain region.

Laser action at 288 nm from LiCAF:Ce sample has been observed as well. The threshold pumping energy flux in nonselective cavity with highly reflecting mirrors was found to be as low as 32 mJ/cm^2 and is the lowest among the known Ce-activated laser media [1-3]. Spectral bandwidth of the radiation emitted in this case was about 2 nm, output pulse duration - 5 ns (pumping pulse duration - 8 ns). Using the nonselective cavity with the plane-parallel mirrors, the output mirror transmission of 68%,

the slope efficiency of 6.5% was reached in this first experiments without any optimization of the device. No visible sample coloration appeared after more than 3 hours irradiation by the pumping source at 12.5 Hz repetition rate. No change in the conversion efficiency was observed with pumping pulse repetition rate.

As the crystals studied did not display any evidence of the ESA in the region of tunable gain, and stable or transient color centers formation under the pumping did not take place, our findings promise the creation of reliable, all-solid-state tunable UV laser source in the nearest future. A careful spectroscopic examination of polarization effects, multisite activation peculiarities of Ce-activated LiCaAlF_6 and its single crystal homologues, as well as detailed tunability studies of the first all-solid-state UV laser, based on rare-earth ion d-f-transitions, are now in progress.

References

1. D.J.Ehrlich, P.F.Moulton et al. Opt. Lett. 4, 184 (1979).
2. D.J.Ehrlich, P.F.Moulton et al. Opt. Lett. 5, 339 (1980).
3. M.A.Dubinskii, R.Yu.Abdulsabirov et al. 18-th Intern. Quant. Electr. Conf. (Vienna, June 14-19, 1992), Techn. Dig., paper FrL2
4. R.Yu.Abdulsabirov, M.A.Dubinskii, B.N.Kazakov, et al., Sov. Phys. Crystallogr. 32, 559 (1987).
5. D.S.Hamilton, in "Tun. Sol.-St. Las." (Spr.-Verl., 1985), p.80.

Tuesday, February 2, 1998

Novel Optical Materials Poster Session

ATuB 9:45am–10:45am
La Salle Ballroom A

CW-lasing of Pr:YAlO₃ at room temperature

A.Bleckmann, F.Heine, J.P.Meyn, K.Petermann and G.Huber

Institut für Laser-Physik , Universität Hamburg

Jungiusstraße 9 - 11 , D 2000 Hamburg 36

Fed. Rep. Germany

FAX 4940-4123-6571

Summary

The interest in solid state lasers based on Pr³⁺ is due to the fact, that Pr³⁺ offers many transitions in the visible and near infrared spectral region. The first pulsed 77 K -laser operation of Pr³⁺ was demonstrated in CaWO₄ by Yariv et al. in 1962 [1]. In the meantime, pulsed 300 K stimulated emission of Pr³⁺ has been reported at several wavelengths in different host crystals [2, 3, 4]. In all these measurements pulsed laser pumping or flashlamp pumping was used. In this paper we demonstrate, that in YAlO₃ from both metastable levels, that is ³P₀ and ¹D₂, cw laser operation is possible under Argon laser excitation.

In our laser experiments we have chosen the host lattice YAlO₃ because these crystals exhibit rather small phonons and can be grown in good laser quality. Furthermore the anisotropy of Pr³⁺:YAlO₃ crystals allows high cross sections in special orientations. As shown in Figure 1 and 2 the absorption and emission spectra depend strongly on the orientation of the crystal. The strongest absorption for argon laser excitation at 476.5 nm is given for $\vec{E} \parallel \vec{c}$ with an effective absorption cross section of $1.4 \cdot 10^{-20} \text{ cm}^2$ (doping level $2 \cdot 10^{20} \text{ cm}^{-3}$).

Laser emission of Pr:YAlO₃ could be obtained at 662.4 nm for $\vec{E} \parallel \vec{a}$, at 613.9 nm and at 753.7 nm for $\vec{E} \parallel \vec{b}$ and finally at 621.6 nm, 719.5 nm, 746.9 nm and 996.0 nm for $\vec{E} \parallel \vec{c}$. This shows the great influence of the orientation upon the possible laserwavelengths of the crystal.

The experimental data have shown slope efficiencies between 1 % and 5 %. In Figure 3 for example the input-output diagram is shown for the $^3P_0 - ^3F_4$ transition at 746.9 nm after excitation with an argon-ion laser operating at 476.5 nm. The first results of our measurements have been 230 mW for the pump power threshold, 12 mW for the maximum output power and 1.1 % for the slope efficiency using mirrors with a transmission of $T = 1.0$ %.

After optimizing the crystal to a length of 5 mm and a doping level of $1.5 \cdot 10^{20} \text{ cm}^{-3}$ we obtained a maximum output power of 30 mW for $T = 10$ % and a slope efficiency of almost 5 % which holds about for all observed laser lines. Further optimization is in progress.

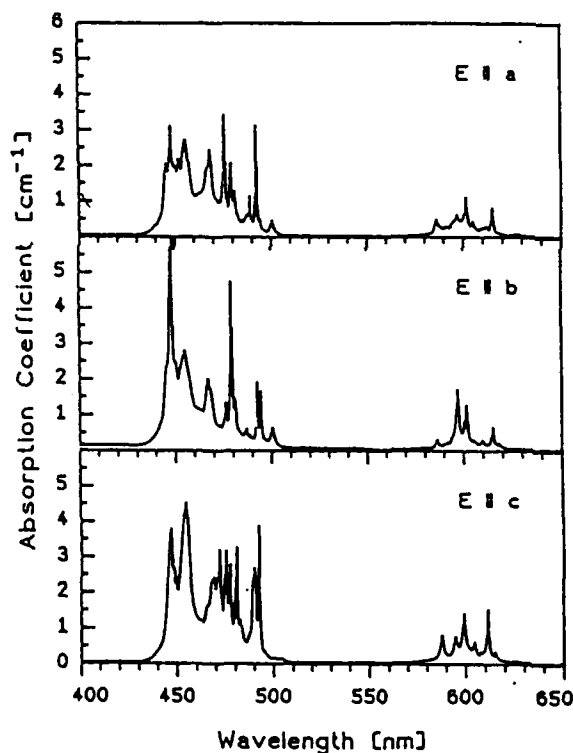


Fig. 1
Absorption spectra of Pr:YAlO₃
along the main crystallographic axes.

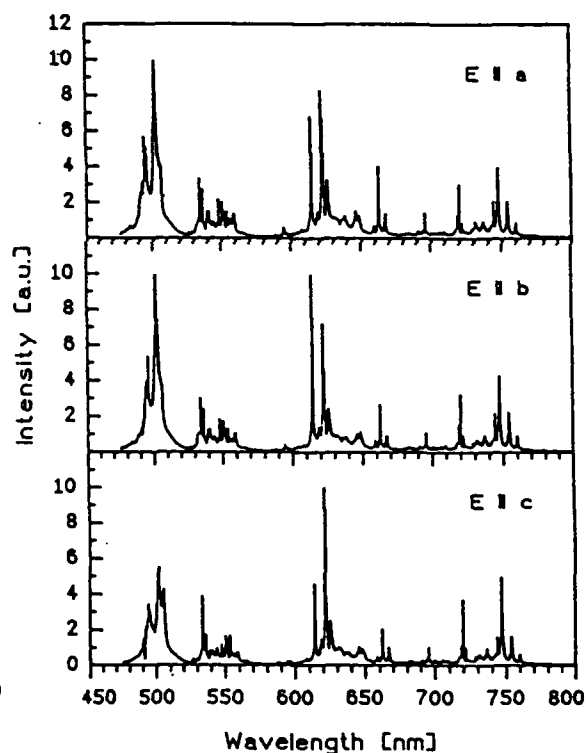


Fig. 2
Fluorescence spectra of Pr:YAlO₃
along the main crystallographic axes.

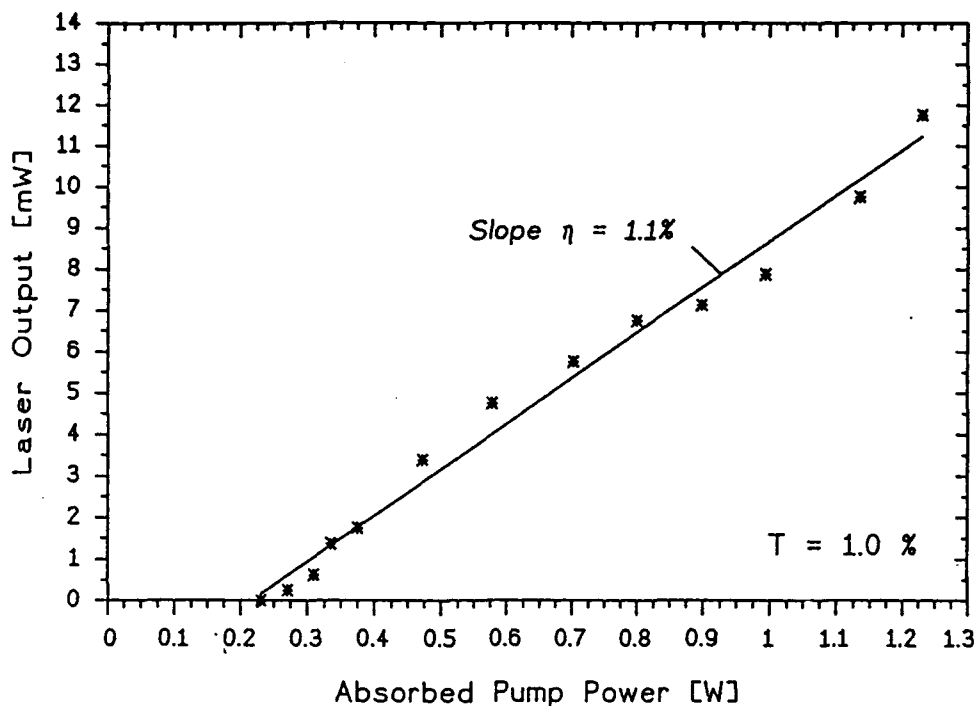


Figure 3.

Input-Output diagram of Pr:YAlO₃ after excitation with an Argon-ion laser operating at 476.5 nm. Laser emission at 746.9 nm.

References

- [1] A.Yariv, S.P.S. Porto and K. Nassan, J.Appl.Phys. 33, p. 2519 (1962).
- [2] Alexander A. Kaminskii, K.Kurbanov, K.L.Ovanesyan and A.G. Petrosyan, phys. stat. sol.(a) 105, p K155-K159 (1988).
- [3] David S.Knowles, Z.Zhang, David Gabbe and H.P.Jenssen, "Laser Action of Pr³⁺ in LiYF₄ and Spectroscopy of Eu²⁺-sensitized Pr in BaY₂F₈" IEEE J. Quantum Electron. QE-24, p. 1118-1123 (1988).
- [4] Esterowitz, R.Allen, M.Kruer, F.Bartoli, L.S. Goodberg, H.P.Jenssen, A.Linz and V.O. Nicolai, "Blue light emission by a Pr:LiYF₄-laser operated at room temperature" J.Appl.Phys. 48, p.650 (1977).

Relative Upconversion Rates in Tm-Ho doped crystals.

K.M. Dinndorf, A.Cassanho, Y.Yamaguchi, and H.P. Janssen

Laboratory for Advanced Solid State Laser Materials
Center for Materials Science and Engineering
Massachusetts Institute of Technology
Cambridge, MA 02139
(617)-253-6878

and

M.Tonelli

Dipartimento di Fisica dell' Universita' Pisa, Pisa, Italy

Introduction

A series of experiments has been conducted in order to compare the potential of different hosts for use in room-temperature Tm-Ho 2 μ m laser systems. The efficient operation of this system depends upon a number of host dependent parameters. One of the main loss mechanisms of the Tm-Ho 2 μ m laser has been identified as $^3F_4 \Rightarrow ^3H_6$, $^5I_7 \Rightarrow ^5I_5$ upconversion (See, for example, [1]). This mechanism acts as a loss by draining the excitations from the upper laser level at high excitation densities. This loss mechanism can be partially offset by the reverse process of cross-relaxation. A simple model which incorporates these as well as other parameters of importance has been used to describe the system and is illustrated in Fig. 1. Using this model, we have been able to extract from experimental data approximate relative values of the upconversion and cross-relaxation coefficients for YLF, BaY₂F₈, and NaYF₄.

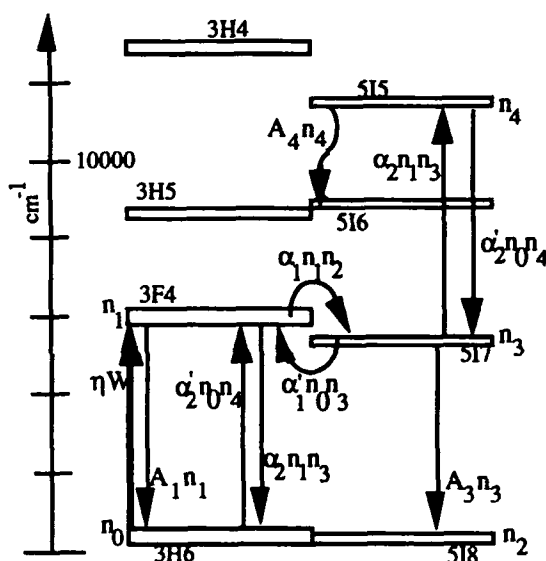


Figure 1. Simplified model for the Tm-Ho 2 μ m system. Spontaneous emission decays omitted.

In this model, η is the effective pumping efficiency of the 3F_4 level of Tm; this can be calculated for 790 nm diode pumping from the cross-relaxation rate of the 3H_4 level of Tm. α_1 and α_1' are, respectively, the parameters for transfer and back-transfer from Tm(3F_4) to Ho(5I_7), α_2 is the upconversion parameter for $^3F_4 \Rightarrow ^3H_6$, $^5I_7 \Rightarrow ^5I_5$ upconversion, and α_2' is the parameter for cross-relaxation. A_1 , A_3 , and

A_4 are the total relaxation rates for singly-doped crystals.

The parameter which we first will discuss in evaluating the potential efficiency of the 2 μm laser is the $^5\text{I}_5$ cross-relaxation rate ($\alpha_2' n_0$). In singly-doped Ho hosts, the primary channel of $^5\text{I}_5$ decay is non-radiative relaxation to $^5\text{I}_6$, while in co-doped materials, other channels become available. Of primary interest is the $^5\text{I}_5 \Rightarrow ^5\text{I}_6$, $^3\text{H}_6 \Rightarrow ^3\text{F}_4$ cross-relaxation that occurs when Ho and Tm are co-doped in a material. Upconversion acts as a loss by promoting an excitation from the Ho $^5\text{I}_7$ level to the $^5\text{I}_5$ level by accepting energy from an excitation in the Tm $^3\text{F}_4$ level, which drops to the $^3\text{H}_6$ state. Thus, two excitations are lost from the upper laser level (the Tm $^3\text{F}_4$ level acts as a reservoir of excitations for the $^5\text{I}_7$ level). Any excitation that returns from $^5\text{I}_5$ via cross-relaxation does not act as loss on the system as this process essentially reverses the upconversion. Excitations which do not return to the $^5\text{I}_7$ - $^3\text{F}_4$ manifolds via cross-relaxation return either by non-radiative relaxation and energy-transfer or by spontaneous emission and are responsible for the loss experienced by the system as, at most, only one excitation returns to the upper level. These processes are described in Fig. 1 by the term $A_4 n_4$. Therefore, to assess the potential loss due to $^5\text{I}_5$ upconversion on the system we can measure the singly-doped decay rate (A_4) and the cross-relaxation rate. The competition between these two rates will determine the potential

loss due to upconversion. It can be seen that a high cross-relaxation rate coupled with a low decay rate can largely offset the loss due to upconversion.

Cross-relaxation

The cross-relaxation rate can be measured by observing the shortening of the Ho $^5\text{I}_5$ lifetime when Tm is co-doped with Ho in the material. The lifetimes are measured by directly pumping the $^5\text{I}_5$ multiplet with a pulsed Ti:Sapphire laser. Table 1 presents the results of these measurements.

Material	Lifetime (initial decay)	Appr. cross- relax. rate
1%Ho:YLF	$18 \pm 2 \mu\text{s}$	0
10%Ho:YLF	$18 \pm 2 \mu\text{s}$	0
6%Tm, 1.2%Ho:YLF	$7 \pm 2 \mu\text{s}$ (~4)	$8.7 \times 10^4 \text{ s}^{-1}$
6%Tm, 0.6%Ho:YLF	$7 \pm 2 \mu\text{s}$ (~4)	$8.7 \times 10^4 \text{ s}^{-1}$
50%Er, 6.7%Tm, 1.7%Ho:YLF	$< 1 \mu\text{s}$	$> 9.4 \times 10^5 \text{ s}^{-1}$
1%Ho:BYF	$50 \pm 4 \mu\text{s}$	0
5%Tm, 1%Ho:BYF	$19 \pm 2 \mu\text{s}$ (~8.5)	$3.2 \times 10^4 \text{ s}^{-1}$
8%Tm, 0.8%Ho:BYF	$8 \pm 3 \mu\text{s}$ (~5.5)	$1.05 \times 10^5 \text{ s}^{-1}$
0.5%Ho:NYF	$130 \pm 5 \mu\text{s}$	0
5%Tm, 0.5%Ho:NYF	$58 \pm 5 \mu\text{s}$ (??)	$9.5 \times 10^3 \text{ s}^{-1}$

Table 1. $^5\text{I}_5$ Cross-relaxation rates for various materials.

The time-dependent fluorescence of the co-doped materials was non-linear in nature, with a fast initial decay which quickly ($\sim < \text{one time constant}$) became approximately linear. The above reported lifetimes represent the time-constants measured in the linear (singly-doped) or nearly-

linear (co-doped) portion of the decays; the initial slope of the fluorescent decay is reported in parentheses for the decays that display a resolvable non-linear decay, with the exception of NaYF₄, for which no numbers were obtained. What inferences can be drawn from these initial slope numbers is not clear at this time; however, they most likely represent an effective cross-relaxation rate for near neighbor pairs (when a Tm ion is nearly adjacent to a Ho ion). This may be of significance in that the $^5I_7 \Rightarrow ^5I_5$, $^3F_4 \Rightarrow ^3H_6$ upconversion process is most likely to occur when the Tm ions are adjacent to the Ho; therefore, it may be that the cross-relaxation process may be more efficient (i.e. have a higher rate) for ions pumped by upconversion than would be predicted from measurements made with simple experiments. As the lifetimes reported represent the nearly-linear portion of the decay, the cross-relaxation rates derived from them (Col. 3, Table 1) represent the cross-relaxation rates as seen by Ho ions in many different environments and therefore serve as a lower limit on the cross-relaxation rate that could be expected for quenching the upconversion. Also note how the cross-relaxation rate increases with increasing Tm concentration for the BaY₂F₈ sample - it may be possible to decrease the loss due to upconversion by increasing the Tm concentration.

Relative Upconversion Rates

Using the cross-relaxation rate and a few assumptions, an approximate measurement of the relative upconversion rates can be made by measuring the 5I_5 and 5I_7 emission intensities as a function of pump power. These measurements are currently underway and the results will be presented at the conference. Preliminary results indicate that the upconversion rate is lower in NaYF₄ than in the other two hosts. In fact, it appears that the upconversion parameter varies from host to host in the same manner as the cross-relaxation parameter. This is expected from simple Forster-Dexter theory as both processes arise from the same mechanism, with some quantitative differences due to the position of the energy levels [2].

To extract the absolute value of the upconversion coefficient for a material, a detailed knowledge of either the 3F_4 - 5I_7 population distribution or of the 3F_4 - 5I_7 transfer coefficients (α_1 and α_1') is required. Measurements to determine this information are currently being planned.

References

1. S.R. Bowman, S. Searles, B.J. Feldman, M.J. Winings, and R.C.Y. Auyeung, "Upconversion studies of Flashlamp-pumped Cr,Tm,Ho:YAG", Proc. of ASSLC, Hilton Head, S.C., 1991.
2. J.C. Wright, in Radiationless Processes in Molecules and Condensed Phases, ed. F.K. Fong, Springer-Verlag, Berlin, 1976, P. 239.

Tunable Erbium-Doped Fiber Ring Laser Using Fiber-Birefringence Tuning Technique

Paul D. Humphrey and John E. Bowers

University of California at Santa Barbara
Department of Electrical and Computer Engineering
Santa Barbara, CA 93106
Tel. (805) 893-4235

Tunable fiber lasers have been made by many techniques, including the use of fiber Fabry-Perot etalon filters [1]-[3], liquid crystal etalon filters [4], fiber grating reflectors [5], external gratings [6], and acousto-optic modulation [7]. Recently, uncontrolled wavelength changes were observed [8] in the output of fiber lasers containing intracavity polarizers during adjustment of intracavity polarization controllers. We report on a simple new technique to controllably tune a fiber laser and we provide a graphical illustration of the tuning process. The method is generally analogous to that used in some tunable Lyot-type filters [9]. A schematic diagram of the laser is shown in Fig. 1. The state of polarization (SOP) at points a-f in Fig. 1 is depicted in the Poincare spheres of Fig. 2(a)-(f) as a function of wavelength.

Recall that on the Poincare sphere, the SOP with azimuth ϕ and ellipticity $\psi = \arctan(b/a)$ is represented as a point with longitude 2ϕ and latitude 2ψ . The effect of a retardance Γ on the SOP of the light passing through it is to rotate the SOP on the Poincare sphere about the axis through the points corresponding to the fast and slow axes of the retardance. The SOP is rotated through an angle equal to Γ , in a CCW sense looking from the fast axis SOP to the slow axis SOP. Linear retarders may be implemented in fiber through the use of controlled bends. A coil of fiber acts as a linear retarder having its fast axis in the plane of the coil.

Let us now consider the effect of the wavelength dependence of the linear retardance. For clarity of explanation we will neglect the wavelength dependence of the refractive index, Poisson's ratio, and the strain-optic coefficients. Then the retardance is inversely proportional to the wavelength, such that longer wavelengths experience less retardance, and thus less rotation on the Poincare sphere, than shorter wavelengths. When a broadband input signal with a linear SOP passes through a linear retarder with its fast axis at 45° to the linear polarization, the output SOP will have constant azimuth but a wavelength-dependent ellipticity. We represent this SOP by a locus of points on the Poincare sphere with constant longitude but wavelength-dependent latitude [10].

We will need to know the amount of retardance $\Gamma(\lambda_0)$ required to transform an incident linear SOP with spectral width $\Delta\lambda = \lambda_+ - \lambda_-$ into a locus of points extending all the way around the sphere so that it closes on itself. Using the simple wavelength dependence described above, we may write the retardance as $\Gamma(\lambda) = \Gamma(\lambda_0) (\lambda_0/\lambda)$. We let λ_0 represent the center of the wavelength range $\Delta\lambda$ of interest, such that $\lambda_0 = 0.5 (\lambda_+ + \lambda_-)$. Finally, we equate the difference in retardance between the extremes of the wavelength range to 2π , representing a complete rotation on the Poincare sphere: $2\pi = \Gamma(\lambda_+) - \Gamma(\lambda_-)$. Solving for λ_0 , we find $\Gamma(\lambda_0) = 2\pi (\lambda_0/\Delta\lambda)$. In other words, the order of the waveplate required is given by $\lambda_0/\Delta\lambda$. For $\lambda_0 = 1550$ nm and $\Delta\lambda = 50$ nm, a 31-wave plate is required.

The general method of the tuning is as follows:

- Pass the light leaving the polarizing isolator through a linear retardance Γ with its fast axis at 45° to the linear polarization and magnitude $\Gamma(\lambda_0) = 2\pi (\lambda_0/\Delta\lambda)$.
- Use two quarterwave coils of fiber to move the SOP locus to the equator.
- Tune the laser by rotating a halfwave fiber coil to bring the SOP of the desired output wavelength nearest to the SOP passed by the input polarizer of the polarizing isolator.

Figure 2 shows the SOP locus as a function of wavelength for each step in this tuning process. In the figures, H and D represent horizontal and diagonal linear polarizations, while R represents right-circularly polarized light. The symbol F is nearest the fast axis end of the axis of

rotation. The SOP locus was plotted for a 45-nm wavelength range, from 1527.5 nm to 1572.5 nm, to approximate the maximum gain bandwidth that might be expected for erbium-doped fiber (EDF).

In Fig. 2(a) the SOP is linear horizontal as the light leaves the polarizing isolator and enters the 31-wave plate provided by the EDF coil oriented at 45°. Fig. 2(b) shows the SOP locus of the light leaving the EDF coil. A random shift is introduced between Fig. 2(b) and Fig. 2(c) to account for uncontrolled bends between the exit of the EDF coil and entrance of the first quarterwave coil. Fig. 2(c) shows the SOP locus as it enters the first quarterwave coil, which is oriented to bring one of the two points where the SOP locus crosses the equator to a pole, such that the locus is again in a polar plane. Fig. 2(d) shows the SOP locus as it enters the second quarterwave coil, which is oriented to bring the polar plane containing the SOP locus to the equatorial plane by rotating about the axis containing the two points where the SOP locus crosses the equator. Fig. 2(e) shows the SOP locus as it enters the halfwave plate, which is used to rotate the SOP of the desired wavelength to the diagonal linear SOP of the input polarizer of the polarizing isolator. The axis of the halfwave rotation is placed such that it bisects the angle between the diagonal linear SOP and the SOP of the desired wavelength. Finally, Fig. 2(f) shows the SOP locus as it enters the polarizing isolator.

A 10-m length of EDF with a core diameter of 3- μ m and a 1- μ m cutoff wavelength was used. Its erbium concentration is estimated to be 440 ppm. The EDF was wound (taking care not to twist the fiber) on a 25-mm diameter rod, introducing an estimated 25-wave retardance. The EDF was reverse pumped by a 30-mW, 1480-nm laser diode. The 10% output coupler provided a slope efficiency of 2%. The laser operated multimode, although one might expect that it would lase in a single longitudinal mode because the effect of spatial hole burning is eliminated in traveling wave operation [6]. The longitudinal mode spacing was 10 MHz.

An optical spectrum analyzer with a 0.1-nm resolution bandwidth was used to measure the laser tuning. A typical spectrum is shown in Fig. 3. The linewidth of the laser was less than 0.1 nm. The tuning curve of output power versus wavelength of operation with constant pump power is shown in Fig. 4. This data was taken with a preliminary laser cavity using a polarizing beamsplitter and a wavelength-independent isolator in place of the polarizing isolator. When the quarterwave coils were optimally positioned, the output wavelength was a monotonic function of the position of the halfwave fiber coil. The optimum quarterwave coil positions were determined through a process of trial and error.

In conclusion, a new method of tuning fiber lasers over a wide range is explained and demonstrated. The laser was tuned from over a 33-nm range by rotation of the halfwave coil.

REFERENCES

- [1] N. Park, J. W. Dawson, K. J. Vahala, and C. Miller, *Appl. Phys. Lett.*, vol. 59, pp. 2369-2371, 1991.
- [2] H. Schmuck, T. H. Pfeiffer, and G. Veith, *Electron. Lett.*, vol. 27, pp. 2117-2119, 1991.
- [3] J. L. Zyskind, J. W. Sulhoff, Y. Sun, J. Stone, L. W. Stulz, G. T. Harvey, D. J. Digiovanni, H. M. Presby, A. Piccirilli, U. Koren, and R. M. Jopson, *Electron. Lett.*, vol. 27, pp. 2148-2150, 1991.
- [4] M. W. Maeda, J. S. Patel, D. A. Smith, C. Lin, M. A. Saifi, and A. Von Lehman, *IEEE Photon. Tech. Lett.*, vol. 2, pp. 787-789, 1990.
- [5] G. A. Ball and W. W. Morey, *Opt. Lett.*, vol. 17, pp. 420-422, 1992.
- [6] G. J. Cowle, D. N. Payne, and D. Reid, *Electron. Lett.*, vol. 27, pp. 229-230, 1991.
- [7] P. F. Wysocki, M. J. F. Digonnet, and B. Y. Kim, *Opt. Lett.*, vol. 15, pp. 273-275, 1990.
- [8] U. Ghera, N. Konforti, and M. Tur, *IEEE Photon. Tech. Lett.*, vol. 4, pp. 4-6, 1992.
- [9] A. M. Title and W. J. Rosenberg, *Opt. Eng.*, vol. 20, pp. 815-823, 1981.
- [10] M. Johnson, *Appl. Opt.*, vol. 20, pp. 2075-2080, 1981.

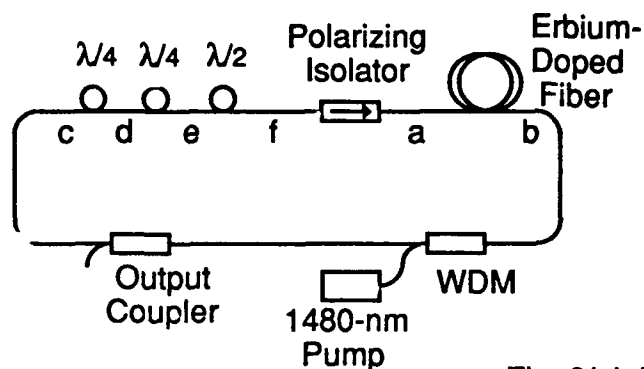


Fig. 1: Tunable Fiber Laser

Fig. 2(a)-(f): Poincaré sphere representation of SOP as a function of wavelength at points a-f in Fig. 1

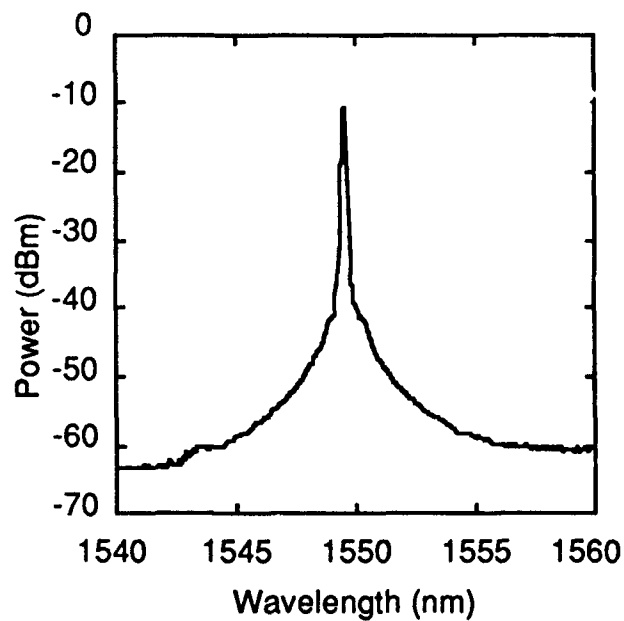
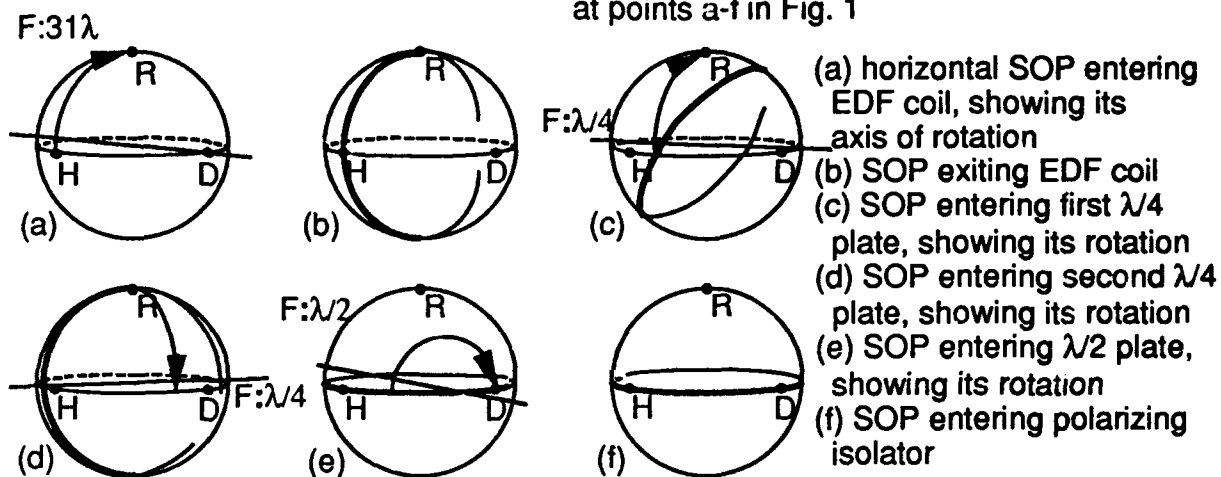


Fig.3: Output optical spectrum

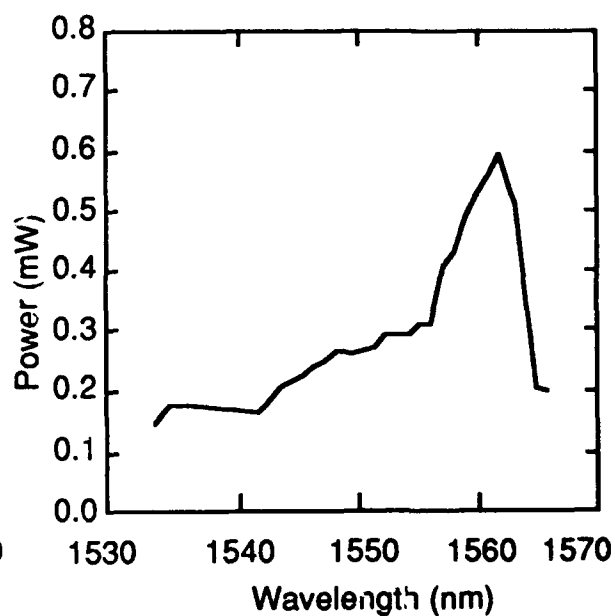


Fig. 4: Laser tuning curve

MODIFIED DYE-DOPED POLYMER ACTIVE MEDIA WITH ADVANCED
LASER DAMAGE RESISTANCE AND PHOTOCHEMICAL STABILITY

V.N.Serova, A.A.Vasil'ev, E.L.Koryagina

Kazan Chemical-Technology Institute;

68 K.Marx St., 420015 Kazan, Russia

M.A.Dubinskii, A.K.Naumov, V.V.Vemashko

Kazan State University; 18 Lenin St., 420008 Kazan, Russia

Dye-doped polymers (DDP) are the cheapest solid-state active media of tunable lasers and have considerable advantages in comparison with a dye solutions /1,2/. Unfortunately, as compared to solid-state crystalline media they have insufficient laser damage resistance (LDR) and photochemical stability. Hence, the search for new polymer laser materials with the advanced operational characteristics is of great importance.

The subjects of our studies were metacrylic copolymers of different chemical composition and structure doped by some Rhodamine dyes. Different modifying additions, such as organic and inorganic acid salts of metals, and P-, N-, S- and O- containing organic compounds have been used. The influence of chemical composition, sub- and supermolecular structure of metacrylic copolymers and the nature of modifying additions on the LDR, photochemical stability (under the pumping conditions) and the efficiency of DDP active elements have been studied. The frequency-doubled radiation of single-mode YAG:Nd Q-switched laser

has been used for pumping.

It was shown that the LDR of widely used for DDP-lasers co-

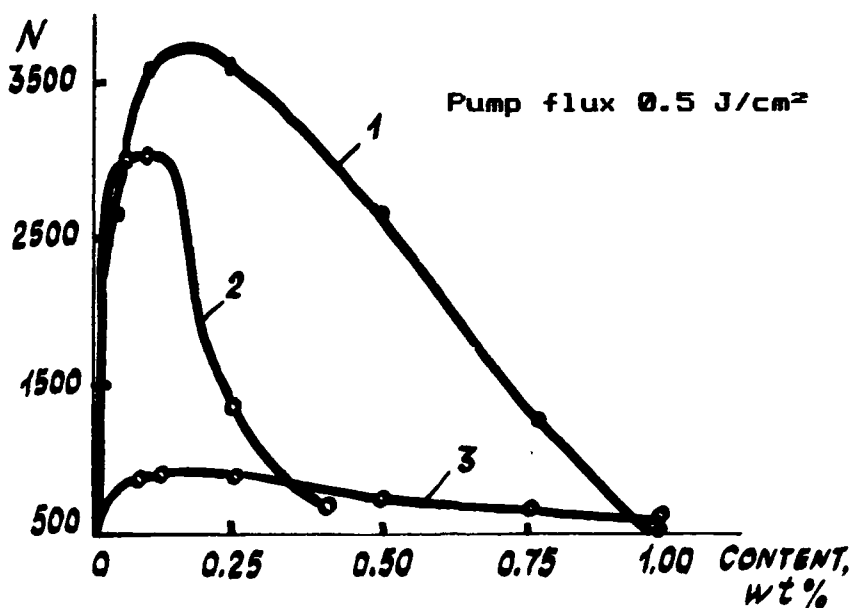
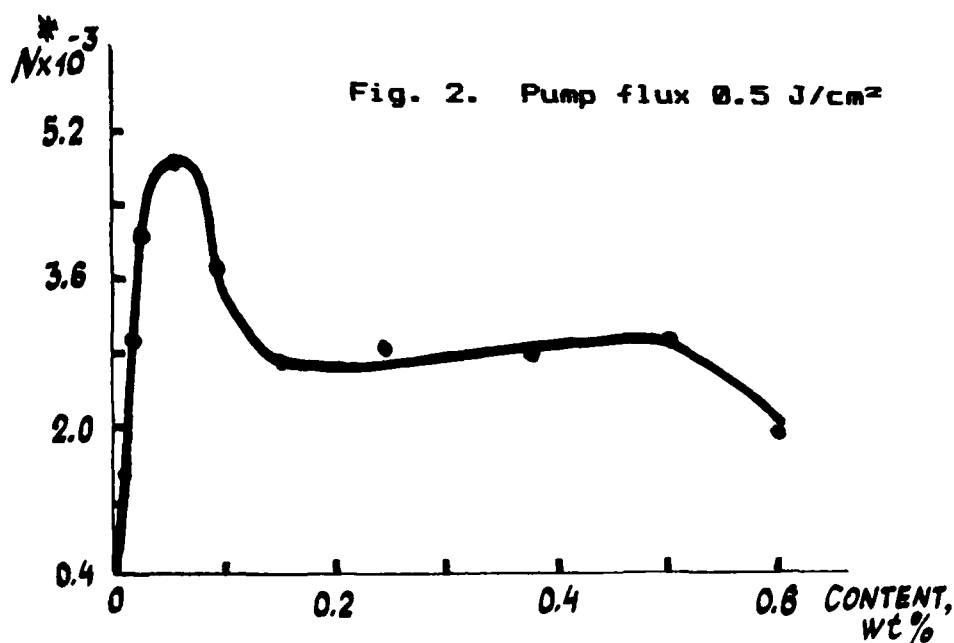


Fig. 1. 1- $\text{Er}_2(\text{CO}_3)_3$; 2- Er-metacrylate; 3- $\text{Ce}(\text{NO}_3)_3$.

polymer of methylmetacrylate with metacrylic acid (MMA-MA) [3/ can be improved by their physical and chemical modifying. In Fig. 1 the dependences of number of laser pumping pulses preceding the first MMA-MA damage (N) on the modifier content are shown. The addition of 0.15 - 0.25 wt% $\text{Er}_2(\text{CO}_3)_3$ or Er-MA improves the LDR more than 7 times. It was revealed also that the LDR of given copolymer can be improved even much more (about 60 times) by adding some N-, S- an O- containing organic modifiers (NSO).

Essential index of practical value for DDP is its photochemical stability under the pumping conditions, defined as a pumping pulse number (N^*) preceding the twofold drop of DDP-laser output energy. The corresponding dependence for Rhodamine-



-66 doped copolymer MMA-MA on the NSO-modifier content is shown in Fig. 2. It is evident that NSO-adding makes it possible more than 10-fold increase of DDP active element photochemical stability. The efficiency of DDP-lasers with the modified media is at an average 1.2 times as high as with the initial ones and reaches 32-35%.

Thus, the new DDP active media with advanced LDR and photochemical stability have been obtained and the possibility to increase significantly the operational characteristics of DDP - based tunable solid-state lasers is demonstrated.

References

1. V.I.Bezrodnij, O.V.Przonskaja et al. - Sov. J. Quant. Electronics 9, 2455 (1982).
2. R.M.O'Connell, T.Saito. - Opt. Engineering 22, 393 (1983).
3. F.Higuchi, J.Muto. - Phys. Lett. 99A, 121 (1983).

Broad Band Thin Film Plate Polarizer for High Power Femtosecond Solid-State Lasers

Donny Mal A. Aminou
Alpine Research Optics Corp.
 2810 Wilderness Place, Unit B, Boulder CO 80301

Jeff Squier
Center for Ultrafast Optics, 2200 Bonisteel, Ann Arbor, Michigan 48109-2099

Abstract

We report the first demonstration of Ultra Broad Band Thin Film Plate Polarizers (UBB-TFP) for femtosecond (fs) / wide band tunable solid-state lasers. By increasing the angle of incidence from the Brewster's angle, we were able to produce very efficient TFPs. Such polarizers dramatically improve the tunability of femtosecond regenerative amplifiers.

Introduction

Compact solid-state femtosecond amplifiers presently rely on chirped pulse amplification techniques to safely extract the stored energy from the gain media. This technique consists of temporally stretching or chirping the pulse prior to amplification, and recompressing to the fourrier transform limit post amplification. The most efficient amplifier for these purposes is a regenerative amplifier. This configuration allows the injected pulse to make any arbitrary number of passes through the gain media in order to fully deplete the stored energy. The most difficult aspect of the regenerative amplifier is that broad band intracavity elements are required to minimize spectral narrowing. The first limiting element is the intracavity polarizer, and care must be taken to ensure that it is appropriately broad. Previous polarizers limited the tunability (for 100 fs pulses) to ~20 nm, and the minimum achievable pulsewidth to ~50 fs. At Alpine Research Optics (ARO), we have developed ultra broad band plate polarizer thin films that are improved upon the best currently available for chirped-pulse amplification. This paper addresses questions regarding the performance of these TFPs, how to improve their efficiency, their

bandwidth and their damage threshold to meet the chirped-pulse amplification requirements.

Overview of various polarizers

Broad band plate polarizers are difficult to fabricate, especially when high power is requested. The most common polarizers are cubes^{1, 2} (MacNeille or Glan-Thomson and Glan-Taylor) and Brewster's angle plate polarizers. The cubes produce high extinction ratios (T_p/T_s) for wider bandwidth. But, they are limited to low energy lasers because of the inherent vulnerability of their optical cement to laser damage. One of the best cubes is the Glan-laser polarizing prism which is air spaced, and has an exit port for the reflected polarization state. Therefore, the power handling ability of these polarizers is determined by the damage resistance of the crystal (calcite). Unfortunately, calcite contains impurities within the crystal. The average power it can handle is around 500 MW/cm² at 1.064 μ m, 10-20 ns pulse, which in general is too low for chirped-pulse amplification. TFPs can withstand higher power laser fluxes and are easier to use. In general, they work at Brewster's angle so that the P-polarization is totally transmitted and the S-polarization totally reflected. However, at this angle of incidence, only

one wavelength can be selected and polarized. This is where our TFPs make the difference.

Principles

The reflectance of a beam on a dielectric multilayer coating at a skew angle of incidence changes with the S and P vibration. One can find geometrical configurations for which $R_S \sim 1$ and $T_P \sim 1$, R_S being the reflectance for the S-vibration and T_P being the transmission of the P-vibration. The base period of the coating is formulated by $(HL)^N H$ or $(LH)^N L$ composed with a stack of two well chosen dielectrics L and H , of low and high indices n_L and n_H repeated N times. The design here, consists of making a table of P and S reflectivities as a function of the layer thicknesses. Those combinations that give the best split of S and P components at a given angle of incidence solve a particular problem.

TFPs at Brewster's angle of incidence are used to separate the S and P planes of polarization of an incident beam. Every interface of the ultra hard multi layer dielectric coating reflects a percentage of the S and transmits the P planes of polarization so that as light passes through the resonant coating stack it becomes progressively polarized. An anti-reflection coating is not necessary as it is already optimized for transmission at Brewster's angle.

In order to fully exploit the bandwidth of a tunable Ti-Sapphire (Ti-S) laser and its chirped pulse^{3, 4, 5} ability (Fig. 1), we designed a wider angle of incidence (68-72°) thin film plate polarizers, which requires an anti-reflection coating on the second side of the plate as the P Plane of polarization reflects up to 4.5% on a fused silica substrate (Fig. 2). Very good polarizing effects are obtained when the Banning¹ conditions are satisfied.

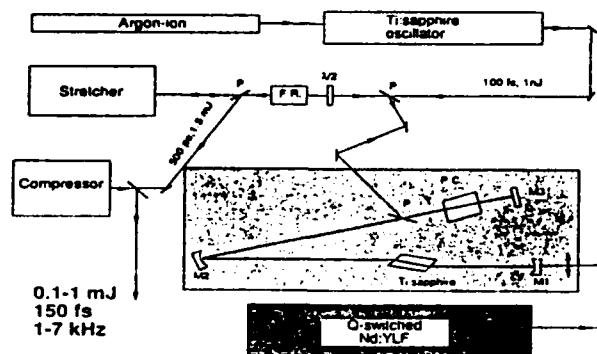


Fig. 1 : Experimental set-up of the chirped-pulse amplification (after ref. 3).

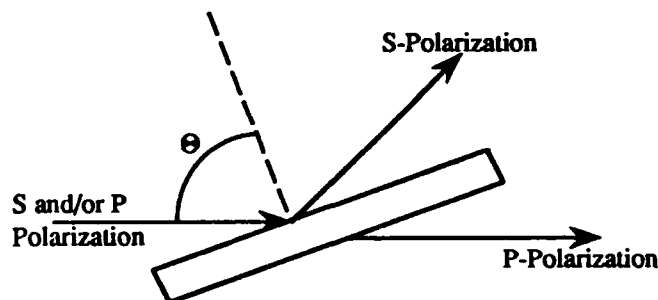


Fig. 2 : Schematic of a TFP.

Results and Discussions

The following performance curves (Fig.3) illustrate the typical spectral range for 2 of our type of polarizers. The ultra-broadband series offer an efficient transmission ($T_P > 98\%$ average) of the P-plane of polarization meanwhile the S-plane is reflected ($R_S > 85\%$) for the entire bandwidth of the Ti-S laser. The broadband series offer a greater extinction ratio (95:1) for an average bandwidth of 50 nm. Both series handle power levels up to $5\text{GW}/\text{cm}^2$ (Ti-S) without damage. A comparison between the broadband and the ultra-broadband mounted intracavity is shown on the figure (FIG.4).

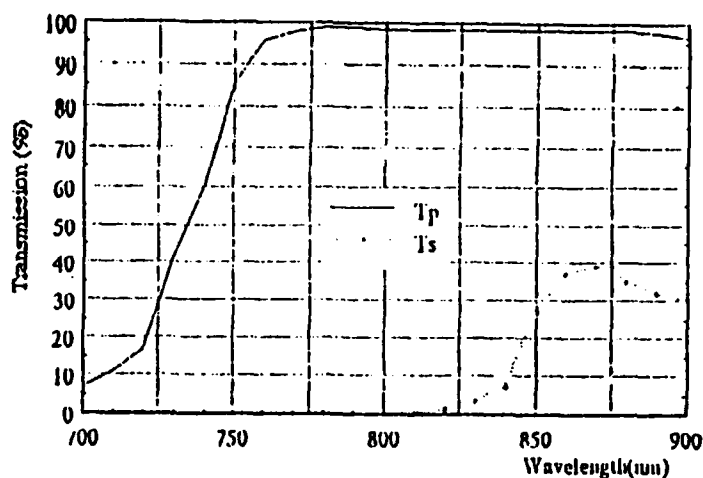
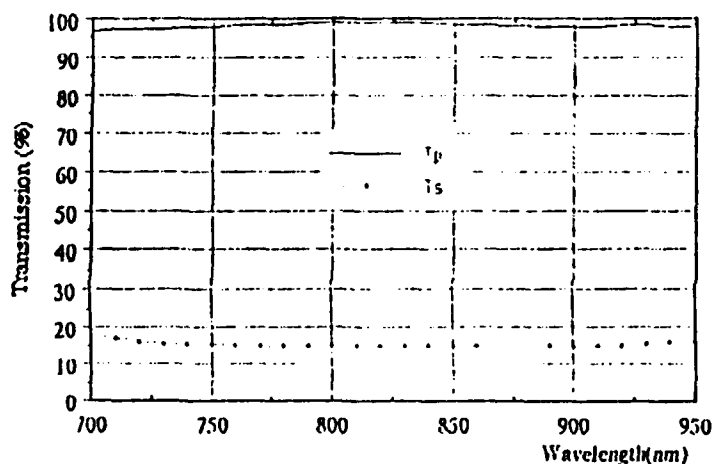
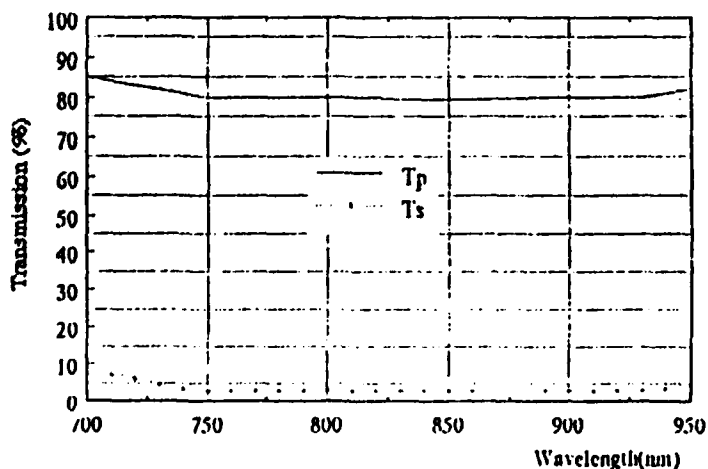
TFP #1, 50nm wide, $\geq 95:1$ extinction ratioTFP #2, Ultra Broadband ≥ 150 nm, T_p biasedTFP #3, Ultra Broadband ≥ 150 nm, R_s biased

Fig. 3: Spectral performance of ARO's thin film plate polarizer.

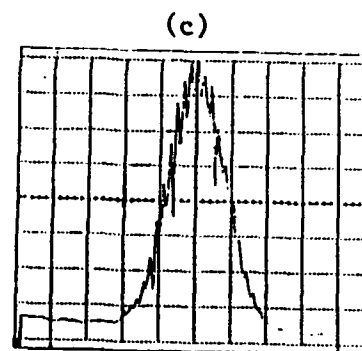
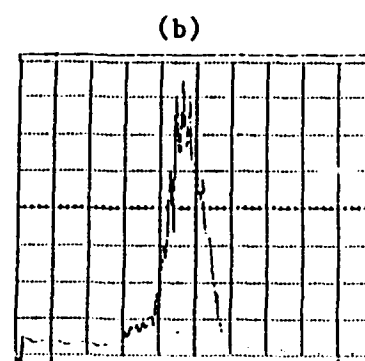
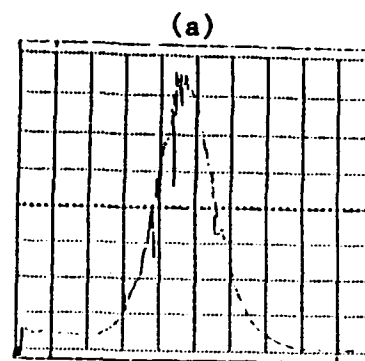


Fig. 4: Output of a Ti-S laser

- a) without an intracavity TFP
- b) with a Brewster's angle TFP;
- c) with ARO's TFP #3

References

- 1- M. Banning, "Practical Methods of Making and using Multilayer Filters", J. Opt. Soc. Am., 37, 792 (1947).
- 2- J. Mouchart, J. Begel and E. Duda, "Modified MacNeille cube polarizer for a wide angular field", App. Opt., 14, 2847 (1989).
- 3- F. Salin, J. Squier, G. Mourou and G. Vaillancourt, OSA proceedings on Advanced Solid-State Lasers, 13, 78 (1991)
- 4- J. Squier, F. Salin, G. Mourou and D. Harter, Opt. Lett., 16, 324 (1991).
- 5- P. Maine, D. Strickland P. Back, M. Passot and G. Mourou, IEEE J. Q. Elec., QE-24, 398 (1988).

Electrooptically fast tunable miniature diode laser pumped
Nd:YAG ring oscillator

I. Freitag, I. Kröpke, H. Welling

Laser Zentrum Hannover e.V.

Hollerithallee 8

3000 Hannover 21, Germany

Summary

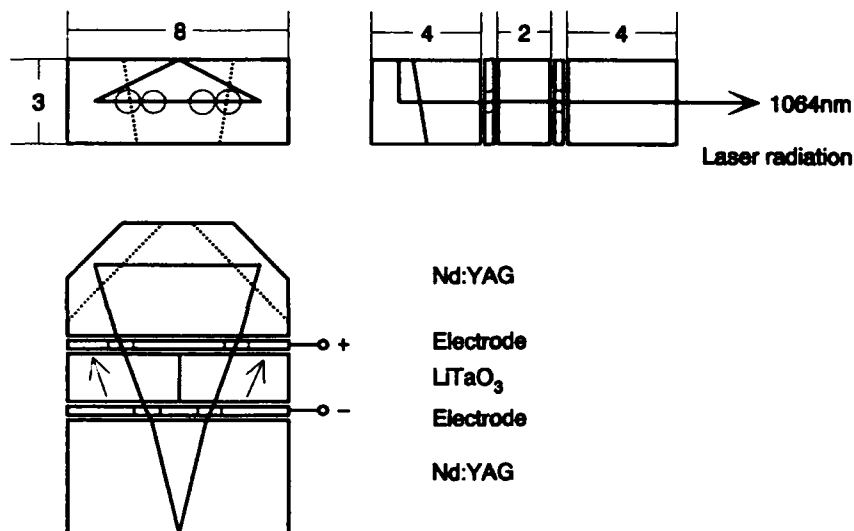
Miniature unidirectional quasi-monolithic diode laser pumped ring oscillators are fast frequency tunable sources of stable single frequency output.

The quasi-monolithic system with a dimension of 3x8x10mm consists of two Nd:YAG and two LiTaO₃ crystals. The design is based on the monolithic unidirectional nonplanar ring laser first reported by T. J. Kane and R. L. Byer (1). Part of the Nd:YAG laser material is replaced by two 2x3x4mm blocks of LiTaO₃ (see figure next page). The beam path inside the crystals is similar to that of the monolithic design. The laser radiation is reflected at the center of the front surface, at the two tilted side surfaces and at the top surface. The plane front surface is coated for a reflectivity of 98% for the s-polarized component of the 1064nm laser radiation and for high transmission of the pump radiation at 809nm. The beam enters and leaves the crystals at 8 surfaces each round trip. To reduce reflection losses this

surfaces are antireflection coated for the laser wavelength of 1064nm. Orientation of the LiTaO_3 crystal c-axis along the direction of the beam path eliminates birefringence.

As in monolithic nonplanar ring lasers an optical diode forces unidirectional and hence single frequency oscillation of the system (2).

Two electrodes made of 35 μm thick copper foils are placed between the Nd:YAG and LiTaO_3 crystals (see figure). An applied



electrical field generates a change of the refractive index inside the LiTaO_3 crystals by the longitudinal electrooptical effect and tunes the laser frequency at a rate of 0.1MHz/V. The measured linewidth is less than 10kHz/100msec with good frequency stability. With a diode laser pump power of 1.7W the output power exceeds 400mW. Conversion efficiency from electrical input power to laser output power is 7%. Further

improvements, especially in tuning coefficient, will be reported with different geometries using the transverse electrooptical effect. Birefringence in LiTaO_3 is small compared to other modulator crystals (for example: $1/20$ of LiNbO_3). First investigations showed that the optical diode can tolerate for this residual birefringence. This allows to orientate the c-axis of the modulator crystals perpendicular to the beam direction, which gives a much larger electrooptical coefficient. In addition this coefficient is proportional to the thickness of the crystal and hence could be easily increased by choosing a thicker modulator. Finally only one LiTaO_3 crystal is necessary, leading to a reduction of components.

With improvements presently in progress this miniature unidirectional quasi-monolithic diode laser pumped ring laser is an attractive source of fast tunable single frequency radiation.

References:

- (1) T. J. Kane and R. L. Byer; Optics Letters 10(85),65
- (2) A. C. Nilsson, E. K. Gustafson and R. L. Byer; IEEE Journal of Quantum Electronics 25(89),767

Multisite Optical Spectra and Energy Levels of Trivalent Thulium-doped Yttrium Scandium Gallium Garnet

Michael D. Seltzer, John B. Gruber, and Marian E. Hills, Code C02354, Naval Air Warfare Center Weapons Division, China Lake, CA 93555, (619) 939-1608; Gregory J. Quarles, Code 6551, Naval Research Laboratory, Washington, D.C. 20375-5000 and Clyde A. Morrison, Harry Diamond Laboratories, U.S. Army Adelphi Laboratory Center, Adelphi, MD 20783-1197

The multisite nature of disordered laser host crystals may play a significant role in enhancing the efficiency and tunability of rare earth ion-doped solid state lasers. Trivalent thulium-doped yttrium scandium gallium garnet ($\text{Tm}^{3+}:\text{YSGG}$), for which tunable 2- μm laser operation has been reported¹, is characterized as a disordered laser crystal because of the occupation of both octahedral and dodecahedral sites in the crystal lattice by Sc^{3+} ions, and the mixed occupancy of octahedral sites by both Sc^{3+} and Ga^{3+} ions. Disorder observed in YSGG is consistent with the crystal composition derived from X-ray diffraction studies:²



where the braces indicate dodecahedral sites, the brackets octahedral sites, and the parentheses tetrahedral sites. In garnets, rare-earth ions preferentially substitute for Y^{3+} ions in dodecahedral sites normally characterized by D_2 symmetry which we shall henceforth refer to as regular D_2 sites. Some dodecahedral sites having symmetry lower than D_2 as a result of mixed occupancy of neighboring octahedral sites may also be occupied by rare-earth ions. These sites shall be referred to as disturbed regular sites. The present paper reports in addition to the optical spectra and energy levels of Tm^{3+} ions in regular D_2 sites in YSGG, spectroscopic evidence from laser excitation experiments that substantiates the presence of Tm^{3+} ions in disturbed regular sites and Tm^{3+} ions in octahedral sites of C_3 symmetry.

The disorder of the YSGG host and subsequent presence of significant numbers of Tm^{3+} ions in sites of other than D_2 symmetry account for absorption spectra with features that are considerably broader than those previously observed in this laboratory in yttrium aluminum garnet (YAG) and similar to those observed in yttrium scandium aluminum garnet (YSAG) hosts. In many instances we observe shoulders on one or both sides of many absorption bands which are due to Tm^{3+} ions in disturbed regular sites as demonstrated in a later section that interprets observed site-selective excitation spectra.

Figure 1 shows the 4 K fluorescence spectrum corresponding to transitions from the 3H_4 manifold to the 3H_6 manifold. We observe that the number of peaks in Fig. 1 exceeds the number of transitions allowed by selection rules from the lowest Stark level in the 3H_4 manifold to the $2J+1$ Stark levels of the 3H_6 ground state manifold. This observation suggests that the spectra shown in Fig. 1 are not exclusively due to fluorescence of Tm^{3+} ions in regular D_2 sites alone.

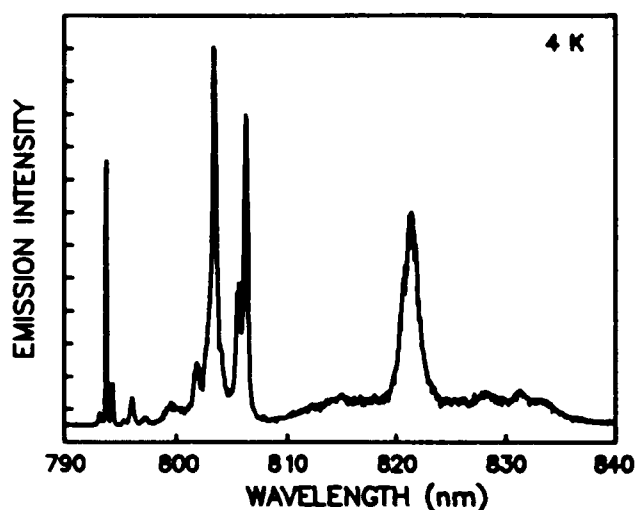


Figure 1. Fluorescence from 3H_4 manifold to 3H_6 manifold at 4 K.

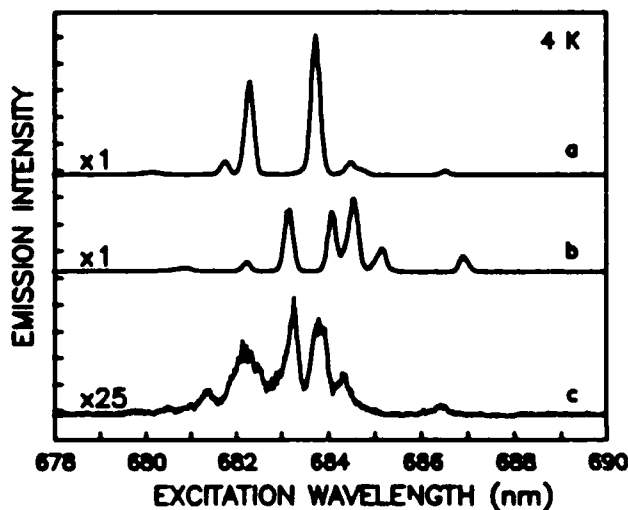


Figure 2. Site-selective excitation of the 3F_3 manifold at 4 K: a. Tm^{3+} ions in regular D_2 sites; b. Tm^{3+} ions in disturbed regular sites; c. Tm^{3+} ions in C_{3i} sites.

The inference that Tm^{3+} ions occupy at least three different sites in YSGG can be made from a detailed examination of both the absorption and fluorescence spectra obtained at 4 K. For example, in absorption, transitions from the ground state (3H_6 , level Z_1) to the lowest Stark level (W_1) in 3H_4 appear as a band containing two peaks (7937.8 Å and 7942.2 Å) and a shoulder at 7932 Å. Three adjacent peaks observed in fluorescence (Fig. 1) are found to match these wavelengths. To establish individual characteristic spectra for Tm^{3+} ions in each site, site-selective excitation scans between 678 and 690 nm were obtained at 4 K and 25 K for the 3F_3 manifold. High-resolution fluorescence detection was carried out successively at 7937.8, 7931.3, and 7943.6 Å and fluorescence intensity was recorded as a function of excitation wavelength as shown in Fig. 2. The figure provides a direct comparison between excitation spectra of Tm^{3+} ions in three distinctly different sites. The relative fluorescence intensities of each scan are also indicated in the figure.

The 4 K excitation spectrum shown in Fig. 2a agrees with the main features of the 3F_3 absorption spectrum obtained over the same wavelength region and is associated with Tm^{3+} ions in regular D_2 sites since the corresponding transitions and those similarly observed at 25 K obey D_2 symmetry selection rules. The excitation spectrum shown in Fig. 2b includes a greater number of peaks than Fig. 2a. For Tm^{3+} ions in sites with symmetry lower than D_2 , all transitions are allowed and therefore more peaks are expected. The abundance of Tm^{3+} ions in disturbed regular sites reflects the disordered nature of YSGG and is consistent with the extensive mixed occupancy of octahedral sites by Sc^{3+} and Ga^{3+} reported in Ref. 2. The excitation spectrum shown in Fig. 2c shows fluorescence that is approximately one twenty-fifth as intense as that shown in Fig. 2a. The relatively short lifetime ($\tau=78 \mu s$) associated with fluorescence depicted in Fig. 2c suggests that the emitting Tm^{3+} ions occupy sites that are entirely different from those associated with Figs. 2a and 2b ($\tau=1.5$ ms). Most notable in Fig. 2c is structure indicative of vibronic coupling between Tm^{3+} ions in octahedral C_{3i} sites and the crystal lattice.

The remaining question concerning the disturbed regular sites occupied by a large fraction of the Tm^{3+} ions in Tm^{3+} :YSGG is their exact nature and symmetry. For Tm^{3+} ions in dodecahedral sites, a range of symmetry possibilities exists depending on the homogeneity of Sc^{3+} ion occupation of neighboring octahedral sites. As a condition for D_2 symmetry, a given dodecahedral site must have its four neighboring octahedral sites occupied exclusively by Sc^{3+} ions. However, where local mixed occupancy of octahedral sites occurs, some of the symmetry operations that define the D_2 point group are precluded for the associated dodecahedral site and therefore its symmetry can be no greater than C_2 .

The spectra and energy levels of Tm^{3+} ions in D_2 sites in YSGG have been analyzed. The levels were used in a crystal-field splitting calculation, the results of which indicated a reasonable agreement between experiment and theory. Spectroscopic evidence from site-selective excitation experiments suggests the presence of a large fraction of Tm^{3+} ions in disturbed regular sites. The abundance of disturbed regular sites is consistent with the intrinsic disorder characteristic of the YSGG host.

References

1. R.C. Stoneman and L. Esterowitz, *Optics Letters* **15**, 486 (1990).
2. G.M. Kuz'micheva, S.N. Kozlikin, E.V. Zharikov, S.P. Kalitin, and V.V. Osiko, *Russ. J. Inorg. Chem.* **34**, 792 (1989).

Comparison of Proton and Gamma Irradiated Nd Doped Materials
Longitudinally Pumped at 0.8 μm

T. S. Rose and R. A. Fields

Electronics Technology Center, The Aerospace Corporation

M2/246, P. O. Box 92957, Los Angeles, CA 90009

Because of the increasing demand for long-lived space qualified optical devices, there is a need to understand the impact of the ambient radiation environment upon solid state laser performance. Exposure to radiation can damage the laser material either by ionizing constituent atoms in the lattice or (in the case of particle radiation) by becoming trapped, thereby disrupting the lattice. In our earlier work¹, it was shown that ^{60}Co gamma rays (ionizing radiation) degrade laser performance of diode pumped Nd:YAG by creating color centers in the material; the decrease in efficiency was specifically attributed to the increase in absorptive loss at the lasing wavelength. Furthermore, it was found that the loss in the material saturated at a value of $\sim .02 \text{ cm}^{-1}$ after an accumulated dose of 100 krad indicating that only certain sites in the lattice are prone to induced defect structures. It was also pointed out that within certain system design criteria, Nd:YAG could effectively perform as a radiation hard laser material, such as Nd:Cr:GSGG. Preliminary results for Nd:YLF indicated a higher susceptibility for radiation induced damage/loss than observed for Nd:YAG. Current work on Nd:YLF indicates that the induced loss does not readily saturate as in Nd:YAG; however the gamma induced damage in Nd:YLF can be annealed at significantly lower temperatures. Some annealing is even observed to occur from the heat deposited when the pump power reaches the level of 2 Watts.

In the past, gamma rays were commonly used to understand radiation effects since they are conveniently obtained from relatively simple sources. While gamma radiation may serve as a good starting point from which to assess the effect of induced ionization effects,

gamma rays are not typically encountered in the ambient space environment. Of more concern are charged particles such as protons, which are mainly derived from solar flares, and electrons which are constituents of the Van Allen belts. It is for this reason that we have continued our studies to include the effect of high energy protons on the performance of longitudinally pumped Nd:YAG, Nd:YLF and Nd:Cr:GSGG. In this current effort we have measured the degradation of the cw performance of longitudinally pumped (at 0.8 μm) Nd:YAG, Nd:YLF and Nd:Cr:GSGG laser crystals upon exposure to relatively high energy protons (49 MeV), in order to assess the ionization damage incurred by the passing of these particle through the material. Proton fluences of 10^{10} (~ 1.5 krad) and 10^{12} cm^{-2} (~ 150 krad) were chosen to simulate exposure levels expected for a 1 and 100 year period in geosynchronous orbit. While no effect was seen for the lower fluence level, exposure to 10^{12} cm^{-2} resulted in ionization damage causing a 20% degradation for both Nd:YAG and Nd:YLF, whereas as Nd:Cr:GSGG remained unaffected. These results are similar to those obtained previously from gamma irradiated samples. A link between the effects of gamma and proton radiation was realized upon the observance of similar color center formation in undoped material via transmission spectra. We are attempting to further correlate the damage induced by the two types of radiation by accurately identifying the color center sites in these materials through electron paramagnetic resonance techniques.

Additionally, we have begun to evaluate the impact of lattice distortions which can be caused by lower energy protons which become trapped in the material. A Nd:YAG crystal was sideways exposed to ~ 21 MeV protons at a fluence level of 10^{12} cm^{-2} so that the protons came to rest midway through the material. Fig. 1 shows the output power of a Nd:YAG sample pumped with 1 Watt of 808 nm light as a function of the transverse position. Aside from the low performance experienced at the very edges of the crystal (resulting from beam clipping and coating nonuniformity), the transverse performance profile clearly depicts a uniform decrease in output across two-thirds of the crystal, with no anomalously large effects occurring in the region where the protons came to rest. While no

distinct damage resulting from trapped protons (as opposed to ionization processes) in Nd:YAG is evident at the current time, further studies regarding this issue are still being pursued.

¹ T.S. Rose, C.L. Fincher, D. Chen, and R.A. Fields, "Laser Performance of Gamma Irradiated Nd Doped Materials Longitudinally Pumped at 0.8 μm ", OSA Proc. on Adv. S.S. Lasers 13, Santa Fe, NM, 1992, p. 285.

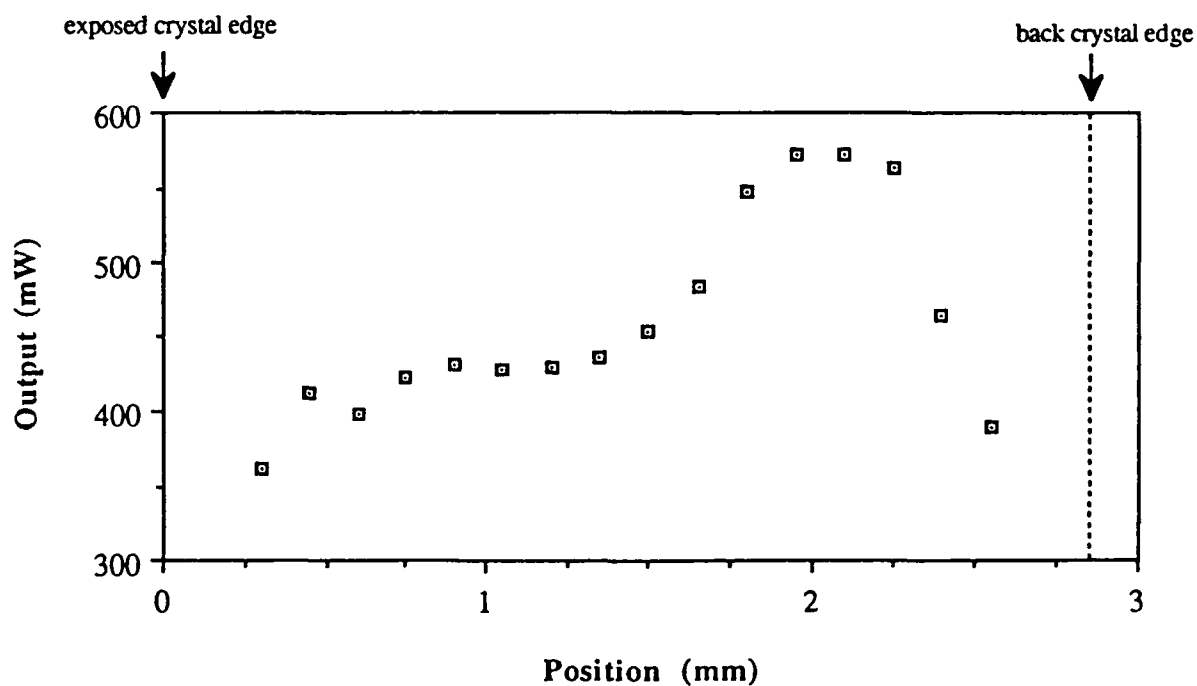


Fig. 1 Output power vs. transverse position of proton irradiated Nd:YAG. The 808 nm Ti:sapphire pump power was held fixed at 1W.

Determination of Laser Efficiencies for Yb-Doped Apatite-Structure Hosts

L. K. Smith, S. A. Payne, W. F. Krupke, L. D. DeLoach, and W. L. Kway
Lawrence Livermore National Laboratory
University of California
P.O. Box 5508, Livermore California 94550
(510) 422-6270

B. H. T. Chai
University of Central Florida
CREOL
12424 Research Parkway, Orlando, Florida 32936

Recently, there has been a renewal of interest in Yb-lasers and in particular, with Yb:YAG, since the development of strained-layer InGaAs laser diodes operating in the 0.9 - 1.1 μm range [1]. This interest has been sparked by the fact that the Yb ion's absorption characteristics are well matched for this type of diode pumping. Furthermore, Yb offers several advantages over Nd, with longer emission lifetimes and the absence of higher-lying excited states that could lead to cross relaxation and upconversion losses. Although the existence of only two electronic states in Yb simplifies our understanding of the system, it suggests, however, that a single group of crystal field-split lines must be used for efficiently pumping and extracting energy from the Yb-doped medium. In order to obtain an efficient laser, we must find a Yb-doped material where the emission cross section is as large as possible, while the pump saturation intensity and thermal population of the lower laser level are minimized.

We have identified three Yb-doped crystals of the apatite structure which possess the characteristics advantageous for laser action [2]. Shown in Table I along with Yb:YAG (for comparison) are $\text{Ca}_5(\text{PO}_4)_3\text{F}$ or C-FAP, $\text{Sr}_5(\text{PO}_4)_3\text{F}$ (S-FAP), and $\text{Sr}_2\text{Ca}_3(\text{PO}_4)_3\text{F}$ (SC-FAP). All three of these crystals have advantages over Yb:YAG in terms of pump cross section (in units of 10^{-20}cm^2 , >3.0 for all apatites and 0.7 for YAG), and emission cross section (>5.0 versus 2.0). They also satisfy the requirements for low pump saturation intensity ($I_{\text{sat}} < 10.0 \text{ KW/cm}^2$) and a low absorbed pump intensity required to achieve net gain ($I_{\text{min}} < 0.5 \text{ KW/cm}^2$). Both of these values are at least 4 times lower than Yb:YAG, the present state of the art. Based on the high cross sections and low I_{min} values characterizing Yb:FAP, we would expect these crystals to serve as useful laser media.

In order to verify this assertion, we set up a laser-pumped laser experiment to measure the actual laser performance of the FAP crystals. Figure 1 shows a CW Ti:sapphire laser tuned to a wavelength between 899 and 905 nm and chopped to a 25% duty cycle to end pump the apatite crystal located at the center of a 10 cm long concentric laser cavity. A 10 cm focal length lens was employed to focus the pump light into the crystal. Several values of output coupling are available to quantify the laser performance of the crystal.

Due to the low pump saturation intensity, we would expect a sizable fraction of the ground state Yb ions to be promoted to the excited state. As a result, the excited state population becomes "clamped" and cannot increase any further, once laser action is initiated in the cavity, as expected on the basis of the principles of fundamental laser physics. This bleaching effect is observed for all the apatite crystals we have studied and serves to complicate the determination of absorbed pump light, which in its simplest form, is a comparison of the pump light incident and transmitted through the crystal. Since we want to determine the fraction of pump light absorbed by the FAP crystal while laser action is occurring in the cavity, we must multiply the fraction transmitted while not lasing, $1-F_{\text{nl}}$, by the ratio of the pump power levels leaking through the output coupler with, P_{l} , and without, P_{nl} , Yb:FAP laser action occurring (accomplished by aligning, then misaligning the output coupler)[3]:

$$(1-F_{\text{nl}})(P_{\text{l}}/P_{\text{nl}}) = 1-F_{\text{l}} \quad (1)$$

The values for F_{nl} and F_l at several input power levels are displayed for a data set of C-FAP taken with 9.5% output coupling in Figure 2. The fraction absorbed while not lasing varies from 86% at very low pump intensity, to 21% at 1.4 W of pump power. The fraction absorbed while lasing, however, corrected for the bleaching effect, is shown to be constant at 80% for this crystal above the laser threshold.

Typical examples of the efficiency results are shown in Figure 3, where one data set obtained for each crystal using the 19.8% output coupling is plotted. The slope efficiency values for the data displayed are noted in the upper corner. The slope efficiencies are rather high (55 to 79%), and the thresholds for laser action are nearly the same [2,3].

In conclusion, spectroscopic studies of crystals of the apatite-structure suggest that they are useful laser media, and laser experiments confirm this to be the case. A total of three apatite-structure crystals doped with Yb have been lased to date. To account for the bleaching effect due to low pump saturation intensity, we have developed methods to determine the fraction of pump light absorbed during lasing. Due to the high efficiencies seen in our experiments, we anticipate that the development of efficient, InGaAs diode laser pumped Yb:FAP laser systems is a reasonable expectation.

This work was performed under the auspices of the U.S. Department of Energy by Lawrence Livermore National Laboratory under Contract No. W-7405-Eng-48.

References

- [1] P. Lacovara, H. K. Choi, C. A. Wang, R. L. Aggarwal, and T. Y. Fan, *Opt. Lett.* **16**, 1089 (1991).
- [2] L. D. DeLoach, S. A. Payne, L. L. Chase, L. K. Smith, W. L. Kway, and W. F. Krupke, "Evaluation of absorption and emission properties of Yb³⁺ doped crystals for laser applications," submitted to *IEEE J. Quantum Electronics*.
- [3] S. A. Payne, L. K. Smith, L. D. DeLoach, W. L. Kway, J. B. Tassano, and W. F. Krupke, "Laser, optical, and thermomechanical properties of Yb-doped fluorapatite," submitted to *IEEE J. Quantum Electronics*.

Table I. Spectroscopic and laser properties of Yb-doped apatite structure crystals.

Crystal	Yb:C-FAP	Yb:S-FAP	Yb:SC-FAP	Yb:YAG
<u>Pump Properties</u>				
λ_{pump} (nm)	905	899	902	942
σ_{pump} (10^{-20}cm^2)	10.0	8.6	3.1	0.8
I_{min} (KW/cm ²)	0.08	0.09	0.39	1.53
I_{sat} (KW/cm ²)	2.0	2.0	7.5	28
<u>Extraction Properties</u>				
λ_{ext} (nm)	1043	1047	1046	1031
σ_{ext} (10^{-20}cm^2)	5.9	7.3	3-5.2	2.03
τ_{em} (msec)	1.10	1.26	0.95	1.08

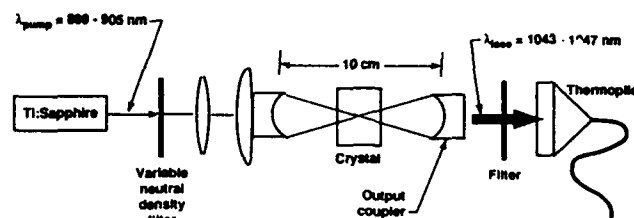


Fig.1. The set up employed to characterize laser performance of the apatite-structure crystals. An Argon laser-pumped Ti:sapphire laser is used to end pump the apatite laser cavity.

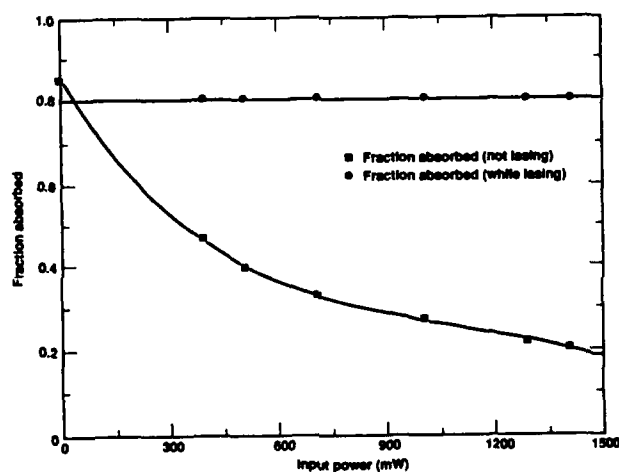


Fig. 2. Plot of absorbed fraction of pump light versus input power. Due to bleaching, the absorbed fraction appears to decrease with increasing input for the non-lasing condition.

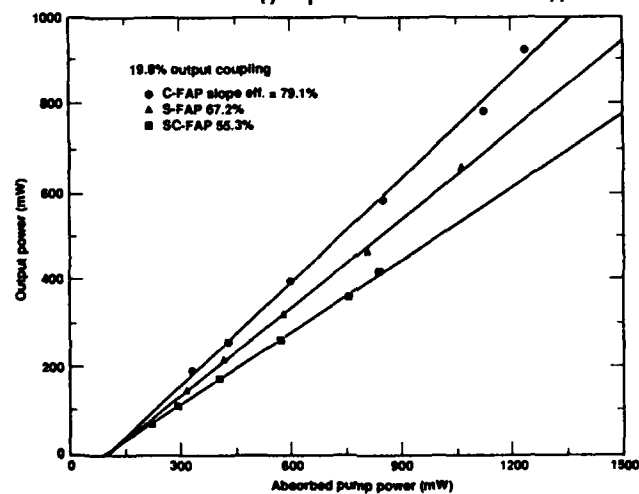


Fig. 3. Examples of typical slope efficiency plots obtained for apatite crystals. These data were obtained with 19.8% output coupling.

ENERGY TRANSFER CALCULATIONS USING A QUANTUM MECHANICAL MODEL

Norman P. Barnes
NASA Langley Research Center
Hampton, VA 23681

Elizabeth D. Filer
Lockheed Engineering and Science Company
Hampton, VA 23666

Clyde A. Morrison
Harry Diamond Laboratories
Adelphi, MD 20783

Summary

Energy transfer is a virtual necessity for Lanthanide series lasers such as Ho, Er, and Tm. With the use of energy transfer, these lasers can be pumped by laser diodes in the visible, and consequently, lase efficiently in the 1.5 to 2.1 μm region. However, energy transfer processes can also lead to deleterious effects which can detract from the efficiency. One such effect in Ho and Tm lasers is commonly referred to as up conversion. On the other hand, up conversion can be used to advantage to create visible solid-state lasers. To accurately model these lasers requires a knowledge of the energy transfer rates. Measurement of the energy transfer rates is complicated by the necessity to accurately determine the excitation density of the various manifolds, especially when laser sources with nonuniform spatial profiles are employed. To obviate these problems, energy transfer rates are calculated using information on the energy levels and the branching ratios. While calculations presented here used a quantum mechanical model to predict these quantities, measured energy levels and branching ratios could be used equally as well.

Results obtained here are significantly different from those obtained using the commonly employed Dexter formalism. In the Dexter formalism, the energy transfer process was averaged over the relative orientation of the participating atoms with respect to each other. Furthermore, an average over the orientation of the individual atoms was also performed. While such an averaging process is a good approximation for liquids, the calculations presented here do not employ this orientational averaging process. As another contrast, the Dexter formalism integrates over the emission and absorption spectra. While this can be done in a straightforward manner for isotropic materials, the process becomes more complicated in birefringent laser materials. Calculations presented here replace the integration process with a sum over the energy levels of the participating

atoms. Polarization properties of the transitions can be taken into account by utilizing branching ratios which have polarization properties built into their definition. As a third contrast, Dexter utilizes an integration over distance to account for the distance between the participating atoms. In this work, to obtain the total energy transfer rate, the calculations include a summation over nearest neighbors, next nearest neighbors, and so forth. In practice, the sum over atoms at various distances converges very rapidly. Because of these differences, the energy transfer rates can be significantly different.

Several general benefits accrue from this process, including a facile method of calculating any energy transfer rate, including rates which are difficult to measure, bidirectional energy transfer rates, and energy transfer rates as a function of temperature. Calculation of any energy transfer rate can be accomplished once the energy levels and branching ratios are known. Even if the branching ratios are not known, they could be roughly approximated with the knowledge of the lifetime of the participating manifolds. For every energy transfer process there is a reverse process; that is, the energy transfer process is bidirectional. Using the theory developed here, the ratio of the energy transfer rates can be readily calculated using a temperature dependent factor. In addition, all energy transfer rates can be readily calculated as a function of temperature. As will be shown, these energy transfer rates can vary widely as a function of temperature. Using this formalism, energy transfer rates are calculated for several laser materials such as Ho:Tm:YAG. General and specific results will be presented.

High-Peak Power, Q-Switched Nd:YLF Laser End-Pumped by a Diode Laser Bar

B. Frei, T. Graf, and J.E. Balmer

Institute of Applied Physics, University of Berne
3012 Berne, Switzerland

Due to their high efficiency and compact size, diode laser-pumped solid state lasers have attracted increasing interest for applications such as micro-machining, remote sensing, micro-surgery, and nonlinear optics. For many of these applications, high peak power, short duration pulses from Q-switched lasers are required. Pulse durations longer than about 4 ns can be obtained by conventional PRM (pulse-reflection mode) Q-switching [1], whereas pulse-transmission mode (PTM) Q-switching is required for pulse durations between about 1 and 10 ns [2]. In the latter mode of operation, the duration of the (trapezoidal) pulse is given by the resonator round-trip time and can so be varied simply by adjusting the resonator length. PTM pulse durations as short as 1 ns can be expected, if the resonator length can be reduced to below ~15 cm. In this work, we report on a diode laser-pumped, PTM Q-switched Nd:YLF laser oscillator producing 1047-nm laser pulses with a variable duration of 2.4 - 8.4 ns and an energy of about 0.1 mJ, corresponding to ~40 kW of maximum peak power. The laser was also operated in the conventional PRM mode, where it produced 3-mJ/14-ns pulses (210 kW of peak power) at an optical efficiency of 15.5% and a (optical) slope efficiency of 18%. To our knowledge, this is the highest peak power and efficiency for end-pumped systems and TEM₀₀ operation reported to date.

Figure 1 shows a schematic of the experimental setup used for PTM operation. In contrast to resonators with conventional output coupling, the PTM laser resonator consists of two highly reflective mirrors (M_1/M_1' and M_2). End-pumping is achieved through the 50-cm radius-of-curvature end of the Nd:YLF rod (AR coated at 800 nm, HR at 1050 nm). For short pulse generation with resonator lengths below about 30 cm, a plane mirror was chosen as M_1 . For long pulses, M_1' was replaced by a 100-cm concave mirror. In order to allow end-pumping of the rod from both sides, a folded resonator was designed. An acousto-optic Q-switch and a LiNbO₃ Pockels cell, driven by a subnanosecond-rise time pulser, serve to produce the PTM pulse. A Fabry-Perot etalon was inserted for partial stabilization of the pulse amplitude.

The Nd:YLF rod is pumped by a 50-W, quasi-cw (400 μ s) diode laser bar at a maximum energy of 20 mJ. A close-coupled fiber-optic cross section transformer (CST) made up of 118, 80/84 μ m diameter, step-index fibers of 0.65 numerical aperture (N.A.) adapts the 1- μ m by 1-cm diode laser emission area to the TEM₀₀ mode of the resonator. The TEM₀₀ mode diameters were calculated to be 1.1 mm (36-cm resonator) and 0.8 mm (120-cm resonator) at the pumped end of the YLF rod. In order to improve the overlap of the pump light distribution and the TEM₀₀ mode as compared to previous work [3],

the CST has been divided into two bundles of 0.72 mm diameter each. The transmission of the CST is 69% without AR coatings. The output from the two CST arms is lens-coupled to the ends of the Nd:YLF rod using commercially available focusing lenses having a N.A. of 0.61. When adjusted for maximum laser output, the losses in the coupling lens were measured to be 26%. This is readily explained by aperture losses due to the insufficient N.A. of the available lenses.

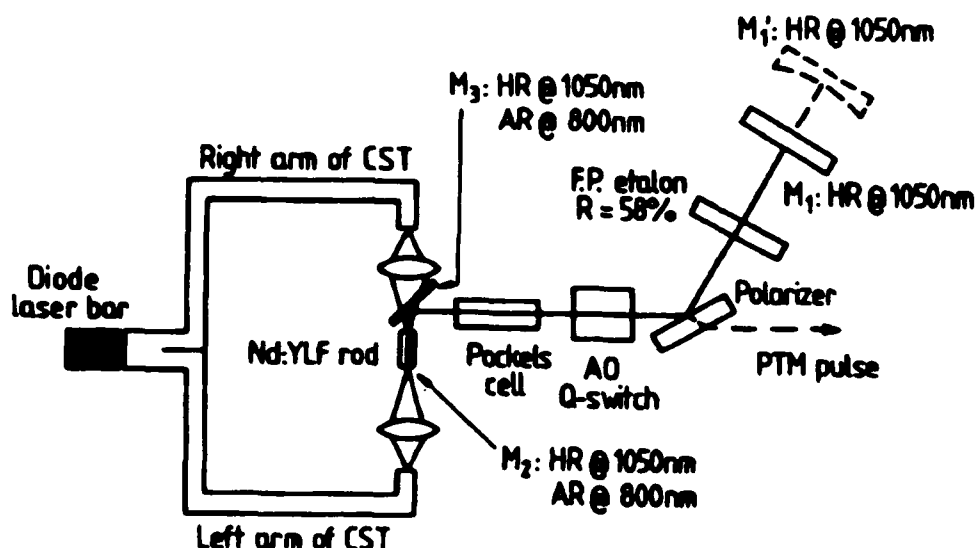


Fig. 1 Experimental setup for PTM operation.

Figure 2 shows the temporal profiles of the PTM pulses as recorded with a PIN photodiode and a 1-GHz oscilloscope with a measured risetime of 400 ps. The duration of the short pulse in Figure 2a) agrees very well with the theoretical FWHM value of 2.4 ns for an optical resonator length of 36 cm. Figure 2b) shows the pulse obtained with the long (120 cm) resonator. The measured pulse duration is 8.4 ns, again in very good agreement with the calculated value.

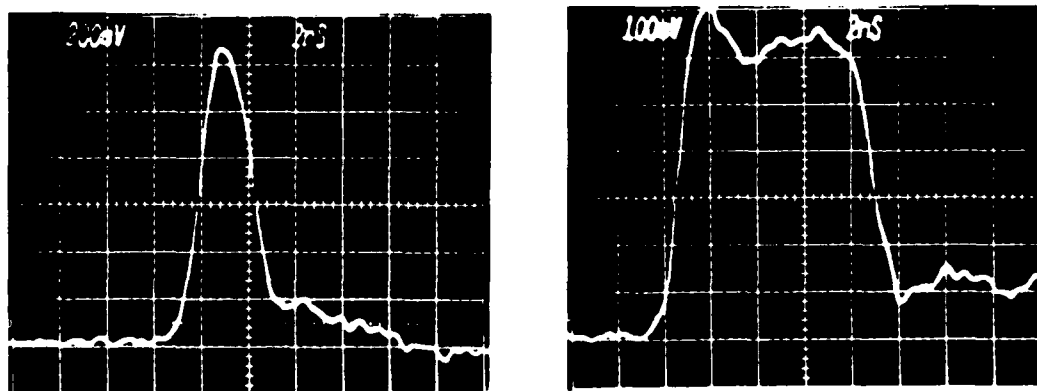


Fig. 2. Oscilloscope traces of the PTM pulse for an optical resonator length of
a) 36 cm and b) 120 cm

The plateau seen on the trailing edge of the pulse is caused by imperfect dumping of the intracavity energy in combination with reflections of the high-voltage pulse at the (high-impedance) Pockels cell. Due to laser-induced damage to the LiNbO_3 Pockels cell, the pump energy had to be limited to 7.5 mJ. Under this condition, a pulse energy of 0.1 mJ was measured, corresponding to a peak power of ~ 40 kW and an optical efficiency of 1.3%.

A marked improvement in optical efficiency was achieved by reducing the N.A. of the diode laser emission. Using a piece of our 84- μm diameter fibers as a collimating microlens between the diode laser bar and the CST, the divergence of the emission from the diode laser could be reduced to a N.A. equivalent of about 0.1. A new, single-arm version of the CST was built using 80/84- μm fibers with a N.A. of 0.14 (see Fig. 3). The measured transmission of this CST/microlens combination was 67% (uncoated). Using the new coupling optics, an electrooptically (EO) Q-switched Nd:YLF laser was set up. With the reflectivity of the output coupler optimized for maximum peak power ($R=80\%$), a TEM_{00} output pulse energy of 3 mJ was obtained at 19 mJ of pump energy from the diode laser, corresponding to an optical efficiency of 15.5%. The optical slope efficiency was 18%. The measured pulse duration was 14 ns, yielding a peak power of 210 kW. These values were obtained at a repetition rate of 10 Hz. The diode laser could be operated at repetition rates of up to 100 Hz, at which value the pulse energy was found to decrease to about 80%.

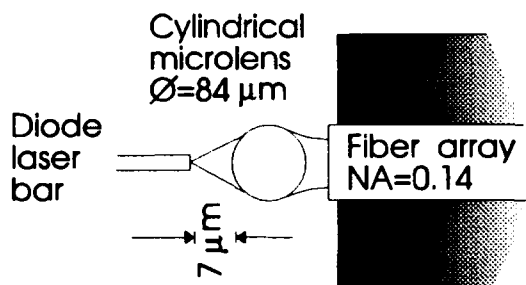


Fig. 3 Schematic of microlens coupling of the diode laser emission into the low-N.A. fiber array

REFERENCES

- [1] D.C. Gerstenberger et al., Conf. on Lasers and Electro-Opt., 1988, OSA Technical Digest (Optical Society of America, Washington, DC 1992), Paper ThB3
- [2] K. Chan, Appl. Opt. 27, 1227 (1988)
- [3] H. Zbinden and J.E. Balmer, Opt. Lett. 15, 1014 (1990)

Thermal properties of Erbium glass lasers

A McInnes and J Richards
Defence Science and Technology Organisation
PO Box 1500
Salisbury
SA 5108
Australia.

Erbium glass lasers operate at the "eye-safe" wavelength of 1.54 μm . This makes them attractive candidates as alternative sources for any Nd:YAG laser-based equipment, which currently suffers restrictions on use due to being hazardous to the eye.

However, Erbium glass lasers are well known to suffer thermal problems^{1,2}. This is primarily due to the high pump input required by three level systems combined with the low thermal conductivity of the glass host. The difficulty of extracting the absorbed heat has so far made practical flashlamp-pumped Er:glass lasers inherently low repetition rate devices. Figure 1 shows the behaviour of the laser output with rod temperature, as it heats up when running uncooled at maximum input (34 J). This is virtually independent of repetition rate.

The work described in this paper explores the relative importance of the various thermally induced effects; lensing, birefringence, rod deformation and gain reduction. These factors have a significant impact on the design of such lasers, and on the potential for improved performance.

The laser consisted of a Kigre QE-7S rod³, 3 mm in diameter x 76 mm long, a concave output coupler and rotating Porro prism Q-switch, which could be replaced with a flat mirror for free running operation. Throughout, the temperature of the rod was varied by changing the amount of cooling applied and/or the repetition rate, and measured using a thermocouple junction in contact with the surface of the rod. Cooling was applied by forcing air through 1.2 mm gaps between the two halves of the pumping enclosure.

Rod deformation was measured by observing the angular deviation of a probe beam reflected from one end of the rod. While bending of up to 1 mrad was observed, it was relatively straightforward to realign the laser to compensate, so this is not a serious limitation for such lasers.

Thermally induced birefringence was measured by passing a probe beam from a plane polarised HeNe laser (543 nm) through the rod and an analyser. Any transmitted signal was monitored using a CCD camera, which allowed the spatial behaviour to be examined. The temporal behaviour of the total signal was also monitored.

Birefringence has a major impact on the Q-switching techniques that can be used. A number of polarisation insensitive techniques are currently in use^{4,5}, so birefringence will not be a fundamental limitation of Er:glass laser performance, but there is considerable interest in the use of electro-optic Q-switching techniques, most of which rely on polarisation for their

operation.

Spatially and temporally resolved birefringence measurements revealed the dynamics of heat flow within the rod; in single shot mode, the birefringence is initially small, then peaks 0.3 seconds after the flash pulse, due to the large thermal gradient between the hot outer surface and cool centre of the rod. However, after running repetitively (uncooled) for a time, the laser reaches a quasi-equilibrium state, and in this mode, the birefringence is initially large, due to a hot centre and cool outer surface, but falls to almost zero 0.4 seconds after the flash, as the thermal gradient is reduced by heating of the outer part of the rod.

This opens up the possibility of effective polarisation based Q-switching in a repetitive, uncooled Er:glass laser. Several problems would have to be addressed, such as the large time difference between the optimum Q-switch delay and the time of minimum birefringence, but careful design may be able to overcome this.

Thermal lensing was measured by two methods. In one, a 543 nm HeNe probe beam was passed through the rod, and changes in the divergence monitored using a CCD camera and laser beam analyser. This allowed calculation of the power of the induced lens as a function of temperature/repetition rate. The greatest lensing observed had an equivalent power of 0.7 Dioptres, equivalent to a focal length of 1.4 metres. This would not be enough to cause the output to drop to zero in a laser such as this, with a cavity length of only 150 mm. Morishige et al⁶ also found thermal lensing to be unimportant, but that was in the case of liquid cooled, athermalised glass.

The other method involved operating the laser without Q switching, and varying the length of the cavity. If lensing were a serious problem, the behaviour of laser output with temperature would be significantly different for different cavity lengths. This is not observed in practice. The distance between rod and rear mirror was varied from 5 to 240 mm, and any variation in output is accounted for through the different mode volumes, and the amount of lensing measured using the technique above.

Thermal gain reduction was measured indirectly, as it was not possible to probe the laser medium with a pulse from another Er:glass laser. The fluorescence at 1.54 μm was measured as a function of temperature, and the result shown in figure 2. From figure 1 we see that the lasing ceases around 170 - 175 C, when pumped with 34 J, uncooled. It can be seen that the fluorescence yield at this temperature has decreased to a level some 85% of the ambient temperature level. If we examine the variation of fluorescence yield with input energy at ambient temperature, we find the 85% level to be equivalent to an input of 25 - 26 J. This is close to the threshold input for this laser at ambient of 23 Joules, suggesting that the change in fluorescence yield with temperature is enough to account for most of the change in output.

Spring et al² found that gain reduction was important in liquid cooled Er:YAG. That taken with this evidence, along with the insufficiency of any of the other effects to explain the observed behaviour, leads to the conclusion that thermal gain reduction is the dominant factor limiting the performance of uncooled, or ineffectively cooled, flashlamp pumped Erbium glass lasers.

In order to attain higher repetition rates from lamp pumped Er:glass lasers without increasing the cooling system to a cumbersome level, efforts must be directed at minimising the heat

absorbed by the glass, for example by filtering and tailoring the flashlamp output. Use of additional claddings and sensitizers to convert otherwise wasted flashlamp energy into the pump bands will also help. Polarisation based Q switching may be possible even in such a highly birefringent system, by allowing the birefringence to build up in such a way that energy input from the lamp causes a decrease rather than an increase.

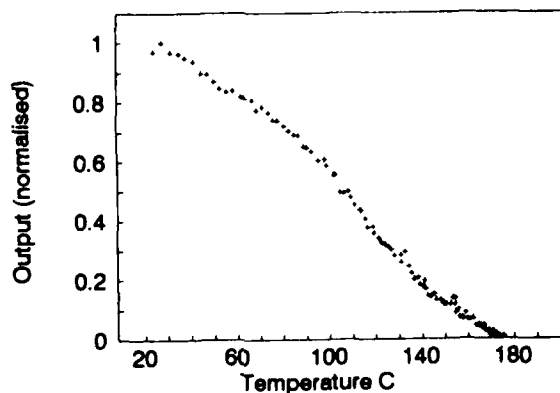


Figure 1. Output vs. rod temperature

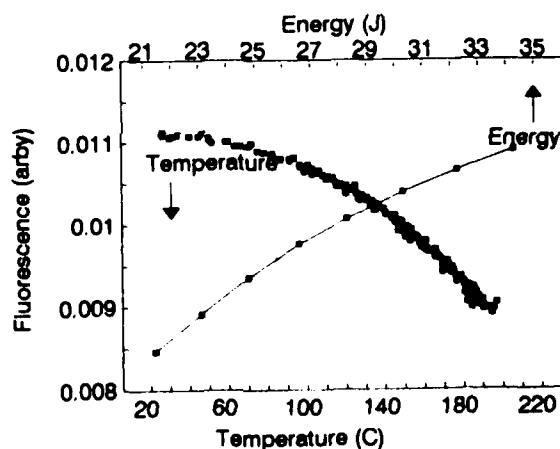


Figure 2. Fluorescence signal vs rod temperature and input electrical energy (laser cold)

References:

- 1) Lukac M and Marincek M, IEEE Jnl of Quantum Electronics, 26, No 10, p1779, October 1990.
- 2) Spring R and Luthy M, J. Appl. Phys. 69, No 2, p581, 15 Jan 1991.
- 3) Kigre Inc, 100 Marshland Rd, Hilton Head Island, SC 29926, USA.
- 4) Asaba K et al, SPIE proceedings 1207, pp 164-171, SPIE, Bellingham 1990.
- 5) Renairi et al, SPIE proceedings 1207, pp 112-123, SPIE, Bellingham 1990.
- 6) Morishige et al, Opt. Lett. 9, No 5, p147, May 1984.

Tuesday, February 2, 1993

Novel Laser Materials 2

ATuC 10:45am-12:00m
La Salle Ballroom B&C

Stephen Payne, *Presider*
Lawrence Livermore National Laboratory

**Sub-picosecond pulse generation from
a laser-diode-pumped, self-starting
additive-pulse mode-locked Nd:LMA laser**

D.W. Hughes, A.A. Majidabadi, J.R.M. Barr and D.C. Hanna,
Optoelectronics Research Centre,
Southampton University,
Southampton,
SO9 5NH,
U.K.

Tel: (0703) 593143

Summary

The technique of additive-pulse mode-locking has recently become well-established for the generation of ultrashort pulses from solid state lasers¹. By combining this technique with laser-diode-pumping, highly efficient, reliable, compact and robust sources of mode-locked pulses have been realised^{2,3}. We have previously reported the generation of sub-picosecond mode-locked pulses from a Ti:Al₂O₃ laser pumped La_{1-x}Nd_xMgAl₁₁O₁₉ (Nd:LMA, or LNA) laser⁴. In this paper we report the generation of 750 fsec pulses from a self-starting additive-pulse mode-locked laser-diode-pumped Nd:LMA laser. This laser is currently being assessed as a seed source for a chirped pulse amplification Nd:glass laser under development at the Rutherford Appleton Laboratory. Nd:LMA is of great interest for this application, since its emission wavelength (1.054 μ m) matches that of the amplifier chain, and its gain bandwidth of 1.3 THz means that it is capable of supporting sub-picosecond pulses. In addition, it has an important advantage over the Nd:glass laser, which is clearly another candidate to be used for the system described above. Although the laser-diode-pumped Nd:glass laser has been shown to be a source of sub-picosecond pulses via additive-pulse mode-locking⁵, it is difficult to scale to higher powers due to its relatively low melting point. Nd:LMA has shown no such catastrophic thermal problems.

The experimental apparatus is shown in figure 1. The pump source was a 3 W laser diode array (SDL 2482). Its output was collimated by the compound collimating lens (L1) and a 15 cm cylindrical lens (L2). The beam was then split into two before being recombined, and focused into the crystal by the lens L3 (focal length 3.2 cm). This splitting and recombination was done in an attempt to improve the quality of the pump beam near the focus, by reducing its divergence in the horizontal plane by a factor of 2 whilst maintaining the horizontal spot size. This brightness enhancing procedure is only possible since the laser diode array is a partially coherent source. The laser medium was a 9 mm long, 5 mm diameter plane-Brewster rod of Nd:LMA with a 9% doping level of Nd ions. The plane surface was coated to give high reflectivity at the lasing wavelength, and high transmission at the pump wavelength. The cavity, which was designed to compensate for the astigmatism caused by the Brewster angle of the laser rod was completed with a 30 cm ROC turning mirror, a plane folding mirror, and an output coupler of 90% reflectivity. A pair of Brewster angled SF10 prisms separated by 92 cm was inserted into the cavity to compensate for the net positive dispersion of the coupled cavity configuration. The total cavity length was 1.4 m. With this arrangement (with the prisms in the

cavity), the maximum output power obtained from the laser was 280 mW for an incident pump power of 2.1 W, a reduction of 12% from the case when the prisms were not included. The output of the laser was at all times single transverse mode.

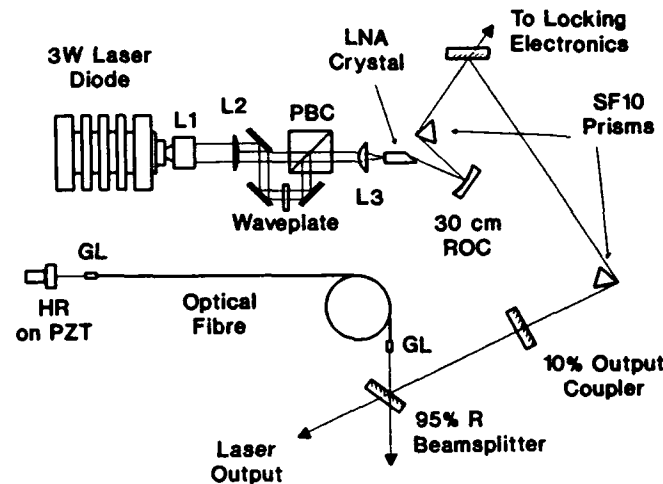


Figure 1: Schematic diagram of the experimental apparatus

The coupled cavity was formed using a 95% reflectivity beamsplitter to direct a portion of the laser output into a single mode optical fibre of length 1.55 m. Coupling into and out of the fibre was accomplished using the GRIN lenses GL, and launch efficiencies in the region of 64-70% were readily achieved. The coupled cavity was completed with a HR mirror mounted on a piezoelectric stack. The total length of the coupled cavity was twice that of the main laser cavity. It should be noted that the parameters used in the coupled cavity (high beamsplitter reflectivity, long fibre length) were originally chosen to facilitate self-starting mode-locked operation, and are not optimized.

When the cavity lengths were correctly matched, mode-locked operation was readily achieved. With a pump power of 2.1 W incident on the crystal, 165 mW was launched into the fibre. At this level, the usable output power was 18 mW. The relative phases of the two cavities were locked using the technique of Mitschke and Mollenauer⁶, and stable mode-locked operation was observed at the cavity round trip frequency of 107 MHz. The threshold for self-starting operation was as low as 36 mW launched into the optical fibre. A typical real-time interferometric autocorrelation trace is shown in figure 2. The pulse duration corresponding to this trace was 750 fsec assuming a hyperbolic secant temporal profile. The high fringe visibility into the wings of the trace indicates that the pulses were not chirped. The optical spectrum corresponding to this autocorrelation trace is shown in figure 3, and has a FWHM of 430 GHz. The time-bandwidth product is thus 0.32. Without the prisms in the cavity, heavily chirped pulses of 1-2 psec duration were obtained, indicating clearly the necessity for intracavity dispersion compensation. Future work will focus on increasing the useful output power from the system and reducing the mode-locked pulse duration to a figure closer to the bandwidth limit of 350 fsec.

We are grateful to Dr Ch Wyon of LETI, Grenoble, France, for supplying us with the Nd:LMA rod used in this experiment. This work was supported by a Science and Engineering Council funded collaboration with the Rutherford Appleton Laboratory.

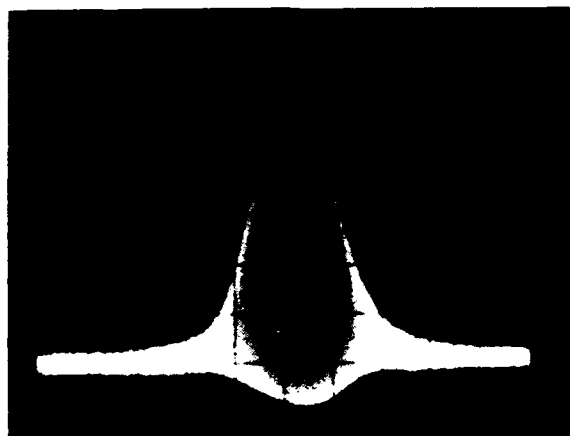


Figure 2: Interferometric autocorrelation trace. Time Delay: 660 fsec/div

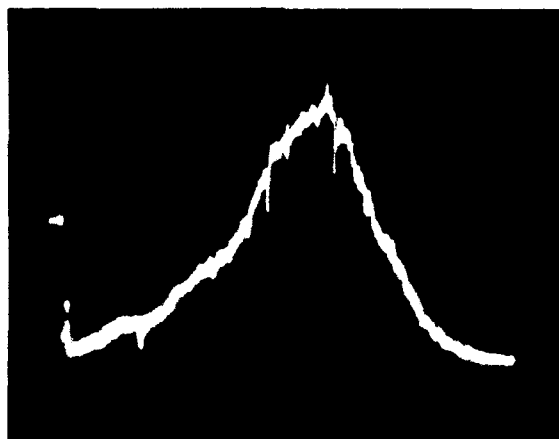


Figure 3: The optical spectrum of the mode-locked laser. Horizontal Scale: 150 GHz/div

References

1. J. Mark, L.Y. Liu, K.L. Hall, H.A. Haus and E.P. Ippen, *Opt. Lett.* **14**, 48 (1989)
2. J. Goodberlet, J. Jacobson, J.G. Fujimoto, P.A. Schulz, and T.Y. Fan, *Opt. Lett.* **15**, 553 (1990)
3. G.P.A. Malcolm, P.F. Curley and A.I. Ferguson, *Opt. Lett.* **15**, 1303 (1990)
4. M.W. Phillips, Z. Chang, J.R.M. Barr, D.W. Hughes, C.N. Danson, C.B. Edwards and D.C. Hanna, "Self-starting additive pulse mode-locking of a Nd:LMA laser", to be published, *Opt. Lett.* (1992)
5. D.W. Hughes, M.W. Phillips, J.R.M. Barr and D.C. Hanna, *IEEE J. Quantum Electron.* **QE-28**, 1010 (1992)
6. F.M. Mitschke and L.F. Mollenauer, *Opt. Lett.* **12**, 407 (1987)

CW pasive mode-locking of a new $\text{Nd}^{3+}:\text{GdVO}_4$ laser

E. Sorokin, I. Sorokina, E. Wintner

Technische Universität Wien, Abt. Quantenelektronik und Lasertechnik

Gusshausstr. 27/359/9, A-1040 Vienna, Austria

Phone : 43-1-58801-3801, Fax : 43-1-5042477

A. I. Zagumennyi, I. A. Shcherbakov

General Physics Institute, Vavilov str. 38, Moscow, Russia

Phone : 7-095-135-11-24 Fax : 7-095-135-02-70

Recently a lot of research efforts were applied to the development and improvement of the new neodymium-doped materials, suitable for diode-pumping. The requirements to the spectroscopic properties of laser materials for diode-pumping are well known: absorption bands should be broad enough to bypass problems with thermal drift of laser diode emission wavelength, while emission lines should be narrow enough to allow higher peak gain. Widely used nearly homogeneously broadened hosts like YAG and YLF have narrow emission and absorption lines. Recently, attention was drawn to a variety of disordered crystalline hosts with the inhomogeneously broadened spectral lines [1], which are suitable for ultrashort-pulse generation as well [2], however at the expense of lower output power and efficiency. We have carried out both spectroscopic and lasing investigations of a new laser material $\text{Nd}^{3+}:\text{GdVO}_4$ (0.9 at. % Nd), which is a Gd analog to an YVO_4 crystal and possesses a unique combination of broad (~ 10 nm) intensive absorption band at 810 nm combined with relatively narrow (~ 1.2 nm) emission line at 1065 nm. In comparison to YVO_4 the new crystal possesses better growth properties and close to unity Nd^{3+} distribution coefficient due to the larger ionic radius of Gd^{3+} .

In this paper we report the first demonstration of a thin-plate $\text{Nd}^{3+}:\text{GdVO}_4$ passively mode-locked laser, pumped by a Kr^+ -laser ($\lambda = 799$ and 752 nm) to simulate diode-pumping. The cavity design is shown schematically in Fig. 1. The active medium was a 1-mm-thick plate, cooled through its side surfaces. The waist diameters inside the crystal were $\sim 15\mu\text{m}$ for resonator beam and $\sim 23\mu\text{m}$ for pump beam. To characterize TEM_{00} -mode CW laser performance, a short cavity, consisting of mirrors M1, M2, M3 and an output coupler at the place of beamsplitter BS was used. The lasing data are summarized in the Table 1.

At maximum available pump power of 2.15 W (1.6 W absorbed), output power of

Table 1:

Output coupling	P_{out}	Slope efficiency
3.5 %	565 mW	41 %
5 %	615 mW	45 %
10 %	645 mW	48 %
16 %	660 mW	51 %

690 mW was obtained without beam profile or efficiency degrading.

For mode-locking experiments a full version of the cavity was used, as shown in Fig. 1. To stabilize interferometrically two arms of a nonlinear interferometer mirror M4 was mounted on a piezoelectrical translator (PZT), controlled by a servo loop. At 1.75 W of pump power (1.3 W absorbed) the laser produced stable train of pulses with $\tau \approx 2.4$ ps (Fig. 2) with output power of 300 mW. The spectral width of the mode-locked laser output was ≈ 0.6 nm (Fig. 3), yielding time-bandwidth product $\Delta\tau\Delta\nu \approx 0.36$. This value is close to that of a transform-limited pulse, indicating that the pulse is almost free of frequency chirp. This can be also seen from an interferometric autocorrelation trace in Fig. 2. These data are obtained without optimization of the fiber length in the nonlinear arm of the resonator, which gives us hope to produce pulses of even shorter duration, utilizing full 1.2-nm-wide linewidth of the material.

In conclusion, we obtained efficient mode-locked operation of the new $\text{Nd}^{3+}:\text{GdVO}_4$ laser material, yielding stable 5 nJ pulses with 2.4 ps duration, which is comparable to that of YAG and YLF. Spectral properties favourable for diode pumping and good CW lasing performance make this new material highly attractive for all-solid-state ultrashort-pulse laser systems.

References

1. M. H. Randles, J. E. Creamer, R. F. Belt, G. J. Quarles, and L. Esterowitz, *Advanced Solid State Laser, Santa Fe 1992, Technical Digest*, p. 289-291 (1992).
2. M. H. Ober, E. Sorokin, I. Sorokina, F. Krausz, E. Wintner, and I. A. Shcherbakov, Subpicosecond Mode-Locking of a Nd^{3+} -doped Garnet Laser, to be published *Opt. Lett.*, 17, 15 September 1992.

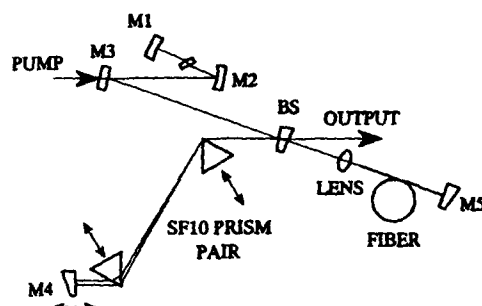


Figure 1: Experimental setup.

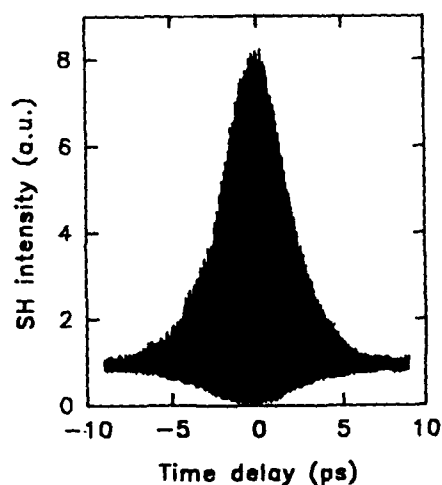
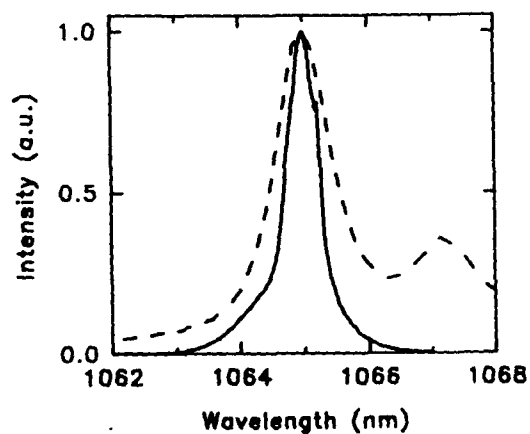


Figure 2: Interferometric autocorrelation trace of a modelocked laser.

Figure 3: Spectrum of a modelocked laser (solid curve). Fluorescence spectrum of $\text{Nd}^{3+}:\text{GdVO}_4$ at room temperature (dashed curve).

Nd³⁺:Ca₂Al₂SiO₇ a New Solid State Laser Material for Diode Pumping

B. Viana, D. Saber, A.M. Lejus and D. Vivien
Laboratoire de Chimie Appliquée de L'Etat Solide (ENSCP)
11Rue P&M Curie 75231 Paris cedex 05 - France
phone# (33)-1-44276707 fax# (33)-1-46347489
R. Romero and C. Wyon
Division Optronique L.E.T.I.- C.E.N.G.
Avenue des Martyrs 85X, 38041 Grenoble Cedex, France

Introduction

Solid state lasers with diode laser pumping are very attractive for producing compact systems with powerful and stable laser emission. In this regard, the disordered gehlenite host Ca₂Al₂SiO₇ (or CASIO) represents a viable candidate material. This paper reviews our work on the optical properties and laser characteristics of Nd³⁺:Ca₂Al₂SiO₇. Laser diode pumping of this material has been achieved and a slope efficiency of nearly 40% has been obtained. Gehlenite possesses a tetragonal crystal cell; Al³⁺ and Si³⁺ statistically occupy tetrahedral sites leading to a structural disorder. The material is readily doped with Nd³⁺ and Ca_{1-x}Nd_xAl₂SiO₇ single crystals with $0 \leq x \leq 0.4$ have been grown by the Czochralski process at a relatively low temperature ($T_f=1580^\circ\text{C}$). The growth axis is perpendicular to the c-axis direction of the structure and laser quality crystals have been prepared. In these samples, the Nd³⁺ distribution is homogeneous and no segregation has been observed.

Optical Properties

Nd³⁺:Ca₂Al₂SiO₇ crystals exhibit broader absorption lines (46Å for the ⁴I_{9/2}->⁴F_{5/2}, ²H_{9/2} transition at 300K) than the more ordered structures activated by Nd³⁺ (5-20Å). Thus the variation of pumping efficiency with respect to the wavelength shift of the laser diode is not as sensitive for CASIO as it is for Nd³⁺:YAG. At 805nm, the oscillator strengths are stronger for the σ orientation (8.1×10^{-6}) than for the π orientation (3.3×10^{-6}). The σ orientation $E \perp c$ is therefore more favorable for diode laser pumping.

From absorption measurements, the Judd-Ofelt parameters have been calculated for Nd³⁺:Ca₂Al₂SiO₇ gehlenite and compared to various Nd³⁺ doped oxide matrices in the table 1

Table 1: Judd-Ofelt parameters for Nd³⁺ doped oxide laser hosts

Laser Host	$\Omega_2 \times 10^{20} \text{cm}^2$	$\Omega_4 \times 10^{20} \text{cm}^2$	$\Omega_6 \times 10^{20} \text{cm}^2$	$X = \Omega_4 / \Omega_6$
Ca ₂ Al ₂ SiO ₇	2.19	2.85	6.77	0.42
Ca ₂ Ga ₂ SiO ₇ ¹	0.82	2.41	6.44	0.37
YAG ²	0.2	2.7	5.0	0.54
YAlO ₃ ³	1.24	4.68	5.85	0.80
LaMgAl ₁₁ O ₁₉ ⁴	1.23	1.75	2.24	0.78

For diode pumping Ω_6 is the most important of the three phenomenological Ω_i parameters. The absorption in the red and near I.R. range depend mainly on this parameter and absorption is enhanced as the value of Ω_6 increases. The Ω_4/Ω_6 ratio governs the branching ratio, the lower the value of the Ω_4/Ω_6 ratio, the stronger the $^4F_{3/2} \rightarrow ^4I_{11/2}$ emission around $1.06\mu\text{m}$. The corresponding fluorescence spectrum for Nd:CASIO exhibits a broad and intensive emission from $1.06\mu\text{m}$ to beyond $1.10\mu\text{m}$ (Fig 1-a). In contrast, the Nd³⁺:YAG emission spectrum under the same experimental conditions consists of narrow lines (Fig 1-b). To our knowledge, Nd³⁺:Ca₂Al₂SiO₇ gehlenite possesses one of the broadest emission bands in this spectral range and offers considerable potential for wavelength tunability.

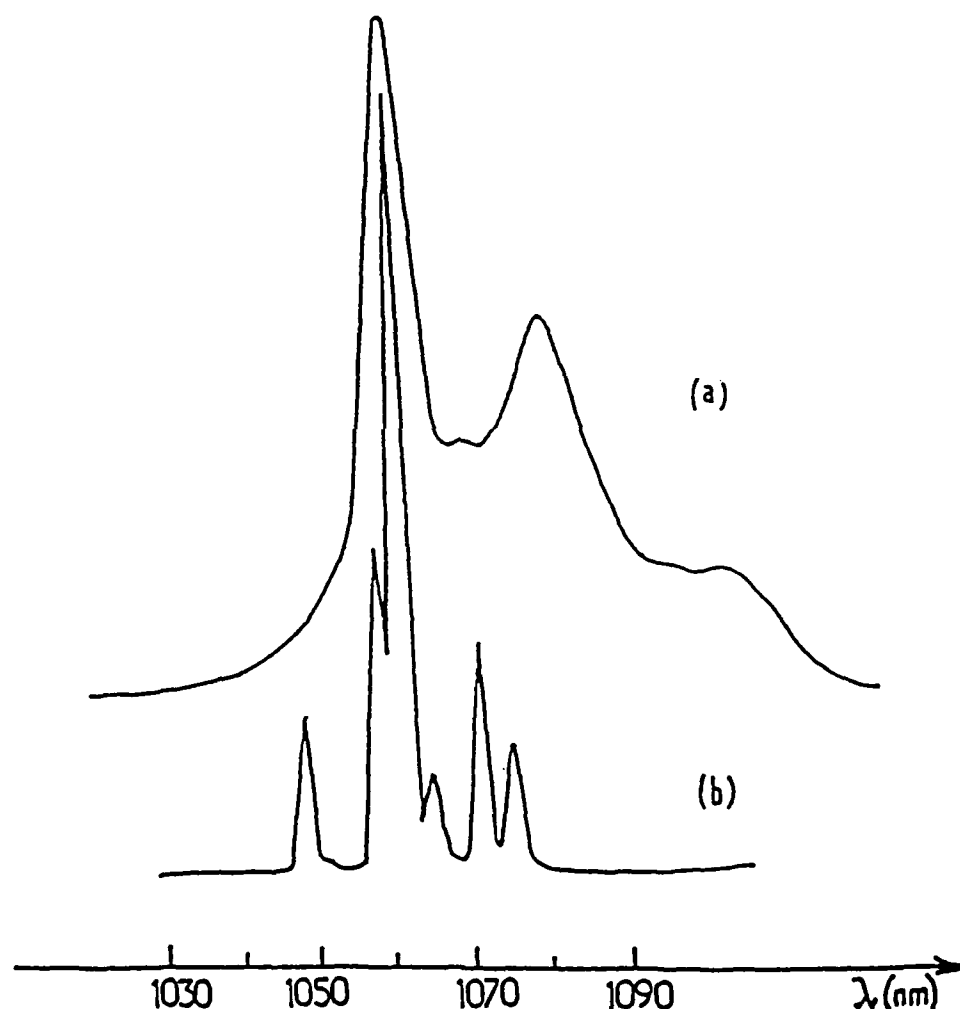


Fig1 : Emission spectra of (a): gehlenite and (b): YAG doped Nd³⁺ laser hosts

The lifetime measurements of the $^4F_{3/2}$ level are in good agreement with the radiative lifetime calculated from the Judd-Ofelt parameters. At low concentration the measured lifetime was $275\mu\text{s}$ ($x=0.005$) with the same value for the calculated radiative lifetime. Furthermore, in Ca_{1-x}Nd_xAl₂SiO₇ crystals for $x \leq 0.03$ (or $\leq 2.2 \times 10^{20} \text{ Nd}^{3+} \text{ cm}^{-3}$), no cross-relaxation was

evident as the fluorescence decay is exponential with a time constant value of $270\mu\text{s}$. At higher concentration Nd^{3+} - Nd^{3+} interactions occur leading to shorter lifetimes and non-exponential decay profiles. For $x = 0.3$, the lifetime is estimated to be around $20\mu\text{s}$.

Laser Characteristics

Laser tests have been performed on a 5mm long laser rod of $\text{Ca}_{1.98}\text{Nd}_{0.02}\text{Al}_2\text{Si}_{0.98}\text{O}_7$. The laser diode pump was horizontally polarized emitting at 805nm, the maximum of the Nd^{3+} absorption. Several laser tests were performed using different output coupling mirrors. The results are shown in Table 2.

Table2: Laser tests on $\text{Ca}_{1.98}\text{Nd}_{0.02}\text{Al}_2\text{Si}_{0.98}\text{O}_7$

Output Mirror Reflectivity (%)	Slope Efficiency μ (%)	$P_{\text{max}}(\text{IR})$ (mw)
98.4	24.2	120
97.5	34	148.5
95.9	35.4	150
94	32.2	122.1
92	39.5	91.6

The efficiencies are calculated according to the formula: $\mu = \frac{P_{\text{IR}}}{P_{\text{abs}} - P_{\text{abs thr}}}$. The values reported in Table 2 are for σ polarization (E_{Lc}) (i.e., the favorable orientation). The threshold is around 180mW (abs) for $R_{\text{out}}=98.5\%$. For $R_{\text{out}}=95.9\%$ the extracted IR laser oscillation is 150mW for a 600mW pump. The optical slope efficiency corresponds to around 35%.

These initial laser tests are extremely encouraging as the crystal growth of the gehlenite has yet to be optimized. Moreover, the prospects of achieving tunability of the laser emission over the range $1.06\mu\text{m}$ - $1.10\mu\text{m}$ are very promising.

This research was supported by the DRET (contract number 90/1202A).

References

- (1) A.A. Kaminskii E.L. Belokoneva, B.V. Mill, S.A. Tamazyan and K. kurbanov
Iz Akad Nauk SSSR, Neorg. Mater. **22**, (1986),1138
- (2) W.F. Krupke, J. Quantum Electron., **7**, (1971), 153
- (3) M.J. Weber , T.E. Varitimas, B.H Mistanger,. Phys. Rev.**B8**, (1973), 47
- (4) A.A. Kaminskii, B.M. Antipenko in the Russian version of "Multilevel Operating Schemes of Crystalline Lasers" M.:Nauka (1989) p159 & p163

Spectroscopic and sensitization analysis of Er, Yb and Cr ions in calcium fluorophosphate

Toomas H. Allik, Science Applications International Corporation,
1710 Goodridge Drive, McLean, VA 22102, (703) 704-3265

John B. Gruber, Department of Physics, San Jose State University,
San Jose, CA 95192

Michael D. Seltzer and Marian E. Hills, Naval Air Warfare Center
Weapons Division, China Lake, CA 93555

Clyde A. Morrison, Harry Diamond Laboratories, U.S. Army Adelphi
Laboratory Center, Adelphi, MD 20783-1197

Bruce H.T. Chai, University of Central Florida, CREOL,
12424 Research Parkway, Orlando, FL 32836

J. Andrew Hutchinson and Larry D. Merkle,
Night Vision and Electro-Optics Directorate, Lasers and Photonics
Division, Fort Belvoir, VA 22060

The development of diode laser pump sources has renewed interest in rare earth ion-doped calcium fluorophosphate $[\text{Ca}_5(\text{PO}_4)_3\text{F}]$ or FAP crystals as a host for stimulated emission in the infrared. For instance, Payne et al. have recently demonstrated efficient laser performance of $\text{Yb}^{3+}:\text{FAP}$ at $1.04 \mu\text{m}$.¹ We believe that $\text{Er}^{3+}:\text{FAP}$ has many desirable properties as an eyesafe laser material at $1.5 \mu\text{m}$. First, FAP possesses high frequency phonons (up to $3,600 \text{ cm}^{-1}$), which should yield rapid nonradiative relaxation processes.² This will reduce upconversion and maximize population in the $^4\text{I}_{13/2}$ level for Er^{3+} . Secondly, the rare-earth site has demonstrated a large crystal-field splitting for the $^2\text{F}_{5/2}$ state of Yb^{3+} which should enhance the activation of the $^4\text{I}_{11/2}$ Er^{3+} manifold by interionic energy transfer. In addition, FAP contains a PO_4^{3-} tetrahedral site which can accept a transition metal such as Cr, and potentially sensitize Er^{3+} directly. Finally, the crystal growth of FAP has been well characterized and lengths up to 25 cm have been obtained.³ To date, we have grown a-axis FAP boules up to 2.5 cm in diameter and $> 10 \text{ cm}$ in length. In this paper we discuss the spectroscopic analysis of $\text{Er}^{3+}:\text{FAP}$ and the sensitization of Er with either Yb or Cr.

We have obtained and analyzed the polarized absorption, fluorescence, and site-selective excitation spectra of $\text{Er}^{3+}:\text{FAP}$ at 4K and higher temperatures. Figure 1 shows the fluorescence spectrum from the $^4\text{I}_{13/2}$ to $^4\text{I}_{15/2}$ states for 1% Er:FAP. The fluorescence lifetime of the $^4\text{I}_{13/2}$ state was measured to be 10.5 ms. Er^{3+} ions occupy three sites, resulting in the observed inhomogeneous broadening. Site-selective polarized excitation was used to establish the spectral features associated with Er^{3+} .

in a given site, and the symmetry of that site. Analysis of the vibronic spectra leads to the conclusion that phonon energies larger than those observed in $\text{Er}^{3+}:\text{YAG}$ are involved. The overall crystal field splitting of the individual multiplet manifolds ($2S+1L_J$) of $\text{Er}^{3+}(4f^{11})$ is larger than the splitting observed in $\text{Er}^{3+}:\text{YAG}$ for at least two of the sites.

The fluorescence quantum efficiency from manifolds higher than $^4I_{13/2}$ (such as $^4S_{3/2}$) appears to be less than observed in other laser host crystals. As in the case of emission, most of the absorption intensity associated with the $^4I_{13/2}$ multiplet is confined to only one or two transitions out of a possible $J + 1/2$ transitions associated with each of the three Er^{3+} sites. Hot bands do not appear until the crystal temperature is nearly 100K indicating the splitting ($\sim 100\text{cm}^{-1}$) between the ground Stark level (Z_1) and the first excited Stark level (Z_2) is much larger than has been reported for Er^{3+} in any host crystal.

We are currently studying the effects of different sensitizers on $\text{Er}:\text{FAP}$. Since Yb^{3+} has been used as an efficient sensitizer for Er^{3+} , we have studied the transfer process for 1-2% Yb , codoped with Er concentrations ranging from 0.1-1.0% in FAP. This energy transfer process in FAP appears promising. In the presence of 0.5% Er^{3+} , the fluorescence lifetime of the (2%) $\text{Yb}^{3+} \ ^2F_{5/2}$ state is reduced by half to 0.6 ms.

For a 0.5% Cr , 1.0% Er sample, the polarized absorption spectrum is shown in Figure 2. This spectrum, with broad spectral features at visible and NIR wavelengths is characteristic of Cr^{4+} in a distorted tetrahedral field.⁴ The fluorescence spectrum of 0.5% $\text{Cr}:\text{FAP}$, without Er^{3+} , is given in Figure 3. The fluorescence of the Cr^{4+} is seen to overlap the Er^{3+} absorption at 1.5 μm . Fluorescence from $\text{Er}^{3+} \ ^4I_{13/2}$ has been observed subsequent to optical excitation of the Cr ion, and the excitation spectra appears in Figure 4. The broad peak centered at 600 nm may be the $^3A_2 \rightarrow ^3T_1$ transition of Cr^{4+} , another oxidation state of Cr or a Cr -related color center. Quantum efficiency measurements will be discussed.

References

1. S.A. Payne, W.F. Krupke, L.D. DeLoach, L.K. Smith, W.L. Kway, and J.B. Tassano, "Laser properties of Yb^{3+} in fluorapatite and other crystalline media," in OSA Annual Meeting Technical Digest, 1992 (Optical Society of America, Washington, D.C., 1992), Vol.23, p.33.
2. A.M. Morozov, L.G. Morozova, A.K. Trefimov, and P.P. Feofilov, Opt. Spektrosk. 29, 1106 (1970).
3. R.C. Ohlmann, K.B. Steinbruegge, and R. Mazelsky, Appl. Opt. 7, 905 (1968)
4. L.D. Merkle, T.H. Allik, and B.H.T. Chai, Optical Materials 1, 91 (1992) and references therein.

Figure Captions.

Figure 1. Polarized room temperature fluorescence spectra of Er^{3+} :FAP.

Figure 2. Polarized room temperature absorption spectra of $\text{Cr}(0.5\%), \text{Er}(1.0\%): \text{FAP}$.

Figure 3. Unpolarized fluorescence spectrum of $\text{Cr}:\text{FAP}$, excited at 620nm.

Figure 4. Excitation spectrum of $\text{Cr}:\text{Er}:\text{FAP}$, emission at 1560 nm.

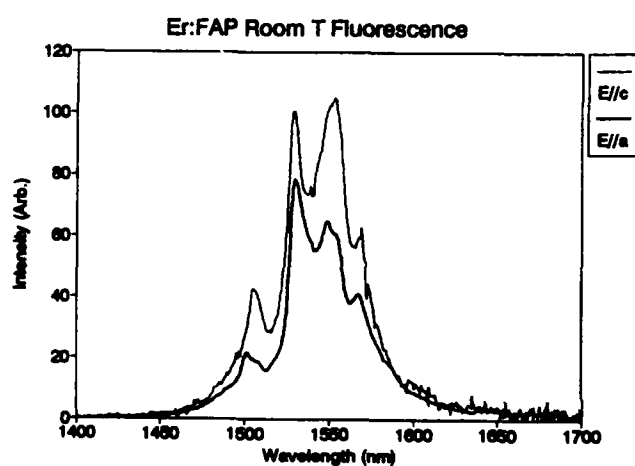


Figure 1.

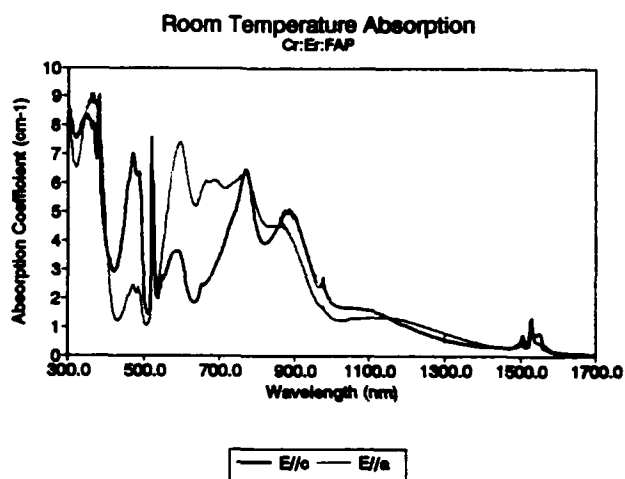


Figure 2.

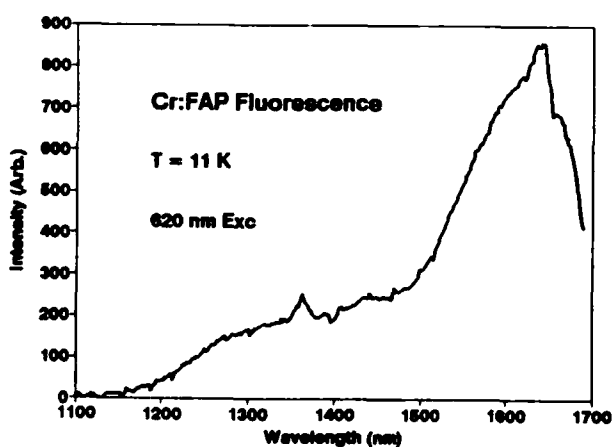


Figure 3.

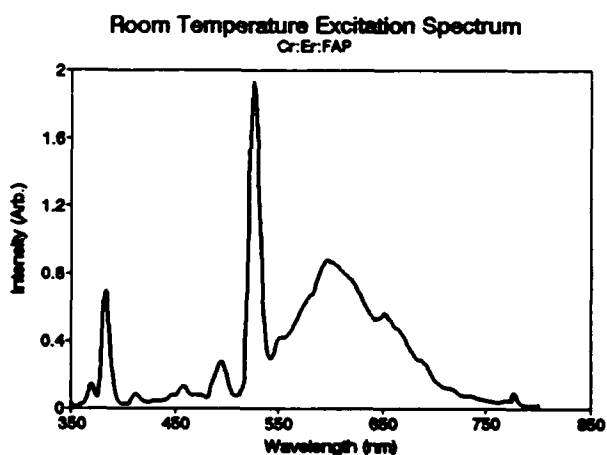


Figure 4.

Next laser glasses for nuclear fusion

T. Izumitani

Izumitani Special Lab., HOYA Corp.
3-3-1, Musashino, Akishima, Tokyo 196 JAPAN

1. Introduction

Nd^{3+} phosphate glass LHG-8 and HAP-4 are well known for nuclear fusion laser glass. But the life time of Nd glasses is about $300\mu\text{s}$ and too short for economical nuclear fusion system. According to Naito¹⁾ (Osaka Univ.), new solid state laser material for nuclear fusion should have the following properties: (a) a thermal shock parameter larger than $3\text{W}/\text{cm}$, (b) saturation parameter of $\sim 10\text{J}/\text{cm}^2$, (c) a fluorescence life time longer than 4ms , (d) a non-linear index of refractive smaller than $3 \times 10^{-13}\text{esu}$.

We examined the rare earth elements except Nd^{3+} , ie, Yb^{3+} , Er^{3+} , Tm^{3+} and Ho^{3+} . The laser wavelength of Tm^{3+} and Ho^{3+} are 1.9μ and 2μ , respectively and very long. Even if we used sensitizer, the emission intensities of Yb-Tm, Er-Tm-Ho and Yb-Tm-Ho doped glasses are too small. $0.8\mu^{21}$ emission of Tm^{3+} -doped glass is very strong but the stimulated emission cross section is too small. Yb^{3+} and Er^{3+} ions satisfy the conditions suggested by Naito.

We calculated the radiative transition probability of Yb^{3+} and Er^{3+} from absorption spectrum. Next, we used the sensitizers Nd^{3+} to Yb^{3+} and Yb^{3+} to Er^{3+} . In order to increase thermal shock resistance, we used low expansion laser glasses such as an aluminate glass or HAP-4 base glass.

2. Experimental

Glass compositions used are shown in Table 1. Nd^{3+} 0.3, Yb^{3+} 2 and Er^{3+} 1cat% were doped.

Table 1 Compositions of glasses (in cat%)

Silicate	49.8SiO_2 - 4.8AlO_2 - $36(\text{LiO}_2+\text{NaO}_2)$ - 9.4SrO
Aluminate	47.9AlO_2 - 36.1CaO - 8MgO - 8BaO
Germanate	57.4GeO_2 - $26.1\text{K}_2\text{O}$ - 16.5BaO
Phosphate	65.2PO_2 - 8.6AlO_2 - $7.5(\text{BaO}+\text{MgO})$ - $18.7\text{K}_2\text{O}$
Fluorophosphate	10PO_2 - 33AlF_3 - 3.8YF_3 - $48.2(\text{MgF}_2+\text{CaF}_2+\text{SrF}_2+\text{BaF}_2)$ - 5NaF

Aluminate glass was melted at 1500°C , for one hour using Pt crucible. Fluorophosphate glass was melted at 900°C for an hour in N_2 atmosphere. Silicate, germanate and phosphate glasses were melted at 1380°C , 1300°C and 1250°C for 2 hours in Pt crucible.

Absorption spectrum was measured with HITACHI-330 spectrophotometer. Emission spectrum was measured with Ge detector or R-2228 photomultiplier for the sample excited with LD 800nm, 980nm or Xe lamp. Life time was measured S-1 photomultiplier or InAs detector for the sample excited with dye laser pumped with YAG laser.

3. Results and discussions

3.1 Nd^{3+} , Yb^{3+} , Er^{3+} singly doped glass

We measured the absorption and emission spectra and life time for the Nd^{3+} , Yb^{3+} and Er^{3+} separately doped glasses. We calculated A-coefficients from absorption spectrum due to Judd-Ofelt treatment using matrix element derived by Carnall²⁾ for Nd^{3+} , Weber³⁾ for Er^{3+} and using Fuchtbauer-Ladenburg⁴⁾ equation for Yb^{3+} . The results are shown in Table 2, 3 and 4.

Table 2 Comparison of laser spectroscopic properties of Nd^{3+} $^4\text{F}_{3/2}$ level in various glasses

	$\nu_e(\text{cm}^{-1})$	$N(10^{20}\text{cm}^{-3})$	$A_e(\text{sec}^{-1})$	$\tau_n(\mu\text{sec})$	$\Delta\lambda(\text{nm})$	$\sigma(10^{-20}\text{cm}^2)$
Aluminate	11274	0.97	3452	292	41	2.33
Fluorophosphate	11521	0.71	871	552	24	1.42
Germanate	11364	0.76	1283	348	24	1.46
Silicate	11377	1.07	1807	248	23	2.54
Phosphate	11455	0.72	2846	255	22	4.37

Table 3 Comparison of laser spectroscopic properties of Yb^{3+} $^2\text{F}_{5/2}$ level in various glasses

	$\nu_e(\text{cm}^{-1})$	$N(10^{20}\text{cm}^{-3})$	$A_e(\text{sec}^{-1})$	$\tau_n(\mu\text{sec})$	$\Delta\lambda(\text{nm})$	$\sigma(10^{-20}\text{cm}^2)$
Aluminate	10225	6.3	1309	1030	64	1.07
Fluorophosphate	10267	4.7	667	2120	67	0.64
Germanate	10267	5.1	750	1190	64	0.58
Silicate	10256	7.1	629	1040	63	0.56
Phosphate	10256	4.9	913	532	66	0.79

Table 4 Comparison of laser spectroscopic properties of Er^{3+} $^4\text{I}_{13/2}$ level in various glasses

	$\nu_e(\text{cm}^{-1})$	$N(10^{20}\text{cm}^{-3})$	$A_e(\text{sec}^{-1})$	$\tau_n(\mu\text{sec})$	$\Delta\lambda(\text{nm})$	$\sigma(10^{-20}\text{cm}^2)$
Aluminate	6506	3.15	117	13.1	33	0.92
Fluorophosphate	6536	2.35	139	12.4	55	0.88
Germanate	6515	2.53	95	7.0	23	1.09
Silicate	6510	3.57	98	5.5	28	1.044
Phosphate	6532	2.41	138	0.9	35	1.224

From the tables, A-coefficient or σ value decreases in the order of $\text{Nd}^{3+} > \text{Yb}^{3+} > \text{Er}^{3+}$ and life time increases in the order of $\text{Nd}^{3+} < \text{Yb}^{3+} < \text{Er}^{3+}$. Change is very remarkable. Therefore, high cross section for stimulated emission will be obtained from Nd^{3+} ion and long life time is given by Yb^{3+} or Er^{3+} . Phosphate or aluminate glass gives high σ values.

3.2 Nd^{3+} - Yb^{3+} codoped glasses.

As shown in Table 2 and 3, A-coefficient of Nd^{3+} is larger than that of Yb^{3+} . Accordingly, it is very useful to use Nd^{3+} ion as a sensitizer for Yb^{3+} active ion. The energy level of Nd^{3+} , $^2\text{F}_{3/2}$ and Yb^{3+} , $^2\text{F}_{5/2}$ exist at 0.88μ and 0.97μ respectively and therefore there is a possibility for overlapping of Nd^{3+} emission and Yb^{3+} absorption spectra.

Fig.1 shows the Nd^{3+} emission and Yb^{3+} absorption spectra in phosphate and aluminate glasses. There is an overlapping between emission and absorption spectra. This means there is an energy transfer⁶⁾ between them. We calculated the energy transfer efficiency⁷⁾ measuring Nd^{3+} life time which is give by equation $\eta = 1 - (\tau_{\text{Nd}^{3+}} - \tau_{\text{Nd}^{3+}})/\tau_{\text{Nd}^{3+}}$. The result is shown in Table 5.

We obtained an aluminate glass doped by sensitizer Nd^{3+} and activator Yb^{3+} , which has higher emission intensity than LHG-8(Fig.2), expansion coefficient 83×10^{-7} , life time 1.04ms and almost satisfies the Naito's requirements.

Table 5 Nd^{3+} 's lifetime (1.06 μm) for Nd and Nd+Yb doped glasses

Glass	Nd^{3+}	lifetime (μs)	Nd^{3+}	Yb^{3+}	lifetime (μs)	η (%)
Aluminate	0.3	292	0.3	2	17.2	94
Silicate	0.3	248	0.3	2	40	83
Germanate	0.3	348	0.3	2	80	80
Fluorophosphate	0.3	552	0.3	2	149	73
Phosphate	0.3	252	0.3	2	69	72

3.3 Yb³⁺-Er³⁺ codoped glasses.

Er³⁺ ions give small A-coefficient and longer life time. In order to make up for small absorption capability, Nd³⁺ or Yb³⁺ which has strong absorption coefficient should be doped. As Er³⁺ makes 3-level laser, wavelength difference between emission and absorption is small, accordingly self-absorption might occur. Therefore, we should use sensitizer. But to use Nd³⁺ is not desirable because of back transfer. Thus, we obtained the glass with high emission intensity by selecting the suitable ratio Nd³⁺:Yb³⁺:Er³⁺=0.5:7.5:0.5⁹⁾ (Fig.3).

In the range of Er³⁺ 0 ~ 0.5 cat%, almost 100% energy transfer occurs from Yb³⁺ to Er³⁺ and the back transfer is negligible. In the range of over 0.5% Er³⁺, the back transfer begins and increases⁹⁾. The reason the Yb-Er phosphate glass shows the highest emission intensity is that the back transfer is negligible.

But we found that Yb³⁺-Er³⁺ codoped glass pumped by 0.98 μ LD gives the stronger emission intensity than Nd³⁺-Yb³⁺-Er³⁺ codoped glass pumped by 0.8 μ LD and by changing the base glass composition to HAP-4 we succeeded to make expansion coefficient smaller.

Table 6 Yb³⁺'s lifetime (at 1.03 μ m) for Yb+Er doped glasses

Glass	Yb ³⁺	(+Nd ³⁺)	lifetime (μ s)	Yb ³⁺	Er ³⁺	lifetime (μ s)	η (%)
Silicate	2	0.3	1040	2	1	91	91
Fluorophosphate	2	0.3	2120	2	1	338	84
Aluminate	2	0.3	1030	2	1	248	74
Germanate	2	0.3	1190	2	1	320	73
Phosphate	2	0.3	532	2	1	27	72

Thus, the new glass with Yb³⁺ 10cat% and Er³⁺ 0.05cat% shows $\sigma=1.65 \times 10^{-20} \text{cm}^2$, $\tau=10\text{ms}$, absorption coefficient 0.04cm^{-1} at 1.54 μ (Fig.4) and expansion coefficient 80.6×10^{-7} and satisfies Naito requirement.

Reference

1. K.Naito, T.Kanabe, S.Nakai et al: Jap. J. Appl. Phys. 31(1992)259.
2. T.Izumitani, B.Peng and X.Zou: applied J. Patent (1992)May.
3. W.T.Canall, P.R.Felds and K.Rajank: J. Chem. Phys. 49(1968)4424.
4. M.J.Weber: Phys. Rev. 157(1967)157
5. W.F.Krupke: IEEE J. Quantum Electronics OE10(1974)450.
6. D.L.Dexter: J. Chem. Phys. 21(1953)836.
7. R.Reisfeld and Y.Kalisky: Chem. Phys. 80(1981)178.
8. T.Izumitani and B.Peng: applied J. Patent (1992)April.
9. T.Izumitani and Y.Lin: Proc. Laser Soc. Japan (1992)Feb.

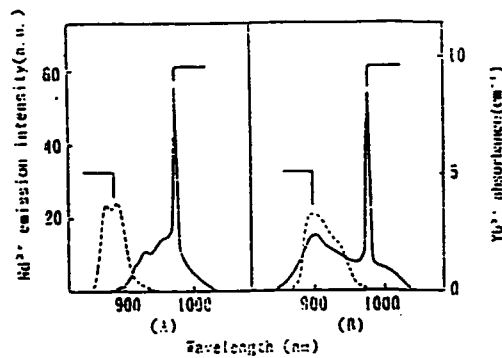


Fig. 1 Spectral overlap of Nd³⁺ emission(${}^4F_{3/2}$ - ${}^4I_{11/2}$) and Yb³⁺ absorption(${}^2F_{7/2}$ - ${}^2F_{5/2}$) in (A) phosphate and (B) aluminate glasses.

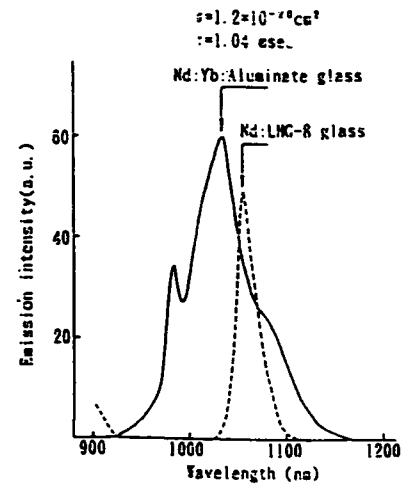


Fig. 2 Emission spectra of 3.1wt% Nd₂O₃ doped LiNG-8 glass and 1Nd₂O₃, 8.8Yb₂O₃ co-doped aluminate glass excited by Xe-lamp.

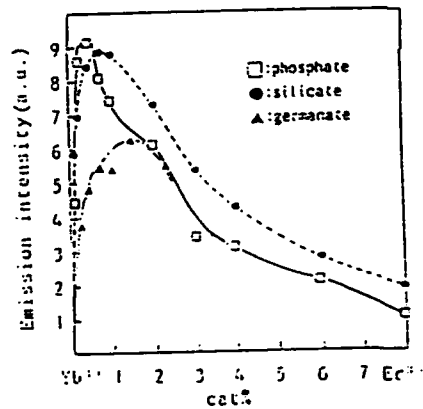


Fig. 3: The emission intensity of Yb³⁺, Er³⁺ codoped silicate and phosphate glasses at 1.54μ. Pumping source is Xenon Lamp

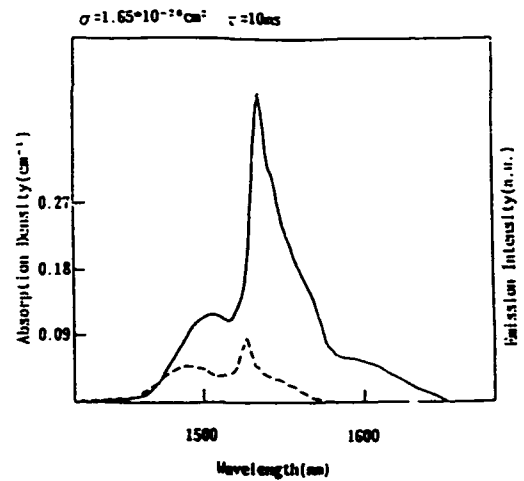


Fig. 4: The emission and absorption spectra of Yb, Er doped phosphate glasses. Yb10cat%, Er0.05cat%

Tuesday, February 2, 1995

Transition-Metal-Ion Lasers 1

ATuD 1:30pm–3:00pm
La Salle Ballroom B&C

William R. Rapoport, *Presider*
Allied-Signal, Inc.

150 fs, 1.5 TW, 10 Hz Ti:Al₂O₃ Laser System

P.H. Chiu, Art Magana, Koichi Yamakawa and John Davis
Continuum (408 727-3240)

and

J.D. Kmetec
Lightwave Electronics (415 962-0755)

We have designed, assembled, and operated a complete solid-state terawatt femtosecond laser system producing 10 Hz pulsed, tunable radiation from 740 to 870 nm. The laser system is similar in design to that described by Kmetec et al. (1). A schematic diagram of the laser system is shown in Fig. 1.

The system was designed to amplify the output pulse from a mode-locked Ti:Al₂O₃ laser and based on regenerative/multi-pass amplifiers using the technique of chirped pulse amplification (2). The low energy seed pulses were obtained from a self mode-locked Ti:Al₂O₃ laser (Mira, Coherent) producing 1 nJ, 120 fs transform limited pulses at 76 MHz repetition rate. These pulses were stretched more than a factor of 1500 by a quadruple pass grating stretcher assembly to approximately 200 ps. The stretcher assembly, consisting of a single 1800 lines/mm holographic grating, a 750 mm focal length achromatic lens, and two 0° gold mirrors, had an effective length of 220 cm and overall throughput efficiency of greater than 50%.

The stretched pulse was then injected into a regenerative amplifier (RA) through a Faraday isolator. The regenerative amplifier was a TEM₀₀ design with cavity length of approximately 1.6 meters. The Brewster cut Ti:Al₂O₃ crystal (7 x 15 mm, 0.15% doping) was end pumped at 10 Hz by 6-7 ns pulses from a Q-switched Nd:YAG laser (NY82-10, Continuum) with a pump fluence of 1.5 J/cm² at 532 nm. The Pockels cell was coated with a sol-gel material to avoid bandwidth narrowing due to etalon effects and the polarizer coating was specially designed to provide bandwidth of 130 nm (1). A thyatron generator capable of producing 7 KV, 5 ns pulses was used to switch the Pockels cell. Both pulse injection and cavity dumping were carried out by the same half-wave electrical pulse by passing it through a delay line. Output energy of 10-12 mJ was observed with seed pulse energies of 0.5 nJ after 12 round trips. The double-pass small signal gain was estimated to be 4.2. Special protection circuitry built into the synchronizing electronics prevented the regenerative amplifier from damage if

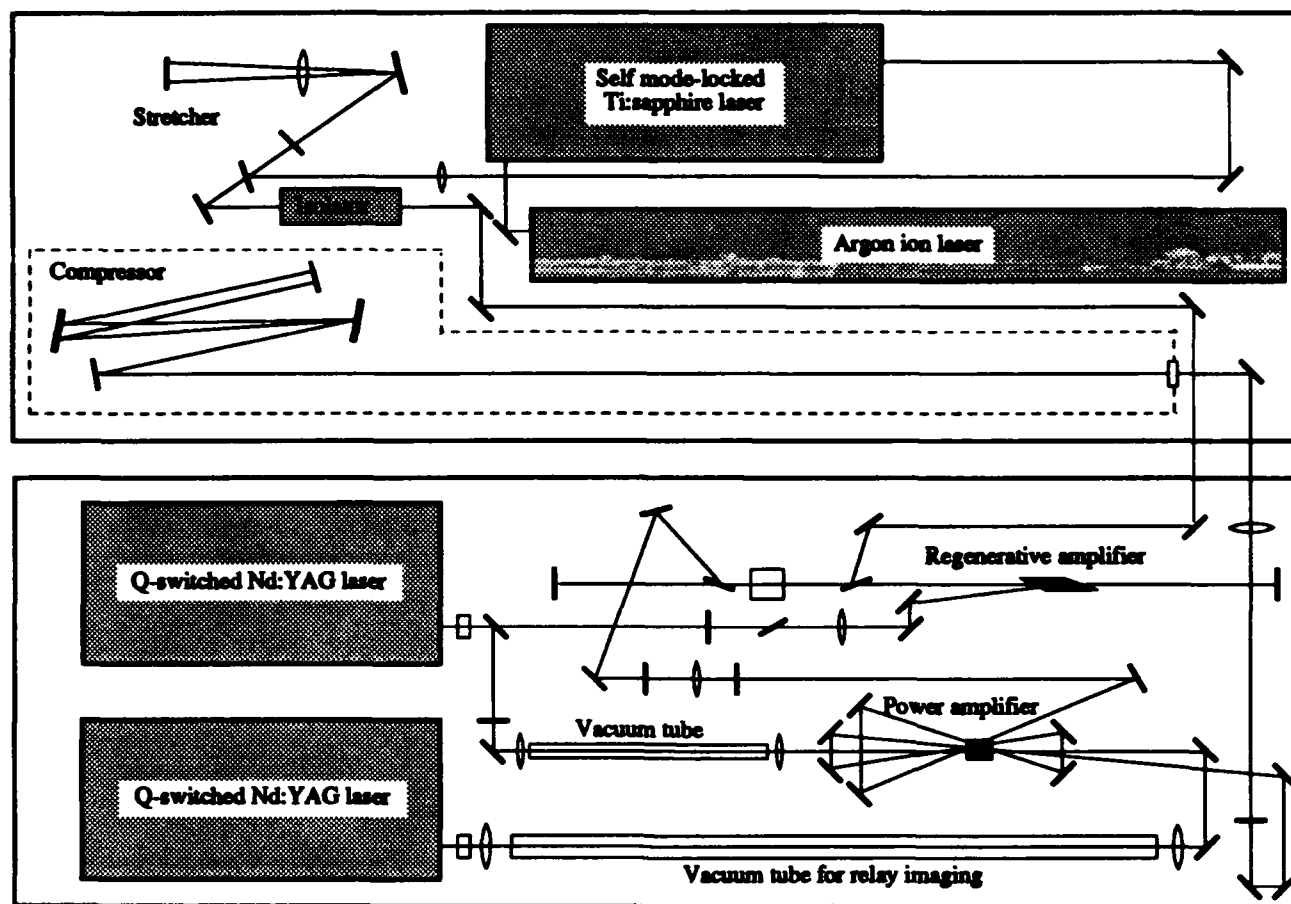


Figure 1. Optical layout of 150 fs, 1.5 TW, 10 Hz Ti:Al₂O₃ laser system

the self mode-locked laser reverted to CW mode. By positioning a dual photo-diode inside the stretcher, the expanded spectrum of the mode-locked beam was monitored through the zero-order of the grating. If the mode-locked laser ran in CW mode, its spectral bandwidth decreased substantially, and triggered shut-off of the complete laser system.

The output from regenerative amplifier was then expanded by a 4 x Galilean telescope to 8-9 mm in diameter before further amplification by a quadruple pass Ti:Al₂O₃ power amplifier. This was pumped by two synchronized high energy 10 Hz Q-switched Nd:YAG lasers. Each pump laser (NY82-10, Continuum) delivered >750 mJ, 7 ns pulses at 532 nm. Image relay

optics were used to provide spatial uniform pump beams at both faces of the amplifiers. The power amplifier Ti:Al₂O₃ crystal was 18 mm in diameter and 15 mm long (0.1% doping) with AR coatings on both faces. Output energies as high as 430 mJ have been generated with input 532 nm pump energies of 550 mJ and 650 mJ for the first and second arm respectively. The single pass gain is then calculated to be 3.

The amplified output from the power amplifier was enlarged in a 8 x Galilean telescope to 70-80 mm diameter and the polarization of the beam converted to vertical by a periscope. The expanded pulse was then double-passed through a grating compressor to remove the positive frequency chirp imposed by the

stretcher. The compressor grating was identical to the expander grating except the ruled area was 110 x 110 mm. The final compressed pulse had energy greater than 230 mJ and the pulsewidth measured with a scanning autocorrelator, gave minimum pulsewidth of 150 fs, assuming a sech² pulse. This corresponds to 1.5 TW peak power. To our best knowledge, this is the highest power reported of any Ti:Al₂O₃ CPA laser system operating at 10 Hz repetition rate. Contrast ratio of 10⁶:1 (between the main and pre-pulse) was achieved by placing a pulse slicer at the output of regenerative amplifier.

Further efforts will focus on the tunability of the system, as well as increasing the output peak power by utilizing a shorter mode-locked seed pulse which is now available. According to the measured free running bandwidth

for our regenerative amplifier, which is greater than 25 nm, the regenerative amplifier can easily support pulses as short as 25 fs at 750 nm. By utilizing the shorter input pulse and a higher energy frequency doubled Nd:YAG pump, we do not anticipate significant technical difficulties in demonstrating >5 TW from a laser system with slight modifications to our existing design. Preliminary results indicate the laser system can be tuned from 740 nm to 870 nm by using three sets of mirrors in the regenerative amplifier.

1. J.D. Kmetec, J.J. Macklin, and J.F. Young, *Opt. Lett.* 12, 1001 (1991).
2. D. Strickland and G. Mourou, *Opt. Commun.* 56, 219 (1985)

High power, gain guided Ti:Al₂O₃ laser: theory and experiment

F. Salin, F. Estable, E. Mottay and L. Brunel *

B.M. Industries
7 rue du Bois Chaland
CE 2901 LISSES
91029 EVRY Cedex - FRANCE

Gain guiding is an old concept, widely used in gas and semi-conductor lasers. The idea is to used the gain gradient obtained for example when a laser medium is pumped by another laser, to concentrate the energy on the resonator axis. This guiding effect can be used in conjunction with an unstable resonator to fill the gain region, and, then efficiently extract the energy, while keeping a good beam quality since no hard aperture is used. This type of resonator is very similar to unstable resonators using a VRM, with the difference that the gain medium is the gaussian aperture which size can be adjusted by changing the pump beam diameter.

We used a code based on the beam propagation method including spatially dependent gain saturation and gain depletion to theoretically study the build-up of the beam in the resonator. We considered a flat-flat resonator containing a Ti:Al₂O₃ rod pumped by a pulsed laser beam (diameter $2w_p=2\text{mm}$). We assumed 40% output coupling and 5% passive loss. For gaussian pump beams we obtained near gaussian output beams which size follows the pump beam size. But, conversely to what was predicted by the ABCD matrix model, we found that the output beam size increases with increasing pump power. This is a clear manifestation of gain saturation which decreases the "gain focusing" effect predicted in a first approximation. We found that the output beam area roughly corresponds to the part of the excited region which is above threshold and then increases with the pump power. We also computed the extraction efficiency defined as the fraction of the energy stored in the excited state which can be extracted. We found that above 4 times threshold (i.e. 1J/cm^2 of stored pump fluence or about 1.7J/cm^2 of pump fluence incident on the Ti:Al₂O₃ rod for our resonator) the extraction efficiency is better than 80%, reaching 90% at 8 times the threshold. This means that virtually all the energy absorbed in the crystal is transferred to the output pulse. Note that this result is independent of the pump beam size and clearly demonstrates the power of gain guiding.

We also tried more sophisticated pump beam profiles. In particular most of the high power Q-switched Nd:YAG lasers (even those using VRM) exhibits modulated beam profile due to diffraction on the YAG rod edges. Figure 1 shows the output beam profile obtained when the Ti:Al₂O₃ laser is pumped by a modulated pump beam. The combined effects of diffraction and gain aperturing actually smooth out most of the modulation leading to a diffraction limited gaussian beam while keeping the extraction efficiency above 80%.

We used gain guiding to obtain tunable high energy pulses in a diffraction limited gaussian beam from a Ti:Al₂O₃ laser. The experimental set-up consisted of a $1\times 1\times 1.5\text{ cm}^3$ Ti:Al₂O₃ crystal surrounded by two flat mirrors. The crystal was pumped from both sides by up to 500 mJ, 532 nm pulses from a B.M. Industries Q-switched Nd:YAG laser model 502 DNS. The gain profile was recorded by imaging the Ti:Al₂O₃ fluorescence on a CCD camera and was approximatively flat-top. With 40% output coupling a maximum of 150 mJ was obtained at 410 mJ of pump energy. The laser was tunable from 690 nm using two prisms in the cavity and a single set of mirrors. More than 100 mJ was

obtained from 720 to 850 nm. Some saturation of the output energy was observed at high pump fluence (fig.2). This saturation can be explained by taking into account the absorption saturation of Ti:sapphire. Using published values of Ti:Al₂O₃ absorption saturation fluence³ (8 J/cm²) plus the small signal absorption of our cristal (92 %) and taking into account the quantum defect (pump wavelength/laser wavelength) we replotted the output energy at 800 nm versus the energy actually stored in the crystal. The curve is given in Fig. 3 and exhibits an slope efficiency of 98 %. Such a high number shows that virtually all the energy stored is actually transferred in the laser beam which means that the mode matching between the pump and laser beam is almost perfect. This is a consequence of gain guiding, since the laser mode "self-adapts" its shape to that of the gain.

The output beam shape was recorded at about 1m from the output coupler using a CCD camera (see Fig.4). As expected the beam is near gaussian despite the non-gaussian nature of the pump. The far field was measured at the focus of a 1 m focal length lens and was gaussian and within about 1.2 x the diffraction limit.

In summary we show both theoretically and experimentally that gain guiding is a very powerful concept. It is presently the simplest way to get high power, high quality beams from laser pumped solid-state lasers. Since the output beam is much smoother than the pump beam, it should be of particular interest in high power diode pumped solid-state lasers.

* L. Brunel was with the Institut d'Optique Théorique et Appliquée, Unité de Recherche Associée au CNRS, Université Paris-Sud, Orsay, France.

1. F. Salin and J. Squier, Opt. Lett., to be published on Sept.15, 1992.
2. F. Estable, E. Mottay and F. Salin, "High energy gain guided Ti:Al₂O₃ oscillator", submitted to Opt. Lett.
3. L.G. DeShazer, J.M. Eggleston and K.W. Kangas, Opt. Lett. 5, 363 (1988).

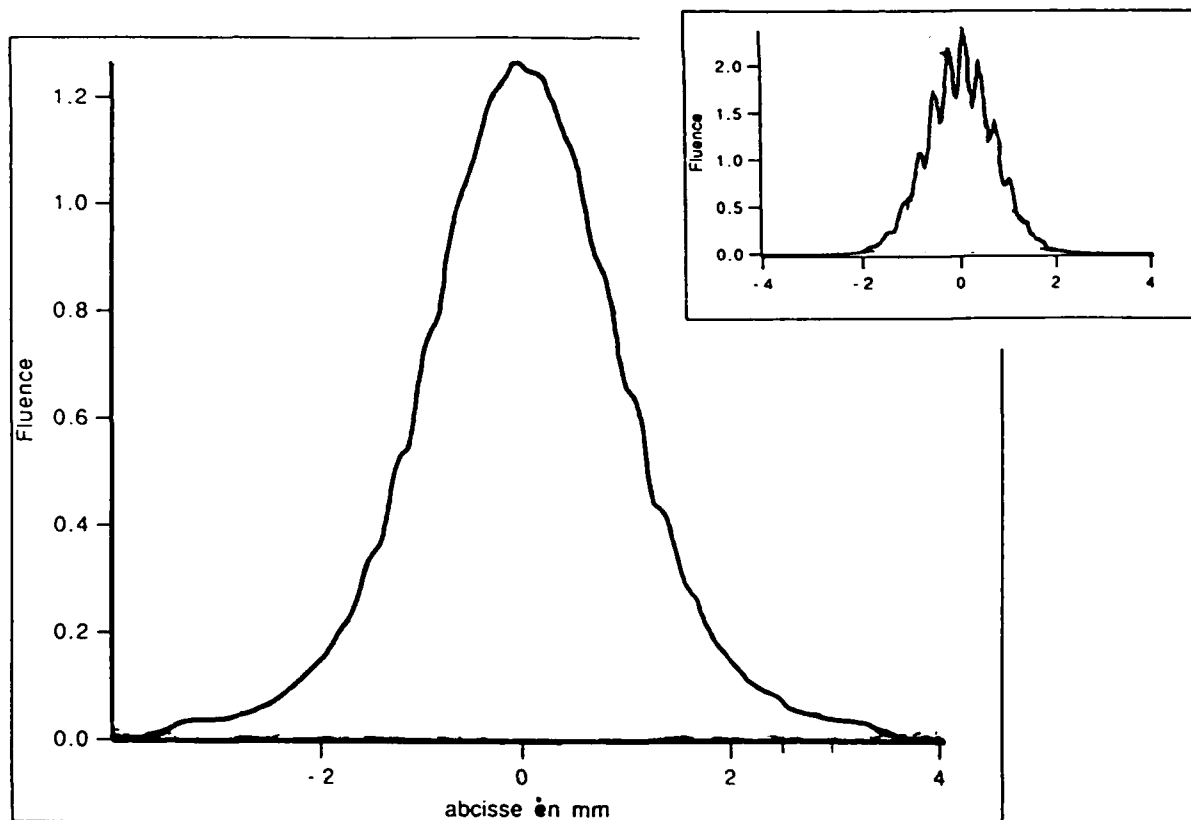


Fig.1: Theoretical output beam profile obtained with the modulated pump beam shown in the inset.

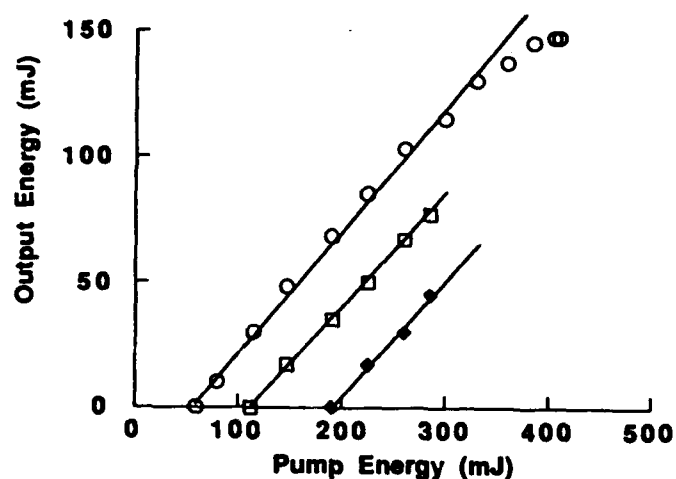


Fig. 2 : Output energy at 790 nm versus pump energy for different output coupler reflectivities : $R = 60\%$ (circles), $R = 30\%$ (squares), $R = 10\%$ (diamonds). In each case the slope efficiency is approximately 50 %.

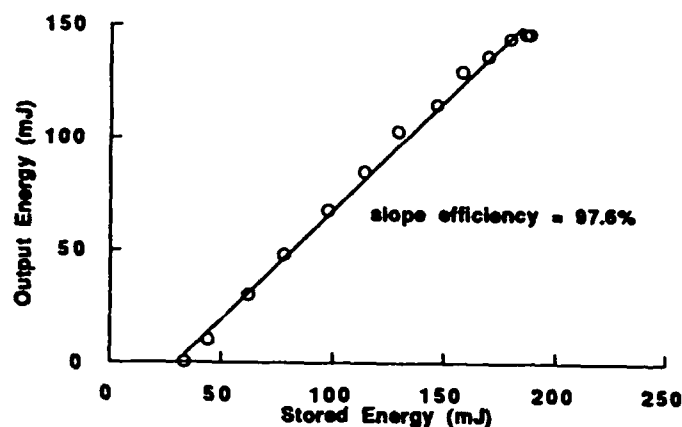


Fig. 3 : Output energy at 790 nm versus energy stored in the upper level of the laser transition. The saturation of the absorption of the $\text{Ti:Al}_2\text{O}_3$ crystal is taken into account.

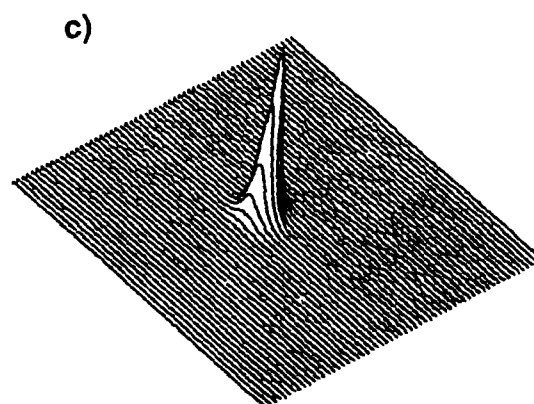
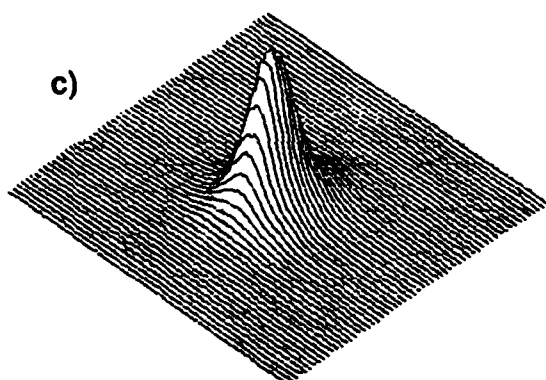
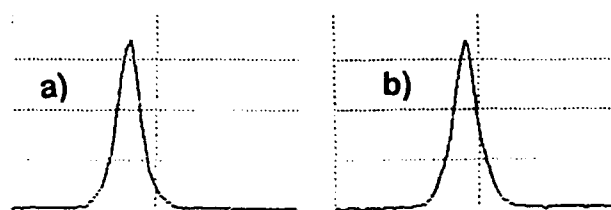
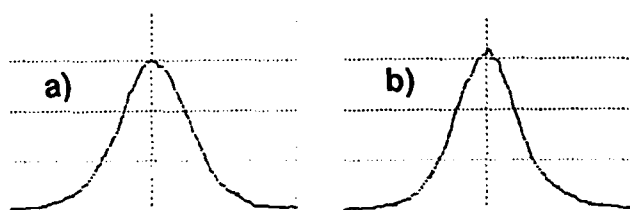


Fig. 4 : Near field (left) and far field (right) profiles of the output beam: (a) horizontal, (b) vertical, (c) 3D plot. This picture is taken at 80 mJ output energy.

Ti:chrysoberyl as a High-Saturation-Fluence Amplification Medium for Ti:sapphire Lasers

Nobuhiko SARUKURA and Yusaburo SEGAWA

Photodynamics Research Center,

The Institute of Physical and Chemical Research (RIKEN),
Minamiyoshinari 6-6-3, Aoba-ku, Sendai, Miyagi 989-32, Japan

Telephone: +81 22 277 3801 Facsimile: +81 22 277 3802

Kiyoshi YAMAGISHI

Corporate R&D Center,

Mitsui Mining and Smelting Company,

Haraichi, Ageo-shi, Saitama 362, Japan

Telephone: +81 48 775 3211 Facsimile: +81 48 775 3210

Rapid progress of Ti:sapphire lasers has enabled a compact tunable high-pulse-energy and high-peak-power laser system.¹ The achievable pulse energy in such systems is determined by the characteristics of the amplification medium: saturation fluence, non-linear reflective index, tuning range matching with the Ti:sapphire, possible pumping methods, and available crystal size and quality. Ti:chrysoberyl is known as a tunable laser material.² Recent efforts have made it possible to fabricate large size (1.5-cm diameter and 7-cm length) and high FOM (~ 100) crystal, and it can be used even for cw-laser operation.³ However, its use as an amplification medium was not studied before. In this presentation, we will describe the high-gain saturation nature of Ti:chrysoberyl, and its application to high gain confocal multi-pass amplifiers.

In order to evaluate its basic properties, the gain for various wavelength and saturation fluence were measured, using 10-nsec, 532-nm pulses from a YAG laser as a pumping source. The gain as wide as that of Ti:sapphire was confirmed at least over 700 nm to 1064 nm, and the gain peak wavelength was 780 nm (Fig. 1). Using a 20-nsec Ti:sapphire laser pulse as a probe, the saturation fluence was evaluated to be 1.6 J/cm^2 at 776 nm, under the assumption of a Frantz-Nodvik relation (Fig. 2), and was higher than that of Ti:sapphire (1.2 J/cm^2).⁴ The corresponding emission cross section was $1.6 \times 10^{-19} \text{ cm}^2$. This results shows that Ti:chrysoberyl promises to be a high-energy amplification medium for Ti:sapphire lasers. Furthermore, ability to use a common pumping source with Ti:sapphire and its well-fitted gain curve are the advantage compared with Cr:LiSAF and LiCAF.

For practical application as a tunable amplifier, we adopted a multi-pass scheme with a confocal lens pair and turning prisms,⁵ which was well-studied as a pre-amplifier in a terawatt-class Ti:sapphire laser system.⁶ The advantages of this confocal multi-pass scheme, compared with a regenerative amplification scheme, are the ease of tuning and operation due to its construction from entirely passive optical components, and no

strict timing requirement for the gain extraction. In this scheme, the following are necessary for high small-signal-gain operation; maximization of the single-pass gain, improvement of pass overlapping, and suppression of self-oscillation. Single-pass gain ($\sim 9\text{dB}$) at a damage-safe pumping level ($\sim 10\text{ J/cm}^2$) on one side of the crystal in Ti:chrysoberyl was smaller than that of Ti:sapphire ($\sim 15\text{dB}$) due to its smaller gain cross section. The single-pass gain was enhanced to $\sim 19\text{dB}$, when 3.3-cm Ti:chrysoberyl crystal ($a_{532}=0.9\text{ cm}^{-1}$) was pumped on both sides by 10-Hz, $\sim 35\text{-mJ}$, 532-nm pulses. Unlike the case of Ti:sapphire,⁵ 6-pass amplification was possible without suffering from self-oscillation due to its smaller gain cross section. The amplifier consisted of a gain medium located at the beam waist of a confocal lens pair, two dichroic mirrors to overlap the input beams with independently focused pumping beams, and three turning prisms for small displacement of each amplification pass (Fig. 3). The confocal lens pair and the prisms allowed the passes to overlap well in a small cylindrical pumped region, and resulted in 52dB gain for the transmitted pulses (Fig. 4). 1.5-psec, 0.24-nJ single-pulse-selected pulses at 796 nm were amplified to $\sim 40\text{ }\mu\text{J}$. It should also be noted the estimated beam breakup parameter (0.6 rad) is small enough for the reported non-linear refractive index value ($2\times 10^{-16}\text{ cm}^2/\text{W}$).⁷ Therefore, there is no need to use chirped pulse amplification for this energy level.

In conclusion, Ti:chrysoberyl has a great potential as an amplification material for Ti:sapphire lasers due to its higher saturation fluence, ability to use a common pumping source, and its well-fitted gain curve. Nevertheless, high gain amplification (52dB) is also possible in a confocal multi-pass configuration. Further research on Ti:chrysoberyl will lead to the development of a compact tunable high energy amplifier.

References

1. P. F. Moulton, J. Opt. Soc. Am. B3, 125 (1986).
2. A. I. Alimpiev, G. V. Bukin, V. N. Matrosov, E. V. Pestryakov, V. P. Solntsev, V. I. Trunov, E. G. Tsvetkov, and V. P. Chebotaev, Sov. J. Quantum Electron. 16, 579 (1986).
3. K. Yamagishi and A. Sugimoto, submitted to J. Appl. Phys.
4. F. Estable, F. Salin, M. Allain, P. George, and A. Brun, Opt. Comm. 72, 235, (1989).
5. N. Sarukura and Y. Ishida, to be published in J. Quant. Electron., Oct., 1992
6. N. Sarukura, K. Yaginuma, K. Kondo, and S. Watanabe, submitted to Opt. Comm.
7. M. J. Weber, D. Milam, and W. L. Smith, Opt. Eng. 17, 463 (1978).

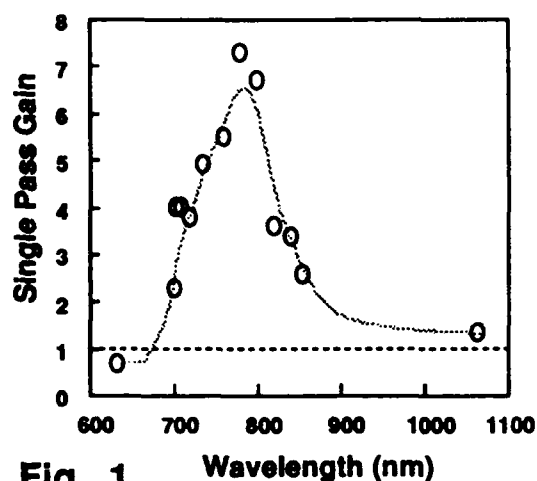


Fig. 1 Wavelength (nm)

The gain curve of Ti:chrysoberyl. The probe light for the measurement of the small-signal gain was provided from mode-locked Ti:sapphire and YAG laser, and a He-Ne laser.

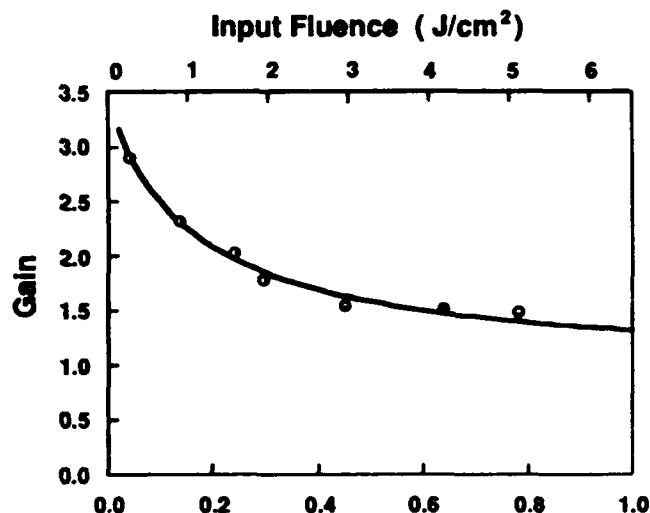


Fig. 2 Input Energy (mJ)

Gain saturation characteristic of Ti:chrysoberyl ($E_s=1.6 \text{ J/cm}^2$, $G_0=3.4$). The beam radius sizes at the crystal surface were $70 \mu\text{m}$ and $500 \mu\text{m}$ for the signal and pumping beams.

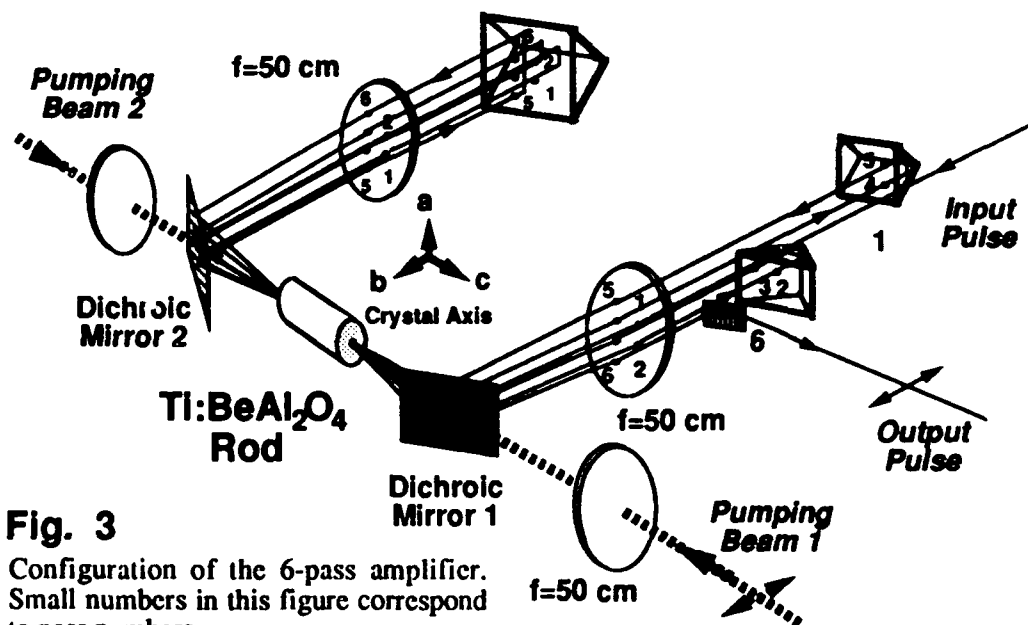


Fig. 3

Configuration of the 6-pass amplifier. Small numbers in this figure correspond to pass numbers.

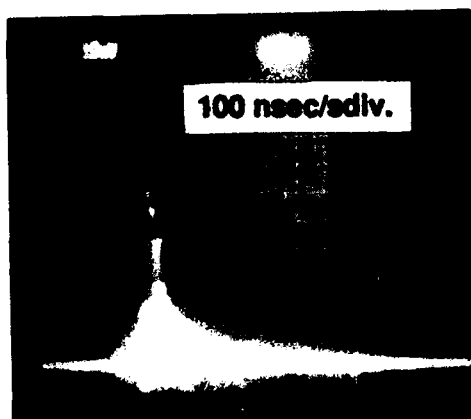


Fig. 4

The pulse train after 6-pass amplification. A gain factor of 52dB was determined with the use of calibrated neutral density filter. Single-pulse selection was not applied to observe temporal gain profile in this case, 80-nsec width of gain shows that there is no strict timing requirement for gain extraction.

Femtosecond Pulses Generated from a Synchronously Pumped Chromium-Doped Forsterite Laser

A. Seas, V. Petričević, and R. R. Alfano

Institute for Ultrafast Spectroscopy and Lasers, and
Center for Analysis of Structures and Interfaces
Departments of Physics and Electrical Engineering
The City College and Graduate School of the City University of New York
138 St. & Convent Avenue, New York, N.Y. 10031, Tel. (212) 650-5531

Summary

Kerr lens mode-locking (KLM) has become a standard method to produce femtosecond pulses from tunable solid state lasers.¹ High power inside the laser resonator propagating through the laser medium with nonlinear index of refraction, coupled with the stability conditions of the laser modes in the resonator result in a passive amplitude modulation which explains the mechanism for pulse shortening. Pulses of 17 fs FWHM were generated using KLM from Ti:Sapphire laser.² Pulses of 50 fs³ and pulses of 150 fs⁴ were also generated from Cr³⁺:LiSrSiF₆ using KLM in combination with a saturable absorber in the cavity and active mode locking, respectively. Recently, chromium doped forsterite was shown to exhibit similar pulse behavior.⁵ Transform limited 60 fs pulses were generated from an actively mode locked forsterite laser using intracavity chirp compensation. The pulses were generated even when the active modulator was turned off, suggesting that KLM technique was operative in the generation of femtosecond pulses from Cr: forsterite laser.

In this presentation, we report on the first successful attempt to generate femtosecond pulses from a synchronously pumped chromium-doped forsterite laser with intracavity dispersion compensation. Stable, transform limited pulses with duration of 105 fs were routinely generated, tunable between 1240 to 1270 nm.

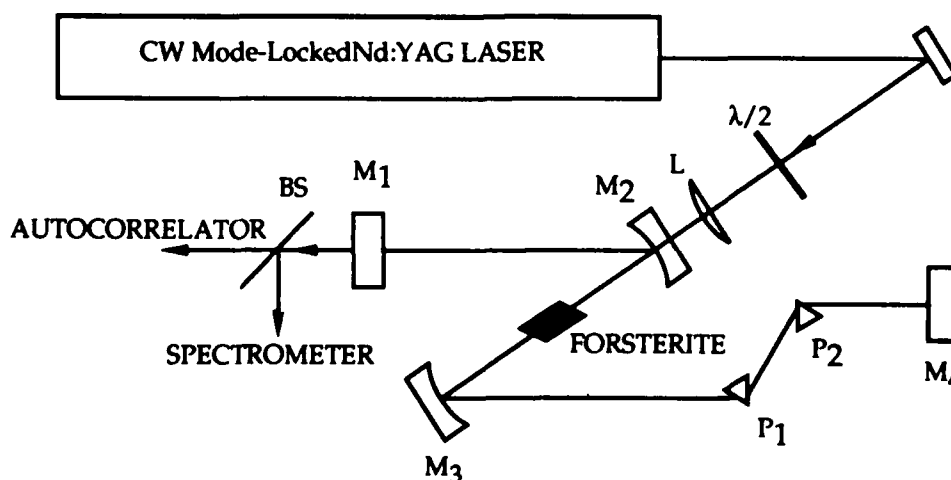


Fig. 1. Schematic diagram of the synchronously pumped mode-locked operation of the Cr:forsterite laser: $\lambda/2$, half-wave plate for 1064 nm; L, focusing lens; M₁, output mirror, M₂, M₃, 10-cm-radius folding mirrors; M₄, back mirror; BS, beam splitter; P₁ and P₂, Schott SF14 glass prisms.

The experimental arrangement is shown in Fig. 1. The Brewster-angle-cut forsterite crystal was placed in a four-mirror, Z-fold astigmatically compensated cavity. The combination of mirrors used was: a flat back mirror, two 10-cm-radius folding mirrors, and a flat output coupler. The transmission of the output coupler was 1% at the lasing wavelength, while the folding mirrors and the back mirror had reflectivity $R=99.9\%$ for the 1200-1300 nm range. The length of the sample was 1.2 cm with absorption coefficient at the pump wavelength of 1064 nm of $\alpha=1.1\text{ cm}^{-1}$. The laser crystal was mounted in a copper block and was cooled by a single-stage thermoelectric cooler. The Cr:forsterite crystal was pumped by an actively mode-locked Nd:YAG laser (82 MHz). The pump beam was focused by a 7.5-cm lens through the 10-cm-radius folding mirror into the crystal. The 1064-nm pump power incident on the forsterite crystal was 5.3 W, of which 3.9 W was absorbed by the crystal. The output of the forsterite laser was monitored with a fast germanium detector and an oscilloscope. The pulsewidth was measured with a noncollinear background free real-time intensity autocorrelator. A collinear interferometric autocorrelator was also used to determine the chirp characteristics of the output pulses. The bandwidth of the mode-locked forsterite laser was measured using a PbS detector coupled to a 50-cm Jarrel Ash monochromator, equipped with variable aperture slits.

Mode locking was observed when the length of the cavity was matched to the length of the mode locked Nd:YAG laser. Once mode-locking was achieved two regimes were observed. In the first we observe long duration pulses (200-300 ps FWHM). By further alignment of the cavity and slightly changing the position of the laser crystal and the distance between mirrors M2 and M3 the pulsewidth was reduced down to 105 fs with a spectral width of the order of 20 nm. The output power of the forsterite laser when femtosecond pulses were generated was 45 mW. An intensity autocorrelation trace and the corresponding spectrum of a typical pulse are shown in Fig. 2 (a) and (b). The pulsewidth shown is 105 fs and the bandwidth is 16 nm. The pulsewidth-bandwidth product $\Delta\tau_p\Delta\nu = 0.32$, indicating transform-limited pulses for a sech^2 pulse. Fig. 3 shows a picture of the interferometric autocorrelation trace of the output pulses. Since there is good visibility of the fringes at the wings of the pulse it is evident from this picture that the pair of prisms compensated for the nonlinear chirp introduced by the forsterite crystal.⁶

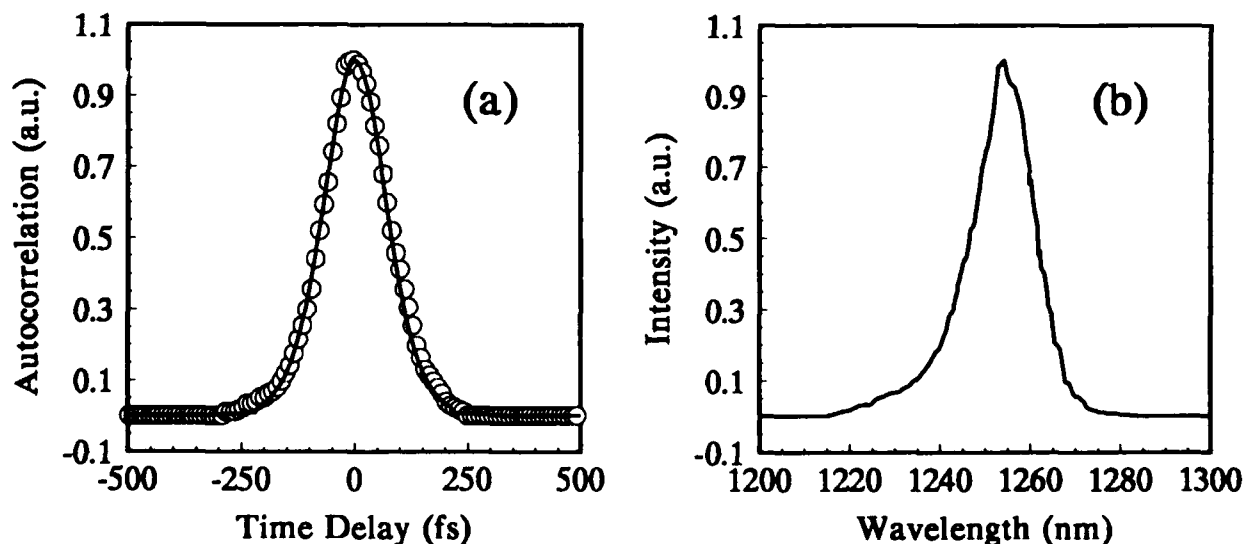


Fig. 2. An autocorrelation trace (a) and spectrum (b) of 105-fs pulses obtained from a Z cavity with glass prisms for chirp compensation. Circles represent experimental data and the solid line is the best fit. sech^2 pulse shape was assumed for fitting. The pulsewidth-bandwidth product $\Delta\tau_p\Delta\nu = 0.32$.

The pair of prisms used in the cavity was made of SF14 Schott optical glass. The optical characteristics of this type of glass for 1250 nm are $n = 1.729$, $dn/d\lambda = -0.02017$, $d^2n/d\lambda^2 = 0.02262$, and $d^3n/d\lambda^3 = -0.0999$.⁷ The optimum distance between the two prisms when stable 105-fs pulses were obtained, was determined to be 35 cm. Carrying out the calculation for the phase derivatives with respect to frequency we get $\partial^2\phi/\partial\omega^2 = -3273 \text{ fsec}^2$ and $\partial^3\phi/\partial\omega^3 = -2170 \text{ fsec}^3$.^{8,9} This indicates that SF14 is not the most appropriate glass for pulse shortening in this wavelength region since it introduces a large cubic phase term. This suggests that by using material which will introduce less cubic phase, shorter pulses will be generated as is the case with Ti:Sapphire. Different types of glass prisms will be discussed which minimize the effect of the cubic phase term.

The passively mode-locked forsterite laser was tuned using an aperture between prism P_2 and mirror M_4 . We were able to continuously tune the laser between 1240 and 1270 nm. The duration of pulses did not vary much throughout the whole tuning range.

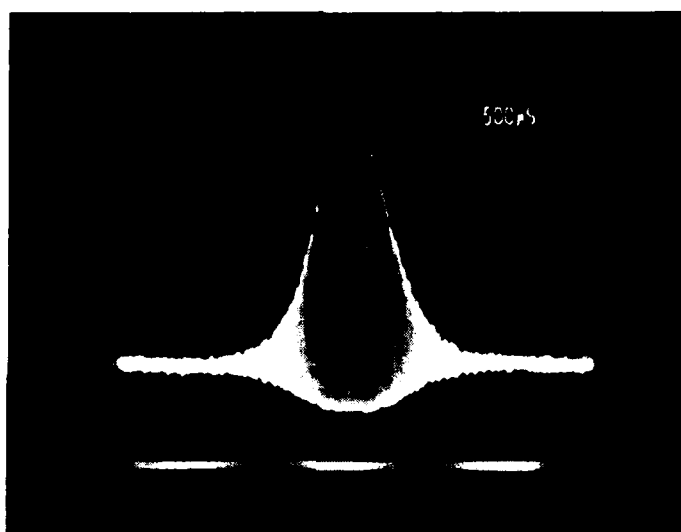


Fig. 4. Interferometric autocorrelation of the output pulses of the forsterite laser

In conclusion, transform-limited femtosecond pulses were generated from a synchronously pumped chromium-doped forsterite laser. Stable 105 femtosecond pulses in TEM₀₀ mode were obtained. The tuning range was of the order of 30 nm, limited only by the coating of the mirrors used and the available pump power.

This research is supported in part by NSF, NASA and ARO.

References

1. T. Brabec, Ch. Spielmann, P. F. Curley, and F. Krausz, *Opt. Lett.* **18**, 1292 (1992), and references therein.
2. Chung-Po, Melanie T. Asaki, Sterling Backus, Margaret M. Murnane, Henry C. Kapteyn, and Howard Nathel, *Opt. Lett.* **18**, 1289 (1992).
3. N. H. Rizvi, P. M. W. French, and J. R. Taylor, *Opt. Lett.* **17**, 877 (1992).
4. A. Miller, P. LiKamWa, B. H. T. Chai, and E. W. Van Stryland, *Opt. Lett.* **17**, 195 (1992).
5. A. Seas, V. Petričević, and R. R. Alfano, *Opt. Lett.* **17**, 937 (1992).
6. Jean-Claude M. Diels, Joel J. Fontaine, Ian C. McMichael, and Francesco Simoni, *Applied Optics* **24**, 1270 (1985).
7. "Optical Glass" Schott Catalog.
8. R. L. Fork, C. H. Brito Cruz, P. C. Becker, and C. V. Shank, *Opt. Lett.* **12**, 483 (1987).
9. R. L. Fork, O. E. Martinez, and J. P. Gordon, *Opt. Lett.* **9**, 150 (1984).

A c.w. mode-locked Cr⁴⁺:YAG laser

P. M. W. French, N. H. Rizvi and J. R. Taylor

Femtosecond Optics Group, Physics Department,
Imperial College, London SW7 2BZ, U.K.
Tel. : 071-589 5111 ext. 6811 Fax. : 071-589 9463 Telex: 929484 IMPCOL G

A. V. Shestakov

R&D Center IRE-POLUS,
1 Vvendenskogo Square, Fryazino, Moscow 141120, Russia

Femtosecond laser physics has been transformed by the advent of the Titanium-doped sapphire laser which has been mode-locked by conventional and novel means [e.g. 1-5], yielding pulses as short as 15 fs [5] from laser oscillators which are stable and can produce several watts of average output power. These mode-locking techniques have been successfully applied to other new laser media including Cr³⁺:LiSAF [6,7] which has the potential to be diode-pumped - thus producing a relatively convenient and compact femtosecond laser system. Consequently the dye laser will be largely superseded in ultrafast laser applications. Recently this trend has been extended to the near infrared spectral region with the generation of femtosecond pulses from Cr⁴⁺:Forsterite lasers using the techniques of Additive Pulse Mode-Locking [8] and Kerr Lens Mode-Locking [9] previously demonstrated with Ti:sapphire lasers. We anticipate that the demonstration of laser action with further vibronic media will extend the spectral coverage of ultrafast solid-state lasers and note that the Cr⁴⁺ ion will be of particular interest in the region from 1 - 2 μm . In time, cryogenic colour-centre lasers may be replaced by convenient room-temperature (diode-pumped) solid-state lasers. Cr⁴⁺:YAG is a laser medium providing gain from 1.34 - 1.56 μm which has been demonstrated as a cw laser at room-temperature, pumped by a Nd:YAG laser in spite of significant excited state absorption [10]. It has an upper state lifetime of $\sim 4 \mu\text{s}$ and a net peak gain cross-section of $\sim 4 \times 10^{-19} \text{ cm}^2$. These parameters are similar to Ti:sapphire and so one may expect that this medium will deliver a similar laser performance. We report here the first mode-locked Cr⁴⁺:YAG laser. This spectral region is clearly of particular interest for optical communications and switching and the potential for a compact diode-pumped laser system delivering tunable femtosecond pulses with watts of average power makes this laser medium very exciting.

The laser crystal used in our experiments was grown at the IRE-POLUS Institute with the optic axis corresponding to the [0,0,1] crystallographic axis and was 20 mm in length and 6 mm in diameter. The absorption coefficient was $\sim 2.5 \text{ cm}^{-1}$ at 1.06 μm corresponding to a Cr⁴⁺ concentration of $\sim 5 \times 10^{17} \text{ cm}^{-3}$ and the laser polarisation was in the [0,1,0] plane. An astigmatically-compensated cavity configuration, similar to that commonly used with Ti:sapphire lasers, was adopted and the laser was pumped by the 1.064 μm output of a cw Nd:YAG laser. Active mode-locking was achieved using a lead molybdate acousto-optic modulator.

The lasing threshold for the complete cavity was 4 W absorbed pump power and the mode-locked laser was typically pumped with 7 W. With no output coupling, modulator or tuning element, the laser threshold was as low as 1.6 W absorbed pump power. A study was made of the performance of the cw laser. A slope efficiency of ~5% was observed for cw pumping. This was thought to be limited by thermal lensing in the laser crystal and by the large amount of scatter in the laser medium. The temperature dependence of the upper-state-lifetime could also have been a contributing factor. When the pump beam was chopped by a ratio of 50:1, the slope efficiency increased to ~12%, suggesting that thermal effects were a problem. We are confident that significantly improved laser efficiency and threshold can be obtained with improved laser crystal quality and more efficient cooling. The laser was tuned using a quartz birefringent tuning wedge and the output power with wavelength is shown in figure 1. The demonstrated tuning range was limited by the dielectric coatings on the cavity mirrors.

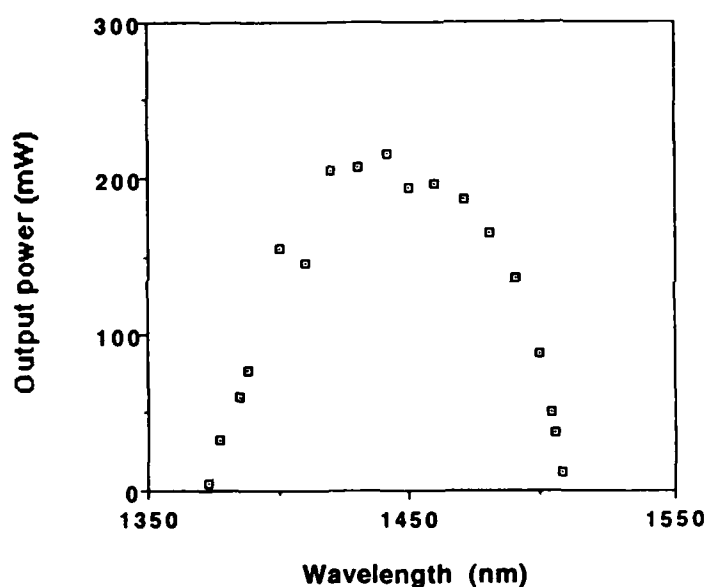


Fig. 1 Variation of output power with wavelength for cw $\text{Cr}^{4+}:\text{YAG}$ laser

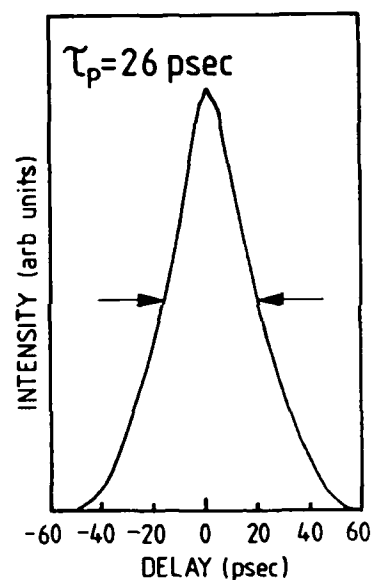


Fig. 2 Autocorrelation trace of the shortest pulses obtained from the actively mode-locked $\text{Cr}^{4+}:\text{YAG}$ laser

In order to demonstrate ultrashort pulse generation, an acousto-optic modulator was incorporated in the cavity. This was a high Q device with a 2 mm aperture which was operated with modulation depths greater than 50%. The RF was applied at ~250 MHz and the laser cavity round-trip time was ~8 ns. When the cavity length was set to the matching point, picosecond pulses at a repetition rate of 125 MHz were observed from 1396 - 1482 nm. This tuning range is reduced compared to the cw laser because of the high insertion loss of the acousto-optic modulator. To generate stable mode-locked pulse trains, the cavity length had to be maintained within ~1 μm of the matching point. Pulses of less than 70 ps duration were observed between 1396 nm and 1478 nm, this duration decreasing to ~30 ps near the peak of

the gain around 1440 nm. Figure 2 shows an autocorrelation trace of the shortest pulses of 26 ps duration (assuming a Gaussian pulse profile) obtained. The pulse spectrum did not exhibit any significant excess spectral broadening - the measured bandwidth being ~ 0.15 nm - close to the resolution limit of our monochromator. Typical average output powers ranged up to 20 mW for 8 W pump power. This low figure is a consequence of the high insertion loss of the modulator. With a larger aperture modulator and an improved laser crystal, average output powers of 100's of mW should be achievable.

When the RF to the modulator was switched off, no mode-locking was observed. This laser is clearly a candidate for KLM and for APM and should yield femtosecond pulses. Until the crystal quality and therefore the intracavity power is improved, APM is likely to prove the more successful approach. Some form of adjustable group velocity dispersion would be desirable to optimise a femtosecond Cr^{4+} :YAG laser. If a standard prism sequence is to be employed, prisms of a transparent material of positive material dispersion around $1.4 \mu\text{m}$ would be required. Work is currently underway to develop a femtosecond Cr^{4+} :YAG laser. We speculate that the presence of excited state absorption, leading to an intensity-dependent loss corresponding to an inverse saturable absorber, may have an impact on passive mode-locking of Cr^{4+} :YAG lasers using the optical Kerr effect.

In conclusion, we have demonstrated an actively mode-locked picosecond cw Cr^{4+} :YAG laser tunable from $1.39 - 1.45 \mu\text{m}$. With further improvement in cavity design and laser crystal quality, we anticipate that this laser medium will yield femtosecond pulses tunable from 1.35 to $1.55 \mu\text{m}$.

References

- 1) N. Sarukura, Y. Ishida, H. Nakano, Opt. Lett. **16**, 153 (1991)
- 2) D. E. Spence, P. N. Kean, W. Sibbett, Opt. Lett. **16**, 42 (1991)
- 3) D. K. Negus, L. Spinelli, N. Goldblatt, G. Feugnet, OSA Meeting on Advanced Solid State Lasers, 1991
- 4) C-P. Huang, H. C. Kapteyn, J. W. McIntosh and M. M. Murnane, Opt. Lett. **17**, 139 (1992)
- 5) Ch. Spielmann, P. F. Curley, T. Brabec, E. Wintner and F. Krausz, Electron. Lett. **28**, 1532 (1992)
- 6) A. Miller, P. LiKamWa, B. H. T. Chai and E. W. Van Stryland, Opt. Lett. **17**, 195 (1992)
- 7) N. H. Rizvi, P. M. W. French and J. R. Taylor, Opt. Lett. **17**, 877 (1992)
- 8) A. Seas, V. Petricevic and R. R. Alfano, Opt. Lett. **17**, 937 (1992)
- 9) A. Sennaroglu, T. J. Carrig and C. R. Pollock, CLEO Paper CTu12 (1992)
- 10) A. V. Shestakov, N. I. Borodin, V. A. Zhitnyuk, A. G. Ohrimtchuk and V. P. Gapontsev, CLEO Paper CPDP11 (1991)

Spectroscopy and Laser Operation of Mn^{5+} -Doped Vanadates

Larry D. Merkle
 Night Vision and Electro-Optics Directorate
 Lasers and Photonics Division
 Fort Belvoir, VA 22060
 (703) 704-1701

Horacio R. Verdun and Bruce McIntosh
 Fibertek, Inc.
 510 Herndon Parkway
 Herndon, VA 22070
 (703) 471-7671

Introduction

There has been considerable interest in materials doped with Cr^{4+} to obtain tunable laser operation around 1200 nm, but this ion's room temperature fluorescence lifetime is typically only a few microseconds, too short for practical pulsed operation under diode pumping.^{1,2} Recently Capobianco, et al, pointed out that the relative positions of the ^1E and $^3\text{T}_2$ states in the isoelectronic ion Mn^{5+} favor much longer lifetimes, and reported single-pass gain in two Mn-doped phosphates whose spectroscopy had been analyzed by Borromei, et al.^{3,4} We are studying several Mn^{5+} -doped crystals, including $\text{Ca}_5(\text{PO}_4)_3\text{F}$, $\text{Sr}_5(\text{PO}_4)_3\text{F}$ and Y_2SiO_5 .

We report here recent results on two Mn-doped orthovanadates: $\text{Mn}:\text{Ba}_3(\text{VO}_4)_2$ (Mn:BOV) and $\text{Mn}:\text{Sr}_3(\text{VO}_4)_2$ (Mn:SOV.) We have succeeded in growing these crystals by two methods: laser heated pedestal growth in a 20% oxygen atmosphere and the Czochralski method in 1% oxygen. The nominal doping levels employed were 0.2 at.% for most boules. The crystals grown so far exhibit an inhomogeneous distribution of Mn ions.

Spectroscopy

The room temperature absorption of Mn:BOV is shown in Figure 1. That of Mn:SOV is very similar. The spectra are consistent with absorption by an ion with d^2 configuration in a very weakly distorted tetrahedral crystal field. The band around 650 nm is due to transitions to states derived from T_d 's $^3\text{T}_1$, and the weak shoulder around 900 nm to the $^3\text{T}_2$, which would be forbidden in perfect T_d symmetry. The sharp line at 1181 nm Mn:BOV (1168 nm in Mn:SOV) is attributable to the ^1E state, and the feature at 772 nm to the $^1\text{A}_1$ state. The polarization dependence is only partly consistent with the weak C_{3v} distortion reported for the vanadium site in this host,⁵ but can be adequately explained by either spin-orbit or vibronic coupling in T_d symmetry.

The fluorescence spectra of both materials, presented in Figure 2, are nearly unpolarized. The dominant peak corresponds well to the ^1E absorption. Comparison of its side peaks in Fig's. 1 and 2 with vibrational analysis of the hosts indicates that they are

of vibronic origin.⁵ For 970 nm excitation the 1E peak exhibits structure, so that at least two sites must be present.

The fluorescence decay of Mn:BOV is dominated by a single exponential, although at low temperatures a weak faster decay component is discernable. The dominant component's decay rate increases roughly linearly with temperature from 790 s^{-1} at 10 K to 2150 s^{-1} at 300 K. The temperature dependence of integrated fluorescence intensity, normalized by the absorbed pump energy, is shown in Figure 3. Simultaneous fitting of the lifetime and intensity data requires the assumption that thermally activated radiative and nonradiative decay processes are both present.

Lacking data on the actual Mn concentration or quantum efficiency in our samples, the spectroscopic stimulated emission cross section cannot be accurately determined. However, saturation of the ground state absorption at 590 nm has been used to estimate the absorption cross section. From this the 1E peak stimulated emission cross section is estimated to be roughly $1 \times 10^{-19} \text{ cm}^2$.

Laser Experiments

Laser-pumped laser experiments have been carried out on both 0.2% Mn:BOV and 0.2% Mn:SOV. The laser cavity consisted of a flat high reflector and an output coupler with 5 cm radius of curvature and 99.0-99.5% reflectivity. The uncoated samples were pumped through the high reflector at 800 nm by a beam of about 0.05 cm radius at e^{-2} intensity, five times the nominal cavity mode radius. The latter was kept so small to facilitate the search for sample regions of satisfactory optical quality. Laser oscillation was observed at room temperature in both materials, with output wavelengths which corresponded to the 1E emission. As seen in Figure 4, the threshold energies incident on the samples were 1.9 mJ for Mn:BOV and 2.6 mJ for Mn:SOV. Their slope efficiencies were 0.0005 and 0.0008, respectively.

Conclusions

Laser operation on the long-lived Mn^{5+} 1E emission has been demonstrated. The observed laser slope efficiencies are quite low, even after correction for the mismatch of mode sizes. This issue requires further study. The absorption spectra and lifetimes of Mn in BOV and SOV are quite attractive for diode or flashlamp pumping. We hope, however, to identify hosts in which the emission has a greater degree of 3T_2 vibronic character, if the cost in reduced lifetime is no worse than a factor of two or three. Such hosts would permit four-level, tunable operation.

References

1. H. R. Verdun, L. M. Thomas, D. M. Andrauskas, T. McCollum and A. Pinto, "Chromium-doped Forsterite Laser Pumped with 1.06 μm Radiation," Appl. Phys. Lett. 53, 2593-2595 (1988).

2. L. D. Merkle, T. H. Allik and B. H. T. Chai, "Crystal Growth and Spectroscopic Properties of Cr^{4+} in $\text{Ca}_2\text{Al}_2\text{SiO}_7$ and $\text{Ca}_2\text{Ga}_2\text{SiO}_7$," *Opt. Mater.* **1**, 91-100 (1992).
3. J. A. Capobianco, C. Cormier, R. Moncorge, H. Manaa and M. Bettinelli, "Gain Measurements of $\text{Mn}^{5+}(3d^2)$ doped $\text{Sr}_5(\text{PO}_4)_3\text{Cl}$ and $\text{Ca}_2\text{PO}_4\text{Cl}$," *Appl. Phys. Lett.* **60**, 163-165 (1992).
4. R. Borromei, L. Oleari and P. Day, "Electronic Spectrum of the Manganate(V) Ion in Different Host Lattices," *J. Chem. Soc., Faraday Trans. 2* **77**, 1563-1578 (1981).
5. L. V. Kristallov, A. A. Fotiev and V. P. Zhukov, "Analysis of the Vibrational Spectra of Strontium and Barium Orthovanadates," *Russ. J. Inorg. Chem.* **26**, 1756-1760 (1981).

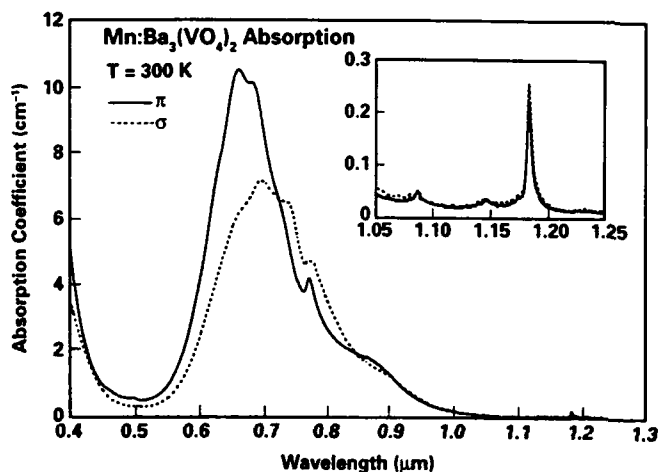


Figure 1. Room temperature absorption of Mn:BOV.

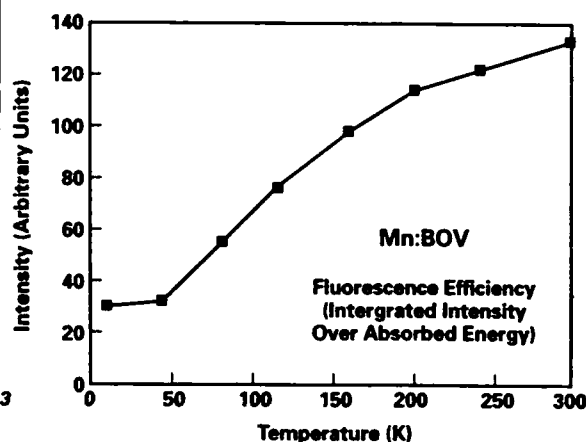


Figure 3. Temperature dependence of Mn:BOV fluorescence efficiency. Excitation is at 970 nm.

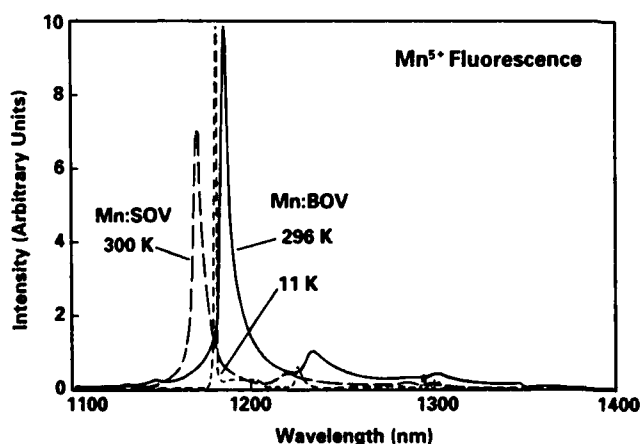


Figure 2. π -polarized fluorescence of Mn:BOV and Mn:SOV.

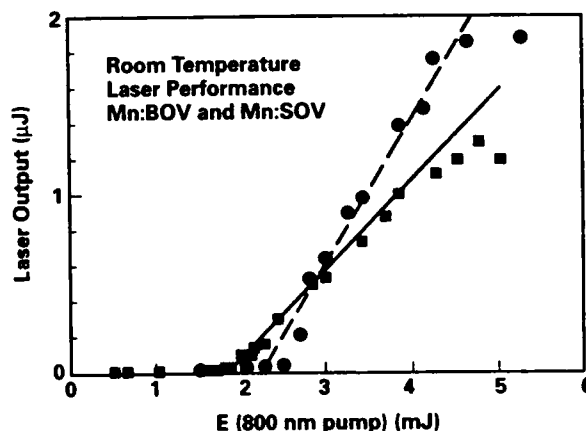


Figure 4. Laser output for pulsed Ti:sapphire pumping. Squares: Mn:BOV; circles: Mn:SOV.

Tuesday, February 2, 1998

Transition-Metal-Ion Lasers 2 Poster Session

ATuE 3:00pm–4:00pm
La Salle Ballroom A

Cr:Mg₂GeO₄ and Cr:CaMgSiO₄: New Potential Tunable Solid-State Laser Crystals

V. Petričević, A. Seas, and R. R. Alfano

Institute for Ultrafast Spectroscopy and Lasers and Center for Analysis of Structures and Interfaces
Departments of Physics and Electrical Engineering
The City College and The Graduate School of The City University of New York
New York, NY 10031

M.R. Kokta

Union Carbide Corporation, 750 South 32nd Street, Washougal, WA 98671

M. H. Randles

Litton-Airtron, Synoptics, 1201 Continental Boulevard, Charlotte, NC 28273

The demonstration of laser operation¹ of chromium-doped forsterite (Cr:Mg₂SiO₄) and subsequent identification of the lasing ion as tetravalent chromium (Cr⁴⁺) residing in tetrahedral environment,²⁻⁸ have generated growing interest in this material, as well as other crystals that may accommodate Cr⁴⁺ in their structure. When potential crystals are considered for the incorporation of Cr⁴⁺ ions into tetrahedral sites, the following conditions should be satisfied by the potential crystal hosts: (1) a tetrahedral site exists containing a tetravalent cation; (2) the ionic size of the site is close to that of Cr⁴⁺; and (3) a good site does not exist for the competing Cr³⁺ ion.

During the past few years several crystals of melilite structure which satisfy the above requirements were grown and investigated for potential laser applications.⁹⁻¹¹ Unfortunately, none of these efforts have produced a new laser material. All the materials that were developed clearly show presence of tetrahedral Cr⁴⁺ in their absorption spectra. However, the luminescence in these materials is either very weak or nonexistent, due to strong nonradiative relaxation. Most recently, low-temperature laser operation of Cr⁴⁺:Y₂SiO₅ has been reported,¹² but its usefulness may be limited since laser operation above 77 K is severely affected by nonradiative processes.

In this paper, we present preliminary results in the development of two new Cr⁴⁺-based laser crystals. We have attempted growth of Cr:Mg₂GeO₄, a germanium analog to forsterite,¹³ and monticellite (Cr:CaMgSiO₄), another end member of the olivine group of crystals,¹⁴ primarily because of the similarity of their crystal structure to the structure of forsterite, although neither of the crystals satisfies all the criteria listed above. In particular, both Mg₂GeO₄ and CaMgSiO₄ have, as forsterite, in their crystal structure sites that may be occupied by the Cr³⁺ ion. In Mg₂GeO₄, Mg²⁺ ions occupy two distinct octahedrally coordinated sites, M1 with inversion (C_i) and M2 with mirror (C_s) point symmetry, while Ge⁴⁺ is tetrahedrally coordinated.¹⁵ In CaMgSiO₄, Mg²⁺ and Ca²⁺ ions are ordered in the M1 and M2 sites respectively, and Si⁴⁺ occupies the tetrahedral site.^{14,16}

The attempt to grow large single crystal of Cr:Mg₂GeO₄ using the Czochralski method was unsuccessful due to volatility of GeO₂ at high temperatures (Mg₂GeO₄ melts congruently at 1855°C).¹³ However, small single crystals were salvaged from the crucible and fabricated into samples suitable for basic spectroscopic measurements. The Cr:CaMgSiO₄ sample was prepared by melting the stoichiometric proportions of oxides in an iridium crucible, followed by slow cooling to produce polycrystalline material which was later cut into slices and polished.

The preliminary measurements of the absorption spectra of Cr:Mg₂GeO₄ for three different crystal orientations, presented in Figure 1, show features that are strikingly similar to those observed in the absorption spectra of chromium-doped forsterite, the only difference being slight red shift. We attribute the dominant absorption bands observed in the spectra to the transitions of the Cr⁴⁺ ion.

The emission spectra of Cr:Mg₂GeO₄ and Cr:CaMgSiO₄ were measured for 625-nm excitation at room temperature and at liquid nitrogen temperature. Both results were compared with the emission of a laser-quality Cr:forsterite crystal for same level of excitation. The measured spectra are shown in Figure 2. All three spectra consist of two broad emission bands, one in the 700-1000 nm region, attributed to the Cr³⁺ ion, and a band due to Cr⁴⁺ spanning the 1000-1500-nm range. Low temperature emission spectrum of Cr:Mg₂GeO₄ is characterized by a sharp zero-phonon line followed by a vibrational sideband very similar to the low-temperature spectrum of Cr:forsterite. Zero-phonon line has been shifted ~20 nm towards the infrared when compared to Cr:forsterite, as expected, due to larger size of the GeO₄ tetrahedron and consequently lower crystal field at the Ge site. Low temperature emission spectrum of Cr:CaMgSiO₄ did not reveal any sharp line structure, with only a hint of a zero-phonon line appearing at ~1125 nm. It is important to note that although of inferior optical quality, both new materials exhibit emission at least as strong as that of Cr:forsterite, for similar pump powers.

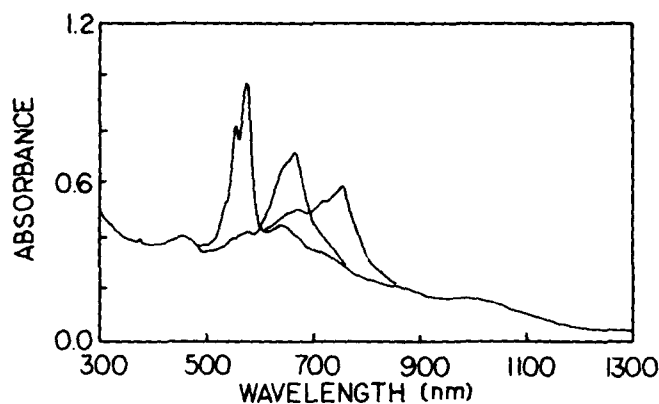


Figure 1. Absorption spectra of $\text{Cr:Mg}_2\text{GeO}_4$ for three different crystal orientations

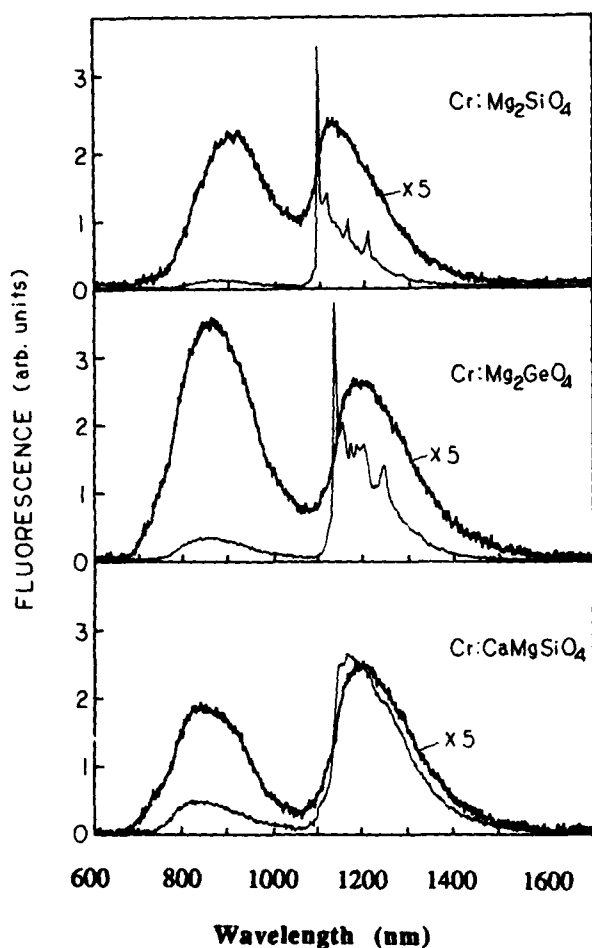
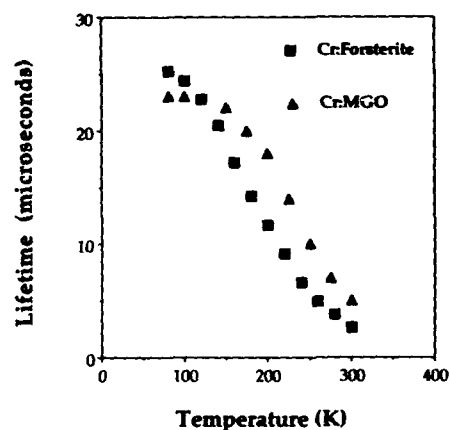
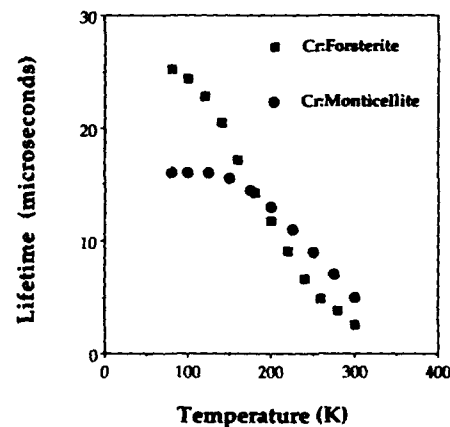


Figure 2. Fluorescence spectra of Forsterite ($\text{Cr:Mg}_2\text{SiO}_4$), $\text{Cr:Mg}_2\text{GeO}_4$ (MGO), and Monticellite (Cr:CaMgSiO_4) for 625-nm excitation, at room temperature (thicker line) and at liquid nitrogen temperature (thin line).



(a)



(b)

Figure 3. Cr^{4+} fluorescence lifetime measured at 1175 nm as a function of temperature of (a) $\text{Cr:Mg}_2\text{GeO}_4$ (Cr:MGO), and (b) Monticellite (Cr:CaMgSiO_4) compared to the fluorescence lifetime of $\text{Cr:Mg}_2\text{SiO}_4$, for 1064-nm excitation.

Fluorescence lifetime has been measured for Cr:Mg₂GeO₄ and Cr:CaMgSiO₄ for 532- and 1064-nm excitation, as a function of temperature. Under 532-nm excitation, in the 800-900-nm range, a lifetime of ~30 μ s, corresponding to Cr³⁺ emission, was measured at room temperature for both materials. These values did not change significantly when the samples were cooled down to 77 K. In Figure 3, fluorescence lifetimes of the Cr⁴⁺ ion, measured at 1175 nm for 1064-nm pump are presented. In Figure 3(a) the temperature dependence of the Cr⁴⁺ emission lifetime of Cr:Mg₂GeO₄ is compared to the lifetime dependence of Cr⁴⁺ in forsterite. Both curves show similar behavior. However, the room temperature fluorescence lifetime of Cr:Mg₂GeO₄ is a factor of two longer than that of Cr:forsterite, indicating that potential room temperature laser operation of this new material may be less affected by nonradiative processes. Temperature dependence of the Cr⁴⁺ emission lifetime in Cr:CaMgSiO₄ at 1175 nm is compared to the emission lifetime of Cr⁴⁺ in forsterite in Figure 3(b). The measured lifetime changes from ~16 μ s at 77 K to ~5 μ s at 300 K, again indicating that this material has a potential for efficient room-temperature laser operation.

In conclusion, basic spectroscopic properties of two crystals, Cr:Mg₂GeO₄ and Cr:monticellite (Cr:CaMgSiO₄) were measured and compared with those of Cr:forsterite. In both crystals the optically active centers were identified as Cr³⁺ and Cr⁴⁺, the latter being responsible for the near-infrared emission in the 1100-1500-nm spectral range. Based on the preliminary measurements, we conclude that Cr:Mg₂GeO₄ and Cr:CaMgSiO₄ represent two promising tunable solid-state laser materials based on the Cr⁴⁺ ion. Monticellite (Cr:CaMgSiO₄) looks particularly promising since it has emission properties similar to those of Cr:Mg₂GeO₄ and significant advantage that its growth does not require special techniques, since none of the oxide compounds are volatile.

This research is supported by NSF, NASA and ARO.

References

1. V. Petrićević, S. K. Gayen, R. R. Alfano, K. Yamagishi, H. Anzai, and Y. Yamaguchi, *Appl. Phys. Lett.* **52**, 1040 (1988).
2. V. Petrićević, S. K. Gayen, and R. R. Alfano, *Appl. Phys. Lett.* **53**, 2590 (1988).
3. H. R. Verdun, L. M. Thomas, D. M. Andrauskas, T. McCollum, and A. Pinto, *Appl. Phys. Lett.* **53**, 2593 (1988).
4. V. Petrićević, S. K. Gayen, and R. R. Alfano, *OSA Proceedings on Tunable Solid-State Lasers*, M. L. Shand and H. P. Jenssen, eds. (Optical Society of America, Washington, D.C., 1989) Vol. 5, pp. 77-84.
5. H. R. Verdun, L. M. Thomas, D. M. Andrauskas, and A. Pinto, *OSA Proceedings on Tunable Solid-State Lasers*, M. L. Shand and H. P. Jenssen, eds. (Optical Society of America, Washington, D.C., 1989) Vol. 5, pp. 85-92.
6. W. Jia, H. Liu, S. Jaffe, and W. M. Yen, *Phys. Rev. B* **43**, 5234 (1991).
7. R. Moncorge, G. Cormier, D. J. Simkin, and J. A. Capobianco, *J. Quantum Electron.* **27**, 114 (1991).
8. K. R. Hoffman, J. Casas-Gonzales, S. M. Jacobsen, and W. M. Yen, *Phys. Rev. B* **44**, 12589 (1991).
9. T. H. Allik, B. H. T. Chai, and L. D. Merkle, *OSA Proceedings on Advanced Solid-State Lasers*, G. Dube and L. L. Chase, eds. (Optical Society of America, Washington, D.C., 1991) Vol. 10, pp. 84-86.
10. A. L. Denisov, E. V. Zharikov, D. A. Zubenkov, M. A. Noginov, V. G. Ostroumov, V. A. Smirnov, M. E. Kholodova, I. A. Shcherbakov, *OSA Proceedings on Advanced Solid-State Lasers*, G. Dube and L. L. Chase, eds. (Optical Society of America, Washington, D.C., 1991) Vol. 10, pp. 82-83.
11. M. H. Garrett, V. H. Chan, H. P. Jenssen, M. H. Whitmore, A. Sacra, D. Singel, and D. J. Simkin, *OSA Proceedings on Advanced Solid-State Lasers*, G. Dube and L. L. Chase, eds. (Optical Society of America, Washington, D.C., 1991) Vol. 10, pp. 76-81.
12. B. H. T. Chai, Y. Shimony, C. Deka, X. X. Zhang, E. Munin, and M. Bass, *OSA Proceedings on Advanced Solid-State Lasers*, L. L. Chase, eds. (Optical Society of America, Washington, D.C., 1992) Vol. 13, pp. 28-30.
13. C. R. Robbins and E. M. Levin, *Am. Jour. Sci.*, Vol. 257, pp. 63-70 (1959).
14. J. D. Birtle, G. V. Gibbs, P. B. Moore, and J. V. Smith, *Amer. Mineral.* **53**, 807 (1968).
15. G. Will, M. Bellotto, W. Parish, and M. Hart, *J. Appl. Cryst.* **21**, 182 (1988).
16. G. A. Lager and E. P. Meagher, *Amer. Mineral.* **63**, 365 (1978).

Absorption and Emission Properties of the New Laser-Active Center Mn^{5+} in Several Crystalline Hosts

Horacio R. Verdún

Fibertek, Inc.

510 Herndon Parkway, Herndon, VA 22070

Tel.: (703) 471-7671 / Fax: (703) 471-5806

Transition-metal ions with the d^2 electronic configuration and in the tetrahedral coordination environment have very special characteristics that make them interesting as potential active centers for solid-state lasers. If the ion is located in a tetrahedral site with T_d point symmetry, the first excited triplet state, 3T_2 , is metastable because electric-dipole transitions between the 3A_2 (ground state) and the 3T_2 state, is symmetry forbidden despite the lack of inversion symmetry. Also, the 1E state (first excited singlet state), which in the systems investigated so far appears to have about the same excitation energy as the 3T_2 state, is also metastable because electric-dipole transitions to or from the ground state are spin forbidden.

Chromium-doped forsterite is the first d^2 -ion system in which laser action was observed due to the $^3T_2 \rightarrow ^3A_2$ transition of Cr^{4+} ,^{1,2} which shows quasi-four-level characteristics due to strong coupling of the 3T_2 electronic state with the lattice. Very recently, Merkle, et al.,³ observed three-level laser action in manganese-doped $\text{Ba}_3(\text{VO}_4)_2$ [barium orthovanadate (BOV)] and in the isostructural crystal $\text{Sr}_3(\text{VO}_4)_2$ (SOV) due to the $^1E \rightarrow ^3A_2$ transition of Mn^{5+} . At difference with Cr^{4+} in forsterite, in the Mn^{5+} center in BOV, the 1E energy level appears to lie below the relaxed 3T_2 level. These two examples illustrate a well-known relationship between relative energy level positions with ionic valence, similar to the one observed in d^3 ions in octahedral sites such as Cr^{3+} and V^{2+} .

One of the frequent causes of poor laser performance of some systems is due to excited state absorption. This effect degrades the performance of Cr:forsterite in the gain-switched mode,⁴ and it may also explain why other Cr^{4+} systems have not shown laser action. Whether or not this effect would also spoil the laser performance of the Mn^{5+} center is one of the issues that would be interesting to investigate. The other important subject is the effect of the host composition and crystalline structure on the coordination environment (anions nature, covalence effects, site configuration and symmetry), which determines the relative position of the energy levels. In particular, it is of interest to investigate if it is possible to find hosts for Mn^{5+} in which the 3T_2 level is the lowest excited state of this

center. Finally, the effect of codopants, which in some hosts may be needed for charge compensation, and other crystal defects on the optical characteristics of the center needs to be understood.

The crystals used in this studied were grown either by the laser-heated pedestal growth (LHPG) method or by the Czochralski method, and in same cases by both. Growth atmospheres contained 1% O₂ for crystals grown by the Czochralski method and up to 20% O₂ for crystals grown by the LHPG method. The hosts that were investigated included crystals with the apatite structure: Ca₅(PO₄)₃F [calcium-phosphor fluorapatite (CPFAP)] and Sr₅(PO₄)₃F (SPFAP); crystals with the palmierite structure: Sr₃(VO₄)₂ (SOV) and Ba₃(VO₄)₂ (BOV). In all these compounds manganese substitutes for either phosphorus or vanadium, all having the same 5-plus ionic valence, and consequently there is no need for charge compensation. Substitution of manganese for silicon with charge compensation was tried in forsterite and yttrium ortho-silicate (YOS). In forsterite, aluminum was used as charge compensator (aluminum substitutes for silicon) and we did not observed spectroscopic evidence of Mn⁵⁺ presence, even in crystals grown in highly oxidizing atmospheres. In this crystal, manganese is incorporated mostly as Mn²⁺ substituting for Mg²⁺ in octahedral sites. Two charge compensation schemes were used for Mn⁵⁺ in YOS: aluminum substituting for silicon and calcium substituting for yttrium. Both cases yielded YOS crystals with the characteristic blue hue of Mn⁵⁺. The absorption spectra of Mn⁵⁺ in all these hosts are very similar. Figure 1 shows the absorption spectra obtained for YOS:Mn,Ca. The emission spectra for a few Mn⁵⁺-doped crystals are shown in Figure 2. With the exception of CPFAP:Mn, for which we did not see any measurable emission a room temperature, all the materials studied show characteristics attributable to an overlap of the emission from the triplet and the singlet states, with the emission from the singlet dominating over the emission from the triplet in different degrees. The system YOS:Mn,Ca shows the strongest triplet emission and the shortest fluorescence lifetime.

References

1. V. Petricevic, S. K. Gayen, R. R. Alfano, K. Yamagishi, H. Anzai and Y. Yamaguchi, *Appl. Phys. Lett.* **52**, 1040 (1988)
2. Horacio R. Verdún, Leonard M. Thomas, Donna M. Andrauskas, Tom McCollum, and Albert Pinto, *Appl. Phys. Lett.* **53**, 2593 (1988)
3. Larry D. Merkle, Albert Pinto, Horacio R. Verdún, and Bruce McIntosh, to be published in *Appl. Phys. Lett.*
4. Horacio R. Verdún and Larry Merkle, *OSA Proceedings on Advanced Solid-State Lasers*, G. Dubé, L. Chase, eds. (Optical Society of America, Washington, DC 1991), Vol. 10, pp. 35.

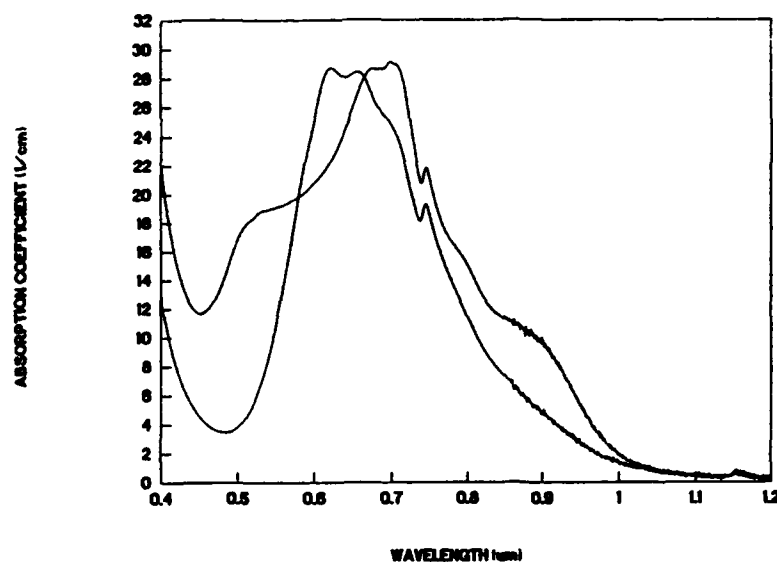


Figure 1. Room temperature absorption of SPFA:Mn²⁺ for two polarizations.

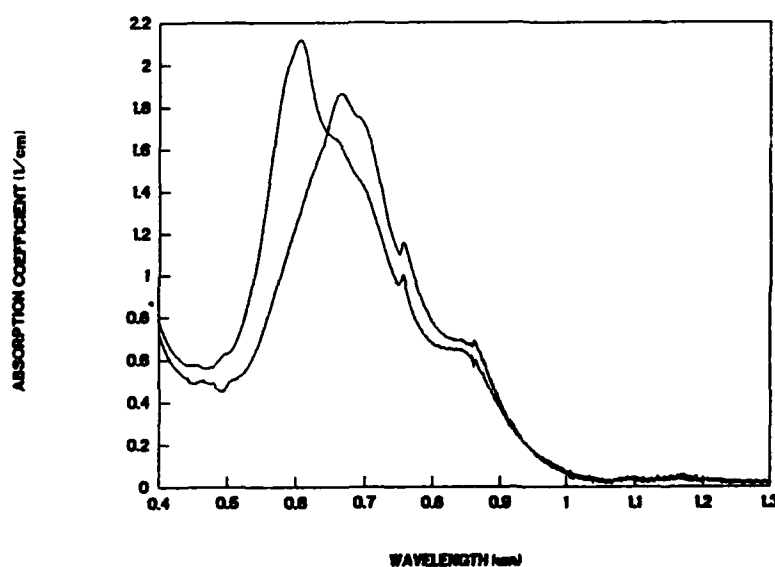


Figure 2. Room temperature absorption of YOS:Mn²⁺ for two polarizations.

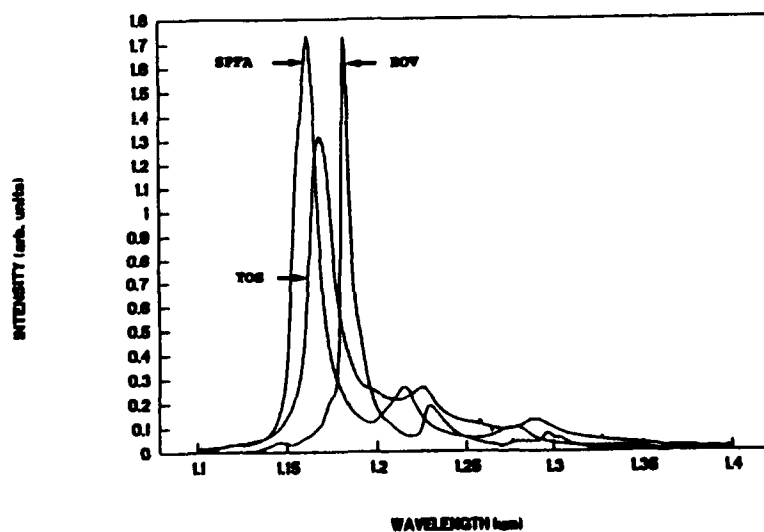


Figure 3. Room temperature emission of Mn²⁺ in three different hosts.

Picosecond Spectroscopy of Excited States
in Transition-Metal-Ion Doped New Laser
Materials

V.P.Mikhailov and N.V.Kuleshov

Institute for Applied Physics Problems, Belarusian State
University, Kurchatov str., 7, Minsk 220064, Belarus
Tel. (0172)-785726

In this paper we report on saturation of absorption and excited state absorption measurements and ultrafast relaxation processes in excited states of transition-metal-ion doped crystals of laser interest.

The kinetics of nonradiative transitions between the pump level 4T_2 and storage level 2E for Cr^{3+} ion was investigated in a number of laser crystals [1]. The nonradiative relaxation times for intra 4T_2 state vibrational transition and for $^4T_2 - ^2E$ electronic transition were measured.

In recent years laser action in near infrared was realized on Cr^{4+} -doped YAG [2] and forsterite [3] crystals. We carried out the saturation of absorption and time-resolved excite-and-probe relaxation measurements on Cr^{4+} ion in a number of crystals, such as Mg_2SiO_4 , YAG, GSGG, GSAG. The picosecond spectrometer based on passively mode-locked Nd-YAlO₃ laser was used for this study. Nonlinear transmission of 1.08 μm 20 ps pump pulses was observed. Absorption cross section of approximately $5 \times 10^{-18} \text{ cm}^2$ in garnets and $2.3 \times 10^{-18} \text{ cm}^2$ in forsterite is estimated for $^3A_2 - ^3T_2$ transition of tetrahedral Cr^{4+} . An upper limit of 8 ps in garnets and 15 ps in forsterite is estimated for intra 3T_2 state vibrational relaxation time. Excited state absorption spectra in visible and near infrared are obtained for Cr^{4+} in garnets. Q-switched and mode-locked neodymium laser action is realized using chromium-doped crystals as the saturable absorbers. The shortest pulses of 80 ps in duration were observed for Nd-YAlO₃ laser with Cr^{4+} :GSGG absorber.

Trivalent vanadium ion has the same $3d^2$ electron configu-

ration as tetravalent chromium. Vanadium doped YAG, which contain tetrahedrally coordinated V^{3+} , has two broad absorption bands in near infrared with peaks at $1.3\ \mu\text{m}$ and $0.83\ \mu\text{m}$ associated with ${}^3A_2 - {}^3T_2$ and ${}^3A_2 - {}^3T_1$ electronic transitions, respectively. In our measurements saturation of absorption was observed for both these transitions. Absorption cross sections and nonradiative relaxation rates are estimated. Mode-locking of Nd-YAG laser at $1.06\ \mu\text{m}$, Nd-YALO laser at $1.34\ \mu\text{m}$ and Ti-Al₂O₃ laser at 780 nm was realized using V^{3+} :YAG crystal as a saturable absorber. The shortest pulses were of about 100 ps at $1.34\ \mu\text{m}$.

The tetrahedral Co^{2+} ion in a number of spinels is characterized by a strong luminescence in visible and near infrared with extremely short radiative lifetime and is suggested to be a possible active ion for laser materials [4]. We investigated excited state dynamics in Co^{2+} :GSGG crystal using pump-probe transmission measurements. Broad absorption bands of tetrahedral Co^{2+} were observed at about $2.3\ \mu\text{m}$, $1.45\ \mu\text{m}$ and 625 nm and were assigned to transitions from 4A_2 to 4T_2 , 4T_1 and ${}^4T_1({}^4P)$ states, respectively. Optical gain followed by excited state transient absorption of $1.06\ \mu\text{m}$ probe pulse was observed after 532 nm pump excitation. The nonradiative lifetime of 4T_1 and ${}^4T_1({}^4P)$ excited states was estimated to be of about 15 ± 5 ps and 35 ± 5 ps, respectively, while an upper limit for intra ${}^4T_1({}^4P)$ state vibrational relaxation time does not exceed 5 ps.

We are grateful to Prof. R.R.Alfano and Prof. J.M.Buchert for cooperation in Co^{2+} :GSGG crystal study.

References

1. S.K.Gayen, W.B.Wang, V.Petricevic, S.G.Demos and R.R.Alfano. J. Luminescence, 47, 181 (1991).
2. N.B.Angert, N.I.Borodin, V.M.Garmash, V.A.Zhitnyuk, A.V.Shestakov. Kvant. Elektron. (USSR), 15, 113 (1988).
3. V.Petricevic, S.K.Gayen, R.R.Alfano. Appl. Phys. Lett., 53, 2590 (1988).
4. B.Henderson, G.F.Imbush. Contemp. Phys., 29, 235 (1988).

Cr⁴⁺:YSGG-Passive Q-Switch for Multispikes Nd-Lasers

Klimov I.V., Shcherbakov I.A., Tsvetkov V.B.

General Physics Institute of Russian Academy of Sciences,
117942 Moscow, Vavilov street, 38, Russia, Fax: (095)135-02-70

Cr⁴⁺-doped garnets with additional absorption band, which peaks near 1.06 μm , are of interest as passive Q-switches for Nd-lasers [1]. High photochemical stability with predictable behavior, good mechanical properties, high thermal conductivity and well-developed inexpensive crystal growth and processing technologies give them considerable advantages as compared with traditional passive Q-switches for Nd-lasers, such as dye cell, acetate films and color-center LiF:F²⁺ crystals. These advantages are especially important for the work at high repetition rates and high light exposures.

Besides, such a modulator allows to realize not only monopulse, but also stable multispikes output at high pumping energies and repetition rates. This regime is interesting from the standpoint of the increase of passive Q-switch laser efficiency and the development of lasers with high both peak and average power.

The multispikes generation using auto-Q-switch mode was demonstrated in [2,3]. Active rods, such as Cr,Nd:GSGG, Cr,Nd:YSGG, Cr,Nd:GSAG containing sensitizer Cr³⁺, active Nd³⁺ and absorption Cr⁴⁺ centers were used in these papers. But additional absorption in the active rod increases its thermoloading and therefore makes the spatial characteristics of the output beam worse.

The subject of this paper is the study of multispikes Q-switch mode using laser cavity scheme with the active rod without Cr⁴⁺-absorption centers and a separate Cr⁴⁺:YSGG passive modulator.

The uncoated Cr⁴⁺:YSGG rod (ϕ 9.3x60mm) grown by the Czochralski method was placed in plane-plane resonator. Three types of active laser rods, such as Nd:YAG (ϕ 6.3x70), Cr,Nd:YSGG (ϕ 6x70), Cr,Nd:GSAG (ϕ 3.7x70) were used in the experiments. The modulator was cooled by distilled water step-by-step with the active crystal. Q-switch initial transmittance $T_0 \sim 60\%$ allowed to obtain stable multispikes output with any active rods employed.

Oscillograms of the obtained output trains of pulses are shown in Fig.1. Fig.2. represents the relation between repetition rate of the output spikes and pumping energy. Strong dependence of output repetition rates on the used active crystal hosts is quite evident. The stimulated emission cross-sections G for transition $^4F_{3/2} \rightarrow ^4I_{11/2}$ (1.06 μm) in the selected active rods, as well as the obtained average output laser parameters are shown in Table 1.

Date of the output characteristics

Table 1.

Active rod	G (relat. to Nd:YAG)	Output rep.rate (kHz)	$\tau_{0.5}$ spike duration (ns)	E_{spike} (mJ)	E_{train} (mJ)
Nd:YAG	1	~ 300	$\sim 80-100$	~ 10	~ 350
Cr,Nd:YSGG	0.43	~ 140	$\sim 60-90$	~ 70	~ 720
Cr,Nd:GSAG	0.26	~ 50	$\sim 30-60$	not measured	not measured

where $E_{\text{pump}} = 70 \text{ J}$, $\tau_{\text{pump}} = 150 \mu\text{s}$, $L_{\text{cavity}} = 1 \text{ m}$, pump rep.rate = 25 Hz.

The relation between the values of output repetition rate are well correlated with the relation between the used crystals cross-section values. The dependence $\text{Output rep.rate}/E_{\text{pump}}$ for the concrete active rod hosts seems to be root and proportional to G and the initial transmittance T_0 of Q-switch (the results of experiments with other values of T_0 are not presented here). Energy of train of pulses reached 57% of free-running mode energy due to multispikes regime. The used uncoated crystal did not permit to make sharper quantitative estimations. The application of such crystals requires sufficiently high accuracy of their mounting, but AR coating eliminates this problem. Due to polarizing insensitivity of Cr^{4+} -Q-switch the polarizing properties of the resonator are not important. In fact, such a Q-switch can be easily placed in any type of Nd-laser cavity without its special preparation. No changes in Q-switch properties have been observed during more than one year of strong use.

Conclusion

We investigated multispikes Q-switch mode for different types of pulsed Nd-lasers using the water-cooled Cr^{4+} :YSGG-passive modulator. The dependence of output spikes repetition rates on pumping pulse energy was studied for three Nd-laser hosts. Due to high stability of the properties and polarizing insensitivity of this modulator, the compact and reliable Q-switch multispikes Nd-laser with high both average and peak power can be constructed. Such lasers could be interesting for application in industry, laser medicine and lidar systems.

We wish to thank P.A.Studenikin, Yu.D.Zavartsev (General Physics Institute, Moscow, Russia) and Dr. I.A.Ivanov ("ELMA", Zelenograd, Russia) for giving Cr^{4+} :YSGG and Cr,Nd :YSGG-crystals, accordingly, at our disposal.

References

1. G.S.Kruglic, G.A.Skripko, A.P.Shkadarevich, "Tunable lasers on active-doped crystals", Minsk, Belorusskii Polytechn. Institute, 1984, p.145, (in Russian).
2. A.A.Danilov, E.V.Zharikov, A.I.Zagumennyi, G.B.Lutts, M.Yu.Nikolskii, V.B.Tsvetkov, I.A.Shcherbakov, "Powerful self-Q-switched laser based on yttrium-scandium-gallium garnet activated with chromium and neodymium", Sov. J. Quant. Electron., v. 16(3), 1989, pp. 474-477.
3. A.L.Denisov, E.V.Zharikov, A.I.Zagumennyi, G.B.Lutts, S.A.Samolova, M.Yu.Nikolskii, V.B.Tsvetkov, I.A.Shcherbakov, "Solid-state lasers based on scandium garnets doped with chromium and neodymium operating in self-Q-switch regime", Izv. Acad. Nauk SSSR, Ser. Fiz., 1991, v. 55, pp. 239-246 (Bull. Acad. of Sciences USSR, Physical Series, v.55, 1991).

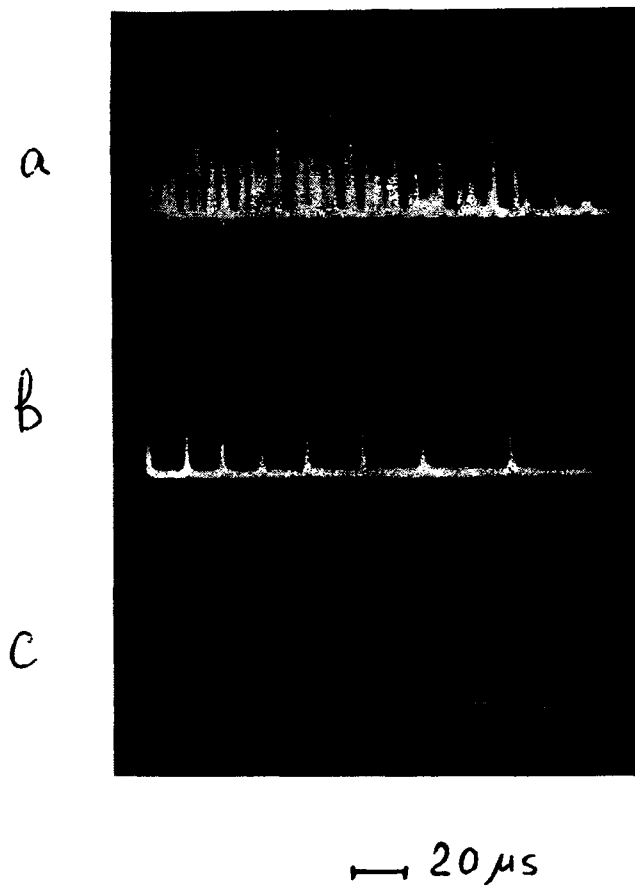


Fig.1. Oscillograms of the laser output for different active media: a-Nd:YAG; b-Cr,Nd:YSGG; c-Cr,Nd:GSAG.

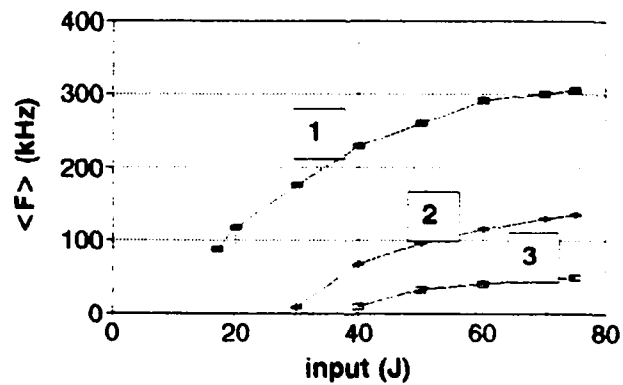


Fig.2. Average repetition rate of spikes in the output pulse for different rods: 1-Nd:YAG; 2-Cr,Nd:YSGG; 3-Cr,Nd:GSAG.

All Solid-State Pulsed-Mode Cr:Forsterite Laser

Ti Chuang and Horacio R. Verdún

Fibertek, Inc.

510 Herndon Parkway, Herndon, VA 22070

Tel.: (703) 471-7671 / Fax: (703) 471-5806

Since the early reports on the Cr:forsterite laser,^{1,2} a significant amount of work has been done to further investigate, characterize and improve its performance. The Cr:forsterite laser has been shown to be a promising solid state laser, tunable in the 1.18-1.35 μm region³ and optically pumpable by 1 μm Nd lasers, currently the most efficient and most advanced solid-state lasers. For applications demanding efficient, compact and reliable laser systems, diode-pumped lasers have been increasingly chosen. It is therefore of interest to develop a forsterite laser system that uses diode-laser arrays as the pumping source for the Nd laser used to pump the Cr:forsterite crystal. We refer to this system as being "all solid-state". In what follows, we report on the performance of what we believe is the first such "all solid-state" Cr:forsterite laser system.

The source of pump radiation chosen for the Cr:forsterite laser was a diode-pumped, Q-switched Nd:YAG laser employing a three-bar high-power diode laser array with coupling optics designed for end-pumping of the Nd:YAG crystal. It is based upon our early work on this type of pumping configuration⁴ with only slight modifications for optimal performance. It uses a 5 cm convex output coupler (OC1) coated for 85% reflection at 1.06 μm , and a KD*P Q-switch (QS). When operated at 50 Hz repetition rate, this laser is capable of delivering more than 2 mJ per pulse at a beam divergence of about two-time diffraction limit and a pulselength shorter than 20 ns.

The resonator for the Cr:forsterite laser consists of a flat end mirror (M) and a 30 cm concave output coupler (OC2), as shown in Fig. 1. The flat mirror is dielectric coated for high transmission at 1.06 μm and high reflection at 1.22 μm . Two output couplers were used, one coated for 85% and the other for 96% reflection at 1.22 μm . For mode matching between the Nd:YAG pumping laser beam and the TEM₀₀ mode of the Cr:forsterite laser resonator, a lens (L) of 50 mm focal length is positioned 7 cm away from the output coupler of the Nd:YAG laser, and the flat mirror of the Cr:forsterite laser is 17 cm from this lens. The forsterite crystal (FC) is about 10 mm long and has a diameter of ~ 1.5 mm. Both ends of this crystal were anti-reflection coated for 1.22 μm . The Cr:forsterite crystal used in this laser was grown using the laser-heated pedestal growth method in 8% O₂ atmosphere, and was codoped with aluminum. Codoping with aluminum seems to increase the incorporation of chromium into the silicon site. The growth axis was oriented along the crystallographic c axis (space group Pbnm). The crystal was oriented with this axis parallel to the resonator

axis. The polarization of the pump radiation coincided with the b axis of the crystal, which is the orientation for which the absorption at $1.064\ \mu\text{m}$ is a maximum. Approximately 70% of the pump radiation was absorbed by the crystal. The cavity length was $\sim 40\ \text{mm}$. The spacing between the flat mirror and the Cr:forsterite crystal is $\sim 5\ \text{mm}$. The laser performance of this forsterite laser is shown in Fig. 2, in which data for the two output couplers tested in this laser are presented.

Since this Cr:forsterite laser is operated in the gain-switched mode, and the pulse formation time is much shorter than the fluorescence lifetime, the asymptote of the input-output curve of the Cr:forsterite laser should pass through the origin.⁵ According to this principle, we extracted the slope efficiencies for two data sets shown in Fig. 2. The slope efficiency is 19.5% for the 85% OC and is 12.5% for the 98% OC. Both data sets in Fig. 2 exhibit the saturation behavior at high absorbed pump energy. This is the result of excited state absorption of the pump radiation, an effect that was studied before.⁶ The temporal profile for the 85% OC is given in Fig. 3, where the small peak is the signal of the residual Nd:YAG laser pump beam. This trace was taken for an absorbed pump energy of about 1.5 mJ. The pulsewidth of the Cr:forsterite laser is $\sim 5.6\ \text{ns}$. The delay time between the pumping laser and the Cr:forsterite laser is approximately 25 ns, which suggests a quite small cavity loss.

We believe an "all solid-state" Cr:forsterite laser system like the one described here will demonstrate its potential in systems requiring tunable pulsed lasers for lidar systems. By tuning the Cr:forsterite laser, and by frequency doubling or tripling its output, several Fraunhofer lines can be reached, allowing the detection of lidar pulses at these wavelengths to be free of the degrading effect of solar background on detector sensitivity.

This work was supported by Fibertek, Inc. through its IR&D program.

References

1. V. Petricevic, S. K. Gayen, R. R. Alfano, K. Yamagishi, H. Anzai and Y. Yamaguchi, *Appl. Phys. Lett.* **52**, 1040 (1988)
2. Horacio R. Verdún, Leonard M. Thomas, Donna M. Andrauskas, Tom McCollum, and Albert Pinto, *Appl. Phys. Lett.* **53**, 2593 (1988)
3. V. Petricevic, S. K. Gayen, and R. R. Alfano, *Appl. Opt.* **28**, 1609 (1989).
4. Horacio R. Verdún and Ti Chuang, *Opt. Lett.* **17**, 1000, (1992)
5. William Wagner and Bela Lengyel, *J. Appl. Phys.* **34**, 2040, (1963)
6. Horacio R. Verdún and Larry Merkle, *OSA Proceedings on Advanced Solid-State Lasers*, G. Dubé, L. Chase, eds. (Optical Society of America, Washington, DC 1991), Vol. 10, pp. 35.

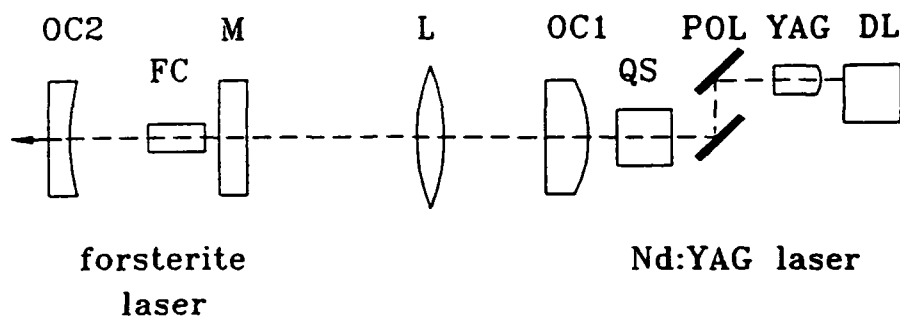


Fig.1. The layout of the "all solid-state" Cr:forsterite laser.
DL: diode laser with optics; YAG: Nd:YAG crystal; POL: folded polarizer set. See text for other explanations.

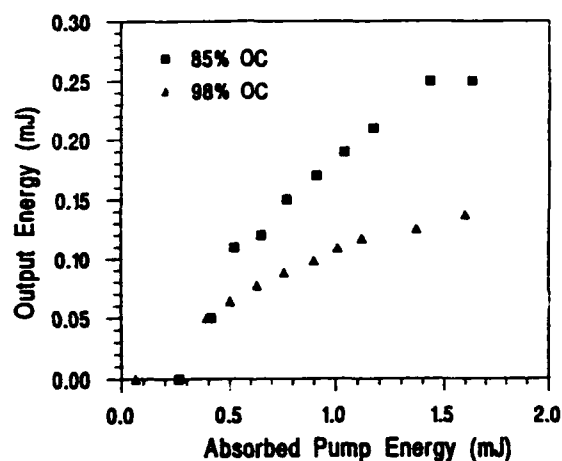


Fig.2. Laser performance of forsterite lasers

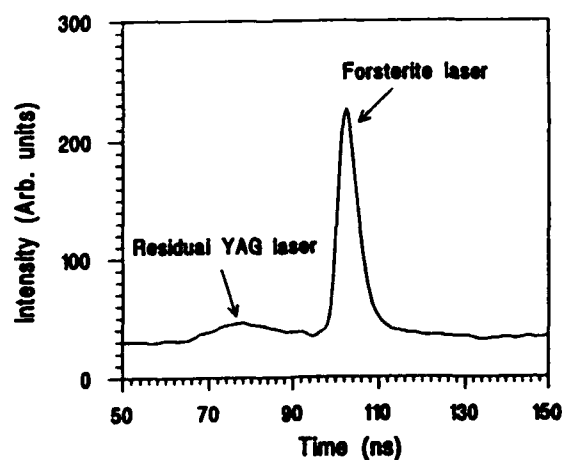


Fig. 3. The temporal profile of the forsterite laser

Spectroscopic and laser studies of Cr⁴⁺-doped garnets and Y₂SiO₅

S. Kück, K. Petermann, U. Pohlmann, G. Huber
Institut für Laser-Physik, Universität Hamburg

T. Schönherr
Institut für Theoretische Chemie, Universität Düsseldorf

In the last years intensive research was made on new tunable solid state lasers. In the infrared spectral region between 1.1 and 1.6 μm the Cr⁴⁺-ion seems to be the most promising laser-ion. Until now, laser action at room-temperature could be achieved in Forsterite (Mg₂SiO₄) [1] and YAG (Y₃Al₅O₁₂) [2]; however, at liquid nitrogen temperature also Y₂SiO₅ is lasing [3]. In all these materials the Cr⁴⁺-ion occupies the tetrahedrally coordinated lattice site.

The absorption and excitation spectra of Cr⁴⁺-doped garnet crystals show three broad bands, fitting excellent to the d⁸ Tanabe-Sugano diagram. The resulting crystal field parameters are compared with those obtained from AOM calculations. The fluorescence is due to the transition ³T₂–³A₂ and shifts to longer wavelengths for lower crystal fields. At the same time the roomtemperature lifetime decreases from 3.4 μsec for YAG down to 1.0 μsec for YSGG. This decrease is caused by higher nonradiative transition rates at low crystal fields.

The low temperature absorption and emission spectra of all Cr⁴⁺-doped garnet crystals show a very complicated structure [Fig. 1 and 2]. We have not been able to find a zero phonon line, because the transition between the ³T₂ and ³A₂ states is symmetry forbidden and a large Stokes shift occurs. So the spectra consist of coupling phonon modes, i.e. a promoting mode, which makes the transition allowed and an accepting mode, which is responsible for the observed progression (see for example the 300cm⁻¹ progression of Cr⁴⁺:GGG in Fig.2).

We also have measured the temperature dependence of the fluorescence lifetime for several Cr⁴⁺-doped garnets. The fluorescence decay is single exponential in the whole temperature range from 4 K to 300 K. From these data the quantum efficiency was calculated using the theory of Struck & Fonger and adding a temperature dependence of

the radiative lifetime. As expected, the best value of nearly 40 % was obtained for Cr^{4+} :YAG assuming a purely radiative lifetime at 4 K.

Until now laser action was achieved only with Cr^{4+} :YAG. With a flashlamp-pumped Cr^{4+} :Nd:GSGG laser (pulse duration 200 μsec) we obtained a slope efficiency of 10.3 % and a threshold of 30 mJ. The laser output strongly depends on the polarization of the pump laser. Best results were obtained for $\vec{E}_{\text{pump}} \parallel \langle 100 \rangle$. This strange behaviour for a cubic crystal like YAG is – in our opinion – due to excited state absorption. The tuning range extends from 1.32 to 1.46 μm and from 1.49 to 1.51 μm . The lack of laser action between these two regions might also be due to ESA-processes. To check this hypothesis polarized excited state absorption spectra will also be presented.

Another promising host material for Cr^{4+} -ions is Y_2SiO_5 because of its tetravalent and tetrahedrally coordinated Si-site; therefore codoping for charge compensation is not required. Furthermore no Cr^{3+} is incorporated, due to the unsuitable octahedral sites. Because Y_2SiO_5 is a monoclinic crystal with spacegroup $C2/c$, the absorption spectrum shows strong polarization effects. The Cr^{4+} -ion emits in the spectral region between 1.1 and 1.6 μm , i.e. at shorter wavelengths than YAG. The lifetime decreases from 11.6 μsec at 4 K down to 1.1 μsec at 300 K; the decay is single exponential. The Struck & Fonger fit yields a quantum efficiency of about 30 %. In comparison with YAG this lower value is caused by the higher phonon energies of the Si-tetrahedra, which leads to higher non-radiative transition rates. As expected from group-theoretical considerations, the low temperature spectra show clearly zero phonon lines similar to those of Cr^{4+} -doped Forsterite.

Literature:

- [1] V. Petricevic et al.
Appl. Phys. Lett. 52 (13), 1040 (1988)
- [2] G.M. Zverew and A.V. Shestakov
OSA Proceedings on Tunable Solid State Lasers Vol. 5, 66 (1989)
- [3] B.H.T. Chai et al.
OSA Proceedings on Advanced Solid State Lasers Vol. 13, 28 (1992)

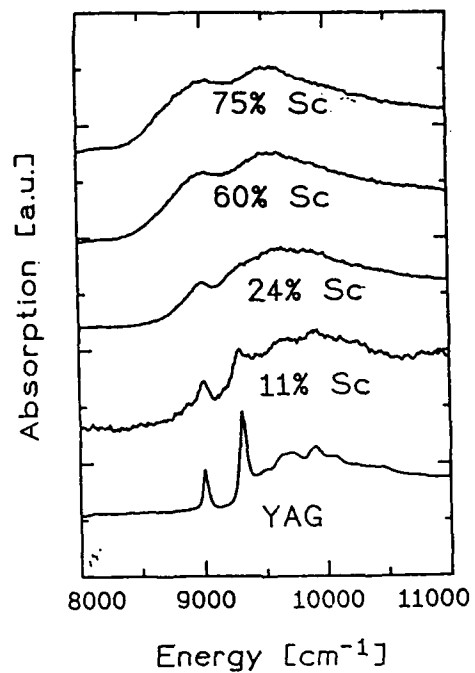


Fig. 1 Low temperature absorption spectra of Cr⁴⁺:YAG and Cr⁴⁺:YSAG with different concentrations of Scandium

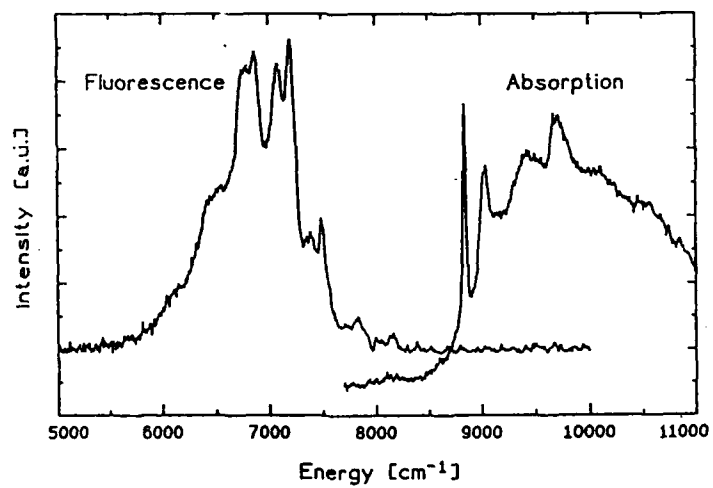


Fig. 2 Low temperature absorption and emission spectra of Cr⁴⁺:GGG

**Photoionization and Excited State Absorption
in $\text{YAlO}_3\text{:Ti}$ Crystals**

S.A. Basun, S.P. Feofilov, A.A. Kaplyanskii
A.F. Ioffe Physico-Technical Institute,
194021, St. Petersburg, Russia

G. Huber, K. Petermann
Institut für Laser-Physik, Universität Hamburg,
Jungiusstraße 11, 2000 Hamburg 36, Germany

$\text{YAlO}_3\text{:Ti}^{3+}$ (YAP:Ti^{3+}) crystals attract attention as an interesting candidate for short-wavelength tunable solid state lasers. Unfortunately, the lasing properties of YAP:Ti appeared to be poor because of the negative role of excited state absorption (ESA) in the spectral range of pumping [1]. In the present work it is directly shown that ESA in YAP:Ti^{3+} is accompanied by the appearance of electric current – this result is significant for the understanding of the nature of electronic transitions in ESA processes.

In our experiments we studied single crystals YAP:0.2\%Ti (A) and $\text{YAP:0.2\%Ti,0.1\%Mn}$ (B) having the same (0.2 %) Ti^{3+} concentration but different Ti^{4+} concentrations (A – $4.9 \cdot 10^{18} \text{ cm}^{-3}$, B – $1.1 \cdot 10^{19} \text{ cm}^{-3}$) as well as a YAP:Ti^{3+} crystal (C) grown in J. Kvapil's group at Turnov, Czechoslovakia. At $T = 77 \text{ K}$ the stationary photoconductivity was studied in thin crystalline wafers with high electric fields E applied by transparent electrodes on the surfaces.

It is found that in YAP:Ti under excitation with cw Ar-laser lines into ${}^2T \rightarrow {}^2E$ band a photocurrent appears which depends quadratically on the pumping intensity P (Fig. 1). It shows that visible light causes the photoionization of Ti^{3+} by a two-step process via the intermediate metastable 2E -state of Ti^{3+} . A similar two-step Ti^{3+} photoionization was observed earlier for $\text{Al}_2\text{O}_3\text{:Ti}^{3+}$ and YAG:Ti^{3+} [2]. In the case of two-step excitation the photocurrent excited by light frequency ν is

$$J(\nu) \sim \left[\sigma_{\text{GSA}}(\nu) \frac{P(\nu)}{h\nu} \right] \left[\sigma_{\text{pi}}(\nu) \frac{P(\nu)}{h\nu} \right]$$

where $\sigma_{\text{GSA}}(\nu)$ is the cross-section of ground state absorption (GSA) $T - E$, which populates the 2E level and $\sigma_{\text{pi}}(\nu)$ is the cross-section of the transition from 2E into the high-lying photoionization state. By parallel measurements of the photocurrent and of the spectral behaviour of $\sigma_{\text{GSA}}(\nu)$ (by observation of Ti^{3+} fluorescence excitation spectrum) $\sigma_{\text{pi}}(\nu)$ was obtained (Fig. 2). In the long-wavelength spectral region $\sigma_{\text{pi}}(\nu)$ has the same shape for the three samples and exhibits some structure; the long-wavelength σ_{pi} decrease is analogous to that of ESA in the 450 – 500 nm region [1]. This demonstrates the connection of the higher ESA state with strongly delocalized (band or weakly coupled) states allowing the spatial charge transport (via a band or tunneling-type respectively) from Ti^{3+} . The experimental result that the photocurrent in sample B (with high Ti^{4+} concentration) is much less than in sample A (Fig. 1) shows that the transfer of an electron released from the step-wise excited Ti^{3+} ion takes place with another Ti^{4+} ion. Indeed, for both mechanisms (band and tunneling) of transport the stationary photocurrent is proportional to the shift \bar{l} of an electron from its generation point (from Ti^{3+}) to a recombination point $e^- + \text{Ti}^{4+} \rightarrow \text{Ti}^{3+}$ and thus is inversely proportional to the Ti^{4+} concentration c . From the experimental $J \sim P^2$ dependence it follows that c is determined by this initial Ti^{4+} concentration in the sample and does not change much under optical excitation of the sample.

The extrapolation of $\sigma_{\text{pi}}(\nu)$ into the "red direction" (Fig. 2) as well as the shape of $\sigma_{\text{GSA}}(\nu)$ (Fig. 5 in [1]) shows that ESA resulting in photoionization begins at energies slightly less than the zero-phonon line energy (540 nm, 18530 cm^{-1} , an arrow in Fig. 2). This might give the possibility of two-step "self-gated" hole burning [3] inside the inhomogeneously broadened zero-phonon line contour in $\text{YAP}:\text{Ti}^{3+}$ due to selective photoionization of Ti^{3+} ions.

References

1. T. Wegner, K. Petermann, Appl. Phys. B 49 (1989) 275.
2. S.A. Basun, S.P. Feofilov, A.A. Kaplyanskii, B.K. Sevastyanov, M.Yu. Sharanov, L.S. Starostina, J. Lumin. 53 (1992) 28.
3. R.M. Macfarlane, J. Lumin. 38 (1987) 20.

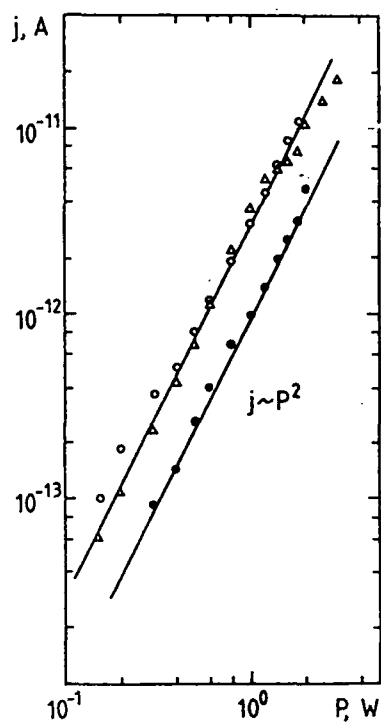


Fig. 1: Pumping dependence of photocurrent in samples A (open circles), B (full circles), and C (triangles) in an electric field of $E = 100$ kV/cm, $\lambda_{\text{exc}} = 488$ nm, beam diameter ≈ 0.5 mm.

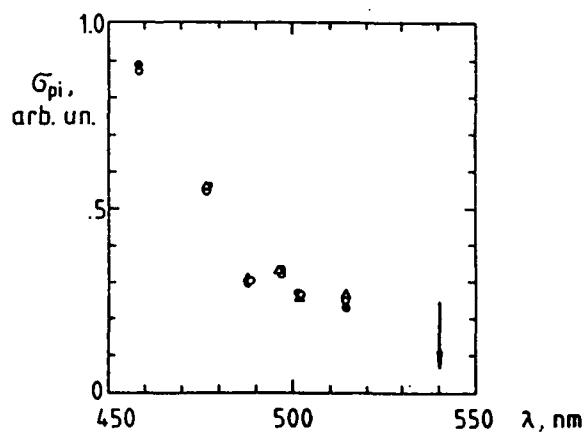


Fig. 2: Spectral dependence of photoionization from the 2E -state cross-section σ_{pi} for samples A (open circles), B (full circles), and C (triangles).

LUMINESCENCE PROPERTIES OF Cr DOPED LiNbGeO_5 LASER CRYSTAL

H. MANAA, R. MONCORGE

Université de Lyon, URA 442 CNRS, 69622 Villeurbanne, France

A.V. BUTASHIN, B. MILL, A.A KAMINSKII

Subnikov Inst. Cryst., Russian Acad. Sc., Moscow 117333, Russia

The discovery of the chromium-doped forsterite $\text{Mg}_2\text{SiO}_4\text{:Cr}$ and yttrium aluminum garnet $\text{Y}_3\text{Al}_5\text{O}_{12}\text{:Cr}$ single crystals as tunable solid-state laser materials in the 1.15 - 1.45 μm range has motivated a great number of studies both in the spectroscopist and laser physicist communities. In particular, though strong presumption exists to assign the lasing center to a Cr^{4+} ion in a tetrahedral environment, some questions still remain unsolved concerning the chemistry as well as the spectroscopy of these systems. That is the reason why many efforts continue to be devoted to that matter either by studying more deeply the above systems or by extending the search to new ones which could bring complementary information and/or better laser properties.

The purpose of this work is precisely to report on the spectroscopic characteristics - absorption, emission, laser excitation, excited-state absorption and fluorescence decay - of the recently discovered $\text{LiNbGeO}_5\text{:Cr}$ laser crystal and to compare these properties with those of the other Cr^{4+} doped crystalline materials.

LiNbGeO_5 is orthorhombic - space group D_{2h}^{16} -. The crystal is biaxial and the Ge^{4+} ions, for which the chromium dopants can substitute, are located on mirror planes in 4c positions (Wyckoff notation), as the Si^{4+} ions in Mg_2SiO_4 , i.e. in distorted tetrahedral sites of C_s symmetry¹.

We summarize the general optical properties of this Cr doped crystal in the figures 1 and 2 and the temperature variation of the emission intensity and of the infrared fluorescence lifetime in figure 3.

The absorption spectra are strongly polarized and they are very similar to that found in Cr doped Mg_2SiO_4 . The emission spectrum extends from about 1100 to 1700 nm providing the possibility of a very broad wavelength tunability.

The fluorescence decays are exponential and they do not vary across the emission band, suggesting the existence of only one kind of emitting center.

More details will be presented at the conference.

Acknowledgements:

The authors wish to thank Prof. G. Boulon for supporting some of us.

References:

1. A.A. Kaminskii, B.V. Mill, E.L. Belokoneva and A.V. Butashin, *Inorganic Materials* 27(9), 1991, p.1899 (russian ref.) and refs therein.

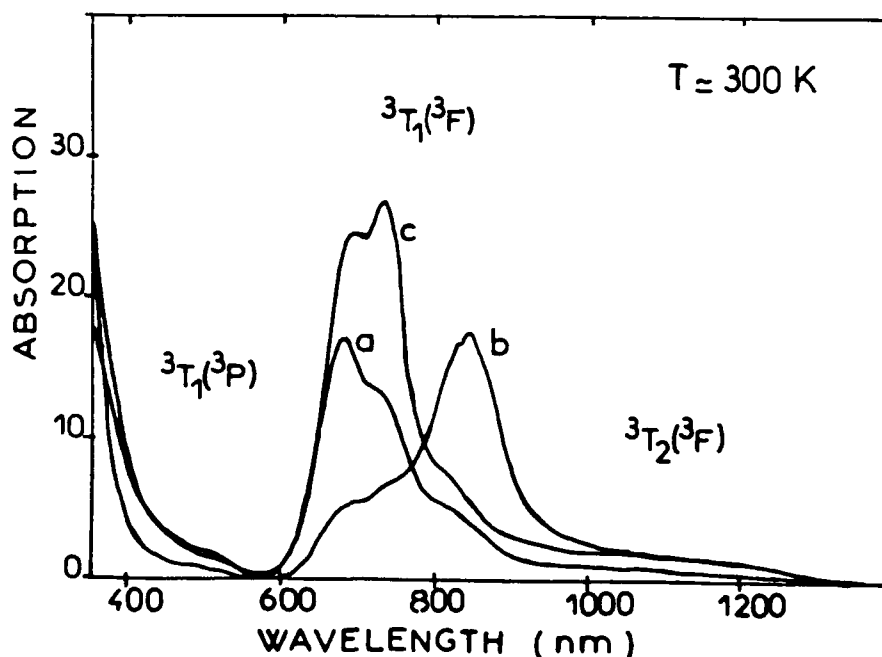


Fig.1: Room temperature polarized absorption spectra of $\text{LiNbGeO}_5:\text{Cr}$ for a) E//a, b) E//b and c) E//c.

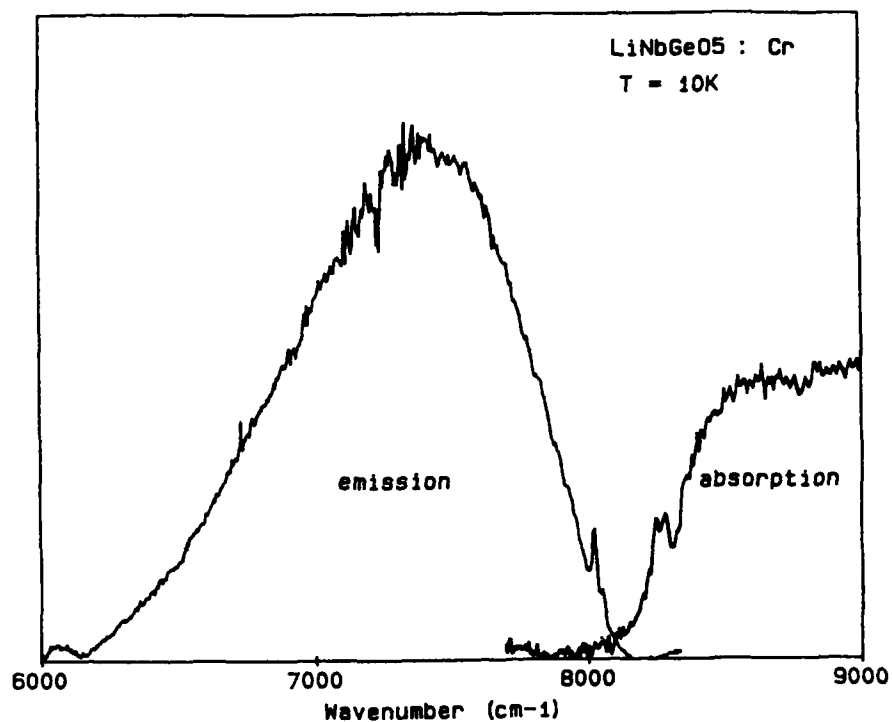


Fig.2: Low temperature infrared absorption and emission spectra (E/c) of LiNbGeO₅:Cr.

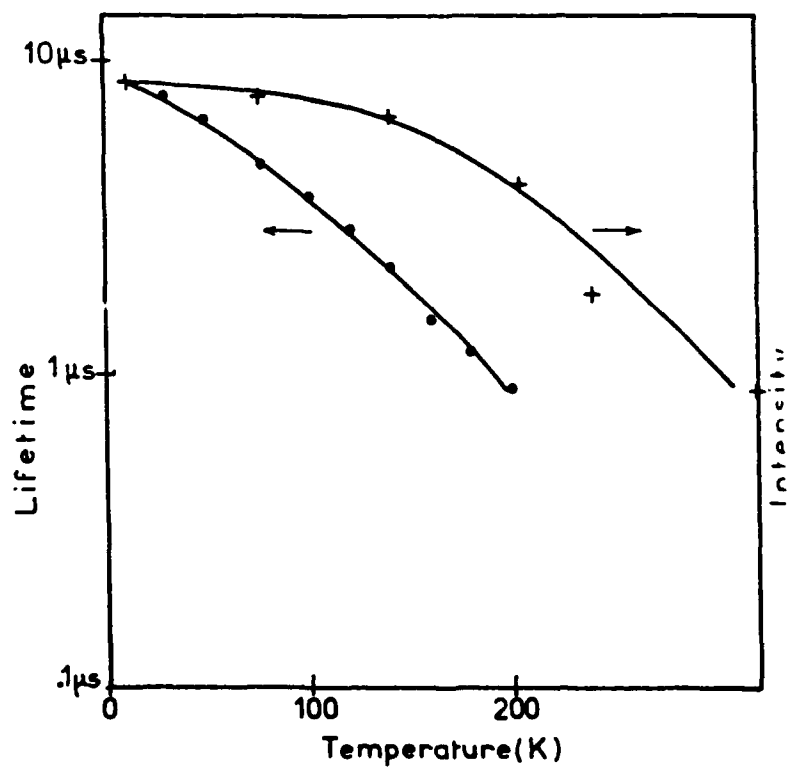


Fig.3: Temperature variations of the infrared emission intensity and lifetime in LiNbGeO₅:Cr.

Gain Measurements and Average Power Limitations in $\text{Cr}^{3+}:\text{LiSrAlF}_6$

F. Hanson and C. Bendall
NCCOSC/RDTE
Code 843
San Diego, CA 92152
(619) 553-5720

Introduction

The chromium doped colquiriites have received considerable attention due to their potential as efficient tunable laser sources in the near-IR which could be frequency doubled into the blue-green spectral region. There is particular interest in the long wavelength tunability of these materials which might allow a single frequency doubled laser to operate in the ocean water transmission window from 450 nm to 500 nm. There are, however, some critical issues which may limit their usefulness in certain applications. Excited state absorption (esa) is present to some degree in all Cr^{3+} based laser materials. Rapoport¹ has measured significant esa in $\text{Cr}:\text{LiSrAlF}_6$ which effectively reduces the cross section by ~40% at 850 nm and indicates that the long wavelength gain may be even more strongly reduced. Excited state upconversion can also reduce efficiency in situations of very strong pumping.¹ In spite of these effects, very efficient $\text{Cr}:\text{LiSrAlF}_6$ lasers have been demonstrated. A more serious problem is the limitation of average power due to the poor thermal conductivity and fracture toughness of this class of materials.²

In a flashlamp pumped rod-geometry we have measured gain for $\text{Cr}:\text{LiSrAlF}_6$ ($\text{Cr}:\text{LiSAF}$) and $\text{Cr}:\text{Li}(\text{Sr}_{1-x}\text{Ca}_x)\text{AlF}_6$ ($\text{Cr}:\text{LiSCAF}$) over a substantially larger wavelength range than has been reported earlier.^{1,3} We also have found a slight gain decrease with flashlamp repetition rate up to the point where thermal fracture occurs. Similar measurements with $\text{Cr}:\text{LiSrGaF}_6$ will also be discussed.

Experiment

The gain measurements were made with a tunable cw Ti:Sapphire probe laser using long wavelength mirrors which allowed operation out to 1000 nm. The 3 x 1/4 inch $\text{Cr}:\text{LiSAF}$ and $\text{Cr}:\text{LiSCAF}$ a-axis laser rods were pumped in a dual lamp diffuse reflecting Kigre pump head. The optical layout is shown in Fig. 1. A nominal half-wave plate was used to rotate the polarization of the cw probe beam and a Glan-Thompson broad-band polarizer gave the desired linear polarization, either parallel or perpendicular to the crystal c-axis. The probe beam was TEM_{00} with a waist diameter of ~3 mm. An integrating sphere and silicon photodiode were placed ~1.5 meter from the laser rod and an aperture and long wave pass filter were used to reduce unwanted light from the flashlamp and fluorescence.

The flashlamps were driven at 40 Joules total energy in ~70 μs long pulses (FWHM) at 4 Hz repetition rate. The relevant signals were averaged on a digital oscilloscope. At each wavelength the cw probe signal intensity was recorded without flashlamp pulses, and the signal during the flashlamp pulse was recorded with and without the probe beam. All signals were averaged for several seconds and peak intensities during the flashlamp pulses were recorded. The flashlamp component was subtracted from the amplified signal and the single pass gain shown in Fig. 2 was obtained.

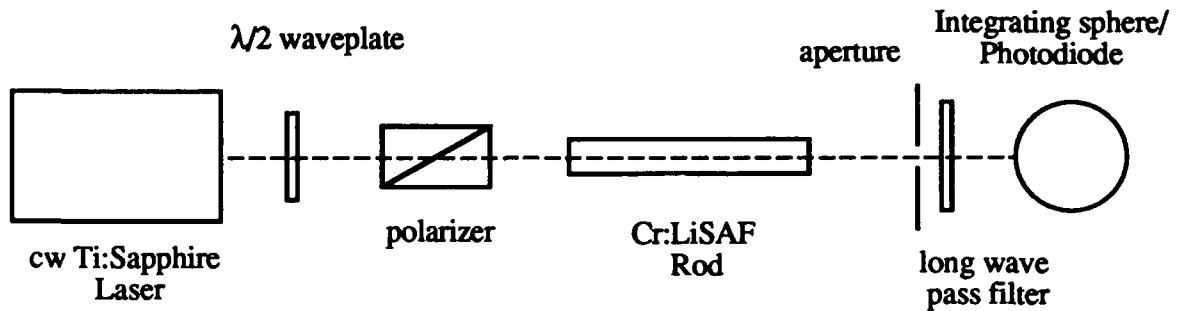


Figure 1. Experimental layout for measuring gain.

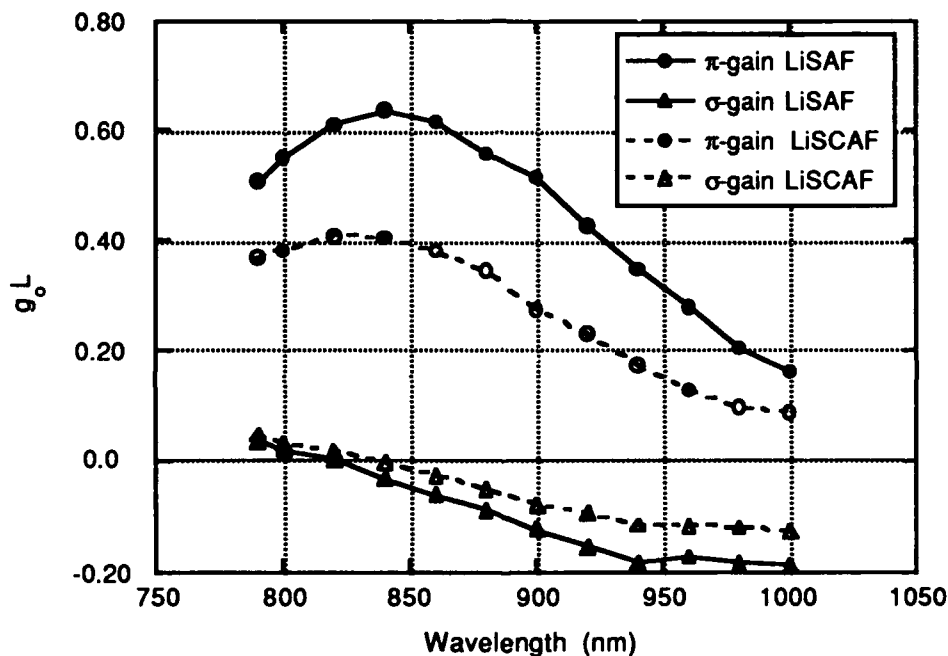


Figure 2. Single pass small signal gain at 40J lamp energy.

It is apparent that substantial gain for π -polarization exists out to beyond 1 μm . For Cr:LiSAF, $g_0 = N(\sigma_\pi - \sigma_{\pi, \text{esa}})$ at 1 μm is 25% of the peak value at 840 nm. This implies that the esa spectrum is not substantially broader than the emission cross section spectrum.⁴ The Cr:LiSCAF material gave similar results although the gain was considerably less because of lower doping. This particular crystal had a high Sr/Ca ratio. Further measurements with Cr:LiSrGaF₆ will be reported.

Thermal issues with flashlamp pumped Cr:LiSAF were examined by measuring small signal gain vs. flashlamp repetition rate. A similar experiment was performed except that a collimated laser diode emitting at 830 nm was used as the signal probe. The flashlamps were run at 40 J and the water/ethylene glycol coolant was maintained at 20°C. The measured gain shown in Fig. 3 decreases slightly with average flashlamp power up to the point of rod fracture which

occurred at 18 Hz. These results are consistent with the known fluorescence quenching with temperature of Cr:LiSAF and the general material properties of the colquiriites.²

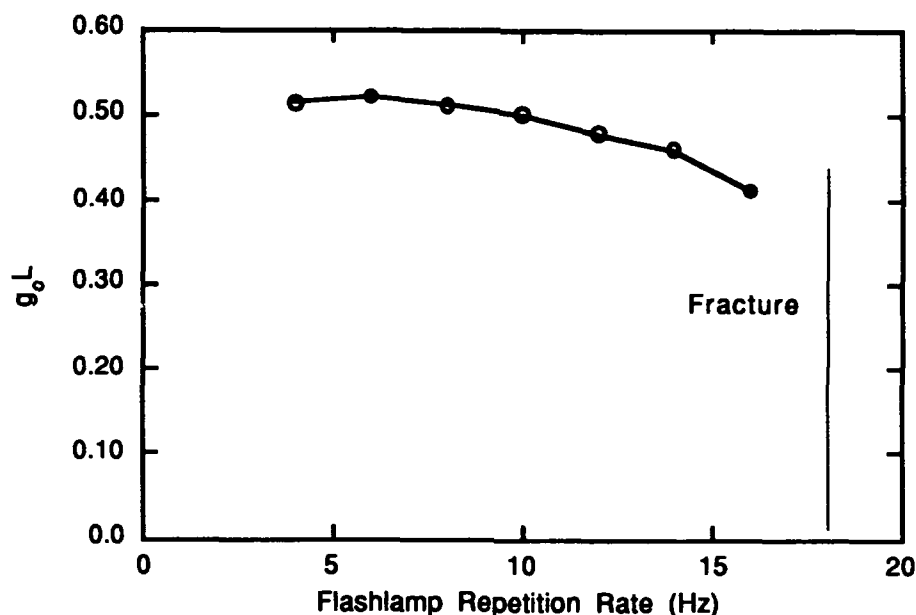


Figure 3. Gain vs. flashlamp repetition rate at 40J lamp energy. Fracture occurred at 18 Hz.

Conclusion

Long wavelength operation of Cr:LiSAF should not be a problem if sufficiently low loss material is used. On the other hand, the problem of thermal fracture effectively limits conventional flashlamp pumped rod geometries to relatively low repetition rates. Alternative geometries using thin slabs would allow higher average power and additional work in this area will be discussed.

References

- ¹ W. R. Rapoport, "Excited State Absorption and Upconversion in Cr:LiSAF," Advanced Solid State Lasers, Santa Fe, NM, (1992)
- ² B. W. Woods, S. A. Payne, J. E. Marion, R. S. Hughes, and L. E. Davis, "Thermomechanical and thermo-optical properties of the LiCaAlF₆:Cr³⁺ laser material," J. Opt. Soc. Am. B, 8, p. 970 (1991).
- ³ P. Beaud, Y.-F. Chen, B.H.T. Chai, and M. C. Richardson, "Gain Properties of LiSrAlF₆:Cr³⁺," Opt. Lett. 17, p. 1064, (1992).
- ⁴ S. A. Payne, L. L. Chase, L. K. Smith, W. L. Kway, and H. W. Newkirk, "Laser performance of LiSrAlF₆:Cr³⁺," J. Appl. Phys. 66, p. 1051, (1989).

Flashlamp Pumped Narrow Linewidth Ti:Al₂O₃ Laser

H.Takeda, F.Kannari, and M.Obara

Department of Electrical Engineering,
Keio University, 3-14-1 Hiyoshi, Kohoku-ku Yokohama 223, JAPAN

Many applications of pulsed Ti:Al₂O₃ laser, e.g. coherent remote sensing such as DIAL or wavelength conversion by nonlinear processes, always require high spectral brightness. A single-longitudinal-mode pulsed Ti:Al₂O₃ oscillator has been developed by using a pulsed laser pumping [1]. However, higher outputs of laser pumped Ti:Al₂O₃ require multiple pump sources and the use of several laser-pumped amplification stages. In contrast, flashlamp-pumped Ti:Al₂O₃ lasers can be scaled to high energies with less difficulty while maintaining a relatively compact and simple system [2, 3]. Moreover, a longer pumping pulsewidth of a flashlamp-pumping than a laser build-up time allows more cavity round trips and easily attains the narrow linewidth operation compared with the laser pumping where lasers are operated in gain switching.

Our studies are directed towards the direct oscillation of a narrow linewidth, tunable, pulsed high power Ti:Al₂O₃ laser with > 100 mJ energy level. The same technologies developed for the Ti:Al₂O₃ material are applicable to Cr:LiSAF or Cr:LiCAF materials that can exhibit more efficient operation with the flashlamp-pumping.

First, we attempted to use a grazing-incident grating cavity with a small incident angle. The grazing-incident grating is usually used at ~89 degree of incident angle [1] to obtain a large angular dispersion. However, such a large incident angle results in a small cavity feedback ~4%. Since a gain-length product of a flashlamp-pumped Ti:Al₂O₃ laser is low $g_0l \sim 2$ [3], ~4% feedback is too small to obtain the efficient laser. Therefore, in our Ti:Al₂O₃ oscillator a 50-mm wide, 1800 grooves/mm holographic grating is applied with a relatively small incident angle of 82 degree, which gives ~25% feedback. The decrease of the angular dispersion at the small incident angle can be compensated by many round-trips allowed in the flash-lamp pumping. The laser output is coupled in zeroth order diffraction because amplified spontaneous emission is still low in our oscillator.

In our flashlamp-pumped Ti:Al₂O₃ oscillator, a 6.35-mm dia., 7.66-cm long (active length of 6.8-cm), [Ti]=0.1 wt.%, FOM=90 (nominal) Ti:Al₂O₃ rod (Union Carbide) is pumped by six Xe-flashlamps with a 5-mm bore dia., 10.2-cm arc length (ILC model 5D4). The pump cavity is a close-coupled type with diffuse reflectors made of PTFE located closely around each lamp. The distance between the lamp and the laser rod is 21 mm. An ethanol solution of laser dye LD490 at 1.0×10^{-3} mol/l is flowed in the space between the diffuse reflector and the rod as a fluorescence converter to shift part of the ultra-violet emission of the flashlamps into the absorption band of Ti:Al₂O₃. The flashlamp excitation circuit consists of a low energy predischage circuit with a 10.2 nF capacitor charged at 18 kV and a main discharge

circuit with a 1 μ F capacitor charged at 6-10 kV, one connected to each lamp. All six main discharge capacitors are discharged by one common spark gap with a few microsecond delay relative to the predischage.

A small-signal net gain was measured to $g_0 \sim 1.75$ at charging voltage of 10 kV by using a diode laser probe at 789 nm. Employing a stable resonator consisting of a 5-m curvature concave total reflector and a 70 % reflectivity plain output coupler with a cavity length of 40 cm, the maximum laser output of 290 mJ at 300 J input energy to the flashlamps. The corresponding slope efficiency 0.1 % was obtained.

In the narrow linewidth operation by using the reduced angle grazing incidence grating, a 5-m curvature concave total reflector was located 60 cm apart from the grating mirror. When the laser was tuned at $\lambda = 794.2$ nm, the maximum laser output energy of 120 mJ with the slope efficiency of 0.06 % was obtained. At reduced input energy of 192 J, the spectral linewidth less than 0.2 nm that is a instrument limit of our spectrometer was obtained.

the theoretical linewidth $\Delta\lambda$ is obtained for the grazing incident grating cavity as [4]:

$$\Delta\lambda = \frac{1}{R} \left(\frac{d \cos \alpha}{2m} \right) \Delta\theta.$$

Here, R is the number of cavity round trips before saturation, d is the groove spacing of grating, α is the incident angle, m is the diffraction order, $\Delta\theta$ is the beam divergence. Applying our cavity parameters together with a measured beam divergence of 3.6 mrad, the theoretical linewidth of $0.14/R$ nm is estimated. The relatively large beam divergence that is ten times larger than the diffraction limit was resulted from the 5-m curvature of the total reflector.

We have also applied an integrated MOPA-type cavity to the flashlamp pumped Ti:Al₂O₃ laser to obtain efficient spectral selection with keeping the high output laser energy. In this system, a central part of the laser rod act as a master oscillator with a convex mirror and a grazing incident grating mirror coupled through a hole opened in a concave total reflector, whereas the peripheral part of the laser rod with confocal mirrors forms an amplifier. Experimental results of this hybrid cavity is also described.

References

- [1] K.W.Kangas, D.D.Lowenthal, and C.H.Muller III, Opt. Lett. 14, 21(1989).
- [2] E.G. Erickson, *Technical Digest of Papers Presented at Topical Meeting on Tunable Solid State Lasers, North Falmouth, MA, 1989*, Optical Society of America, Washington(1989) , Paper MCI-1.
- [3] A.J.W. Brown, C.H. Fisher, K.W. Kangas, C.H. Muller III, and D.D. Lowenthal, presented at the Conference on Lasers and Electro-Optics, Anaheim, California, 21-25 May 1990.
- [4] F.J. Duarte and L.W. Hillman ed. *DYE LASER PRINCIPLES* , ACADEMIC PRESS,INC.

Mode-Locking of Near Infrared Lasers with
 V^{3+} :YAG Crystal as a Saturable Absorber

V.P.Mikhailov, N.I.Zhavoronkov, N.V.Kuleshov,
 V.A.Sandulenko, K.V.Yumashev and P.V.Prokoshin

Institute for Applied Physics Problems, Belarusian State
 University, Kurchatov str. 7, Minsk 220064, Belarus

Tel. (0172)-785726

Saturation of near infrared absorption was investigated recently in tetravalent chromium doped garnets [1] and forsterite [2]. These systems were shown to be effective solid state saturable absorbers for neodymium lasers. In this paper we report on vanadium doped YAG as a new solid state passive shutter for near infrared laser systems.

Tetrahedral V^{3+} ion which has $3d^2$ electron configuration is characterized by two strong broad absorption bands in near infrared region with peaks at $1.3 \mu m$ and $0.83 \mu m$ (Fig.1). These bands are assigned to transitions from 3A_2 ground state to the excited states 3T_2 and 3T_1 , respectively. Saturation of absorption was observed for both these transitions. The results for crystal transmittance as a function of incident energy density of 20 ps mode-locked Nd-YAlO₃ laser beam at $1.08 \mu m$ is depicted in Figure 2. The best fit of the theoretical curve calculated from modified Frantz-Nodvik equation [3] to the experimental points was obtained for the saturation energy density of about $0.024 \pm 0.002 \text{ J/cm}^2$. This results in the absorption cross section value at $1.08 \mu m$ of about $8.2 \pm 0.8 \times 10^{-18} \text{ cm}^2$.

An upper limit for intra 3T_2 state vibrational relaxation

time was estimated to be 10 ± 5 ps from picosecond pump-and-probe relaxation measurements.

Mode-locked and Q-switched laser operations were obtained using V^{3+} :YAG as a saturable absorber for Ti-Al₂O₃ laser at 770 nm and Pr-YAlO₃ laser at 747 nm. $^3A_2 - ^3T_1$ transition of the absorber was excited by the emission of these lasers. Ultrashort pulses observed were 0.3 - 0.5 ns in duration and 0.5 mJ in energy for both these lasers. Q-switched pulses with energy up to 5 mJ were 50 - 80 ns in duration for Pr-YAlO₃ laser and of about 300 ns for Ti-Al₂O₃ laser.

Mode-locked laser operation was realised also for 1.34 μ m Nd-YAlO₃ and 1.06 μ m Nd-YAG lasers. Train of ultrashort pulses with total energy of about 8 mJ was observed at 30 J pump energy for Nd-YAlO₃ laser. Single pulses were 0.1 - 0.3 ns in duration.

References

1. M.I.Demchuk, N.V.Kuleshov, V.P.Mikhailov, A.I.Mitkovets, P.V.Prokoshin, V.A.Sandulenko, A.P.Shkadarevich, and K.V. Yumashev. Zh. Prikl. Spektrosk. (USSR), 51, 377 (1989).
2. M.I.Demchuk, V.P.Mikhailov, N.I.Zhavoronkov, N.V.Kuleshov, P.V.Prokoshin, K.V.Yumashev, M.G.Livshits, and B.I.Minkov. Opt. Lett. 17, No 13 (1992).
3. W.Rudolph and H.Weber. Opt. Commun. 34, 491 (1980).

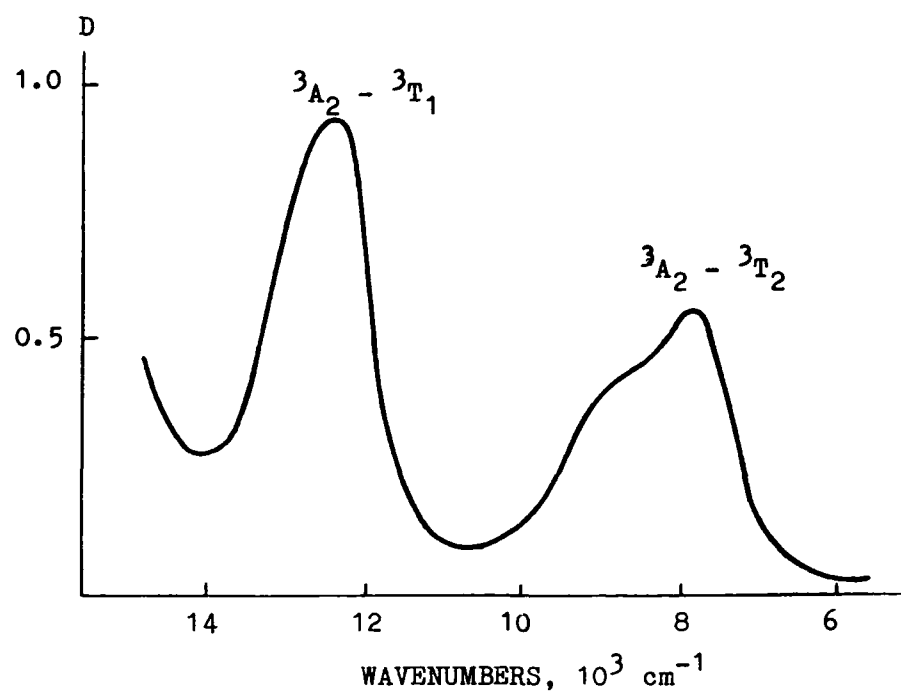


Fig. 1. Absorption spectrum of V³⁺:YAG

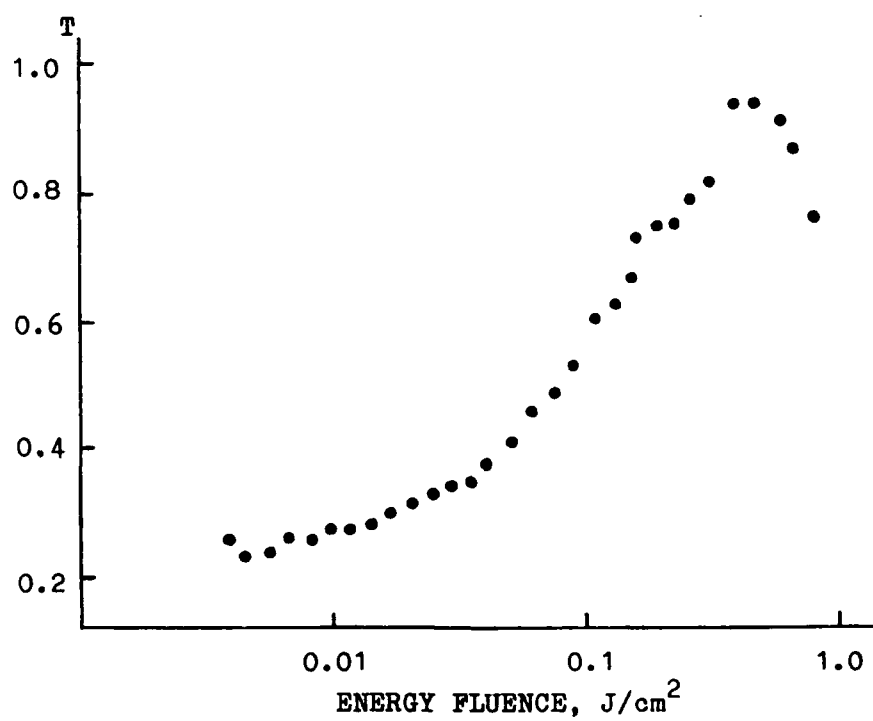


Fig. 2. Saturable absorption data.

Tuesday, February 2, 1993

LiSAF Lasers

ATuF 4:00pm–5:30pm
La Salle Ballroom B&C

James C. Barnes, *Presider*
National Aeronautics & Space Administration

Terawatt Cr:LiSrAlF₆ Laser System

T. Ditmire, H. Nguyen, and M. D. Perry

Lawrence Livermore National Laboratory
P.O. Box 808, L-395, Livermore, CA 94550

Summary

The development of the new solid state laser material, Cr:LiSAF¹, offers an important alternative for short pulse laser applications. Like Ti:Sapphire, LiSAF exhibits a broad bandwidth, and is tunable from 760 to 950 nm. Unlike Ti:Sapphire, it has a long upper state lifetime of approximately 60 μ sec and, therefore, can be flashlamp pumped. This advantage, couple with the fact that LiSAF has a low nonlinear refractive index and low thermal lensing, make it an ideal candidate for high-power, femtosecond laser systems.

Using the technique of chirped pulse amplification we have developed a one hundred femtosecond laser system capable of producing peak powers in excess of a terawatt. Since the effective gain cross section is low, (3.3×10^{-20} cm²), a multipass amplifier is required to achieve the gains necessary to raise pulse energies to the multi-millijoule level. We have developed a Cr:LiSAF regenerative amplifier that produces a pulse energy above 8 mJ at a repetition rate of 5 Hz.³ These pulses are then further amplified at 1 Hz in two Cr:LiSAF power amplifiers, yielding 300 mJ. Recompression produces a 150 mJ pulse with a near transform limited pulsewidth of 135 fsec.

The optical layout of the LiSAF system is shown in Fig 1. We start with a 76 MHz pulse train of 100 fsec pulses from a self mode-locked Ti:Sapphire oscillator pumped by 8W from an argon-ion laser. The oscillator is tuned to 825 nm, the gain peak of LiSAF. These 5 nJ pulses are four passed through an 1800 line/mm grating pair pulse stretcher. The stretcher produces a positively chirped pulse close 400 psec in duration.

The beam then enters a TEM₀₀ stable ring regenerative amplifier cavity. The seed pulses enter the cavity through a brewster angle polarizer. A single crystal $\lambda/2$ Pockels cell acts as a pulse selector and also switches the pulse out of the cavity after amplification. The stretched single pulse is amplified in a 4mm diameter LiSAF rod which has a single pass small signal gain of 3.2. The pulse is passed around the cavity 34 times bringing the energy to 8 mJ before cavity dumped. At this level we remain well below the saturation fluence of LiSAF. This is important so as to prevent pulse shape distortion resulting from gain saturation which would result in a corresponding spectral distortion of the temporally chirped pulse. Avoiding this is necessary to maintain a clean, high contrast pulse form upon recompression. Gain narrowing in the LiSAF is negligible for a net gain in the regenerative amplifier of 10^7 .

The pulse from the regenerative amplifier is then passed through a serrated aperture which clips approximately 50% of the input energy. The image of this aperture is then relayed with magnification through the remainder of the amplifier system. This scheme permits us to amplify a near flattop beam in the laser rods allowing a larger fill of the rod diameter and greater energy extraction. After being clipped in the serrated aperture, the pulse passes through an air spatial filter that expands the spatial profile of the pulse by a factor of 3. The pulse is double passed through a 9.5 mm diameter LiSAF rod. A polarizer, Faraday rotator, and half waveplate serve to extract the pulse after the second pass.

This amplifier is pumped with four flashlamps by 600 J of electrical energy. The flashlamp intensity pulse shape has been specifically tailored to the upper state lifetime of the Cr:LiSAF to give maximum energy extraction efficiency. We achieve a double pass net gain of this amplifier of approximately 45. Pulse energies after this amplifier exceed 100 mJ. The pulse is then single passed through another 9.5 mm LiSAF rod. Pumped in a two flashlamp pump head by 180 J of electrical energy, this amplifier yields a single pass gain of 3.2. Output energy after this amplifier is 300 mJ.

A vacuum spatial filter expands the pulse which is then injected into a grating pair pulse compressor. A double pass through the 1800 lines/mm grating pair has an energy efficiency of 55%. The result is recompressed pulse energies of 150 mJ. Autocorrelation of the recompressed pulse, shown in figure 2, indicates a FWHM pulse width of 135 fsec. The amplified pulse spectrum is shown in figure 3. The time bandwidth product of the amplified pulse is .36 indicating a transform-limited pulse. The system repetition rate is 1 Hz.

- ¹ S. A. Payne, L.L. Chase, L. K. Smith, W.L. Kway, and H. W. Newkirk, J. Appl. Phys. **66**, 1051 (1989).
- ² D. Strickland and G. Mourou, Opt. Commun. **56**, 219 (1985).
- ³ M. D. Perry, D. Strickland, T. Ditmire, and F.G. Patterson, Opt. Lett. **17**, 604 (1992).

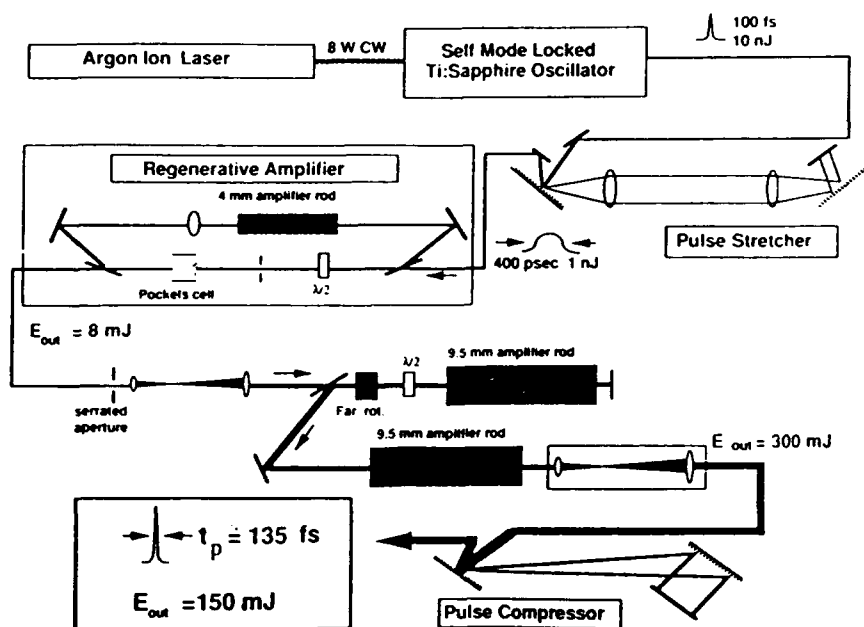


Figure 1. Cr:LiSAF Laser System Layout

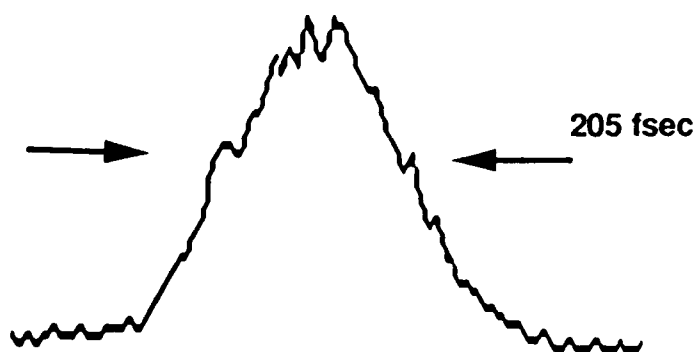


Figure 2. Recompressed Pulse Autocorrelation

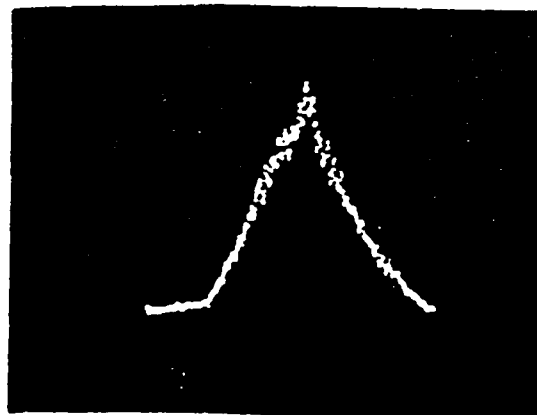


Figure 3. Amplified Pulse Spectrum (Centered at 825 nm)

Generation Of Tunable Pulses As Short As 33 Fs From Cr:LiSrAlF₆ Lasers

N. H. Rizvi, P. M. W. French and J. R. Taylor

Femtosecond Optics Group, Physics Department,
Imperial College, London SW7 2BZ, U.K.

Tel. : 071-589 5111 ext. 6811 Fax. : 071-589 9463 Telex: 929484 IMPCOL G

The recent demonstrations of femtosecond Titanium-doped sapphire lasers yielding pulses as short as ~15 fs [e.g. 1-4], fuel the excitement in the quest for new broadband solid-state laser media. The dye laser will be largely superseded in ultrafast laser applications where, with the same pump laser, the Ti:Al₂O₃ laser offers superior performance in terms of convenience, stability, pulse duration and energy.

Cr³⁺:LiSrAlF₆ is an attractive alternative to Ti:sapphire, lasing across almost the same spectral range (760-920 nm) but exhibiting a longer upper-state lifetime and red-shifted absorption profile, permitting it to be efficiently pumped by laser diodes at 670 nm and by flash-lamps or arc-lamps. In principle, an all-solid-state diode-pumped tunable femtosecond laser system could be realised - with Cr:LiSrAlF₆ providing the gain media in both amplifiers [5] and oscillators where the relatively long upperstate lifetime confer higher energy storage and lower laser threshold than Ti:Al₂O₃. Mode-locked operation and intracavity frequency doubling would permit the construction of a compact, diode-pumped efficient blue laser source.

The observation of self-mode-locking in Ti:Al₂O₃ has led to the realisation that the nonlinear refractive index of the laser medium can be used to provide both amplitude

modulation, through self-focussing or "Kerr Lens Mode-locking" (KLM) [2], and phase modulation which, together with group velocity dispersion, can lead to further pulse compression. These mode-locking techniques are generally applicable to vibronic solid-state laser media eg. krypton ion-pumped Cr:LiSrCaAlF₆ [6].

Here we report on a c.w. Cr³⁺:LiSrAlF₆ laser pumped, for the first time, by the 488 nm output from a low power argon ion laser. This laser was passively mode-locked through the optical Kerr effect and the mode-locking was initiated using a dye jet stream of neocyanine. For absorbed pump powers of only 500mW (within the reach of diode lasers), pulses of less than 50 fs were routinely generated. The laser was self-starting and exhibited excellent stability. After optimising the second and third order dispersion of the system, close-to-transform-limited pulses as short as 33 fs duration, assuming a sech^2 pulse profile, were obtained. Figure 1 shows a typical interferometric autocorrelation trace. The Cr:LiSrAlF₆ laser rod used in these experiments was 20 mm long and doped to a molar Cr³⁺ concentration of 1.5 %. We note that Cr:LiSrAlF₆ does not exhibit concentration quenching and that doping levels as high as 20 % are not unreasonable. This should permit our 20 mm long laser rod to be replaced by a rod of ~ 1 mm with the corresponding reduction in the net intracavity third order dispersion [4]. Thus it should be possible to generate considerably shorter pulses using this laser medium. What is more significant for most laser users, however, is that the femtosecond pulses were generated for as little as 500 mW pump power - well within the range of reported 670 nm diode lasers. [7]

In this Cr:LiSrAlF₆ laser, the saturable absorber in the laser cavity (which exhibits a low-level absorption loss of only 1 %) appears to provide a weak modulation, sufficient to initiate the pulse formation, and also tends to stabilize the laser by suppressing the evolution of unwanted satellite structures. Using a fast saturable absorber, rather than relying only on KLM, means that the laser is not critically sensitive to alignment and can be routinely switched on with femtosecond pulse generation. Evidence of self-focussing acting to compress the pulses, however, has been noted and this mechanism certainly plays a role in the generation of

sub-100 fs pulses. We will describe the optimisation of this Cr:LiSrAlF₆ laser and will report on our recent work with alternative Cr³⁺-doped parents.

References

- 1) N.Sarukura, Y.Ishida, H.Nakano, Opt.Lett. **16**, 153-155 (1991)
- 2) D.K.Negus, L.Spinelli, N.Goldblatt, G.Feugnet, OSA Meeting on Advanced Solid State Lasers, 1991
- 3) C-P Huang, H. C. Kapteyn, J. W. McIntosh and M. M. Murnane, Opt.Lett. **17**, 139-141 (1992)
- 4) Ch. Spielmann, P. F. Curley, T. Brabec, E. Wintner and F. Krausz, Electron. Lett. **28**, 1532 (1992)
- 5) F. Balembois, P. Georges, F. Salin, G. Roger, and A. Brun, Ultrafast Phenomena conference, PDP FC28, 1992
- 6) P. Li Kam Wa, B. H. T. Chai, A. Miller, Electron. Lett. **27**, 2350-2351 (1991).
- 7) H. B. Serreze, C. M. Harding and R. G. Waters, Electron. Lett. **27**, 2246 (1991)

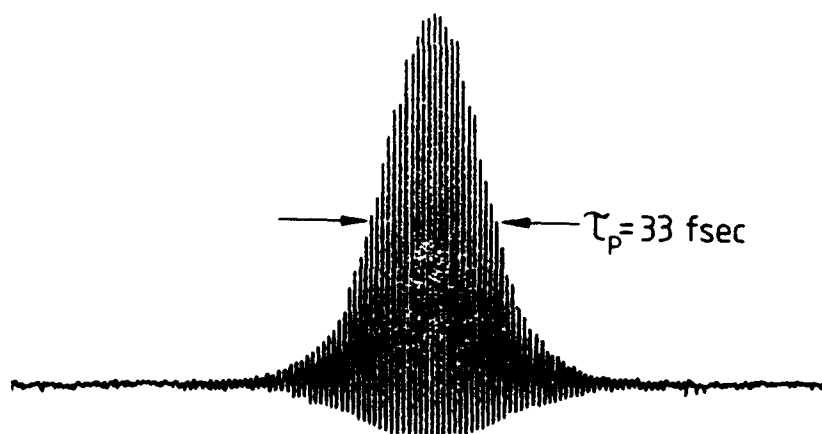


Figure 1 Interferometric autocorrelation trace of 33 fs pulses obtained from the passively mode-locked Cr:LiSrAlF₆ laser

High Repetition Rate CW Pumped Cr:LiSAF Femtosecond Regenerative Amplifier

**François Balembois, Patrick Georges, François Salin,
Gérard Roger and Alain Brun**

Institut d'Optique Théorique et Appliquée
Unité de Recherche Associée au CNRS N°14
Université Paris-Sud
B.P. 147

91403 Orsay Cedex, France

Ph: 33-1-69 41 68 56

Fax: 33-1- 69 41 31 92

Jean Luc Tapié

COHERENT Scientifique

Domaine Technologique de Saclay

4 rue René Razel

91892 Orsay Cedex, France

Since its first demonstration by Payne et al at the Lawrence Livermore National Laboratory [1], the $\text{Cr}^{3+}:\text{LiSrAlF}_6$ (LiSAF) crystal has proved to be a promising laser medium. This crystal combines a large fluorescence bandwidth (750-950 nm) with an absorption band in the red between 600 and 700 nm making it particularly suitable for the development of an all solid state diode pumped tunable laser. Due to its extremely large emission band, Cr:LiSAF is well suited to the generation and amplification of ultrashort pulses. Self mode-locking to produce femtosecond pulses has already been demonstrated in Cr:LiSAF [2,3]. Unlike Ti:Sapphire, the long upper state lifetime (67 μs) enables flashlamp pumping and Cr:LiSAF regenerative amplifiers have been developed to produce pulses of several millijoules at low repetition rates [4]. There is now great interest in increasing the repetition rate from amplifier systems. Recently T. Norris demonstrated a regenerative Ti:Sapphire amplifier working at a repetition rate up to 250 kHz and producing 2 μJ amplified pulses [5]. Considering that the long upper state lifetime of the Cr:LiSAF allows a higher energy storage compared to Ti:Sapphire, we have developed a Cr:LiSAF regenerative amplifier pumped by a cw Krypton ion laser. This amplifier operates at 5 kHz and produces 11 μJ pulses.

The schematic of the amplifier is as follows (fig.1). A 15 mm long, Brewster angle cut Cr:LiSAF crystal (from Lightning Optical Corporation) was used in a three mirror linear cavity. These mirrors had a high reflective dielectric coating centered at 820 nm. The length of the cavity was around 1 meter corresponding to a 7 ns cavity round trip time. The crystal was pumped by the red lines of a cw Krypton ion laser and its absorption was around 97%. In order to reduce the thermal load, the pump laser was chopped at 200 Hz with a 1/4 duty cycle. A Pockels cell and a broadband polarizer were used to trap and dump the pulses. Without injection (i.e. in a free running Q-switched configuration), the amplifier produced 11 μJ , 7 ns pulses at 5 kHz and around 830 nm for a pump power of 4 W on the Cr:LiSAF crystal. The spectrum of these pulses was 20 nm wide indicating that the amplifier can support femtosecond pulses. Note that the repetition rate is limited to 5 kHz by the Pockels cell and it should be possible to operate at 14 kHz (corresponding to the inverse of the upper state lifetime) without any decrease in the pulse energy.

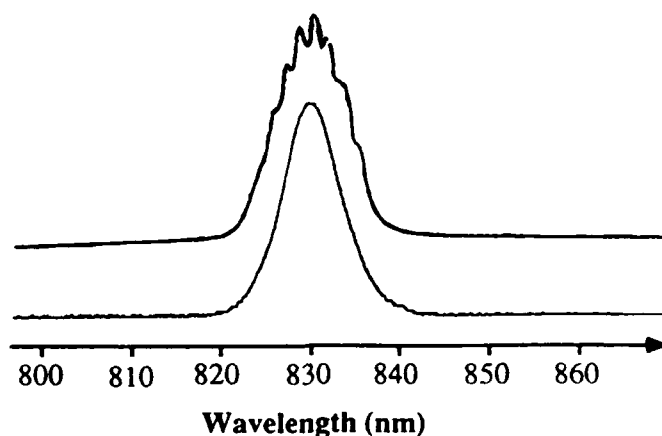


Fig.4: Output spectrum of the amplified pulses (upper curve) and initial pulses (lower curve).

Figure 4 shows that the amplified spectrum matched the spectrum of the MIRA laser pulses. Due to group velocity dispersion in the intracavity elements, the pulses were stretched to around 10 ps. We tried to compress the pulses back to their initial duration with a pair of gratings (2000 T/mm). We obtained a compression to 600 fs but it was not possible to reduce this duration due to space problems between the two gratings. However, without recompression, the amplified beam focused in a water cell can generate a white light continuum.

We observe that, at 4 W pump power the peak power density of the amplified pulses in the LiSAF crystal was so high that the threshold for continuum generation was reached at the end of the amplification. At higher pumping level it will be therefore necessary to increase the spot diameter inside the crystal.

In conclusion, we believe that this high repetition rate Cr:LiSAF regenerative amplifier used in combination with a self mode-locked Cr:LiSAF oscillator will lead in the future to an **all solid state** (including the pump lasers) femtosecond system producing up to 5 μ J pulses at around a 10 kHz repetition rate.

Acknowledgements :

The authors wish to thank the LOA-ENSTA (Palaiseau) and especially J.P. Chambaret for the loan of the Pockels cell.

References :

- [1] S. Payne, L. Chase, L. Smith, W. Kway and H. Newkirk
J. App. Phys, 66 1051 (1989).
- [2] A. Miller, P. LiKamWa, B. Chai and E. Van Stryland
Opt. Lett. 17, 195 (1992).
- [3] N. Rizvi, P. French and J. Taylor
Opt. Lett. 17, 877 (1992)
- [4] M. Perry, D. Strickland, T. Ditmire and F. Patterson
Opt. Lett. 17, 604 (1992)
- [5] T.B. Norris
Ultrafast Phenomena 8, paper MB6 (8-12 June 1992)
- [6] D. Strickland and G. Mourou
Opt. Comm. 56, 219 (1985)

Upconversion in Cr:LiSGaF and Cr:LiSAF.

M. A. Noginov, H. P. Jenssen and A. Cassanho
Center for Materials Science and Engineering
Massachusetts Institute of Technology
Cambridge Ma 02139
Tel.: (617) 253-6878

Chromium doped LiSrAlF₆ (LiSAF)¹ and LiSrGaF₆ (LiSGaF)^{2,3} are emerging new materials for tunable lasers and lasers for ultra short pulses. In these materials the ground state absorption also extends into the region where laser diode pumping is feasible. Strong upconversion has been identified as a potential problem in achieving high inversion levels^{4,5}, especially for the high Cr concentrations needed for laser diode wing pumping.

In the experiments described here, slab samples of Cr:LiSGaF (N_{Cr}=3 to 100%) and Cr:LiSAF (N_{Cr}=7.4%) were excited with a chopped Ar laser beam ($\lambda=488$ nm) at low duty cycle. The maximum available power was equal to ≈ 2 W. The pulse duration was varied from $\approx 10\mu\text{s}$ (short pulse) to $\approx 400\mu\text{s}$ (long pulse). The Ar laser emission was focused to pump the crystal. The minimum spot size diameter was equal to $\approx 40\mu\text{m}$. For low temperature measurements the crystal was placed in a cryostat which allowed the temperature to vary in the range of 77 to 300K.

The Cr luminescence decay curves for 10% and 100% Cr doped LiSGaF at T=300K are shown in Fig. 1. At low excitation density (curves 1 and 4) the decays are exponential with life times $t \approx 85\mu\text{s}$ and $70.5\mu\text{s}$ respectively. Curves 2, 5 and 3, 6 correspond to higher pump density; pump pulse widths were equal to $11\mu\text{s}$ and to $350\mu\text{s}$ respectively. In both cases the maximum Cr population was kept the same, $\approx 5 \cdot 10^{18} \text{ cm}^{-3}$. The experimentally observed shortening of the effective decay time is typical for systems with upconversion.

It has been shown⁶, that in the case of a static upconversion process (no energy migration) a linear relationship should result when we plot:

$$\frac{n_0 \exp(-t/\tau)}{n(t)} - 1 \text{ vs } \text{erf}(\sqrt{t/\tau}) \quad (1)$$

In the case of migration controlled upconversion a linear relationship results when we plot:

$$\frac{n_0 \exp(-t/\tau)}{n(t)} - 1 \text{ vs } 1 - \exp(t/\tau) \quad (2)$$

where τ is the life time in the absence of upconversion; $n_0=n(0)$ is the population of excited ions at the end of the pump pulse.

The results for the short pump pulse and moderately high excitation density ($n_0 \approx 5 \cdot 10^{18} \text{ cm}^{-3}$) are shown in Fig. 2. As can be seen in Fig. 2a we have a linear relationship for the 100% Cr when the kinetics is plotted according to (2) and far from linear when plotted according to (1). From this we can conclude that in this particular case the upconversion is the migration controlled process, the rate of upconversion can be described in terms of αn^2 . The value of the upconversion parameter α (obtained from the tangent of angle ϕ in Fig. 2a) is equal to $\approx 2.2 \cdot 10^{-15} \text{ cm}^3/\text{s}$. This value is in good agreement with the value published in Ref. 5 ($3 \cdot 10^{-15} \text{ cm}^3/\text{s}$).

In lower doped crystals the luminescence kinetics behave quite differently. Figure 1 shows that in 10% Cr:LiSGaF crystal the luminescence kinetics after the short pump pulse (curve 5) has a shorter effective decay time than the kinetics after the long pump pulse (curve 6). In this case, as in the case of Cr(100%):LiSGaF, the initial population level n_0 was kept the same for both curves 5 and 6. Note that in this crystal the upconversion kinetics after the short pulse does not give a linear relationship for either (1) nor (2) (Fig.2b). Thus, in this crystal we have some intermediate case between static and migration controlled upconversion energy transfer. For the range of Cr concentrations used it was found that the lower the concentration is the further we move away from the migration controlled upconversion. The upconversion constant α is only defined if we have a linear relationship when the kinetics is plotted according to (2). Since the value of α is proportional to $\tan \phi$, we see from Fig. 2b (10% Cr) that we can have an error of three times depending on how we fit the data to a straight line. The dependence of the effective values of α , with the appropriate error bars, vs. Cr concentration in LiSGaF is presented in Fig.3. The value of α we measured in Cr(7.4%):LiSAF, $\alpha=1.1 \cdot 10^{-15} \text{ cm}^3/\text{s}$, is comparable to, within the same error bars, the value in Refs. 4 and 5.

The value of the upconversion micro parameter $C_{da}=1.2 \cdot 10^{-37} \text{ cm}^6/\text{s}$ evaluated from the luminescence kinetics ($\tan \delta$ in Fig. 2b) with the assumption of the dipole-dipole mechanism for the energy transfer, seems to be unusually high. Nevertheless, this value is reasonable taking into account the high value of the upconversion parameter α as measured in Cr:LiSGaF crystals.

Low temperature measurements of LiSCrF₆ shows that the effect of upconversion decreases with decreasing temperature. The low temperature luminescence kinetics plotted according to (1) and (2) look more like the curves of Fig. 2.b than the curves of Fig 2.a. Moreover, the measured values of the upconversion micro parameter C_{da} decrease with the decrease of temperature, Fig. 4. Thus, apparently, both a decrease in the migration rate and a decrease in C_{da} are responsible for the low efficiency of upconversion in the low temperature case.

As it was stated above, at room temperature and at moderate levels of populations ($n_0 < 1 \cdot 10^{19} \text{ cm}^{-3}$) the upconversion in the Cr(100%):LiSGaF is a migration controlled process. Nevertheless, at higher excitation density ($n_0 \approx 2 \cdot 10^{19} \text{ cm}^{-3}$) the average distance between excited ions becomes smaller, and the contribution from the direct upconversion to the net kinetics becomes comparable with the migration one. This leads to the changing of the luminescence decay curve shape: it looks similar to the case of Fig. 2.b but not to Fig. 2.a.

In conclusion we have shown that the use of an upconversion constant is not always valid. In our case it is only valid for 100% Cr, for a moderate population density and at near room temperature. In all other cases the upconversion rate can not be described by αn^2 .

1 S. A. Payne et al. IEEE J.Q.E. 24, 2243 (1988)

2 S.A.Payne, et al. in OSA Proceedings on Advanced Solid-State Lasers, 1991 Vol. 10, pp 14-17.

3 A. Cassanho et al. in OSA Proceedings on Advanced Solid-State Lasers, 1992 Vol. 13, pp.2-4.

4 M. A. Noginov et al. in OSA Proceedings on Advanced Solid-State Lasers, 1991 Vol. 10, pp.21-24.

5 W. R. Rapoport in OSA Proceedings on Advanced Solid-State Lasers, 1992 Vol. 13, pp.21

6 D. A. Zubenko et. al., Laser Physics (to be published).

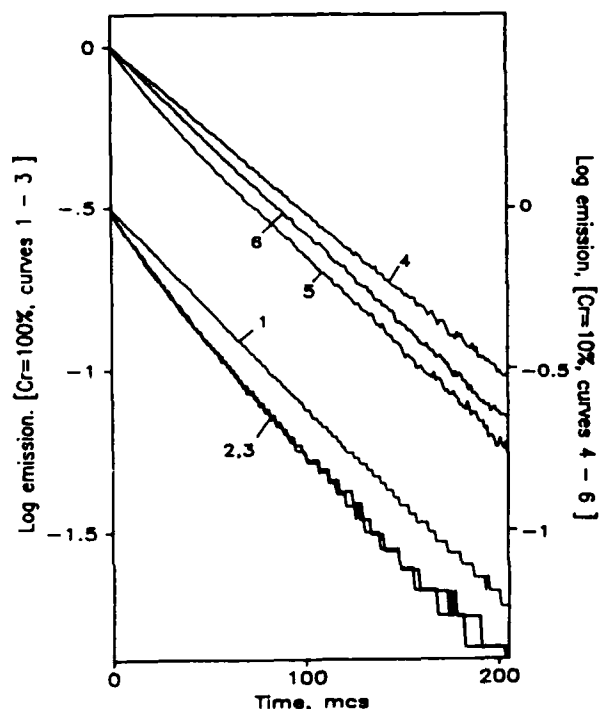


Figure 1. Kinetics of Cr luminescence in Cr:LiSGaF after short pump pulse $\sim 11 \mu\text{s}$ (curves 1,2,3,4) and after long pump pulse $\sim 350 \mu\text{s}$ (curves 3,6) at room temperature. 1,2,3 - $N_{\text{Cr}}=100\%$; 4,5,6 - $N_{\text{Cr}}=10\%$; 1,4 - weak pumping; 2,3,5,6 - relatively strong pumping; the maximum population of excited ions was kept the same in both cases of 2 and 3 and in both cases of 5 and 6.

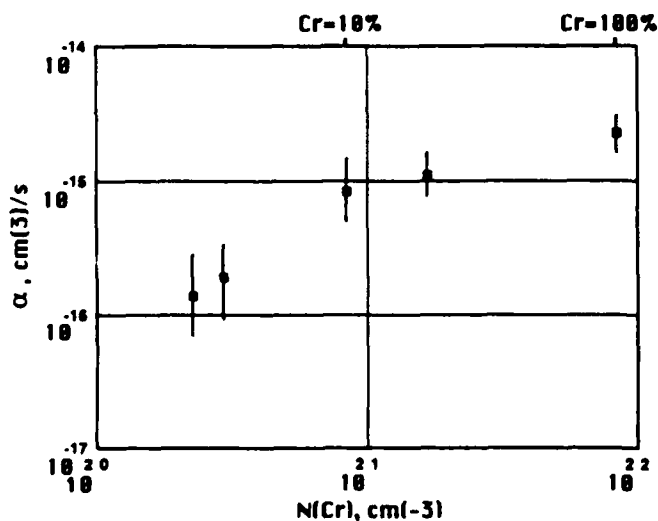


Figure 3. The dependency of upconversion parameter α on Cr concentration in Cr:LiSGaF.

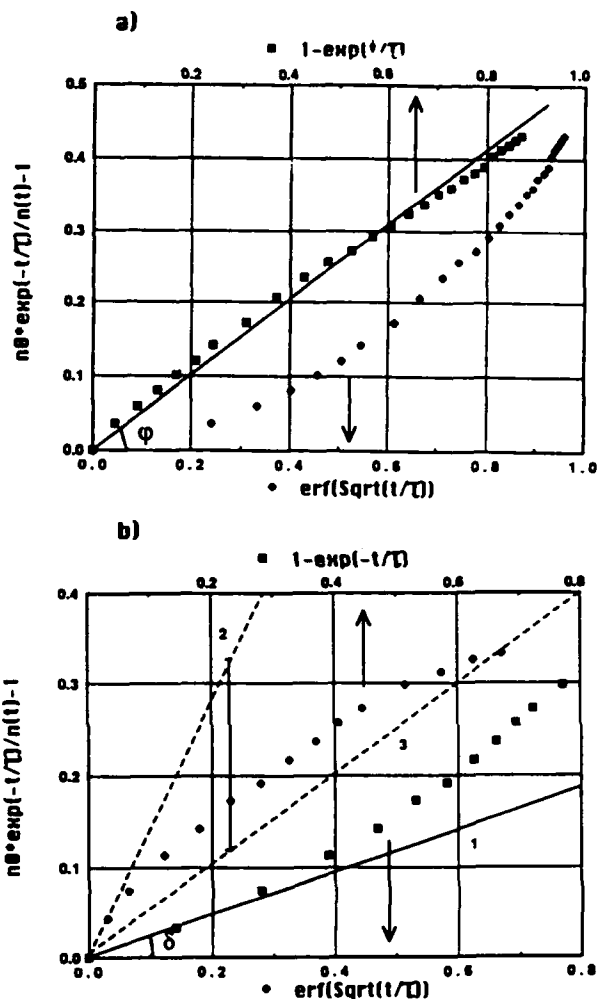


Figure 2. The room temperature kinetics of Cr luminescence in Cr:LiSGaF after a short pump pulse; $n_0 \exp(-t/\tau)/n(t)-1$ is plotted both versus $(1-\exp(-t/\tau))$ and $(\text{erf}(\sqrt{t/\tau}))$. a) - $N_{\text{Cr}}=100\%$; the tangent of ϕ can be used to determine the upconversion parameter α ; b) - $N_{\text{Cr}}=10\%$; the tangent of δ is used to evaluate C_{da} (Ref. 6); lines 2 and 3 represent the limits for the angle ϕ for the given Cr concentration.

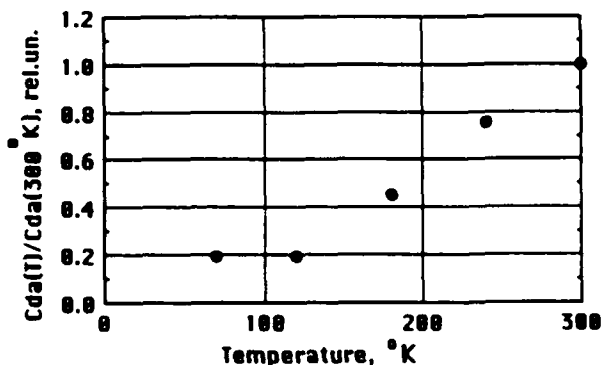


Figure 4. Relative temperature dependencies of the upconversion micro parameter C_{da} in Cr(100%):LiSGaF.

Optical and Physical Properties of the LiSrAlF₆:Cr Laser Crystal

S. A. Payne, W. F. Krupke, L. D. DeLoach,
L. K. Smith, J. B. Tassano, and W. L. Kway

Lawrence Livermore National Laboratory
P.O. Box 5508
Livermore, CA 94550
510-423-0570

Cr-doped LiSrAlF₆, or Cr:LiSAF, has recently been demonstrated to serve usefully in several types of laser technologies. While the early reports entailed assessments of the laser- and flashlamp-pumped efficiencies and of tuning ranges,^{1,2} researchers later pursued both diode and alexandrite laser pumping schemes.^{3,4,5} Cr:LiSAF has also been found to function usefully as an ultrashort pulse regenerative amplifier, and as a self-starting mode-locked system.^{6,7} These efforts to deploy Cr:LiSAF in actual systems have led, however, to the recognition of several limitations exhibited by this crystal. In order to further develop the emerging technologies, it is necessary to understand and characterize the phenomena responsible for these limitations. In particular, we have pursued measurements of the thermomechanical properties, water durability, and pump-induced upconversion losses.

The thermal and mechanical properties of Cr:LiSAF appear in Table I, including the thermal conductivity (κ), expansion coefficient (α), Young's modulus (E), fracture toughness (K_{Ic}), and the overall figure-of-merit defined as

$$R_T = \frac{\kappa K_{Ic} (1 - \nu)}{\alpha E} \quad (1)$$

where ν is Poisson's ratio. The listed R_T values of LiSAF, LiCAF (LiCaAlF₆), and YLF (LiYF₄), suggest that all three materials are much weaker than typical oxides (where $R_T > 3$), and that LiSAF is similar to LiCAF but somewhat weaker than YLF. It is important to note that the actual heat loading that may be tolerated is strongly dependent on both the surface finish, and on the cooling techniques employed. It is therefore believed that all three materials listed in Table I can be successfully utilized in appropriately engineered systems.

The durability results are listed in Table II, in terms of milligrams of material lost, per cm² of surface area during one day. The measurements were all conducted under a set of standard conditions, in which the sample was immersed in an unstirred beaker of fluid held at 50°C. It is apparent that LiSAF is considerably less durable ($D_w = 2.6 \text{ mg/cm}^2 \cdot \text{day}$), than either LiCAF (0.22) or YLF (0.04). The substitution of Sr for Ca

leads to higher solubility in water, as is also the case for CaF_2 and SrF_2 . The replacement of Ga for Al (LiSGAF) degrades the durability from 2.6 to 5.0 $\text{mg}/\text{cm}^2 \cdot \text{day}$. We also found that the partial substitution of Ca for Sr (LiSCAF) did not improve the durability significantly. We did notice, however, that lowering the temperature had a significant impact (2.6 at 50°C versus 0.64 at 25°C), as did using a 50/50 ethylene glycol/water mixture (0.20 $\text{mg}/\text{cm}^2 \cdot \text{day}$ at 50°C).

It has recently been reported that Cr-doped crystals suffer pump-induced losses, as a consequence of Auger upconversion processes.⁸ Here, two excited states of Cr annihilate so as to promote one of the ions to a more highly excited state while returning the other to the ground state, thereby leading to the loss of one quantum of energy. This mechanism may be phenomenologically modeled with the equation:

$$dN/dt = -N/\tau - \gamma N^2 \quad (2)$$

where N is the excited state population, τ is the emission lifetime, and γ is the Auger upconversion coefficient. The results of our analyses are plotted in Fig. 1, where it is clear that γ increases substantially, depending on the Cr atomic fraction, X_{Cr} , in the crystal $\text{LiSrAl}_{1-x}\text{Cr}_x\text{F}_6$. The fit to the data yields

$$\gamma = 0.8 \times 10^{-15} \text{ cm}^3 \text{ s}^{-1} + (17 \times 10^{-15} \text{ cm}^3 \text{ s}^{-1}) X_{\text{Cr}} \quad (3)$$

The dependence on X_{Cr} suggests that the upconversion process is strongly enhanced by migration of the excited states among the Cr ions. A completely independent calculation based on the spectral overlaps of the Cr emission band, with its ground and excited state absorptions, provides a migration-assisted upconversion slope of $25 \times 10^{-15} \text{ cm}^3 \text{ s}^{-1}$. This value agrees reasonably with the slope of eq. (3), and provides evidence that the mechanism of Auger upconversion is adequately understood.

In summary, we have measured and discussed the properties of Cr:LiSAF that impact three important areas during actual laser operation, including the thermal fracture limit, the durability, and the pump-induced Auger upconversion rates. Appropriate consideration of these and other issues should aid in the design and operation of useful Cr:LiSAF laser systems.

References

1. S. A. Payne, L. L. Chase, L. K. Smith, W. L. Kway, H. W. Newkirk, *J. Appl. Phys.* **66**, 1051 (1989).
2. M. Stalder, B. H. T. Chai, and M. Bass, *Appl. Phys. Lett.* **58**, 216 (1991).
3. R. Scheps, *Opt. Mater.* **1**, 1 (1992).
4. S. A. Payne, W. F. Krupke, L. K. Smith, W. L. Kway, L. D. DeLoach, and J. B. Tassano, *IEEE J. Quant. Electron.* **28**, 1188 (1992).
5. D. Harter and J. Squier, presented in *Advanced Solid-State Lasers*, Santa Fe, NM, February 17-19, 1992.
6. M. D. Perry, D. T. Strickland, T. Ditmire, and F. G. Patterson, *Opt. Lett.* **17**, 604 (1992).

7. N. H. Rizvi, P. M. W. French, and J. R. Taylor, Opt. Lett. **17** (1992).

8. M. A. Noginov, V. G. Ostroumov, I. A. Shcherbakov, V. A. Smirnov, and D. A. Zubenko, OSA Proceeding for Advanced Solid-State Lasers, eds. G. Dubé and L. Chase, March 18-20, 1991, Hilton Head, SC.

This work was performed under the auspices of the U.S. Department of Energy by Lawrence Livermore National Laboratory under Contract No. W-7405-Eng-48 and was funded under Defense Advanced Research Projects Agency orders 6874 Am 9.

Table I. Thermal and mechanical properties of several crystalline laser materials
($E_{ave} = 1/3(2C_{11} + C_{33})$; $\nu \sim 0.3$; κ and α quantities listed for $\parallel c$, then $\perp c$)

Property	LiSAF	LiCAF	YLF
κ , [W/(m°C)]	2.9	5.1, 4.6	5.8, 7.2
α , ($10^{-6}/^{\circ}\text{C}$)	-10, 19	3.6, 22	8, 13
E_{ave} , (GPa)	109	107	75
K_{IC} , ($\text{MPa} \cdot \text{m}^{1/2}$)	0.42	0.31	0.27
R_T , ($\text{W}/\text{m}^{1/2}$)	0.41	0.42	1.1

Table II. Durability results for LiSAF and other fluoride crystals in water at 50°C
(unless otherwise noted)

Crystal	D_w (mg/(day \cdot cm ²))
LiSAF	2.6
LiSAF	0.64 (25°C, H ₂ O)
LiSAF	0.20 (ethylene glycol/H ₂ O, 50°C)
LiCAF	0.22
LiSGAF (LiSrGaF ₆)	5.0
LiSCAF (LiSr _{0.8} Ca ₂ AlF ₆)	2.3
YLF	0.04
CaF ₂	0.10
SrF ₂	0.29

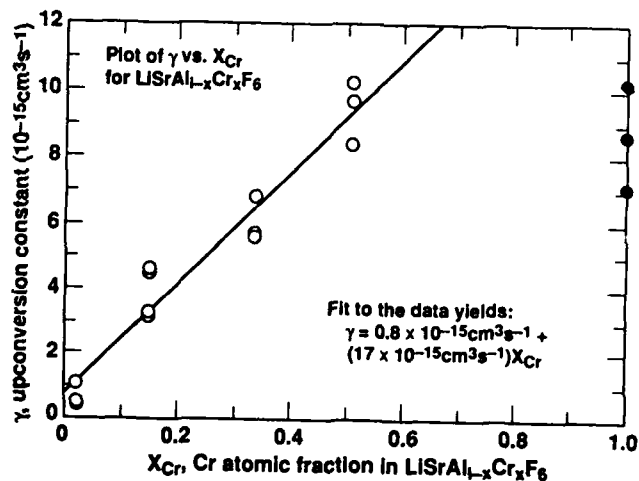


Fig. 1: Plot of the Auger upconversion constant against the atomic fraction of chromium in LiSAF

Higher Average Power Operation of Cr:LiSAF and Cr:LiSGaF Pumped by Alexandrite

W. R. Rapoport
Allied-Signal Inc
Morristown, NJ

There has been significant interest in Cr:LiSAF ^{1,2} due to its high emission cross-section (Peak $\approx 4.8 \times 10^{-20} \text{ cm}^2$), relatively long fluorescence lifetime ($\sim 69 \text{ } \mu\text{sec}$), broad tuning range (760-1010 nm), high quality (scatter loss of $\sim 0.1\%/ \text{cm}$ in selected rods ³), and there is a very small reduction in lifetime for Cr doping up to its stoichiometric limit. Cr:LiSGaF is similar to Cr:LiSAF where gallium is 100% substituted for aluminum. The material exhibits a slightly lower emission cross-section (Peak $\approx 3.3 \times 10^{-20} \text{ cm}^2$)⁴, longer fluorescence lifetime ($\sim 88 \text{ } \mu\text{sec}$), similar tuning range (760->1000 nm), high quality (scatter loss of $< 0.05\%/ \text{cm}$ in selected rods⁵). The 4T_2 absorption band wing extends out beyond 800 nm making these materials candidates for diode or red laser pumping ² which is particularly useful because these materials are not as robust as that of many oxide crystals so flashlamp pumping may have significant limitations. An excellent laser pump for these materials is alexandrite which has a significant overlap with the Cr:LiSAF and Cr:LiSGaF absorption wings.

Preliminary measurements of alexandrite pumped Cr:LiSAF produced slope efficiencies of $\sim 50\%$ in long pulse operation, with low loss material and near the peak of the emission cross-section, indicating that Cr:LiSAF is one of the more efficient Cr doped lasers. Further testing revealed the limitations imposed by the poor thermo mechanical behavior of both materials. Thermal fracture limits the average power loading for a given size rod.

Several different heat exchanger systems were investigated. They consisted of traditional water cooled geometries and modified conductively cooled methods. These geometries were modeled by a finite element analysis routine, which indicated the areas under highest tensile stress and the thermal fracture points. Modification of the heat exchanger geometry allowed for significant average power loading increases in the material. Figure 1 shows 9.2 Watts emitted from a 5 mm diameter system with a slope efficiency of 58%. This result was limited by the amount of available pump power, not by the thermal loading on the material. Results from the models and possible improvements will be presented.

Average power testing of Cr:LiSAF and Cr:LiSGaF showed that the failure point of Cr:LiSGaF is $\sim 75\%$ that of Cr:LiSAF. The test was conducted with identically prepared samples of low scatter material, and approximately the same absorption profiles. The Cr:LiSGaF showed a marked increase in positive thermal lensing just prior to failure. The failure modes appear to be thermal in nature and originate in the areas of highest tensile stress.

A Q-switched alexandrite laser was used to generate 125 ns pulses at 746 nm in a TEM₀₀ spatial profile with a maximum output energy of 120 mJ/pulse. The Cr:LiSAF (2.0% Cr, 5.9 cm length, 94% absorption) and Cr:LiSGaF (3% Cr, 2.9 cm length 75% absorption) crystals were carefully oriented between crossed polarizers for maximum extinction ($> 200:1$) and were excited in the π polarization. A cw Ti:Sapphire laser, tuned from 780-915 nm, served as the probe. The polarization state of the cw source was rotated for probing the π and σ polarizations. Under low repetition rate conditions, so thermal effects could be neglected, the gain ($g_{\pi, \sigma}$) was measured for a constant pump input and is shown in Figure 2. The detector was located far enough away so that the fluorescence signal was small. The gain is sometimes negative in the σ polarization indicating the presence of excited state absorption (ESA). ESA

cross-sections, σ_{esa} , are estimated from this data using the emission cross-sections, $\sigma_e^{\pi,\sigma}$ (known from fluorescence data ¹) and using $g_0^{\pi,\sigma} = N^*(\sigma_e^{\pi,\sigma} - \sigma_{esa})$ where N^* is the average excited state population density. In fact N^* is a decreasing function of distance, x , into the samples. In these experiments the probe beam sampled only the upper 85% intensity points of the pumped area and the wings of the cw probe laser were clipped at the detector. N^* is obtained by measuring the spatial profile of the beam and the amount absorbed. For these estimates, ESA of the pump and upconversion were neglected. Figures 3 a,b shows the estimated values of $\sigma_{esa}^{\pi,\sigma}$ as well as $\sigma_e^{\pi,\sigma}$. The error bars are $\pm 20\%$ on the values of the σ_{esa} due to experimental inaccuracies in determining the true value of the excited state density. The results, when correcting for the differences in absorption, indicate that the relative emission cross-section of Cr:LiSGaF is $\sim 70\%$ that of Cr:LiSAF and that the emission peak is slightly blue shifted.

Acknowledgements

I wish to acknowledge J. Fleming for preparing the samples and H. P. Jenssen, M. L. Shand, and F. Hansen for the many discussions. The samples were provided by Allied-Signal, Lightning Optical and MIT.

References

1. S. A. Payne, L. L. Chase, L. K. Smith, W. L. Kway, and H. W. Newkirk, "Laser Performance of $\text{LiSrAlF}_6:\text{Cr}^{3+}$ ", J. Appl. Phys. 66, 1051, 1989
2. S. A. Payne, W. F. Krupke, L. K. Smith, W. L. Kway, L. E. Davis and J. B. Tassano. "752 nm Wing-Pumped Cr:LiSAF Laser", JQE, Vol 28, No. 4, April 1992, pp. 1188-1196.
3. Lightning Optical and Allied-Signal samples.
4. L. K. Smith, S. A. Payne, W. L. Kway, L. L. Chase and B. H. T. Chai. "Investigation of the Laser Properties of $\text{Cr}^{3+}:\text{LiSrGaF}_6$ ", JQE, Vol 28, No 11, November 1992
5. Sample provided by A. Cassanho and H. P. Jenssen from MIT

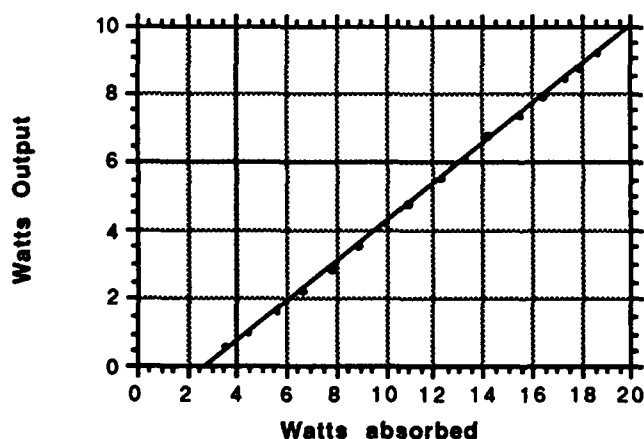


Figure 1: Alexandrite pumped Cr:LiSAF output/absorbed input at 10 hz

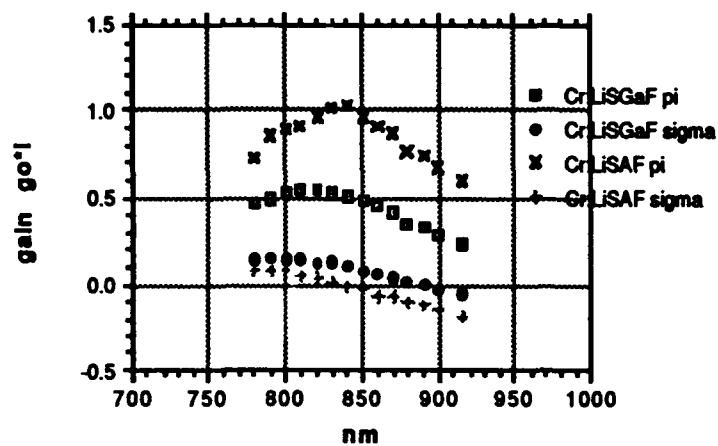


Figure 2: Measured values of g_0^l for π , σ polarizations for Cr:LiSAF and Cr:LiSGaF

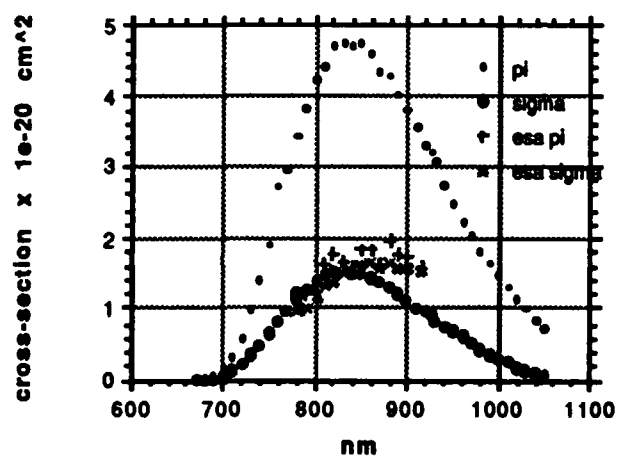


Figure 3a: Estimated values for ESA in Cr:LiSAF

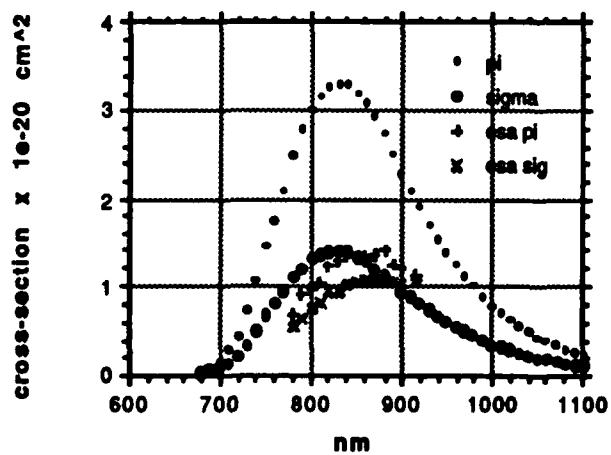


Figure 3b: Estimated values for ESA in Cr:LiSGaF

Tuesday, February 2, 1993

Applications of Compact Blue-Green Lasers 1

CTuA 10:30am–12:00m
Pelican Ballroom

Mark W. Dowley, *Presider*
Liconix

Compact blue-green lasers for future optical disk systems

Shigeo Kubota, Michio Oka and Hisashi Masuda

Kubota Opto-Electronics Laboratory
Corporate Research Laboratories, Sony Corporation
6-7-35, Kitashinagawa, Shinagawa-ku, 141 Tokyo, Japan
Tel: 81-3-3448-5621 Fax: 81-3-3448-5634

Summary

Diode-pumped, intracavity-doubled Nd:YAG, Nd:YVO₄ green lasers, KTiOPO₄ (KTP) sum frequency mixing, KNbO₃ resonant ring doubler, periodically-poled KTP and LiNbO₃ waveguide blue lasers, and II-VI blue laser diodes are promising sources for future 4 to 5 time pit density optical disks. Although the blue diode (460nm) is expected to reduce the intersymbol interference in read out signal from higher density optical disks, considering its probable beam aspect ratio, astigmatism, and the spectral sensitivity of a Si PIN photodetector, at least 5mW room temperature cw output will be required for its future application. Efficient blue harmonic generation of Ti:Sapphire lasers in a periodically-poled LiNbO₃ waveguide and in a Cerenkov-radiation mode Ta₂O₅/KTP waveguide were also demonstrated. Their efficient stable coupling with a diode will be next key issue. Only applications of bulk nonlinear frequency conversion to actual optical disk systems have been demonstrated so far.

TEM₀₀ mode 10mW cw output was obtained from a miniature-integrated SHG green laser (mi-green laser) pumped by a 250mW Sony broad area diode (SLD302). The retardation change with temperature in an intracavity 2.5mm-thick KTP allowed the low noise operation (RIN= -140 dB/Hz at 5MHz) of the mi-green laser over a temperature range of 3K. Separately we measured dN/dT of the KTP prism by minimum deviation angle method, which well explained the retardation change observed. In read out of an optical disk rotating at linear velocity of 8.3m/s by using a compact mi-green pickup, carrier to noise ratio of 62 dB at 10MHz carrier frequency was obtained [1].

We have developed a variable length block coding called VFM, which is well suited for 6 time areal bit density (6.9 bit / μm^2) recording on a 5 inch optical disk, where the minimum pit length which corresponds to 2 bits, is 0.36 μm and track pitch is 0.8 μm .

Using a pickup equipped with the mi-green laser and a glass biaspheric lens ($NA=0.6$), one hour play back time at bit rate of 10 Mbit/s was achieved. Since the read out system is well diffraction-limited and also disk-noise-limited by virtue of the aberration-free, low noise laser, the optical frequency response of the pickup was effectively equalized by using a transversal filter, which enabled data retrieval at symbol error rate of 10^{-6} [2]. Fourth harmonic generation of a diode-pumped Nd:YAG laser by using an external resonant BBO ring doubler is a next generation source for such ultra high density master disk recording. High speed (20kHz servo bandwidth), sub-angstrom positioning of a BBO cavity mirror by a novel voice-coil-motor (VCM) realized far more than 100mW cw diffraction-limited 266nm generation [3,4].

Efficient 459nm generation by sum frequency mixing of a diode-pumped Nd:YAG laser and a 808nm single-longitudinal mode diode laser in a flux-grown KTP as well as in a hydro-thermally grown KTP was observed. Current modulation of the diode (150 mW) allowed up to 50 Mbit/s modulation of 15 mW blue output. Combining the blue source with a magnetically-induced super resolving disk (MSR), which realized a read out of signal with bit length of $0.3\mu\text{m}$ at byte error rate of 10^{-4} by using a 780nm diode [5], more than 20 time enhancement of areal bit density is expected.

In summary, we described extra 1.5 time enhancement of bit density in a 5 inch high density optical disk by using a novel coding scheme VFM and a waveform equalizer combined with a miniature-integrated SHG green laser. According to Hartley and Shannon's information theory which tells us that channel capacity is determined by the signal to noise ratio and frequency bandwidth of the channel, this enhancement of bit density originated mainly from improvement of the laser source in terms of aberration and noise compared with conventional diode sources. We also reported direct modulation of up to 50 Mbit/s of efficient sum frequency mixing in KTP.

References

1. H.Masuda, F.Maeda, M.Oka, Y.Kaneda, M.Sugiura and S.Kubota: "Miniature integrated SHG green laser," in digest of Compact Blue-Green Lasers 1992, Vol.6, 94/FA3-1.
2. Y.Shinpuku, A.Akiyama, T.Kashiwagi, H.Ino and Y.Chaki: " A new channel coding and SHG green laser for high density optical disk," in digest of Optical Memory Symposium 1992, pp.67-68 (in Japanese).

3. M.Oka and S.Kubota," Second harmonic generation green laser for high density optical disks," JJAP Series 6, Proc. Int. Symp. on Optical Memory, 1991, pp.135-140.
4. M.Oka, N.Eguchi, H.Masuda and S.Kubota:"All-solid-state continuous wave 0.1-W untra-violet laser," in 1992 Conference on Lasers and Electro-Optics vol.7 OSA Technical Digest Series (Optical Society of America, Washington, DC 1992), paper CWQ7.
5. A.Fukumoto and S.Kubota: " Super resolution of optical disk using a small aperture," JJAP Series 6, Proc. Int. Symp. on Optical Memory, 1991, pp.153-157.

DISPLAYS, HIGH DEFINITION TELEVISION AND LASERS

William E. Glenn

Director, Imaging Systems Laboratory, Florida Atlantic University, Boca Raton, Florida, USA

Introduction

High definition television for both commercial and consumer use is critically dependent on the development of new display technology that can be manufactured at a reasonable price. There is a strong demand for new high definition displays for the theatre conference rooms and for other commercial applications. These applications need inexpensive high resolution projection displays with 3,000 to 10,000 lumens output. Only light-valve projectors have been able to come close to the technical requirements - but at a very high cost.

All of the components needed for consumer distribution of high definition television are now available except for an acceptable display. Most of the cost of a consumer HDTV installation is in the cost of the display because of the large size and high resolution.

If efficient solid-state lasers can be produced inexpensively in all three primary colors this could lead to a solution to the display requirements for high definition television.

Requirements

First let us consider the requirements of a consumer HDTV display. HDTV was originally designed to provide the same viewing experience (sharpness, contrast, field of view etc.) as the motion-picture theatre⁹.

When an observer is viewing a moving image, there is an optimum resolution on the viewer's retina. The preferred viewing distance for standard or high definition television or the motion picture has the limiting resolution of the system - about 22 cycles per degree on the viewer's retina.

For an interlaced television system, the vertical resolution is determined by the scan line spacing. As shown in Figure 1, at a given viewing distance, the scan line spacing (in millimeters) will be the same. The HDTV image will be larger simply because it has more lines. HDTV is really the same resolution image in the viewer's retina with a larger field of view.

The consequences of this fact are indicated in Figure 2. At a typical 9 foot viewing distance, a 24" diagonal display is optimum for 525 line television while a 63" display is optimum for HDTV. It is obvious that the traditional shadow mask CRT will not meet the cost, size and weight objectives for this application.

In addition to size, there are several other factors that need to be considered. Figure 3 shows the other characteristics that a display should have.

Flicker is of particular concern for HDTV displays. Flicker perception increases with increased brightness and with increased eccentricity from the center of the field of view. For displays such as CRT's or laser scanners there is a very high amplitude of brightness change at the field rate of the scan. At an eccentricity of 15°, the frequency at which flicker cannot be detected is about 10% higher than on axis perception².

Fortunately, matrix addressed light-valve displays (such as active-matrix liquid crystal projectors) have a very low brightness variation at the field repetition rate. Consequently they do not have visible flicker even with bright, wide field viewing.

Light-valve projectors, however, must be progressively addressed at 50 Hz or higher in order to get good motion rendition and high efficiency.

In satisfying the requirements for an HDTV display, one must consider the optical efficiency that is achievable and the potential manufacturing cost in large quantities. Figure 4 gives a few options that are in various stages of development. Figure 5 gives a few examples of light-valve projectors that are either commercially available or have operating prototypes. If the objectives of Figure 3 are to be met, the display needs an optical efficiency of over 3 lumens per watt. All of the displays listed in Figure 5 fall short of that objective.

Projectors

In the near future, projectors promise to be the most attractive option for inexpensive large displays. CRT projectors are available with a rather minimum light output. Light-valve projectors, like the G.E. Talaria,^{3,4} have adequate light output for consumer use but at too high a price.

In the near term, the active-matrix LCD projector seems to be the most promising light-valve technology for projectors. Current HDTV projectors of this technology have been able to get efficiencies of about one lumen per watt.

Active-matrix transmission liquid crystal projectors have an advantage in that the technology is heavily supported by the market for small direct-view active-matrix liquid crystal displays, primarily laptop computers and small television sets. This high level of technology support is a considerable advantage for this technology since it is relatively competitive in other respects with the other light-valve options.

In the future one must consider the possibility of the solid-state laser as an attractive light source for projectors. Their high efficiency in producing a coherent monochromatic light beam is certainly very appealing. In recent years considerable progress has been made in achieving good efficiency in all three primary colors. While there is more work to be done in this area, this option looks very desirable. Solid state lasers are presently very expensive. However, in quantity production there is no basic reason why this should remain the case.

Lasers can be used in laser scanners using a combination of mechanical and Bragg diffraction scanning. They can also be used as light sources for active-matrix LCD projectors or deformable light-valves. A coherent, efficient monochromatic light source would greatly improve the performance and cost of the LCD projector.

Conclusion

In the near term, active-matrix LCD light-valve projectors with improved efficiency and improved screen design promise to be the leading candidates for HDTV consumer and commercial displays.

In the long term, projectors using solid-state lasers as a light source are an attractive option if the present rate of improvement in performance and cost continues.

References

1. Ichiro Yuyama, "II Fundamental Requirements for High Definition Television Systems, Large Screen Effects," *NHK Technical Monograph*, 32, June 1982.
2. G. Murch, D. Mead, "Flicker in Displays," *In Human Factors Research Report*, Techtronix, 1984.
3. W.E. Glenn, "Principles of Simultaneous Color Projection Television Using Fluid Deformation," *J. SMPTE*, 79, p. 788, 1970.
4. E. Bauman, "The Fischer Large Screen Projection System," *J.SMPTE*, 50, p.344, 1953.

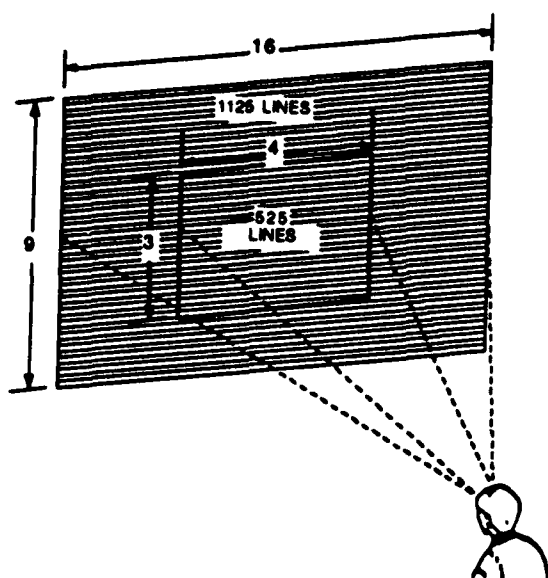


Figure 1. Relative size of standard and high definition images at the same optimum viewing distance.

Relative Size of Displays

(9' viewing distance)

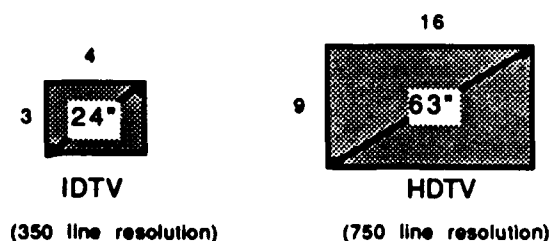


Figure 2. Relative sizes of a 525 and 1125 line television set when viewed at a distance of 9 feet.

Display Requirements

	Consumer Display	Theatre Display
Resolution	> 750 TV lines	> 750 TV lines
Light Output	1000 lumens	10,000 lumens
Cost	<\$2,000	< \$50,000
Response Time	< 10 mS	< 10 mS
Power Consumption	< 300 W	< 3,000 W
Small Area Uniformity	± 0.25%	± 0.25%
Contrast Ratio	> 90:1	> 90:1
Flicker	Undetectable	Undetectable

Figure 3. Performance requirements for HDTV displays for consumer and commercial use.

Display Efficiency and Power Consumption

Display	Efficiency (lumens/watt)	Power Required (Watts) Consumer Display (1,000 lumens)	Theatre Display (10,000 lumens)
Gas Laser Scanner	0.03	30,000	300,000
CRT Projector	0.5	2,000	20,000
Light Valves	1	1,000	10,000
Light Valves	4	250	2,500
Solid State Lasers (3%)	10	100	1,000

Figure 4. Optical efficiency and power requirements for projections with various light sources.

Light Valve Projectors

Display	Manufacturer	Light Output (Lumens)	Resolution (TV lines per picture height)	Efficiency (Lumens per W)
Eidophor 525-line	Gretag A.G.	7,000	375	0.44
Eidophor 1125-line	Gretag A.G.	4,200	800	0.26
Talaria	General Electric	1,350	325	0.77
2LV Talaria	General Electric	2,300	800	0.92
3LV Talaria	General Electric	3,600	800	1
AMLCD	Sharp Mitsubishi Seiko-Epson Phillips Others	~200	325-800	1

Figure 5. Approximate light output, resolution and efficiency of commercially available light-valve projectors.

**Imaging and Analysis of Semiconductor Surfaces with
a Blue-Green Laser Scanning System**

**Bruce Worster
Ultrapointe Corporation**

A system to provide 3-D images of submicron surface structure, composition, and defects on semiconductor wafer surfaces using a multiwavelength blue-green laser is described.

Tuesday, February 2, 1993

Applications of Compact Blue-Green Lasers 2

CTuB 1:30pm–2:45pm
Pelican Ballroom

Daniel Guillot, *Presider*
Uniphase Corporation

The Use of Air-Cooled Argon Ion Lasers in Automated Genetic Analysis

Mel N. Kronick, Applied Biosystems, Inc., Foster City, CA 94404, (415)-570-6667

Significant advances in our understanding of biological function and dysfunction have been made possible over the last several years by the development of techniques to sequence and analyze DNA. Automation has been introduced to increase the speed and accuracy of such sequencing and analysis and to make the processes less laborious and less costly. Today, the method of choice of such automation utilizes laser excitation to detect, in real time, fluorescently labeled DNA fragments as they are electrophoretically driven through a separating gel medium (1). The fluorescence-based technology for analysis has been applied to many current problems in medical and biological research with great success. It is now routinely used in hundreds of laboratories worldwide to sequence DNA in a wide variety of biotechnology research projects including programs such as the Human Genome Initiative. Applications to the mapping and diagnosis of genetic disorders as well as to the use of DNA for forensic purposes have also been amply demonstrated (2,3). An even wider acceptance of the technology has unfortunately been significantly inhibited by its high price.

Primarily because of its modest size, output power and output wavelength, the air-cooled argon ion laser has been the laser source of choice. The cost, finite tube life, large power supply and high power consumption of such lasers are viewed, however, as significant liabilities. In fact, the laser itself represents the most significant cost component of the automated systems. Further developments in blue-green laser technology which could lower the price of available lasers while improving efficiency and reliability have the potential to increase dramatically the utilization of these fluorescence-based analyses. The output wavelengths of such lasers must, however, take into account the desirable features of and the technology investment in the fluorescent

dyes employed today. Years of chemical research have gone into the development of highly fluorescent dye derivatives that are compatible with the very few naturally occurring enzymes that can be used for genetic analysis (4). Both at present and in the future, the dependence of automated genetic analysis upon blue-green lasers can thus not be underestimated.

1. G. L. Trainor, "DNA Sequencing, Automation, and the Human Genome," *Analytical Chemistry* (1990) **62**, 418-426.
2. P. E. Mayrand et al., "The Use of Fluorescence Detection and Internal Lane Standards to Size PCR Products Automatically," *Applied and Theoretical Electrophoresis* (1992) **3**, 1-11.
3. K. M. Sullivan et al., "Automated DNA Profiling by Fluorescent Labeling of PCR Products," *PCR Methods and Applications* (1992) **2**, 34-40.
4. L. G. Lee et al., "DNA Sequencing with Dye-Labeled Terminators and T7 DNA Polymerase: Effect of Dyes and dNTPs on Incorporation of Dye-Terminators, and Probability Analysis of Termination Fragments," *Nucleic Acids Research* (1992) **20**, 2471-2483.

Short Wavelength Gas Lasers – Future and Applications

William T. Silfvast
CREOL—University of Central Florida
12424 Research Parkway
Orlando, FL 32826

An overview of short wavelength gas lasers will be presented including a summary of their characteristics, new developments in the field, and existing and potential future applications.

Laser Induced Fluorescence Detection in Capillary Electrophoresis with a Blue Frequency Doubled Light Source

Fredrik Laurell

Institute of Optical Research, 100 44 Stockholm, Sweden

Mårten Jansson and Johan Roeraade

Dept. of Analytical Chemistry, Royal Institute of Technology, 100 44 Stockholm, Sweden

Introduction

Capillary electrophoresis (CE) is a rapid and efficient separation technique for small volume samples, which has attracted much attention. Combined with laser induced fluorescence (LIF) detection, extraordinary sensitivity can be achieved. Lasers, emitting light in the visible as well and in the UV have been used in recent studies to detect biomolecules, *e.g.*, amino acids, DNA¹ or proteins². Compared to classical electrophoresis, CE offers better possibilities for automated analysis where a compact and reliable detection unit is necessary. An all solid state laser for LIF would be the ideal light source. Compared to gas lasers, which have been employed, the solid state laser is more compact, stable and has a lower power consumption. Moreover, the reliability and the minimum maintenance requirement of a solid state laser would be an important advantage³. Frequency doubled diode lasers using quasi-phase matching (QPM) waveguides are interesting candidates as light sources for LIF, as the output wavelength could be chosen to match the absorption band of the fluorescing analyte. Also, sufficient power (in the order of mW) in the blue light region could be generated⁴.

In this report we describe a CE system, with LIF detection using frequency doubled blue light generated in a segmented KTP waveguide, which was used to separate NDA-labeled amino acids. An absolute detection limit of $4 \cdot 10^{-17}$ mol was achieved with a signal to noise ratio of 3:1. This concept is a promising candidate for compact automated capillary electrophoretic systems with high sensitivity.

Instrumentation

A schematic of the experimental set-up is shown in fig.1. The light source consisted of a cw Ti:sapphire laser endfire coupled to a KTP waveguide and tuned to phase matching. At the output of the waveguide the blue light was collimated and the remaining fundamental radiation was absorbed in two IR filters. The blue beam was reflected by a dichroic beamsplitter and focused on the capillary by a 60 X 0.8 NA microscope objective. Fluorescent light was collected by the same objective and passed through the dichroic beamsplitter⁵. Standard spatial and spectral filters were used to eliminate stray light and remnant pump light. The signal light was finally collected by a PMT (Hamamatsu, R4220). The capillary could be translated in three dimensions to adjust for maximum signal while the other parts of the optical system were not altered after initial alignment. The blue light beam was chopped and the signal from the PMT was connected to a phase-locked amplifier (PLA) to obtain an improved signal to noise ratio at low light levels. The PLA signal was recorded on a Chromatointegrator (Hitachi).

Three criteria decided the choice of wavelength of the frequency doubler; 1) absorption bands of the suitable fluorophores, 2) available wavelengths for high power diode lasers, and 3) possible wavelengths in existing KTP waveguides. In this work we decided to build our system for a 424 nm fluorophore pump wavelength; the wavelength corresponding to frequency doubling in KTP QPM waveguides with a 4 μ m QPM period. For the fundamental wavelength (848 nm) high power

frequency diode lasers are commercially available. The waveguides on the 5 mm long KTP sample were fabricated by standard ion-exchange procedure described by van der Poel *et al*⁶.

The CE unit was built in-house and consisted of a high voltage d.c. power supply (Model 225, +/- 30 kV, Bertan) and a custom made timer controlled injector. Fused-silica capillary tubing (360 μm O.D. and 50 μm I.D., total length 64 cm, distance between injector and detector 57 cm) was obtained from Polymicro Technologies (Phoenix, AZ, USA). The detector end was modified to accommodate the on-column laser detection set-up. The electrophoresis run buffer consisted of 100 mM H_3BO_3 pH 9.3. The amino acids Arginine-DL, Methionine-DL, Alanine-DL and Glutamic acid-DL and KCN (used in the derivatisation) were obtained from Sigma (St. Louis).

Experiments

The fluorophore, naphthalene-2,3-dicarboxaldehyde (NDA, Molecular Probes, Eugene, OR, USA) was used to tag the amino acids⁷. The ratio of NDA to total amount of amino acid content was 12.5. The original concentration of each amino acid was 71 μM . Reactions were carried out with the NDA/KCN solution (ca 0.5 h) and serially diluted in times of 10 to 7 nM with H_3BO_3 buffer. NDA attached to primary amines have a strong absorption band in the 400-450 nm region and a broad fluorescence around 450-525 nm. The products were electrokinetically injected into the capillary column (4 sec. at an injection voltage of 6 kV). Next, the capillary was placed in the run buffer vial and a high voltage (typically 30 kV) was applied for the electrophoretic run. Due to their difference in migration and the high field strengths applied (470 Volts/cm) a fast separation was accomplished. 170 mW of IR was used to excite the KTP waveguide, resulting in 1.2 mW of blue light which was focused on the capillary. A typical electropherogram is shown in fig. 2. With the present set-up, the concentration detection limit proved to be 6 nL injection of a 7 nM sample, *i.e.*, an absolute detection limit of $4 \cdot 10^{-17}$ mol. In this case the signal to noise ratio was 3:1.

Conclusions

A CE system with blue light LIF detection has been constructed. It was possible to detect $4 \cdot 10^{-17}$ mol of analyte. Orders of magnitude improvement in detection sensitivity are expected with more carefully designed optical and electrical detection system. Work is now in progress to replace the Ti-sapphire laser by a diode laser to obtain a compact light source for the detection system.

References

- ¹ J. Z. Zhang, D. Y. Chen, S. Wu, H. R. Harke, and N. Dovichi, *Clin. Chem.* **37** (1991) 1492-1496.
- ² D. F. Swaile, and M. J. Sepaniak, *J. Liq. Chromatogr.* **14** (1991) 869-893.
- ³ T. Higashijima, T. Fuchigami, T. Imasaka, and N. Ishibashi, *Anal. Chem.* **64** (1992) 711-714.
- ⁴ M. G. Roelofs, F. Laurell, and J. D. Bierlein, in *Compact Blue-Green Lasers Technical Digest 1992* (Optical Society of America, Washington, D.C., 1992), Vol. 6, pp. 127.
- ⁵ L. Hernandez, J. Escalona, N. Joshi, and N. Guzman, *J. Chromatogr.* **559** (1991) 183-196.
- ⁶ C. J. van der Poel, J. D. Bierlein, J. B. Brown, and S. Colak, *Appl. Phys. Lett.* **57** (1991) 2074.
- ⁷ T. Ueda, F. Kitamura, R. Mitchell, and T. Metcalf, *Anal. Chem.* **63** (1991) 2979-2981.

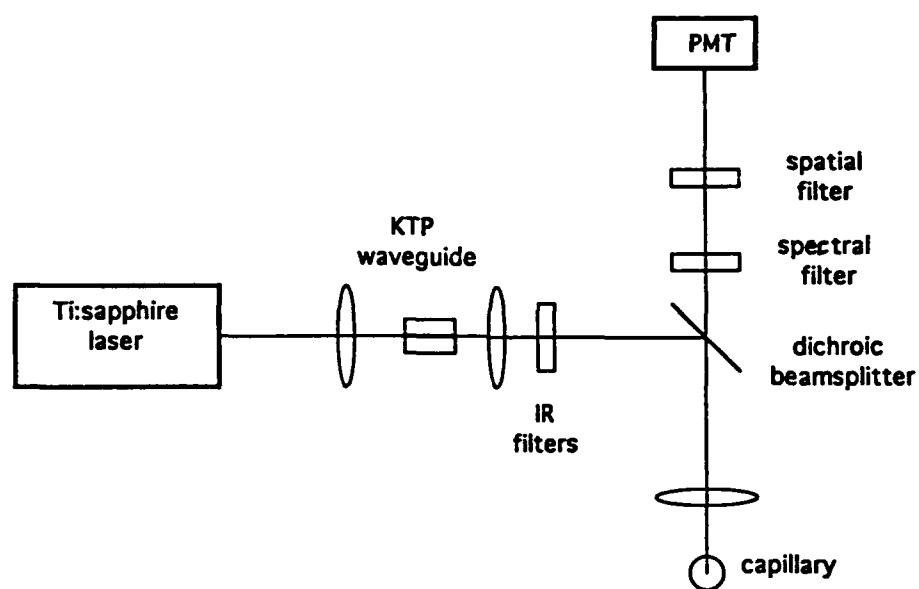


Fig. 1. Experimental set-up for LIF detection in capillary electrophoresis.

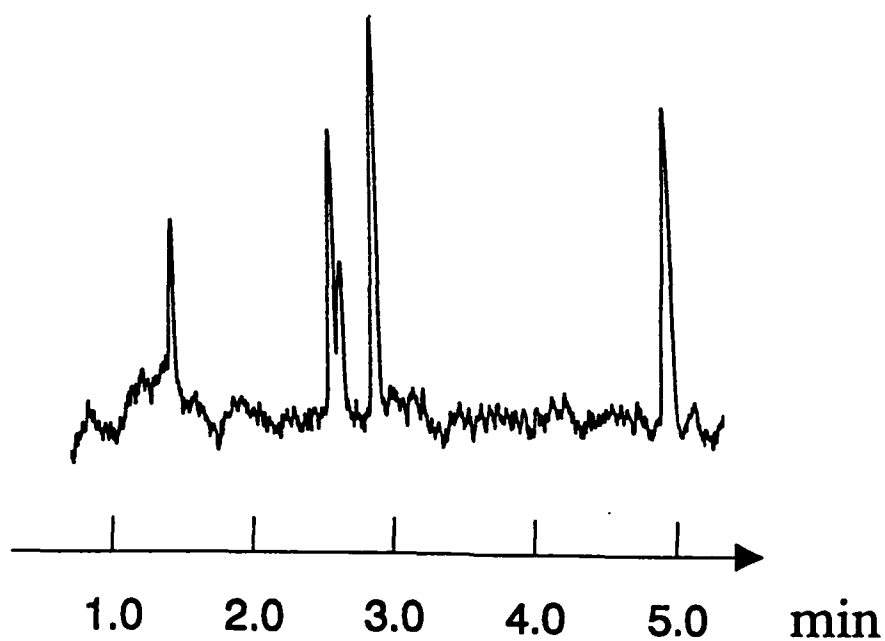


Fig. 2. Electropherogram of a sample consisting of four NDA-labeled amino acids. The sample concentration was 70 nM, and the injection volume 6 nl. The microscope was a 20 X 0.4 NA, other conditions see text.

Tuesday, February 2, 1993

Blue-Green Semiconductor Lasers

CTuC 3:15pm–4:45pm
Pelican Ballroom

James M. DePuydt, *Presider*
3M Company

Growth of ZnMgSSe and Fabrication of Blue Laser Diodes

K. Akimoto, H. Okuyama, T. Miyajima, Y. Morinaga, F. Hiei and M. Ozawa

Sony Corporation Research Center, 174 Fujitsuka, Hodogaya, Yokohama, 240 Japan

Fax No: 045-334-6934

For decades, wide gap II-VI semiconductors have been intensively studied for application to visible light emitting devices. Recently some research groups have fabricated laser diodes that emit blue-green light from a ZnCdSe/ZnSSe single and multi quantum well active layer¹. However, emission of genuinely blue light can not be obtained from these type of structures. When we use Zn(S)Se as an active layer material, blue light can be obtained. But there have not been candidates for a cladding layer material, that is lattice-matched to the substrate and has sufficient band-gap energy. In this paper, we firstly propose a new material, ZnMgSSe. This material meets the requirements of the cladding layer of Zn(S)Se for fabricating a blue laser diodes. Secondly, we report the successful CW operation of ZnSe/ZnMgSSe multi quantum well and double-heterostructure blue lasers at 77K for the first time.

ZnMgSSe films were grown on (100)GaAs substrate by molecular beam epitaxy. The source materials were elemental Zn(6N), Se(6N), Mg(4N) and a compound ZnS(6N). The growth temperature was 240 C. Composition x and y of $\text{Zn}_x\text{Mg}_{1-x}\text{S}_y\text{Se}_{1-y}$ were determined by electron-probe microanalysis. The lattice constant was determined from X-ray diffraction (400) peaks. The band-gap energy was estimated from the band-edge emission in the photoluminescence spectrum at 77K.

In the X-ray diffraction pattern, tetrahedral (400) reflection was observed. The pattern showed that ZnMgSSe has a zincblende structure. Although the lattice constants of MgS and MgSe (NaCl structure) have been reported, the lattice constants of the zincblende structure have not. Figure 1 shows the relationship between band-gap energy and lattice constant of various II-VI semiconductors containing MgS and MgSe. It can be seen that band-gap energy of ZnMgSSe can be varied from 2.8 eV to near 4 eV, maintaining lattice-matching to a (100)GaAs substrate².

Based on the discussion of common cation and common anion rule, the heterostructure of

efficiently. The refractive index of ZnMgSSe is smaller than that of Zn(S)Se, and decreases as the band-gap energy increases. It is expected that light confinement is possible in this double heterostructure. Thus far, Zn(S)Se/ZnMgSSe meets the requirements of a double heterostructure of blue-light laser diodes.

To fabricate a blue laser diodes, we studied n- and p-type doping into ZnMgSSe and the design of an optimised laser structure. The n-type doping into ZnMgSSe was carried out using ZnCl_2 as a dopant source. The carrier concentration was controlled from 10^{16} cm^{-3} to 10^{18} cm^{-3} . The p-type doping was achieved using nitrogen plasma, which was produced by electron cyclotron resonance.

The schematic structure of the blue laser diode is shown in Fig. 2. The active layer of multi quantum well was composed of six quantum well (ZnSe, 6 nm) and five barrier layers (ZnMgSSe, 10 nm). The composition of ZnMgSSe of the cladding layer was the same as that of the barrier layer. The composition x and y were 0.90 and 0.18, respectively. In photoluminescence measurements at 77K, the energy of the band-edge emission of ZnSe and ZnMgSSe were 2.78 and 2.97 eV, respectively. An Au/Pd electrode was evaporated on the p-type cap layer. Although good ohmic characteristics were not obtained, the adhesion of Au/Pd is good and the turn-on voltage of Au/Pd is 7V.

The relation of the light output power to the DC current is shown in Fig. 3. The threshold current I_{th} was 45 mA, which corresponds to a threshold current density J_{th} of 230 A/cm^2 . When the intensity of the light output abruptly increased, strong polarisation characteristics were observed, which is further evidence of lasing.

Fig. 4 shows the emission spectrum for the laser diode under continuous wave operation at 77K. The driving current was just above I_{th} . The lasing wavelength was 447 nm and many longitudinal modes were observed³.

We also fabricated the ZnSe/ZnMgSSe double heterostructure laser diodes. The threshold current density of this type of lasers were about 20% higher than that of the multi-quantum-well lasers, which might be a result of quantum effects involving the excitonic nature of the lasing.

REFERENCES

1. M.A.Haase, J.Qiu, J.M.DePuydt, and H.Cheng, Appl. Phys. Lett. 59 (1991) 1272.
2. H.Okuyama, K.Nakano, T.Miyajima and K.Akimoto, Jpn. J. Appl. Phys. 30 (1991) L1620.
3. H.Okuyama, T.Miyajima, Y.Morinaga, F.Hiei, M.Ozawa and K.Akimoto, Electron. Lett. 28 (1992) 1798

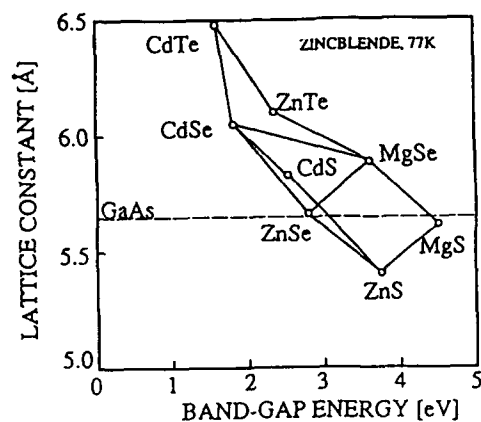


Fig. 1 Relationship of band-gap energy at 77K and lattice constant of II-VI semiconductors containing MgS and MgSe.

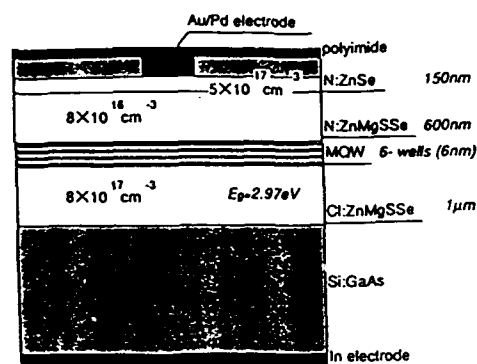


Fig. 2 Schematic structure of the blue laser diode.

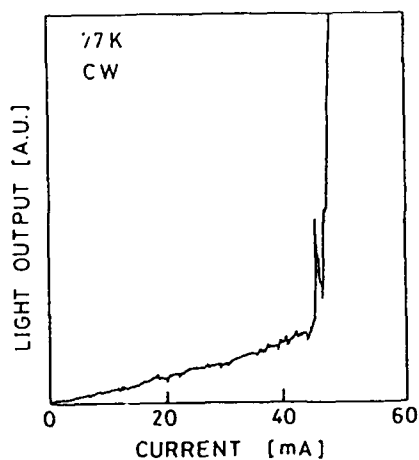


Fig. 3 Relationship of the light output power to the dc current. The threshold current is 45 mA, which corresponds to $J_{th} = 230\text{ A/cm}^2$.

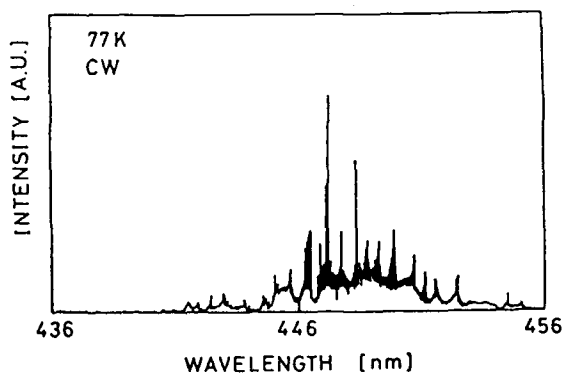


Fig. 4 Emission spectrum for the multi-quantum-well laser under continuous wave operation at 77K.

Advances in II-VI Blue-Green Laser Diodes

C.T. Walker, J.M. DePuydt, M.A. Haase, J. Qiu and H. Cheng

3M Company, 201-2S-05 3M Center, St. Paul, MN 55144, USA

Telephone: (612) 736-9815 FAX: (612) 737-2590

Significant progress toward the development of viable blue and green II-VI laser diodes (LDs) was made since the initial demonstration of these devices in our laboratory nearly 2 years ago [1]. Lasing was obtained in the pulsed mode at room temperature [2] with threshold current densities less than 1000 A/cm^2 and continuous wave devices have been operated at 80 K. It is also important to note that several other laboratories succeeded in confirming laser oscillation in related structures [4-10]. Some recent advances in II-VI laser diodes include the development of electrical contacts to *p*-type ZnSe with lower contact resistances, the growth of high quality lattice matched ternaries and the realization of increased efficiencies in $\text{Cd}_x\text{Zn}_{1-x}\text{Se}$ quantum wells grown by atomic layer epitaxy.

To gain some perspective of the status of II-VI diode lasers it is useful to compare the performance of these devices with the minimum requirements that must be met by a laser in optical recording systems. A working definition of a practical laser and the performance of current II-VI devices made in our laboratory are shown in table I.

Lasing under pulsed current injection is possible up to room temperature. In devices with a $\text{Cd}_x\text{Zn}_{1-x}\text{Se}$ active layer within ZnSe or $\text{ZnS}_{0.07}\text{Se}_{0.93}$ barriers the emission wavelengths at room temperature are in the range 508 - 535 nm. These devices are typically operated with 50 - 500 nsec pulses at about 1kHz repetition rates. The output power during the pulse for 50 nsec pulses is as large as 70 mW. The voltage at lasing threshold in recent devices is 9 - 10 V; this is

smaller than in early devices where threshold occurred at about 20 - 25 V. The primary reason for the reduction in operating voltage is advances in the electrical contact to the *p*-side. The major shortcoming of these LDs is their short lifetimes; the best devices have lifetimes about 1 hour when operated near threshold.

	Working Definition of a Practical Laser Diode	Status of Today's Devices
Continuous Operation	1-3 mW at RT	1-3 mW at 80K
Pulsed Operation	50 nsec	50 nsec
Pulse Rep. Rate	6 MHz at RT	<1 KHz at RT
Output Power in Pulse	30 mW at RT	70 mW at RT
Operating Temperature	25 °C	Pulsed to RT, CW at 80K
Device Lifetime	10,000 Hours	1 Hour pulsed at RT 1 Hour CW at 80K

Table I. Comparison of the current status of our II-VI laser diodes with the most basic requirements which must be met by a device for it to be considered useful.

True continuous wave devices have been demonstrated at 80 K; CW operation was achieved up to 125 K, but only for very short times. The emission wavelengths at 80 K from the $\text{Cd}_x\text{Zn}_{1-x}\text{Se}$ single quantum well devices are 490 - 512 nm. The CW output power is 1-3 mW. The threshold current density is about 100 A/cm^2 and the onset of lasing occurs at 9 - 10 V. Again the most significant shortcoming of the devices under CW operation is their short lifetime; the diodes often last less than 1 hour even when operated only slightly above threshold.

The electroluminescence from single quantum well light emitting diodes was studied in order to identify the cause of the short device lifetimes.

Topographs were constructed using an optical microscope and a CCD camera. Two types of dark line defects (DLDs) were observed during these studies. The first DLD has a projection onto the (001) plane along the $\langle 110 \rangle$ direction. The second DLD originally appears as a dark spot that elongates during operation in the $\langle 100 \rangle$ direction when viewed from the (001) surface. Devices that had $\text{ZnS}_x\text{Se}_{1-x}$ barriers lattice matched to the GaAs substrate had lifetimes that were increased by several orders of magnitude. The X-ray rocking curves from the long-lived LEDs had FWHM about 30 arcsec, this is approximately one order of magnitude smaller than the FWHM from devices with ZnSe barriers. The dominant reason for the increased lifetime appears to be the reduction of the $\langle 100 \rangle$ DLD. In order to have good optical confinement it is necessary to have heterostructures with a large difference between the optical indices. Unfortunately high quality lattice matched II-VI heterostructure providing such optical confinement have not been developed at this time.

In addition to the requirements listed in table I, LDs for optical recording systems must operate in a single lateral mode. Index guided devices made in our laboratory have lased in a single lateral mode and CW devices have also been observed to lase in a single longitudinal mode.

Although tremendous progress has been made in II-VI laser diodes over the past 18 months significant problems remain to be solved before useful blue and green LDs can be made. Additional improvements to the electrical contact to *p*-type ZnSe are needed in order to reduce heating. The growth of other ternaries and quaternaries with low dislocation densities needs to be mastered in order to fabricate lattice matched heterostructures with good optical confinement. Finally additional process development like die bonding and facet coating is needed.

- [1] M. A. Haase, J. Qiu, J. M. DePuydt and H. Cheng, *Appl. Phys. Lett.* **59**, (1991) 1272.
- [2] H. Cheng, J.M. DePuydt, M.A. Haase and J. Qiu, *LEOS Topical Meeting on Epitaxial Materials and In-situ Processing for Optoelectronic Devices*, Newport Beach, CA (July, 1991)
- [3] J.M. DePuydt, M.A. Haase, J Qiu and H. Cheng, *Compact Blue-Green Lasers*, OSA 1992 Tech. Dig. Ser. Vol. 6 (1992).
- [4] H. Jeon, J. Ding, W. Patterson, A.V. Nurmikko, W. Xie, D.C. Grillo, M. Kobayashi and R.L. Gunshor, *Appl. Phys. Lett.* **59**, (1991) 3619.
- [5] D.J. Olego (Philips Research Laboratories) *1992 March Meeting of the American Physical Society*, 16-20 March, Indianapolis, IN.
- [6] J.F. Schetzina (North Carolina State University), private communication.
- [7] K. Ohkawa, et al. (Matsushita Electric Industries) *53rd Spring Meeting, (1992) of The Japan Society of Applied Physics.*
- [8] T. Ohno, et al. (Matsushita Electric Industries) *53rd Spring Meeting, (1992) of The Japan Society of Applied Physics.*
- [9] S.Y. Wang I. Hauksson, J. Simpson, H. Stewart, S.J.A. Adams, J.M. Wallace, Y. Kawakami, K.A. Prior and B.C. Cavenett, *Appl. Phys. Lett.* **61** (1992) 506.
- [10] H. Okuyama, T. Miyajima, Y. Morinaga, F. Hiei, M. Ozawa and K. Akimoto, *Electronics Letters* **28** (1992) 1798.

THERMAL CHARACTERISATION OF A II-VI BLUE SEMICONDUCTOR LASER

R.R. Drenten, T. Marshall, J. Gaines, J. Petruzzello

Philips Laboratories
North American Philips Corp.
345 Scarborough Rd.
Briarcliff Manor, NY 10510
tel. (914) 945 6524

Introduction

After proper p-doping in ZnSe became possible, several authors have reported on lasers in the II-VI semiconductor system [1,2]. The first results were obtained using a pulsed power supply and at liquid nitrogen temperature. Steady progress has been made since then, but one of the main problems is still the electrical contact to the p-doped semiconductor. The generally used metal contact acts as a reverse-biased Schottky junction. The breakdown voltage is of the order of ten volts, therefore considerable power dissipation takes place there, which makes CW room temperature operation difficult. In this work characterisation of the thermal behavior of such a II-VI semiconductor laser is presented. The results contribute to the understanding of the feasibility of CW operation.

Experimental

Laser diodes with an emission wavelength of 487nm at 80K have been grown on n-GaAs substrates, using molecular beam epitaxy. The layer structure is depicted in Fig.1. The n- and p-doping are provided using Cl and N respectively. The stripe is defined using polyimide insulation; the top-contact is formed by a 2000 Å Cr/Au layer. Voltage-contrast measurements performed in a scanning electron microscope [3] show that the voltage-drop across this junction mainly determines the voltage-drop across the entire diode. After growth and application of the patterned polyimide and the Cr/Au contact, the wafer is thinned to 100 µm, a Cr/Au back contact is applied and 300 µm long laser chips are cleaved out. For the measurements, the diodes are soldered substrate-down to copper cubes, using In solder, and cooled to liquid-nitrogen temperature. A 10^{-4} duty-cycle pulsed power supply is used. The stripe width is 10 µm, giving a threshold current of approximately 17mA at 80K; the operating current is 15mA higher.

In Fig.2 the spectral positions of the longitudinal modes are plotted as a function of the controlled temperature of the laser mounting block. The drive pulse width is 20ns. For each temperature the strongest mode, which approximately gives the gain maximum, is indicated. A shift to longer wavelengths of 0.067nm/K for the gain maximum and of 0.02nm/K for the longitudinal modes is seen with increasing temperature. The shifts are found to be linear with temperature in the 80-100K range.

To investigate the intra-pulse heating, gated spectra are measured, using a boxcar integrator. These are plotted, together with a time-integrated spectrum, in Fig.3. The drive pulse length was 230ns. The gate times are given; the gate width was 10ns in all cases. The broader spectrum at 30ns can be explained by a slight decrease in the current through the laser in that interval, caused by reflections in the 50 Ω coax power supply line between the pulse generator and the laser. The gain maxima as a function of the gate time, are plotted in Fig.4. During the first 20ns of the pulse, the wavelength stays constant; after that it increases approximately linearly with time, which is the expected behavior due to heating of the active region by a source at the top contact. The linear wavelength shift with time corresponds to a temperature rise of 0.16K/ns.

The current through the laser I_l also varies with time in the pulse. It follows the dotted line in Fig.4. This is most likely due to the temperature rise in the top contact itself, which lowers the avalanche breakdown voltage [4]. Since the power-supply is a constant voltage source with an internal impedance of 75 Ω, this decreasing voltage across the

diode induces a current increase.

Once the temperature of the active region can be determined from the lasing wavelength, the heat-resistance from the active- and top-contact-region to the laser mounting block for these lasers can be determined [5]. In the experiment pulses of 85ns drive the laser and a small superimposed dc current is used for the heating. The spectra at different heating power levels are given in Fig.5. As can be seen, the induced wavelength shift is linear with the applied power at a slope of 4.3 nm/W. Using the known shift of the gain maximum with temperature of 0.05nm/K, a heat resistance of $R_t = 85$ K/W, which is comparable to values seen in GaAs/AlGaAs lasers [6], can be derived.

Discussion

From numerical data in the literature [7], the thermal conductivity and specific heat of ZnSe can be estimated. Using these values in a simple thermal model for a semi-infinite solid [8], the temperature development with time at the position of the active region, 1.5 μm under the surface, can be calculated. The model shows that, after a delay of 20ns, the temperature ramps up at a rate of 0.13K/ns. The similarity between this value and the measured one confirms that the observed phenomena are mainly thermal.

When the short-pulse threshold current as a function of temperature and the thermal resistance are known, the conditions for CW operation can be derived. Assume that the threshold current follows $I_{th} = k \exp(T/T_0)$, with k a constant. T_0 has been determined to be 80K in the lasers of this study. For a certain CW current injection level, the difference $\Delta T = T_0 \ln(I_t/k) - T_{base} - R_t V I_t$ between the temperature at threshold and the induced temperature in the active layer by that current has to be positive for lasing. T_{base} is the mounting block temperature and V is the voltage drop in the vicinity of the active region. For example, for the $I_{th} = 17$ mA at 80K and $T_{base} = 80$ K, there is a current range for which ΔT is positive, making CW operation possible, for $R_t V \leq 1700$ K/A. For $T_{base} = 300$ K, $R_t V \leq 100$ K/A is necessary, which could be obtained by a $R_t = 30$ K/W (mounting substrate-up [5]) and $V=3.5$ V (improved top contact). Of course, these values are dependent on the T_0 and the needed injection level (factor k). Also, deviations of the I_{th} from the exponential law will change the needed $R_t V$ values.

In conclusion the wavelength spectrum of a II-VI-based semiconductor laser under pulsed conditions has been studied. A monotonic thermal shift that starts 20ns after the beginning of the pulse is seen, indicating that most of the heat is produced at the p-contact region. The thermal shift rate with time, at the beginning of the drive pulse, and the thermal resistance from the epitaxial region to the ambient are as expected from the geometry and literature data on material thermal parameters. From these characteristics, conditions for CW operation can be derived and will be discussed.

References

- [1] M.A. Haase, J. Qui, J.M. DePuydt, H. Cheng; Appl. Phys. Lett. 59, 1272 (1991).
- [2] H. Jeon, J. Ding, W. Patterson, A.V. Nurmikko, W. Xie, D.C. Grillo, M. Kobayashi, R.L. Gunshor; Appl. Phys. Lett. 59, 3619 (1991).
- [3] J. de Poorter; private communication.
- [4] S.M. Sze; Physics of semiconductor devices; 2nd ed., Wiley, New York (1981).
- [5] J.S. Manning; J. Appl. Phys. 52, 3179 (1981).
- [6] J.J.L. Horikx; unpublished.
- [7] Y.S. Touloukian et al.; Thermophysical properties of matter; vol.1&5, IFI/Plenum, New York - Washington

(1970).

[8] H.S. Carslaw, J.C. Jaeger; Conduction of heat in solids, 2nd ed., Oxford University Press, London (1959).

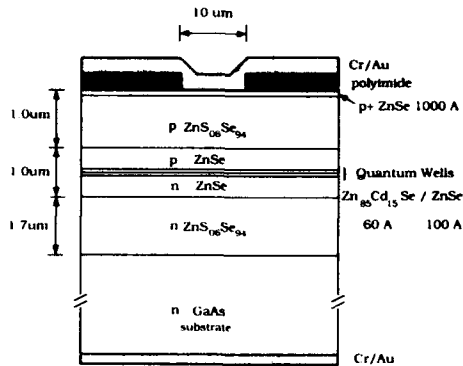


Fig. 1. Schematic cross-section of the used semiconductor lasers.

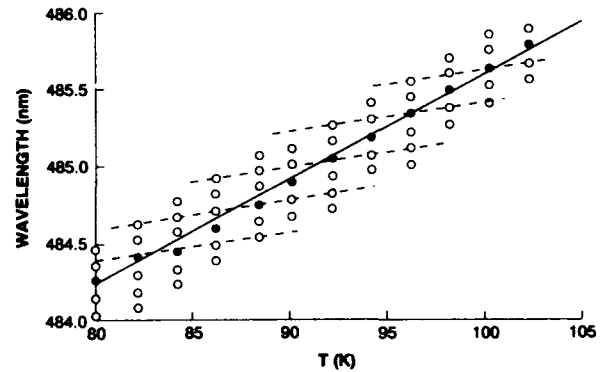


Fig. 2. Spectral positions of the longitudinal modes as a function of the temperature of the laser. The solid circles represent the strongest modes (gain maximum). The solid and dashed lines give the temperature shifts of the gain maximum and of the modes respectively.

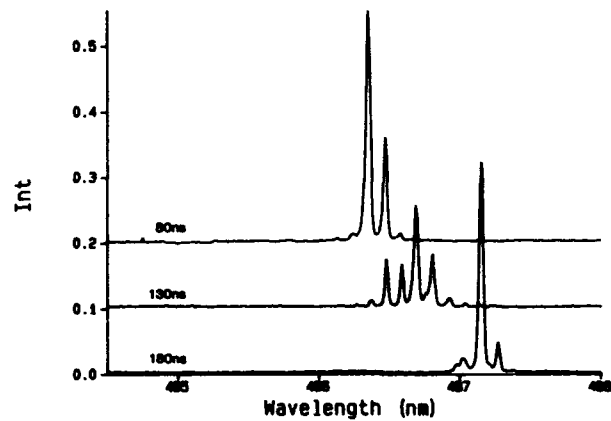
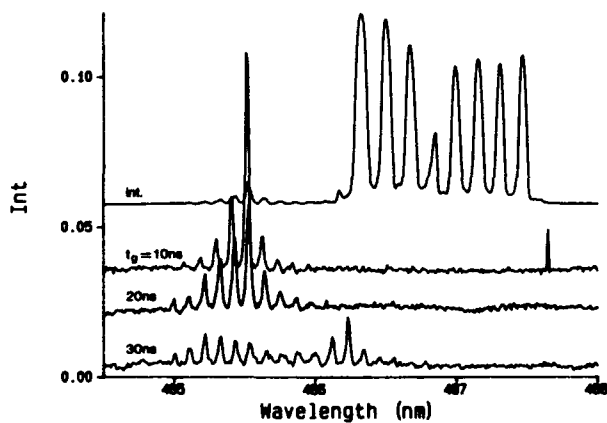


Fig. 3. Gated spectra and a time-integrated spectrum for 230ns drive pulses at twice the threshold current. Gate width is 10ns.

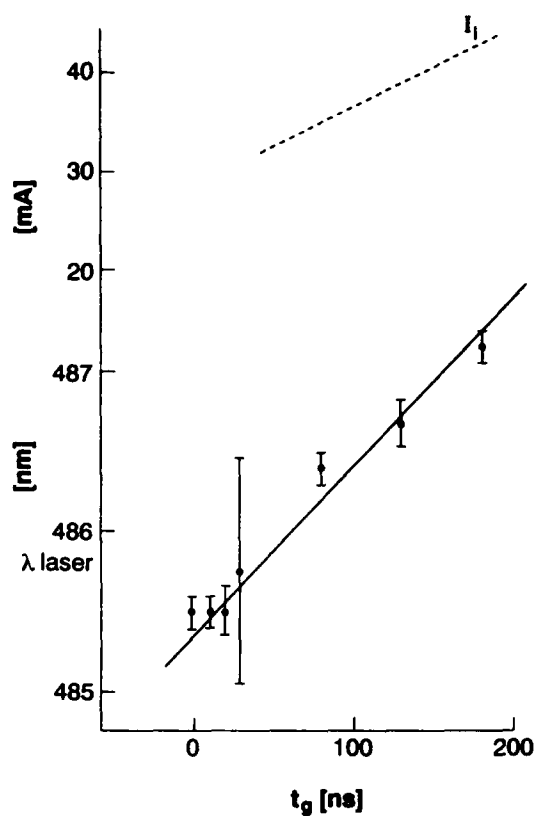


Fig. 4. Center-wavelength as a function of gate-time from the gated spectra (points with error bars, indicating spectral widths). The dotted curve gives the current through the laser after it has become steady.

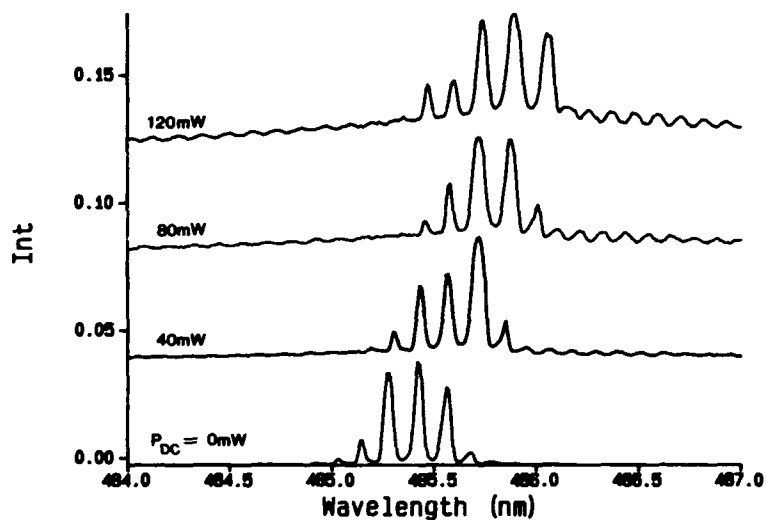


Fig. 5. Wavelength spectra under various dc-heating conditions (20ns drive pulse).

**Digital Alloy Quantum Wells of CdSe/ZnSe: New Structures
for Blue-Green Lasers**

H. Luo, S. Short, N. Samarth, A. Yin, A. Pareek, M. Dobrowolska, and J.K. Furdyna
Department of Physics, University of Notre Dame, Notre Dame, IN 46556

P. Ahrenkiel and M. Al-Jassim
National Renewable Energy Laboratory, 1617 Cole Blvd. Golden, CO 80401

F.C. Peiris and J.R. Buschert
Department of Physics, Goshen College, Goshen, IN 46556

SUMMARY

Rapid progress in ZnCdSe/ZnSe wide-gap semiconductor heterostructures has demonstrated the feasibility for applications such as blue-green semiconductor lasers. There are, however, still various problems that have to be resolved, among which is the quality of ZnCdSe alloy that comprises the quantum well region. A search of quantum wells with better optical characteristics lead to our study of digital quantum wells of CdSe/ZnSe. One of the advantages of CdSe/ZnSe digital alloys is the ordered crystal structure in the quantum well regions that might decrease alloy scattering of charge carriers. Most of the current interest in ZnCdSe/ZnSe prompted by applications is in the blue-green region, corresponding to Cd concentrations of less than 25%. We therefore focused our attention to structures consisting of various numbers of periods of 1 monolayer (ml) of CdSe and 3ml of ZnSe, which have an effective Cd concentration of 25%.

Because of the ultrathin (monolayer) nature of the digital alloy structures, migration enhanced epitaxy (MEE) was used as the growth technique. All samples were

grown on (100) GaAs substrates with 1 μ m ZnSe buffer layer grown by MBE at 300°C. The growth temperature for the digital alloy regions was set between 175°C to 300°C. The CdSe/ZnSe digital alloy quantum wells grown (by MEE) were embedded in ZnSe barriers, which were grown by MBE. Since there is at any time only one shutter open during MEE growth, we studied the effect of various lengths of time for each shutter opening, which is shown to depend on the sticking coefficient of the element deposited. We also varied the length of interruption between the deposition of successive elements. The process of re-evaporation not only during, but also after, deposition was observed to be very strong for Cd and Se, both of which have smaller sticking coefficients than that of ZnSe.

Photoluminescence (PL) and photoluminescence excitation (PLE) were used for characterizing the samples. The ground state transition energies obtained from the PL spectra provide a good measure of the monolayer coverage in the digital alloy quantum wells, as well as their *quantum efficiency*. The monolayer structures can be resolved in transmission electron microscopy (TEM) images. The periodicity of the digital alloy was also studied by X-ray diffraction.

Variations of the MEE growth technique were experimented. This includes eliminating the interruption between successive depositions, and also having a short overlap between depositions of cations and anions. Such experiments resulted in improved monolayer coverage and optical characteristics.

All samples were studied by PLE, which shows a clear correlation between the monolayer coverage and the electron-phonon coupling through the number of observable phonon replicas. Such a correlation is also reflected in the temperature dependence of the ground state PL peaks. For the samples with the highest coverage, the phonon peaks in the PLE spectra can be totally eliminated. Those samples also demonstrated the best room temperature behavior. Plotted in Fig. 1 is a room temperature PL

spectrum, showing peaks from the 7, 4 and 2 periods of CdSe(1ml)/ZnSe(3ml) quantum wells (labeled A, B and C, respectively). Peak D is from the ZnSe buffer layer. By fitting the line shapes of the PL peaks, the full width at half maximum of the peaks are 28meV, 32meV, and 38meV for the 7, 4, and 2 period quantum wells, respectively, which are the narrowest room temperature PL peaks from structures with similar well widths and Cd concentrations.

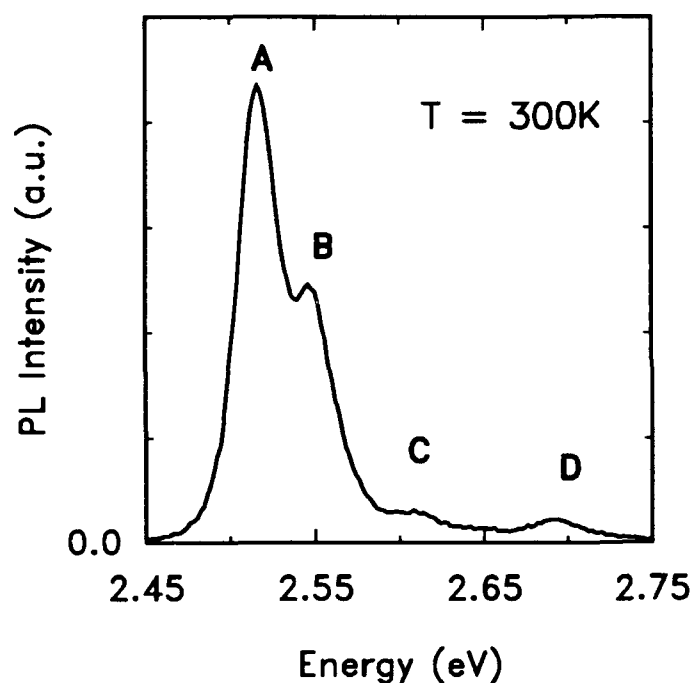


Figure 1. Room temperature PL peaks from the 7, 4 and 2 periods of CdSe(1ml)/ZnSe(3ml) quantum wells (labeled A, B and C, respectively). Peak D is from the ZnSe buffer layer.

Wednesday, February 3, 1993

Mid-IR Lasers 1

AWA 8:00am–9:30am
La Salle Ballroom B&C

Donald J. Smith, *Presider*
U.S. Air Force

Pulsed Gain Measurements and 3- μ m CW Laser Operation in Er³⁺-Doped Crystals

B. J. Dinerman*, P. F. Moulton, and D. M. Rines

Schwartz Electro-Optics

45 Winthrop Street, Concord, Massachusetts 01742-2052

(508) 371-2299

Summary

Recent research into 3- μ m-wavelength erbium lasers has shown that efficient operation can be achieved in both the pulsed and cw modes of operation, despite the population bottleneck that arises due to a long lower laser state lifetime. This, we believe, is due in part to the upconversion acting within the system that effectively removes ions from the lower laser state and repopulates the upper state. In a past paper, we reported the first cw operation in monolithic Er³⁺-doped YAG, GGG, and YSGG via resonant excitation into the ⁴I_{11/2} upper laser state (Figure 1). [1] We now report further investigations into these materials, with the addition of BYF and YLF, that include studies of the 3- μ m gain properties under conditions of pulsed pumping.

Using a cw Ti:Sapphire laser for preliminary laser investigations, we obtained laser thresholds as low as 5 mW, slope efficiencies greater than 30%, and outputs approaching 200 mW. We also achieved CW laser action using one or two 1-W, 964-nm strained-quantum-well diode lasers, where the diode laser emissions were coupled into the erbium laser crystal using identical lenses to collimate and focus the light. Higher thresholds and lower efficiencies resulted from the multimode and asymmetrical nature of the pump beam. Table 1 presents the results from Ti:Sapphire-pumped and diode-pumped erbium.

Using a 0.25-m monochromator with a 300-groove/mm grating blazed at 2 μ m, we investigated the spectral nature of the laser output. In operation well above threshold, the spectral widths were typically \sim 1.5 nm, including 2-5 longitudinal modes. Er:BYF was the only material which appeared to operate on a single longitudinal mode for operation as high as 6 \times threshold.

The spectral nature of the output may also be affected by operating temperature. We chose Er:YAG as a representative material to study this dependence. We mounted the monolithic laser crystal in a variable-temperature, liquid-nitrogen-cooled, evacuated Dewar. The 2.937- μ m line steadily increased in intensity as we cooled the system from room temperature, but near 180 K, this line decreased and two new lines, one at 2.858 μ m and one at 2.899 μ m, appeared. At 77 K, these two lines gained strength and laser action ceased entirely at 2.937 μ m.

More recently, we have begun investigating the 3- μ m wavelength laser gain of these erbium-doped materials using a "pump-probe" method. We side-pumped sample crystals with a pulsed, 970-nm Cr:LiSAF laser, and probed gain using our cw, diode-pumped monolithic lasers. The flashlamp-pumped Cr:LiSAF laser was excited by a transistor-switched variable-pulsewidth lamp driver in order to observe the effect of pump pulsewidth on gain.

To date, we have conducted gain measurements for Er-doped YSGG, GGG, BYF, and YLF. We conducted the measurements for each sample as a function of pump pulse duration and pump energy. We studied the temporal dependence on a digital oscilloscope, and the values we used to calculate gain were recorded directly from this measurement. Figure 2 shows gain measurements for Er:YSGG for two different pump energies.

Results of the measurements show that the gain signal remains fairly linear throughout the range of energies, indicating that gain saturation has not yet occurred. We anticipate that at higher energies, saturation would occur due to upconversion processes affecting the upper laser level at high excitation densities. [2] Upconversion adds a term quadratic in upper-state population to the system rate equations, and has the effect of reducing the apparent storage time as pump levels increase. Results of gain measurements for 30%-doped Er:YSGG are shown in Figure 3. We plan

to determine the upconversion coefficients for all the materials to be studied by fitting our gain data to a rate-equation model. We expect the garnet crystals to have similar properties, but the coefficients for the fluoride crystals may be substantially lower.

In summary, we have studied the cw laser properties of Er-doped YSGG, GGG, YAG, BYF, and YLF. Low thresholds and high efficiencies have been demonstrated. In addition, we have conducted gain measurements near $3\text{ }\mu\text{m}$ for each material. Large gains have been observed under high-power, short-pulse pumping.

*corresponding author

References:

- [1] B. J. Dinerman and P. F. Moulton. "CW Laser Operation from Er:YAG, Er:GGG and Er:YSGG." OSA Proceedings on Advanced Solid-State Lasers. Santa Fe, New Mexico. February, 1992.
- [2] V. A. Smirnov and I. A. Shcherbakov. "Nonlinear Interactions in Scandium Garnets Doped by Chromium and Erbium Ions." OSA Proceedings on Tunable Solid State Lasers. North Falmouth, Massachusetts. May, 1989.

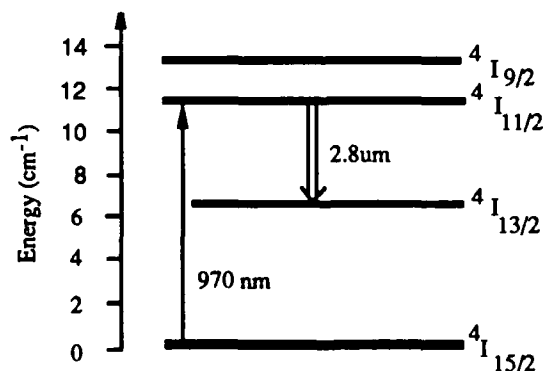


Figure 1. Relevant energy states of Er^{3+} .

	Er:YSGG	Er:GGG	Er:YAG	Er:BYF	Er:YLF
laser wavelength (nm)	2797	2821	2937	2800	~2800
laser threshold (mW)	5 (70)	7 (250)	40 (410)	6 (10)	-
slope efficiency (%)	31 (26)	27 (19)	26 (12)	20 (13)	-
laser output (mW)	190 (511)	155 (293)	143 (190)	104 (163)	95

Table 1. Performance summary of 3- μ m erbium lasers. Values in parentheses indicate results from double 1-W-diode pumping. All other values from Ti:Sapphire pumping.

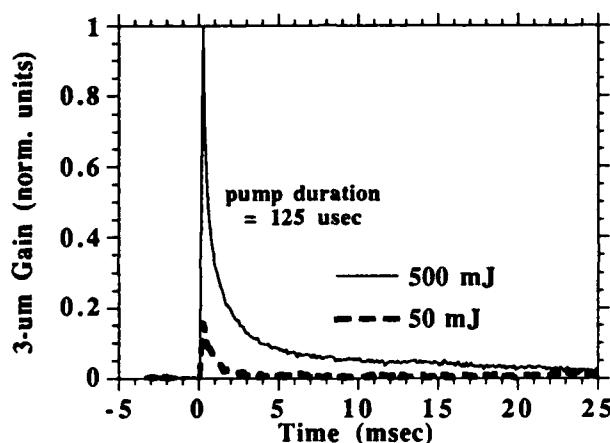


Figure 2. Gain measurements for Er:YSGG using a 125- μ sec pump pulse. (The DC baseline has been subtracted for purpose of presentation.)

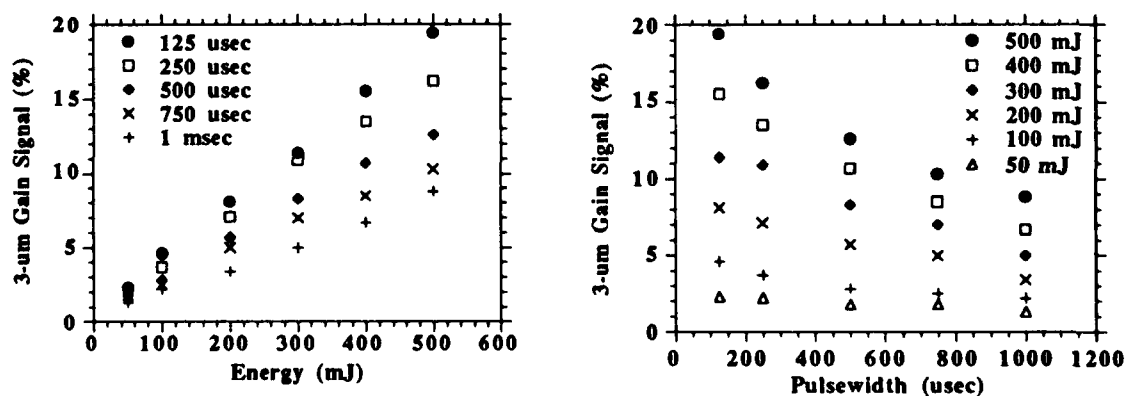


Figure 3a,b. Results of gain measurements for Er:YSGG as functions of pump energy and pulsewidth.

Cw-cascade laser operation in Er:YLF and Er:KYF at room temperature

B. Schmaul, G. Huber, R. Clausen

Institut für Laser-Physik, Universität Hamburg, Jungiusstr.11, 2000 Hamburg 36
Germany

B. Chai, M. Bass

Center for Research in Electro Optics and Lasers and Department of Physics,
University of Central Florida, Orlando, FL 32816, USA

For cascade laser operation several suggestions were made [1,2]. In Tm,Ho:YLF cascade lasing was observed [3,4]. In this work cascade cw-laser emission was obtained at 300K from 1% and 0.5% doped Er:YLF at 2810 nm and 1620 nm and also from Er:KYF at 2804 nm and 1612 nm using the $4I_{11/2} - 4I_{13/2}$ and the $4I_{13/2} - 4I_{15/2}$ transitions. The lower level of the 2810 nm transition is the upper level of the 1620 nm transition. The combination of a low concentration of Er^{3+} ions and the YLF or KYF host enabled cascade lasing at room temperature on both transitions. The fact that the lifetime of both the $4I_{11/2}$ and the $4I_{13/2}$ levels of Er^{3+} in YLF are comparable, 2.9 msec and 10 msec [5], respectively, is thought to make this result possible.

The Er:YLF rods used had an atomic concentration of 1 % and 0.5% and were coaxially pumped by a krypton ion laser operating at 647 nm. The pumped lengths were 6.9 mm (Er[1%]:YLF), 11mm (Er[0.5%]:YLF and 9.3mm (Er[1%]:KYF) along the crystal's a-axis. The laser resonator was a nearly concentric cavity formed by one 5 cm and one 10 cm radius mirror with high reflectivity for both transitions. The laser radiation was analyzed with the aid of a 1/4 m monochromator employing a 300 grooves/mm grating blazed at 2000 nm and an InSb detector cooled to 77 K. Signals from this detection apparatus were monitored with an oscilloscope (Tektronix Model 2440) and stored in a computer.

Fig. 1 shows the simultaneous cw-operation at both 2810 and 1620 nm for Er[1%]:YLF. It also shows the temporal waveform of each wavelength while lasing. A mechanical chopper was used to reveal the appearance of the first laser pulse at 2660 nm (upper trace). After the lower Stark level of the 2660 nm transition is filled the laser operation shifts to the longer laser wavelength at 2810 nm. When this transition is in steady state operation the 1620 nm transition starts to lase (lower trace). Because the 1620 nm laser is near threshold, its lasing starts approximately 10 msec after the onset of pumping.

Fig. 2 shows the output-vs-input power curve for all wavelength operation in continuous wave mode (without chopping). The pump laser beam was focused with a 5 cm lens and the resonator consisted of the mirrors described above. From the definition of slope efficiency, the mirror transmissions and the measured slope efficiency we calculate the cavity losses at 2810 nm to be 6%. The threshold for the 2810 nm wavelength couldn't be measured directly because the krypton laser pump source couldn't stably emit at very low power, but is estimated to be 20 mW.

The threshold for the 1620 nm wavelength is estimated to be 200 mW of absorbed pump power. Unfortunately the maximum pump power of the krypton pump laser corresponded to about 230 mW of absorbed power. The slope efficiency is about 0.4 % for the 2810 nm transition alone and about 1.3 % for both wavelengths lasing simultaneously [Fig.2]. The ratio between the 2810 and 1620 nm laser output power is estimated from the oscilloscope traces to be about 12:1. As cascade lasing begins the increase in lasing efficiency is due to the rapid depletion of the lower level population of the 2810 nm transition by the onset of lasing at 1620 nm.

References:

- [1] A.A.Kaminskii, *Laser Crystals*, (Springer, Berlin, 1981), 49-52.
- [2] N.P. Barnes and K.E. Murray, *Tunable Solid State Lasers*, (1989) 161-166.
- [3] R.C. Stoneman and L. Esterowitz, *Advanced Solid State Lasers*, (1990) 267-270.
- [4] G. Kintz, L. Esterowitz and R. Allen, *Tunable Solid State Lasers*, (1987) 20-22.
- [5] J. Rubin, A. Brenier, R. Moncorge, and C. Pedrini, *Journal of Luminescence* 36 (1986) 39-47.

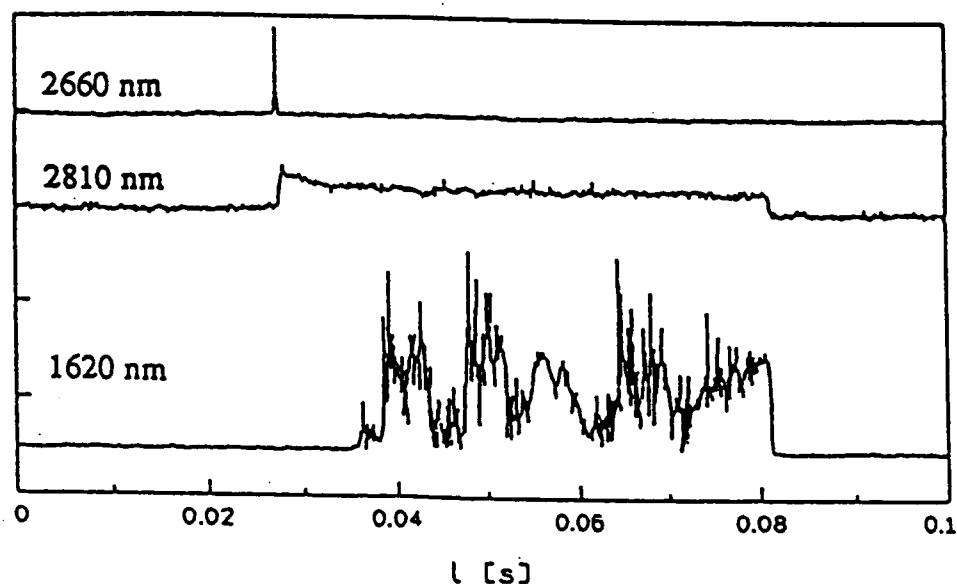


Figure 1. Cascade laser activity is shown. After an initial laser pulse at 2660 nm the 2810 nm transition starts to lase. With a delay of approximately 10 msec the 1620 nm laser appears and both transitions lase simultaneously. The intensity for each wavelength is shown in arbitrary units.

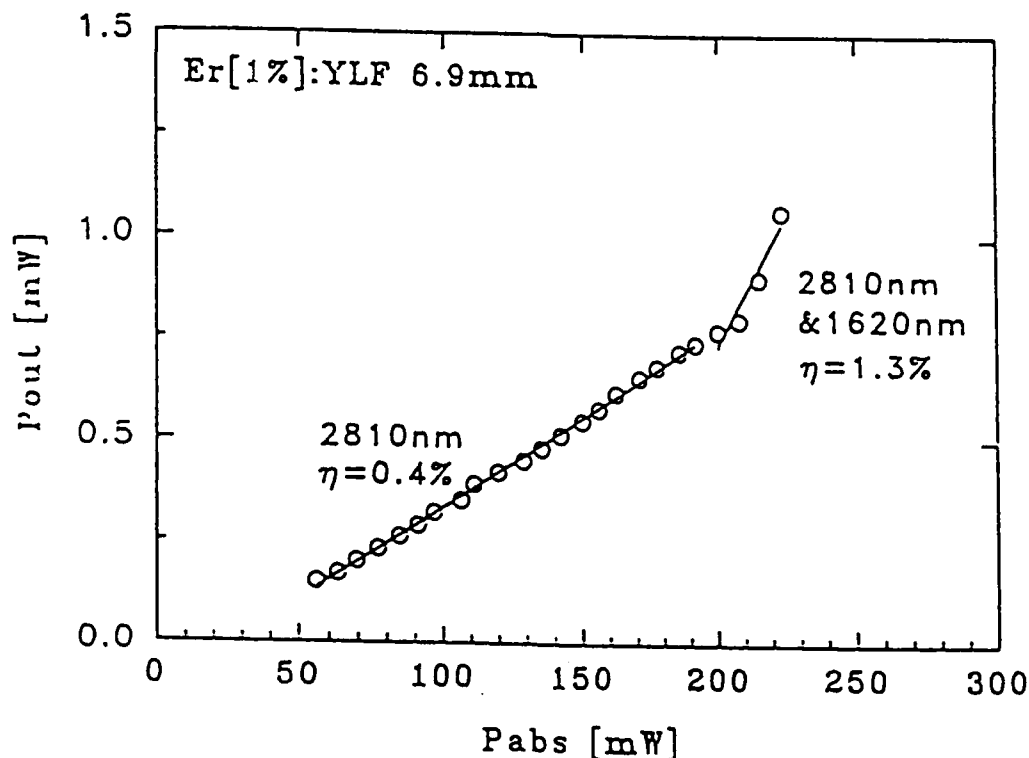


Figure 2. The output-vs-input power curve for Er[1%]:YLF for 647 nm krypton laser excitation is given. In the first part of the curve the output power is related to the 2810 nm transition. During cascade lasing (right side of the curve), the measured output power is the sum of that for both wavelengths.

All Optical Modulation of a 2.7 μm Erbium-Doped Fluorozirconate Fiber Laser

Ch. Frerichs

Institut für Hochfrequenztechnik, Technical University of Braunschweig, Post Box 3329,
D-W-3300 Braunschweig, Germany; Phone: 49-531-391 2423, Fax: 49-531-391 5841.

Mid-infrared lasers at 2.7 μm are attractive devices for medical and sensor applications, since in this range there is a strong absorption band of OH-radicals /1/. Fiber lasers at this wavelength are favourable because of their potentially low threshold powers and high efficiencies, due to the large power densities in the fiber core. The most promising candidate in this field is an Er^{3+} -doped fiber laser based on the fluoride glass ZBLAN, the most stable and easily fabricated IR-glass.

Er^{3+} -doped ZBLAN fiber lasers at 2.7 μm , resulting from the transition $^4\text{I}_{11/2} \rightarrow ^4\text{I}_{13/2}$, were first published in 1988 /2/ and have already been realized with very low threshold powers and high efficiencies /3/. As Er^{3+} has absorption bands pumpable with semiconductor lasers, such devices at 800 nm have been used to pump fiber lasers at 2.7 μm /4/.

For applications in medicine, and particularly in sensing, it may be necessary to modulate the laser. It is also a great advantage to have the feasibility of all-optical switching, as there may be applications which prevent the use of mechanical, electro-optical or acousto-optical switches. In this paper, a novel method of modulating a 2.7 μm fiber laser is presented, whereby the lower $^4\text{I}_{13/2}$ laser level is saturated through pumping with a laser diode at 1550 nm.

The experiments were carried out with a configuration shown in Fig. 1. The pump diode was a 500 mW STC single strip AlGaAs-MQW-Laser (LQ05P-KM78) emitting at 800 nm. Its beam was collimated and converted to a circular cross-section by an anamorphic prism pair. The signal diode was an OKI OL503A-65 at 1550 nm with a peak power of 65 mW, which was collimated. The signal laser was modulated directly. Both beams having approximately the same diameter, they were superposed with a dichroic beamsplitter and focussed into the fiber through the input mirror. The fiber was a 0.8 m long ZBLAN fibre made by *Le Verre Fluoré*, doped with 1000 ppm Er^{3+} . The core diameter was 30 μm and numerical aperture 0.15. The endfaces were butted against the resonator mirrors. The reflectivities of input and output mirror at 2.7 μm were 100% and 97%, respectively. The output was focussed through an IRGN6 lens and a high pass filter on to a PbS-detector, the signal of which was shown on a storage oscilloscope and recorded on a computer. The signal was monitored with a Ge-photodiode.

Pumping the fibre laser at 800 nm yields a 2.7 μm CW-laser. When pumping simultaneously at 1550 nm, the power of the 2.7 μm laser decreases with increasing power at the signal wavelength. At certain signal powers, depending on the pump power, the 2.7 μm

laser operation expires. The amount of signal power necessary to extinguish the 2.7 μm laser is approximately 2/3 of the pump power.

The temporal behaviour of the modulated 2.7 μm fibre laser is shown in Figs. 2 and 3. The signal is plotted inversely. Upon switching on the signal, the 2.7 μm operation almost immediately disappears. After switching off the signal, a delay of 0.2 to 1 ms is observed - depending on the modulation frequency - before the 2.7 μm operation recommences with relaxation oscillations. It was possible to modulate the 2.7 μm fiber laser at up to 2.5 kHz. At these high frequencies only one spike of relaxation oscillations was observed emitting a pulse with a duration of some tens of micro-seconds.

Fig. 4 shows the energy level scheme of Er^{3+} with the absorption, ESA and lasing transitions. The switching effect occurs due to the pumping of the lower laser level at 1550 nm. Thus inversion between the $^4\text{I}_{11/2}$ and the $^4\text{I}_{13/2}$ -level is terminated. The switching-off effect is rather rapid because the absorption of the $^4\text{I}_{13/2}$ -level is a stimulated process which is not dependent on the fluorescence lifetime of this level. The switching-on effect occurs after inversion is re-established. This occurs through depletion of the $^4\text{I}_{13/2}$ -level by spontaneous emission and by excited state absorption to the $^2\text{H}_{11/2}$ -level. The former process is dependent on the fluorescence lifetime of this level of approximately 9 ms and hence rather slow, whereas the latter is a stimulated process and therefore rapid. It is therefore assumed to be the dominant process because of the switching-on time of 1 ms or less.

Improvement of this modulation technique should be possible by optimisation of the pump and modulation wavelength and of the fiber geometry (e.g. by using a shorter fiber in order to get shorter relaxation spikes). The optimum pump wavelength ought to be that of the strongest ESA from the $^4\text{I}_{13/2}$ -level. Lastly, there would be much greater absorption of the modulation signal at wavelengths below 1550 nm.

In conclusion, a novel method has been presented to modulate a fiber laser at 2.7 μm by co-pumping with a 1550 nm-laser. This technique is a simple, all-optical method potentially allowing modulation of a 2.7 μm fiber laser via a communications fibre without any intra-cavity elements. It may find application in sensing and medicine.

References

- /1/ L. Esterowitz: Diode Pumped Solid State Lasers at 2 and 3 micron for the Biomedical Field; Proc. SPIE Vol. 1182, pp. 49, 1988.
- /2/ Brierley, M.C.; France, P.W.: Continuous Wave Lasing at 2.7 μm in an Erbium-doped Fluorozirconate Fibre; El.Lett. 24, pp. 935, 1988.
- /3/ Wetenkamp, L.; Frerichs, Ch.; West, G.F.; Többen, H.: Efficient CW operation of tunable fluoro-zirconate fibre lasers at wavelengths pumpable with semiconductor laser diodes; J. of Non-Crystalline Solids 140, pp.19, 1992.
- /4/ Allen, R.; Esterowitz, L.; Ginther, R.J.: Diode-pumped single-mode fluoro-zirconate fiber laser from the $^4\text{I}_{11/2} \Rightarrow ^4\text{I}_{13/2}$ transition in erbium; Appl. Phys. Lett. 56, pp. 1635, 1990.

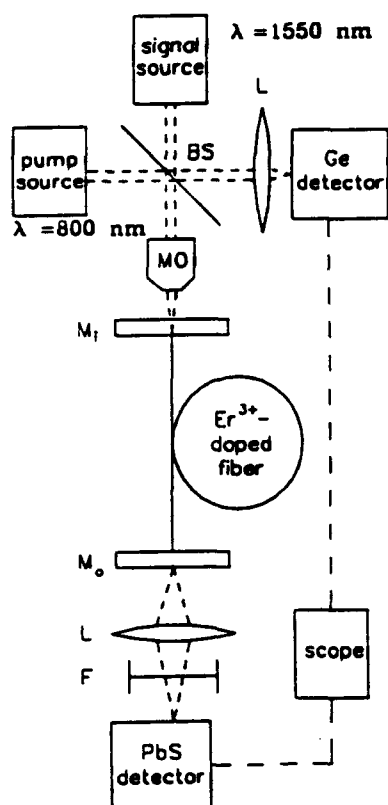


Fig. 1: Experimental configuration
(MO = microscope objective, L = lens, F = filter,
M = mirror (input/output), BS = beamsplitter)

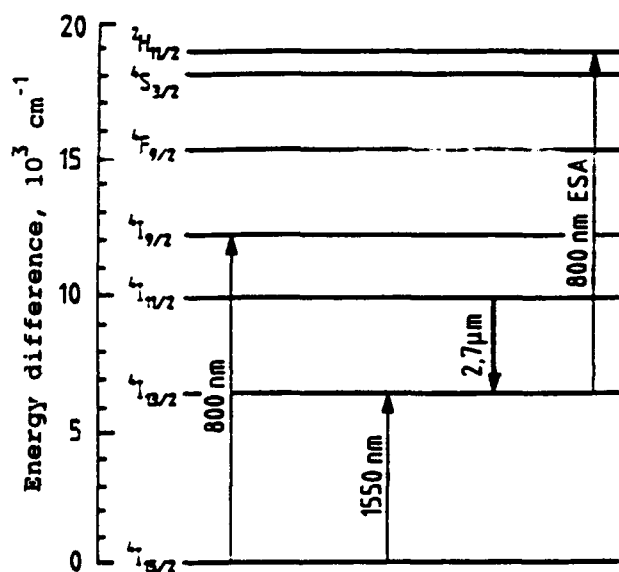


Fig. 4: Energy level diagram of Er^{3+} with transitions

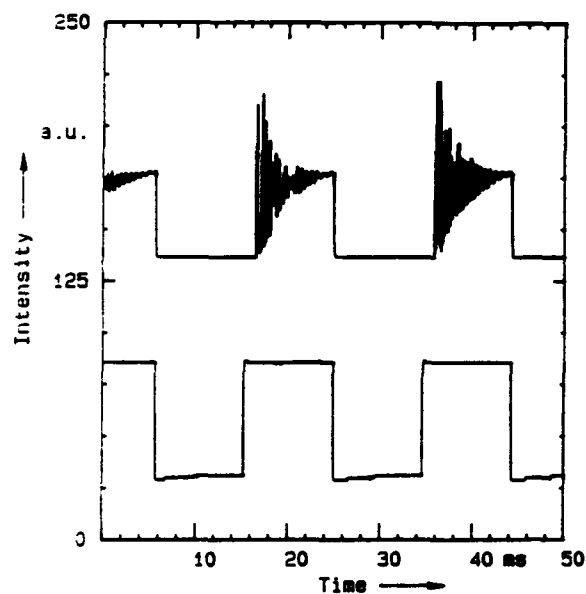


Fig. 2: Fiber laser signal (above) and modulation signal (below, inversely plotted).

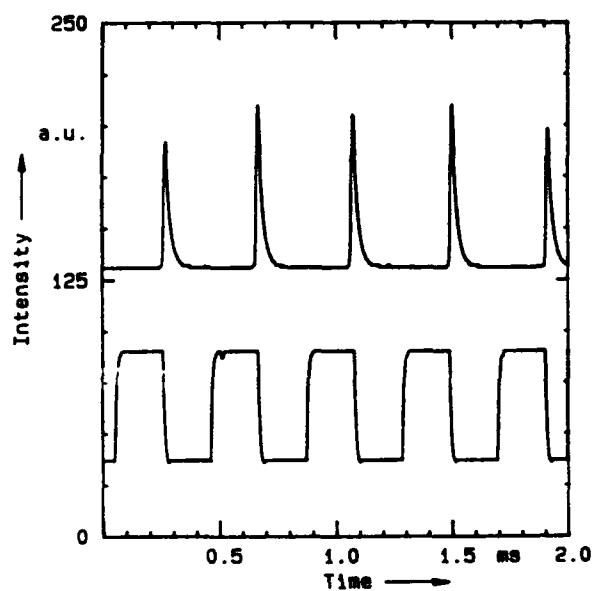
$$f_{\text{mod}} = 50 \text{ Hz}, P_{\text{pump, abs}} = 17 \text{ mW}, P_{\text{sig, abs}} = 12,5 \text{ mW}$$


Fig. 3: Fiber laser signal (above) and modulation signal (below, inversely plotted).

$$f_{\text{mod}} = 2,4 \text{ kHz}, P_{\text{pump, abs}} = 17 \text{ mW}, P_{\text{sig, abs}} = 12,5 \text{ mW}$$

Diode-pumped Single Frequency Ho:Tm:YLF

John P. Deyst

Science Applications International Corporation, Hampton, VA

Grady J. Koch

NASA/Langley Research Center, Hampton, VA

Mark E. Storm

Hughes/STX Corporation

I. Introduction

Lasers with a wavelength of $2\mu\text{m}$ are useful for applications that require eyesafe propagation through the atmosphere.^{1,2} This Letter discusses a single frequency laser that could be used as an injection locking source for a high power oscillator, or as a local oscillator source for a coherent receiver. The monolithic design of this laser is especially appealing because of its compactness, ruggedness, stability, and simplicity.

We chose Ho:Tm:YLF for our work because this 2-micron laser material has demonstrated high gain amplification.^{3,4} Previous researchers have demonstrated multi-mode lasing of Ho:Tm:YLF at or near room-temperature using external cavity resonators.^{5,6} Single-frequency lasing in a monolithic Ho:Tm:YAG lasers has also been reported.⁷⁻⁹ This paper reports the first demonstration of single-frequency lasing performance using Ho:Tm:YLF near room temperature. Continuous tunability over 5.6 GHz is also demonstrated.

II. Experimental Setup

Single frequency lasing was achieved with a plano/convex crystal with mirror coatings applied to its ends. The crystal was 1mm in thickness and 3mm in diameter, and a 1meter radius of curvature was used on the convex side. It was doped with 5% thulium and 0.5% holmium. The pump side was flat

and coated for maximum reflectivity at $2.06\mu\text{m}$ and maximum transmission at 780nm. The output coupler was a 98% reflective coating on the convex side. The laser crystal was mounted on a thermoelectric cooler and operated at temperatures down to -25 C.

The laser was end pumped by a Sony 303XT laser diode which had a maximum output power of 500mW, and a 780nm output wavelength. Since the $2\mu\text{m}$ lasing spectrum is strongly influenced by the optical coupling to the crystal resonator mode volume, careful attention was paid to the size and shape of the pump spot. The elliptical, highly divergent beam from the laser diode was collimated and circularized with a triplet lens and an anamorphic prism pair. The collimated beam was then focused by a 25mm focal length achromatic doublet to an elliptical spot of 15 by $90\mu\text{m}$ in diameter, much smaller than the crystal resonator's beam waist diameter which was $240\mu\text{m}$.

Ho:Tm:YLF is birefringent and exhibits different absorption and emission features on the two orthogonal axes. This laser was pumped with the laser diode polarization parallel to the c-axis of the crystal because absorption is quite strong in this orientation at 780nm.

III. Experimental Results

The crystal lased at a wavelength of $2.050\mu\text{m}$ polarized parallel to the c-axis. The lasing wavelength and polarization was independent of the pump polarization. The

crystal could be made to lase on a single or multiple longitudinal modes.

The number of longitudinal modes could be changed by altering the position of the pump focus along the length of the crystal. Maximum power was obtained from three longitudinal modes with the pump focus close to the HR mirror. Figure 1 shows the multi-mode laser power emitted for several different crystal temperatures versus the amount of pump power absorbed by the crystal. The maximum power obtained was 20 mW at a crystal temperature of -25 C. At this temperature the slope efficiency was 30.2%.

By moving the position of the pump focus closer to the center of the crystal, single frequency operation could be obtained. Stable single frequency operation was obtained and 6 mW of single frequency power was generated, with a slope efficiency of 18.6%. Single longitudinal mode operation was verified using a 3/4 meter monochromator, which could easily resolve the 1.4 nm longitudinal mode spacing. A scanning Fabry-Perot was next used to search for any higher order transverse modes--none were found. The Fabry-Perot had an adjustable mirror separation of 1 to 15 cm; one of the mirrors was mounted on a piezo electric transducer. The effective finesse of this device after alignment was 25. Based on the resonator geometry, any transverse modes would be spaced at approximately 1.25 GHz. Figure 2 shows a scan through two free spectral ranges with the mirror separation set at 5cm (FSR=3 GHz). A transverse mode associated with the single longitudinal mode would have appeared between the peaks marking the ends of the free spectral ranges. Similar measurements were made over the 1 to 15 cm mirror separation range--no higher order modes were found. A high speed photodiode was used to check for any low frequency spatial mode beating. No beating was observed within the 250 MHz bandwidth of this detector.

The Fabry-Perot scans also give some indication of the laser's linewidth. The width of the Fabry-Perot feature in Figure 2 shows

that the laser's wavelength spans 120MHz. This is not the linewidth of the laser, however, but the passband of the Fabry-Perot inteferometer. The measurement is still resolution limited after using the smallest possible passband of 40 MHz, corresponding to a mirror separation of 15cm. The measured linewidth is therefore less than 40 MHz. We expect the laser bandwidth to be significantly less than 1 MHz, comparable to other diode-pumped solid-state lasers.

Frequency tuning was achieved by temperature tuning the length of a similar plano/plano single frequency resonator. The laser tuned over 0.8 Angstroms (5.7GHz) between -30 and -26C. No longitudinal mode hopping was seen since the 14 Angstrom mode spacing is much greater than the tuning range. This tuning corresponds to a rate of 1.5 GHz per Celsius degree. This is consistent with the calculated value of 1.7 GHz per Celsius degree using published values for linear expansion coefficient and variation of refractive index with temperature.¹⁰ We believe a much larger tuning range is possible.

IV. Conclusions

We have demonstrated single frequency lasing of Ho:Tm:YLF at 2.050 μ m using a monolithic plano/convex resonator. This laser produced 6 mW of single mode power with a slope efficiency of 18.6%. The laser was frequency tuned continuously over 5.6 GHz by thermally changing the laser resonator length. The laser frequency tuning rate was measured to be 1.5 GHz/C.

The lasing spectrum of the Ho:Tm:YLF laser was strongly dependent on the position of the diode-laser pump beam focus along the length of the laser crystal. One, two, or three longitudinal modes could be made to lase by shifting the focal point of the pump laser inside the crystal. This behavior is attributed to the coupling of the pump beam to the laser's mode volume. The single frequency characteristics of this laser could be used to seed a high power oscillator. Such a laser system would be useful for eyesafe

atmospheric sensing.^{1,2,4}

References

1. M. E. Storm, "Coherent $2\mu\text{m}$ Sources Burst into Wind Shear Detection", *Laser Focus World*, 27, 4, 117-122, Apr. 1991.
2. M.J. Kavaya, S.W. Henderson, E.C. Russell, M.R. Huffaker and R.G. Frehlich, "Monte Carlo computer simulations of ground-based and space-based coherent DIAL water vapor profiling," *Appl. Opt.*, 28,5, 840-851, Mar. 1989.
3. M.E. Storm and J.P. Deyst, "Gain and Energy Storage in holmium YLF," *IEEE Trans. Phot. Tech. Lett.*, 3, 11, 982-985, Nov. 1991.
4. M. E. Storm, "Ho:Tm:Er:YLF amplifier performance and the prospects for multi-joule energies using diode-laser-pumping," accepted for publication in *IEEE Journal of Quantum Electronics*. Also see the references within this paper.
5. H. Hemmati, "2.07 μm cw diode-laser-pumped Tm,Ho:YLiF₄ room-temperature laser," *Opt. Lett.*, 14, 9, 435-437, 1 May 1989.
6. B. T. McGuckin and R. T. Menzies, "Efficient CW Diode-Pumped Ho:Tm:YLF Laser with Tunability Near 2.067 μm ," *IEEE J. Quant. Elect.*, 28, 4, 1025-1028, April 1992.
7. M. E. Storm and W.W. Rohrbach, "Single-Longitudinal-Mode Lasing of Ho:Tm:YAG at 2.09 μm ," *Appl. Opt.*, Vol. 28, No. 23, 4965-4967, 1 Dec. 1989.
8. M.E. Storm, Grady Koch and W.W. Rohrbach, "Single-Mode Lasing of Ho:Tm:YAG at 2.091 μm in a Monolithic Crystal," *OSA Proc. Adv. Solid-State Lasers*, vol. 6, Salt Lake City, UT, March 5-7, 1990, pp. 140-143.
9. T. J. Kane and T. S. Kubo, "Diode-Pumped Single-Frequency Lasers and Q-Switched Laser Using Tm:YAG and Tm,Ho:YAG," *OSA Proc. Adv. Solid-State Lasers*, vol. 6, Salt Lake City, UT, March 5-7, 1990, pp. 136-139.
10. N.P. Barnes and D. J. Gettemy, "Temperature Variation of the Refractive Indices of Yttrium Lithium Fluoride", *J. Opt. Soc. Am.*, 70, 10, 1244-1247, Oct. 1980.

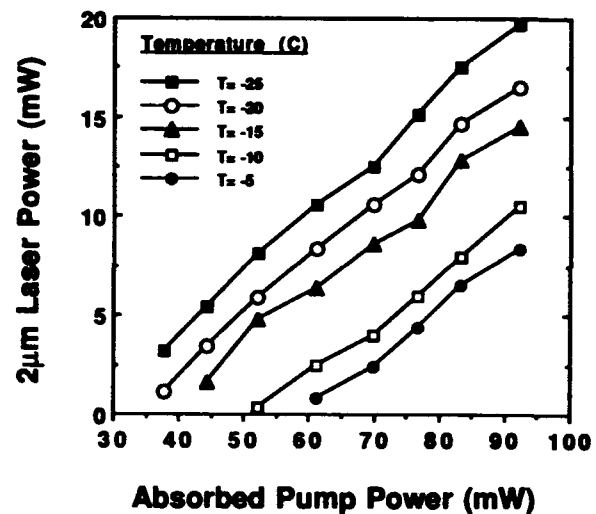


Figure 1: 2 μm laser power versus absorbed pump power for several crystal temperatures.

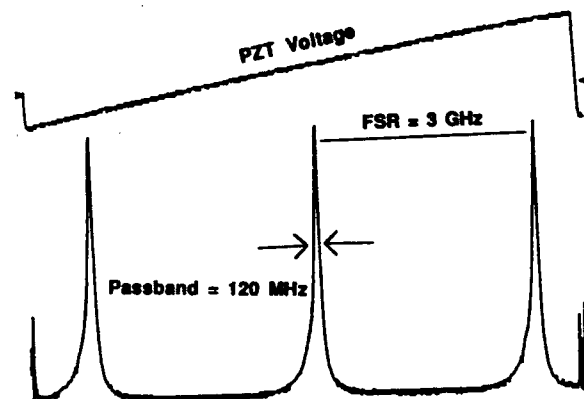


Figure 2: Fabry-Perot spectrum of single-frequency Ho:Tm:YLF laser

**Design and Performance of a High-Power, Diode-Pumped
2.1 μm Tm,Ho:YAG Laser**

G.J. Quarles, S.R. Bowman, J.G. Lynn,
C.L. Marquardt, S.K. Searles, and B.J. Feldman
Naval Research Laboratory
Washington, DC 20375-5320
Phone (202) 404-8609

INTRODUCTION

In this paper we describe the latest developments in the design and operation of a high average power, diode-pumped, 2.1 μm laser. We have designed and tested a Tm,Ho:YAG resonator which utilizes direct transverse pumping of the Tm using high-power, quasi-CW, 785 nm laser diode arrays. Each array is impingement cooled, and consists of a three bar stack which emits a total of 180 W of peak power. These diodes are each 1 cm in length and are mounted in a seven-fold symmetry and butt-coupled around a cooling jacket which surrounds a 3mm ϕ x 33mmL Tm,Ho:YAG laser rod. A mixture of water and methanol flows between the cooling jacket and the laser rod to provide a means of extracting the excess heat. The laser resonator is illustrated in Figure 1 and consists of two laser rods, each of which is 33 mm in length.

Surrounding each laser rod are three 1 cm wide rings of seven diode arrays. For this demonstration the Ho ion concentration is 0.36% and the Tm concentration is 6%. A previous study of this lasers performance characteristics as a function of Tm concentration has been reported previously.¹ Thermal lensing is quite significant in these materials and severely limits the designs that can be utilized for the resonator. When operating each individual laser rod at a 3% duty cycle (ie, 20 Hz, 1.5 ms diode pulse time) we measured thermal focal lengths as short as 20 cm. To compensate for this lensing, the rod closest to the high reflector was fabricated with a concave curvature on one end. This compensation reduced the convergence of the beam and allowed the

two rods to be brought within close proximity to each other with no bulk or coating damage due to the thermal lens. This compressed resonator design, which is shown in Fig. 1, allows the cavity length to be reduced to 25 cm. Compensation for the losses due to thermal depolarization effects has been accomplished through the placement of a half-wave plate between the two laser rods. This component is critical for achieving high average power under Q-switched operation. The Q-switch used in this demonstration was a Brewster-cut, water-free, fused silica acousto-optic modulator. For use in pumping an optical parametric oscillator, a plano-concave lens was placed approximately 30 cm from our output coupler to collimate the 2.1 μm laser beam. We have studied the 2 μm to 4 μm conversion efficiency and damage thresholds for two different nonlinear crystals, AgGaSe_2 and ZnGeP_2 . The largest conversion slope efficiency measured was 33%, and was achieved at room temperature with a multimode beam in the AgGaSe_2 .

This laser has been operated in a multi-burst, Q-switched mode which was previously demonstrated at NRL for flash-pumped $\text{Cr}:\text{Tm}:\text{Ho}$ laser systems.² Multimode, long pulse output energies as high as 370 mJ at 25 Hz with a 1.2 ms diode pump pulse have been achieved with $T = 0^\circ\text{C}$ for the laser rod coolant. The multi-burst, Q-switched energy extracted under the same conditions was 327 mJ total in 11 Q-switched pulses, thus extracting >90% of the available long pulse energy. Electrical-to-optical efficiencies for this system as high as 3.1% have been measured. Because of the thermal-optic distortions in the $\text{Tm}:\text{Ho}:\text{YAG}$, the average power of the laser is very repetition rate dependant. As seen in Figure 2, the average power of the laser peaks at 24 Hz before rolling off. A continued increase in the repetition rate drives the laser to become unstable.

REFERENCES

1. S.R.Bowman, G.J.Quarles, J.G.Lynn, S.K.Searles, and B.J.Feldman, at ILS-VIII 8th Interdisciplinary Laser Science Conference, paper TuMM2 (1992).
2. S.R.Bowman, M.J.Winings, S.Searles, and B.J.Feldman, IEEE J.Quantum Electron. 27, 1129 (1991).

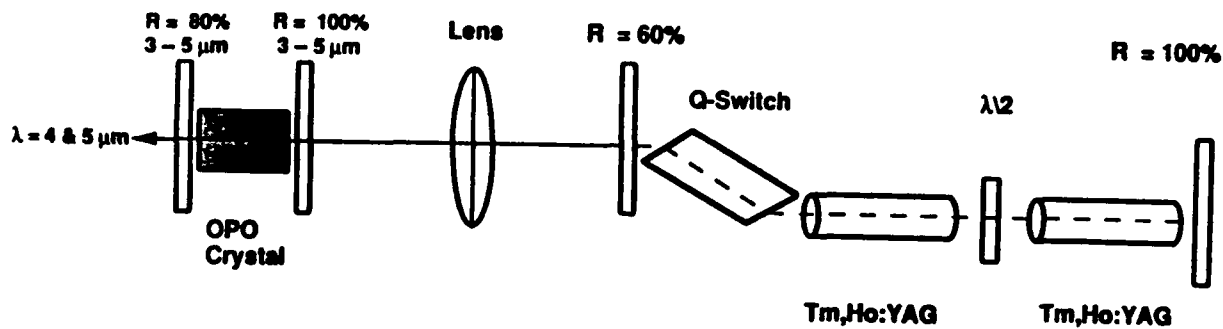


Figure 1. Schematic of the Diode-Pumped $2.1 \mu\text{m}$ Laser and Optical Parametric Oscillator.

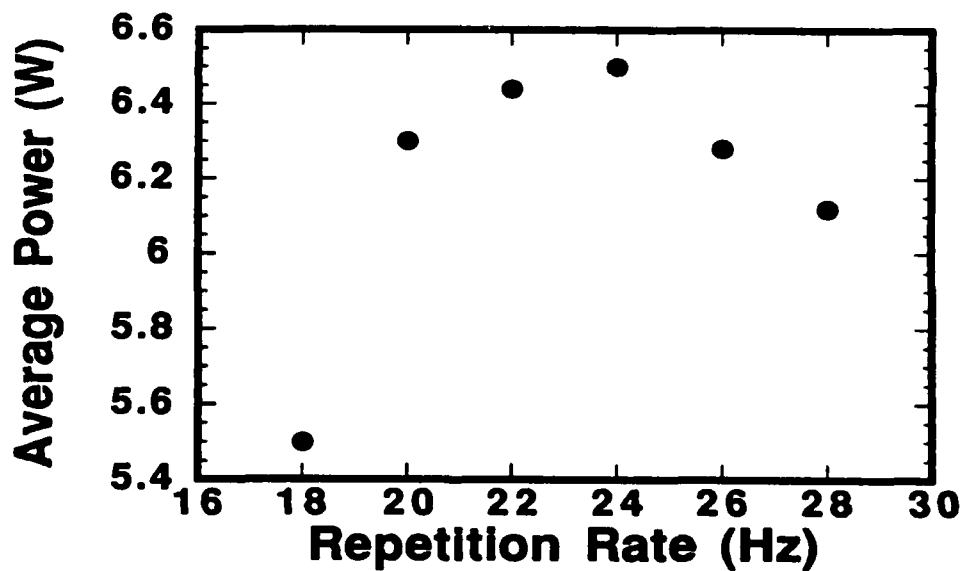


Figure 2. Room Temperature Average Power Output from $2.1 \mu\text{m}$ Laser versus Diode Repetition Rate.

Self-mode-locking properties of Tm:YAG-Lasers

Frank Heine, Ernst Heumann, Günter Huber,
 Institut für Laser-Physik,
 Jungiusstr.11,
 2000 Hamburg 36,
 Germany
 (Tel.:01149-40-4123-5241)

During the last 2 years the method of Kerr-Lens-Mode-locking (KLM), originally discovered by Spence et al.[1], was also tried in laser materials other than Ti:Sapphire [2]. Recently Cr^{4+} :Forsterite was successfully mode-locked by this powerful method [3] to reach the fsec time domain with wide spectral range solid state laser materials.

We report what we believe to be the first self-mode-locked operation of Tm:YAG, giving subnanosecond pulse width without using any additional active or passive elements.

The length of the Cr,Tm:YAG crystal was 6.2 mm, it was grown in our group using the Czochalski technique. Doping concentration were $1.85 \cdot 10^{20} \text{ cm}^{-3}$ and $1 \cdot 10^{21} \text{ cm}^{-3}$ for Cr^{3+} and Tm^{3+} respectively. The experimental setup consisted of a folded astigmatically compensated 3-mirror cavity, similar to that described in ref.[5]. The Kr-laser was focused with a lens of 10cm focal length through the first resonator mirror ($R=10\text{cm}$, HT @ 647 and 676nm, HR @ 2013nm), the crystal was inclined to Brewsters angle to prevent etalon effects. The folding mirror (same parameters as mirror 1) collimates the beam to the output coupler. Self-mode-locking could be achieved by using transmissions between 1% and 8%, the pulse formation process was optimized using transmissions of 3% and 5%. Pump energy was delivered by absorbing 2 watts of a Kr-laser at 647 and 676 nm matching the absorption bands of Cr or Tm respectively. The beam profile and the spectral bandwidth were controlled by using a scanning beam-analyser and a confocal Fabry-Perot-Interferometer. For determination of the absolute wavelength, a 0.5 meter spectrometer was used. The total optical length of the resonator was 1.05 meter and could be varied over $\pm 20\text{cm}$. In contrast to the typical setup for Ti:sapphire- lasers, a longer cavity could not stabilize the mode-locking. A one plate birefringent filter (1.48mm thickness) was used to control bandwidth.

The alignment of the resonator to the beginning of excessive mode beating decreases the output power from 250 mW to 140 mW (3% transmission of the output coupler). The Tm:YAG output consisted of pulse trains with durations of several hundred microseconds (Fig.1), in which the pulse width continuously decreases from the start to the amplitude maximum. This regime was stable for several hours before realignment was necessary. It should be noted that the appearance of KLM was restricted to the edges of stability regime of the resonator, in agreement with ref.[4].

Due to the oscillatory behaviour we were not able to perform an autocorrelation measurement, the pulse widths could only be estimated to lie between 800 and 400 psec. The upper limit is the time resolution of our fast detector-oscilloscope combination, the lower limit is related to the measured bandwidth (850 MHz), assuming chirp-free pulse structure. With active modelocking, pulsewidths between 30 and 40 psec has been obtained using acousto-optical modulation [5],[6]. It was possible to "switch" the repetition rate between single and double roundtrip frequency (143 MHz) by alignment of the laser resonator (see fig.2,3). Changing the distance between crystal and folding mirror by approx. $100\mu\text{m}$ and changing the position of the beam waist of the pump laser relative to the Thulium crystal by several microns led to the emission of pulsetrains with double roundtrip frequency. This mode-locking regime was found to be stabilised by performing weak nonresonant extracavity feedback, such as diffuse reflection from a sheet of paper behind the output coupler. The physics of this phenomenon are still under investigation. The beam profile was measured to become elliptic in the self-mode-locked regime (horizontal to vertical 1 to 0.85). When we suppressed mode-locking by coupling an external cavity or by inserting an etalon into the cavity, the beam become circular. This ellipticity indicates the existence of higher order transversal modes in the KLM-regime, the same result as found in reference [1].

We argue that the instability of the self-synchronisation process is mainly caused by thermal lensing

effects. In comparison to sapphire the relation of thermal lensing parameter to Kerr lensing parameter was estimated to be 6 times larger in YAG [4]. The main reason for this is dn/dT in YAG, which is 10 times larger than in sapphire [7]. Another contribution to thermal lensing effects is the heating of the crystal by reabsorption of the laser radiation. The reabsorption losses could reach 7%/cm at the laser-wavelength (2013 nm) [8], and with increasing peak-power even a partial bleaching of this reabsorption will change the index of refraction. This reabsorption induced lensing is in the same order of magnitude as the pump-power induced change in the refractive index. The reabsorption induced thermal lensing could be seen by blocking the Tm-laser and measure the change of divergence of the Kr-laser transmitted through the folding mirror. All these thermal effects are very sensitive to pump-power instabilities. The reabsorption losses of Tm^{3+} in YAG are 10 times larger than the losses due to the parasitic absorption in commercially available Ti:sapphire laser crystals having a Figure of Merit of ~ 300 . Even a small change in the pump-power or in the laser output will alter resonator and beam properties. In contrast to Ti:sapphire the implementation of an adjustable slit in the cavity has no stabilizing effect on the Kerr-lensing. Reducing the slit-width results in decreasing the output power without noticeably changing the mode-locking process.

Using a host crystal where dn/dT is smaller than in YAG (such as YLF) [9] in connection with a "quiet" pump source (an actively stabilised Kr-laser or laser diodes) should increase the stability of the mode-locking process, and therefore give rise to shorter pulse lengths.

In conclusion we have demonstrated self-mode-locking of cw- pumped Cr:Tm:YAG-lasers with repetition rates of 143MHz and 286MHz. Pulse widths between 400 and 800 psec in trains of several hundred microseconds have been obtained simply by alignment of the laser resonator very close to the stability regime.

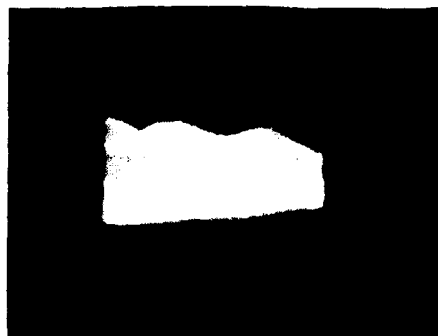


Fig.1: Envelope of self-mode-locked pulsetrains, 20 μ sec/div



Fig.2: Cr:Tm:YAG pulses at 143 MHz repetition rate



Fig.3: Cr;Tm:YAG pulses at 286 MHz repetition rate

References

- [1] D.E.Spence, P.N.Kean, W.Sibbet, *Opt. Lett* **16**,42 (1991)
- [2] G.B.A.Malcolm, A.I.Ferguson *Opt. Lett* **16**,1967 (1991)
- [3] T.J.Carring, A.Sennaroglu, C.R.Pollok, Advanced Solid-State Lasers , 1992, Technical Digest Series, MB4-1 / p.29-31.
- [4] D.Georgiev, J.Herrmann, U.Stamm, to be published in *Opt. Comm.*
- [5] F.Heine, E.Heumann, G.Huber, K.L.Schepler, *Appl. Phys. Lett.* **60**, 1161 (1992)
- [6] J.F.Pinto, L.Esterowitz, G.Rosenblatt, *Opt. Lett.* **17**,731 (1992)
- [7] A.A.Kaminskii, *Laser Crystals* (2nd edition), Springer Verlag New York, Berlin, Heidelberg (1990) p.321
- [8] T.Becker, R.Clausen, G.Huber, E.W.Duczynski, P.Mitzscherlich in Tunable Solid State Lasers, Vol.5 of the OSA Proceeding Series, M.L.Shand and H.P.Jensen, eds.(Optical Society of America, D.C.1989), pp 150-153.
- [9] J.L.Emmet, W.F.Krupke, J.B.Trenholme, *Physics of laser fusion Vol IV*, Lawrence Livermore National Laboratory, Livermore, Calif. ucrl-533344 (1982),p.26

Wednesday, February 8, 1995

Mid-IR Lasers 2 Poster Session

AWB 9:35am–10:30am
La Salle Ballroom A

Single-Longitudinal-Mode and Q-Switched
Diode-Pumped Tm,Ho:YLF Oscillators

Charley P. Hale, Sammy W. Henderson, and Paul J. M. Suni

Coherent Technologies, Inc.
3300 Mitchell Lane, Suite 330
Boulder, CO 80301
(303) 449-8736

Remote sensing applications have prompted intensive research and development of efficient eyesafe ($\lambda > 1.4 \mu\text{m}$) solid-state laser sources in recent years. Coherent laser radar experiments using Tm,Ho:YAG lasers at $2.1 \mu\text{m}$ wavelength have shown much promise for making very accurate, long-range measurements of wind speed and direction.¹ It has been shown that Tm,Ho:YAG suffers from considerable lifetime shortening due to up-conversion. This strongly limits its energy storage capability (at least for CW pumping), and hence how much energy can be extracted. Because of its weaker non-linearities Tm:YAG has become the material of choice in systems where high pulse energies are needed. This material is still not ideal for all lidar applications; the emission wavelength ($2.0 \mu\text{m}$) falls into an atmospheric attenuation region which is not as clean as around $2.1 \mu\text{m}$, and the small emission cross-section forces such high fluences in the cavity that damage may occur. Yttrium Lithium Fluoride (YLF) co-doped with Thulium and Holmium has received considerable recent attention^{2,3} as a possibly superior laser for certain applications. Compared to YAG lasers with similar Tm,Ho dopant concentrations, Tm,Ho:YLF appears to exhibit lower upconversion losses.⁴ The relatively high emission cross-section also permits operation at low fluences. As a result there is great potential for damage-free, high pulse energy operation of Q-switched Tm,Ho:YLF. In addition, the greater cross-section means that it will be far easier to develop efficient amplifiers in Tm,Ho:YLF than in, e.g., Tm:YAG.

We have concentrated our efforts in two distinct directions that will be reported here: the development of very stable, single-frequency CW Tm,Ho:YLF oscillators with laser crystals operating near and above room temperature, for use as tunable master oscillators in coherent lidar systems; and the more recent investigation of high-power CW and Q-switched Tm,Ho:YLF oscillators operating across a range of temperatures, pumped with 6 W of CW diode laser power centered at 792 nm.

A number of rod lengths, dopant concentrations, and crystal temperatures were investigated in the master oscillator development effort. Figure 1 shows the performance of a 4 mm-long, 6 % Tm, 0.5 % Ho:YLF crystal at two rod temperatures, 10° C and 35° C, as a function of diode pump power and longitudinal mode control. In all cases, the crystal is axially pumped in a 12 cm-long near-hemispheric cavity using a Spectra Diode Labs 3 W CW diode laser temperature-tuned to 792 nm wavelength and linear polarization oriented parallel to the 'c'-axis of the naturally birefringent YLF crystal. The 2 μ m laser spatial mode is TEM₀₀, with a minimum pump spot size formed inside the laser rod of \sim 200 μ m (10-90 % diameter). No intracavity line-narrowing elements are used in the multi-longitudinal-mode (MLM) cases, and the laser operates on many longitudinal modes near 2065 nm. When an 18 % R, 0.5 mm-thick etalon and an uncoated 75 μ m-thick etalon are introduced into the cavity, single-line operation was observed at full pump power, at both rod temperatures. The laser is highly linearly polarized without introduction of any polarizing element, due to the birefringent nature of YLF. While single-frequency slope efficiency is relatively low at 35° C, this mode of operation is very attractive in many applications due to the ease and simplicity of temperature stabilization necessary in very high frequency stability lasers.

Figure 2 shows the same laser's behavior when the output is tilt-tuned across the full 19.6 nm (1390 GHz) free spectral range of the thin etalon (with the 0.5 mm-thick etalon removed). Clearly, the flatness and absence of "frequency pulling" near the ends of the etalon range suggest that a thinner tuning etalon or appropriate birefringent tuning element would produce an even wider tuning range than demonstrated above.

High-power experiments are being conducted using two 3 W CW diode lasers, arranged to pump from either end of the laser rod. Results will be presented on short cavity, high-power CW lasers at various rod temperatures and dopant concentrations, and on long-cavity, acousto-optically Q-switched Tm,Ho:YLF lasers.

References

1. S. W. Henderson, C. P. Hale, J. R. Magee, M. J. Kavaya, and A. V. Huffaker, *Opt. Lett.* **16**, 773 (1991).
2. B. T. McGuckin and R. T. Menzies, in *Conference on Lasers and Electro-Optics*, Vol. 12 of 1992 OSA Technical Digest Series, pp. 24-25.
3. P. A. Budni, M. G. Knights, J. R. Mosto, and E. P. Chicklis, in *Advanced Solid-State Lasers*, Vol. 13 of 1992 OSA Technical Digest Series, pp. 380-383.
4. M. E. Storm and J. P. Deyst, *IEEE Phot. Tech. Lett.* **3**, 982 (1991).

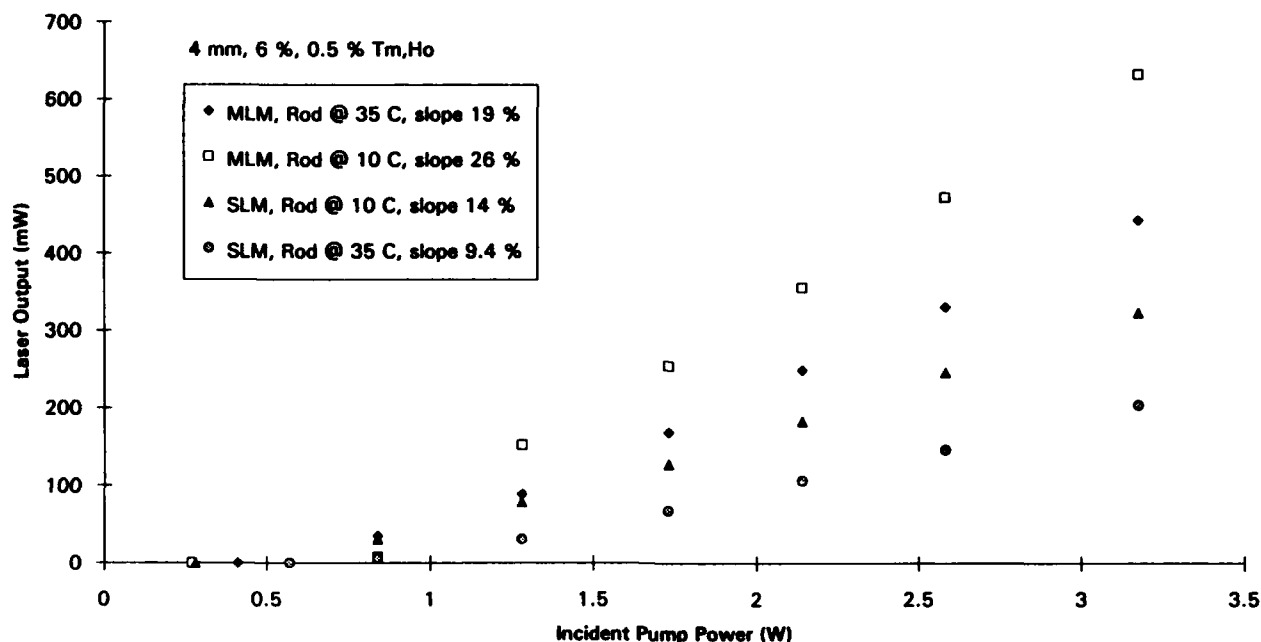


Figure 1. Tm,Ho:YLF Laser output versus diode laser pump power incident on the laser rod. Both multi-longitudinal-mode (MLM) and single-frequency (SLM) results are plotted for two different rod temperatures.

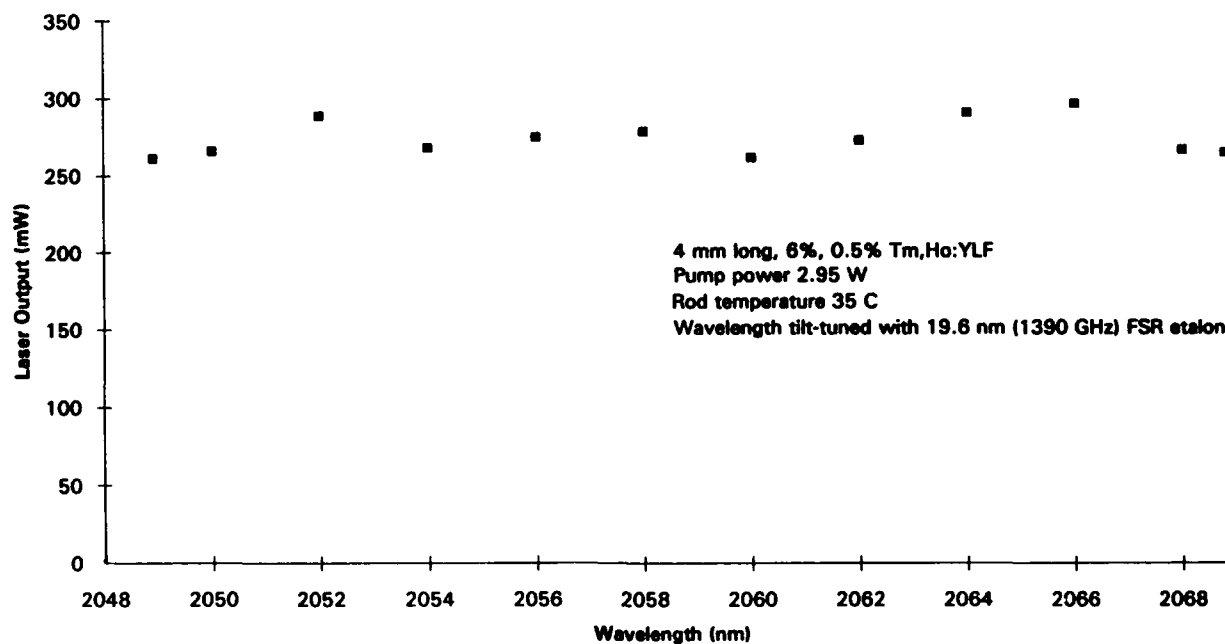


Figure 2. Tm,Ho:YLF output power versus wavelength. A 75 μm -thick uncoated silica etalon was tilted inside the laser cavity to tune the laser output across 19.6 nm near 2060 nm.

SPECTROSCOPY AND LASING IN Ho:Tm:Lu₃Al₅O₁₂

Elizabeth D. Filer
Lockheed Engineering and Science Company
Hampton, VA 23666

Norman P. Barnes
NASA Langley Research Center
Hampton, VA 23681

Felipe E. Naranjo
Science and Technology Corporation
Hampton, VA 23681

Milan R. Kokta
Union Carbide Corporation
Washougal, WA 98671

Summary

Lasing has been demonstrated in what the authors believe is a new laser material, Ho:Tm:Lu₃Al₅O₁₂ or Ho:Tm:LuAG. Laser performance of a Ho laser which is sensitized with Tm is highly dependent on the particular laser material. As with other Lanthanide series lasers, such as Nd, the stimulated emission cross section depends heavily on the selection of the laser material. However, in a Ho laser operating on the ⁵I₇ to ⁵I₈ transition, the lower laser level is in the ground manifold. As such the thermal population of the lower laser level must be overcome to reach threshold. Since which specific energy level within the lower laser manifold is the lower laser level as well as its thermal occupation is dependent on the laser material, selection of the laser material becomes more critical. In addition, in a Ho laser material which is sensitized with Tm, both favorable and deleterious energy transfer processes are material dependent. Thus, the selection of the particular laser material becomes very critical. To screen the multitude of potential laser materials, a quantum mechanical model was used to evaluate relevant parameters, and a figure of merit was used to select the most favorable candidates. LuAG was one of the two garnet materials of choice. One of the three transitions predicted to have the lowest threshold was also predicted to have a wavelength of 2.100 μm.

Lasing in Ho:Tm:LuAG was achieved by using a Ti:Al₂O₃ laser pump in a longitudinal pumping configuration. As much as 30 mJ of pump energy was focused to a beam radius of about 0.36 mm in the Ho:Tm:LuAG laser material. Pump energy density for these experiments was kept less than about 7.0 J/cm². Initial experiments utilized a short length of Ho:Tm:LuAG, only 1.4 mm. A

resonator consisting of a 0.3 m radius of curvature HR mirror and a flat output mirror was used to produce a beam radius of 0.32 mm in the Ho:Tm:LuAG. A nearly collinear pumping arrangement allowed the pump beam to be directly incident on the Ho:Tm:LuAG sample rather than being transmitted through one of the mirrors forming the resonator.

Using an output mirror with a reflectivity of 0.992, a threshold of about 8 mJ of incident energy was achieved. Lasing wavelength was measured as 2.1004 μm in good agreement with the quantum mechanical prediction. Lasing was also achieved with several other output mirrors having lower reflectivity. Using an output mirror with a 0.978 reflectivity, the slope efficiency was 0.0524. Since the Ho:Tm:LuAG sample was so short, only a fraction of the incident pump energy was absorbed. If the slope efficiency is calculated using the absorbed energy rather than the incident energy, the slope efficiency is 0.36.

Threshold increased with the negative logarithm of the output mirror reflectivity, while the slope efficiency increased asymptotically, as expected. An observed slope efficiency less than the photon energy limit results from limited absorption of the pump beam and a limited overlap of the pumped volume and the mode volume. Limited overlap results from the disparity in size and the noncollinear nature of the pumping arrangement. Further data will be presented on the germane spectroscopic parameters as well as more information on the laser performance.

A Comparative Study of Diode Pumped Two Micron Laser Materials

S.R. Bowman, G.J. Quarles, J.G. Lynn and B.J. Feldman

Laser Physics Branch, Code 5540,

Naval Research Laboratory, Washington, D.C. 20375-5000

Phone (202) 767-9418

The potential applications in medicine and remote sensing have generated substantial recent interest in 2 μm lasers. In this paper, we have extended our previous work on flashlamp pump Tm:YAG and Tm,Ho:YAG [1-4] to characterize these materials using laser diode pumping. Laser diode pumping of these materials holds the promise of higher average power and more reliable laser sources at 2 μm .

All laser crystals tested were 3x33 mm rods with AR coated faces and polished barrels. A nominally 6% Tm:YAG sample was compared to 0.36%Ho,Tm:YAG samples containing 4%, 6% and 9% thulium doping. The Tm:YAG 2.02 μm laser properties were compared to the 2.09 μm laser properties of Ho,Tm:YAG.

The laser diodes bars used in these experiments pumped into the thulium absorption bands at 781 and 785 nm. The laser diodes emit pulses of 60 W per bar for up to 2 msec and at duty cycles up to 8%. The diodes were arranged in close coupled radial pumping geometry with 21 diode bars per centimeter along the full length of the laser rod. Laser diode pumping with this geometry is ideal for material studies since it produces a nearly top-hat temporal and spatial pump profile.

Using a short flat/flat cavity, measurements of the laser thresholds, long pulse energies, average powers and thermo-optic distortions were conducted for all the concentrations as a function of output coupling, sample temperature and firing rate. Figure 1 shows a comparison of the long pulse energies for the samples at 293 K and 10 Hz firing rate. Additionally, measurements

of the Tm and Ho fluorescence buildup and decay were studied and compared with laser rate models. These studies reveal the Tm concentration dependence of laser diode coupling, Tm-Ho energy transfer rates and Tm-Ho upconversion losses. The results of these studies will be discussed.

References:

- [1] Gregory J. Quarles, Annette Rosenbaum, Charles L. Marquardt and Leon Esterowitz, "Efficient room-temperature operation of a flash-lamp-pumped Cr,Tm:YAG laser at 2.01 μm ," *Opt. Lett.*, vol. 15, no. 1, pp. 42-44, 1990.
- [2] S.R. Bowman, M.J. Winings, R.C.Y. Auyeung, S. Searles and B.J. Feldman, "Laser and Spectral Properties of Cr,Tm,Ho:YAG at 2.1 μm ," *IEEE J. Quantum Electron.*, vol. 27 pp. 2142-2149, 1991.
- [3] S.R. Bowman, M.J. Winings, S. Searles and B.J. Feldman, "Short-Pulsed 2.1 μm Laser Performance of Cr,Tm,Ho:YAG," *IEEE J. Quantum Electron.*, vol. 27 pp. 1129-1131, 1991.
- [4] S.R. Bowman, G.J. Quarles and B.J. Feldman, "Upconversion Losses in Flashlamp-Pumped Cr,Tm:YAG," *OSA Proceedings on Advanced Solid-State Lasers*, Lloyd L. Chase and Albert A. Pinto, eds. Vol. 13, pp. 169-173.

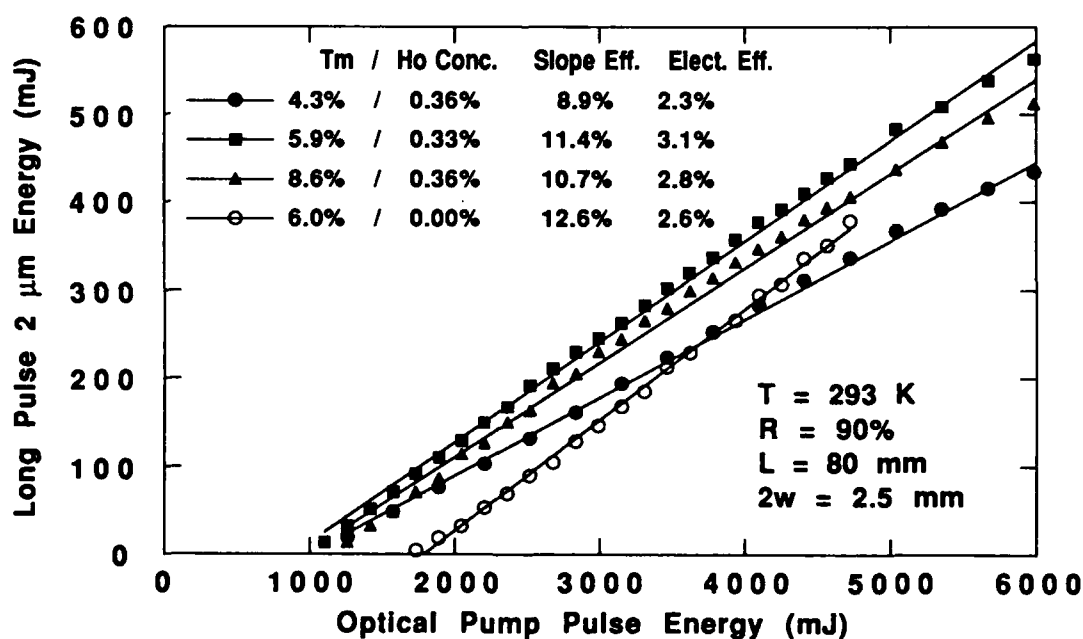


Figure 1.

Room Temperature 2 μ Laser Action of Ho³⁺ doped YSGG, GSAG, YSAG and YAG Crystals.

I.V.Klimov, I.A.Shcherbakov, V.B.Tsvetkov

General Physics Institute, Russian Academy of Sciences
Russia, 117942, Moscow, Vavilov str. 38, Fax: (095)135-02-70

Since 1985 a number of Ho-doped active media have been developed [1-7] on the basis of the scheme using the energy transfer on the way $\text{Cr}^{3+} \rightarrow \text{Tm}^{3+} \rightarrow \text{Ho}^{3+}$ ions [1]. The best achieved laser characteristics (slope efficiency 5.1% and total - 4.5% in 1 Hz repetition rate mode) brought up 2 μ Ho-laser close to industrial and medical application. However, the main question is the possibility of the effective laser operation with pulse repetition rates up to 20 Hz at least.

Formerly it was shown that the efficiency of energy transfer [1] $\text{Cr}^{3+} \rightarrow \text{Tm}^{3+} \rightarrow \text{Ho}^{3+}$ is almost equivalent in crystal host of YAG and scandium garnets [4,6]. The advantage of scandium garnets is the possibility of easy growing the crystals highly doped with Cr ions. In the case of YAG it is difficult to do so. The disadvantage of this kind of crystals is worse thermal conductivity in comparison with YAG host. This fact leads to higher temperature of the active rod under pumping and deterioration of laser parameters.

The present paper is devoted to the comparative study of a series of YSGG, GSAG, YSAG and YAG crystals doped with Cr, Tm and Ho ions (Table 1).

Table 1. The data of the specimens.

No	Crystal host	Concentration: Cr ³⁺ Tm ³⁺ Ho ³⁺ (10 ²⁰ /cm ³)	Rod sizes (mm): diameter length			
1	YSGG	2.5 8.0	0.5	4.0	76	
2	GSAG	2.0 4.0	0.5	5.2	84	
3	YAG	1.0 4.0	0.5	6.3	100	
4	YSAG	2.0 4.0	0.5	5.0	84	
5	YAG	2.0 8.0	0.5	5.0	60	

Notes: 1. Dopants concentrations are determined by their content in the initial charge before growing process.

2. The crystals were grown by G.B.Lutts, S.P.Kalitin, A.I.Zagumennyi and E.V.Zharikov (General Physics Institute, Moscow, Russia)

For all the laser rods heat deposition measurements were made. The interferometric calorimeter was employed to determine these data for single pulse pumping mode. The measuring values proved to be about $K = 10.5\%$ (the accuracy was 15%) for all the investigated crystals, despite different Cr concentration and cross-section in different hosts. It is interesting to note that the value of heat load for Ho-crystals is less than for Cr,Nd:YSGG ($K \sim 15\%$ with the same accuracy of measurements), although Stokes shift is approximately two times less for Nd-active medium. This effect can be explained by the influence of the cross-relaxation process in Tm ions. This process is involved in the energy transfer from Cr to Ho ions and doubles the pumping quantum efficiency.

The next step was the measurements of the laser output of different Ho-lasers for different repetition rates of pumping pulses (Fig.1a-1d). This study was carried out using water-cooled silvered elliptical pump chamber. The resonator length was 33 cm. The output couplers were chosen optimal for every type of active medium ($R = 50\%$ - YSGG; 70% - GSAG, YSAG; 80% - YAG).

Two main processes - thermoactivated depopulation of two bounded levels 3F_4 (Tm) and 5I_7 (Ho) and thermolensing effect - influence the laser characteristics dependence on the pump repetition rate. The results of the thermolensing study under 10 Hz repetition rate are shown in Fig.2. One can see that the minimum value for thermal lens is observed for YAG laser rod. YSAG crystal host results are very close to the YAG, and for YSGG and GSAG thermolensing effect is too high. This is connected with the value of thermal conductivity of these crystals: YAG - 12.9; YSGG - 7.9; GSAG - 5.6 W/m K [8]. By the way, GSAG crystal possesses two times smaller value of temperature gradient of the refraction coefficient dn/dt than YSGG and this fact explains a little bit better thermolense behavior.

Thus, 2 μ Ho-lasers based on Cr,Tm,Ho doped YAG and YSAG crystals are very close in the laser parameters. However it is possible to grow high optical quality YSAG crystals highly doped with Cr ions. The good way for 2 μ Ho-lasers could be the search of optimum compositions of YSAG crystal host and simultaneously the optimization of Tm concentration the same way as [9].

References

- [1] B.M.Antipenko, A.S.Glebov, T.I.Kiseleva, V.A.Pis'mennyi, Soviet Tech.Phys.Lett. 1985, v.11, p.284.
- [2] B.M.Antipenko, A.S.Glebov, L.I.Krutova, V.M.Solntsev, L.K.Sukhareva, Sov.J.Quant.El. 1986, v.16, p.995.
- [3] A.N.Alpat'ev, E.V.Zharikov, S.P.Kalitin, A.F.Umyskov, I.A.Shcherbakov, Sov.J.Quant.El. 1987, v.7, p.587.
- [4] V.A.Smirnov, I.A.Shcherbakov, Quantum Electronics, 1988, v.24, p.949.
- [5] A.N.Alpat'ev, E.V.Zharikov, A.I.Zagumennyi et al. Kvantovaya elektronika, 1989, v.11, p.2176.
- [6] G.J.Quarles, A.Rosenbaum, I.D.Abella, C.L.Marquardt, L.Esterowitz, Optical and Quantum Electronics, 1990, v.22, p.S141.
- [7] T.Becker, G.Huber, H.-J.v.d.Heide, P.Mitzscherlich, B.Struve, E.V.Duczynski, Optics Communications, 1990, v.90, p.47.
- [8] P.A.Popov, N.N.Sirota, E.V.Zharikov, A.I.Zagumennyi, I.A.Ivanov, G.B.Lutts, Laser Physics, 1991, v.1, p.437.
- [9] B.M.Antipenko, A.A.Nikitichev, Izvestia AN SSSR, seria phys., 1991, v.55, p.267.

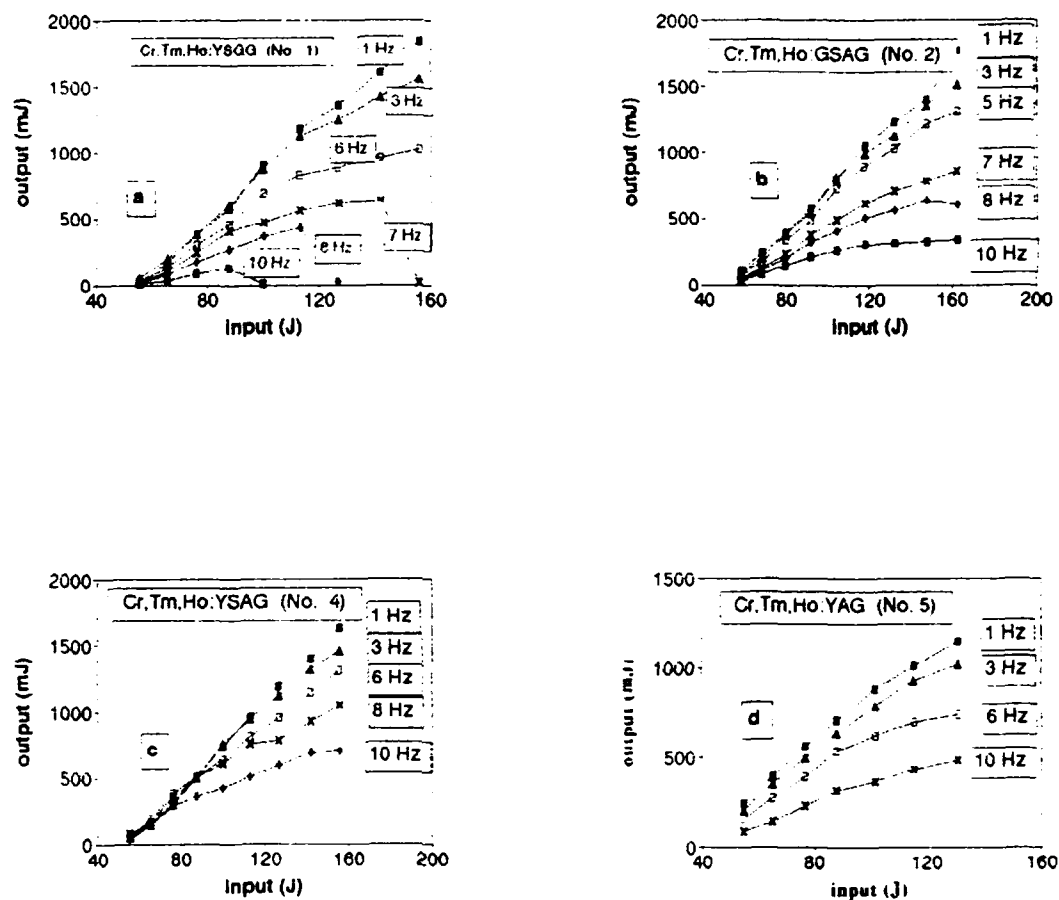


Fig. 1. Input/output curves for Cr,Tm,Ho doped garnets: (a)-CTH:YSGG; (b)-CTH:GSAG; (c)-CTH:YSAG; (d)-CTH:YAG.

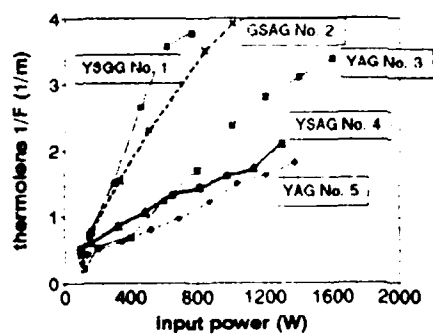


Fig. 2. Thermolens characteristics for Cr,Tm,Ho doped garnets.

LONG PULSELENGTH TWO MICRON LASERS FOR LAWS APPLICATION

**Mahendra G. Jani
Science and Technology Corporation
101 Research Drive, Hampton, VA 23666
(804)-864-8067**

**Norman P. Barnes and Keith E. Murray
MS-474, NASA Langley Research Center
Hampton, VA 23681
(804)-864-1630**

Long pulselengths, on the order of 1.0 microsec, allow Ho lasers to generate relatively high peak powers efficiently. Ho laser materials are usually characterized by relatively low effective stimulated emission cross sections. For many optical components energy density at which laser induced damage threshold occurs increases with the pulselength. Hence, by utilizing nominal microsecond pulselengths, the laser induced damage threshold can be increased about an order of magnitude when compared with more common Q-switched pulselengths. Operation at an increased energy density permits efficient operation of laser materials with modest gains, such as Ho laser materials. Long pulselength, efficient, two micrometer lasers are needed for remote sensing applications. In recent years, ground-based and airborne lidars have been utilized to meet growing need for measuring various atmospheric parameters, such as wind velocity. An example of such a system is the prospective Laser Atmospheric Wind Sounder (LAWS) , which is currently under development by National Aeronautics and Space Administration (NASA). Two different wavelengths, 9.1 micrometer CO₂ laser and emerging 2 micrometer laser

technology are being seriously considered for LAWS application. We report experimental and theoretical analysis of flashlamp pumped 2 micrometer laser systems.

We have investigated flashlamp pumped Ho:Tm:Cr:YAG and Ho:Tm:Er:YLF laser systems to obtain long pulselengths. A four meter ring resonator with an acousto-optic Q-switch was utilized to obtain Q-switched pulses and unidirectional operation. A low output mirror reflectivity was used to avoid high internal circulating power densities in the resonator. Variations in the laser output energy and the pulselengths were measured as a function of input pump energies. Results for the ring resonator are shown in Fig. 1 for flashlamp pumped Ho:Tm:Cr:YAG laser system. Laser output energy and pulselengths for 1 meter and 2 meter standing wave resonators are shown in Fig. 2.

Theoretical calculations using a model for three-level Q-switched lasers were performed. Results of theoretical calculations are represented by solid lines in Fig. 1 and Fig. 2 for ring resonator and standing wave resonator, respectively.

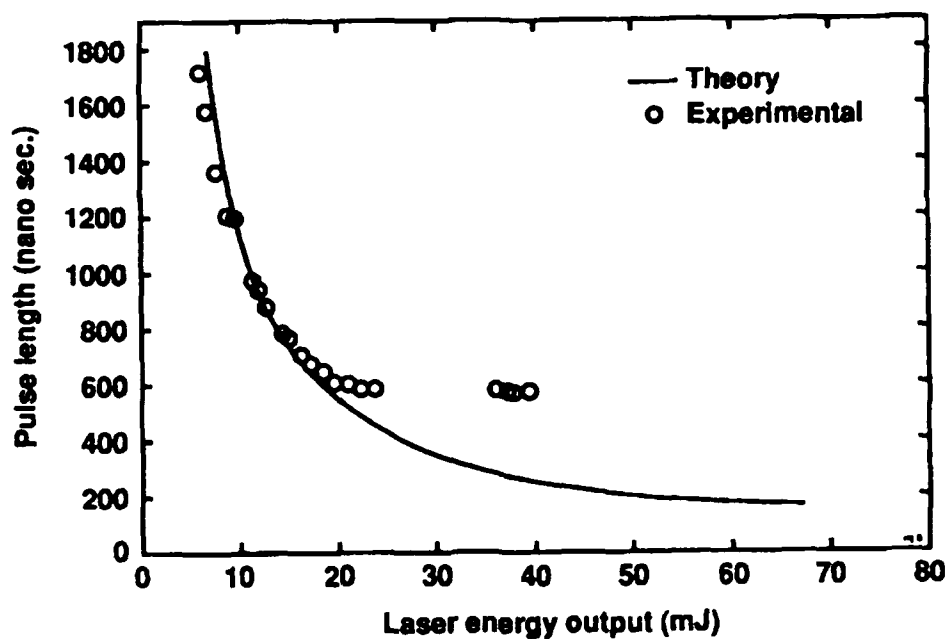


Fig. 1 Results for a Ho:Tm:Cr:YAG Four-Meter Ring Resonator. Data below 25 mJ is bidirectional operation while data above 35 mJ is unidirectional operation.

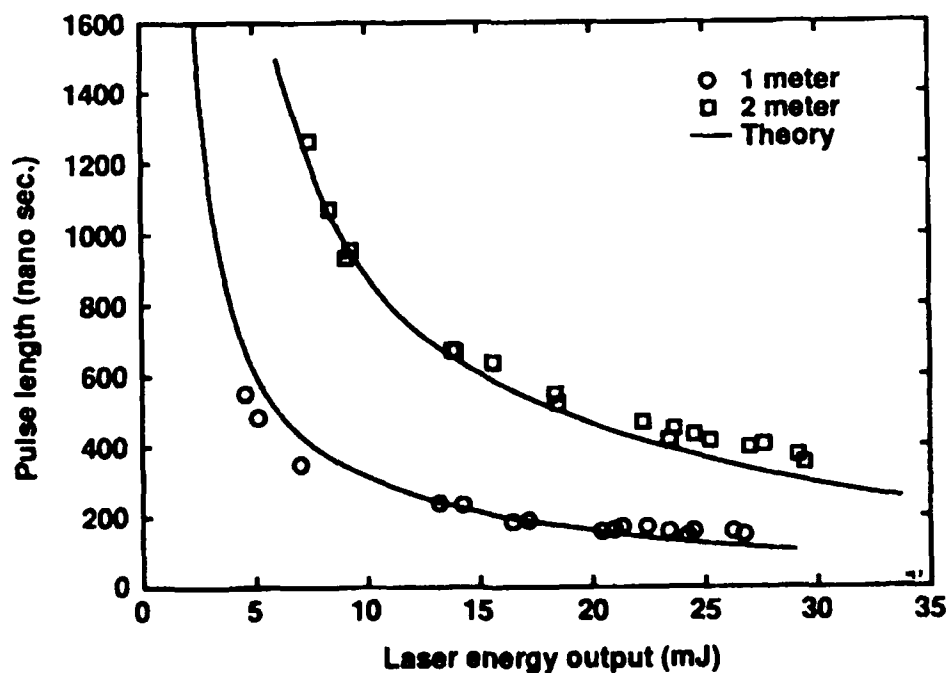


Fig. 2 Results for a Ho:Tm:Cr:YAG Standing Wave Resonator.

Alexandrite Laser Pumped Ho:Tm:YLF Laser Performance

Chang J. Lee and Gooywan Han

Physics Department, Hampton University, Hampton, Virginia 23668

(804-864-8614)

Clayton H. Bair, Norman P. Barnes, Philip Brockman and Robert V. Hess

NASA - Langley Research Center, Hampton, Virginia 23681 (804-864-1608)

The development of laser diode pumped all solid state 2 μm lasers for ground-, aircraft-, and space-based remote sensors is of interest because of their compact, reliable, and eye-safe operation potential. With the increased availability of laser diodes and laser diode arrays, a greater number of researchers are gaining access to the tools necessary to construct and test such devices; however, the difficulty in collecting and propagating the laser diode output energy still inhibits systematic investigation of some potentially useful pump geometries. We have used an Alexandrite laser as a laser diode simulator to longitudinally pump Ho:Tm:YLF crystals having a variety of lengths and dopant concentrations to enable us to compare their performance in an end-pumped configuration.

The laser rods used in this investigation were operated at room temperature and varied in Ho dopant concentrations from 0.5% to 1.5%. Rods of each concentration were fabricated with lengths ranging from 4 mm to 6 mm. In the experimental set-up, shown in figure 1, the Alexandrite laser output passes through a half-wave plate/ polarizer combination in which the half-wave plate is rotated to vary the incident pump energy. The polarizer is oriented such that the pump polarization is aligned parallel to the YLF crystalline c-axis. A computerized data acquisition system allows simultaneous readings of the pump energy monitor and 2 μm laser output signals for real time display of output vs input

energy and data storage for later processing.

Slope efficiencies, measured with respect to absorbed pump energy, as a function of output coupling for two 5 mm Ho:Tm:YLF rods using a 200 μ s Alexandrite laser pump pulselength are shown in figure 2. The improved performance at the higher Ho dopant concentration, which also has been observed in CW pumped geometries and reduced temperatures (1), may have a significant impact in the design of high energy systems required in remote sensing applications.

The results of a series of experiments in which the crystal length and Ho concentration, along with the pump pulselength and energy, were varied will be presented. Experimental results will be compared those of a comprehensive rate equation model describing the energy transfer and laser dynamics. The performance of Ho:Tm:YLF pumped by an Alexandrite laser will be compared to previously obtained results for comparable Ho:Tm:YAG experiments (2).

References

1. A. Di Lieto, A. Neri, P. Minguzzi, M. Tonelli, and H. P. Jenssen. Technical Digest XVII International Quantum Electronics Conference, PWe120, June 14-19, 1992, Vienna, Austria.
2. C. J. Lee, G. Han, C. H. Bair, N. P. Barnes, and R. V. Hess. OSA Annual Meeting, MJJ5, Sep. 20-25, 1992, Albuquerque, NM.

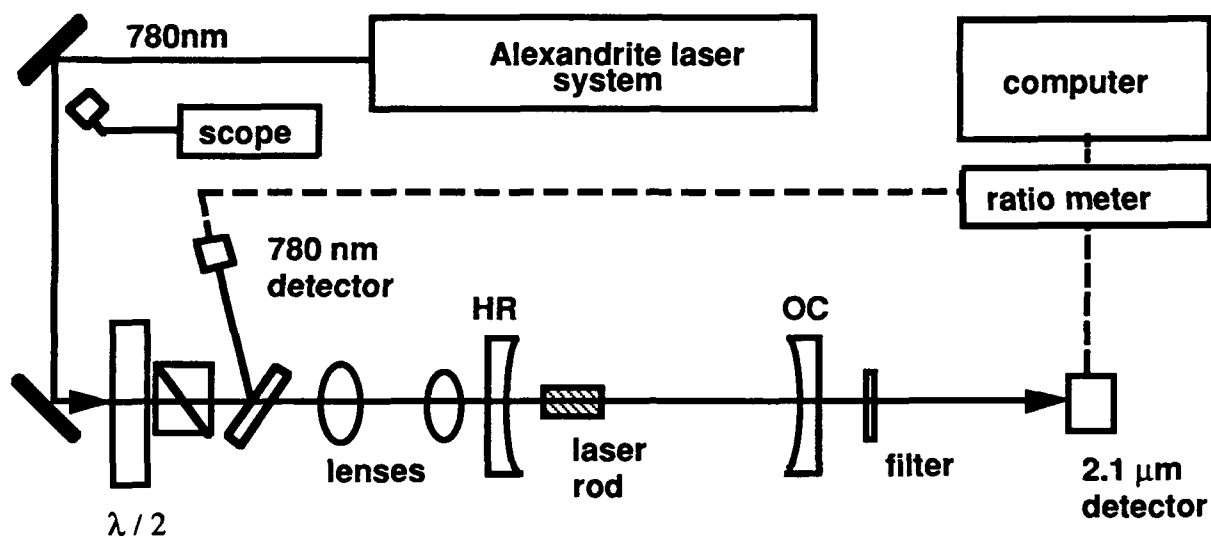


Fig. 1 Schematic of experimental set-up for Alexandrite laser pumped 2 μm laser.

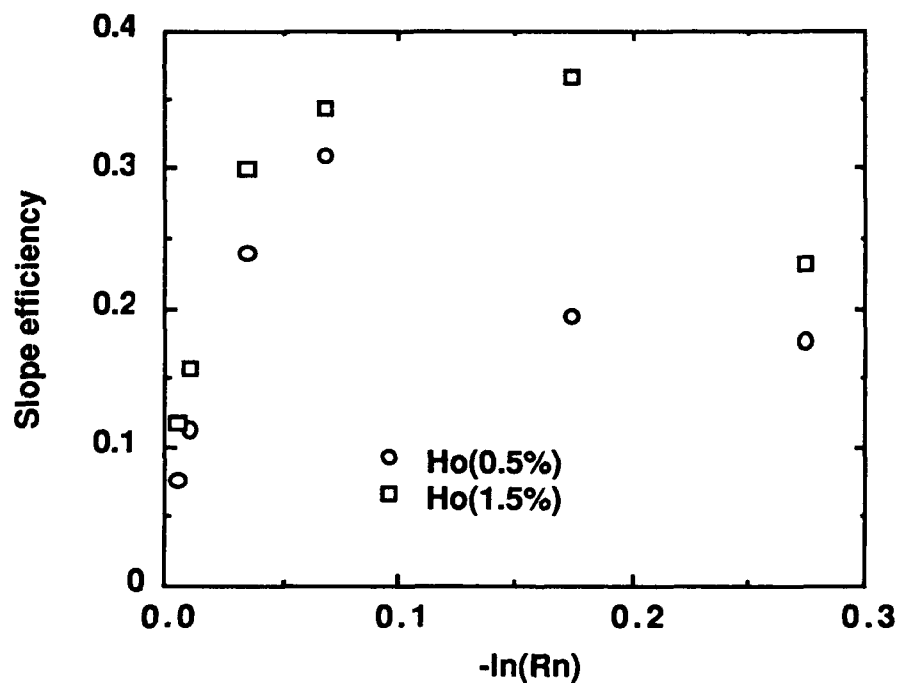


Fig. 2 Slope efficiency for Ho(0.5%):Tm(4%):YLF and Ho(1.5%):Tm(4%):YLF as a function of outcoupling for a 200 μs pump pulselength.

PUMP SATURATION FOR THE 2 μ m Tm LASER

Christian Hauglie-Hanssen* and N. Djeu
 Department of Physics
 University of South Florida
 Tampa, FL 33620-5700

Diode pumping of the 2 μ m Tm laser usually takes place on the 3H_6 - 3H_4 band near 800 nm. The 3F_4 upper laser level is then populated by cross relaxation of the excited 3H_4 level. When the 3F_4 density becomes sufficiently large, upconversion to 3H_5 , followed by multiphonon relaxation can be a significant channel for energy loss. The saturation of the pump beam is influenced by the latter process. We have obtained an approximate expression for the saturation of the pump in the presence of upconversion loss for this laser system. We have also applied this result to the analysis of pump absorption saturation data in Tm:YVO₄.

The starting rate equations for the derivation of the generalized saturation formula are the following:

$$\frac{dN_1}{dt} = -2U_{12}N_1^2 - 2U_{13}N_1^2 - A_1N_1 + 2C_{31}N_3N_2 + R_2N_2$$

$$\frac{dN_2}{dt} = -R_2N_2 + U_{12}N_1^2$$

$$\frac{dN_3}{dt} = -C_{31}N_3N_2 + U_{13}N_1^2 + (N - N_1) \frac{\sigma I}{h\nu}$$

Here N_1 , N_2 , and N_3 are the densities of the 3F_4 , 3H_5 , and 3H_4 levels, N is the total Tm³⁺ density, U_{12} and U_{13} are the upconversion rate constants from 3F_4 to 3H_5 and 3F_4 to 3H_4 , C_{31} is the cross relaxation rate constant from 3H_4 to 3F_4 , A_1 is the radiative rate of 3F_4 , and R_2 is the net multiphonon and radiative rate from 3H_5 to 3F_4 . Also, σ is the absorption cross section, $h\nu$ the energy of the pump photon, and I the intensity of the pump beam. Note that the simplifying assumption that all the ions are in either the ground state or the metastable 3F_4 state has been made.

When the rate equations are solved together, one finds that the pump saturates as

$$\alpha = \left[1 - \frac{1}{b} (\sqrt{(1+aI)^2 + 2abI} - (1+aI)) \right] \alpha_0$$

where

$$a = \frac{2\sigma}{h\nu A_1}$$

$$b = \frac{2U_{12}N}{A_1}$$

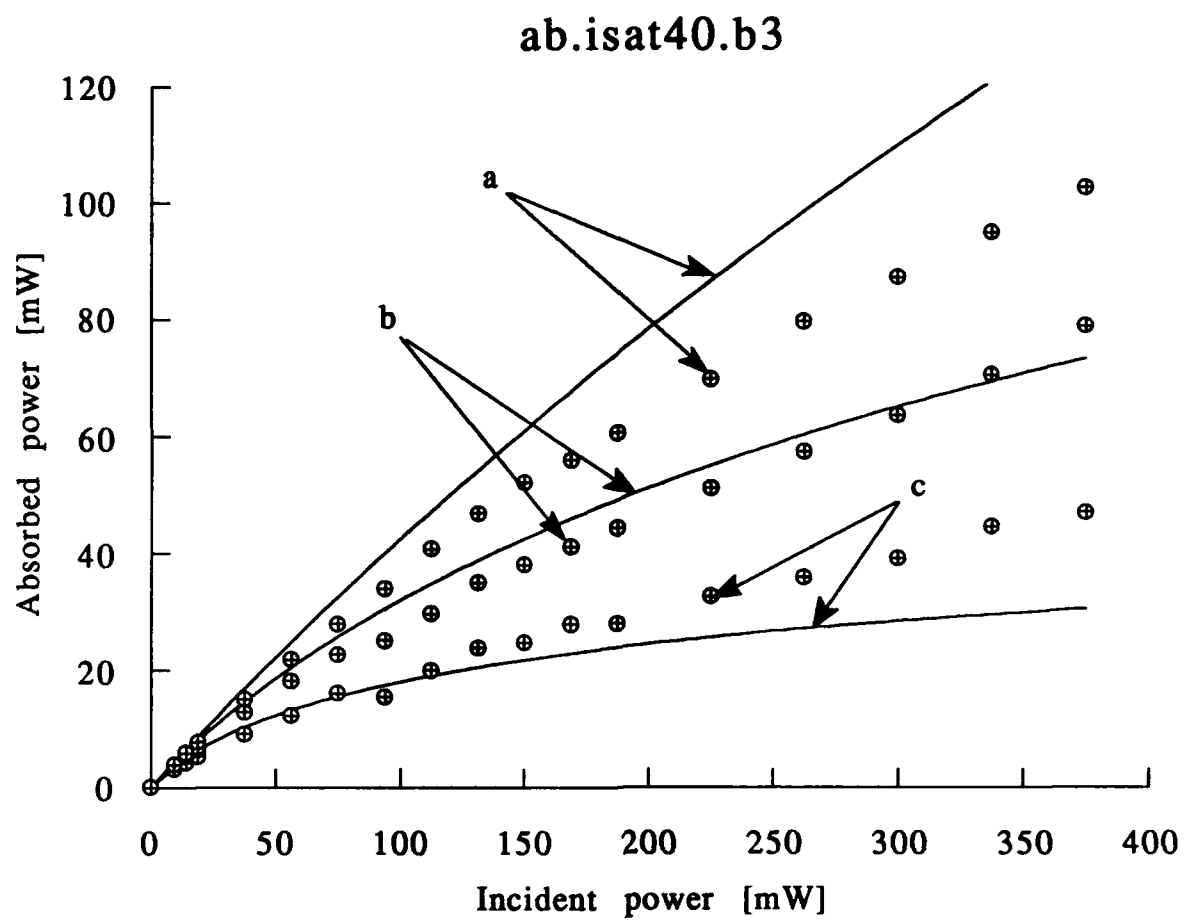
and $\alpha_0 = \sigma N$ is the unsaturated absorption coefficient. In the limit of $b \rightarrow 0$, one obtains the familiar saturation formula

$$\alpha = \frac{\alpha_0}{1+aI}$$

if the identification of a with $1/I_s$ is made.

We have performed pump saturation measurements in Tm:YVO_4 . The data shown in the accompanying figure were taken on a 0.21 mm thick sample with 5% doping for the π polarization. The labels a , b , and c stand for beam radius of $49\mu\text{m}$, $21\mu\text{m}$ and $10\mu\text{m}$ respectively. Numerical calculations using the generalized saturation formula were made in the plane wave approximation, taking into account the Gaussian profile of the pump beam. The provisional best fit to the data, shown in the figure, was obtained for $1/a = 4 \text{ kW cm}^{-2}$ and $b = 3$. Efforts to improve the fit are continuing. Work is also underway to obtain a simultaneous fit to the $2\mu\text{m}$ emission data, and the results will be reported.

* Present address: Simrad Optronics, P.O. Box 6114, Etterstad, 0602 Oslo 6, Norway.



DEPENDENCE OF HO UPCONVERSION RATE CONSTANTS IN YAG ON DOPANT CONCENTRATION

L. B. Shaw, X. B. Jiang, R. S. F. Chang, and N. Djeu

Department of Physics
University of South Florida
Tampa, FL 33620-5700

In an earlier work we have shown that by measuring the time dependent densities of the Ho 5I_7 , 5I_6 , and 5I_5 levels following the direct pulsed excitation of 5I_7 , one can determine the upconversion rate constants from 5I_7 to 5I_5 and 5I_6 individually.¹ A 10% Ho:YAG sample was used in that initial study. We have now extended these measurements to other dopant concentrations. The variations in the upconversion rate constants with Ho doping are reported here.

It was shown in Ref. 1 that under quasi-steady-state conditions the densities in 5I_5 and 5I_6 are related to the 5I_7 density by

$$N_3 = \frac{U_{13}}{C_{31}N_o + R_3} N_1^2 \quad (1)$$

$$N_2 = \frac{1}{C_{21}N_o + R_2} \left(U_{12} + \frac{M_{32} + A_{32}}{C_{31}N_o + R_3} U_{13} \right) N_1^2 \quad (2)$$

Where

- N_o = density of 5I_8 ground state
- N_1 = density of 5I_7 level
- N_2 = density of 5I_6 level
- N_3 = density of 5I_5 level
- C_{31} = cross relaxation rate const. from 5I_5 to 5I_7
- C_{21} = cross relaxation rate const. from 5I_6 to 5I_7
- U_{13} = upconversion rate const. from 5I_7 to 5I_5
- U_{12} = upconversion rate const. from 5I_7 to 5I_6
- M_{32} = multiphonon relaxation rate from 5I_5 to 5I_6
- A_{32} = radiative rate from 5I_5 to 5I_6
- R_2 = net radiative and multiphonon rate from 5I_6
- R_3 = net radiative and multiphonon rate from 5I_5

Once the cross relaxation, multiphonon, and radiative rates are known, the upconversion rate constants can be determined.

The samples used in our measurements were approximately 1 mm in diameter and several hundred microns in thickness. They were pumped by the central portion of a near Gaussian beam at $1.91\mu\text{m}$ to ensure uniform excitation throughout the volume. Emissions from the levels of interest were monitored through an $1/8\text{ m}$ monochromator and appropriate filters. The absolute density for $^5\text{I}_7$ was deduced from the known volumetric absorption at $1.91\mu\text{m}$ and the initial $^5\text{I}_7$ signal level. The absolute densities for the $^5\text{I}_5$ and $^5\text{I}_6$ levels were calculated by comparison with signals resulting from the direct excitation of these levels at $1.13\mu\text{m}$ and 872 nm respectively.

Representative plots of upconverted state density vs $^5\text{I}_7$ density for $^5\text{I}_5$ and $^5\text{I}_6$ are given in Figs. 1 and 2. From our own measured multiphonon and cross relaxation rates and calculated radiative rates the upconversion rate constants were determined. The dependence of the latter on Ho concentration for upconversion to $^5\text{I}_5$ is shown in Fig. 3. The apparent linear dependence with extrapolation through the origin suggests that upconversion to the $^5\text{I}_5$ level can only proceed via excitation migrations. This is analogous to the case of cross relaxation processes which show a quadratic dependence on the dopant concentration.² In contrast Fig. 4 shows the variation of the rate constant for upconversion to $^5\text{I}_6$ with dopant concentration. Here the upconversion rate constant starts out with a linear dependence on dopant concentration and then levels off. This is reminiscent of cross relaxation processes which transition from a quadratic dependence to a linear dependence with increasing dopant concentration.² The latter regime is entered when superfast migration is attained.

-
1. L. B. Shaw et.al., "Upconversion of $^5\text{I}_7$ to $^5\text{I}_6$ and $^5\text{I}_5$ in Ho:YAG and Ho:YLF," Paper ME9, Advanced Solid State Lasers, Santa Fe, NM, 1992.
 2. A. A. Kaminskii, Laser Crystals, (Springer-Verlag, Berlin, 1981).

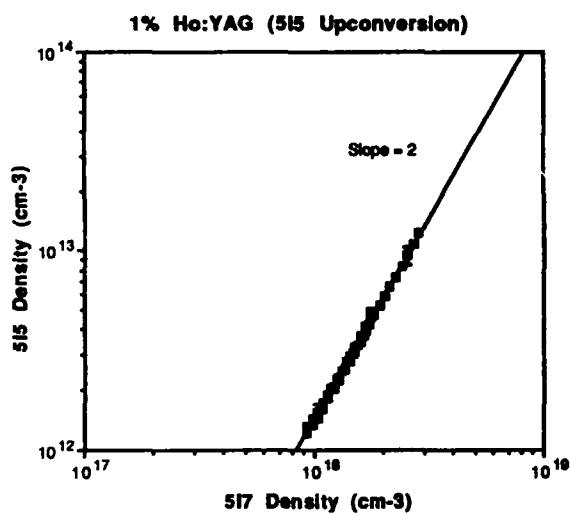


Figure 1

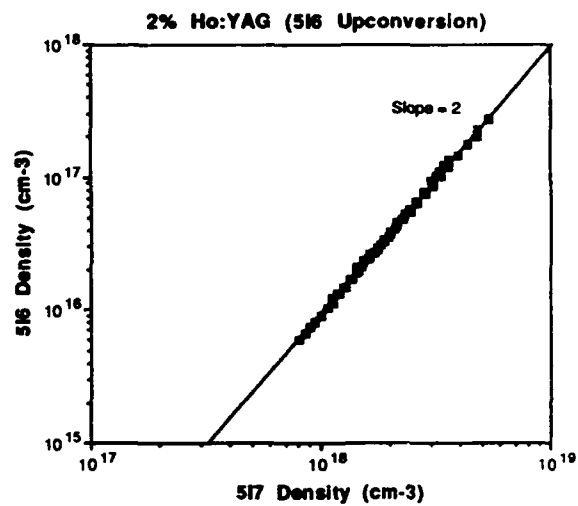


Figure 2

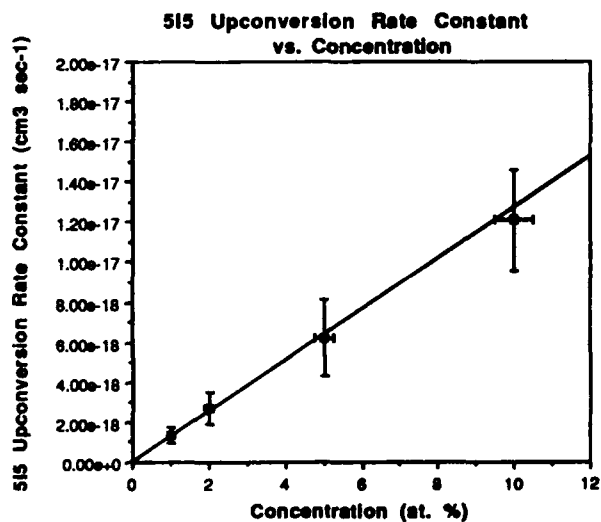


Figure 3

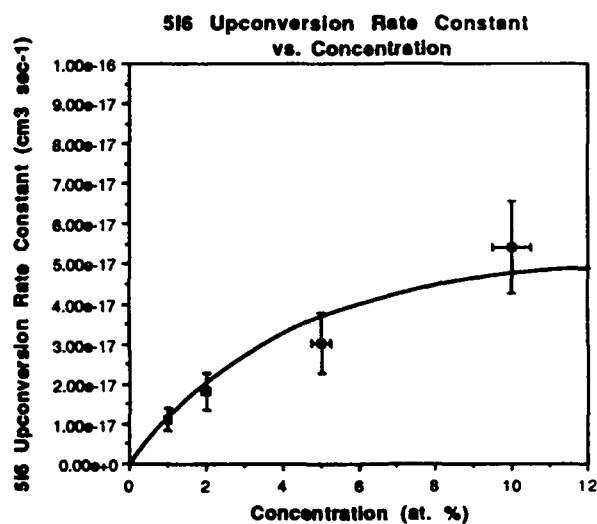


Figure 4

Tm, Ho doped Alumino-zirco-fluoride glass sensitized with Yb ions.

T. Izumitani, B. Peng and X. Zou

Izumitani Special Lab., HOYA Corporation
3-3-1, Musashino, Akishima, Tokyo 196 JAPAN

1. Introduction

Tm³⁺, Ho³⁺ doped glasses and crystals have been investigated for upconversion laser (blue, green, red) and Eye-safe laser. We applied Yb³⁺ ions as a sensitizer to Tm³⁺, Ho³⁺ doped alumino-zirco-fluoride glasses which were pumped with 0.98 μ laser diode and obtained 2.85 μ laser glass containing Yb, Ho as laser mess, 0.88 μ and 2 μ laser glasser containing Yb, Tm and Yb, Ho respectively as eye-safe laser and 0.8 μ laser glass containing Yb, Tm for femto-sec laser amplifier.

2. Experimental

Glass compositions used is shown in Table 1.

Absorption spectrum was measured with HITACHI-330 spectrophotometer. Emission was measured with InAs detector for 1.88, 2.0 and 2.84 μ and R-2228 photomultiplier for 0.8 μ for the sample 25x25x5mm pumped with 680nm, 790nm and 980nm laser diodes. Life time was measured with InAs detector for 1.88, 2.0 and 2.84 μ and S-1 detector for 0.8 μ for the sample pumped with a dye laser pumped by Nd:YAG laser.

3. Results and discussions

3.1.1 Yb³⁺-Tm³⁺ doped glasses

We calculated intensity parameter Ω values from absorption spectrum and the electric dipole line strength S_{ed} and magnetic dipole line strength S_{md} using the matrix elements given by Canal¹⁾. Table 2 and 3 shows intensity parameter (Ω) and radiative transition probability(A). Table 4 and 5 shows the life time and emission intensity. Fluoride glass has longer life time and shows the max. emission intensity at Tm³⁺ 8 cat%.

As the emission spectrum of Yb³⁺(²F_{5/2}-²F_{7/2}) and absorption spectrum of Tm³⁺(³H₆-³H₅) are overlapped, energy transfer occurs between Yb³⁺:²F_{5/2} and Tm³⁺:³H₅ as shown in Fig.1 and 2.

In AZF glasses, 1.88 μ emission intensity increases with Yb³⁺ concentration. Regarding to Tm³⁺ content, the highest emission intensity is given at 4 cat%. Fig.3 shows the emission spectrum of Yb³⁺ 1% and Tm³⁺ 2% codoped AZF glass.

3.1.2 Yb-Tm-Ho doped glasses

Intensity parameters of Ho³⁺ are shown in Table 6. Radiative transition probabilities(A) calculated using matrix elements given by Weber²⁾, are shown in Table 7. The A coefficient of Ho³⁺(⁵I₇-⁵I₈) of AZF glass is small but the life time is very long because of small phonon energy.

As the energy level of Tm³⁺:³H₄ is very close to that of Ho³⁺:⁵I₇, and 1.88 μ emission spectrum of Tm³⁺(³H₄-³H₅) overlaps with 2.0 absorption spectrum of Ho³⁺:⁵I₈-⁵I₇, energy transfer occurs between them. At 1 cat% Ho³⁺ content, 2.0 μ emission intensity increases with increasing Tm³⁺ content and shows the max. at 8%. At 8% Tm³⁺ content, 2.0 μ emission intensity increases with Ho³⁺ content and gives the max. at 2% Ho³⁺. Fig.4 shows the emission spectrum of the AZF glass containing 8 cat% Tm³⁺ and 2 cat% Ho³⁺. The glass gives higher emission intensity than Cr-Tm-Ho doped YSGG.

Energy transfer also occurs from Yb³⁺ to Tm³⁺, and then Tm³⁺ to Ho³⁺ by pumping with 0.98 μ LD as shown in Fig.5. Energy transfers from Yb³⁺:²F_{5/2} to Tm³⁺:³H₅, then relaxes from ³H₅ to ³H₄. Next, energy transfers from Tm³⁺:³H₄ to Ho³⁺:⁵I₇. The absorption coefficient of Yb³⁺(²F_{7/2}-²F_{5/2}) is stronger than

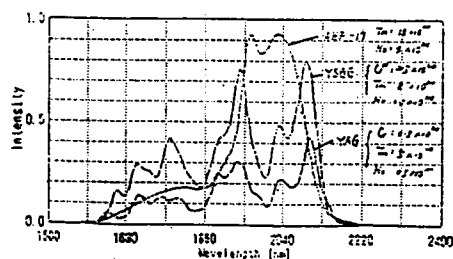


Fig. 4

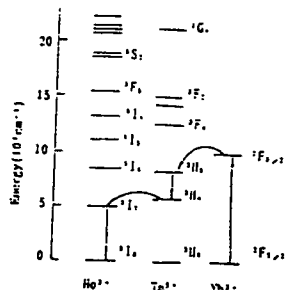


Fig. 5 The energy transfer of Ho³⁺, Ta³⁺, Yb³⁺ system

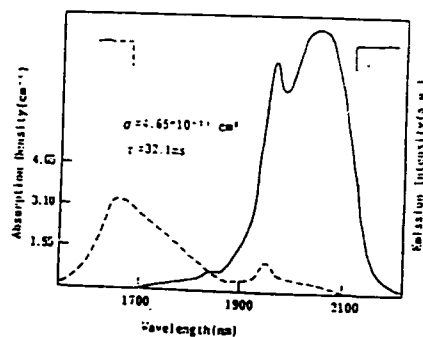


Fig. 6 The emission and absorption spectra of Yb, Ta and Ho doped fluoride glass.

Yb12.5cat%, Ta5.5cat%, Ho1cat%



Fig. 7: The energy transfer of Yb, Ho system in fluoride glasses

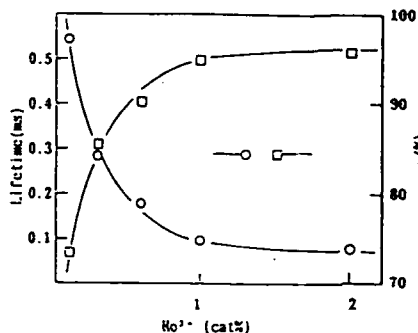


Fig. 8: The lifetimes of Yb³⁺ (²F₇/₂ → ²F₅/₂) versus concentration of Ho³⁺ in Yb³⁺ 16cat% doped fluoride glasses and the energy transfer efficiency of Yb to Ho.

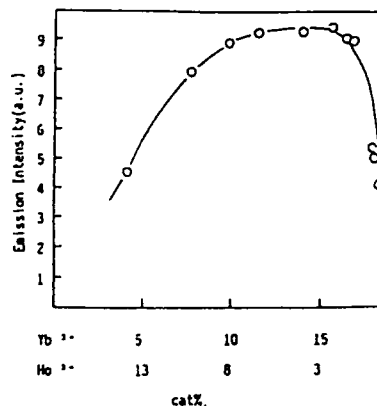


Fig. 9: The emission intensity of Ho(⁵I₄ → ⁵I₃) in Yb³⁺, Ho³⁺ codoped fluoride glasses

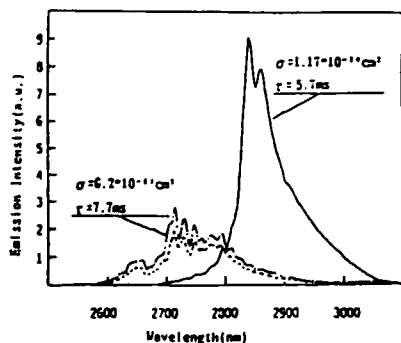


Fig. 10: The emission spectra of Ho(⁵I₄ → ⁵I₃) in Yb, Ho codoped fluoride glass, Er(⁴I₁₃/₂ → ⁴I₁₅/₂) in Yb, Er codoped fluoride glass and Er(⁴I₁₃/₂ → ⁴I₁₅/₂) in Er doped fluoride glass.

— (Ho(⁵I₄ → ⁵I₃) in Yb16cat%, Ho2cat%)
 — (Er(⁴I₁₃/₂ → ⁴I₁₅/₂) in Yb2cat%, Er10cat%)
 - - - (Er(⁴I₁₃/₂ → ⁴I₁₅/₂) in Er10cat%)

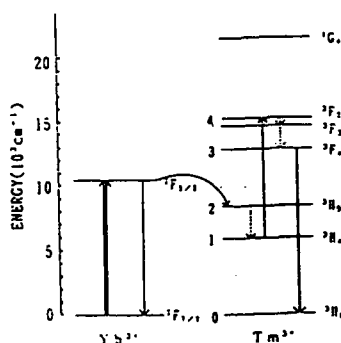


Fig. 11

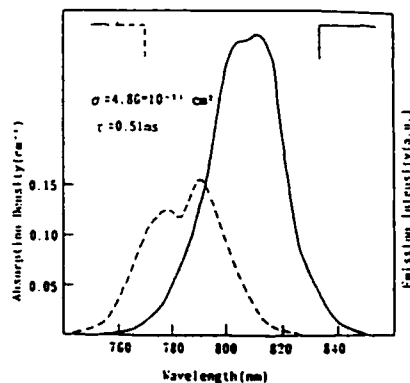


Fig. 12: The emission and absorption spectra of Yb, Tm doped fluoride glass.

Yb16cat%, Tm8.3cat%

On the Optical Center in Cr^{4+} doped YAG

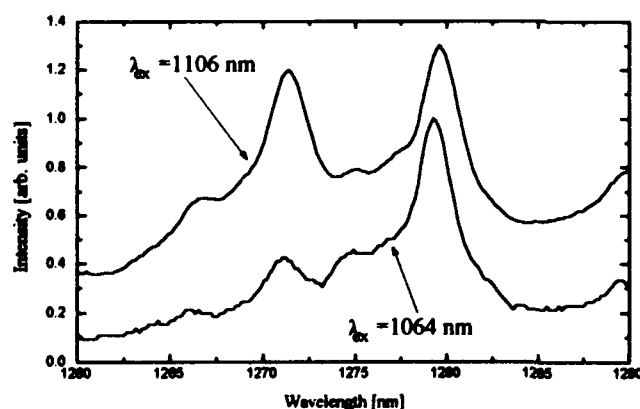
Hergen Eilers, Uwe Hömmerich, Stuart M. Jacobsen and William M. Yen

Department of Physics & Astronomy, University of Georgia,

Athens, GA 30602, Tel.(706) 542-3427

There has been a great interest in Cr^{4+} doped materials as emitting sources in the near infrared in the last few years. Cr:Forsterite and Cr:YAG show laser action at room temperature [1-4]. For both materials it is believed that Cr^{4+} in a tetrahedral site is the optical center. However, there is still some uncertainty about the interpretation of the optical spectra of these materials. We found, that Cr:YAG has more than one site which is responsible for the near infrared emission. Fig. 1 shows the fluorescence of the zero phonon lines in the 1280 nm region. Excitation with 1064 nm Nd:YAG laser shows the well-known emission peak at 1279.6 nm and its hot-band at 1275 nm. At higher energies some smaller peaks with a shorter lifetime are visible [5]. Excitation at 1106 nm from a tunable Malsan 203 color center laser increases the emission from the higher energy center at 1271.4 nm and

its hot-band at 1266.9 nm.



The emission from the 1271.4 nm center is also highly polarized as can be seen in fig. 2. The excitation spectrum, seen in fig. 3, shows that the 1279.6 nm emission can be excited at 1115 nm, while the 1271.4 nm emission can be best excited at

Fig. 1: Fluorescence of Cr,Ca:YAG for different excitation wavelength.

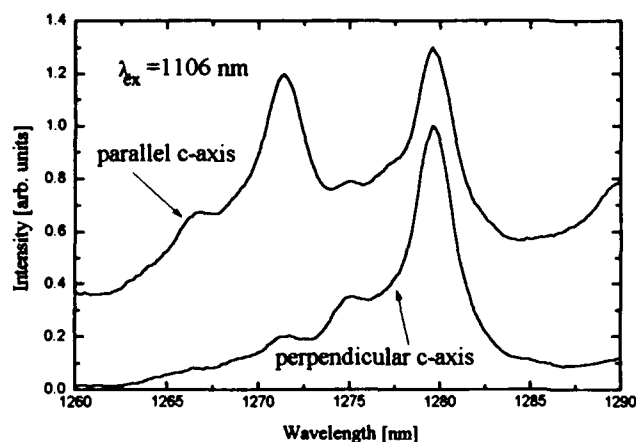


Fig. 2: Polarization dependence for the Cr,Ca:YAG emission

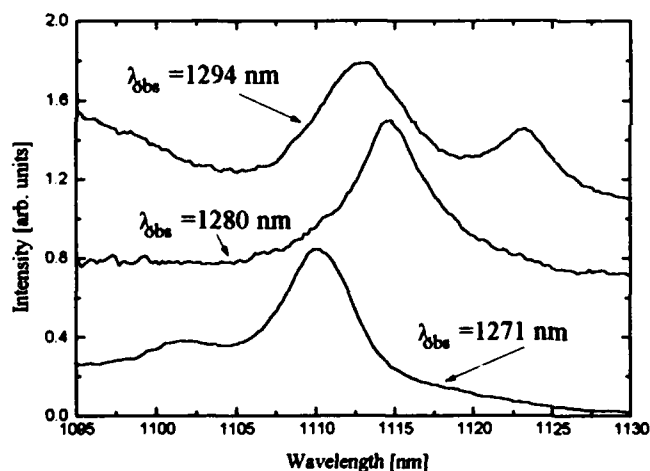


Fig. 3: Excitation spectrum of Cr,Ca:YAG for different observation wavelength.

References:

- 1) V. Petricevic, S.K. Gayen and R.R. Alfano, "Laser action in chromium-activated forsterite for near-infrared excitation: Is Cr^{4+} the lasing ion?", Appl. Phys. Lett. **53**, 2590 (1988)

1110 and 1102 nm. A further excitation spectra, also seen in fig. 3, reveals another center that can be excited at 1113 and 1123 nm and that emits between 1293 and 1294 nm. The lifetimes of these different centers at 10 K are between 27 and 31 μs . At room temperature the lifetimes show no difference. Our first thought, that the co-dopant ion Ca^{2+} is responsible for the different centers, was not correct. Samples with Mg^{2+} as the co-dopant ion show exactly the same energy levels. We will discuss possibilities to explain the different centers and their behavior.

- 2) H.R. Verdun, L.M. Thomas, D.M. Andrauskas and T. McCollum, "Chromium-doped forsterite laser pumped with 1.06 μm radiation", *Appl. Phys. Lett.* **53**, 2593 (1988)
- 3) N. I. Borodin, V.A. Zhitnyuk, A.G. Okhrimchuk and A.V. Shestakov, "Oscillation of a $\text{Y}_3\text{Al}_5\text{O}_{12}:\text{Cr}^{4+}$ Laser in wave length region of 1.34-1.6 μm ", *Izvestiya Akad. Nauk SSSR, Ser. Fizicheskaya*, **54** (8), pp. 1500-1506 (1990)
- 4) W. Jia, H. Eilers, W.M. Dennis, W.M. Yen and A.V. Shestakov, "The Performance of a $\text{Cr}^{4+}:\text{YAG}$ Laser in the near infrared", *OSA Proceedings on Advanced Solid-State Lasers*, Lloyd L. Chase and Albert A. Pinto, eds. (Optical Society of America, Washington, DC 1992), Vol. 13, pp.31-33.
- 5) K.R. Hoffman, U. Hömmerich, S.M. Jacobsen and W.M. Yen, "On the emission and excitation spectrum of the NIR laser center in $\text{Cr}:\text{YAG}$ ", *J. Lumin.* **52**, 277 (1992)

Spectroscopic investigations of the NIR center in Cr doped Y_2SiO_5

U. Hömmerich, H. Eilers, S.M. Jacobsen and W. M. Yen
 Department of Physics and Astronomy, University of Georgia
 Athens, GA 30602
 (706) 542-3427

W. Jia and Y. Wang
 Department of Physics, University of Puerto Rico
 Mayaguez, PR 0078

Summary

Near infrared (NIR) laser action in Cr: Forsterite and Cr: YAG has been attributed to Cr^{4+} in tetrahedral coordination [1,2]. However, in both these systems an adequate theoretical description of the energy levels and other important parameters is still lacking. Also, further complexity arises due to the coexistence of Cr^{3+} in octahedral symmetry and due to charge compensation problems [3,4]. The newest Cr^{4+} laser material is Cr doped Y_2SiO_5 (YSO), but so far laser action has been achieved only up to 257 K [5]. In contrast to Cr:Forsterite and Cr:YAG, Cr:YSO is supposed to be a pure Cr^{4+} system and no charge compensation is required [6]. Therefore Cr:YSO provides a useful system to study the optical properties of the new NIR lasing center.

We are currently engaged in detailed spectroscopic investigations on Cr: YSO. High resolution NIR excitation, emission measurements and piezo spectroscopic investigations will be reported in this paper.

Low temperature absorption and emission spectra of Cr: YSO are shown in Fig.1. The absorption spectrum is dominated by strong absorption bands in the visible region and only a very weak NIR absorption. The absorption bands are broad and without any sharp features. The low temperature emission spectrum shows a broad band peaking at 1225nm accompanied by a sharp emission peak at around 1150nm. The high resolution emission spectrum reveals two lines at 1148.2nm and 1143.6nm (Fig.2). Since the NIR absorption is only very weak we used the H_2 - Raman shifted output of a Nd:YAG pumped dye laser to perform NIR excitation measurements. With this tunable NIR laser we can observe two sharp peaks which match up with the lines observed in emission (Fig.2). The lines can therefore be identified as being electronic origins. The temperature dependence of the zero phonon lines in emission and excitation reveal that the splitting of 35cm^{-1} is an excited state splitting. The assignment of the zero phonon lines to the spin orbit splitting of the $^3\text{T}_2$ level is supported by piezo spectroscopic studies. Only very little stress is necessary to split up the original zero phonon line at 1148.2nm into two lines. The sensitivity of the zero phonon lines toward uniaxial stress (Fig.3) is a factor of 100 greater than the R-line shift in ruby. This splitting of the zero phonon line is due to different oriented sites.

References:

1. V. Petricevic, S.K. Gayen, R.R. Alfano, K. Yamagishi, Y. Anzai and Y. Yamaguchi, Appl. Phys. Lett. 52 (1988) 1040.
2. W. Jia, H. Eilers, W. M. Dennis, W.M. Yen and A.V. Shestakov, in OSA Proceedings of Advanced Solid State Lasers, eds. L. Chase and A. Pinto (Optical Society of America, Santa Fe, NM, 1992) Vol.13 p.31.
3. R. Moncorge, G. Comier, D.J. Simkin, and J. Capobianco, IEEE Journal of Quantum Electronics 27, (1991) 114.
4. S. Kück, K. Petermann, and G. Huber, in OSA Proceedings of Advanced Solid State Lasers, eds. G. Dube and L. Chase (Optical Society of America, Hilton Head, SC, 1991) Vol.10 p.92.
5. B.H.T. Chai, Y. Shimony, C. Deka, X.X. Zhang, E. Munin, and M. Bass, in OSA Proceedings of Advanced Solid State Lasers, eds. L. Chase and A. Pinto (Optical Society of America, Santa Fe, NM, 1992) Vol.13 p.28.
6. C. Deka, M. Bass, B.H.T. Chai, and X.X. Zhang, in OSA Proceedings of Advanced Solid State Lasers, eds. L. Chase and A. Pinto (Optical Society of America, Santa Fe, NM, 1992) Vol.13 p.47.

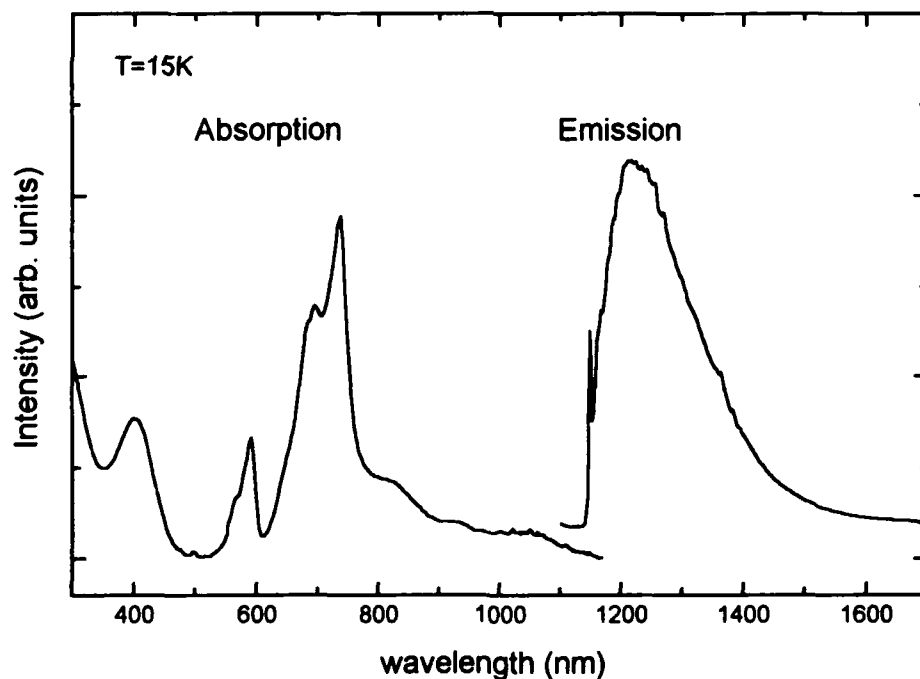


Figure 1. Low temperature absorption and emission of Cr: Y_2SiO_5

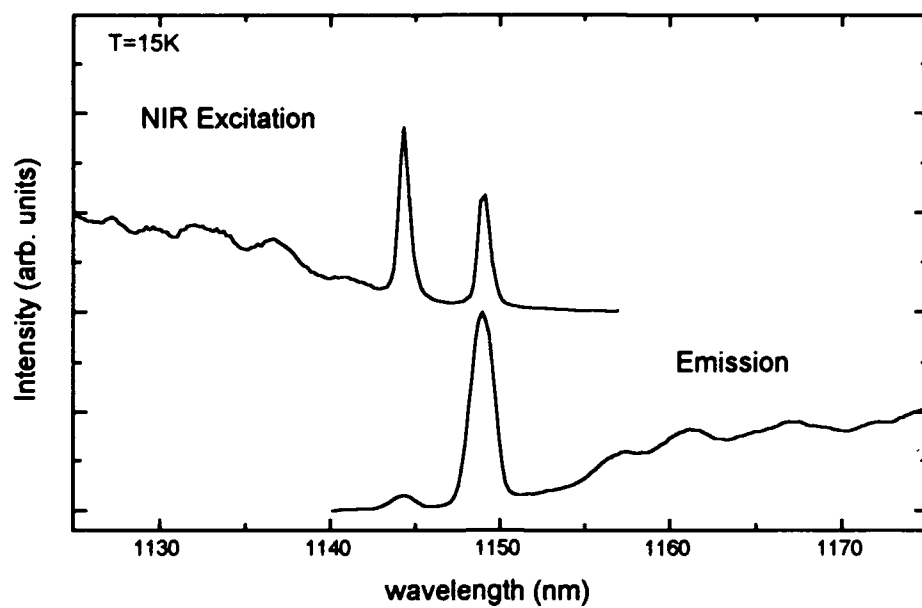


Figure 2. High resolution NIR excitation and emission spectrum on Cr:Y₂SiO₅

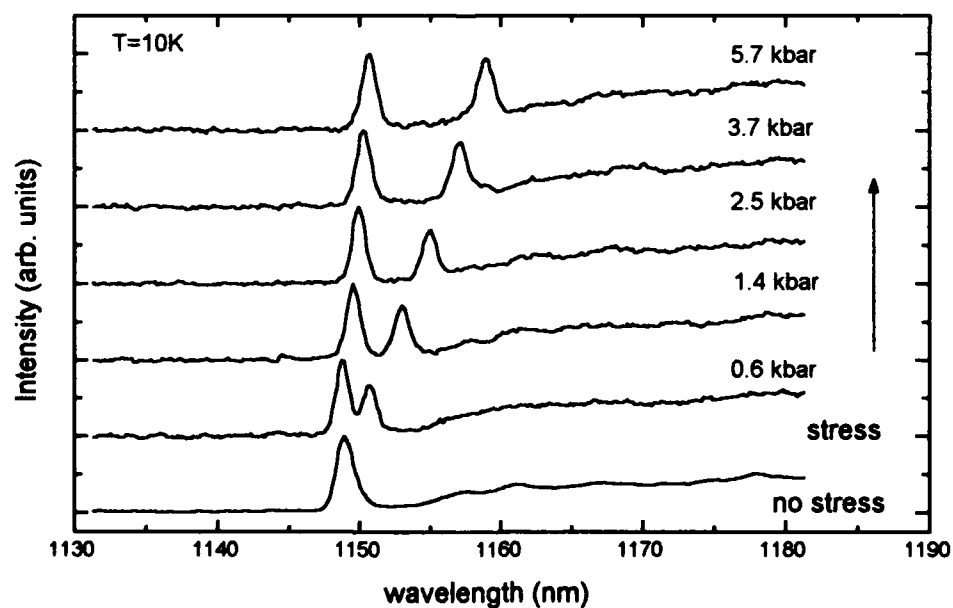


Figure 3. Uniaxial stress experiment on Cr: Y₂SiO₅

Upconversion Studies in Laser Diode Pumped Tm,Ho:YLiF₄

G. Hansson, A. Callenäs and C. Nilsson

National Defense Research Establishment
Dept of information technology
P.O.Box 1165, S-58111 Linköping, Sweden
Tel. (int)+46 13 11 80 00

Introduction

The development of high power, laser diode pumped solid state lasers using Thulium or Thulium, Holmium doped crystals is very promising. The laser wavelength, 2 μm , is eyesafe and has great potential in several applications. However there is a problem with an upconversion process which depletes the upper laser level and thereby increases the laser threshold. Today there are primarily two crystal hosts used for these systems, Y₃Al₅O₁₂ (YAG) and YLiF₄ (YLF). A cw model for this process based on a rate equation approach has been presented together with measurements on a Tm,Ho:YAG crystal [1]. The model defines a rate constant for the upconversion process which can be used to compare different host materials. More recent measurements have shown a weaker upconversion process in YLF systems compared to YAG [2] but no value for the rate constant has been presented.

In this paper we present fluorescence measurements on a Tm,Ho:YLF crystal pumped by a GaAlAs laser diode. The measurements were made for different crystal temperatures and pump powers. Upconversion rate constants were calculated from the experimental results using the model described in ref. 1.

Experimental

The laser crystal used in the measurements was a 2 mm length, 7 mm diameter, 6.0 % Tm, 0.4 % Ho doped YLF crystal grown by Airtron. The pump beam from the laser diode, a 1 W array from Laser Diode inc., was focused into the crystal using a simple arrangement with an aspheric and a cylindrical lens. Measurements showed that the spot size was fairly circular with a radius of 75 μm . Temperature control of the crystal was accomplished by a pair of thermoelectric coolers integrated in the crystal holder. To avoid water condensation dry nitrogen was sprayed on the crystal surfaces. The lowest temperature obtained was 256 K, limited by heat conduction back into the crystal mount and heating from the gas flow. The laser diode was wavelength controlled to the 792 nm absorption band using a thermoelectric cooler mounted inside the casing. Crystal absorption were measured at 256 K, 273 K and 295 K to establish the absorption coefficient α . Spectral measurements were made with a Bomem DA2 fourier transform spectrometer. The space between the crystal and the instrument was filled with dry nitrogen to reduce the water vapor absorption in the 1.8 - 1.9 μm band. The pump radiation had to be blocked by a color filter, Schott UG6, to avoid saturation in the spectrometer. The spectra were compensated for detector response and filter transmission using a blackbody as reference. Spectra of the fluorescence were obtained for the temperatures mentioned above and for different pump levels. Results obtained at 256 K is showed in figure 1. Tm fluorescence is found in the 1.65-1.94 μm band and Ho fluorescence in the 1.87-2.08 μm band. The energy transfer takes place in the spectral overlap between the two ions.

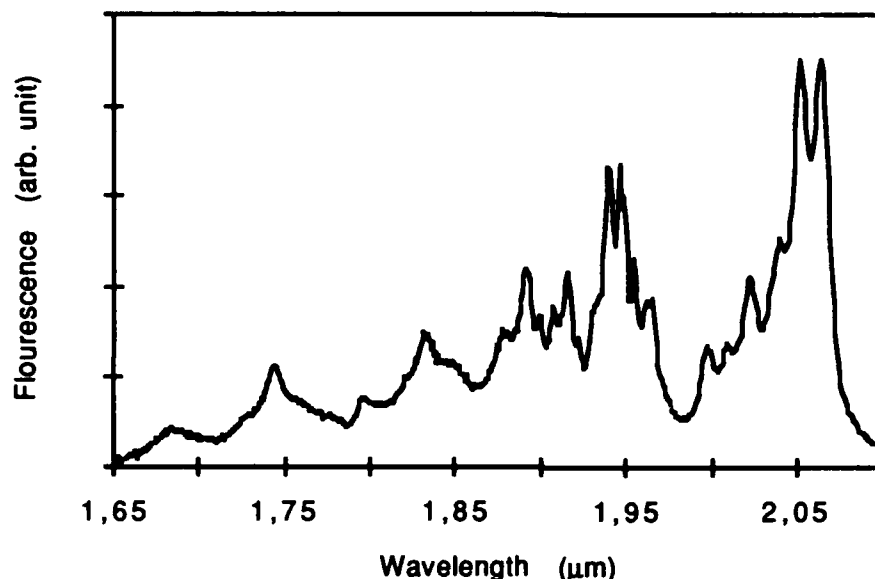


Figure 1. Fluorescence spectra obtained at a crystal temperature of 256 K.

Results and discussion

The total population N_{tot} at (r,z) of the 5I_7 level of Ho and 3F_4 level of Tm are given by

$$N_{\text{tot}}(r,z) = \frac{1}{q\tau f_{\text{Tm}}f_{\text{Ho}}} \left[\sqrt{1 + 2q\tau^2 f_{\text{Tm}}f_{\text{Ho}} \frac{\eta_p P_{\text{abs}}}{h\nu_p} r_p(r,z)} - 1 \right]$$

where q is the upconversion rate constant, τ is the coupled lifetime of the levels, f_{Tm} and f_{Ho} are the equilibrium Boltzmann distribution factors at the current temperature, η_p is the pump quantum efficiency, ν_p is the pump frequency, h is Planck's constant and $r_p(r,z)$ is the pump intensity distribution.

$N_{\text{tot}}(r,z)$ must be integrated over the pump volume to give a value proportional to the fluorescence. The pump distribution was assumed to be gaussian with a waist radius $\omega_p = 75 \mu\text{m}$. The peak fluorescence at $2.06 \mu\text{m}$ from the 5I_7 level in Ho were obtained from the measured spectra and plotted against absorbed power. For $\tau = 12 \text{ ms}$, $\eta_p = 1.76$ and using the data in table 1 curves fitting the data points were calculated giving a value for the upconversion rate constant q for each temperature. The fluorescence data and the curves from the model are plotted in fig 2.

Table 1. The temperature dependent parameters used in the model with the corresponding q values.

Temp. (K)	f_{Tm}	f_{Ho}	$\alpha \text{ (cm}^{-1}\text{)}$	$q \text{ (cm}^3\text{/s)}$
256	0.28	0.72	3.8	1.3×10^{-18}
273	0.32	0.68	3.5	1.5×10^{-18}
295	0.37	0.63	3.1	1.8×10^{-18}

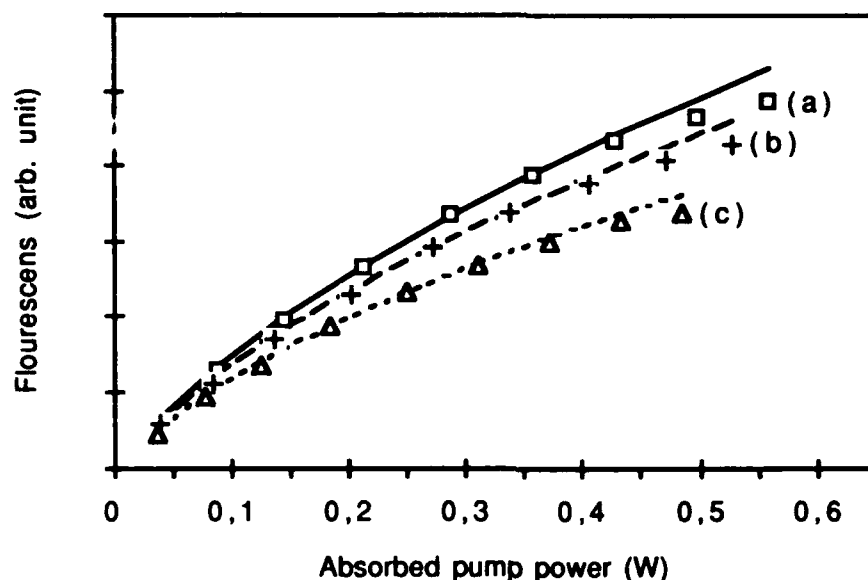


Figure 2. Fluorescence data as a function of absorbed pump power at temperature (a) 256 K, (b) 273 K and (c) 295 K with the corresponding curvefit, solid line $q=1.3 \times 10^{-18} \text{ cm}^3/\text{s}$, dashed line $q=1.5 \times 10^{-18} \text{ cm}^3/\text{s}$, dotted line $q=1.8 \times 10^{-18} \text{ cm}^3/\text{s}$.

The values of q are one order of magnitude smaller for this crystal compared to YAG which was found to be $2.4 \times 10^{-17} \text{ cm}^3/\text{s}$ in ref 1. The model is a good description for the fluorescence at moderate pump levels. At higher pump levels saturation effects becomes evident. The variation of temperature in the measurements results in a moderate change in the q value. The difference in Ho fluorescence is therefore largely given by the temperature dependence of the Boltzmann equilibrium distribution factors, f_{Tm} and f_{Ho} .

Summary

We have studied upconversion in the $^5\text{I}_7$ level in Ho codoped with Tm in YLF pumped by a laser diode. Measured data were fit to a steady state model and the upconversion rate constant was found to be one order of magnitude smaller compared to Tm,Ho:YAG. These results show that YLF has an advantage over YAG as a host for laser diode pumping of Tm,Ho systems.

References

1. T. Y. Fan, G. Huber, R. L. Byer, "Spectroscopy and diode laser pumped operation of Tm,Ho:YAG", IEEE JQE, vol. 24, no. 6, June 1988, p. 924-933.
2. G. Armagan, A. M. Buoncristiani, A. T. Inge, B. Di Bartolo, "Comparison of spectroscopics properties of Tm and Ho in YAG and YLF crystals", OSA Proceedings on Advanced Solid-State Lasers, vol. 10, 1991, p. 222-226.

Wednesday, February 3, 1993

Organic Nonlinear Materials

CWA 8:45am-9:30am
Pelican Ballroom

Shinsuke Umegaki, *Presider*
Keio University

Enhanced Second-Harmonic Generation with a Periodically Poled Nonlinear Organic Copolymer

Heihachi Sato, Yuji Azumai and Iwao Seo*

Department of Electrical Engineering, National Defense Academy, Yokosuka 239, Japan [Tel. (0468)41-3810].

*Advanced Materials Laboratory, Mitsubishi Petrochemical Co. Ltd., Ibaraki 300-03, Japan [Tel. (0298)87-1015].

Summary

In second-harmonic generation (SHG) perfect phase-matching cannot be essentially satisfied between fundamental and second-harmonic (SH) waves for organic polymers or copolymers as done in inorganic crystals. Thus, it is quite required to take the phase-matching by some means. In order to overcome this disadvantage the inter-mode and the Cerenkov radiative phase-matchings have been often adopted in a slab or channel waveguide with mainly nonlinear optical (NLO) organic and inorganic crystals[1]-[3]. However, since the attainable SHG power is necessarily limited, a periodic corrugation of the NLO susceptibility $\chi^{(2)}$ is induced into the waveguide for the phase-matching or quasi-phase matching by using the technique of domain-inversion in inorganic crystals[4],[5].

In this paper we shall thus demonstrate both the inter-mode quasi phase-matching and the Cerenkov radiative phase matching to enhance the SHG power extremely with the periodically corrugated NLO susceptibility into the slab-waveguide made of

VDCN/VAc copolymer. The enhancement factor of these schemes will also be evaluated to the SHG power from a uniform $\chi^{(2)}$ bulk specimen.

The experimental schematic diagram and close up of slab-waveguide are, respectively, depicted in Fig. 1(a) and (b). As a fundamental wave source, a pulsed Nd:YAG $1.06 \mu\text{m}$ was used. The fundamental beam was incident on the slab-guide by a prism coupler. The slab-guide has been composed of the corrugated $\chi^{(2)}$ VDCN/VAc copolymer, fused silica and gold evaporated fused silica as the guiding, the upper and lower layers, respectively. After the mode analysis based on the refractive indices at each layer, this slab-guide can be used for either the inter-mode quasi-phase matching or the Cerenkov radiative phase-matching. Since the SHG power will be effectively enhanced if the wave number of the corrugation period Λ is exactly equal to the difference of the wave-numbers between the fundamental and SH waves. Thus the Λ was chosen to be 60

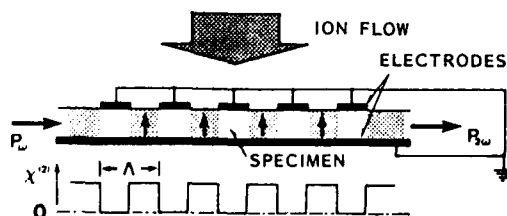


Fig. 2 Processing a periodic $\chi^{(2)}$ corrugation onto spin-coated VDCN/VAc copolymer film using corona discharge.

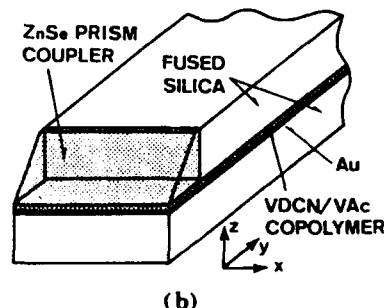
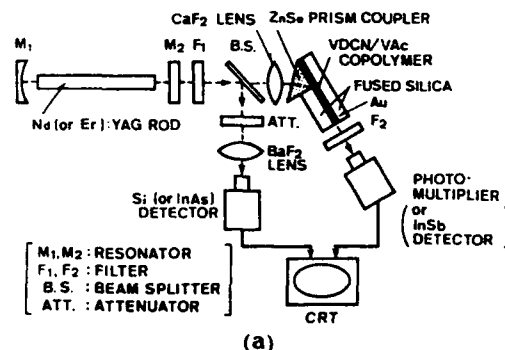
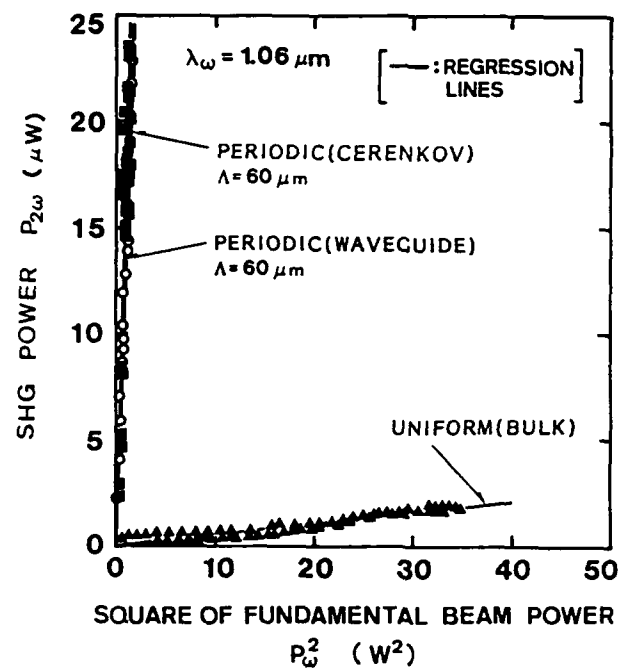


Fig. 1 Experimental setup: (a) schematic diagram and (b) close up of NLO slab-guide portion.

μm , with introduced the periodic $\chi^{(2)}$ into the copolymer having the thickness of $\sim 1.5 \mu\text{m}$ by the corona-discharge (see Fig. 2). The specification of the corrugated copolymer is summarized in Table I, together with a uniform $\chi^{(2)}$ specimen.



Dependence of Fig. 3 Linear dependence of SHG the SHG power $P_{2\omega}$ on power $P_{2\omega}$ on the square of the the square of the fundamental power P_{ω}^2 are illustrated in Fig. 3 for both the inter-mode quasi phase-matching and Cerenkov phase-matching, showing good linear characteristics as expected in the theory. In the Cerenkov scheme with a quasi sinusoidal $\chi^{(2)}$ corrugation, the SHG power tends to radiate along two directions as shown in Fig. 4. Comparing with SHG power obtained from a uniformly distributed $\chi^{(2)}$ bulk VDCN/VAc copolymer, the en-

Table I Specification of VDCN/VAc copolymer with a periodic $\chi^{(2)}$ corrugation.

Molecular formula	$\left[\begin{array}{c} \text{CN} \\ \\ -\text{CH}_2 - \text{C} - \text{CH}_2 - \text{CH} - \\ \quad \quad \\ \text{CN} \quad \quad \text{OCOCH}_3 \end{array} \right]_n$	
Molecular weight	470,000	
Phase	Amorphous	
Glass transition temperature	182 °C	
Poling	Corona discharge(7 kV/cm)	
	Uniform poling	Periodic poling ($\Lambda = 60 \mu\text{m}$)
Thickness	1.43 μm	1.5 μm

hancement factors (E.F.) of 480 and 410 are obtained at 1.06 μm , respectively, for the inter-mode and Cerenkov schemes. These E.F. values are smaller by the factor of ~ 2 than the theoretical estimates. This is considered due to actually a quasi sinusoidal $\chi^{(2)}$ corrugation even though the square $\chi^{(2)}$ corrugation was intended with a comb-shape electrode by a corona discharge.

The SHG power obtained from both the inter-mode and the Cerenkovian phase-matchings with the periodic $\chi^{(2)}$ corrugation are theoretically derived, especially emphasizing on the enhancement factor overwhelming to the uniform $\chi^{(2)}$ bulk material. In addition, comparison of several schemes will also be described, together with practical problems.

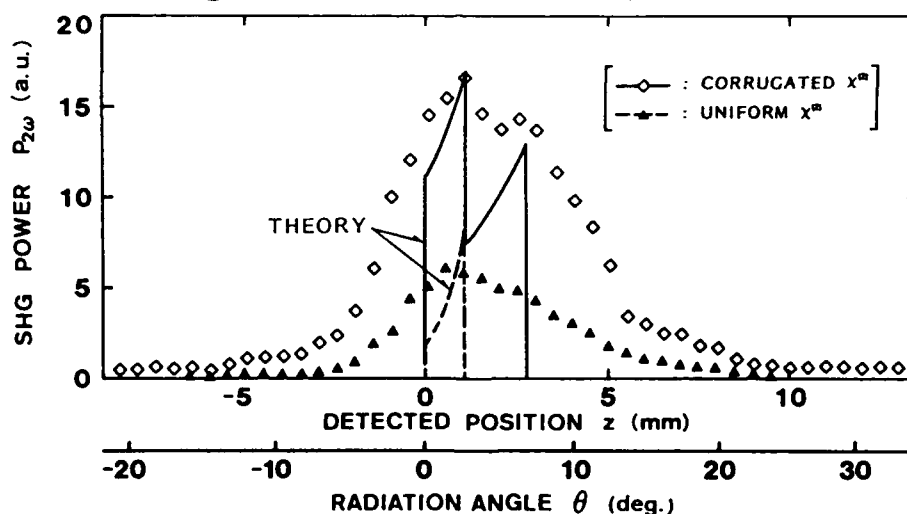


Fig. 4 SHG power as a function of the Cerenkov radiation angle θ .

References

- [1] P. K. Tien, R. Ulrich and R. J. Martin, Appl. Phys. Lett. 17, 447(1970).
- [2] N. A. Sanford and J. M. Connors, J. Appl. Phys. 65, 1429(1989).
- [3] Y. Azumai, I. Seo and H. Sato, Nonlin. Opt. 1, 129(1991).
- [4] G. A. Margel, M. M. Fejer and R. L. Byer, Appl. Phys. Lett. 62, 108(1990).
- [5] Y. Azumai, M. Kishimoto and H. Sato, Jpn. J. Appl. Phys. 31, 1358(1992).

**An Organic Crystal
3,5-dimethyl-1-(4-nitrophenyl)pyrazole
for Compact Visible Light-sources**

**H. Hyuga, C. Goto, Y. Okazaki, A. Harada, S. Mitsumoto
and**

K. Kamiyama

**Miyanodai Technology Development Center,
Fuji Photo Film Co., Ltd.,
798, Kaisei-machi, Ashigarakami-gun, Kanagawa 258, Japan
(TEL: 465-85-2027, FAX: 465-85-2031)**

S. Umegaki

**Department of Electrical Engineering,
Faculty of Science and Technology, Keio University
3-14-1, Hiyoshi, Kouhoku-ku, Yokohama-shi, Kanagawa 223, Japan
(TEL: 45-563-1141, FAX: 45-561-8838)**

The advent of blue-green II-VI semiconductor lasers[1] is stimulating the research activity in more efficient frequency-conversions of III-V semiconductor-laser sources. In almost all cases of the conversions, inorganic materials are being used. On the other hand, organic materials have been developed and expected to give more efficiencies in the conversions because of their higher figures of merit in comparison with the inorganics.

This paper reports the guided-wave and bulk devices using an organic nonlinear-optical crystal of 3,5-dimethyl-1-(4-nitrophenyl)pyrazole(DMNP) [2], which can be grown from the melt as a single bulk crystal of good optical quality and as a single core-crystal in a glass-capillary. The relatively large nonlinear coefficient d_{32} , whose value is 90 pm/V, can be used in both devices.

1. Simultaneous Generation of a Red, a Green and a Blue Light-wave in a Crystal-cored Fiber

Previously, we reported the generation of blue light by frequency doubling using a DMNP-cored fiber[3]. The phase-matched second-harmonic power of wavelength 484 nm reached 0.21 mW from the only 13.4 mW incident fundamental power. In the case of the Cerenkov-radiation type frequency-doubling, the phase-matching is easy to attain and the optimum design for high efficiency is possible by selection of a cladding glass and of a core-radius with practical tolerance.

We succeeded in simultaneously generating a red, a green and a blue light-wave by using an InGaAsP and an AlGaAs semiconductor laser as fundamental light-sources, whose wavelengths were 1300 nm and 890 nm, respectively. The length, the core-diameter and the cladding glass of the DMNP fiber used were 7 mm, 1.2 μm and superflint SF15, respectively.

The experimental setup is illustrated in Fig.1. The half-wave plates were used for the polarization-directions of the two fundamental lasers to coincide with the crystallographic y-axis of DMNP, since the nonlinear coefficient used was d_{32} . The prism pair was required to circularize the radiated-beam pattern in the case of the AlGaAs laser, but not in the case of the InGaAsP laser used in telecommunications. Both lasers were coupled into the fiber by an objective lens. The propagation loss for 1300 nm and for 890 nm were estimated by the cut-back method to be 1.5 dB/cm and 1.7 dB/cm, respectively.

The wavelengths generated were 650 nm(red), 530 nm(green) and 445 nm(blue). The blue and the red light-wave corresponded to frequency doubling of 890 nm and of 1300 nm, while the green light-wave to sum-frequency mixing of both. The conversion efficiencies calibrated for the 40 mW-fundamental powers into the blue, the red and the green were 1.4 %, 0.5% and 2.6 %, respectively.

2. Non-critically Phase-matched Generation of a Blue Light-wave in an Nd:YAG Laser Cavity

A DMNP crystal is biaxial and its nonlinear coefficient d_{32} is non-critically phase-matchable for the second-harmonic generation of Type I at a wavelength of 472 nm. A doubled wavelength of a 946 nm-Nd:YAG laser fits this wavelength.

However, considering a possibility of direct modulation of a converted light, we attempted to generate a blue light-wave by non-critically phase-matched sum-frequency mixing of a semiconductor laser with an 809 nm-laser-diode pumped Nd:YAG laser by using a bulk crystal internal to the laser cavity. Actually, the non-critically phase-matching is possible in generating a 471 nm-light-wave by sum-frequency mixing of 844 nm and 1064 nm.

The experimental setup is shown in Fig.2. The 844 nm-semiconductor laser to be mixed was made propagated coaxially with the 809 nm-semiconductor laser to pump the YAG laser by the polarization beam-splitter and focused through a lens into the DMNP crystal and the Nd:YAG plate with 5 mm thickness. The DMNP crystal was so cleaved as the cleavage plane involved the crystallographic y- and z-axes. After being ground by a diamond-turning machine, the flat surfaces, whose flatness was evaluated by a microscopic Fizeau's interferometer to be less than $\lambda/4$, were anti-reflection coated at wavelengths of 1064 nm, 807~840 nm and 471 nm. The dimensions of the obtained crystal were 5 mm in diameter and 4 mm in length. The crystal was so set that its crystallographic y-axis should coincide with the polarization direction of the 844 nm-semiconductor laser. In spite of no polarizer in the cavity for the 1064 nm-oscillation of the YAG laser, its polarization direction was parallel to the y-axis of DMNP.

The blue output power was 0.1 mW for the absorbed pump-power 110 mW of the 809 nm-semiconductor laser and the mixed power 50 mW of the 844 nm- semiconductor laser. The reason of the relatively low efficiency was mainly attributed to a high insertion loss of the DMNP crystal reaching 13 % and also to mismatching of the transverse mode of the YAG laser oscillated at 1064 nm with the profiles of the mixed 844 nm-semiconductor laser and the pumping 809 nm-semiconductor laser.

REFERENCES

- [1] M.A.Haase, J.Qiu, J.M.DePuydt, and H.Cheng, *Appl.Phys.Lett.* **59**, 1272 (1991).
- [2] M.Okazaki, H.Fukunaga, and S.Kubodera, *J.Synthetic Organic Chem.Japan* **47**, 457 (1989).
- [3] C.Goto, A.Harada, K.Kamiyama, S.Umegaki, in *Conference on Laser and Electro-Optics* Vol.12, 1992 OSA Technical Digest series. (Optical Society of America, Washington DC, 1992), paper CThA4.

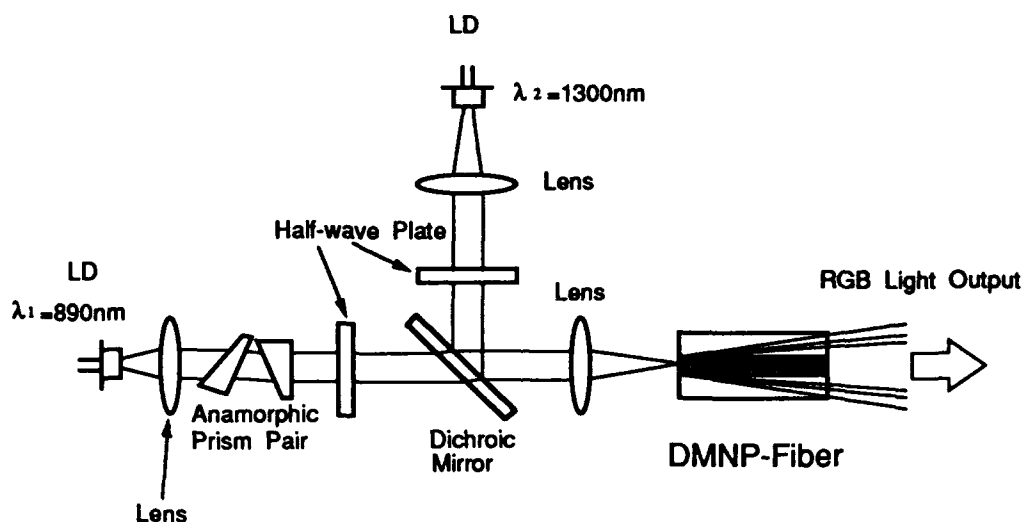


Figure 1. The experimental setup for simultaneous generation of a red, a green and a blue light-wave in a crystal-cored fiber.

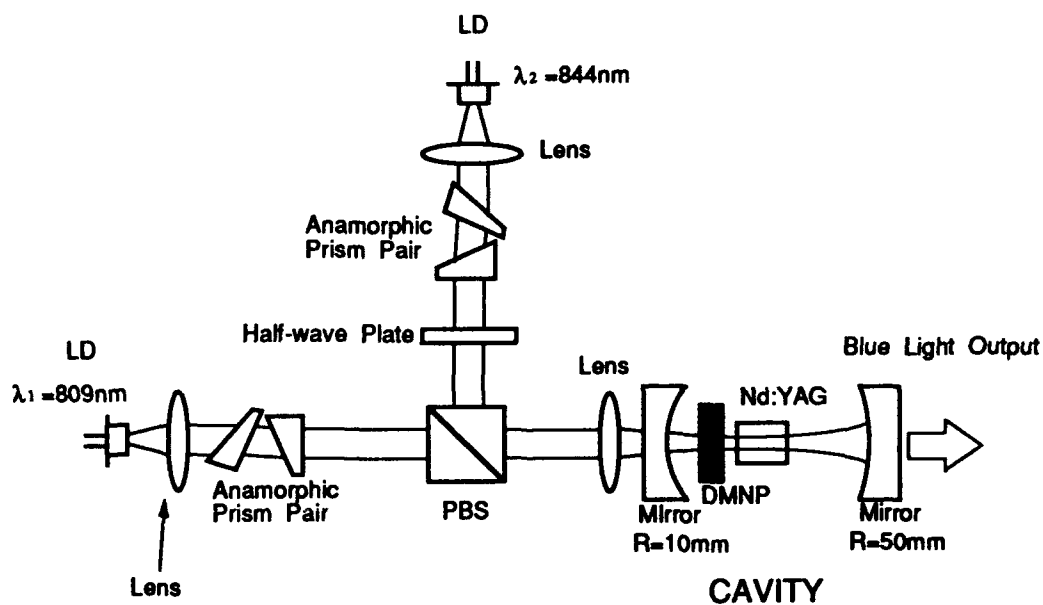


Figure 2. The experimental setup for non-critically phase-matched generation of a blue light-wave in an Nd:YAG laser cavity.

Wednesday, February 8, 1998

Joint Session on Inorganic Nonlinear Materials

JWA 10:30am–11:30am
La Salle Ballroom B&C

Peter F. Bordui, *Presider*
Crystal Technology, Inc.

PERIODIC DOMAIN-INVERTED NONLINEAR OPTICS

Hiromasa ITO, Choichi TAKYU, and Motoki OHASHI

Research Institute of Electrical Communication, Tohoku University

2-1-1, Katahira, Aoba-ku, Sendai 980, Japan

tel: +81-22-227-6200 fax: +81-22-263-9848

Abstract

An e-beam method is developed for the fabrication of domain reversed volume grating in LiNbO_3 and LiTaO_3 . Blue SHG experiment was performed to demonstrate high efficient nonlinear interactions. Periodic domain inverted structure has wide potentials for the various nonlinear optical interactions.

INTRODUCTION

The quasi-phases-matching (QPM) method has attracted much attention recently for efficient nonlinear optical process at relatively low power level. Various methods have been reported to fabricate periodic domain inverted structures. The inverted region is usually restricted near the surface, so that most of the nonlinear applications are limited to use the optical waveguide structure.

We report here a new fabrication method of periodic volume domain grating by means of the electron beam writing to LiNbO_3 and LiTaO_3 crystals at room temperature. The generation of blue second harmonic light is also reported.

PERIODIC DOMAIN FABRICATION

The structure change for the domain flip of the LiNbO_3 crystal corresponds to the symmetrical displacement of the Li ion site only at 0.14 nm along the z axis in connection with the oxygen triangle¹⁾. If the internal field is large enough to pull down the Li ion site, the domain is easily exchanged. For this purpose, we use the electron beam irradiation to the -z surface to give the local charge with arbitrary patterns².

The scanning electron microscope (SEM) (HITACHI S570) was used as an electron beam exposure system. The personal computer controls the beam position to expose the arbitrary pattern with arbitrary dose. Prior to the electron beam treatment, +z surface of LiNbO_3 is coated with Cr metal, and the electron beam is exposed on the -z surface. The penetration depth of the electron into LiNbO_3 sample depends on the electron beam energy, and it is estimated about few micron meter at an accelerating voltage of few tens of kilovolt.

Figure 1 shows the etching pattern of the +z surface of the LiNbO_3 substrate after the electron beam treatment, where the beam irradiated surface is 500 μm away. Surprisingly, a regular domain grating pattern is clearly seen at the other end of the surface; the volume domain grating is formed. The period of the grating is 6.4 μm for this case, and the accelerat-

ing voltage was 25 kV with the beam current of 4×10^{-10} . The electron beam was scanned along the x-axis of the crystal. The characteristic of the domain inversion depends on the beam current, the accelerating voltage, the beam scanning speed, the crystal orientation, the crystal temperature, and so on. Typical exposing conditions are followings : sample thickness of 0.5 mm, accelerating voltage of 20–30 kV, the dose of electrons of 2×10^9 electrons/sec, the electron charge of 0.5×10^{-12} C per 1 μm for the scanning condition and all the process was done at the room temperature without any external DC bias.

Possible mechanism for the domain inversion by the electron beam exposure is as follows: The spontaneous polarization P_s of LiNbO_3 is about 0.7 C/m^2 at room temperature, and this charge should induce the electric field as high as $8 \times 10^{10} \text{ [V/m]}$, however, this is neutralized by ions and electrons adsorbed at the surface. Due to the electron beam, positive charge is neutralized by the electron to give the internal electric field. At the certain strength of the internal electric field ($\sim 30 \text{ kV/mm}$ or more) the domain flips, and meanwhile the surface charge is also neutralized by electrons.

QPM CONDITION and SHG EXPERIMENT

The QPM condition for SHG is given by

$$T = 2m \times \lambda_{\text{SH}} / (n_{\text{SH}} - n_{\text{F}}) \quad (1)$$

where T is a domain period, λ_{SH} is harmonic wavelength in vacuum, n_{F} and n_{SH} are the refractive indices at the fundamental and harmonic wavelength, respectively, and m is an integer for the order of the QPM.

The m th order of the effective nonlinear coefficient is expressed by

$$d_{\text{eff}}^{(m)} = (2d / m \pi) \sin(m \pi (1 - \xi)) \quad (2)$$

Figure 2 shows the square of effective nonlinear coefficient for the periodic domain structure as a function of the duty ratio of the domain inversion ξ .

To investigate the basic performance of the device, QPM SHG was tested using a $\text{Ti:Al}_2\text{O}_3$ laser as a source. The dimension of the domain grating under test was typically $0.5(\text{W}) \times 1.4(\text{L}) \times 0.5(\text{T}) \text{ mm}^3$.

The QPM condition was measured using various samples with different domain periods. Observed QPM data are summarized in Fig. 3 for domain period vs. fundamental wavelengths. Solid lines represent the calculated values.

About 20 μW of blue output was obtained with the length of the domain grating of 1.4 mm under the fundamental power of a hundred milliwatt. This bulk structure gives a relatively high efficiency to verify the usefulness of this structure. LiTaO_3 substrate was also investigated and we obtained the similar result of LiNbO_3 . Under the confocal focusing condition, the conversion efficiency of 24 % / W-cm is expected for QPM-SHG at the fundamental wavelength of 800nm.

This structure is quite useful for the various nonlinear parametric interactions, such as

parametric oscillation and difference frequency generation not only in the blue and green region but also infrared and even in the submillimeter wave region.

- 1) P. W. Haycock and P. D. Townsend, *Appl. Phys. Lett.*, **48**, 698 (1986).
- 2) H. Ito, C. Takyu, and H. Inaba, *Electron. Lett.*, **27**, 1221 (1991).

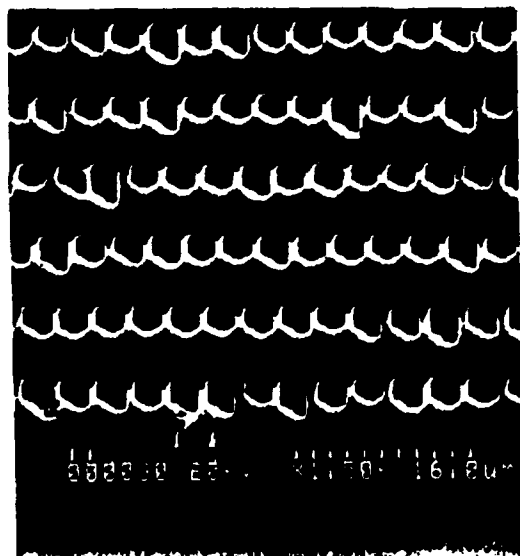


Fig. 1 Magnified view of etched pattern of domain reversal grating of LiNbO_3 . The grating period is $6.4 \mu\text{m}$, and the mean interval of dots is about $3 \mu\text{m}$, due to the c-beam scanning mechanism.

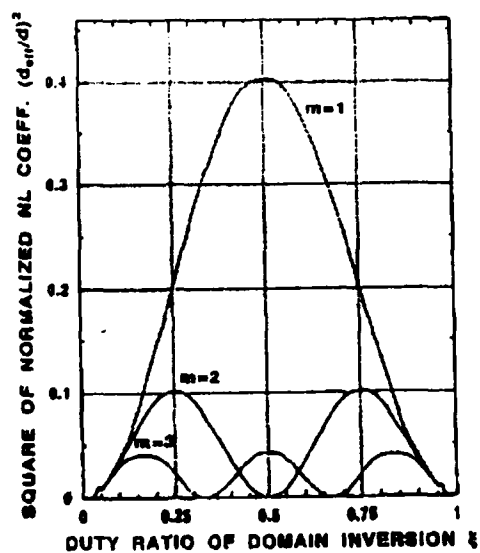


Fig. 2 Square of effective nonlinear coefficient for a periodic domain structure as a function of the duty ratio of domain inversion ξ . The parameter m refers the order of the QPM.

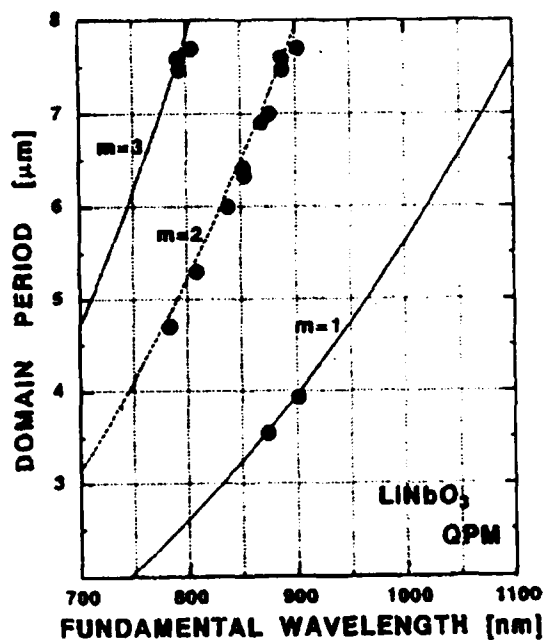


Fig. 3 QPM domain periods against fundamental wavelengths.

Comparative experimental study of KTA and KTP for the SHG at 1.32 μm and 1.064 μm

B. Boulanger, G. Marnier, J.P. Fève, B. Ménaert and X.Cabirol
Laboratoire de Minéralogie-Cristallographie et Physique Infrarouge, URA CNRS 809, Université
de Nancy I, Faculté des Sciences, BP 239, 54506 Vandoeuvre Cedex, France.
Tél : 83 91 22 68

C. Bonnin and P. Villeval
Cristal Laser S.A., BP 44, 54230 Chaligny, France.
Tél : 83 47 01 01

We report the first experiment, to our knowledge, of type II phase-matching SHG at 1.32 μm in KTiOAsO_4 (KTA) [1,2]. The phase-matching directions are measured in an orientated sphere of the studied crystal placed at the center of an Euler circle and illuminated by the focused beam at the fundamental wavelength [3]. The KTA and KTP crystals which we study are grown using a flux of alkali metal halide [4]. The crystals are cut in a sphere with a diameter of 2.45 mm for KTA and 5.12 mm for KTP. The spherical coordinates (θ , ϕ) of the phase-matching directions measured are given in figure 1.

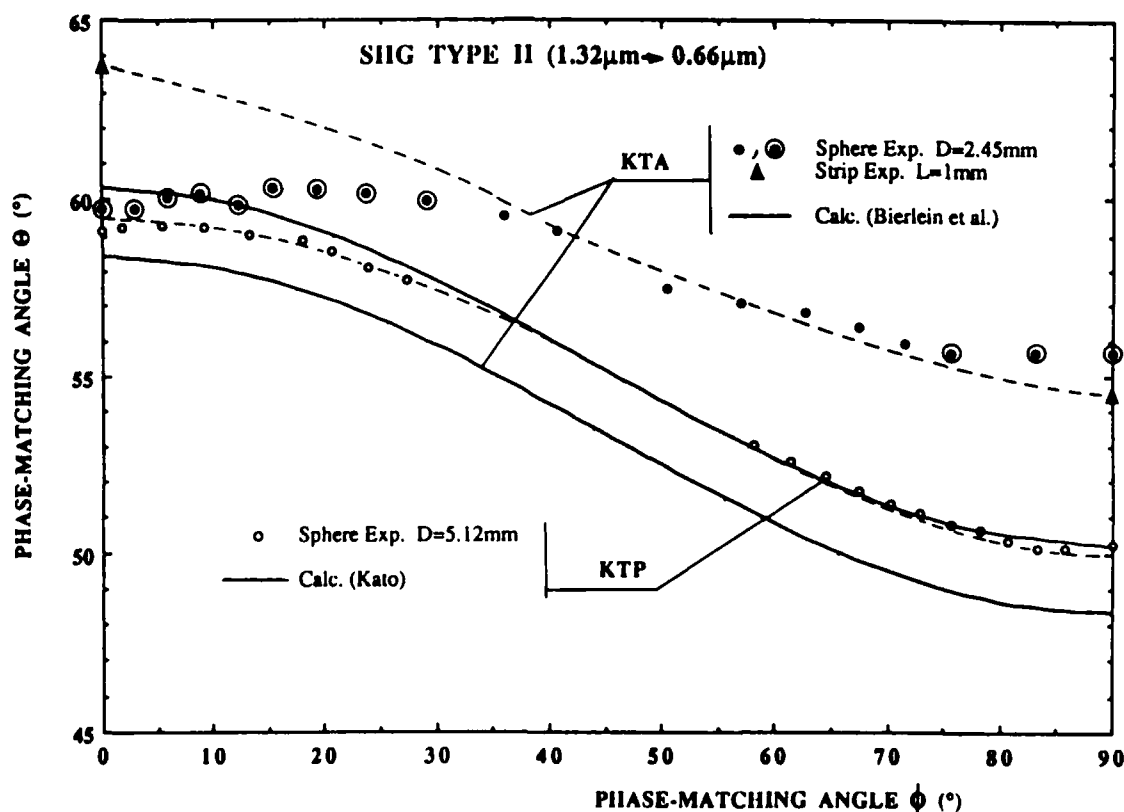


Figure 1 : Phase-matching angles of type II SHG at 1.32 μm . Comparison between KTP and KTA. Comparison between experiment and calculation. The experimental points symbolized by \odot are distorted because of the asphericity.

The maximum efficiency is obtained in the x-z plane at $\theta = 65^\circ$ for KTA and $\theta = 59.3^\circ$ for KTP. The measurements of the power generated at $0.66 \mu\text{m}$ in two uncoated 1mm-thick strips cut perpendicular to these directions indicate that KTA has a figure of merit (d_{eff}^2/n^3) about a factor 1.4 larger than KTP, that is to say a ratio of about 1.25 between the χ_{24} coefficients (figure 2).

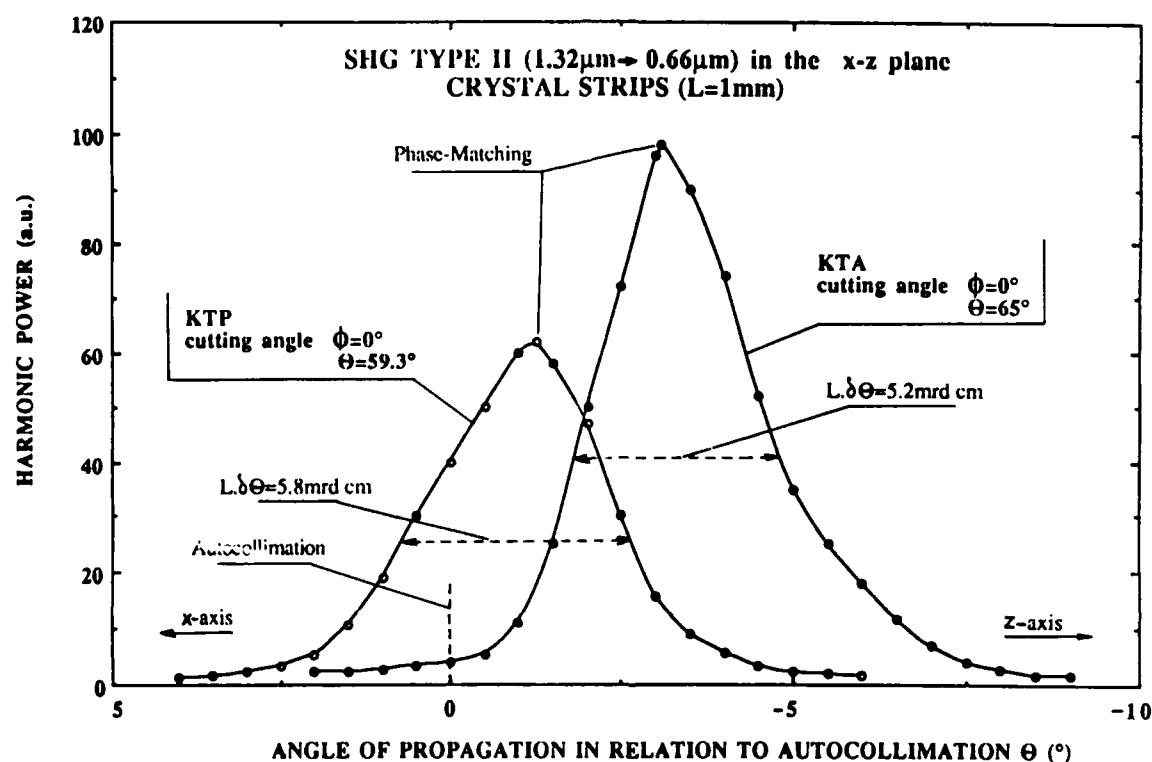


Figure 2 : Power generated at $0.66 \mu\text{m}$ compared for KTP and KTA as a function of the θ external angle in the x-z plane around the phase-matching directions for the same fundamental power. The origin at $\theta = 0$ is defined by the autocollimation of the two strips.

The same study in the y-z plane indicates a ratio of about 1.15 between the χ_{15} coefficients of KTA and KTP.

The experiments give also the possibility of estimating the ratio χ_{24}/χ_{15} which is found equal to 1.9 for KTP and 2 for KTA.

The sphere of KTA in which we detect type II phase-matching SHG at $1.32 \mu\text{m}$ is also used for the study of type II SHG at $1.064 \mu\text{m}$ with the same experimental procedure.

The maximum of type II SHG efficiency at $1.064 \mu\text{m}$ in KTA is obtained along the y-axis. We give in figure 3 the generated power at $0.532 \mu\text{m}$ measured as a function of the direction of propagation in the x-y plane.

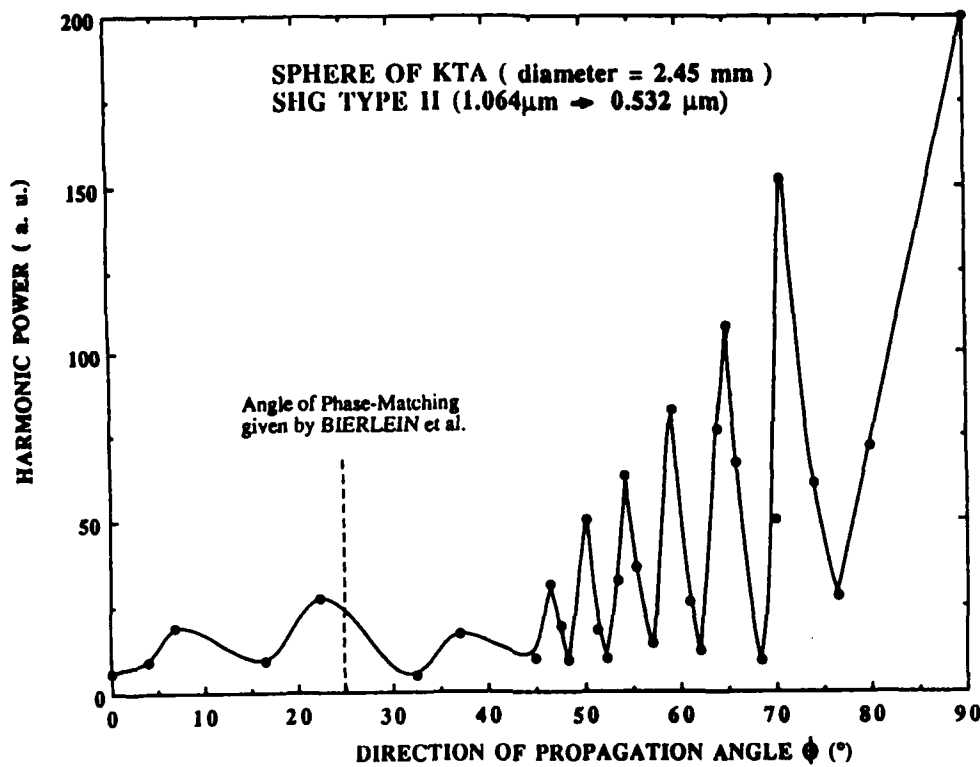


Figure 3 : Power generated at 0.532 μm in KTA as a function of the Φ angle in the x-y plane.

The fringes system of the curve of figure 3 is described by the interference function $I(\Phi)$:

$$I(\Phi) = \text{sinc}^2(\Delta k(\Phi).L/2). \quad (1)$$

L is the optical length and has the same value, equal to the sphere diameter, for all direction of propagation from the x-axis ($\Phi=0^\circ$) to the y-axis ($\Phi=90^\circ$). In fact the sphere method allows the study in normal incidence of all direction of propagation of the crystal that is different from a Maker fringe experiment [3]. Thus, the argument of the interference function varies with Φ only by the mismatch parameter $\Delta k(\Phi)$ which is given by the following relation for a Type II configuration of polarization in the x-y plane of a biaxial crystal :

$$\Delta k(\Phi) = n_z^\omega + n_{xy}^\omega(\Phi) - 2 n_{xy}^{2\omega}(\Phi) \quad (2)$$

$$\text{where } n_{xy}(\Phi) = [\cos^2\Phi / n_y^2 + \sin^2\Phi / n_x^2]^{-1/2}. \quad (3)$$

From our experiments, it is quite obvious that the maximum of type II SHG efficiency at $1.064\mu\text{m}$ obtained along the y-axis of KTA is not phase-matched ($\Delta k \neq 0$) : the efficiency is 40% less than type II phase-matching SHG efficiency at $1.32\mu\text{m}$ for the same fundamental power in the same sphere. In more the comparison between type II SHG at $1.064\mu\text{m}$ of KTA, along the y-axis, and KTP, along the phase-matching direction of greater efficiency ($\theta=90^\circ$, $\Phi=23.3^\circ$), on two 2.18mm-thick strips samples indicates that KTP has an efficiency about a factor 50 larger than KTA.

Thus, no phase-matching ($\Delta k=0$) is observed even at about $\phi = 25^\circ$ in the x-y plane where its detection have been reported by Bierlein et al. [5].

Then, we conclude that type II phase-matching at $1.064\mu\text{m}$ is forbidden by the birefringence and the dispersion in frequency of the refractive indices of KTA and that for all fundamental wavelength lower than $1.064\mu\text{m}$. Complementary experiments at higher fundamental wavelengths will allow to determine the fundamental cutoff wavelength of KTA for type II phase-matching SHG. In more, our experiments show also that KTA is more efficient than KTP when the phase-matching exists.

This work allows also to question the powder screening. In fact, measurements of SHG at $1.064\mu\text{m}$ in KTA powders lead El Brahim and Durand [6] in 1986 to conclude that the phase-matching at $1.064\mu\text{m}$ is possible.

The absolute measurements of the coefficients of the second order electric susceptibility tensor $\chi^{(2)}$ is under study on KTP and will also be reported.

This work is supported by the contract : MENJS-DRED 901331 and CNRS-PIRMAT 90N83/0045 GZ 86.

Bibliography :

- [1] B. BOULANGER, G. MARNIER, B. MENAERT, X. CABIROL, J.P. FEVE, C. BONNIN and P. VILLEVAL, submitted to Nonlinear Optics, June (1992)
- [2] B. BOULANGER, G. MARNIER, B. MENAERT, X. CABIROL, J.P. FEVE, C. BONNIN and P. VILLEVAL, OEC'92, Tokyo, Post-deadline Paper P-D7, July 15-17 (1992)
- [3] G. MARNIER and B. BOULANGER, Opt. Commun. **72** (3-4), 139-143 (1989)
- [4] G. MARNIER, US Patent, n° 146928 (22.01.88)
- [5] J.D. BIERLEIN, H. VANHERZEELE and A.A. BALLMAN, Appl. Phys. Lett., **54**(9), 783-785 (1989).
- [6] M.EL BRAHIMI and J.DURAND, Rev. Chim. Miner. **23**,146-153 (1986).

Second-order Optical Nonlinear Properties in Corona-poled Glass Films

A.Okada, K.Mito*, and K.Sasaki

Department of Material Science, Faculty of Science and Technology, Keio
University, 3-14-1 Hiyoshi, Kohoku-ku, Yokohama 223, JAPAN.

(Tel)+81-45-563-1141 ext.3306

*Department of Physics, Faculty of Science and Technology, Keio University,
3-14-1 Hiyoshi, Kohoku-ku, Yokohama 223, JAPAN.

(Tel)+81-45-563-1141 ext.3994

Due to their optically isotropic properties inorganic glasses are not expected to exhibit second-order optical nonlinearity $\chi^{(2)}$. However, we have observed that $\chi^{(2)}$ can be induced in radio-frequency(rf) sputtered Corning 7059 glass films by corona poling and realized phase-matched second-harmonic generation(SHG) in a corona-poled glass film waveguide.¹ To elucidate the mechanism responsible for the induced $\chi^{(2)}$ in the corona-poled glass films is not only interesting from a physical point of view but also serves to develop new glass films with a large $\chi^{(2)}$.

In this paper, we carried out several experiments to elucidate the origin of the induced $\chi^{(2)}$ in the corona-poled glass films. These include the dependence of the second-order nonlinear coefficient d_{33} value on the kinds of the substrates, time decay of d_{33} , and poling at room temperature.

The glass films used in this study were fabricated by rf sputtering Corning 7059 glass on five different kinds of glass substrates(Pyrex glass, fused quartz, soda-lime glass, Corning 7059 glass and indium-tin-oxide(ITO) coated Pyrex glass). The thickness of the films were $\sim 1.8 \mu\text{m}$. The glass films were corona poled using the needle-to-plane electrode configuration. A voltage of approximately 5 kV was applied to the needle. The values of d_{33} of the glass films were determined by the Maker-fringe method.

Table 1 shows the results of the dependence of the d_{33} value on the kinds of the substrates. The SHG signal was not observed or negligibly small for the glass films deposited on the fused quartz and Corning 7059 glass substrates. These results are similar to those observed in poled polymer films in which case the

difference in the electric field strength in the films among the substrates account for the results.² However, from the considerably rapid decay of d_{33} observed in the glass films on the soda-lime glass substrate (Table 2), we consider that charges accumulated at the interface of the glass film and the substrate contribute to the creation of the $\chi^{(2)}$ in the glass film. A possible mechanism deduced from this consideration is that the $\chi^{(2)}$ is induced through the $\chi^{(3)}$ process in which the internal electric field set up by the accumulated charges at the interface acts on the third-order nonlinearity of the glass film. In order to verify this model, we derived the accumulated planar charge density σ by considering a simplified equivalent circuit (Fig.1) for corona poling and examined the experimental results on the basis of it. The planar charge density can be evaluated from the following equations.

$$-\epsilon_f E_f(t) + \epsilon_s E_s(t) = \sigma(t) / \epsilon_0 \quad (1)$$

$$d_f E_f(t) + d_s E_s(t) = V \quad (2)$$

$$\partial \sigma / \partial t = J_f - J_s \quad (3)$$

$$J_f = E_f / \rho_f, \quad J_s = E_s / \rho_s \quad (4)$$

where the subscripts f and s have the meanings a glass film and a substrate respectively.

The values of d_{33} for glass films on the Pyrex glass substrate as a function of poling time at room temperature is shown in Fig.2. Different samples were used at each poling time. The d_{33} value grew gradually with poling time and approached the value of 0.5 pm/V. Considering this phenomena in terms of σ , it corresponds to the charge accumulation process at the interface. By fitting the time dependent σ derived from Eq.1-4 to the experimental data, a curve was obtained as depicted in Fig.2. Figure 3 shows the time decay of d_{33} for a corona-poled Corning 7059 glass film and a SiO_2 film ($d_{33}=0.25$ pm/V). In both cases the d_{33} values are likely to approach the same value. This result can be expected since the films are deposited on the same kind of substrate. The rather rapid decay observed initially after the poling is considered to be due to the decay of charges on the surface of the films.

In conclusion, we have confirmed that the induced $\chi^{(2)}$ is closely related to the accumulated charges at the interface of the glass film and the substrate.

References

1. A.Okada, K.Ishii, K.Mito, and K.Sasaki, Appl.Phys.Lett.60,2853(1992).
2. A.Suzuki, Y.Matsuoka, and A.J.Ikushima, Jap.J.Appl.Phys.30,L1493(1991).

Substrate	d_{33} (pm/V)	
	Poling Temperature	
	100°C	300°C
Pyrex glass	$0.55 \pm .07$	$0.57 \pm .02$
Fused quartz	~ 0	~ 0
Corning7059 glass	~ 0	~ 0
Soda-lime glass	$0.24 \pm .02$	—

Table 1 Dependence of d_{33} on the kinds of the substrates.

Substrate	Time decay of d_{33}
Pyrex glass	3 days \rightarrow 77 %
Soda-lime glass	2 hours \rightarrow 46 %

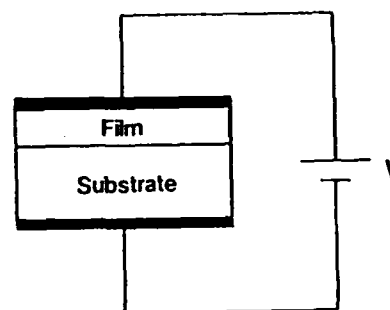
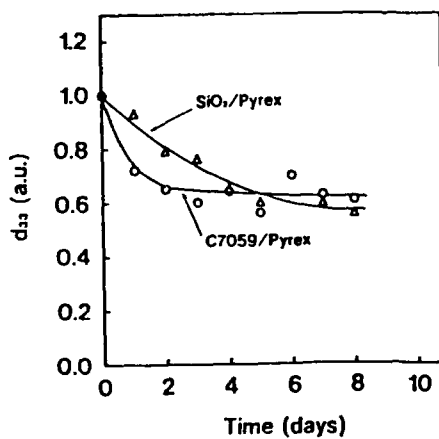
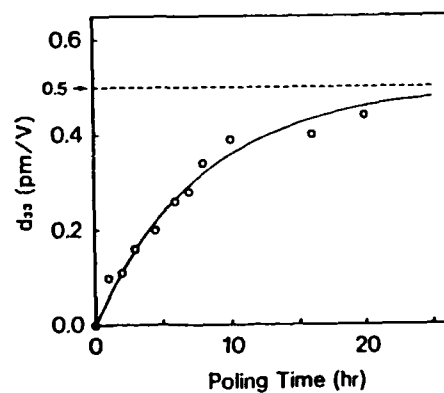
Table 2 Time decay of d_{33} .

Fig.1 Equivalent circuit for corona poling.

Fig.2 Time decay of d_{33} .Fig.3 The values of d_{33} as a function of poling time at room temperature.

Wednesday, February 3, 1993

Joint Session on Frequency Upconversion in Bulk Devices 1

JWB 12:30pm–2:00pm
La Salle Ballroom B&C

David C. Hanna, *Presider*
Southampton University, United Kingdom

Overview of Bulk SHG Activities in Japan

Takatomo SASAKI

Faculty of Engineering, Osaka University

2-1 Yamadaoka, Suita, Osaka 565, JAPAN

(TEL)+81-6-877-5111 EXT.4562, (FAX)+81-6-875-0506

The developement of compact blue-green laser sources by frequency conversion is being energetically done for mainly high density optical memories. In Japan, the bulk type SHG devices using internal cavity resonant method with the combination of the Nd:YVO₄ microchip lasers and the nonlinear optical crystal KTP are popular because the system is simple, compact and easy to get transverse and longitudinal single mode and promising for practical devices. The present status and the problems for practical use of bulk type SHG devices using Nd:YVO₄, NYAB, organic nonlinear crystals and other crystals, which have being developed in Japan will be presented.

**Diode Laser Upconversion in Bulk Nonlinear Resonators—
An Overview of Recent Progress**

**G. J. Dixon
Department of Electrical Engineering
and
Center for Research on Electro-Optics and Lasers
Orlando, FL 32826**

Recent progress in the fields resonant sum frequency generation and external resonant diode doubling will be discussed. The possibilities for watt-level visible devices and the issues separating bulk nonlinear devices from the commercial marketplace will be detailed.

**Stable and Efficient Generation of Green Light
by Intracavity Frequency Doubling of Nd:YVO₄ Lasers**

Y.KITAOKA, S.OHMORI, K.YAMAMOTO, and M.KATO
Optical Devices Research Laboratory
Matsushita Electric Industrial Co.,Ltd.
3-1-1, Yagumo-nakamachi, Moriguchi, Osaka 570, Japan
06-906-2420

T.SASAKI
Department of Electrical Engineering
Faculty of Engineering, Osaka University
2-1, Yamadaoka, Suita, Osaka 565, Japan
06-877-5111

Compact laser sources of shorter wavelengths offer the potential for high-density optical recording, but they also require low noise and a high-power light beam (over 10 mW). It was recently reported that a continuous wave green laser diode (LD) of II-VI groups oscillated at the Nitrogen temperature and also emitted pulsed wave at room temperature.¹ Nonetheless, further efforts are required for practical application of II-VI lasers.

Coherent light sources, on the other hand, based on intracavity second harmonic generation (SHG) of LD-pumped solid-state lasers have been investigated intensively by a number of researchers.^{2,3} Intracavity SHG has been achieved with Nd:YVO₄ lasers operating at 1.064 μm (laser transition). The Nd:YVO₄ crystal is a promising material offering several advantages such as a high-emission cross section and a large absorption coefficient.^{4,5} Efficient frequency doubling in the KTP (KTiOPO₄) intracavity has so far demonstrated for an Nd:YVO₄ laser pumped by a single longitudinal mode LD,³ which, unfortunately, suffered from serious noise attributed to the multimode oscillation and the LD mode hopping. To solve this problem, we must look at previous works on external cavity LDs with diffraction grating for optical communication application. Grating external cavity LDs can be applied to, for example, wavelength division multiplexing systems to stabilize the longitudinal modes of LDs.⁶ Several of these LDs with a grating feedback system have already been confirmed to provide such advantages as a narrow spectrum width and high wavelength selectivity of LDs.

In this paper, we report on a stable and efficient green light obtained by frequency doubling in the KTP intracavity of Nd:YVO₄. In our method, diffraction grating feedback optics is employed to stabilize the wavelength of LDs in the absorption spectrum of Nd:YVO₄.

Figure 1 is a schematic diagram showing intracavity SHG of Nd:YVO₄ pumped by an LD with a grating feedback optical system. A narrow-striped and single longitudinal mode LD was used in the experiment. A part of the collimated light beam was fed back to the active layer of the LD as the first order diffracted light from the grating, and the zeroth order diffracted beam conveniently served as the pumping beam. The pitch and the diffraction efficiency of the grating were 0.8 μm and 5 %, respectively. The proposed optical system is advantageous over previous grating feedback optics systems⁶ since a commercially available LD can be used, and a conventional reflection-type grating can be applied with no appreciable loss in light power. The reflected light was focused at a facet of Nd:YVO₄. The Nd:YVO₄ had an Nd³⁺ concentration of 3 at.%, as selected by the authors, to get the absorption coefficient of the crystal of 111 cm^{-1} , which is much higher than that for Nd:YAG.⁵ It should be noted

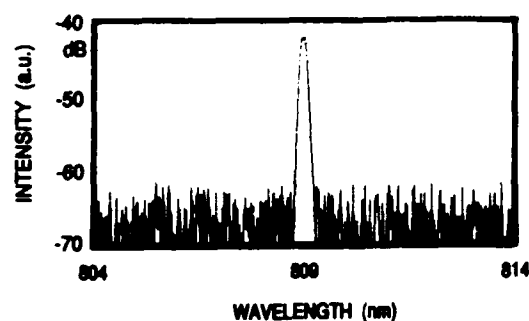
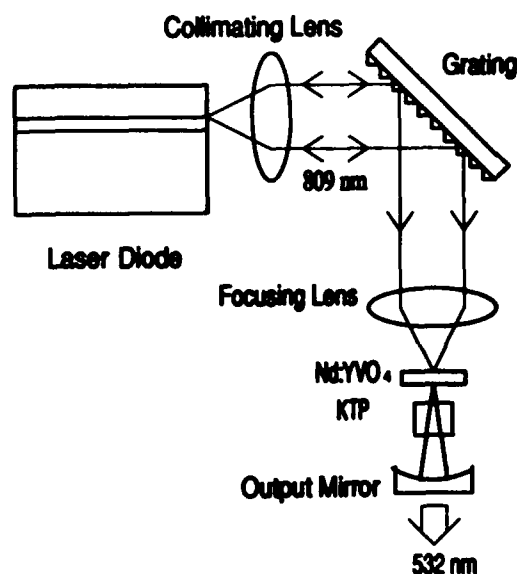


Figure 2. The longitudinal mode spectrum of LD with grating feedback system.

Figure 1. The schematic diagram of KTP intracavity SHG of Nd:YVO₄ pumped by LD with grating feedback system.

that stable and efficient single longitudinal mode oscillation might be possible by using 3 at.% Nd:YVO₄ with a shorter absorption length.^{4,5} The Nd:YVO₄ was coated on the LD side (A-plane) for high reflectivity at wavelengths of 1.064 μm and 0.532 μm and for anti-reflectivity at 0.809 μm , and was coated on the opposite side (B-plane) of the crystal for anti-reflectivity at 1.064 μm and 0.532 μm . The laser cavity consisted of the A-plane and an output mirror with a 50 mm radius of curvature, which was coated for high reflectivity at 1.064 μm . A 5-mm-thick KTP was inserted to the cavity; it is a birefringent crystal and was used for Type II phase matching in this experiment. Because Nd:YVO₄ oscillates with linear polarization, the KTP was temperature-controlled at 23 $^{\circ}\text{C}$ to maintain linear polarization of 1.064 μm oscillation.⁴

Figure 2 shows the longitudinal mode spectrum of LD with grating feedback optics. As shown in Fig.2, the grating firmly fixed the wavelength of LD at the center of the absorption spectrum (809 nm). When the temperature of the LD was changed within the range of 23 ± 10 $^{\circ}\text{C}$ (at casing), the longitudinal mode remained unchanged. Another advantage of using grating feedback optics is that the wavelength of the LD is kept stable against changes in the power of the LD, from the threshold level to 70 mW. After the grating was removed, however, the spectrum had the multimode condition and mode hopping resulted from light reflected from the facet of Nd:YVO₄. Furthermore the wavelength of the LD shifted at a rate of 0.2 nm/ $^{\circ}\text{C}$ when the temperature of the LD was changed. For an average wavelengths of 809 nm, the oscillated wavelengths of commercial LDs are known to differ within the approximate range of ± 15 nm. Therefore adjusting the wavelength of LD to the center of the absorption spectrum by grating feedback optics is an essential and practical way of achieving efficient pumping.

The experiment of the green light generation using an LD with a grating feedback system as the pumping source was performed for 0.3-mm thick and 0.5-mm thick 3% Nd:YVO₄. A continuous wave green light of 11 mW was generated from 50 mW of LD input power. For

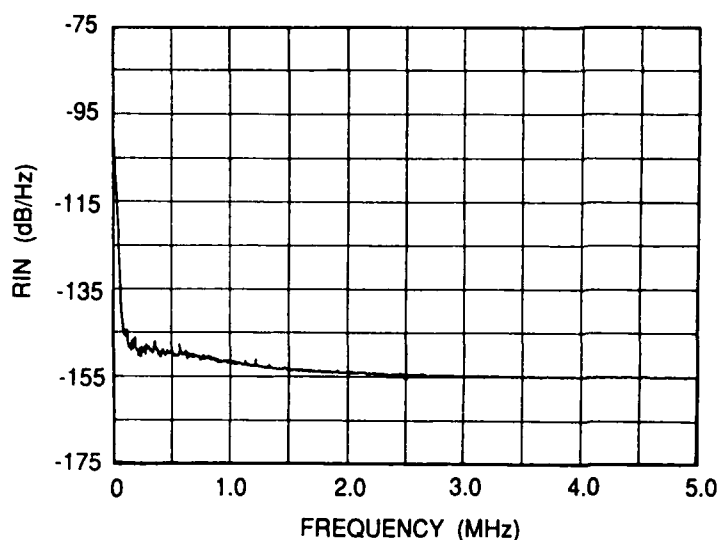


Figure 3. The RIN spectrum of green light as pumping by LD with grating feedback system.

the 0.5-mm-thick 3% Nd:YVO₄, a conversion efficiency of 22 % was achieved. The fluctuation of the green light was less than $\pm 3\%$. The fundamental wave was able to oscillate in a single mode, as measured by a scanning Fabry-Perot interferometer.

Figure 3 presents noise spectrums of green light output. Figure 3 shows the noise spectrum of 9.8 mW green light, pumped by 50 mW, for 0.3-mm-thick 3% Nd:YVO₄, when the LD has a grating feedback system. The power of the obtained light was large enough to measure the noise by use of an Si-PIN photo diode. The measurement was carried out at the resolution band width of 30 kHz. Figure 3 indicates that if single longitudinal mode oscillation of the pumping source is maintained, the noise level is held very low in the frequency region higher than 100 kHz, and so the relative intensity noise (RIN) less than -145 dB/Hz is obtainable to be sufficient for the optical disk specifications, which can be maintained in the temperature range of ± 10 °C. On the other hand, for the multi-mode condition, the noise level was increased and the RIN was less than -100 dB/Hz.

In conclusion, we have demonstrated stable and highly efficient intracavity SHG of Nd:YVO₄ pumped by an LD with grating feedback optics. By using Nd:YVO₄ with an Nd³⁺ concentration of 3%, green light of 11 mW (maximum), for an incident pumping power of 50 mW, was obtained as well as a high conversion efficiency of 22%. The noise level of this green light was very low corresponding to the RIN of less than -145 dB/Hz. One promising application of this green light source is the high-density optical disk.

References

- (1) M.A. Haase, J. Qiu, J.M. DePuydt, and H. Cheng, *Appl. Phys. Lett.* **59** 1272 (1991).
- (2) T. Baer and M.S. Keirstead, in *Digest of Conference on Lasers and Electro-Optics* (Optical Society on America, Washington DC, 1985), paper ThZZ1.
- (3) K. Tatsuno, T. Andou, S. Nakatsuka, T. Miyai, M. Takahashi, and S. Hermfrid, in *Digest of Conference on Lasers and Electro-Optics* (Optical Society On America, Washington DC, 1992), paper CWQ8.
- (4) T. Sasaki, T. Kojima, A. Yokotani, O. Oguri and S. Nakai, *Opt. Lett.* **16** 1665 (1991).
- (5) G.J. Kintz and T. Baer, *IEEE J. Quantum Electron.* **26** 1457 (1990).
- (6) H. Sato, K. Itoh, M. Fukai, and N. Suzuki, *IEEE J. Quantum Electron.* **QE-18** 328 (1982).

Characterization for the Single-Mode-Operation of Diode-Pumped Nd:YVO₄ Lasers for Intracavity Doubling

K. Tatsuno, S. Helmfrid, T. Andou, and T. Miyai*

CRL, Hitachi, Ltd., 1-280 Higashi-koigakubo, Kokubunji, Tokyo 185, JAPAN

Tel: 81-423-23-1111, Fax: 81-423-27-7705

* Hitachi Metals, 5200 Mikajiri, Kumagaya-shi, Saitama 360, JAPAN

Summary

Intracavity frequency doubling of diode-pumped Nd:YVO₄ lasers is expected to be a promising approach for an optical source of the future optical disk systems. In the previous paper, we have shown ultra high storage density erasable magneto-optical recordings of HDTV pictures played back by a stable compact green laser (CGL) consisting of Nd:YVO₄ and KTP[1, 2]. The conversion efficiency of the CGL was up to 10% (50mW-diode laser to 5mW green output) due to large emission cross section and absorption coefficient of the Nd:YVO₄ gain medium. In the CGL, single axial- and polarization-mode operation is important to avoid fluctuations in the green output power due to the nonlinear coupling between the modes[3,4]. To confirm a long term stability of the CGL, perturbations in cavity parameters for the single-mode operation must be considered.

In this paper, experimental measurements and analysis have been carried out to characterize the perturbations in cavity parameters. The parameters treated here are thickness of the gain medium, cavity length, energy migration and birefringence of the cavity components. The analysis[5] is based on the following extended equation of reference [6]. The ratio r , between multimode threshold and the single-mode threshold is

$$r = f^{-1} \left(\frac{1 - \exp(-d/l)}{2 - (d^2/l^2 + 2d/l + 2)\exp(-d/l)} \left(\frac{\lambda^2}{\pi n_{gm} l \Delta\lambda_0} \right)^2 \right), \quad f^{-1}(x) = \frac{1}{2} (1+x)(2+x), \quad (1)$$

where d is the thickness of the gain medium, l is the $1/e$ absorption depth, λ is the wavelength of the fundamental radiation, n_{gm} is the refractive index of the gain medium and $\Delta\lambda_0$ is the FWHM of the small-signal gain curve.

The multimode threshold depends on the thickness of the gain medium. If the thickness is chosen to be of the same order as the absorption depth, the multimode threshold can be

significantly increased at the expense of a reduced output power. This is due to the different distribution along the Nd:YVO₄ of the gain of the first mode and the excess gain close to the nodes of the first mode that other modes use to compensate for their lower small-signal gain.

The one longitudinal cavity mode is not always located with its frequency in the center of the gain curve. Figure 1 shows a simulated results of the cavity-length shift dependency to the ratio, r , for both cases as with and without the energy migration effect[7] into account. When the energy migration effect is assumed, the FWHM of the peak is increased and reduces the sensitivity, but in the mode-hop region that occurs for each half-wavelength shift in the optical path length, multimode oscillation will always occur.

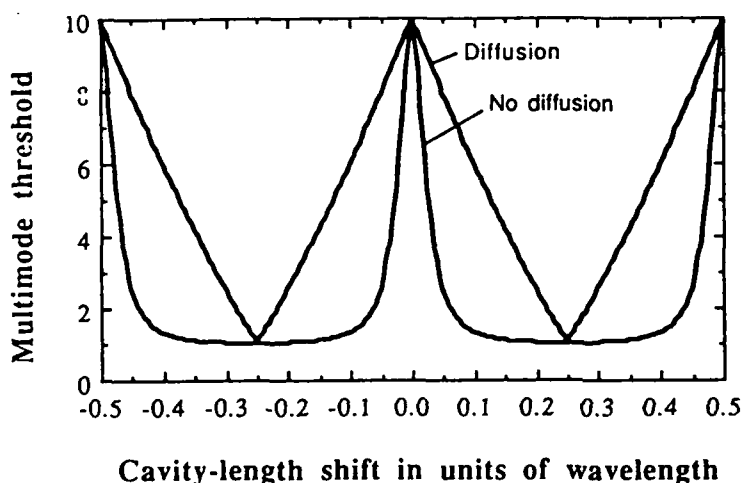


Fig. 1 Multimode threshold as function of shift in the cavity length, with and without energy migration (diffusion).

Fig. 2 (a) shows a measurement results of the single-axial mode operation. Figure 2 (b) is indicating that when the cavity temperature changes, the second mode starts to set in. It is shown that the device is very sensitive to such fluctuations. Control of the cavity length is, therefore, essential for good long-term stability.

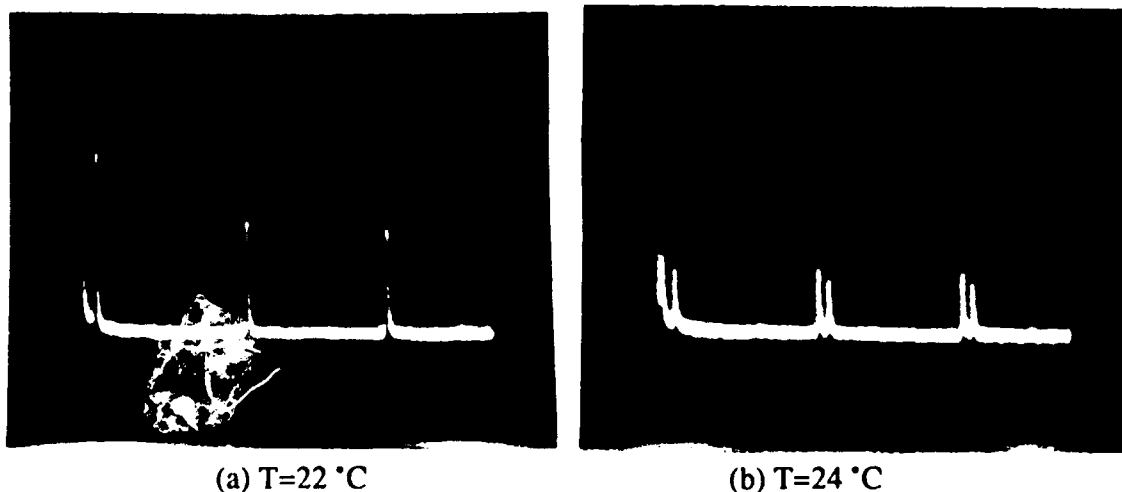


Fig. 2 Cavity-length shift dependence of diode-pumped Nd:YVO₄ laser axial-mode

Coupling between different polarization modes in the cavity also cause chaotic output at the second-harmonic generation[3]. Since Nd:YVO₄ is a birefringent material with a higher emission cross-section along the c-axis, it is advantageous to use a cavity with polarization modes parallel and orthogonal, respectively, to that axis. In type-II phase-matched second-harmonic generation, the KTP crystal axes should be in 45° to the axes of the Nd:YVO₄ crystal. If the KTP crystal acts as a half-wave plate, which can be achieved by temperature tuning, it does not influence the polarization of the cavity modes because the total effect after two passages is equivalent to a whole-wave plate. Therefore, the polarization modes are polarized along the axis of the Nd:YVO₄ crystal and the output is stable[2]. The influence of the birefringence of the Nd:YVO₄ crystal is also important. If this crystal acts as a half-wave plate, the polarization modes are degenerate. A slight shift in the birefringence of the KTP crystal will, close to the degenerate case, result in modes polarized along the axes of KTP. Therefore, two polarization modes in 45° angle to the axes of the Nd:YVO₄ crystal will oscillate. A more general analysis shows that the most stable configuration is when the Nd:YVO₄ is a quarter-wave plate. In experiments we have observed that there is a long-term drift in the output polarization of our devices. Control of the temperature of Nd:YVO₄ is important to avoid this problem.

In conclusion, we have shown that a thin gain medium, in combination with a short absorption depth, can be used to enhance the threshold for multimode operation of intracavity-doubled lasers at expense of a reduced output power. The total optical path length of the cavity and the birefringence of the Nd:YVO₄ crystal both have influence on the threshold for multimode operation. Control of these parameters is essential for good long-term stability.

References

- [1] K. Tatsuno, M. Takahashi, H. Sugiyama, T. Andou and T. Miyai : Techn. Digest, *Optical Memory '92* (Yokohama) p7 (in Japanese)
- [2] K. Tatsuno, T. Andou, S. Nakatuka, T. Miyai, M. Takahashi and S. Helmfrid : *CLEO'92*, Vol. 12, OSA Technical Digest (OSA), CWQ8, 374 (1988)
- [3] T. Baer : *J. Opt. Soc. Am.* B3, 1175 (1986)
- [4] M. Oka and S. Kubota : *Opt. Lett.* Vol.13, No.10(1988) p805
- [5] S. Helmfrid, K. Tatsuno, T. Andou and T. Miyai : Techn. Digest, *Japan Optics '92* (Kyoto)
- [6] G. J. Kintz and T. Baer, *IEEE J. Quantum Electron.* QE-26, 1457 (1990)
- [7] T. Sasaki, T. Kojima, A. Yokotani, O. Oguri and S. Nakai, *Opt. Lett.* 16, 1665 (1991)

Wednesday, February 3, 1993

Joint Poster Session

JWC 2:00pm–4:15pm
La Salle Ballroom A

Comparative spectroscopy of Ho^{3+} and Yb^{3+} in KYF_4 , BaY_2F_8 , and YLiF_4

R. E. Peale¹, X. X. Zhang², M. Bass^{1,2,3}, and B. H. T. Chai^{2,4}

¹Department of Physics, ²Center for Electro-Optics and Lasers, ³Department of Electrical Engineering, ⁴Department of Mechanical Engineering, University of Central Florida,
Orlando, FL 32816
Tel. (407) 823-5206

A recent comparison of Yb, Ho upconversion energy transfer in different fluoride crystals has been performed[1]. The purpose was to demonstrate the promise of Yb,Ho:KYF₄ as a green upconversion laser as compared with similarly doped BaY₂F₈ (BYF) and YLiF₄ (YLF). We compare here high resolution, low temperature absorption spectra for the three crystals and our determination of the energy levels.

We have measured polarized, temperature dependent, transmission spectra of Ho³⁺, and Yb³⁺ in the three hosts KYF₄ (KYF), BYF, and YLF from 500 to 22,000 cm⁻¹ at a resolution of 1 cm⁻¹ using a Bomem DA8 Fourier spectrometer. The advantage of the Fourier technique to characterization of upconversion laser materials is its high frequency accuracy, being 0.004 cm⁻¹ at 2000 cm⁻¹ for the Bomem. With the energy levels extracted from these data, a meaningful comparison of upconversion energy transfer in the three hosts is possible. For this purpose, results from grating spectroscopy are unreliable, since systematic errors due to faulty calibration are often greater than the measured line widths.

Figure 1 presents the green region of the polarized spectrum Ho³⁺ in the three fluoride crystals at sample temperatures of 80 K. These are the $^5\text{I}_8 \rightarrow ^5\text{F}_4$, $^5\text{S}_2$ transitions; $^5\text{S}_2$ is the state from which green laser emission potentially will occur in the upconversion process. For YLF (π polarized) and BYF(E || z), energy levels are determined directly from the pattern of thermal replicas without recourse to theory. The π -polarized KYF spectrum reveals a complicated set of overlapping peaks and shoulders which occupy a wider spread of frequencies than for either YLF or BYF. Many of the lines are better resolved in sigma polarization, revealing the simultaneous presence of widely spaced broad peaks and sharp (FWHM < 1 cm⁻¹) closely spaced lines. Due to the complexity of the spectrum and indications that the dopant ions sit at more than one site in the crystal[2], determination of energy levels will require measurements at liquid helium temperatures.

Figure 2 presents the Ho³⁺ $^5\text{I}_8 \rightarrow ^5\text{I}_6$ transitions for the three fluoride crystals (same polarizations as Fig 1). Energy from excited Yb³⁺ ions transfers to the $^5\text{I}_6$ levels in the first stage of the upconversion process. Once again the YLF and BYF spectra are similar and easily analyzed. The KYF data again presents a problem with widely-spaced broad lines and a closely-spaced set of three extremely sharp lines at the center of the spectrum.

Finally, we present the $^2F_{7/2} \rightarrow ^2F_{5/2}$ transitions of Yb^{3+} in each of the three crystals. These are the infrared transitions which are pumped to initiate the upconversion process. All three spectra are similar.

We will present liquid helium temperature data for the three hosts, our determination of the levels of Ho^{3+} and co-dopant Yb^{3+} , and a discussion of the relevance of these data to upconversion energy transfer.

References:

1. X. X. Zhang, M. Bass, B. H. T. Chai, and R. E. Peale, proceedings of this conference.
2. J. Sytsma, S. J. Kroes, G. Blasse, and N. M. Khaidukov, J. Phys: Condens. Matter **3**, 8959 (1991).

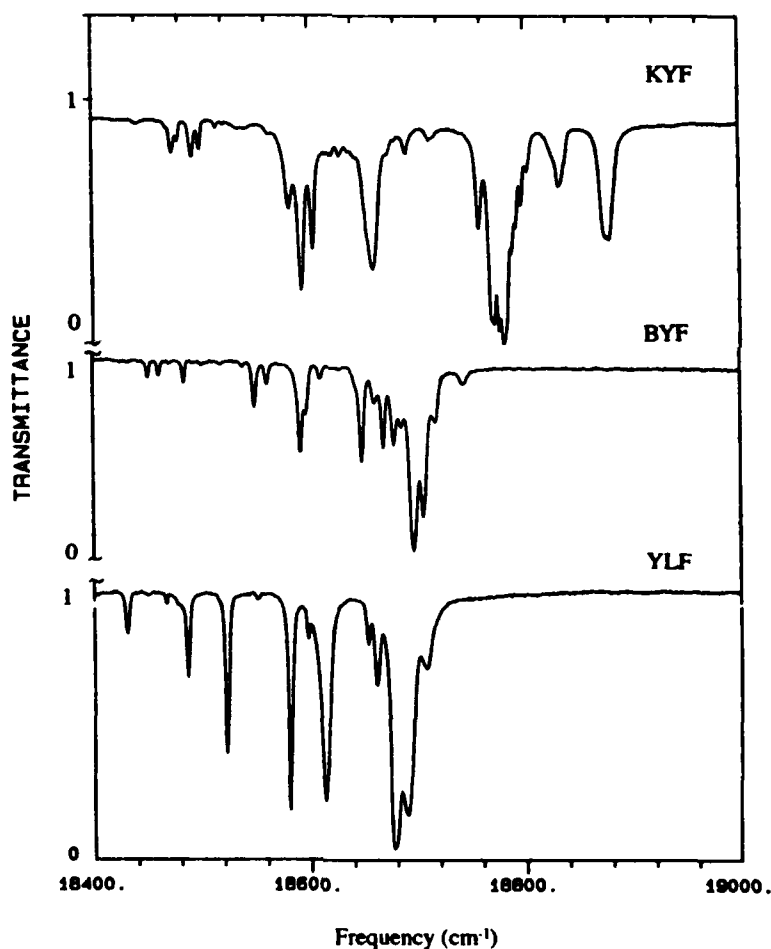


Figure 1. $^5I_8 \rightarrow ^5F_4, ^5S_2$ transitions of Ho^{3+} . The sample temperatures are 80 K and the resolution 1 cm^{-1} .

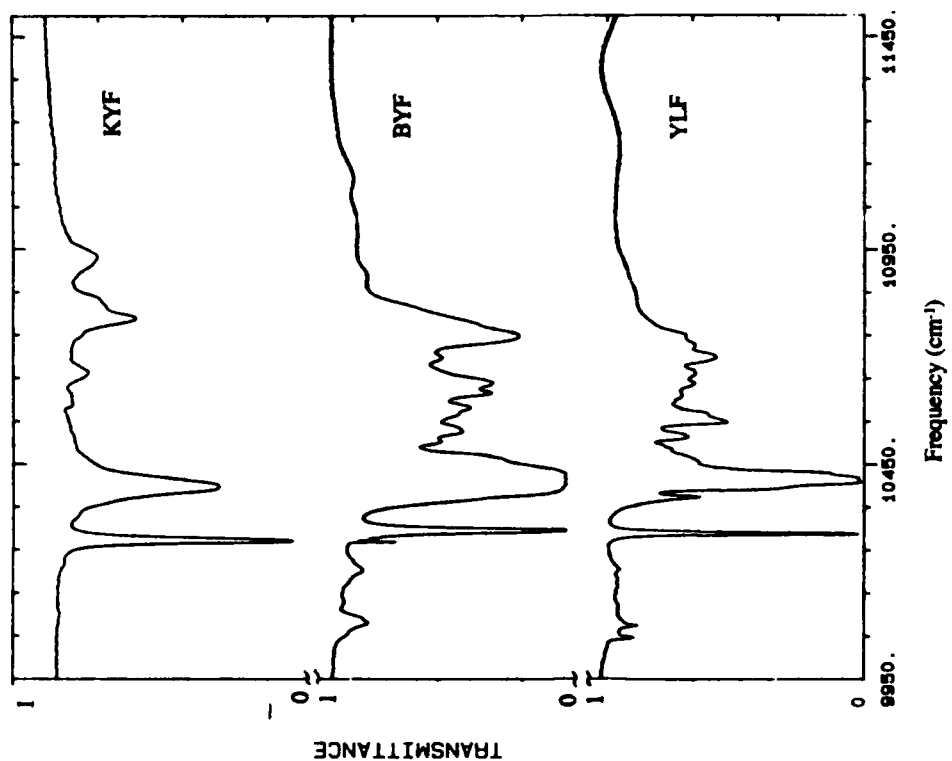


Figure 3. $^2F_{7/2} \rightarrow ^2F_{5/2}$ transitions of Yb^{3+} . The sample temperatures are 80 K and the resolution 1 cm^{-1} .

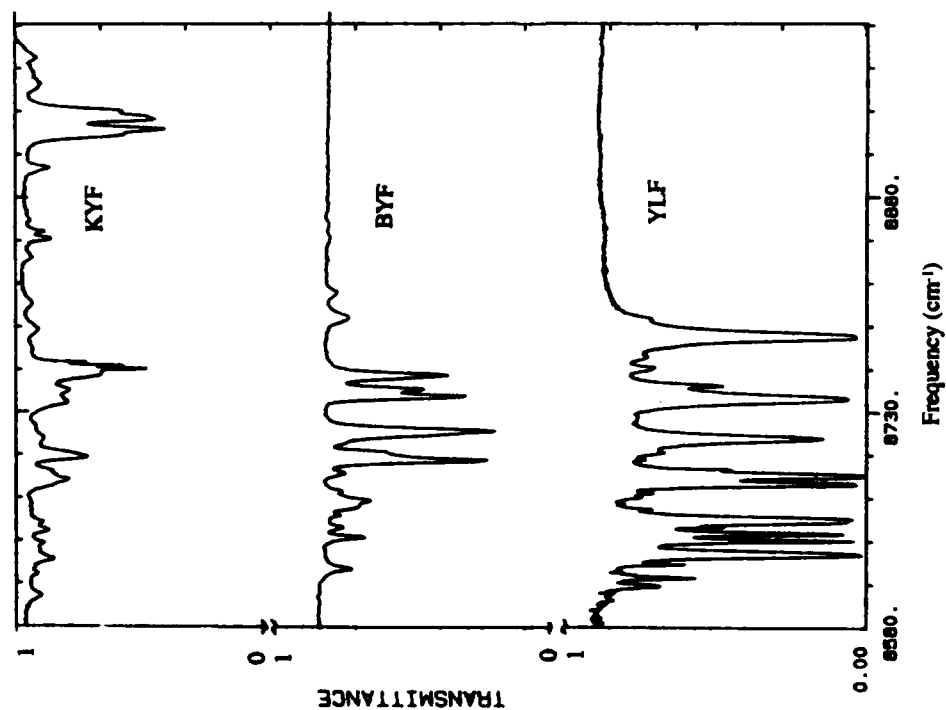


Figure 2. $^5I_8 \rightarrow ^5I_6$ transitions of Ho^{3+} . The sample temperatures are 80 K and the resolution 1 cm^{-1} .

**Pairwise Visible to UV Up-Conversion in
 Ho^{3+} and Tm^{3+} Doped CsMgCl_3**

Ali Gharavi, Gary L. McPherson

Tulane University, New Orleans, Louisiana

Up-Conversion is observed at 11 K when $^1\text{G}_4(\text{D})$ state of Tm^{3+} and $^5\text{F}_5(\text{D})$, $^5\text{F}_4(\text{E})$, $^5\text{F}_3(\text{F})$, $^5\text{F}_2(\text{G})$ and $^3\text{K}_8(\text{H})$ states of Ho^{3+} are pumped. These states absorb between 655 and 450 nm. The dynamics and pathways are studied which reveal a pairwise energy transfer between distinct pairs of Ho^{3+} or Tm^{3+} in crystals.

Ho Concentration Dependence of Yb, Ho Upconversion Energy Transfer in KYF₄

X.X. Zhang, M. Bass, and B.H.T. Chai
Center for Research in Electro-optics and Lasers
University of Central Florida
12424 Research Parkway, Orlando, FL 32826
Tel. (407) 658-6800

We have found that the Yb \rightarrow Ho upconversion process in KYF₄ (KYF) is much more efficient than in either BaY₂F₈ or YLiF₄ [1] under the same doping conditions. Long lifetime, low phonon energy, weak self-absorption, and some other unique spectroscopic features make KYF a promising host for an Yb, Ho upconversion green laser. In order to optimize the upconversion efficiency, we have carried out a detailed study on the Ho concentration dependence of the Yb \rightarrow Ho transfer processes in KYF.

Large, high optical quality, single crystals of KYF were grown by a modified Czochralski pulling technique in our crystal growth facilities. In all the samples studied in this report the concentration of Yb was fixed at 20%. The Ho concentration ranged from almost zero to 0.8 % (~0.005%, 0.05%, 0.1%, 0.2%, 0.4%, and 0.8%). We worked with 20% Yb because, for a fixed Ho concentration, samples with 20% Yb showed stronger upconversion than those with either 10% or 40%.

The typical room temperature π -polarization visible to near infrared emission spectrum of Yb, Ho: KYF, with IR excitation at about 970 nm, is shown in Fig. 1. The σ -polarization emission, spectrum not shown in the figure, is at least three times weaker than that of π -polarization. As a result we concentrate on the π -polarization as it is a better candidate to lase. The integrated intensity of the green emission as a function of the Ho concentration is plotted in Fig. 2. It can be seen that the integrated intensity of the green emission increases dramatically with Ho concentration up to about 0.2%, it then remains nearly constant. We will explain why above 0.4% the green intensity may be expected to decrease with increasing Ho concentration.

The decay time of the singly doped 20% Yb:KYF at room temperature is 4.75 ms. It decreases monotonically with Ho concentration due to the Yb \rightarrow Ho energy transfer. The decay time of Yb is only 245 μ s when codoped with 0.8% Ho in KYF. The transfer rate W_{tr} can be calculated with the following equation:

$$W_{tr} = \frac{1}{\tau} - \frac{1}{\tau_0}$$

where τ is the measured decay time of Yb in the presence of Ho and depends on the Ho concentration, and τ_0 is the decay time of Yb alone. The resulting energy transfer rate as a function of Ho concentration is given in Fig. 3. It can be seen that the transfer rate increases linearly with Ho concentration.

The energy transfer efficiency η can also be calculated with the following equation:

$$\eta = 1 - \frac{\tau}{\tau_0}$$

and is plotted as a function of Ho concentration in Fig. 2. One can see from Fig. 2 that the intensity of the green emission and the transfer efficiency have a direct correlation.

More detailed results will be presented and the energy transfer model will be discussed.

References:

1. X. X. Zhang, M. Bass, B.H.T. Chai, and R. Peale, "Comparison of Yb, Ho upconversion energy transfer in different fluoride crystals," submitted to Advanced Solid-State Lasers Topical Meeting, Feb. 1993

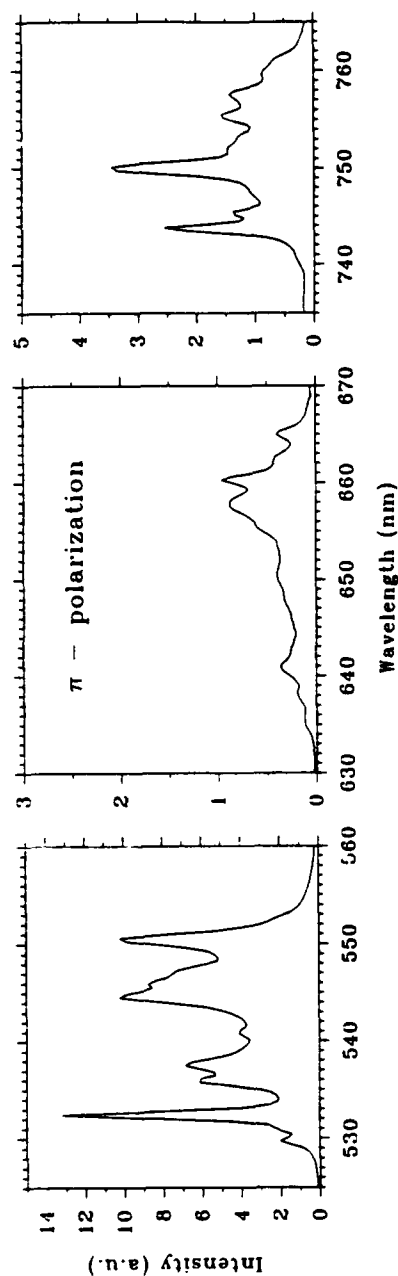


Fig.1. Room temperature emission spectrum of 20%Yb,0.1%Ho:KYF under 970 nm excitation

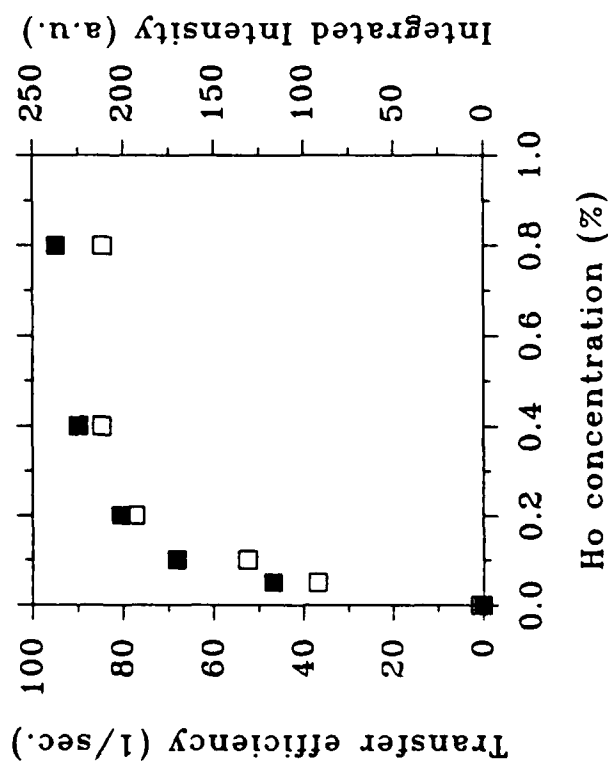


Fig.2. Green integrated intensity (□) and transfer efficiency (■) as a function of Ho concentration

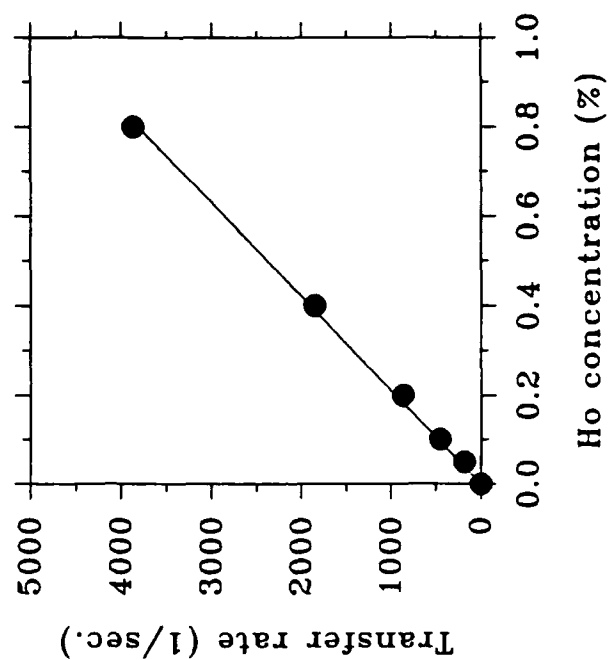


Fig. 3. Energy transfer rate as a function of Ho concentration

Blue, green and red, Tm^{3+} , Ho^{3+} doped upconversion laser glasses, sensitized by Yb^{3+} and Er^{3+}

T. Izumitani, B. Peng and Y. Lin

Izumitani Special Lab., HOYA Corporation
3-3-1, Musashino, Akishima, Tokyo 196 JAPAN

1. Introduction

In order to get blue, green and red laser beam, we applied upconversion process¹⁾. We used Tm^{3+} , Ho^{3+} ions which give three energy level lasers. As the difference between emission and absorption peak wavelength is small, the sensitizers were applied to get higher emission intensity. The base glass was fluoro-zirco, aluminate glass(AZF)²⁾, because the phonon energy is small and the chemical durability is excellent.

2. Experimental method

Melting: We added the active ions Tm^{3+} or Ho^{3+} and the sensitizer ions Yb^{3+} or Er^{3+} to the base glass AlF_3 25.1, ZrF_4 12.8, YF_3 11.1, CaF_2 15.4, MgF_2 3.7, SrF_2 13.6, BaF_2 12.6, NaF 5.6 cat%. The glasses were melted at 950°C in graphite carbon crucible for one hour.

Measurement: Absorption was measured by HITACHI330 spectro photometer. Emission was measured with Ge-detector or R-2228 photomultiplier pumping with 0.98 μ or 0.8 μ LD. Lifetime was measured with R-2228, pumping by Nd:YAG pumped dye laser. Cross section for stimulated emission was calculated by Judd-Ofelt theory.

3. Result and discussions

3.1 Yb-Tm blue light emission(0.47 μ)

0.47 μ blue light was obtained from Tm^{3+} ions sensitized with Yb^{3+} ions. The emission mechanism considered as follows: As shown in Fig.1, the blue light is obtained by three step upconversions³⁾. By pumping with 0.98 μ LD, Yb^{3+} ions are excited from $^2F_{7/2}$ to $^2F_{5/2}$ and energy transfers from $^2F_{5/2}(\text{Yb}^{3+})$ to $^3H_5(\text{Tm}^{3+})$. After thermally relaxed from 3H_5 to 3H_4 , the upconversion occurs from 3H_4 to $^3F_{2,3}$. After thermally relaxed from $^3F_{2,3}$ to 3F_4 , the upconversion again occurs from 3F_4 to 1G_4 . 0.47 μ emission is produced by radiative transition from 1G_4 to ground state, 3H_6 .

Fig.2 shows the max. emission intensity is obtained at 0.06% Tm^{3+} and 19 cat% Yb^{3+} . The glass shown $\sigma = 1 \times 10^{-21} \text{cm}^2$, $\tau = 0.76 \text{ms}$ from Judd-Ofelt treatment and the lifetime measurement.

3.2 Yb-Ho green light emission(0.54 μ)

Energy transfer occurs between $\text{Yb}^{3+} (^2F_{5/2} - ^2F_{7/2})$ and $\text{Ho}^{3+} (^5I_6 - ^5I_7)$. As shown in Fig.4, Yb^{3+} is pumped with 0.97 μ LD and energy is transferred from $\text{Yb}^{3+} : ^2F_{5/2}$ to $\text{Ho}^{3+} : ^5I_6$. The upconversion occurs from 5I_6 to 5S_2 . 0.55 μ emission is produced by radiative transition from 5S_2 to 5I_7 . Fig.5 and 6 show the 0.1 Ho^{3+} and 12cat% Yb^{3+} gives the max. emission intensity. Because the high content Yb^{3+} and low content Ho^{3+} give the highest energy transfer from Yb^{3+} to Ho^{3+} and suppress the back transfer. Lower content of Ho^{3+} give the longer lifetime. The glass give $\sigma = 1.47 \times 10^{-20} \text{cm}^2$ and $\tau = 1.08 \text{ms}$.

3.3 Er-Tm and light emission (0.67μ)

Energy transfer occurs between $\text{Er}^{3+} : {}^4\text{F}_{9/2}$ and $\text{Tm}^{3+} : {}^3\text{F}_2$. As shown in Fig.7, 0.8μ or 0.98μ LD excites Er^{3+} ions to ${}^4\text{I}_{9/2}$ or ${}^4\text{I}_{11/2}$ relaxing to ${}^4\text{I}_{13/2}$. Upconversion occurs from ${}^4\text{I}_{13/2}$ to ${}^4\text{F}_{9/2}$ and then energy is transferred ${}^4\text{F}_{9/2}$ (Er^{3+}) to ${}^3\text{F}_2$ (Tm^{3+}). 0.67μ emission is produced by radiative transition from ${}^3\text{F}_2$ to ${}^3\text{H}_6$.

From Fig.8 and 9, Er^{3+} 15 cat% and Tm^{3+} 0.5 cat% gives the max. emission intensity. The glass shown $\sigma = 2.11 \times 10^{-21} \text{cm}^2$ and $\tau = 0.12 \text{ms}$.

Reference

1. S.Tanabe, K.Hirao and H.Toratani: Solid State Phys. 27(1992)186.
2. T.Izumitani, T.Yamashita and M.Tokida: Halide glasses for infrared fiber optics(1987)187.
3. D.C.Hanna et al: Optics communications 78(1990)187.
4. X.Zow and T.Izumitani: Non-cryst. solid(to be published)

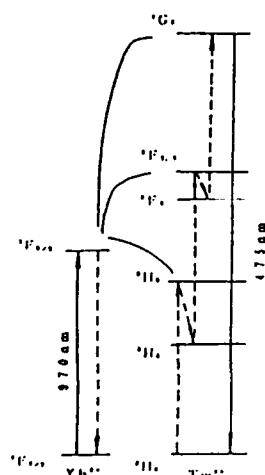


Fig1: The energy transfer of Yb, Tm system in fluoride glasses

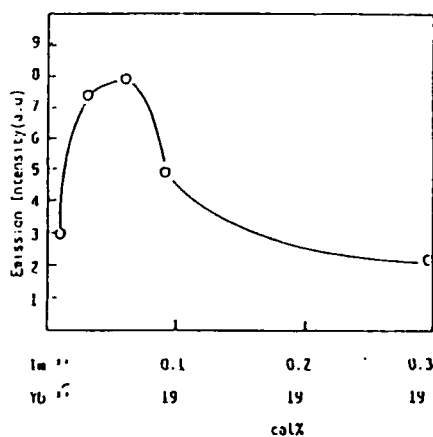


Fig2: The emission intensity of $\text{Tm}^{3+} ({}^6\text{G}_{7/2} \rightarrow {}^6\text{H}_{5/2})$ in Yb^{3+} , Tm^{3+} codoped fluoride glasses

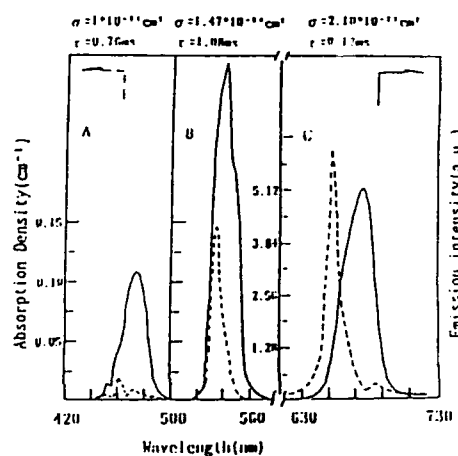


Fig3: The emission and absorption spectrum of Yb, Er sensitized Tm, Ho doped fluoride glasses.

A: Yb19cat% Tm0.01cat%
B: Yb12cat% Ho0.1cat%
C: Er15cat% Tm0.5cat%

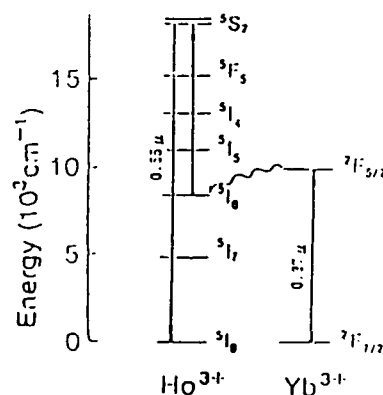


Fig4: The energy transfer of Yb, Ho system in fluoride glasses

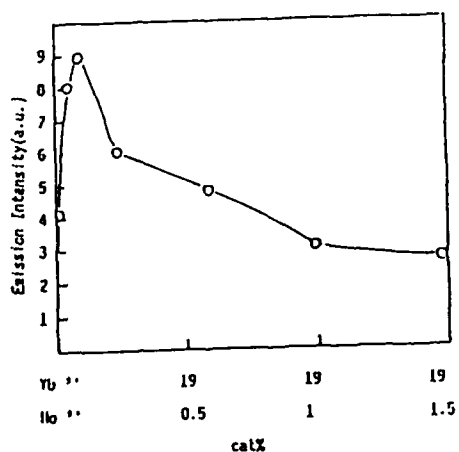


Fig5: The emission intensity of Ho($^5F_7 \rightarrow ^5I_8$)
in Yb³⁺, Ho³⁺ codoped fluoride glasses

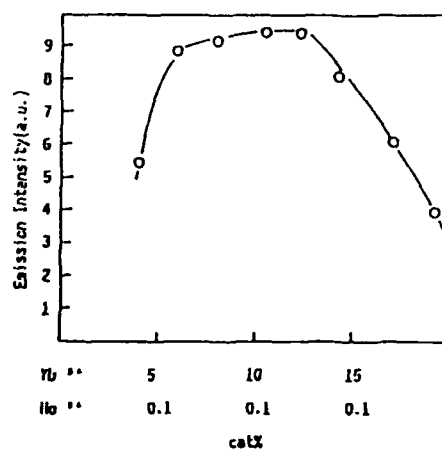


Fig6: The emission intensity of Ho($^5F_7 \rightarrow ^5I_8$)
in Yb³⁺, Ho³⁺ codoped fluoride glasses

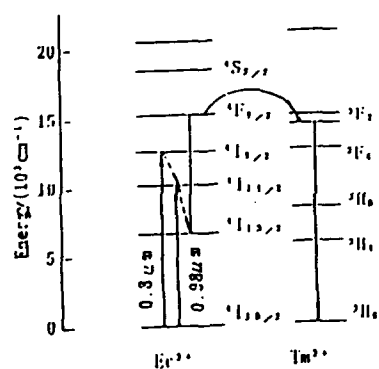


Fig7: The energy transfer of Er³⁺, Tm³⁺ system.

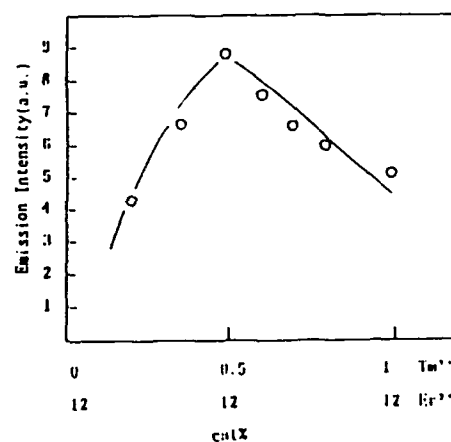


Fig8: The emission intensity of Tm³⁺($^3F_4 \rightarrow ^3F_6$) in
Tm³⁺, Er³⁺ codoped fluoride glass

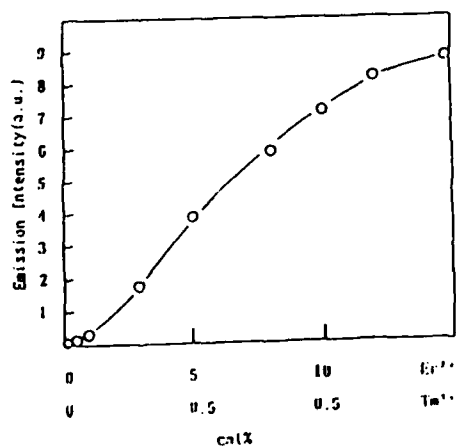


Fig9: The emission intensity of Tm³⁺($^3F_4 \rightarrow ^3F_6$) in
Tm³⁺, Er³⁺ codoped fluoride glass

Non-uniformity of the Phase Matching Angle in Flux Grown KTP Crystal

Takatomo SASAKI, Akio MIYAMOTO, and Sadao NAKAI

Faculty of Engineering and Institute of Laser Engineering, Osaka University,

2-6 Yamada-Oka, Suita, Osaka 565, JAPAN

TEL +81-6-877-5111 (ext.4562)

Atsushi YOKOTANI

KIMURA Metamelt Project, ERATO, Research Development Corporation of Japan.

5-9-9 Tohkohdai, Tsukuba 300-26 JAPAN

Tel +81-298-47-5191

We grew KTP crystals of which size is over 8.5 cm in the *c*-axis from flux, and measured distribution of refractive indices which affects on the phase matching angle in the grown crystal. As a result, we have found that the phase matching angle in the crystal changed considerably corresponding to the change in the refractive indices. As the refractive indices of KTP crystal grown by flux change due to the growth condition, it seems to be difficult to determine the phase matching angle precisely.

KTP crystals were grown using the $K_6P_4O_{13}$ (K6) as a flux.^{1,2)} A platinum crucible, 150 mm in diameter and 150 mm in height was located at the center of an electric furnace. An electronic load cell with a sensitivity of 0.1g was used in order to monitor the weight of the crystal during growth. Amount of starting solution was approximately 2 l in volume. The saturation temperature of the starting solution was approximately 950°C. The top seeded solution growth (TSSG) was carried out using a seed of several cubic millimeters. The seed was rotated at 60 rpm and direction of the rotation was inverted every 30 sec. The temperature falling rate was regulated from 0 to 3°C/day so that the bulk growth rate estimated from the signal of the load cell did not exceed 1 mm/day. After a total growth period of 40 days, a KTP crystal with a dimension of 32x42x87 mm³ was successfully obtained without liquid inclusion.

Optical homogeneity in KTP crystals was evaluated by means of interferometry with a He-Ne laser ($\lambda=0.6328\mu\text{m}$). Figure 1 shows a photograph of a large aperture KTP sample plate finished for TypeII second harmonic generation (SHG) of Nd:YAG laser, which was cut from the grown crystal. The orientation was $\theta=90^\circ$, $\phi=24^\circ$ and the thickness was 7 mm. A zygo interferometer Mark-IVxp was used. Figure 2(a) shows an interferogram of wavefront distortion in transmission of the sample taken with circular polarized wave and Fig 2(b) shows a schematic drawing of growth sector structure in the sample. Interference fringes are parallel



Fig.1 KTP Sample plate.
Size: 53x42x7t (mm³)

to the sample edges and they are sharply kinked at the growth sector boundaries. This means that the refractive index of each sector of the crystal gradually changed along the growth direction.

We also observed interferograms of this sample using linearly polarized wave in order to estimate the change of refractive indices more precisely. By using a horizontally polarized wave, we can observe the relative distribution in the index for the Z-polarized wave (n_z). In the case of the vertically polarized wave, we can observe the change in index of the wave whose polarization direction lies in X-Y dielectric plane (n_{xy}). The results are shown in Fig. 3(a) and(b). From these figures, it was found that the change of n_z was much larger than that of n_{xy} . By using a computerized analysis, the former was estimated to be 1.6×10^{-4} and latter, 7.1×10^{-6} . The value of n_z decreased from the seed to the edge of the crystal. This tendency of change in the indices was almost the same in other KTP crystals grown from other runs where the growth conditions are almost the same.

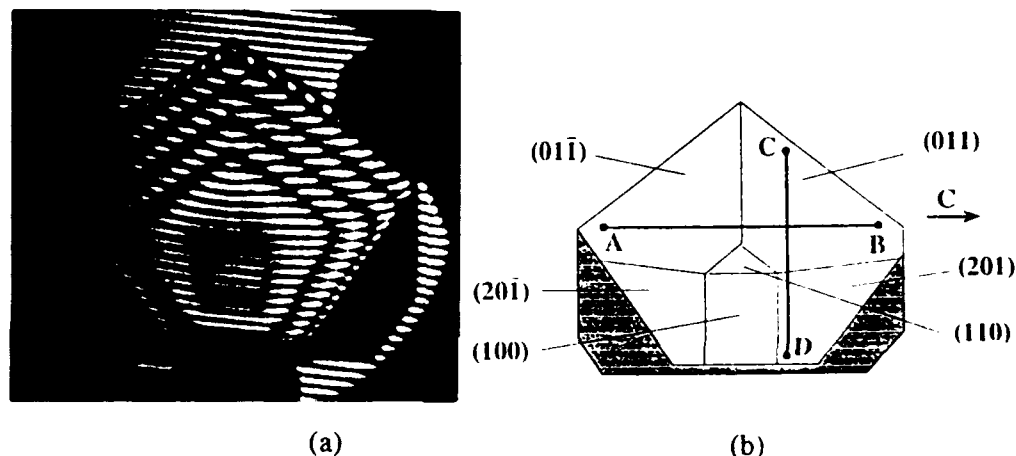


Fig.2 (a) Interferogram of the KTP plate taken with circular polarized wave.
(b) Sector structure of the sample.

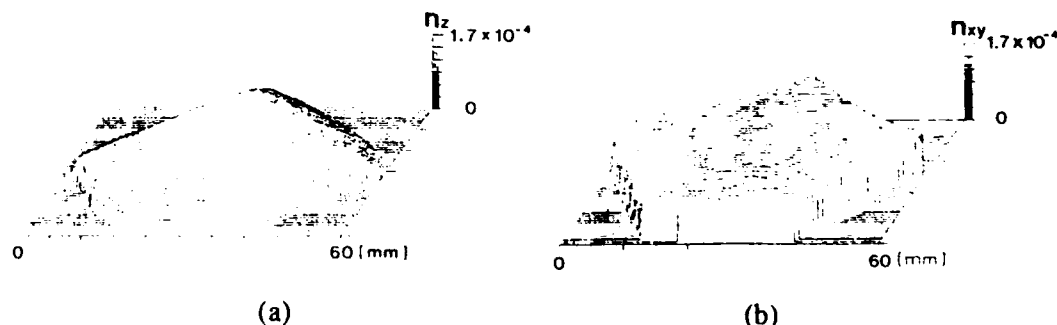


Fig.3 Wavefront distortion in transmission of the KTP plate taken with the linearly polarized waves. (a) Z-polarized wave. (b) XY-polarized wave.

We investigated an influence of variation of the refractive indices on the phase matching angles using a Q-switched Nd:YAG laser. The beam size was reduced to 1mm^{ϕ} in order to increase spatial resolution. The crystal sample was attached to a

ϕ - θ goniometer on a y-z stage and the second harmonic(SH) wave was generated. For a constant value of θ ($\theta=90^\circ$), changing the ϕ -angle, a direction where the SH wave was generated at maximum intensity was determined with an accuracy of ± 3 arcminutes. The measuring position was moved along the lines A-B and C-D indicated in Fig.2(b) in order to measure the local variation of the phase matching direction. The results are shown in Fig.4. Moving from the point A to the point B, the phase matching angle ϕ became smaller and took the minimum value at the central portion of the plate and became larger again. As a result, the ϕ values at the points A and B became almost the same. The difference between the maximum and the minimum values was approximately 0.36 degrees. Similar measurements were carried out along the line C-D indicated in Fig.2(b). In this case, ϕ only decreased as moving from the points C to D. The difference between the maximum and the minimum values was 0.38 degrees. These angle differences agreed well with the values estimated from the calculation of the phase matching angle using the change of indices measured above. Since the acceptance angle in full width at half maximum (FWHM) of the SHG of KTP is approximately 1°cm , these variations in the phase matching angle will give rise to a reduction of the conversion efficiency of the SHG.

In summary, we have grown large KTP crystals and measured the non-uniformity of the phase matching angle in the crystal. The phase matching angle in one crystal varies up to 0.38 degrees corresponding to the change of n_z . Relationship between this variation of refractive indices and crystallographic defects, lattice parameters, growth conditions *etc.* and the reason of the nonuniformity of refractive indices will be presented.

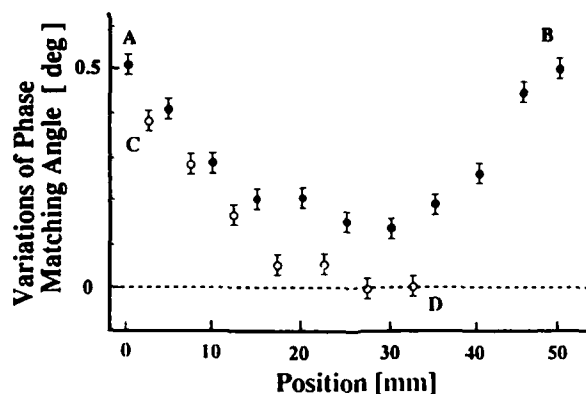


Fig.4 Change of the phase matching angle in the KTP plate. Alphabets (A,B,C and D) in this figure correspond to the positions indicated in fig.2(b). The ordinate shows variations of the phase matching angle for each measuring points, which were normalized by a value at the point D.

References

- 1) A.Yokotani, A.Miyamoto, T.Sasaki and S.Nakai: *J. Cryst. Growth* 110, 963 (1991).
- 2) T.Sasaki, A.Miyamoto, A.Yokotani and S.Nakai: *J. Cryst. Growth*, (Special issue for ICCG-10, in press.)

RADIATIVE TRANSITION PROBABILITIES OF TRIVALENT RARE-EARTH IONS IN LiYF_4 .

C. Li, Y. Guyot, C. Linarès, R. Moncorgé and M. F. Joubert

Laboratoire de Physico-Chimie des Matériaux Luminescents,
Université Claude Bernard Lyon 1
Unité de Recherche Associée CNRS n°442
Bât. 205, 43 boulevard du 11 novembre 1918,
69622 Villeurbanne CEDEX, FRANCE.
phone number: 72-44-83-39.

Lithium yttrium fluoride (LiYF_4) doped with different rare-earth ions has been the subject of several studies. Its IR laser applications are well known [1] and, as an upconversion laser, it is now the object of extensive investigations [2]. In particular, the exact knowledge of the values of the radiative probabilities of the intraconfigurational 4f transitions of the rare-earth ions in this crystal is always a matter of discussion [3, 4] and this is the reason why we try to clarify this point in this paper in the case of Nd^{3+} , Er^{3+} , Tm^{3+} and Ho^{3+} doped LiYF_4 .

The radiative transition probabilities may be evaluated using the Judd-Ofelt theory [5, 6] which is a phenomenological approach. This treatment assumes equal population and negligible J mixing of all the crystal field levels so that it is based on measured absorption line strengths at high enough temperature. For an electric dipole transition, the matrix elements $U^{(t)}$ for a given trivalent rare-earth ion, which are necessary for the calculations, vary only slightly from host to host and may be considered unchanged, so we used the values given in the literature [8-11]. The host dependent part of the line strengths is contained in the so-called Judd-Ofelt intensity parameters Ω_t ($t = 2, 4$ and 6).

The absorption spectra were recorded very accurately at room temperature in the σ and π polarizations. The refractive index of LiYF_4 is 1.47 and the rare-earth ion concentrations of the crystals used for this study are $\text{LiYF}_4:1.5\text{at\%Nd}^{3+}$, $\text{LiYF}_4:1\text{at\%Er}^{3+}$, $\text{LiYF}_4:1\text{at\%Ho}^{3+}$ and $\text{LiYF}_4:1\text{at\%Tm}^{3+}$. The Judd-Ofelt intensity parameters resulting from this investigation in the case of Nd^{3+} , Er^{3+} and Ho^{3+} are given in the table 1.

	Ω_2 (10^{-20}cm^2)	Ω_4 (10^{-20}cm^2)	Ω_6 (10^{-20}cm^2)	δ (10^{-20}cm^2)
LiYF ₄ : Nd ³⁺	1.22	2.10	4.65	0.18
LiYF ₄ : Er ³⁺	1.70	1.06	1.24	0.195
LiYF ₄ : Ho ³⁺	0.96	2.05	1.43	0.177

Table 1: Calculated Judd-Ofelt intensity parameters Ω and RMS δ .

Using these Ω_i parameters, we derived the calculated radiative transition probabilities W_{calc} and these values were compared with the experimental relaxation probabilities W_{exp} (inverse of fluorescence lifetime). As an example, we show the results obtained in the case of LiYF₄:0.013at%Er³⁺ and LiYF₄:0.1at%Nd³⁺ in table 2.

For the $^4S_{3/2}$ and $^2P_{3/2}$ manifolds of Er³⁺, which have relatively large energy gaps to the next lower levels (2961 cm⁻¹ and 3200 cm⁻¹ respectively), it appears clearly that the experimental relaxation rates are essentially radiative. The same conclusion may be given for the Nd³⁺ $^4F_{3/2}$ manifold (gap: 5109 cm⁻¹). In the case of the $^2F(2)_{5/2}$ manifold of Nd³⁺ which also has a large energy gap to the next lower level (3932 cm⁻¹), the experimental relaxation probability is much greater than the calculated radiative probability. This may be due to the possibility of a cross relaxation process between two neighboring Nd³⁺ ions or, more probably, to the uncertainty of the Judd-Ofelt calculation for such a high energy level.

LiYF ₄ :0.1at%Nd ³⁺			LiYF ₄ :0.013at%Er ³⁺		
	$W_{\text{calc}}(\text{s}^{-1})$	$W_{\text{exp}}(\text{s}^{-1})$		$W_{\text{calc}}(\text{s}^{-1})$	$W_{\text{exp}}(\text{s}^{-1})$
$^4F_{3/2}$	1672	1742	$^4I_{9/2}$	93	$14.92 \cdot 10^4$
$^4G_{7/2}$	3436	$\geq 10^8$	$^4F_{9/2}$	971	$12.35 \cdot 10^3$
$^2P_{1/2}$	1709	$\geq 10^8$	$^4S_{3/2}$	1748	1637
$^2P_{3/2}$	1733	$20 \cdot 10^3$	$^4F_{5/2}$	2488	$11.76 \cdot 10^6$
$^4D_{3/2}$	$16.13 \cdot 10^3$	$76.92 \cdot 10^4$	$^2H_{9/2}$	2336	$76.92 \cdot 10^3$
$^2F(2)_{5/2}$	$29.41 \cdot 10^3$	$68.49 \cdot 10^3$	$^4G_{11/2}$	8475	$13.89 \cdot 10^6$
			$^2P_{3/2}$	3937	4367

Table 2: Calculated radiative probabilities W_{calc} and experimental relaxation probabilities W_{exp} in the cases of LiYF₄:0.013at%Er³⁺ and LiYF₄:0.1at%Nd³⁺. The experimental lifetimes, measured at T=6K, are evaluated with an error of $\pm 6\%$.

More detailed data about these calculated radiative transition probabilities and measured relaxation rates, including the cases of $\text{LiYF}_4:\text{Tm}^{3+}$ and $\text{LiYF}_4:\text{Ho}^{3+}$, will be given at the conference, and a subsequent paper will be devoted to their interpretation [12].

References.

- [1] A. A. Kaminskii, in " Laser Crystals ", Springer Series in Optical Sciences, Vol. 14, edited by D. L. MacAdam, New York 1981.
- [2] W. Lenth et al., Advances in laser science III eds. A. C. Tam, J. L. Gole and W. C. Stwalley, AIP Conference Proceedings No 172, 8 (1988); F. Tong W. P. Risk, R. M. Macfarlane and W. Lenth, Electr. Lett. 25 (20), 1389 (1989); R. A. McFarlane, Appl. Phys. Lett. 54, 2301 (1989); F. Tong, R. M. Macfarlane and W. Lenth, QUEL'89; W. Lenth and R.M.Macfarlane, J. Lum. 45, 346 (1990); D. C. Nguyen et al., Appl. Optics 28 (17), 3553 (1989); D. C. Nguyen et al., SPIE 1223, 54 (1990); T. Hebert, R. Wannemacher, W. Lenth and R.M.Macfarlane, Appl. Phys. Lett. 57 (17), 1727 (1990); R. M. Macfarlane, R. Wannemacher, T. Hebert and W. Lenth, Digest of Conference on Lasers and Electro-Optics CLEO-90, Anaheim, California, page 250, paper CWF-1.
- [3] A. M. Tkachuk, Opt. Spectrosc.68, 775 (1990).
- [4] S. Hubert, D. Meichenin, B. W. Zhou and F. Auzel, J. Lumin. 50, 7 (1991).
- [5] B. R. Judd, Phys. Rev. 127, 750 (1962).
- [6] G. S. Ofelt, J. Chem. Phys. 37, 511 (1962).
- [7] W. T. Carnall, P. R. Fields and K. Rajnak, J. Chem. Phys. 49, 4412 (1968).
- [8] W. T. Carnall, private communication.
- [9] M. J. Weber, Phys. Rev. 157, 262 (1967).
- [10] W. T. Carnall, H. Crosswhite and H. M. Crosswhite, special rep. 1977, Chemistry Division, Argonne National Laboratory, Argonne IL.
- [11] M. J. Weber, B. H. Matsinger, V. L. Donlan and G. T. Surratt, J. Chem. Phys. 57, 562 (1972).
- [12] B. Jacquier, M. F. Joubert and R. M. Macfarlane, to be published.

POWER AND SPATIAL CHARACTERISTICS OF
ELECTRON-BEAM-PUMPED SEMICONDUCTOR LASER
EMITTERS MADE BY DIFFERENT TECHNOLOGIES

A.L.Gurskii, S.V.Davydov, E.V.Lutsenko, I.I.Kulak,
A.I.Mitcovets, G.P.Yablonskii

Institute of Physics, Acad. Sci. of Belarus,
F.Skaryna av. 70, 220072 Minsk, Belarus
Tel.(0172)395352

Recently [1] it was shown that the creation, by means of chemical etching [2], of certain microrelief on the anion surfaces of laser wafers instead a totally reflecting silver mirror permits increasing the output power of lasers based on CdS_{Se} compounds by about one order of magnitude compared to the multi-component emitters with the silver mirrors.

In this paper we report more detailed results of investigation of output power dependences from pump intensity and also of spatial characteristics of radiation for laser wafers based on CdS, ZnCdS, ZnSe, CdTe, and GaAs, with different kinds of mirrors and different thickness.

To make multielement emitters with longitudinal electron-beam excitation, commercial semiconductor crystals were used. The emitters were 0,2 mm thick wafers 50 mm in diameter cemented onto quartz substrates, and 1,2 mm thick wafers without substrates. The wafers were crystallographically oriented in basal plane. For some wafers preliminarily dielectric reflective coatings with the reflection coefficient $R=30-70\%$ or special interference coatings were placed on the A-surface of the wafers. The thin wafers were cut into 0,5-1 mm square elements to a depth of 180 mkm, and the thick wafers to a depth about 2/3 of total thickness.

Some selected dependences of output energy E_o from pump intensity I_p for excited area about 1 cm^2 are given in Fig.1.

Characteristically for all dependences corresponded to thin wafers with microrelief is the saturation of output energy with increasing of pump intensity (curves 1,3,5,7), and for thick wafers with microrelief the output energy at pump intensity 250 mJ/cm is the same as for thin wafers, which probably caused by absorption saturation in passive area, and there isn't saturation of output energy in thick wafers (curve 9).

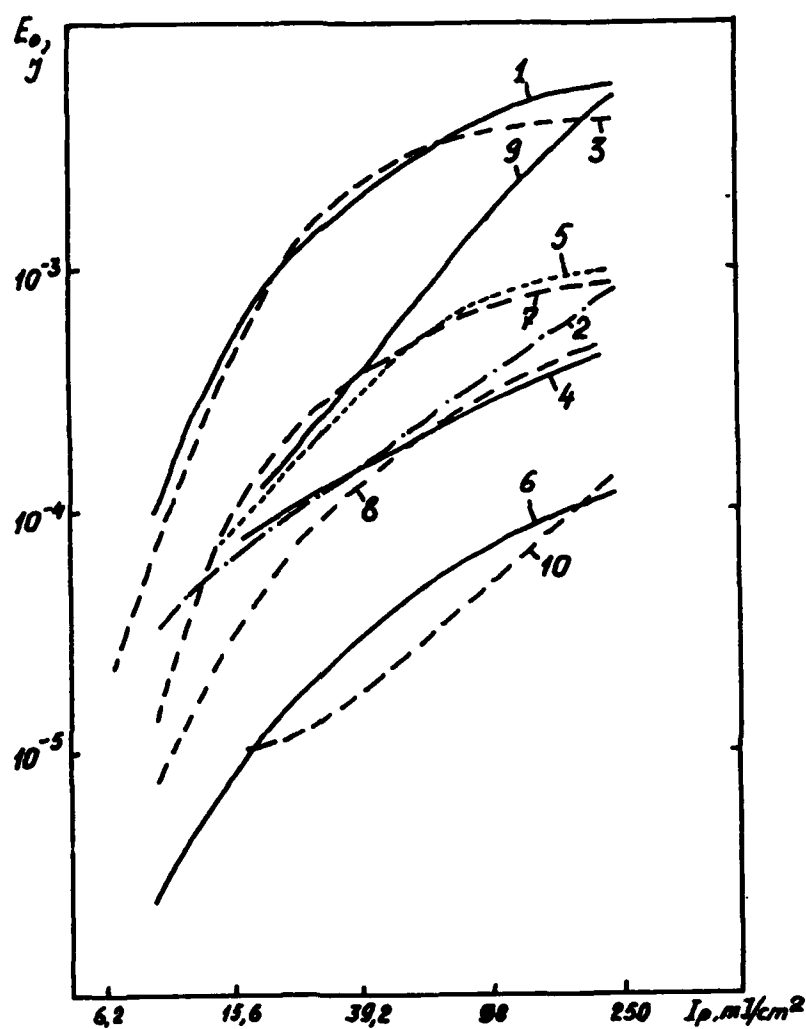


Fig.1. The dependences of output energy from pump intensity for different samples:

- 1- CdS, 0,2 mm, microrelief, 2- CdS, 0,2 mm, Ag-coating,
- 3- ZnSe, 0,2 mm, microrelief, 4- ZnSe, 0,2 mm, Ag-coating,
- 5- ZnCdS, 0,2 mm, microrelief, 6- ZnCdS, 0,2 mm, Ag-coating,
- 7- GaAs, 0,2 mm, microrelief, 8- GaAs, 0,2 mm, Ag-coating,
- 9- CdS, 0,2 mm, microrelief, 10- CdS, 0,2 mm, Ag-coating.

For GaAs crystals the efficiency of using of microrelief is smaller than for II-VI compounds because of worse quality of obtained microrelief (curves 7,8).

The spatial distribution of radiation intensity depends from pump intensity and from kind of mirrors. The presence of microrelief leads to expanding of spatial diagram. It is probably conditioned by the fact that the angle of microprism apex is different from 45° . It is possible to modify the spatial diagram of emitters by deposition of interference coatings onto wafer surfaces.

The use of these lasers made it possible to create non-cooled lasers based on some promising active media [3].

The possible causes of saturation of output energy increasing in thin wafers with a microrelief, the particularities of spatial diagrams and methods of their improvement are discussed.

1. A.L.Gurskii, S.V.Davydov, I.I.Kulak, A.I.Mitcovets, A.A.Stavrov, A.P.Shkadarevich, G.P.Yablonskii. Abstracts of 8th International Conference on Ternary and Multinary Compounds, Kishinev (SU), 1990, p.335.
2. V.P.Gribkovskii, V.V.Grusinskii, A.L.Gurskii, S.V.Davydov, I.I.Kulak, A.I.Mitcovets, A.A.Stavrov, A.P.Shkadarevich. Inventor's certificate SU No 1653514, IPC H01S 3/18.
3. I.I.Kulak, A.I.Mitcovets, A.P.Shkadarevich, G.P.Yablonskii. Proc. Conf. "Advanced Solid-State Lasers", Santa-Fe, New-Mexico, 1992, p. 162-164.

Generation of 369.4 nm Radiation By Efficient Doubling of a Diode Laser

A. Williams, D. J. Seidel, and L. Maleki

Jet Propulsion Laboratory, California Institute of Technology,
4800 Oak Grove Drive, Pasadena, California 91109
(818) 354-3688

The trapped ytterbium ion frequency standard^{1,2} under development at JPL requires at least $10\ \mu\text{W}$ of continuous-wave (cw) laser radiation at 369.4 nm. Only diode lasers meet the requirements of low power consumption and small size for use aboard spacecraft¹, but diode lasers are not currently available at this wavelength. It is therefore necessary to employ frequency doubling methods to reach 369.4 nm with diode lasers.

In order to overcome the low doubling efficiency associated with continuous-wave operation and milliwatt input powers, we have designed a buildup ring cavity for the 738.8 nm fundamental radiation (Fig. 2). The cavity is also designed to take advantage

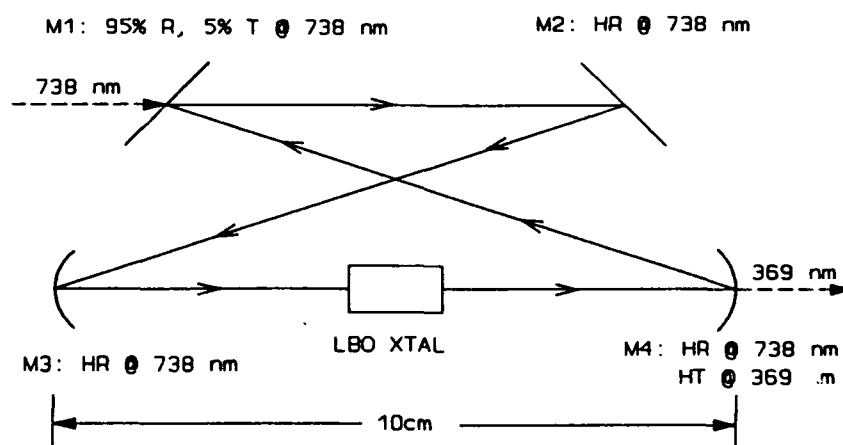


Figure 1: Design of optical buildup cavity for generation of 369.4 nm light.

of the increase in doubling efficiency with tight focusing of the input beam by employing curved mirrors M3 and M4 to focus the fundamental beam to a waist of $25\ \mu\text{m}$ in the doubling crystal. In order to accommodate such tight focusing, we chose a doubling crystal of lithium triborate (LBO) due to its large acceptance angle. The small folding

angle ($\sim 5^\circ$) reduces astigmatism and makes the cavity size compatible with constraints on spacecraft instrumentation.

The custom antireflection coatings on the mirrors and crystal are expected to allow a buildup factor of approximately 15; therefore, a diode laser with output power of 10 mW will provide 150 mW of fundamental radiation to the doubling crystal. At this input power and fundamental beam waist, we expect greater than 0.5% conversion efficiency, thus producing more than 35 μ W of 369.4 nm laser radiation. We will present results obtained with diode lasers at the required 738.8 nm fundamental wavelength provided by the Micro Devices Laboratory at JPL, which we have found to produce cw power of 10 mW or more.

The research described here was carried out at the Jet Propulsion Laboratory, California Institute of Technology, under contract sponsored by the National Aeronautics and Space Administration.

References

1. D.J. Seidel, A. Williams, R.W. Berends, and L. Maleki, "The Development of a Ytterbium Ion Frequency Standard," *Proc. of the 46th Annual Freq. Control Symp.*, to be published 1992.
2. R. Casdorff, V. Enders, R. Blatt, W. Neuhauser, and P.E. Toschek, "A 12-GHz Standard Clock on Trapped Ytterbium Ions," *Annalen der Physik*, vol. 48, no. 1-3, pp. 41-55, 1991.

Self-Frequency-Doubling laser crystal Nd: β -BaB₂O₄

T.Ebihara, Y.Matsuoka and H. Toratani
Materials Research Laboratory, HOYA Corporation,
3-3-1 Musashino, Akishima, Tokyo 196, Japan
Phone +81(425)46-2743

Liu Lin
Institute of Physics, Chinese Academy of Science,
P.O.Box 603(26), 8, Nansanjie, Zhongguancun, Beijing, China
Phone 289131-503

Summary

A self-frequency-doubling crystal, Nd_{1-x}Y_xAl₃(BO₃)₄ (NYAB) and Nd:MgO:LiNbO₃, is a crystal which combines laser properties and nonlinear optical properties. We report a new self-frequency-doubling crystal Nd: β -BaB₂O₄.

Nd doped β -BaB₂O₄ crystal was prepared in the melt growth technique which had been successfully applied for β -BaB₂O₄ crystal¹⁾. Taking account of charge compensation and ionic radius matching, Nd ion was incorporated together with monovalent ion. In melt quenching experiments we found that the substitution of Ba with Nd+(K,Cs) up to 5wt% was possible and no significant degradation was observed in S.H.G. efficiency measured by powder method. Crystal growth experiments were carried out in a resistant heating furnace (Fig.1). A water cooling coil was set just above the melt surface to obtain a sufficient temperature gradient which is needed to prevent the formation of α -phase BaB₂O₄ instead of β -phase BaB₂O₄. Temperature gradient required to obtain β -phase was larger than approximately 100°C/cm. Seeding temperature was about 1100°C which was much higher than that reported for β -BaB₂O₄. In our experiment this seeding temperature was adequate also for growing β -BaB₂O₄ although it was not readily explained by previously proposed theory. By optimizing growth conditions such as seeding temperature, temperature gradient

above the melt, growth rate, starting materials etc., a relatively good crystal of approximately 10mm in diameter by 5mm in length were obtained. However the cell structure and some cracks were developed as the crystal size was increased. Since the segregation coefficient of Nd ion in the crystal is lower, the crystal quality becomes poorer as Nd concentration in the melt is increased. Consequently we were able to obtain good crystals only in very light Nd doping. On the other hand, Nd: α -BaB₂O₄ crystal was rather easily obtained in larger size with better optical quality. Nd:BaB₂O₄ glass was prepared by slightly increasing Nd+(K,Cs) substitutions. Fluorescence spectra of Nd: β -BaB₂O₄ crystal was measured with laser diode excitation at 800nm in comparison with Nd: α -BaB₂O₄ crystal and Nd:BaB₂O₄ glass (Fig.2). These spectra are quite distinct each other. Nd:BaB₂O₄ glass has a broad band of peak wavelength at 1061nm representing the inhomogeneous structure as expected. Nd: α -BaB₂O₄ crystal shows a spectra with rather fine structure in which stark splitting is obvious. The peak wavelength of the largest band is at 1068nm. Nd: β -BaB₂O₄ crystal has less obvious splitting and the peak wavelength is at 1053nm. It suggests that Nd: β -BaB₂O₄ crystal has a much more disordered structure than Nd: α -BaB₂O₄ crystal. The 4-circle X-ray diffractometer analysis indicates that Nd ion occupies Ba ion site of β -BaB₂O₄ crystal in a random manner. Fluorescence lifetime of these crystals and the glass for Nd concentration of 1wt% in batch were 50 μ s to 80 μ s although the Nd concentrations of the obtained crystals were not certain, but less. A 7x3x2mm³ size c-axis Nd: β -BaB₂O₄ crystal of good optical quality was cut and polished for further spectroscopic measurements. Crystal growth condition, second order nonlinear optical efficiency of Nd: β -BaB₂O₄ crystal are reported. Lasing experiments using both α - and β -BaB₂O₄ crystals are under consideration.

References :

- 1) K. Ito, F. Marumo and Y. Kuwano ; Journal of Crystal Growth, 106, (1990) 728-731

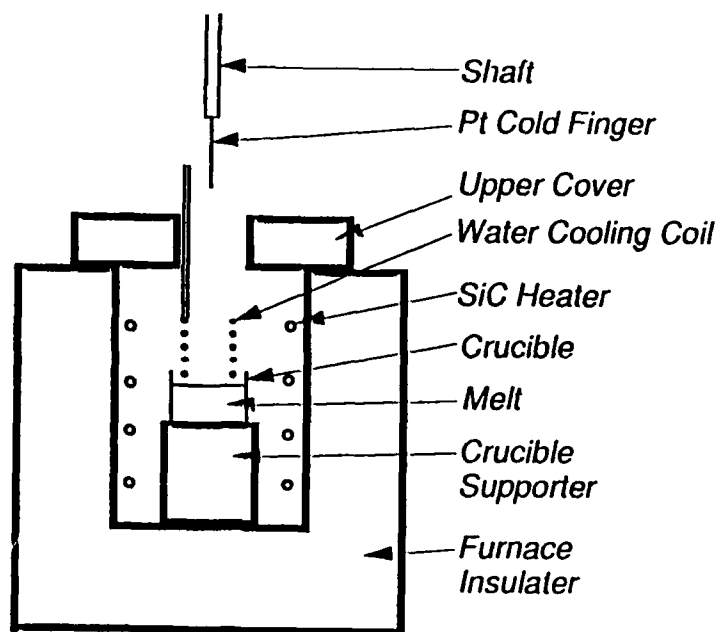


Fig.1 Schematic drawing of crystal growth setup.

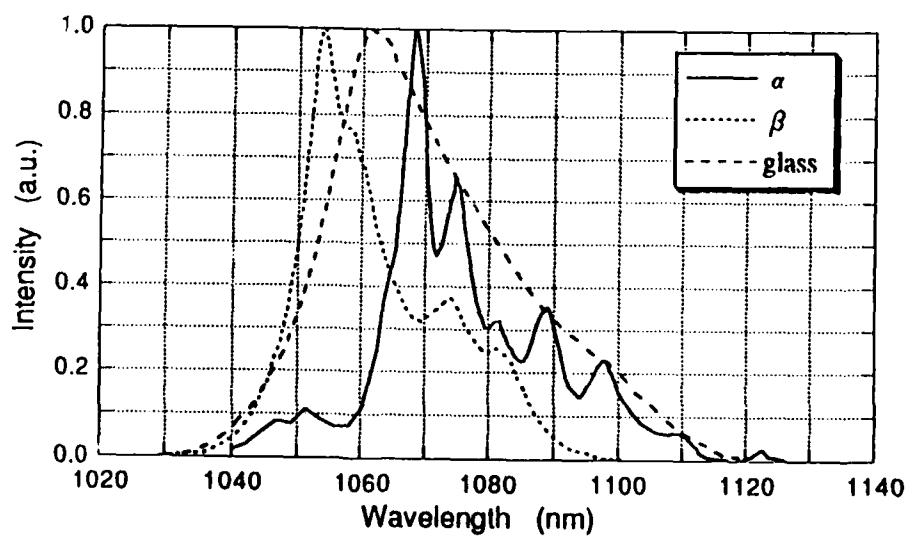


Fig.2 Fluorescence spectra of Nd:α-, β-, glass-BaB₂O₄ excited with 800nm laser diode.

Tunable blue light source by intracavity frequency doubling of a Cr-doped LiSAF laser

François Balembois, Patrick Georges, François Salin,
Gérard Roger and Alain Brun

Institut d'Optique Théorique et Appliquée
Unité de Recherche Associée au CNRS N°14
Université Paris-Sud
B.P. 147
91403 Orsay Cedex, France

Ph: 33-1-69 41 68 56
Fax: 33-1- 69 41 31 92

Compact solid state lasers emitting in the blue-green wavelength range are expected to be the key components for optical recording and underwater communications or as spectroscopic sources. To develop such lasers, several approaches are under study at numerous laboratories around the world. Possible solutions include up-conversion lasers [1,2], green or blue diode lasers [3], sum frequency mixing techniques [4] or frequency doubled near IR sources [5] that produce blue or green light at fixed wavelengths. Compact sources generating tunable blue light could be particularly useful for spectroscopic experiments. One possibility is an optical parametric oscillator pumped by the third harmonic of a YAG laser but this solution requires high peak power from the pump laser [6].

In this letter, we report on a tunable blue source using an intracavity frequency doubled, Q-switched, cw pumped, $\text{Cr}^{3+}:\text{LiSrAlF}_6$ (Cr:LiSAF) laser. Cr:LiSAF was discovered in 1989 by Payne et al. at the Lawrence Livermore National Laboratory [7]. It has an absorption band in the red between 600 and 700 nm and can be pumped by red diode lasers [8]. Its large fluorescence bandwidth leads to tunable laser emission between 760 and 1000 nm [9]. A compact tunable blue laser source can thus be obtained by intracavity second harmonic generation of a Cr:LiSAF laser.

In order to simulate diode pumping, we used the red lines (647 and 676 nm) of a cw krypton ion laser to pump our 15 mm long Cr:LiSAF crystal. The Cr^{3+} concentration was 0.8 % in weight and the absorption was 97 % of the pump power. Cr:LiSAF, in comparison to titanium sapphire, is of relatively poor thermomechanical quality and we observed thermal damage to our sample for 2 W cw pump power. Therefore, for higher pumping rates, the krypton laser was chopped at 200 Hz with a 25 % duty cycle. The laser configuration is shown in figure 1. The krypton ion laser beam was focused by a 10 cm focal lens through a dichroic mirror M_1 (high transmission in the 600-700 nm range and high reflection between 800 and 900 nm) into the Cr:LiSAF crystal. M_2 is a high reflector in the 800-900 nm range. A birefringent filter was used to tune the laser wavelength. A 1 mm long LiIO_3 crystal was introduced at the focal point of a second cavity formed by two mirrors M_3 and M_4 . These mirrors had a high reflectivity between 760 and 830 nm and were dichroic coated to allow maximum transmission in the blue. In order to increase peak power and to produce more blue radiation, the LiSAF laser was used in Q-switched operation with the aid of an acousto-optic

crystal operating at 125 MHz. This crystal was used to modulate the intracavity losses. Since the cavity mode spacing was 190 MHz, the acousto-optic modulator did not act as a modelocker (requiring 250 MHz cavity mode spacing), but rather as a loss source. At a repetition rate of a few kHz, we switched off the RF power and thereby decreased the losses and allowed the laser to produce nanosecond pulses.

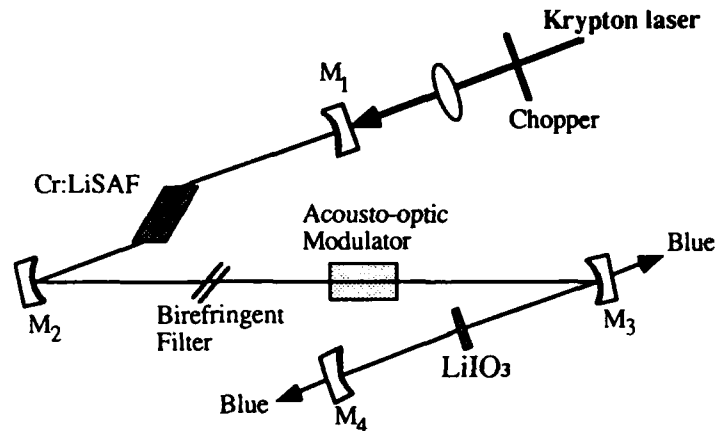


Figure 1 : Experimental set up.
M₁ and M₂ are R=100 mm, M₃ and M₄ are R=150 mm.

The infrared pulses were 280 ns long while the blue pulses produced in the LiIO₃ crystal were 230 ns long at 407 nm. The decrease in pulse length is consistent with the fact that the second harmonic intensity is proportional to the square of the fundamental intensity. Blue light could be observed on the mirrors M₃ and M₄. Counting both outputs, we obtained blue pulses of 0.74 μ J at 407 nm at a repetition rate of 10 kHz. This corresponds to 7.4 mW average blue power at 3.3 W pump power incident on the Cr:LiSAF crystal [10]. We could tune the blue emission wavelength by simultaneously adjusting the birefringent filter to vary the infrared wavelength and modifying the LiIO₃ crystal orientation to preserve phase matching. We observed blue light generation between 395 nm and 435 nm (fig.2). The decrease around 415 nm is due to the cavity mirrors as their transmission increases above 830 nm. This lead to a decrease in energy in the cavity and a corresponding decrease in blue generation.

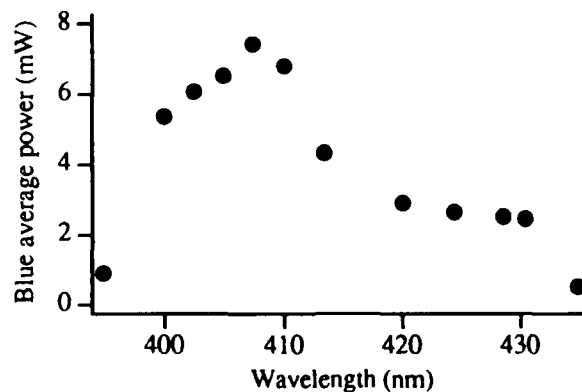


Figure 2 : Tunability in Q-switched operation at 3,3 W pump power.

We considered the effect on the efficiency of blue generation of the infrared spot size on the LiIO_3 crystal (diameter of 100 μm for the configuration described in figure 1). We tried two other configurations with different radii of curvature for the mirrors of the second cavity leading to spot sizes of 70 μm and 200 μm . However these configurations lead to a weaker output of blue than the initial one.

Several possibilities for improving this laser exist. With better adapted mirrors, it should be possible to tune the laser between 380 nm and 500 nm, corresponding to the entire emission band of the Cr:LiSAF crystal. Our experiment could be improved by minimizing intracavity losses through the use of a nonlinear crystal with antireflection coatings in both the blue and the infrared range. Finally, it could be modified so as to have only one blue output by introducing a flat mirror between the two cavities (HR around 830 nm and HT around 415 nm) and using two mirrors with HR at 830 nm and 415 nm mirrors for the second cavity.

In conclusion, we describe a blue laser source with 40 nm tunability (395 nm-435 nm) producing up to 7 mW average power around 407 nm. We believe we could reach 10 mW average power by using mirrors with optimized coatings and by using more efficient nonlinear crystals such as KNbO_3 in place of our LiIO_3 crystal. Many applications such as optical data storage or spectroscopy of biological media require around 10 mW of blue laser light. Thus, once the krypton pump laser is replaced by laser diodes, this source will be suitable for a number of sensors and instruments.

Acknowledgements : We thank B. Deveaud (CNET Lannion) for the loan of the LiIO_3 crystal.

References :

- [1] J.Y. Allain, M. Monerie and H. Poignant
Electron. Lett. 26 (1990) 166-168
- [2] R.M. Mcfarlane, F. Tong, A.J. Silversmith and W. Lenth
Appl. Phys. Lett., 52 (1988) 1300
- [3] M.A. Haase, J. Qiu, J.M. Depuydt and H. Cheng
Appl. Phys. Lett., 59 (1991) 1272-1274
- [4] J.C. Baumert, F.M. Schettenberg, W. Lenth, W.P. Risk and G.C. Bjorklund
Appl. Phys. Lett., 51 (1987) 2192
- [5] G.J. Dixon, C.E. Tanner and C.E. Wieman
Opt. Lett. 14 (1989) 731-733
- [6] J.T. Lin
Opt. and Quantum Electronics 22 (1990) S283-S313.
- [7] S.A. Payne, L.L. Chase, L.K. Smith, W.L. Kway and H.W. Newkirk
J. Appl. Phys. 66, 1051 (1989).
- [8] R. Shep, J.F. Myers, H.B. Seneze, A. Resenberg, R.C. Morris and M. Long
Opt. Lett. 16, 820 (1991).
- [9] M. Stalder, B.H.T. Chai and M. Bass
Appl. Phys. Lett. 58 (1991) 216.
- [10] F. Balembois, P. Georges, F. Salin, G. Roger and A. Brun
submitted to Appl. Phys. Lett. (July 92)

Comparison of Yb, Ho Upconversion Energy Transfer in Different Fluoride Crystals

X.X. Zhang¹, M. Bass^{1,2,3}, B.H.T. Chai^{1,4}, and R.E. Peale²

University of Central Florida, Orlando, FL 32816

¹ Center for Research in Electro-optics and Lasers, ² Department of Physics

³ Department of Electrical Engineering, ⁴ Department of Mechanical Engineering

Tel. (407) 658-6800

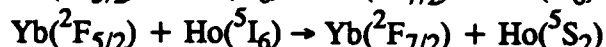
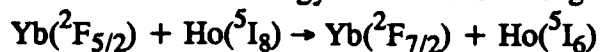
Recently, there is a renewed interest in obtaining short wavelength solid state lasers through upconversion schemes. Yb sensitized upconversion energy transfer is specially attractive for this purpose because of the ability of high power InGaAs diode lasers to pump Yb. Yb, Ho upconversion energy transfer is relatively simple compared to upconversion involving other rare earth ions. Although a Yb sensitized Ho green laser has been realized at 77 K in BaY_2F_8 [1], no such lasing has been achieved at room temperature. In searching for a more suitable host for the room temperature Yb, Ho green upconversion laser we have carried out a systematic spectroscopic study on the Yb, Ho upconversion processes in BaY_2F_8 (BYF), KYF_4 (KYF), and LiYF_4 (YLF). Based on the detailed absorption, emission and fluorescence decay data, KYF is shown to be a promising host.

The spectra of the green emission of these crystals at room temperature are given in Fig. 1. They were obtained with the same pump power from a Ti:sapphire laser tuned to the center absorption wavelength of Yb ions in each crystal at around 960 to 970 nm. The integrated intensities of the green emission at room temperature for different samples are given in Table 1. The green integrated intensity of 20%Yb, 0.1%Ho:KYF is 4.4 times higher than that of BYF of the same concentration and it is 5.2 times higher for 20%Yb, 0.2%Ho:KYF than for similarly doped YLF. Fluorescence decay times at 12 K, obtained with the pulse excitation from an 80 ns Q-switched Cr:LiSAF laser, are also given in Table 1. From the table we can see that, the respective transfer efficiency of the Yb excitation due to the Yb \rightarrow Ho energy transfer is 65% and 34% for KYF and BYF having concentrations of 20%Yb and 0.1%Ho; 79% and 12% for KYF and YLF having concentrations of 20%Yb and 0.2%Ho. It appears that the IR to green conversion in KYF is much more efficient than in either BYF or YLF.

The green emission of Ho originates from the transition from the $^5\text{S}_2$ level to the $^5\text{I}_8$ ground state. Therefore the emission and the absorption spectra overlap with

each other, as seen in Fig. 1. Due to the strong absorption the only line which could possibly lase is the one at the longest wavelength (about 551 nm). Comparing the emission and the absorption spectra of the three crystals one can see that the relative emission intensity of this peak in KYF is particularly strong and the absorption coefficient of this peak in KYF is particularly low. These properties make KYF attractive as a host for Yb, Ho green laser.

Yb ions transfer the excitation energy to Ho ions through the following two successive steps:



For efficient upconversion energy transfer to take place it is important that the lifetimes of the intermediate state of Ho ($^5\text{I}_6$) as well as the excited state of Yb ($^2\text{F}_{5/2}$) are sufficiently long. However, this depends on the multiphonon relaxation rate and, therefore, critically on the phonon energy. The absorption edge due to the lattice vibration (phonon) of these three crystals (having the same length) is given in Fig. 2. It can be seen that the maximum phonon energy in KYF appears to be the lowest and may explain why the lifetime in KYF is the longest. However, since these energy transfer processes are phonon-assisted, the energy mismatch between the transferring levels is critical. Detailed energy level positions will be presented. Discussions of the energy transfer mechanism will also be given.

Table 1. Spectroscopic data of Yb, Ho codoped crystals

Crystal	BYF	KYF	KYF	YLF
Doping concentration	20% Yb 0.1% Ho	20% Yb 0.1% Ho	20% Yb 0.2% Ho	20% Yb 0.2% Ho
Integrated intensity of green emission(a.u.)	15.5	68	100	19.4
Yb decay time without Ho, τ_0 (ms) at 12 K	2.4*	4.98	4.98	1.95
Yb decay time with Ho, τ (ms) at 12 K	1.58	1.75	1.04	1.71
Transfer rate (s^{-1}) = $\tau^{-1} - \tau_0^{-1}$ at 12 K	216	371	761	72
Transfer efficiency $\eta(\%) = 1 - \tau/\tau_0$ at 12 K	34	65	79	12

*estimated from Ref. 2 room temperature data

References:

1. L.F. Johnson and H.J. Guggenheim, "Infrared-pump visible laser," Appl. Phys. Lett. **19**, 44 (1971)
2. L.F. Johnson, H.J. Guggenheim, T.C. Rich, and F.W. Ostermayer, "Infrared-to-visible Conversion by Rare-Earth Ions in Crystals," J. Appl. Phys. **43**, 1125 (1972)

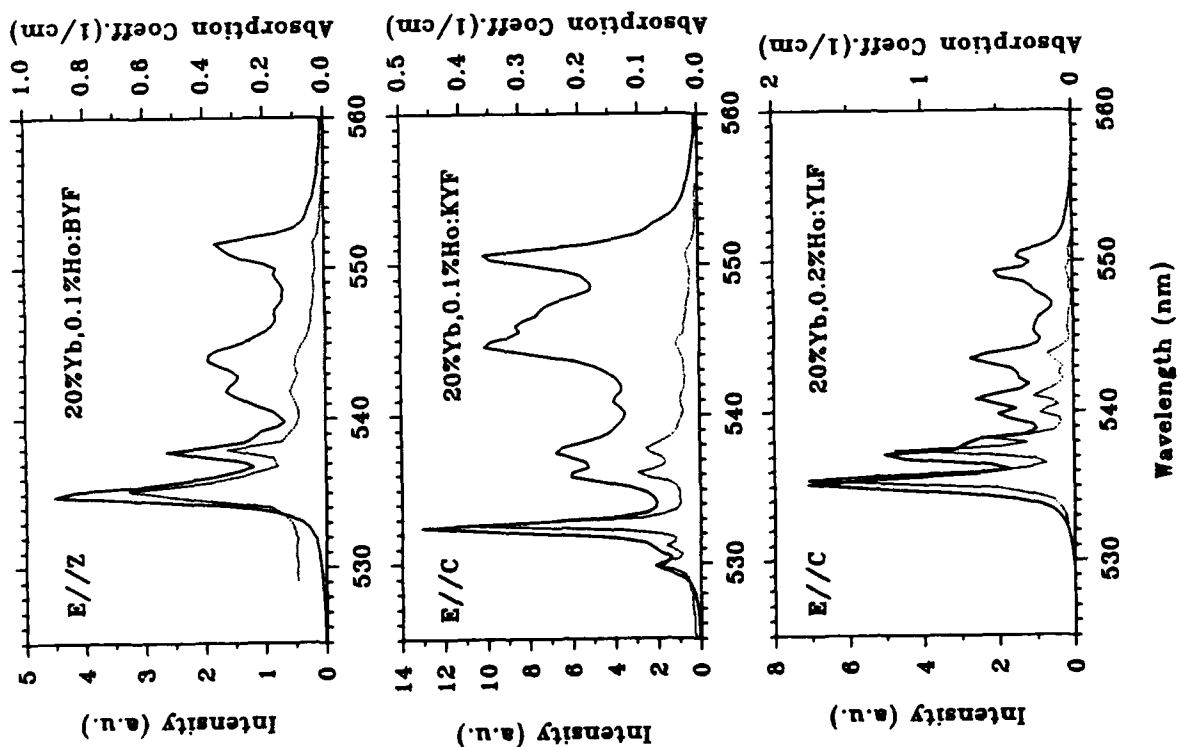


Fig. 1. Green emission (—) and absorption (---) spectra of Ho in different Yb, Ho codoped crystals at room temperature. The emission was excited by a Ti:sapphire laser pumping at the Yb ions at 960–970 nm

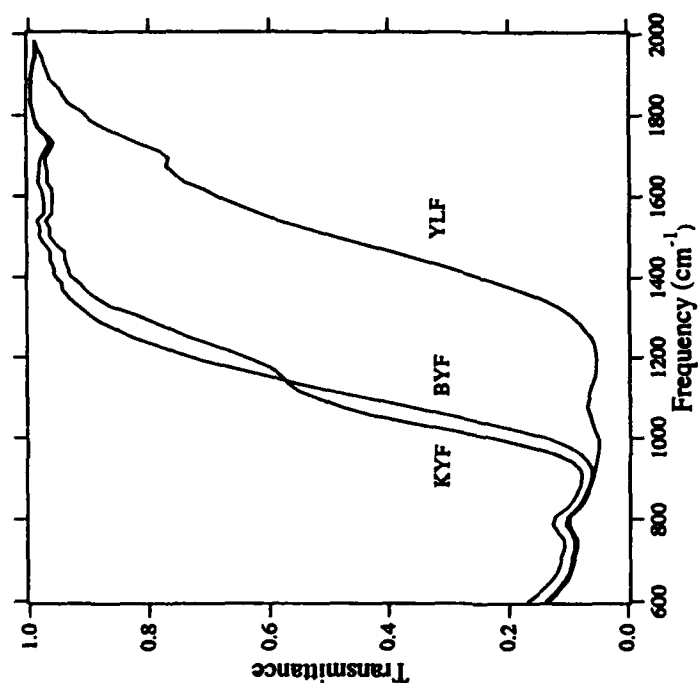


Fig. 2 Transmittance vs. frequency for KYF, BYF and YLF showing the lattice vibration absorption edge

Wednesday, February 3, 1993

Joint Session on Frequency Upconversion in Bulk Devices 2

JWD 2:30pm–3:45pm
La Salle Ballroom B&C

Thomas M. Baer, *Presider*
Spectra-Physics Laser Diode Systems

Controlling Chaos in an Intracavity Doubled Nd:YAG Laser

Rajarshi Roy
School of Physics
Georgia Institute of Technology
Atlanta GA 30332
(404-894-5265)

A Nd:YAG laser with an intracavity frequency doubling crystal displays irregular intensity fluctuations for certain ranges of operating parameters.^{1,2} Analysis of the laser system shows that these fluctuations are chaotic in nature, and that it is possible to operate the laser stably in selected parameter regimes.^{2,3} It has also been shown experimentally that dynamical control of such a laser system is possible, and that a variety of periodic waveforms as well as the unstable steady state can be stabilized through an appropriate feedback technique called occasional proportional control.^{4,5} In this technique, tiny kicks are given to the pump excitation, that depend in amplitude on the difference of the output intensity from a chosen reference level, and with a period related to the relaxation oscillation period. The laser may be maintained in a stabilized steady state over a wide range of pumping if a tracking procedure is used that makes suitable changes in the control circuit parameters as the pump level is altered.

References:

1. T. Baer, J. Opt. Soc. Am. B3, 1175 (1986).
2. (a) M. Oka and S. Kubota, Opt. Lett. 13, 805 (1988). (b) G.E. James, E.M. Harrell II, C. Bracikowski, K. Wiesenfeld and R. Roy, Opt. Lett. 15, 1141 (1990).
3. C. Bracikowski and R. Roy, Chaos 1, 49 (1991).
4. E.R. Hunt, Phys. Rev. Lett. 67, 1953 (1991).
5. R. Roy, T.W. Murphy, Jr., T.D. Maier, Z. Gills and E.R. Hunt, Phys. Rev. Lett. 68, 1259 (1992).

Fundamental Walk-Off Compensation in KTP

J. L. Nightingale

Coherent Laser Group

Palo Alto, CA 94304

(415) 858-7605

Intracavity-frequency-doubled, diode-pumped lasers are attractive sources of visible light. The best characterized materials for a diode-pumped, frequency-doubled system are Nd:YAG as the laser medium and KTP as the nonlinear medium. Since frequency doubling of a 1064 nm fundamental wavelength in KTP requires Type II phasematching, both fundamental polarization states must be excited to generate the second harmonic. Poynting vector walk-off between these fundamental polarization states can introduce resonator loss.¹ By orienting the KTP at an oblique angle of incidence within the resonator and fabricating the KTP so that the phasematching condition is satisfied, this loss can be eliminated.

Figure 1(a) illustrates the problem typically encountered for a KTP crystal oriented for Type II phasematching of a 1064 nm fundamental beam. The crystal is fabricated to phasematch at normal incidence, implying the end face normals are 23.3° from the x-crystallographic-axis and 90° from the z-crystallographic-axis.² In this figure, the beam polarized in the KTP's x-y crystallographic plane is denoted with subscript 1 and the beam polarized perpendicular to this plane (the z-direction) is denoted with subscript 2. The wave vectors, Poynting vector, and displacement vectors for the fundamental radiation are denoted \mathbf{k}_1 and \mathbf{k}_2 , \mathbf{S}_1 and \mathbf{S}_2 , \mathbf{D}_1 and \mathbf{D}_2 , respectively. For this orientation, \mathbf{S}_1 walks-off from \mathbf{k}_1 by 0.2° and

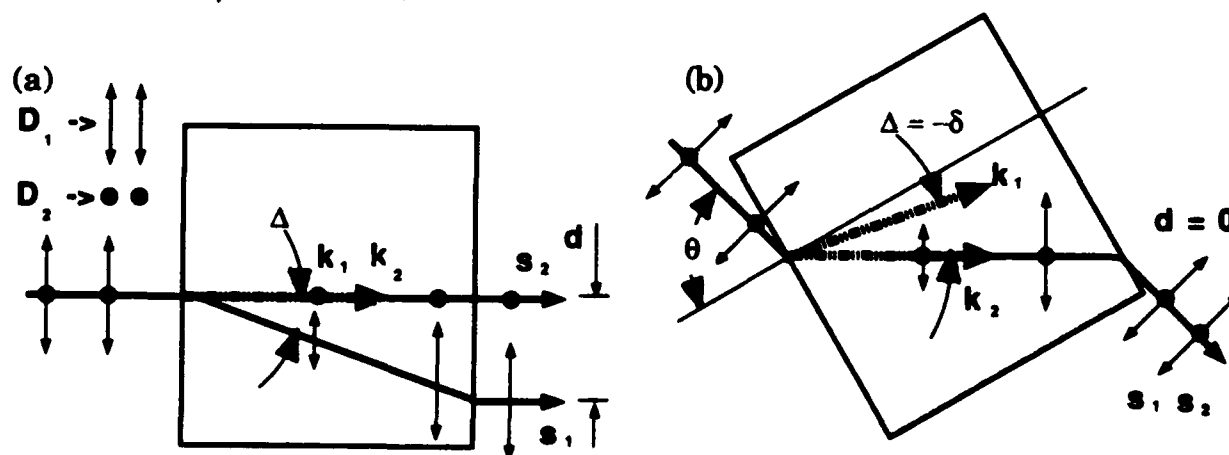


Figure 1 - (a) Poynting vector walk-off in KTP for a normal incidence fundamental beam. (b) Elimination of the spatial separation due to Poynting vector walk-off by orienting the KTP at an oblique angle of incidence.

S_2 experience no walk-off from k_2 . Since for normal incidence k_1 and k_2 are parallel, the beams angular separation due to walk-off (Δ) is 0.2° . For a 5 mm long KTP crystal, the separation between the two orthogonally polarized beams (d) is 17 microns. In a resonator the depolarizing effects of this spatial separation may lead to additional resonator loss, which is particularly deleterious for low-power, diode-pumped systems.¹

The effects of Poynting vector walk-off of the two fundamental beams can be compensated by orienting the KTP at an oblique angle of incidence.³ At the interface between the KTP and surrounding air, the wave vectors for each polarization state, k_1 and k_2 , independently satisfy Snell's Law. The orientation of this difference is in the plane of incidence and the magnitude of this difference, δ , is given by the formula

$$\delta = \arcsin(\sin(\theta)/n_1) - \arcsin(\sin(\theta)/n_2)$$

where θ is the angle of incidence and n_1 and n_2 are the refractive indices associated with the two polarization states. By correctly choosing the angle and plane of incidence, the difference in the initial orientation of the wave vectors can be used to compensate for the Poynting vector walk-off. In the case of KTP for second harmonic generation of 1064 nm radiation, $\Delta = -\delta$ for $\theta = 7^\circ$ oriented in the x-y crystallographic plane. This condition is depicted in Figure 1(b). It should be noted that this orientation does not address the related, but independent, second harmonic walk-off.

In order to simultaneously satisfy the phasematching condition, the KTP is fabricated with end face normals 27.5° from the x-axis and 90° from the z-axis. This allows the wave vectors to satisfy the phasematching condition simultaneous with a 7° angle of incidence to satisfy the walk-off compensation condition. The exact numerical values for the phasematching condition and the walk-off compensation condition are somewhat uncertain because of uncertainties in the refractive indices of KTP.

Figure 2 illustrates the efficacy of this technique in minimizing depolarization of a transmitted fundamental beam. The data in this figure were obtained using a linearly polarized 1064 nm beam with a 50 micron beam radius incident on a KTP crystal fabricated with end faces normals 27.5° from the x-axis and 90° from the z-axis. The plane of incidence was 90° from the z-axis and was varied in the x-y plane by rotating the crystal. At each orientation, waveplate

effects were nulled out by adjusting the KTP temperature so that the KTP was an integer λ waveplate. The polarization components of the transmitted beam amplitude parallel and perpendicular to the incident initial polarization state were measured and the depolarization calculated as the ratio of the two quantities. A pronounced minimum in the depolarization occurs at an angle of incidence near 7° , as expected from the preceding analysis.

The utility of this walk-off compensation technique has been demonstrated in diode-pumped, intracavity-frequency-doubled lasers. KTP crystals oriented for walk-off compensation and conventionally oriented KTP crystals have been used in the refractively closed ring resonator shown in Figure 3.⁴ The efficiency of green generation improves by more than a factor of two using the walk-off compensated crystal. With a 5-mm-long, walk-off-compensated crystal, 264 mW of single-mode, single-frequency, 532 nm radiation was obtained with 1200 mW of 808 nm laser diode pump radiation. This represents 22% conversion efficiency, verifying the utility of the walk-off compensation technique described here.

Figure 2 - Experimental verification of walk-off compensation.

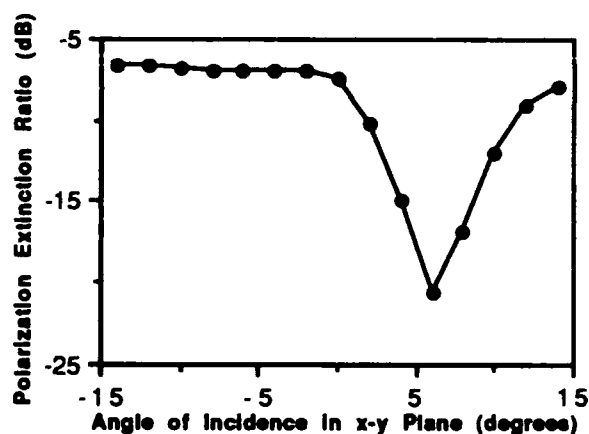
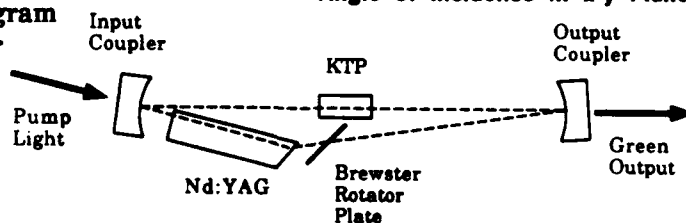


Figure 3 - Schematic diagram of the diode-pumped laser resonator.



References:

1. D. W. Anthon, D. L. Sipes, T. J. Pier & M. R. Ressel, *IEEE J. Quantum Electronics*, **28**, 1148 (1992).
2. R. A. Stolzenberger, *Applied Optics*, **27**, 3883 (1988).
3. J. L. Nightingale, U. S. Patent 5,136,597, (1992).
4. J. L. Nightingale & J. K. Johnson, Proceedings of the Conference on Lasers and Electro-Optics 1992, 54 (1992).

Second Harmonic Generation of a High Power Coherent Laser Diode

Robert Waarts, Ross Parke, Derek Nam, David Welch, David Mehuys,
Amos Hardy, Robert Lang, Steve O'Brien, Don Scifres

Spectra Diode Labs, 80 Rose Orchard Way, San Jose CA 94301

Tel: (408) 943-9411

Summary:

Frequency doubling of laser diodes has been demonstrated in bulk crystals, bulk crystals in a resonant cavities as well as in periodically poled waveguides. The output power available from the frequency doubling schemes however, has been limited by the relatively low output powers available from laser diodes. Frequency doubling of laser light requires a high brightness diffraction limited input beam with single spectral mode. Coherent output power from a semiconductor laser has been limited for many years to 100-200 mW, However, recently over 1 Watt cw diffraction limited output power has been obtained from a monolithically integrated flared master oscillator power amplifier (MOPA)¹.

In this paper we report on frequency doubling in a bulk KNbO₃ crystal with a novel, high power, monolithic laser diode. The laser diode operates at a single frequency with a diffraction limited output beam throughout its operating range. In addition, the output from the laser diode does not exhibit any steering as a function of changes in the injection current. A schematic diagram of the MOPA is shown in Figure 1. The MOPA consists of a DBR master oscillator with two second order gratings. The output from the laser is coupled into a flared amplifier. The taper of the flared amplifier is matched to the approximately 6 degrees divergence of the beam emitted from the oscillator. The signal is amplified along the length of the flared amplifier such that the peak intensity remains nearly constant and the increase in output power is a result of the expanding aperture of the amplifier. The light is coupled out of the amplifier through the anti-reflection coated cleaved facet. The light output from the oscillator as a function of the injection current to the oscillator is shown in Figure 2 and the far field at different output power levels is shown in figure 3. The differential efficiency is 60 % and the device operates in a single spectral mode at 955.5 nm at all output power levels.

A schematic diagram of the set up for frequency doubling of the output from the MOPA is shown in figure 4. The MOPA is similar to the MOPA discussed previously however a different device with a wavelength of 988 nm is used such as to be properly phase matched in KNbO_3 near room temperature². The output from the MOPA is i) collimated in the direction perpendicular to the junction by an objective lens with a focal length of 6.5 mm and $\text{NA}=0.6$ and ii) corrected for astigmatism as well as circularized with a 200 mm focal length cylinder lens. The output from the cylinder lens is focussed with a 100 mm focal length lens into a spot with 20 and 30 micron FWHM in the direction perpendicular and parallel to the junction respectively. A 7 mm long b-cut KNbO_3 crystal is positioned at the focussed beam.

We obtained 1.2 mW blue-green output power from single pass SHG at an input power to the crystal of 0.5 Watt and at a crystal temperature of 34 degrees C. This is about a factor of 2 smaller as compared to the results obtained in an a-cut KNbO_3 crystal with a $\text{Ti:Al}_2\text{O}_3$ laser and slightly smaller as compared to the results obtained with a broad area GaAs laser amplifier³.

This is the first demonstration of single pass frequency doubling of a monolithic high power diode laser capable of output power exceeding 1 Watt. The advantages of this system include modulation to 1 GHz, simple alignment tolerances and ease of fabrication.

References:

- 1) D. Welch, R. Parke, D. Mehuys, A. Hardy, R. Lang, S. O'Brien, D. Scifres, "1.1 W, cw, diffraction-limited operation of a monolithically integrated flared amplifier master oscillator power amplifier", to be published in electronics letters.
- 2) Biaggio, P. Kerkoc, L. S. Wu, Peter Gunter, Beat Zysset "Refractive indices of orthorhombic KNbO_3 II. Phase matching configurations for nonlinear-optical interactions.", Journal of Optical Society of America B. vol. 9, pp. 507-517 (1992)
- 3) L. Goldberg L. Busse and D. Mehuys, "Blue light generation by frequency doubling of AlGaAs broad area amplifier emission", Appl. Phys. Lett. vol. 60, pp. 1037-1039 (1992)

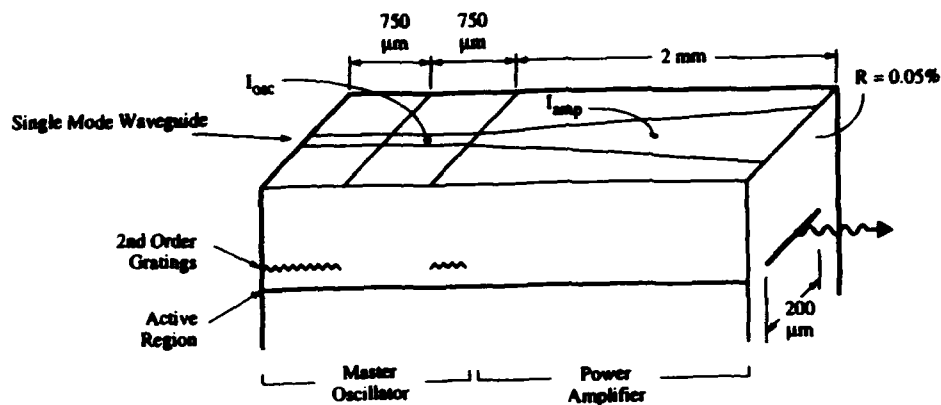


Figure 1: Schematic diagram of the MOPA

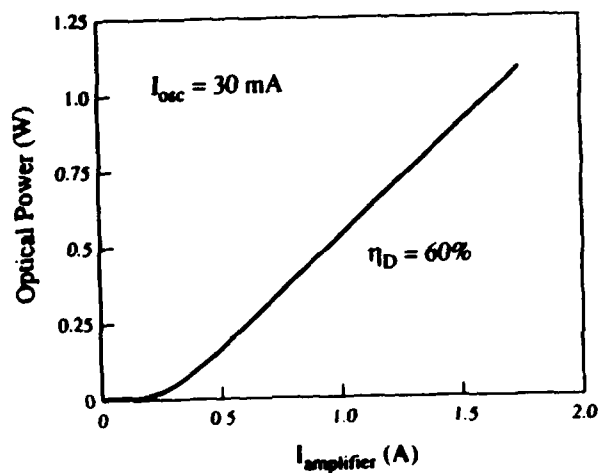


Figure 2:
Light output versus input
current to the amplifier.

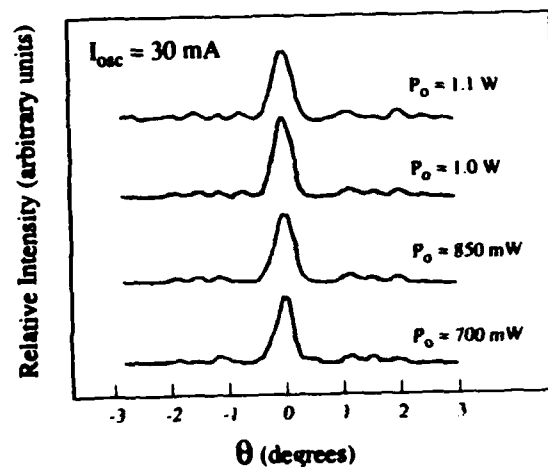


Figure 3:
Far field from the MOPA.

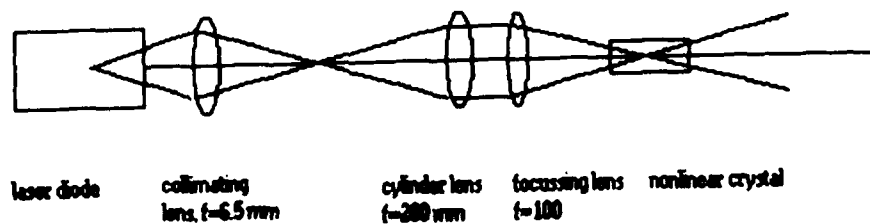


Figure 4:
Schematic diagram of
the experimental set up.

Low Threshold Quasi-Three-Level 946nm Laser Operation of an Epitaxially Grown Nd:YAG Waveguide

D.C.Hanna, A.C.Large, D.P.Shepherd, and A.C.Tropper
Department of Physics and Optoelectronics Research Centre
University of Southampton
Southampton SO9 5NH, U.K.
Tel +44 703 595000
Fax +44 703 585813

I.Chartier, B.Ferrand, and D.Pelenc
Laboratoire d'Electronique de Technologie et d'Instrumentation
Department Optronique
Commissariat à l'Energie Atomique
Centre d'Etudes Nucleaires de Grenoble
85X 38041 Grenoble Cedex, France
Tel +33 76884047
Fax +33 76885157

Summary

There has recently been much work on fabricating waveguide lasers based on crystal hosts by methods such as crystal fibre growth¹, ion-exchange², in-diffusion³, ion-implantation⁴, and epitaxial growth⁵. Despite the confinement of pump and signal beams to a few microns spot size, in general these lasers have not shown a clear advantage over bulk lasers in terms of thresholds due to propagation losses of the order of 0.1dB/cm or higher. Here we identify laser systems in which crystal waveguides will show great advantages over bulk lasers, namely 3 level and quasi-3 level transitions, and as an example describe the low threshold operation of a 946nm Nd:YAG epitaxial waveguide laser. The extra cavity loss arising from using a waveguide is less significant in (quasi-) three level systems as re-absorption loss from the lower laser level is present.

There has been much interest in the laser operation of the 946nm ${}^4F_{3/2}$ - ${}^4I_{9/2}$ transition in Nd:YAG⁶⁻⁸ as a means to obtaining a diode pumped blue laser source (after frequency doubling). One of the problems associated with this transition is that the lower laser level is the upper 857cm⁻¹ crystal field component of the ground state manifold containing 0.7% of the population at room temperature. Here we report a waveguide laser that despite only having confinement in one direction and a laser transition which only has a relatively small percentage of the population in the lower laser level still shows thresholds lower than those achieved in equivalent bulk systems. The prospects for operation of other (quasi-) three level systems are also discussed.

We have recently reported that Nd:YAG waveguides can be fabricated by liquid phase epitaxial growth of Nd:YAG layers on pure YAG substrates, followed by the growth of a pure YAG cladding layer⁵. Such waveguides exhibit very low loss for a crystal waveguide

($\leq 0.05\text{dB/cm}$) but rely purely on the Nd doping to achieve the refractive index difference required for guidance. In order to take full advantage of the waveguide geometry, guides of just a few microns width should be fabricated but this requires a larger index difference than can be produced by 1at. % Nd doping alone. The mixed crystal $\text{Y}_3(\text{Al}_{1-x}\text{Ga}_x)_5\text{O}_{12}$ is known to maintain the garnet crystal structure while having a controllably higher refractive index⁹. We report here for the first time the demonstration of a waveguide laser using the enhanced index difference caused by Ga doping. The waveguide described in this experiment has an active layer co-doped with 12at. % Ga, and 35at. % Lu (which compensates for the size mis-match between Ga and Al), increasing the refractive index difference to 1.4×10^{-2} (at 633nm). This guide has two modes for both TM and TE polarisations at 946nm with a calculated fundamental mode spot size ($1/e^2$ half-width of intensity) of $2.0\mu\text{m}$.

The laser thresholds observed when operating Ga,Lu,Nd doped guides of various widths at $1.064\mu\text{m}$ indicated losses of 0.1-0.2 dB/cm, taking into account the fact that the stimulated emission cross-section at $1.064\mu\text{m}$ is reduced by a factor of two at this doping level⁹. Despite the somewhat increased propagation loss and the reduced stimulated emission cross-section, the fact that smaller spot sizes can be produced by these guides meant that the $1.064\mu\text{m}$ threshold for a $3.8\mu\text{m}$ width guide (propagation loss 0.15dB/cm) is similar to that found in the original waveguides⁵ and that the expected threshold at 946nm is lower for these guides because the propagation loss is less significant for the quasi-three level system.

For the experiment described here a cladded, $3.8\mu\text{m}$ active layer thickness guide was end polished to a length of 0.95mm to allow longitudinal pumping by an R6G dye laser at 588nm. This was slightly shorter than intended as only $\sim 45\%$ of the pump light was absorbed in a single pass. Thus the incident threshold power will not be the optimum value which would occur when the guide length was nearer to an absorption length. The laser cavity was formed by butting two thin light-weight mirrors against the polished end faces. These mirrors were held in place by the surface tension of a drop of fluorinated liquid although, in future, direct coating of the end faces would be preferred. The mirrors were highly reflecting at 946nm and had 81 % transmission at 588nm. No attempt was made to feedback the unabsorbed pump light as we were interested in directly comparing our results to a similar experimental set up with bulk lasers⁶. The mirrors had $\sim 95\%$ transmission at $1.064\mu\text{m}$ to avoid oscillation at this wavelength. The pump light was end-launched using a X10 microscope objective forming a $\sim 2\mu\text{m}$ circular waist at the input face.

Laser oscillation at 946nm was observed at a power incident on the input mirror of 4.0mW. Taking into account the mirror transmission and subtracting the pump power observed to emerge from the output end (due to less than 100% absorption and launch efficiency) we calculated an absorbed power threshold of 1.2mW. The output, observed with a CCD camera and image analyser (Big Sky Software Corporation beamview analyser), was single mode in both the guided and unguided planes with measured spot sizes of $\sim 2\mu\text{m}$ and $\sim 35\mu\text{m}$ respectively. This result compares favourably to the bulk laser result of Fan and Byer⁶ who found an incident power threshold of $\sim 5.7\text{mW}$ despite having a better optimised length crystal and using a more favourable pumping wavelength (808nm). Using the measured spot sizes and propagation loss,

and using standard Nd:YAG material constants, we calculated an absorbed power threshold of 0.9mW. The small discrepancy between this value and the experimentally observed value of 1.2mW may be due to some reduction in the 946nm stimulated emission cross-section from that of standard Nd:YAG, as has been observed at $1.064\mu\text{m}^9$. The same calculations suggest that if channel waveguides could be fabricated, perhaps by ion-implanting low refractive index side walls or by etching, without greatly increasing the loss from the current level of 0.15dB/cm then thresholds of $<100\mu\text{W}$ should be achieved. Further improvements could be made by choosing an output mirror that strongly reflects the unabsorbed pump light or using a cavity that resonates a single frequency pump source⁸.

The prospects for low threshold operation of waveguide lasers in other (quasi-) three level system is also most promising. For example the $1.03\mu\text{m}$ laser transition in Yb:YAG terminates at 613cm^{-1} in the ground state manifold and has $\sim 5\%$ of the population in the lower laser level. Using the material constants quoted in ref.12 and similar spot sizes and losses to the guide used in this experiment we would predict an absorbed power threshold of $\sim 4\text{mW}$ for a 1.65mm long crystal and a 10% output coupler. This is to be compared with an experimentally observed bulk laser threshold of 71mW¹⁰. Other well known transitions such as the $\sim 2\mu\text{m}$ line of Ho^{3+} ^{11,12} and the $\sim 1.6\mu\text{m}$ of Er^{3+} ¹³ are equally promising, as are a number of other transitions not normally considered for bulk lasers because of their highly 3-level nature.

References

1. M. J. F. Digonnet, C. J. Gaeta, D. O'Meara, and H. J. Shaw, IEEE J. Lightwave Technol. **LT-5**, 642 (1987).
2. E. Lallier, J. P. Pochelle, M. Papuchon, M. P. De Micheli, M. J. Li, Q. He, D. B. Ostrowsky, C. Grezes-Besset, and E. Pelletier, IEEE J. Quantum Electron. **Qe-27**, 618 (1991).
3. R. Brinkmann, W. Sohler, and H. Suche, Electron. Lett. **27**, 415 (1991).
4. S. J. Field, D. C. Hanna, A. C. Large, D. P. Shepherd, A. C. Tropper, P. J. Chandler, P. D. Townsend, and L. Zhang, Electron. Lett. **27**, 2375 (1991).
5. I. Chartier, B. Ferrand, D. Pelenc, S. J. Field, D. C. Hanna, A. C. Large, D. P. Shepherd, and A. C. Tropper, Opt. Lett. **17**, 810 (1992).
6. T. Y. Fan and R. L. Byer, Opt. Lett. **12**, 809 (1987).
7. W. P. Risk and W. Lenth, Opt. Lett. **12**, 993 (1987).
8. J. P. Cuthbertson and G. J. Dixon, Opt. Lett. **16**, 396 (1991).
9. R. K. Watts and W. C. Holton, J. Appl. Phys. **45**, 873 (1974).
10. P. Lacovara, H. K. Choi, C. A. Wang, R. L. Aggarwal, and T. Y. Fan, Opt. Lett. **16**, 1089 (1991).
11. R. Allen, L. Esterowitz, L. Goldberg, J. F. Weller, and M. Storm, Electron. Lett. **22**, 947 (1986).
12. T. Y. Fan, G. Huber, R. L. Byer, and P. Mitzscherlich, Opt. Lett. **12**, 678 (1987).
13. E. W. Duczynski, G. Huber, K. Petermann, and H. Strange, in *Digest of Topical Meeting on Tunable Solid State Lasers* (Optical Society of America, Washington, D.C., 1987), p.197.

Wednesday, February 3, 1993

Joint Session on Upconversion Lasers

JWE 4:15pm–5:30pm
La Salle Ballroom B&C

Bruce Chai, *Presider*
University of Central Florida

Upconversion Fiber Lasers

Stephen G. Grubb
AT&T Bell Laboratories
PO Box 636
Murray Hill, NJ 07974-0636
(908) 582-2678

Over the past two years, the uniform, high-intensity pumping advantages of the single-mode fiber geometry have been realized in demonstrating several new visible upconversion laser transitions. To date 11 different CW, room-temperature visible upconversion laser/pumping combinations have been demonstrated with visible laser powers of up to 200 mW. Perhaps the most dramatic demonstration of an upconversion laser to date was the CW, room-temperature operation of a Pr^{3+} -doped ZBLAN fiber at 5 visible wavelengths¹. An additional advantage of the fiber geometry for upconversion lasers is that the fiber laser is the only laser geometry where the pump spot size and resonator length are decoupled. This extra degree of freedom is extremely important in the upconversion process where the ground-state absorption (GSA) and one or more excited-state absorptions (ESA) must be balanced in order to efficiently populate the upper laser level. For example, the three-photon pumped Tm^{3+} upconversion laser discussed in this paper would not be possible in a Tm^{3+} -doped crystal due to the extremely weak GSA. The long resonator lengths possible in fiber lasers also allow the minimization of concentration quenching effects while distributing the absorption to facilitate heat removal.

Visible laser emission has been demonstrated in Tm^{3+} , Ho^{3+} , Er^{3+} and Pr^{3+} -doped ZBLAN fibers via 2 photon pumping schemes. Blue upconversion fiber lasers have been demonstrated in both Tm^{3+} and Pr^{3+} -doped ZBLAN fibers, but the Tm^{3+} version required pumping with two different visible wavelengths and operation at 77 K², while the Pr^{3+} fiber laser required the use of two widely spaced infrared wavelengths. Recently we reported the first single-wavelength pumped, CW, room-temperature blue upconversion laser in a Tm^{3+} -doped ZBLAN fiber using a 3 photon pumping scheme, as shown in Figure 1. The pump source was a Nd:YAG laser operating in the 1.12 μm spectral region. A lasing threshold of 25 mW of absorbed pump and a slope efficiency of 32% versus absorbed pump power has been observed up to a maximum output power of 57 mW at 480 nm. Lasing on the red laser transition ($^1\text{G}_4 \rightarrow ^3\text{F}_4$) has also been observed at 650 nm in a Tm/Yb co-doped ZBLAN fiber. We were not able to achieve red lasing in the Tm^{3+} only doped ZBLAN fiber. We hypothesize that Yb^{3+} is necessary to depopulate the lower $^3\text{F}_4$ level, which is typically a self-terminating laser transition.

Recent results with fiber lasers suggest that the output power should be scalable to very high output powers. A diode pumped 1123 nm Nd:YAG laser was constructed and used as the fiber laser pump source which led to a blue laser output power of 35 mW. High power diode laser- pumped single-mode fiber lasers are generally a problem due to the requirement that the pump sources be diffraction limited. The diode-pumped solid state laser functions as a brightness converter and readily allows the power scaling of the fiber laser output with

increasing pump array power. A Nd:YAG pumped Yb^{3+} fiber laser operating at $1.12\ \mu\text{m}$ has also been used as a pump source for a Tm^{3+} blue upconversion fiber laser. ⁴

We have obtained ESA spectra of both Tm^{3+} -doped fluoride and oxide fibers following excitation into the $^3\text{H}_4$ state at 785 nm. The ratio of white light absorption of the fibers (pumped/unpumped) is shown in Figure 3. Values above 1 are regions dominated by excited state absorption, while values below 1 are regions of predominately GSA. The fluoride fiber exhibits ESA peaks at approximately 1060 and 1130 nm. The oxide fiber exhibits only a single peak at 1075 nm presumably due to the extremely short lifetime of the $^3\text{H}_4$ state in an oxide host. The efficiency of blue laser operation versus pump wavelength is an extremely sharp function. In spite of the existence of strong ESA at 1064 nm, we have not been able to observe blue upconversion lasing when pumped with over 1 Watt of power with a Nd:YAG laser at 1064 nm due to the lack of sufficient GSA. At 1100 nm we observed lasing, but the threshold was several hundred milliwatts of absorbed power. The laser threshold drops to 25 mW at 1123 nm. A more complete wavelength dependence is difficult to obtain due to the lack of tunable CW laser sources in this spectral region.

This work was performed while the author was employed by the Amoco Technology Company.

References:

1. Smart, R.G., Hanna, D.C. Tropper, A.C., Davey, S.T., Carter, S.F. and Szebesta, D., "CW Room-Temperature upconversion lasing at blue, green, and red wavelengths in infrared-pumped Pr^{3+} -doped fluoride fibre", *Electron. Lett.*, 1991, **27**, pp. 1307-1308.
2. Allain, J.Y., Monerie, M., and Poignant, H., "Blue upconversion fluorozirconate fibre laser", *Electron. Lett.*, 1990, **26**, pp. 166-167.
3. Grubb, S.G., Bennett, K.W., Cannon, R.S., and Humer, W.F., "CW room-temperature blue upconversion fibre laser", *Electron. Lett.*, 1992, **28**, pp. 1243-1244.
4. Hanna, D.C. et. al., submitted to *Electronics Letters*.

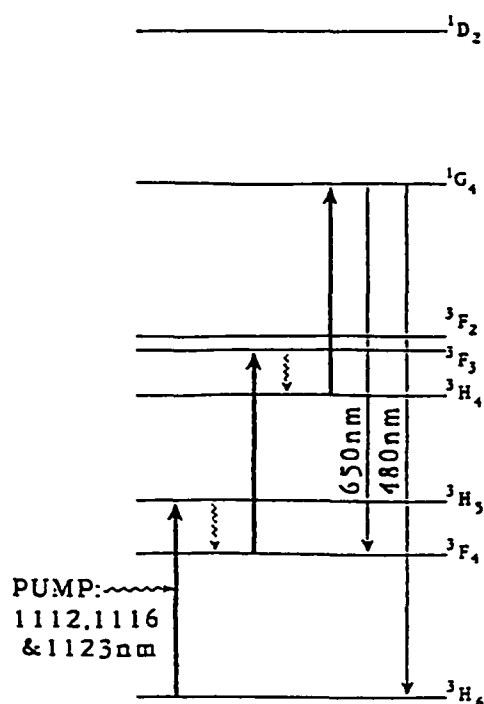


Figure 1: Energy level diagram of Tm^{3+} showing upconversion laser pumping scheme

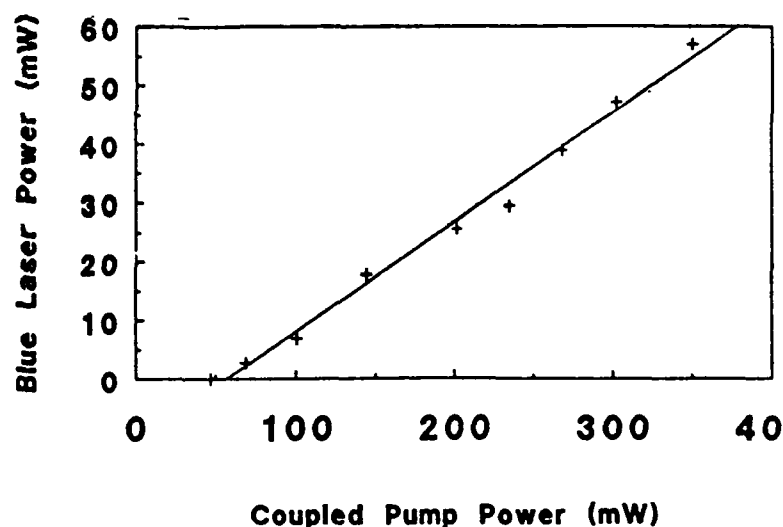


Figure 2: Laser characteristic for 1.12 μm pumped Tm^{3+} blue upconversion fiber laser

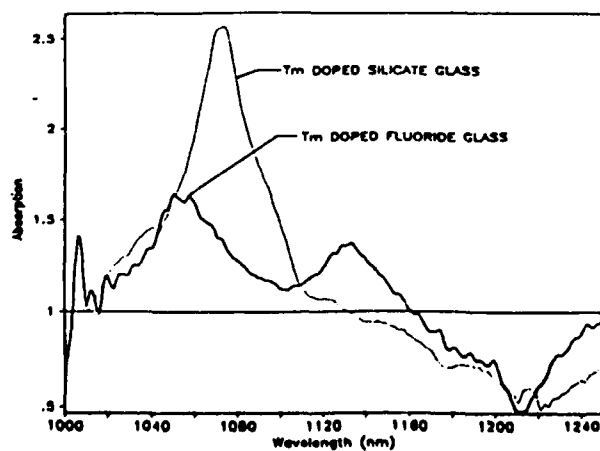


Figure 3: Excited state absorption spectra of Tm^{3+} -doped silica and fluoride (ZBLAN) fibers

Ho-Yb fluoride glass fiber for green lasers

A. Shikida, H. Yanagita and H. Toratani

Materials Research Laboratory

HOYA Corporation

3-3-1 Musashino, Akishima, Tokyo 196, Japan

Phone +81(425)46-2748

Ho^{3+} upconversion emission at 543nm ($^5\text{S}_2$ - $^5\text{I}_8$) is a potential candidate for realizing a red-diode pumped green laser. However, this emission is of three-level system, so that lower doping is needed to achieve lower lasing threshold. A long, low loss single mode fiber is usually adopted for this type of laser to obtain a sufficient pump absorption without much cavity loss [1]. To make a compact device, it is necessary to increase the pump absorption efficiency. Yb has been known as an effective sensitizer for Ho in many crystals when the diode emitting around 980nm is used for excitation [2]. We report effects of host glass composition and Yb sensitizer concentration on the Ho green upconversion emission and the pump power dependence of the excited population density for fiber lasers.

Glasses were prepared by melting fluorides mixture in a glassy carbon crucible under Ar/ Cl_2 gas atmosphere which was followed by quenching and annealing. Samples for spectroscopic property measurements were cut and polished to the size of 23x12x3mm. The host glass compositions (Table1) were chosen in order to see effect of the phonon frequency on the emission. The multiphonon decay rate is given by [3]

$$W_{\text{MPR}} = W(0) \exp(-\alpha \Delta E / \hbar \omega) \quad (1)$$

where $W(0)$ is the decay rate at zero energy gap, α is a parameter including the electron-phonon coupling constant, ΔE is the energy gap between emitting level and next lower level (3030cm^{-1}) and $\omega/2\pi$ is the effective phonon frequency. The phonon frequency becomes larger in the sequence ZBLAN, AZF and AYZ (Table2).

We observed that the upconversion emissions at 410, 545, 670nm of Er system were stronger for ZBLAN than for AZF while the spontaneous emission probability was nearly the same for these glasses (Table 3). It indicates that these emissions are primarily governed by the multiphonon decay of the emitting level. The upconversion excitation occurs through the resonant energy transfer in which no phonon plays a role.

On the other hand, ZBLAN has a lower upconversion emission efficiency than AZF and AYZ in Ho-Yb system. The Stokes emission intensity with the 485nm excitation is increased with decreasing effective phonon frequency of glasses, which suggests that the multiphonon decay of $^5\text{S}_2$ level affects the emission efficiency. However, in the upconversion emission a

reverse trend is observed. Since the energy transfer from $^2F_{5/2}$ state of Yb^{3+} to 5I_6 state of Ho^{3+} is phonon-assisted (energy gap is about 1540cm^{-1}), the transfer efficiency is largely affected by the phonon frequency of the host glass [3]:

$$W_{\text{ET}} = W_0 \exp(-\beta \Delta E / \hbar \omega) \quad (2)$$

where W_{ET} is the nonresonant transfer rate, W_0 is the resonant transfer rate, β is a parameter similar to α but nearly half the value, $\omega/2\pi$ is the effective phonon frequency and ΔE is the energy gap between the donor and the acceptor levels. Actually the energy transfer efficiency in Yb-Ho estimated from the fluorescence lifetime measurement is about 0.52 in AZF, which is much higher than 0.33 in ZBLAN. This is due to the phonon frequency in AZF higher than ZBLAN. The upconversion emission intensity seems to be predominantly determined by the energy transfer efficiency in the excitation process in Yb-Ho system. On the other hand, the multiphonon decay probability from the emitting level in the emission process increases with the increasing of the phonon frequency. Therefore, there should be some appropriate phonon frequencies which enhance the energy transfer but still suppress the multiphonon decay. In this work we chose AZF as a host glass.

The dependencies of the emission intensity on sensitizer (Yb) and the activator (Ho) concentrations are shown in Fig.1. Maxima are observed at about 6mol% YbF_3 for both 0.1mol% and 0.5mol% HoF_3 concentrations. Keeping YbF_3 concentration constant at 6mol%, the maximum emission was obtained around 0.1mol% HoF_3 . To reduce the threshold for population inversion, Ho concentration is preferred to be as low as possible. Therefore, we employed a glass containing 0.05mol% HoF_3 and 6mol% YbF_3 for the lasing experiment. The fiber is a core diameter of $13\mu\text{m}$, NA of 0.17 and loss of 4dB/m at 514.5nm.

Using this fiber, the population density of lasing level was measured as a function of pump power. The experimental setup is shown in Fig.2. A Ti:Sapphire laser was employed as a pump laser and an Ar ion laser (543.5nm) as a probe laser. Comparing the transmitted power of the probe beam through a 5mm fiber with or without pumping, the threshold pump power for the population inversion was estimated to be about 14mW in the 975nm excitation. We observed that the 420nm fluorescence from 5G_4 level increases with pump power: It depends on the pump power cubic, while the 543nm fluorescence depends quadratically. It suggests that the upconversion from 5S_2 to higher energy levels takes place which may suppress the 5S_2 population build-up. For a longer fiber (96mm), the 5S_2 population saturates before reaching the inversion. The optical length for 90% pump absorption is less than 5mm, therefore the rest of the fiber simply acts as an absorbed medium for the emission. This is why the population inversion was never achieved for the longer fiber.

The lasing experiment is on the way. The results for this fiber as well as single mode fibers with a double clad structure to improve pumping efficiency will be given.

References:

- [1] J.Y.Allain, M.Monerie and H.Poignant : Electron. Lett. 26, 262 (1990)
- [2] L.Esterowitz, J.Noonam and J.Bahler : Appl.Phys.Lett. 10, 126 (1967)
- [3] T.Miyakawa and D.L.Dexter : Phys.Rev. B1, 2961 (1970)

Table 1. Glass compositions.

ZBLAN	53.0ZrF ₄ - 20.0BaF ₂ - 1.62LaF ₃ - 3.0AlF ₃ - 20.0NaF - 0.11HoF ₃ - 2.27YbF ₃
AZF	25.1AlF ₃ - 12.8ZrF ₄ - 9.1YF ₃ - 3.7MgF - 15.4CaF ₂ - 13.6SrF ₂ - 12.6BaF ₂ - 2.8NaF - 2.8NaCl - 0.1HoF ₃ - 2.0YbF ₃
AYF	36.0AlF ₃ - 12.13YF ₃ - 8.3MgF - 25.0CaF ₂ - 8.3SrF ₂ - 8.3BaF ₂ - 0.09HoF ₃ - 1.88YbF ₃

Ho³⁺ of 2.08X10¹⁹ ions/cc and Yb³⁺ of 4.15X10²⁰ ions/cc were doped in all of the above glasses.

Table 2. Comparison of upconversion emission between ZBLAN and AZF.

glass	phonon* energy(cm ⁻¹)	upconversion emission	Stokes emission	energy transfer efficiency 1- (τ ₁ / τ ₂)**
ZBLAN	506	5.7	24.5	0.33
AZF	625	9.1	24	0.52
AYF	630	8.5	17	0.41

* : estimated by FTIR

** : τ₁ is the lifetime in Ho³⁺-Yb³⁺ codoped samples, and τ₂ is in the Yb³⁺ single doped samples.

Table 3. Comparison of upconversion emission between ZBLAN and AZF.

	Er ³⁺ blue(410nm)	green(545nm)	red(670nm)	Ho ³⁺ -Yb ³⁺ green(541nm)
emission intensity ratio (ZBLAN / AZF)	1.17	1.32	1.12	0.62

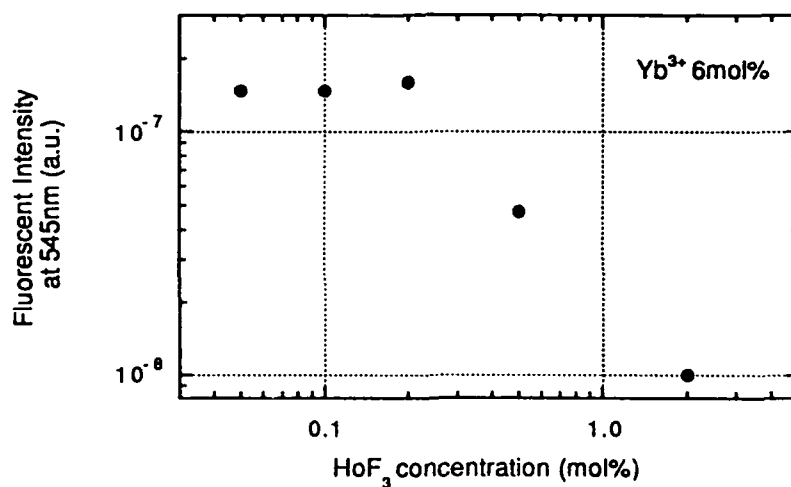
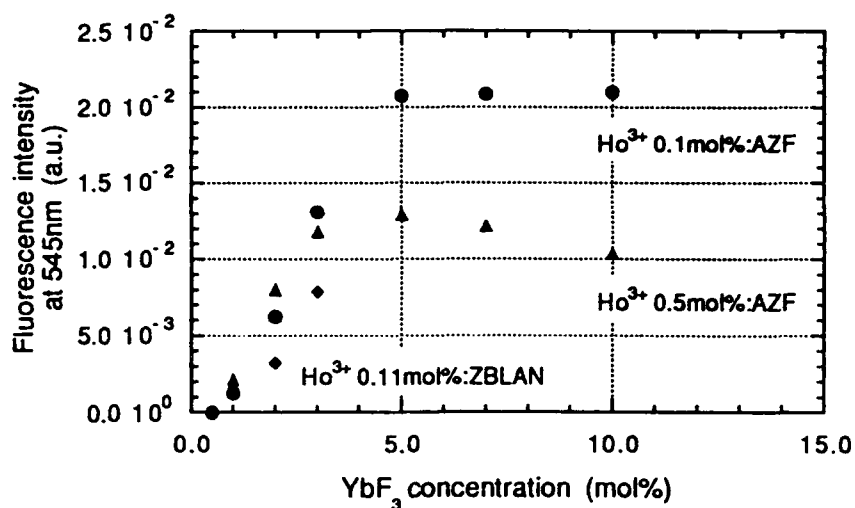


Fig. 1 Dependencies of the emission intensity of sensitizer(Yb) and activator(Ho) concentrations.

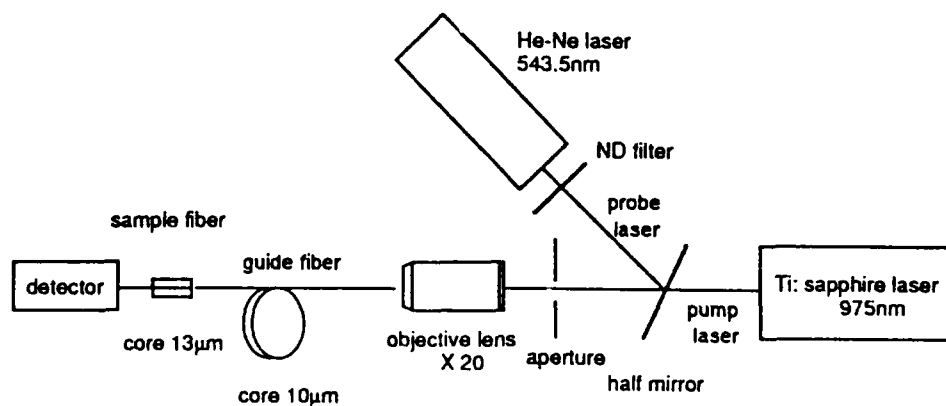


Fig. 2 Schematic diagram of experimental setup for evaluating population inversion.

COOPERATIVE ENERGY TRANSFER IN A Yb-Pr DOPED ZBLAN FIBER

A.Remillieux, B.Jacquier and H.Poignant*

U.R.A. 442 du C.N.R.S. UNIVERSITE LYON

43 Boulevard du 11 Novembre 1918

69622 Villeurbanne Cédex FRANCE

Phone number 33 72 44 83 36

Upconversion pumping of rare earth doped materials has been extensively studied over the two past decades. Most of mechanisms for converting infrared radiation to short wavelength output are quite well known and relative strengths of these processes have already been reported in bulk materials [1]. However, due to length of interaction of laser light with luminescent centers in a fiber, Excited State Absorption (E.S.A.) can dominate the Addition of Photons by Energy Transfer (so-called A.P.T.E.). This is mainly true because of low doping of fibers. Such low concentration is required to prevent from clustering or aggregation which causes losses along the fiber.

Recently, CW room temperature red upconversion laser actions have been reported in a Yb³⁺ sensitized Pr³⁺ ZBLAN fiber pumped at 850 nm [2]. Absorption of a first photon into the phonon sideband of Yb³⁺ ion absorption band is followed by fast non radiative relaxation to its lowest excited state (²F_{5/2}(1)) and non radiative energy transfer to the ¹G₄ state of Pr³⁺ ions, then a second photon of the same frequency is absorbed to promote Pr³⁺ ions into the ³P₁ or ¹I₆ states (figure 1 and table 1). This was probed by recording the excitation spectrum of the ³P₀ blue fluorescence [3].

Experiments reported here have been performed with the same co-doped ZBLAN fluoride fiber used in ref.2 (2% Yb³⁺ and 0.1% Pr³⁺), experimental techniques have already been presented elsewhere.

* LAB-OCM C.N.E.T. BP 40, 22301 Lannion FRANCE

Under pulsed laser excitation, blue upconversion fluorescence is only observed when Yb^{3+} ions are resonantly pumped into the Stark components of the $^2\text{F}_{5/2}$ state. Low temperature absorption data of table 1 indicate that there is no resonance between the photon energy and excited state absorption transitions $^1\text{G}_4 \rightarrow ^3\text{P}_j, ^1\text{I}_6$. Only the path is to note that the energy of $^3\text{P}_0$ is roughly two times the energy of the $^2\text{F}_{5/2(2)}$ Stark component of Yb^{3+} ions. Then two excited Yb^{3+} ions can transfer their energy to a single Pr^{3+} ion as a result of a cooperative energy transfer (figure 1). To probe this energy transfer mechanism, we have recorded fluorescence decays of various Stokes emissions of a low concentrated Pr^{3+} material under resonant excitation (see table 1 for the results).

The blue antistokes fluorescence decay pumped at 933 nm, represented in figure 2, exhibits an initial rise followed by a long decay, the full line represents the best fit with a biexponential law, the time constants being 22 μs and 404 μs respectively.

Enlargement of the short time part of figure 2 shows that no feeding of the $^3\text{P}_0$ state occurs during the pulse which, again, rules out an E.S.A. process via the $^1\text{G}_4$ state. The rate equation model predicts a similar profile assuming a single exponential decay of donor ions (Yb^{3+}). However, the adjusted time constants does not fully verify the lifetimes $\tau(^3\text{P}_0)$ in the initial rise and $\tau(^2\text{F}_{5/2})/2$ in the long tail, reported in table 1, because of the two following reasons. The long tail of the $^3\text{P}_0$ fluorescence decay is affected by fast diffusion among Yb^{3+} ions and energy transfer between excited Yb^{3+} ions and the $^1\text{G}_4$ state of Pr^{3+} ions. The initial rise is shortened due to back transfer from Pr^{3+} ions in the $^3\text{P}_0$ state and two ytterbium ions which has already been pointed out [4].

REFERENCES

- [1] F.Auzel in "Radiationless Processes" ed. by B.DiBartolo, Plenum Press p213 (1980)
- [2] J.Y.Allain,M.Monerie,H.Poignant Electron.Lett. Vol.27(13) p1156 (1991)
- [3] B.Jacquier,A.Remillieux,M.F.Joubert,P.Chritensen,H.Poignant to appear in J.of.NonCrystalline Solids
- [4] J.Y.Allain,M.Monerie,H.Poignant Electron.Lett. Vol.27(12) p1012 (1991)

Energy levels (identification)	Frequency ν (cm ⁻¹)	Lifetime τ (μs)
³ H ₅ Fluo 300 K	2200	
³ H ₆ Abs. 6 K	4284	
³ F ₂ Abs. 6 K	5155	
³ F ₃ Abs. 6 K	6553	
³ F ₄ Abs. 6 K	6964	
¹ G ₄ Abs. 6 K	9901	100
¹ D ₂ Abs. 6 K	17065	360
³ P ₀ Abs. 6 K	20964	46
³ P ₁ , ¹ I ₆ Abs. 6 K	21505	48
³ P ₂ Abs. 6 K	22719	
² F _{7/2} Fluo 4,5 K	155	
Fluo. 4,5 K	301	
Fluo 4,5 K	480	
² F _{5/2} Abs. 300 K	10250	1650
Abs. 300 K	10423	
Abs. 300 K	10719	

P R A S E O D Y M I U M

Y T T E R B I U M

Tableau 1. Positions and lifetimes of the energy levels of a co-doped Yb - Pr ZBLAN material.

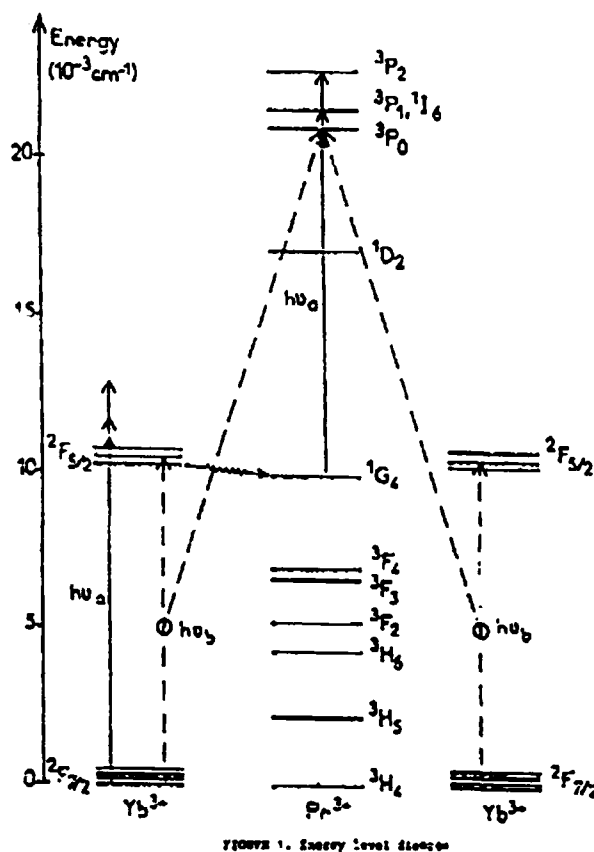
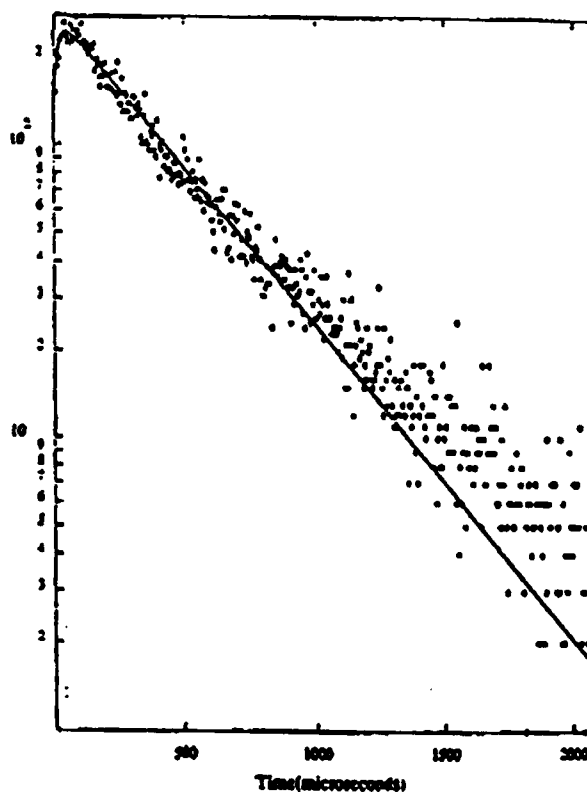


FIGURE 1. Energy level diagram



Photoluminescence decay curve of the ³P₀ state pumped at 933 nm with the best fit: $\tau_{\text{fast}}(1) = 22$ microseconds, $\tau_{\text{slow}}(2) = 404$ microseconds

FIGURE 2

Near Infrared Pumped ZnSe and ZnSSe Blue Lasers

X.H. Yang, W. Shan, J.M. Hays, and J.J. Song

Center for Laser Research and Department of Physics, Oklahoma State University,
Stillwater, Oklahoma 74078

Tel: (405)744-5809

ZnSe and ZnSe-based materials are receiving a great deal of attention for their potential blue opto-electronic applications.^{1,2} We have previously reported observations of room temperature blue laser oscillations from ZnSe and ZnSSe single crystals employing the above-the-band-gap one-photon pumping method.^{3,4} Here we report our recent study of blue laser action in these crystals where optical pumping was achieved via two-photon transitions. In particular, we have used near-infrared (~850 nm) excitation with two photon energies in the vicinity of the fundamental energy gaps in these wide gap materials.

Lasing was observed at 446 nm from ZnSe, and 438 nm from $\text{ZnS}_{0.05}\text{Se}_{0.95}$ at 10 K. These lasing peak positions are approximately the same as those for the one-photon pumping case. An increased blue shift is expected in $\text{ZnS}_x\text{Se}_{1-x}$ with greater concentrations of sulfur. Strong blue laser emission was observable to the naked eye even at 200 K. With an increase in temperature, the lasing peak position was found to shift to lower energies at a faster rate than the band gap change. At 180 K, the lasing occurred at 460 nm in ZnSe, and the energy position decreased by 85 meV corresponding to an about 50 meV decrease in the band gap.

The ZnSe and $\text{ZnS}_{0.05}\text{Se}_{0.95}$ samples used in this work were single crystals grown by seeded physical vapor-phase transport (SPVT) technique. Small bar-like samples with cavity length 300-500 μm were cleaved from mechanically polished, and then chemically etched wafers. The parallel cleaved sample edge facets form a laser cavity with no optical coating necessary. The optical pumping source used in this work was a tunable pulsed dye laser pumped by the second harmonic of a Nd:YAG laser (10Hz, 10nsec). Experimental configurations are similar to those in refs. 3 and 4.

Figure 1 shows the emission spectra of ZnSe taken at three different excitation intensities. The pumping wavelength was 830 nm. Essentially the same spectra were measured in $\text{ZnS}_{0.05}\text{Se}_{0.95}$ except that the emission peaks shift to higher energies due to the alloying effect. The lasing threshold was found to be $\sim 16 \text{ MW/cm}^2$ in ZnSe. In Figure 2, we show the laser emission intensity versus the excitation power density for the same sample used for Figure 1. As the sample temperature increases from 10 to 200 K, the lasing threshold increases only about a factor 3, and the emission linewidth changes from ~ 5 to 7.5 meV. We have also studied the pumping wavelength dependence by tuning the near infrared dye laser. The lasing was observed from ZnSe in the pump wavelength from 830 nm to ~ 867 nm. Since these wavelengths are readily accessible with commercial GaAs-based compact diode lasers, our work demonstrates the feasibility of packaging very compact blue lasers. Furthermore, ZnSe-based materials can be grown on top of GaAs substrates using thin film growth methods such as MBE. Therefore, our work suggests the exciting possibility of monolithically integrating ZnSe-based devices with GaAs-based laser devices. The work presented here can also be extended to

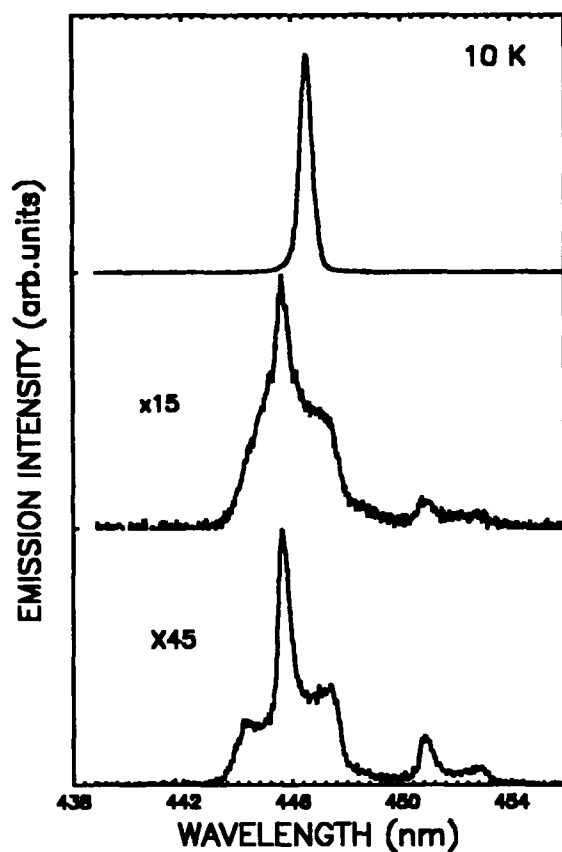


Fig.1 Emission spectra of a ZnSe sample with 430 μm cavity length taken at 10 K under different excitation densities. The pumping wavelength is 830 nm.

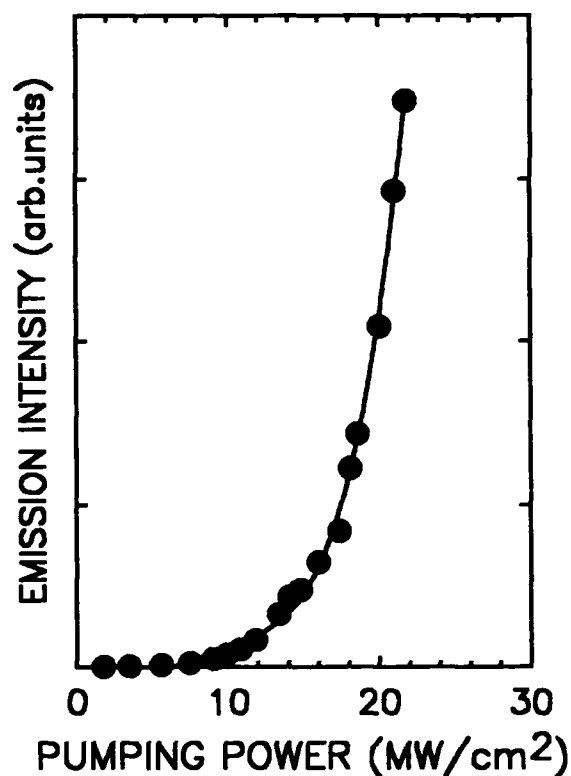


Fig.2 Dependence of the ZnSe laser emission intensity on the excitation power density.

heterostructures such as ZnSe/ZnSSe, ZnSe/ZnCdSe quantum wells.

1. R.A. Reynolds, J. Vac. Sci. Technol. A7, 269(1989).
2. R.N. Bhargava, J. Cryst. Growth, 86, 873(1988).
3. X.H. Yang, J.M. Hays, W. Shan, J.J. Song, E. Cantwell, and J. Aldridge, Appl. Phys. Lett. 59, 1681(1991).
4. X.H. Yang, J.M. Hays, W. Shan, J.J. Song, E. Cantwell, and J. Aldridge, Appl. Phys. Lett. 60, 926(1992).

Thursday, February 4, 1993

Frequency Upconversion in Waveguide Devices 1

CThA 8:30am–10:15am
Pelican Ballroom

Martin M. Fejer, *Presider*
Stanford University

Quasi-phasematched waveguides periodically poled by applying an external field for efficient SHG

M. Yamada, N. Nada, M. Saitoh, and K. Watanabe

Applied Magnetic Research Department
Corporate Research Laboratories
Sony Corporation

6-7-35, Kita-Shinagawa, Shinagawa-ku, Tokyo, 141, Japan
Phone: 81-3-3448-2547

The realization of a compact and low cost blue coherent light source is essential for high-density optical data storage, laser printing, and color display applications. So far laser-diode-based second-harmonic-generation (SHG) devices seems to be the most convenient way of making a violet or blue light sources. The conversion efficiency of quasi-phasematching (QPM) SHG is highest when the periodic reversal of the sign of the nonlinear coefficient d of the material occurs in the phasematching period[1]. The QPM-SHG allows the use of any component of the nonlinear susceptibility tensor, and by selecting the period of the sign inversion of the d coefficient, light with arbitrary wavelengths within the transparency range of the nonlinear materials can be generated. A high conversion efficiency QPM-SHG device has the following requirements: 1) it should be composed of materials with large nonlinear coefficients and good transparency, 2) its waveguide should have low loss with strong mode confinement, 3) a good overlap between the fundamental and the second harmonic field, and 4) the periodically inverted domain structure should be obtainable at any depth in the waveguide suitable for first order QPM. The last requirement, in particular, is most important for taking full advantage of the materials.

A variety of fabrication methods for ferroelectric domain inversion in numbers of materials have been reported such as 1) anisotropic diffusion of Ba ions for potassium titanyl phosphate (KTiOPO₄ or KTP)[2], 2) proton exchange and heat treatment below the Curie temperature for lithium tantalate (LiTaO₃)[3], 3) Ti in-diffusion [4] or Li₂O out-diffusion[5] near the Curie temperature for lithium niobate (LiNbO₃) and 4) electron beam bombardment at room temperature on the negative c-face of lithium niobate[6], and so on. In spite of the high nonlinear coefficient in lithium niobate, the conversion efficiency of the actual waveguide device previously has been lower than those of KTP and lithium tantalate[2,7]. This was mainly due to the fact that the indiffusion or outdiffusion technique previously used was only capable of creating the (nonideal) shallow triangular domain boundary which itself could only yield third order QPM thus dropping the effective conversion

efficiency substantially. In our research we have successfully developed a method to easily invert the ferroelectric domains of lithium niobate by applying an external electric field[8]. Using this method the spontaneous polarization of lithium niobate was inverted by applying a pulsed external field through a sample thin enough to prevent catastrophic electron avalanche damage. This method not only enables the fabrication of ideal laminar domain structures for first order QPM-SHG as shown in Fig. 1 but also has eliminated the propagation loss due to the periodical changes in the refractive indices. The device fabricated by this method allowed us to achieve a high power of $>20\text{mW}$ at the blue wavelengths and a high conversion efficiency of $> 600\%/W\text{-cm}^2$.

In this paper we will present current results about our QPM-SHG device fabricated by applying the external field method.

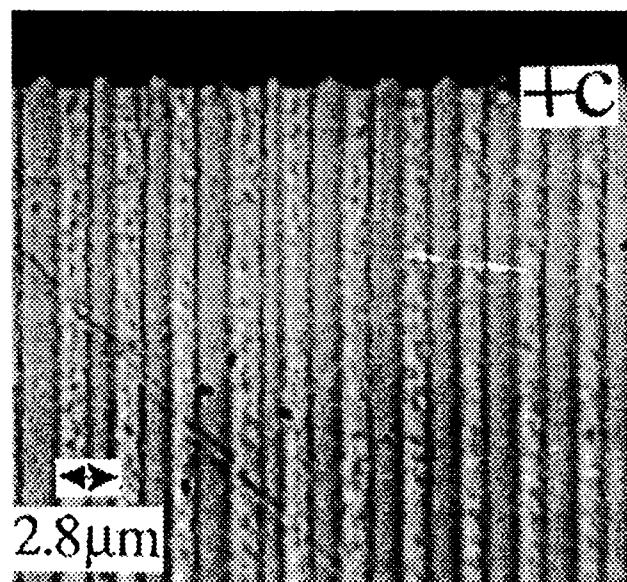


Fig. 1 The cross-section of the periodically inverted domain structure in lithium niobate fabricated by applying an external electric field.

References

- 1 J. A. Armstrong, N. Bloembergen, J. Ducuing, and P.S. Pershan, *Phys. Rev.*, **127**, 1918(1962)
- 2 C. J. van der Poel, J. D. Bierlein, J. D. Brown, and S. Colak, *Appl. Phys. Lett.*, **57**, 2074(1990)
- 3 K. Nakamura, and H. Shimizu, *Appl. Phys. Lett.* **56**, 1535(1990)
- 4 E. Lim, M. Fejer, and R. L. Byer, *Electron. Lett.*, **25**, 174(1989)
- 5 J. Webjorn, F. Laurell, and G. Arvidsson, *IEEE Photonics Technol. Lett.*, **1**, 316(1989)
- 6 M. Yamada, and K. Kishima, *Electron. Lett.*, **27**, 828(1991)
- 7 K. Yamamoto, K. Mizuuchi, and T. Taniuchi, *Opt. Lett.*, **16**, 1156(1991)
- 8 M. Yamada, N. Nada, and K. Watanabe, *Integrated Photonics Research Meeting*, April 1991, New Orleans

Linear and Nonlinear Optical Properties of Annealed Proton Exchanged LiNbO₃ Waveguides

M. L. Bortz, L. A. Eyres, and M. M. Fejer

E. L. Ginzton Laboratory
Stanford University
Stanford, California 94305
415-725-2282

Quasi-phasematched frequency conversion in LiNbO₃ waveguides is an efficient method for the generation of short wavelength radiation from infrared laser diodes. While many techniques are used to form the ferroelectric domain grating necessary for quasi-phasematching, waveguide confinement is usually provided by the annealed proton exchange (APE) process. The optical properties of APE waveguides are not well understood and accurate models relating the modes of the waveguide to processing parameters are not available. Also, effects of the APE process on the nonlinear optical properties of LiNbO₃ have yet to be understood. In this presentation we discuss two sets of experiments. First, we report a nonlinear diffusion coefficient for protons in LiNbO₃ and the relationship between concentration and index change, which allow a quantitative prediction of the modes of APE waveguides.¹ Second, we report depth profiling of the d₃₃ nonlinear coefficient in proton exchanged (PE)² and APE waveguides which, in conjunction with the optical modes, allows accurate calculation of the overlap integrals and normalized conversion efficiencies for guided wave nonlinear optical interactions. These models make possible the optimization of APE waveguides for maximum normalized conversion efficiency, noncritical phasematching, or efficient coupling to a laser diode for any guided wave nonlinear optical interaction.

To understand the properties of channel APE waveguides, studies were performed on planar waveguides on both x and z-cut LiNbO₃. PE-LiNbO₃ waveguides fabricated in benzoic acid had abrupt step-like refractive index and H⁺ concentration profiles with depths (d_e) determined from the literature.³ Exchange temperatures and depths varied from 160 °C to 220 °C and 0.15 to 0.8 μm, respectively. Annealing was performed at 333 °C for times (t_a) ranging from 1 to 40 hrs. Prism coupling was used to obtain the mode indices and inversion of the mode indices to obtain refractive index profiles was performed using two techniques⁴ which produced similar results for the surface index change (Δn_a) and 1/e depth (d_a) of the profiles. When normalized to d_e, the area under the index profiles was constant to within several percent, indicating a near-linear relationship between concentration and index change. To analyze the data we introduce the following normalized variables: a normalized diffusion time $\tau = t_a/d_e^2$, a normalized surface index change $\Delta n_a/\Delta n_e$ (where Δn_e is the surface index change prior to annealing), and a normalized waveguide depth d_a/d_e. Shown as data points in Figure 1 are Δn_a/Δn_e and d_a/d_e vs $\sqrt{\tau}$ for x and z-cut LiNbO₃ waveguides. The dashed lines show the results assuming linear diffusion theory with D₀ = 0.55 μm²/hr, the asymptotic limit observed in our data, and a linear relationship between index change and concentration. Clearly this modeling approach is insufficient to predict the properties of APE waveguides. That the data fall on a single line indicates that over the range of fabrication parameters investigated, the APE process may be modeled by the diffusion equation; however, a concentration dependent diffusion coefficient must be used to reproduce the results. We have found empirically that $D(C) = D_0[(1-a) + a \cdot e^{-bC}]$ with a = 0.9, b = 12, and the concentration C = 1 corresponding to the initial PE condition, reproduces the data, as shown by the solid lines in Figure 1. This diffusion model and a linear relationship between index and concentration also accurately reproduce the shape of the experimental index profiles.¹

SIMS profiling of the H⁺ concentration was also performed on x-cut PE and APE LiNbO₃ waveguides. SIMS data, normalized for matrix effects, showed x = 0.7 in H_xLi_{1-x}NbO₃ prior to annealing, in good agreement with previous estimates.⁵ Shown in Figure 2 are SIMS H⁺ profiles of APE waveguides exchanged to 0.35 μm and annealed for 4, 8, and 16 hrs. The solid lines are the results of the nonlinear diffusion model. The absolute SIMS concentration is scaled to the calculated relative concentration (C = 1 for PE) using a constant that is independent of anneal time. No other free parameters are used to compare the SIMS profiles with the diffusion model derived from

the optical data. The model accurately reproduces the H^+ profile, which is substantially different from that predicted by linear diffusion theory, especially in the wings. In the presentation, this work will be compared with previously published models for the diffusion of protons and the index change vs. concentration in the $H_xLi_{1-x}NbO_3$ system.

The planar diffusion models for z and x-cut $LiNbO_3$ described above can be combined into a two-dimensional diffusion model for computation of the H^+ concentration profile and, with the dispersion data for Δn_e given in Ref. 1, the modes of channel APE waveguides. Even if the masking process used to delineate the channel waveguides affects the PE depth the annealing process will still be described by the above model, but the actual PE depth must be determined. The waveguide fabrication parameters necessary for achieving noncritical phase-matching or optimal coupling to a laser diode can then be determined. Practical aspects of the design of channel waveguides will be discussed in the presentation.

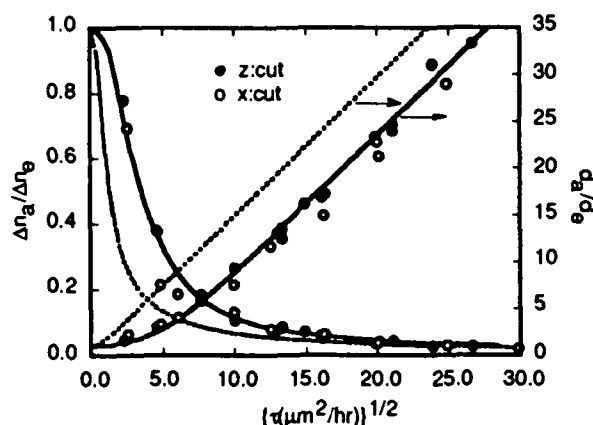


Figure 1. Normalized index change and waveguide depth vs. the normalized anneal time. The lines are described in the text.

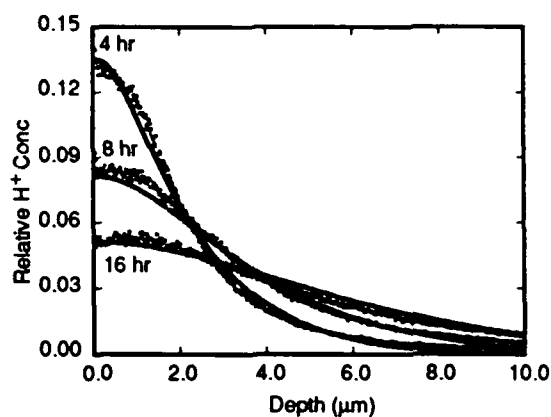


Figure 2. Comparison between H^+ SIMS profiles and the nonlinear diffusion model described in the text.

The nonlinear optical properties of PE and APE waveguides have been a source of controversy over the past several years.^{6,7} We have used reflection second harmonic generation (SHG) as a probe of the d_{33} nonlinear coefficient in both PE and APE- $LiNbO_3$. Since the PE- $LiNbO_3$ system has an abrupt boundary at the waveguide-substrate interface, it is well suited to reflection studies at wavelengths at which the crystal is transparent. Reflected SH fields are generated at the air-waveguide and the waveguide-substrate interface, and the interference between the two reflected second harmonic (SH) fields as a function of incident angle can be used to measure the d_{33} coefficient of the PE film. Comparison of the angular dependence of the total reflected 532 nm SH field with theory revealed that d_{33} of PE- $LiNbO_3$ is $< 1\%$ the bulk $LiNbO_3$ value.² This agrees with guided wave experiments which show that annealing is necessary to produce efficient frequency conversion.

Measurement of the d_{33} coefficient in APE waveguides is complicated by the graded refractive index profile and the unknown spatial variation in the d_{33} coefficient. The d_{33} coefficient of APE- $LiNbO_3$ was studied using depth resolved reflection SHG with a 532 nm fundamental and a 266 nm SH field. Since the SH wavelength is above the APE- $LiNbO_3$ band edge, only SH generated within the 50 nm⁷ absorption depth of the surface is observed in reflection. As shown in Figure 3, the sample was angle lapped to project depth into lateral position, with a wedge angle of < 2 mrad determined using surface profilometry. A depth resolution of < 0.05 μm was achieved by focussing the Q-switched 532 nm fundamental radiation, polarized along the z-axis, to a 20 μm diameter spot. The focussed spot was scanned across the surface and the reflected 266 nm SH was measured vs. lateral position and normalized to the signal from bulk $LiNbO_3$. Shown in Figure 4 is the normalized signal vs. depth for x-cut APE waveguides exchanged to 0.44 μm and annealed at 333 $^{\circ}C$ for 3, 5, and 9 hrs. The waveguide $1/e$ depths were approximately 0.9, 1.4, and 2.1 μm , respectively. For the 3 hr anneal no signal is observed within the original PE

depth, while an abrupt increase to near the bulk LiNbO_3 value occurs between 0.4 and 0.5 μm . This is in agreement with the 1064 nm to 532 nm reflection SHG experiment previously discussed. For increasing anneal times d_{33} vs. depth has a similar form, but the position at which the signal abruptly increases to the bulk value moves towards the surface. However, even for very long annealing times (> 60 hr) no reflected signal is observed from the actual surface. This is in agreement with previous experiments on unwedged APE- LiNbO_3 waveguides in which a reflected 266 nm signal was never observed, even after very long anneal times.⁷ The data show that the original PE waveguide has no d_{33} coefficient, but LiNbO_3 retains significant nonlinearity throughout the annealing process at depths greater than the original PE depth.

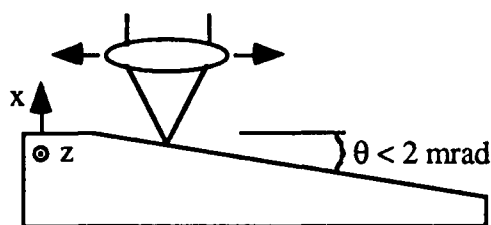


Figure 3. Diagram of the wedged sample and technique used for depth profiling of the d_{33} coefficient in APE- LiNbO_3

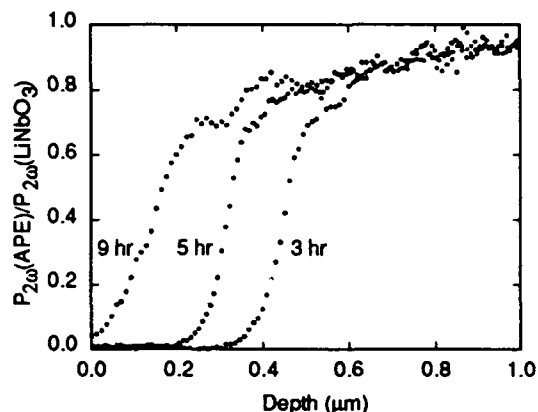


Figure 4. Normalized reflected second harmonic vs. depth for different waveguide annealing times.

The above data demonstrate that the variation in conversion efficiency of guided wave QPM devices with waveguide annealing time is due to a variation in the overlap integral with the d_{33} coefficient in the guide. For PE waveguides the fundamental and SH modes are fully contained in the original PE depth and the conversion efficiency is very low since $d_{33}=0$ in the waveguide. For intermediate anneals the modes extend deeper into the substrate where they encounter the d_{33} coefficient of LiNbO_3 , and the conversion efficiency is maximized. For long anneals the modes are spread out and lower peak intensities reduce the conversion efficiencies. *Thus the variation in conversion efficiency with annealing is not so much due to a restoration in the d_{33} coefficient of the APE waveguide as a variation in the overlap integral due to a spatial redistribution of the modal fields.* Detailed conversion efficiency calculations based on the model for the modal properties of APE waveguides and the d_{33} measurements described above will be presented.

The authors thank Karl Kissa of the Charles Stark Draper Laboratory for the SIMS data.

- 1 M. L. Bortz and M. M. Fejer, Opt. Lett. 16, 1844 (1991).
- 2 M. L. Bortz and M. M. Fejer, Opt. Lett. 17, 704 (1992).
- 3 For z-cut LiNbO_3 , D. F. Clark, A. C. G. Nutt, K. K. Wong, P. J. R. Laybourn, and R. M. De La Rue, J. Appl. Phys. 54, 6128 (1983). For x-cut LiNbO_3 , T. Maciak and M. Sokolowski, Optica Applicata 19, 423 (1989).
- 4 J. M. White and P. F. Heidrich, Appl. Opt. 15, 151 (1976). K. S. Chiang, J. Lightwave Tech. LT-3, 385 (1985).
- 5 C. E. Rice, J. L. Jackel, and W. L. Brown, J. Appl. Phys. 57, 4437 (1985). M. M. Howerton, W. K. Burns, P. R. Skeath, and A. S. Greenblatt, J. Quantum Electron. 27, 593 (1991).
- 6 R. A. Becker, Appl. Phys. Lett. 43, 131 (1983). T. Suhara, H. Tazaki, H. Nishihara, Electron. Lett. 25, 1326 (1989). X. Cao, R. Srivastava, R. V. Ramaswamy, and J. Natour, IEEE Photon. Tech. Lett. 3, 25 (1991).
- 7 F. Laurell, M. G. Roelofs, and H. Hsiung, Appl. Phys. Lett. 60, 301 (1992).

Phase-matched and Cerenkov-type second harmonic blue light generation in ion-implanted KNbO₃ waveguides

D. Fluck and P. Günter

Institute of Quantum Electronics, Swiss Federal Institute of Technology
ETH Hönggerberg, CH-8093 Zürich, Switzerland.

M. Fleuster and Ch. Buchal

Institut für Schicht- und Ionentechnik
Forschungszentrum Jülich, D-5170 Jülich, Germany.

Several approaches have been described for generating blue light by frequency doubling near infrared laser sources in nonlinear optical materials [1]. KNbO₃ has been shown to have excellent nonlinear optical properties making it particularly attractive for nonlinear optics [2]. Thanks to its large nonlinear optical susceptibilities, its room-temperature phasematchability between 860 nm and 980 nm by angle tuning, its transparency down to 390 nm, and its very high threshold to optical damage, KNbO₃ proved to be one of the most promising materials for high-efficiency frequency doubling of near infrared laser radiation into the blue and green spectral range [3-5].

Second harmonic generation (SHG) using optical waveguides is very attractive due to the tight beam confinement over long interaction lengths enabling to achieve very high conversion efficiencies even on the power level of presently available DLs. Conventional methods for waveguide formation such as ion indiffusion and ion exchange, which have been used in other oxides have not yet been demonstrated to be successful in KNbO₃, mainly because of its low diffusion constant at temperatures below the structural phase transition at 217 °C. Ion implantation and sputter deposition are the only methods so far reported to produce crystalline low-loss optical waveguides in KNbO₃ [6-11]. We have reported for the first time phase-matched (PM) and Cerenkov-type SHG in ion-implanted planar and channel KNbO₃ waveguides [12,13].

The KNbO₃ waveguides used in this work have been produced by using low-dose MeV He ion implantation because for these conditions low-loss planar and channel waveguides have been produced [6,10]. The SHG experiments were performed with a cw titanium sapphire laser with a linewidth of less than 5 GHz. The waveguide input coupling was accomplished in an end-fire geometry using microscope objectives. The mode coupling insertion loss was 4-5 dB.

The SH power was measured as a function of the input power for different planar and channel waveguides. We have found that SHG was achieved in a mode-to-mode

conversion in the planar waveguides whereas in the channel waveguides we observed Cerenkov-type SHG where the blue light is radiated into the substrate.

With a maximum fundamental power of 165 mW in a 5.6 mm long and 5.4 μm thick planar waveguide a power of 2.4 mW of SH blue light at 433 nm was generated, which is equivalent to a normalized conversion efficiency of 16 %/Wcm. The mode conversion was between the TM_0 mode and the TE_1 mode of the planar waveguide.

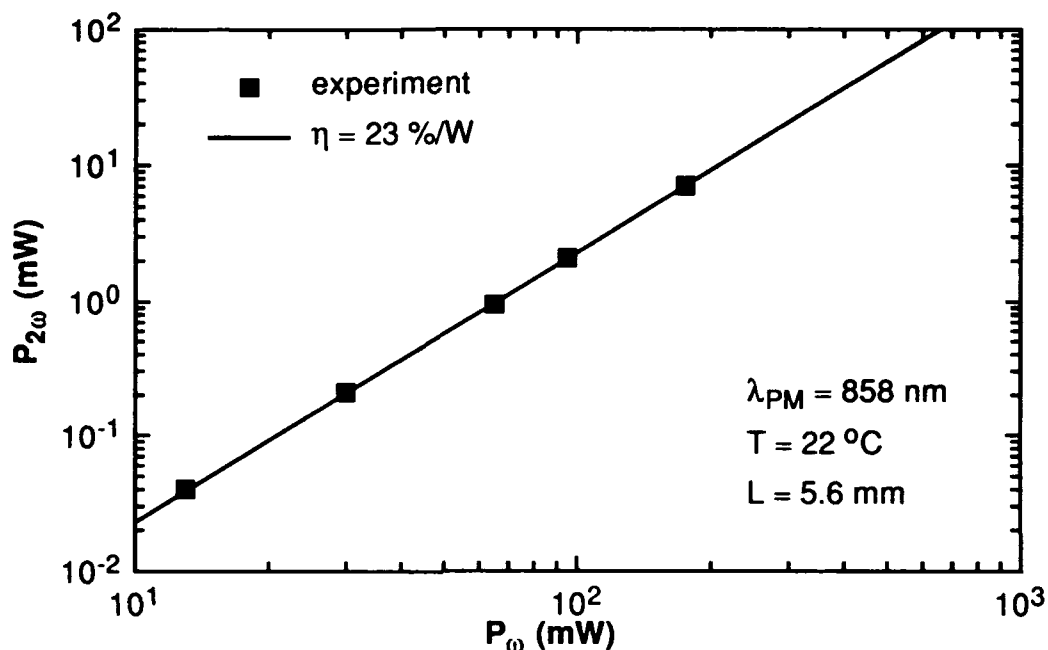


Figure 1: Power of the SH blue light at 428 nm as a function of the fundamental power for Cerenkov-type frequency doubling in a 5.4 μm x 7.5 μm ion-implanted KNbO_3 channel waveguide of 5.6 mm length.

A maximum power of 176 mW at 856 nm was coupled into a 5.4 X 7.5 μm^2 channel waveguide of 5.6 mm length providing a blue light output power of 7.1 mW at 428 nm. Figure 1 shows the quadratic dependence of the SH power at 428 nm measured as a function of the fundamental power. The theoretical curve corresponds to a normalized conversion efficiency of 41%/Wcm. The SH radiation was emitted under a Cerenkov angle of less than 5 degrees into the bulk crystal.

We will present results on the fabrication and tailoring of optical waveguides in KNbO_3 by ion implantation and report current results on PM as well as Cerenkov-type SHG in ion-implanted KNbO_3 waveguides.

Acknowledgements: We gratefully thank H. Wüest for the crystal growth and J. Hajfler for the excellent crystal polishing.

REFERENCES

- 1 e. g. G. I. Stegeman and C. T. Seaton, "Nonlinear integrated optics", J. Appl. Phys. **58**, R57 (1985).
- 2 P. Günter, "Near infrared noncritically phase-matched second-harmonic generation in KNbO₃", Appl. Phys. Lett. **34**, 650 (1979).
- 3 P. Günter, P. M. Asbeck, and S. K. Kurtz, "Second-harmonic generation with Ga_{1-x}Al_xAs lasers and KNbO₃ crystals", Appl. Phys. Lett. **35**, 461 (1979).
- 4 J.-C. Baumert, P. Günter, and H. Melchior, "High efficiency second-harmonic generation in KNbO₃ crystals", Opt. Commun. **48**, 215 (1983).
- 5 H. Jaeckel, G.-L. Bona, P. Buchmann, H. P. Meier, P. Vettiger, W. J. Kozlovsky, and W. Lenth, "Very high-power AlGaAs SQW-GRINSCH ridge laser with frequency-doubled output", IEEE J. Quantum Electron. **QE-27**, 1560 (1991).
- 6 F. P. Strohkendl, P. Günter, Ch. Buchal, and R. Irmscher, "Formation of optical waveguides in KNbO₃ by low dose MeV He⁺ implantation", J. Appl. Phys. **69**, 84 (1991).
- 7 D. Fluck, R. Irmscher, Ch. Buchal, and P. Günter, "Optical strip waveguides in KNbO₃ formed by He ion implantation", Appl. Phys. Lett. **59**, 3213 (1991).
- 8 F. P. Strohkendl, D. Fluck, P. Günter, R. Irmscher, and Ch. Buchal, "Nonleaky optical waveguides in KNbO₃ by ultralow dose MeV He ion implantation", Appl. Phys. Lett. **59**, 3354 (1991).
- 9 D. Fluck, R. Irmscher, Ch. Buchal, and P. Günter, "Tailoring of optical planar waveguides in KNbO₃ by MeV He ion implantation", Ferroelectrics **128**, 79 (1992).
- 10 D. Fluck, M. Fleuster, Ch. Buchal, and P. Günter, "Low-loss optical channel waveguides in KNbO₃ by multiple energy ion implantation", J. Appl. Phys. **72**, 1671 (1992).
- 11 S. Schwyn Thöny, P. Günter, and H. W. Lehmann, "Sputter deposition of epitaxial waveguiding KNbO₃ thin films", Appl. Phys. Lett. **61**, 373 (1992).
- 12 D. Fluck, B. Binder, M. Küpfer, H. Looser, Ch. Buchal, and P. Günter, "Phase-matched second harmonic blue light generation in ion implanted KNbO₃ planar waveguides with 29% conversion efficiency", Opt. Commun. **90**, 304 (1992).
- 13 D. Fluck, J. Moll, M. Fleuster, Ch. Buchal, and P. Günter, "Blue light generation by frequency doubling cw diode laser radiation in KNbO₃ channel waveguides", Electron. Lett. **28**, 1092 (1992).

Fabrication of periodically inverted domain structures in LiTaO₃ using proton exchange

Satoshi Makio, Fumio Nitanda, Kohei Ito, and Masayoshi Sato

Magnetic and Electronic Materials Research Laboratory,
Hitachi Metals, Ltd., 5200 Mikajiri, Kumagaya, Saitama 360, Japan

1. INTRODUCTION

Optical storage and laser printer applications require a compact solid-state blue source to achieve greater versatility. One method to obtain this blue light is via Quasi phase matched (QPM) second harmonic generation (SHG).^{1,2} With QPM we are able to fabricate a high-efficiency blue light source. By inverting the spontaneous polarization with an appropriate period it is possible to phase match any arbitrary wavelength. Several methods have been used to fabricate periodic domain inversion in LiNbO₃ and LiTaO₃. Ti indiffusion³ or Li outdiffusion⁴ near the Curie temperature are well-known techniques to reverse the polarization in LiNbO₃. Electron beam bombardment^{5,6,7} has also been employed to make "well"-shaped inverted domains. Periodically poled structures in LiTaO₃ can be realized through selective proton exchange (PE) followed by heat treatment near the Curie temperature⁸. A few micron deep semi-circular shaped domains with a first-order period has been fabricated using proton exchange and a quick heat treatment near the Curie temperature, generating 15mW of blue light⁹.

We report on the formation of long ($>50 \mu\text{m}$), "spike-like" inverted domains in LiTaO₃ using heat-treatments well below the Curie temperature. These domains are formed by proton exchange in conjunction with one-directional heating, and their behavior during post-PE annealing is examined. These domains have straight walls and the same period as the proton exchanged grid, which are favorable conditions to obtain a first-order QPM device.

2. EXPERIMENTAL

A 30nm thick Ta mask was deposited on the c- face of 0.5mm thick LiTaO₃ substrate using an electron beam deposition method. The first-order periodic pattern with a $3.2 \mu\text{m}$ period was fabricated on the Ta mask by conventional photolithography and CF₄ dry etching, forming windows to allow proton exchange. A small amount of pyrophosphoric acid was dropped on the Ta mask side of the substrate, which was then placed on already heated (260 °C) hot plate for 30 minutes, namely one-directional heating from the rear surface of the substrate. After removal of the Ta mask, some specimens were cut into strips, polished and etched with HF and HNO₃ to examine the

proton exchange and domain inversion. Others underwent heat treatment between 300°C and 600°C, and were then etched to observe the change in the inverted domains.

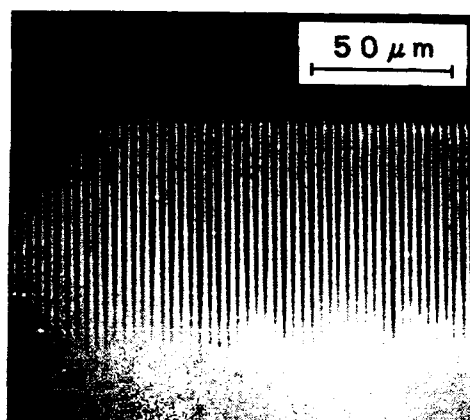


Figure 1. Cross-sectional micrograph of periodically inverted "spike-like" domains fabricated on LiTaO₃, proton exchanged at 230°C for 30 minutes and post PE annealing at 440°C for 0.5 minute.

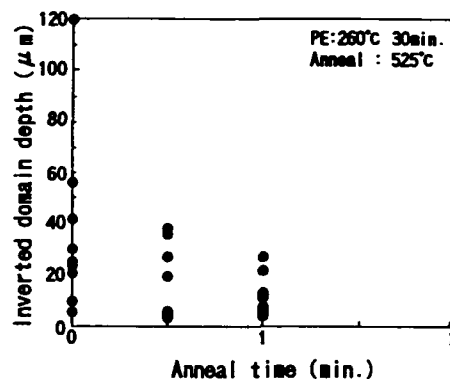


Figure 2. Measured domain inversion depth plotted against the heat treatment time.

3. RESULTS and DISCUSSION

Domain inversion in proton exchanged LiTaO₃ had previously been considered to occur during the post PE annealing step near the Curie temperature⁸. Using our process we found that the polarization reversing during the proton exchange process, far below the Curie temperature. Figure 1 shows a cross-sectional view of a LiTaO₃ sample, proton exchanged at 260 °C for 30 minutes with post PE annealing at 440 °C for 0.5 minute. Although the proton exchanged layer is less than 1 μm thick, inverted domains expanded from the proton exchanged region to deep inside the substrate. The domains look like "spikes", with thin and sharp ends.

These "spike-like" domains seem to be similar to the so-called "needle-shaped" microdomains¹⁰ which are common in poled crystals as residual anti-domains, usually being isolated and randomly distributed. In our case inversion mechanism is not clear, but we think the periodic stress due to proton exchange is likely to trigger the growth of the anti-domains, which is in turn accelerated by the thermal gradient.

Because previous report of domain inversion via proton exchange in LiTaO₃ were achieved near the Curie temperature, we were interested in the thermal stability of the domains during the post PE annealing. From a practical point of view it is essential for the domains to survive the 350-380°C heat treatment in order to fabricate waveguides on the substrate by the annealed proton exchange (APE) method. Figure 2 shows the domain inversion depth as a function of heat treatment time. Heat treatment was carried out at 525°C for up to 2 minutes. Although there is some scatter in the data, the

general tendency is for the domains to become shorter and finally vanish as the heat treatment time increases. At lower temperature, though, they survive longer heat treatment time.

To fabricate a single-mode APE waveguide after inverting the "spike-like" domains, PE was carried out at 260 °C for 16 minutes in pyrophosphoric acid and post PE annealed at 380 °C for 5 minutes. Using a tunable cw Ti:sapphire laser with end-fired coupling into a 3 μm width and 9mm long waveguide, we demonstrated blue light SHG exiting from the waveguide. Figure 3 shows the relation between the fundamental power and the output power. The second-harmonic power was quadratic with the fundamental power at less than 23mW, and the normalized conversion efficiency was $12.3\% \text{W}^{-1} \text{cm}^{-2}$. At fundamental power greater than 23mW the waveguide suffered from optical damage. This damage caused the refractive index to change and altered the phase matching conditions. Therefore the output SH power decreased with time. The dependance of the output power on the fundamental wavelength is shown in Figure 4. The FWHM in the tuning curve was 0.15nm. The poor conversion efficiency could be attributed to changes in the domain inversion ratios due to the APE waveguide process and not enough optical confinement.

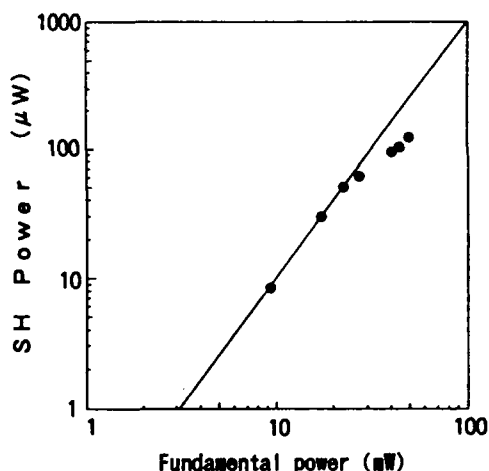


Figure 3. Measured SHG output plotted against the fundamental power.

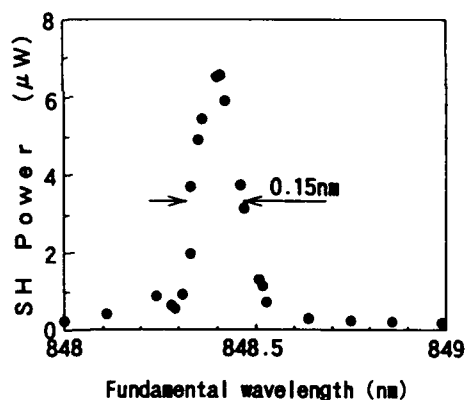


Figure 4. Experimental wavelength tuning curve for QPM-SHG waveguide.

4. CONCLUSION

We fabricated deep ($>50 \mu\text{m}$) inverted periodic domain structures with a 3.2 μm period using selective proton exchange with one-directional heating at 260 °C for first-order QPM in LiTaO₃. The domain inversion occurred during the proton exchange process, far below the Curie temperature, and the domains stemmed and stretched toward the non-proton-exchanged area from the proton exchanged layer. Though the inverted domains shrank and finally vanished through post PE annealing, they were

stable enough to survive the temperature of the waveguide fabrication process. We demonstrated blue light SHG with APE waveguides, but occurred optical damage in LiTaO_3 . Higher efficiency may be obtained by optimizing the parameters of the APE waveguide fabrication process.

References

- 1 J. A. Armstrong, N. Bloembergen, J. Ducuing, and P. S. Pershan, *Phys. Rev.* **127**, 1918 (1962)
- 2 S. Somekh and A. Yariv, *Opt. Commun.* **6**, 301 (1972)
- 3 S. Miyazawa, *J. Appl. Phys.* **50**, 4599 (1979)
- 4 J. Webjorn, F. Laurell, and G. Arvidsson, *IEEE Photon. Technol. Lett.*, **1**, 316 (1989)
- 5 R. W. Keys, A. Loni, R. M. De La Rue, C. N. Ironside, J. H. Marsh, B. J. Luff, and P. D. Townsend, *Electron. Lett.*, **26**, 188 (1991)
- 6 M. Yamada and K. Kishima, *Electron. Lett.*, **27**, 828 (1991)
- 7 H. Ito, C. Takyu, and H. Inada, *Electron. Lett.*, **27**, 1221 (1991)
- 8 K. Mizuuchi, K. Yamamoto, and T. Taniuchi, *Appl. Phys. Lett.*, **58**, 2732 (1991)
- 9 K. Mizuuchi and K. Yamamoto, *Appl. Phys. Lett.*, **60**, 1283 (1992)
- 10 N. Ohnishi, T. Iizuka, *J. Appl. Phys.*, **46**, 1063 (1975)

Frequency Doubling of Laser Diode using Periodically Domain-inverted LiTaO₃

K.Yamamoto, K.Mizuuchi, Y.Kitaoka, and M.Kato
Optical Devices Research Laboratory,
Matsushita Electric Industrial Co., Ltd.,
Yagumo-nakamachi 3-1-1, Moriguchi, Osaka, 570 Japan
06-906-2420

As compact, solid-state sources for blue coherent light, laser diode-based second harmonic generation (SHG) devices hold great potential for use in high-density optical disk and laser printer applications. In such applications, the primary concerns for the blue light sources are those of stability and high power generation over several milliwatts.

Quasi-phase matched (QPM) SHG is an attractive method to gain the blue light sources, because phase-matching of an arbitrary wavelength is obtainable by appropriate periodic modulation of the nonlinear polarization^{1,2}. QPM-SHG devices using a waveguide are capable of realizing high-conversion efficiencies; a large nonlinear coefficient such as d_{33} can be used and the waveguide can also attain strong optical confinement with long interaction length³⁻⁵.

The authors have previously demonstrated periodically domain-inverted structure in LiTaO₃ waveguide⁶ and obtained high efficiency (157%/W) using a Ti:Al₂O₃ laser⁷. LiTaO₃ is thus confirmed to be less susceptible to optical damage, and it has a large nonlinear coefficient. Therefore, the QPM-SHG waveguide device in LiTaO₃ is a hopeful candidate for compact blue-light source.

However, one has to overcome several difficulties before successful generation of blue-light over several milliwatts is attained using frequency doubling of laser diodes. Firstly, a higher conversion efficiency must be fulfilled, because currently available laser diode power is still limited. Secondly, the lasing wavelength of a conventional Fabry-Perot laser diode must be stabilized, so that the wavelength of the laser diode is stably maintained within the allowance range of the QPM-SHG.

In this paper, we report on a new approach to stable and high power blue-light generation by frequency doubling of a laser diode, wherein is employed a QPM-SHG device of LiTaO₃ with a periodically domain-inverted region and proton-exchanged waveguide. High efficiency SHG has been obtained by optimizing both a deep domain-inverted region and a low-loss waveguide with strong confinement⁷. We also propose to apply grating feedback technique to maintain single longitudinal mode oscillation of the laser diode, and so to match the lasing wavelength with phase-matching wavelength of the QPM-SHG. Generation of stable blue light up to 3mW was attained by frequency doubling of the laser diode.

The periodically domain-inverted regions are arranged so that a channel waveguide traverses the regions. The period of the domain-inverted regions was 3.8 μ m. The domain-inverted region was fabricated using a selective proton-exchange and quick heat treatment technique below the Curie temperature. Pyrophosphoric acid was used for proton-exchange. The fabricated domain-inverted depth was 1.9 μ m. Further, a quick heat treatment technique was also made use of to fabricate a strong confinement waveguide. The fabricated waveguide was of 1.9 μ m depth, 4 μ m width, and 10mm length. The waveguide depth was the same as

the depth of the domain-inverted region, so that the guided mode was able to overlap efficiently with the domain-inverted region. The propagation loss of the channel waveguide was 0.8dB/cm.

To evaluate the characteristics of this device in detail, a widely tunable Ti:Al₂O₃ laser was used as the fundamental wave source. Maximum blue light power of 31mW was obtained for 145mW of fundamental power. The normalized conversion efficiency of this device was 220%/W. The FWHM wavelength acceptance bandwidth was 0.12nm.

We further carried out experiments on laser diode frequency doubling using grating feedback technique. Figure 1 shows the experimental setup for frequency doubling of a GaAlAs laser diode with a grating feedback optical system. The output power of the laser diode was 120mW. The light beam from the laser diode was collimated using a lens of N.A.=0.55, and the beam was focused using a lens of N.A.=0.6. A half-wave plate was inserted to rotate the polarization of the beam to achieve maximum mode matching in transverse magnetic (TM) propagation of the waveguide. The maximum power of 44mW was coupled into the waveguide. A part of the fundamental light as the first order diffracted light at grating (0.56μm pitch) was fed back to the active layer of the laser diode through the waveguide. A dichroic mirror was inserted to reflect only generated harmonic wave. The proposed optical system is advantageous over previous grating feedback optical systems⁸⁾, in that a conventional reflection-type grating and commercially available laser diode can be applied with no appreciable loss in both fundamental and harmonic wave.

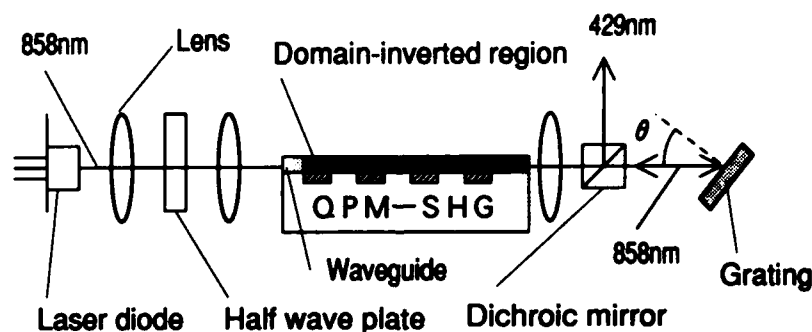


Fig.1. Experimental setup for frequency doubling of a laser diode with grating feedback system.

Under these conditions, the laser diode could maintain single longitudinal mode oscillation, and no mode hopping was observed. Figure 2 shows the lasing wavelength dependence on the grating angle. As grating angle θ was varied from 49.5 to 50.8°, the lasing wavelength accordingly changed from 845 to 861nm. The grating firmly fixed the wavelength of laser diode at the phase matching wavelength. The generated second harmonic power versus the input fundamental power is shown in Fig.3. Blue light of 3.1mW was generated for 44mW of fundamental power with a conversion efficiency of 7%. When the temperature of the laser diode casing was changed from 17 to 35°C, the longitudinal mode remained unchanged and

stable SHG was obtained. Furthermore, the time fluctuation of generated second harmonic power was within $\pm 1.5\%$, when the temperature was fixed.

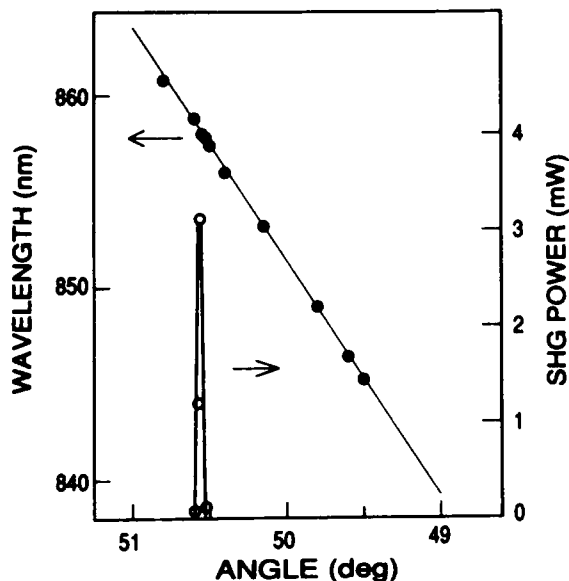


Fig.2. Lasing wavelength and second harmonic power plotted against grating angle.

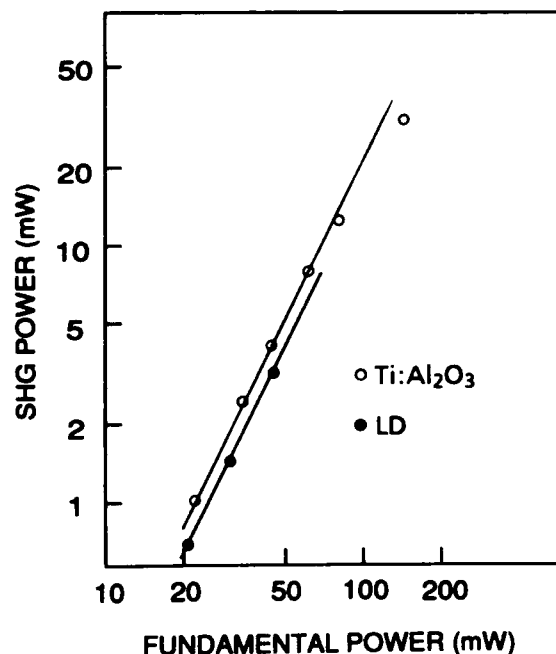


Fig.3. Generated second harmonic power versus input fundamental power. Fundamental sources are Ti:Al₂O₃ laser and laser diode (LD).

In summary, we have succeeded in fabricating a high conversion efficiency QPM-SHG device in LiTaO₃, in which the deep domain-inverted region and the strong confinement waveguide were formed by proton-exchange and quick heat treatment. Locking the lasing wavelength by grating feedback technique is proposed and 3.1mW of blue light (429nm) for 44mW of fundamental power has been demonstrated. Furthermore it was shown that the generated second harmonic power was stable, varying temperature of the laser diode and over a long time period. This QPM-SHG device with grating feedback system has been shown to be a candidate for a compact blue light source applicable to optical disks and laser printers.

References

- (1) J.A.Armstrong, N.Bloembergen, J.Ducuing, and P.S.Pershan, Phys. Rev., 127 (1962) 1918
- (2) S.Somekh and A.Yariv, Opt. Commun., 6 (1972) 301
- (3) E.J.Lim, M.M.Fejer, R.L.Byer, and W.J.Kozlovsky, Electron.Lett., 25 (1989) 731
- (4) J.Webjorn, F.Laurell, and G.Arvidsson, IEEE Photon. Technol. Lett., 1 (1989) 316
- (5) C.J.van der Poel, J.D.Bierlein, J.B.Brown, and S.Colak, Appl.Phys.Lett., 57 (1990) 2074
- (6) K.Mizuuchi and K.Yamamoto, Appl. Phys. Lett, 60 (1992) 1283.
- (7) K.Yamamoto and K.Mizuuchi, IEEE Photon Technol. Lett. 4 (1992) 435
- (8) H.Sato, K.Itoh, M.Fukai, and N.Suzuki, IEEE J.Quantum Electron. QE-18 (1982) 328

Thursday, February 4, 1993

Frequency Upconversion in Waveguide Devices 2

CThB 10:45am–12:00m
Pelican Ballroom

John D. Bierlein, *Presider*
E. I. DuPont de Nemours Company

QUASI-PHASE-MATCHING (QPM) IN THE CHANNEL Rb:KTP WAVEGUIDES.

Eugene A. Shcherbakov, Vladislav A. Maslov
 General Physics Institute, RAS,
 38 Vavilov str., 117942 Moscow, Russia
 tel.: (095) 132-82-31; fax: (095) 135-81-39

In recent years, several techniques of formation the periodic domain-inverted grating (PDIG) in the different ferroelectric crystals were examined extensively. Mainly, the variety of the techniques was concerned with LiNbO_3 and LiTaO_3 crystals [1]. It was well established that formation of ferroelectric domains had strong dependence of the quality, conductivity and other physical properties of the crystals.

In the case of KTP crystal, the domain-inverted structures for QPM were created only by the ion exchange of Rb/Ba for K through the suitable mask [2]. By this technique, the segmented channel waveguide was formed in KTP simultaneously. It is known that at room and higher temperatures KTP resembles a superionic conductor and conductivity, which possibly assisted by K^+ and O^{2-} vacancies, can vary by 4 order of magnitude from 10^{-10} to $10^{-6} \Omega^{-1}\text{cm}^{-1}$ [3]. Therefore, the periodic variation of KTP surface conductivity can result in the formation PDIG. From this point of view, we have used the periodic dielectric film cladding, heating and cooling for fabrication of PDIG in KTP crystal.

Recently, this technique based on ferroelectric-domain inversion induced by SiO_2 cladding was used in LiNbO_3 [4].

Our preliminary measurements have indicated that for the Rb:KTP channel waveguide ($w = 5\mu\text{m}$) and the $9.6\mu\text{m}$ period of PDIG (third order QPM) the SHG ($\lambda = 400\text{nm}$) efficiency was $29\% \text{W}^{-1}\text{cm}^{-2}$.

References

1. G. Arvidsson, OSA Topical Meeting on Compact Blue-Green Lasers, Santa Fe, NM, Feb. 1992.
2. C. J. v. d. Poel, J. D. Bierlein, J. B. Brown, and S. Colak, Appl. Phys. Lett., 57, 2074 (1990).
3. G. d. Stucky, M. L. F. Phillips, and T. E. Gier, Chem. of Mater. 1, 492, (1989).
4. M. Fujimura, T. Suhara, H. Nishihara, Electron. Lett., 27, 1209 (1991).

KTP segmented waveguides as concurrent Bragg reflectors and second harmonic generators.

M. G. Roelofs, W. Bindloss, A. Suna, J. D. Lee, and J. D. Bierlein

Science and Engineering Laboratories, E. I. du Pont de Nemours & Co,
Experimental Station, Wilmington, DE 19880-0328

A periodic modulation of optical nonlinearity by means of ferroelectric domain reversal has led to the generation of blue light by quasi-phase matching in waveguides of, e.g. lithium niobate ^{1,2}, lithium tantalate ^{3,2}, and potassium titanyl phosphate (KTP) ⁴. When the linear optical constant (index) is also periodically modulated along the propagation direction, these waveguides may serve also as distributed Bragg reflectors ^{5,6}. The back reflection of light in a narrow band of wavelengths, subject to the Bragg condition, has been utilized to stabilize a diode laser pump, forcing it to oscillate in a narrower band of wavelengths suitable for second harmonic generation.

Thus we are led to the problem of a) designing a waveguide which will meet the Bragg condition at a wavelength λ_{Bragg} near to the quasi-phase matching at wavelength λ_{QPM} and b) ensuring that the intensity of the Bragg reflection is sufficient to 'lock' the diode laser to it. In Rb/Ba-diffused waveguides in KTP, temperature tuning allows one to shift the relative position of λ_{Bragg} and λ_{QPM} by 0.035 nm/°C, so if one is constrained to temperature tuning the KTP waveguide by ± 10 °C, then at the center of the temperature band λ_{Bragg} and λ_{QPM} should match within some 0.35 nm. An additional constraint is assumed in that the mechanics of making the photomask limits one to certain dimensions for the sections of the waveguide. For example, at 0.1 μ addressing, all dimensions on the mask must be integer multiples of 0.1 μ .

The key to achieving the above has been to create structures with superperiods much longer than the minimum required for first-order QPM, allowing one to go to high orders (e.g. 275) in the Bragg reflection. The waveguide is composed of a pattern of N segments, each segment

having length h_i composed of an 'on', or diffused, section and an 'off', or undiffused section. The pattern repeats itself after N segments with a superperiod, or repeat distance, of Λ_{sp} . The average period of the N segments over the pattern is then $\Lambda_{avg} = \Lambda_{sp}/N$, which for frequency doubling light of 846 nm wavelength, is near to 4.00 μ . However, the individual segments may deviate somewhat from that required for perfect QPM, so that some are a few tenths of a micron longer, some a few tenths shorter. This can be done without serious loss of blue output. Also, the superperiod allows one to change λ_{QPM} in small increments, and thus bring it close to the lasing wavelength of a given diode laser. The difference in λ_{QPM} for a 0.1 μ change in Λ_{sp} is 5.7 nm. However, in a superperiod of $N=16$ segments with $\Lambda_{sp} = 64 \mu$, adding 0.1 μ to only one of the 16 segments increases Λ_{avg} by only 0.00625 μ , which allows tuning of λ_{QPM} in 0.36 nm increments.

Having chosen an average period to achieve a given λ_{QPM} , various combinations of the number of segments N and the various Bragg orders are examined. At, e.g., $N=1$, the 17th and 18th orders of Bragg reflections are separated from each other by 47 nm, and a match to an arbitrary λ_{QPM} is unlikely. However, by $N=10$, the 174th order Bragg reflection occurs at 847.6 nm, and the 173rd order reflection occurs at 852.4 nm, only 4.8 nm apart. Usually one can find a match (within the temperature tuning tolerance) of λ_{Bragg} to λ_{QPM} by going no higher than $N=8$. The smallest N possible is the desirable one: if N is too large, then the Bragg peaks are spaced too closely together, and the diode laser will not 'lock' to one of them, but will hop back and forth between adjacent Bragg peaks.

In order to maintain a high intensity of the Bragg reflection, the segments should be close to an integer multiple of 1/2 wave in optical path length, while the individual sections (both the on and the off section) should be close to an odd integer multiple of 1/4 wave in optical path length. For Rb/Ba-diffused waveguides in KTP and λ_{QPM} near 850 nm, segments of lengths 3.7, 3.9, 4.4, and 4.6 are close to 1/2 wave, and can be used to construct the superperiod. Thus $N=4$ and $\Lambda_{sp} = 4.025 \mu$ can be achieved with 3 segments of 4.0 μ and 1 segment of 4.1 μ ; but it can

also be achieved, and with higher Bragg intensity, using 3 segments of $3.9\ \mu$ and 1 segment of $4.4\ \mu$. Though the Bragg order is very high, this technique allows all $2N$ interfaces of the superperiod to contribute, albeit imperfectly, to building reflected intensity.

Calculations for a 5 mm long waveguide show that all the light should be reflected when the Bragg condition is met (even for Bragg orders of 275 with $64\ \mu$ superperiods), yet measurements of the guides yield typically 0 to 20% reflected intensity. The desired intensity to lock the diode is in the range of 5 to 10% reflectance. Factors which might lower the measured intensity and have been investigated are a) random fluctuations in the position of the interfaces, b) systematic variation in the position of the interfaces (caused e.g. by imperfect contact of KTP and photomask during exposure), c) variation in the segment length (caused e.g. by aberration in the e-beam lens used to write the mask, and d) boundary roughness due to imperfect photolithography. Both b) and c) reduce the observed intensity while also significantly broadening the Bragg peak. Peak broadening is observed in the measured waveguides, but not to an extent sufficient to explain the reduced intensity. The effect of d), roughness of the order of $0.1\ \mu$ in the edges of the sections, does in calculations lead to a substantial lowering of intensity without broadening the peak, in agreement with the measurements.

References

1. J. Webjorn, F. Laurell, and G. Arvidsson, IEEE J. Lightwave Technol. **7**, 1597 (1989).
2. E. J. Lim, S. Matsumoto, M. L. Bortz, and M. M. Fejer, Proc. SPIE-Int. Soc. Eng. **1561**, 135 (1991).
3. K. Mizuuchi and K. Yamamoto, Appl. Phys. Lett. **60**, 1283 (1992).
4. C. J. v. d. Poel, J. D. Bierlein, J. B. Brown, and S. Colak, Appl. Phys. Lett. **57**, 2074 (1990).

5. K. Shinozaki, T. Fukunaga, K. Watanabe, and T. Kamijoh, Appl. Phys. Lett. **59**, 510 (1991).
6. M. G. Roelofs, J. D. Bierlein, and F. Laurell, presented at the Opt. Soc. of Am. Compact Blue-Green Lasers topical meeting, Feb. 4 (1992).

Generation of 425 nm light by waveguide frequency doubling of a GaAlAs laser diode in an extended-cavity configuration

W.P. Risk, W. J. Kozlovsky, W. Lenth, S.D. Lau

IBM Research Division
Almaden Research Center
650 Harry Rd., MS K69/803
San Jose, CA 95120

G.L. Bona, H. Jaeckel, D.J. Webb

IBM Research Division
Zurich Research Laboratory
8803 Ruschlikon, Switzerland

There is currently considerable research on compact blue light sources that use periodically-poled waveguides for quasi-phased-matched frequency doubling of GaAlAs laser diodes.^{1,2} For such devices to become practical, they must be configured in such a way that optical feedback from the SHG waveguide or the other optical elements does not adversely affect the spectral characteristics or increase the amplitude noise of the diode laser. Although optical isolators can be used to reduce feedback, this approach does not lend itself to miniaturization of such devices. A more attractive alternative is the use of a configuration that includes the frequency doubling waveguide and all other optical elements within an "extended" laser cavity. In this configuration, lasing due to the reflectivity of the diode laser output facet is suppressed by anti-reflection (AR) coating, and strong feedback is intentionally provided by an external mirror or grating to produce laser oscillation.

To form such a cavity (Figure 1), the output facet of a single-spatial-mode, 850-nm GaAlAs SQW-GRINSCH laser diode^{3,4} was AR-coated using a $\lambda/4$ layer of Si_3N_4 . The residual facet reflectivity was determined to be less than 0.4%. The back facet was coated to produce a reflectivity of ~90%. Light from the laser was collimated, circularized, rotated 90° in polarization, and coupled into a periodically-poled KTP waveguide. Both the input and output facets of the KTP substrate were AR-coated with a $\lambda/4$ layer of MgF_2 , and this reduced the ~9% Fresnel reflectivity of each uncoated facet to $\leq 0.2\%$. The periodically-poled KTP

waveguide (commercially available from DuPont) had a period of 4 μm , a channel width of 4 μm , and a length of 4.5 mm. The light emerging from the KTP waveguide was collimated and directed onto a diffraction grating (1200 lines/mm, blazed for 6328 Å). The grating was used in Littrow mode for retro-reflection of the incident beam. At 850 nm, the grating reflected approximately 43% of the incident light. A low ($\sim 6.5\%$) reflectivity beamsplitter was used to sample the signal immediately in front of the grating to determine the infrared and blue powers present inside the cavity.

Lasing threshold for the extended-cavity laser was measured to be 28 mA. For a given alignment of the grating, the frequency remained unchanged (within the 0.8 Å resolution of the spectrometer) as the current was increased. By tilting the diffraction grating, the frequency of the laser could be tuned over a range of several nanometers. When tuned to the peak phasematching wavelength, 0.21 mW of 425-nm light was generated from 22 mW of 850-nm light present in the cavity. Hence, the conversion efficiency was $\sim 1\%$, and the normalized conversion efficiency was 214%/W-cm².

The spectral width of the extended-cavity laser was examined and found to be less than the 0.8 Å resolution of the spectrometer, indicating that no residual laser diode "chip" modes (~ 1.5 Å spacing) were present; this narrow spectral width is compatible with the ~ 2 -3 Å wide phasematching bandwidth of the 4.5-mm long KTP waveguide. The number of extended-cavity modes having ~ 0.012 Å spacing could not be observed directly due to the limited resolution of the spectrometer. The measured conversion efficiency of 214%/W-cm² is less than the 275%/W-cm² efficiency obtained using a broadband ($\Delta\nu < 2$ GHz) titanium:sapphire laser, but greater than the 100%/W-cm² efficiency obtained using a single-frequency ($\Delta\nu < 500$ kHz) titanium:sapphire laser. These differences in conversion efficiency are probably due to the spectral content of each individual laser. Since sum-frequency mixing between longitudinal modes of a multimode source can yield a higher conversion efficiency than that obtained with a single-mode source⁵, it is likely that the extended-cavity laser oscillates in several longitudinal modes.

Instead of a bulk diffraction grating, frequency-selective feedback can be obtained using the periodic waveguide itself as a distributed Bragg reflector. We fabricated 9-mm-long segmented channel waveguides having 4.5 μm width and 5.5 μm period in flux-grown KTP. For this geometry, the 24th order TM-mode Bragg reflection occurs at 845.3 nm, which is within the gain-bandwidth of the laser diode. When light was coupled into the waveguide, lasing occurred

with a threshold current of 33 mA. The spectral width was measured to be 0.8\AA or less. Blue light generation was not observed in this case because the period was incorrect for phasematched SHG of the 845.3 nm laser wavelength. Operation of the extended-cavity laser using the waveguide as a DBR structure is under further investigation.

Improved performance of device is being pursued using a dichroic beamsplitter to permit more efficient extraction of the blue light. In addition, the blue power can be increased by driving the diode at higher current and by temperature tuning the laser diode to optimize power at the wavelength required for phasematching.

1. M.G. Roeloefs, F. Laurell, J.D. Bierlein, in *Compact Blue-Green Lasers Technical Digest 1992*, Optical Society of America, Washington, D.C., 1992), Vol. 6, p. 127.
2. Kazuhisa Yamamoto and Kiminori Mizuuchi, *IEEE Photon. Technol. Lett.*, **4**, 435, (1992).
3. C. Harder, P. Buchmann, H. Meier, *Electron. Lett.*, **22**, 1081 (1986).
4. Heinz Jaeckel, Gian-Luca Bona, Peter Buchmann, Heinz P. Meier, Peter Vettiger, William J. Kozlovsky, Wilfried Lenth, *IEEE J. Quantum Electron.*, **QE-27**, 1560, (1991).
5. Sten Helmfrid and Gunnar Arvidsson, *J. Opt. Soc. Am. B*, **8**, 2326, (1991).

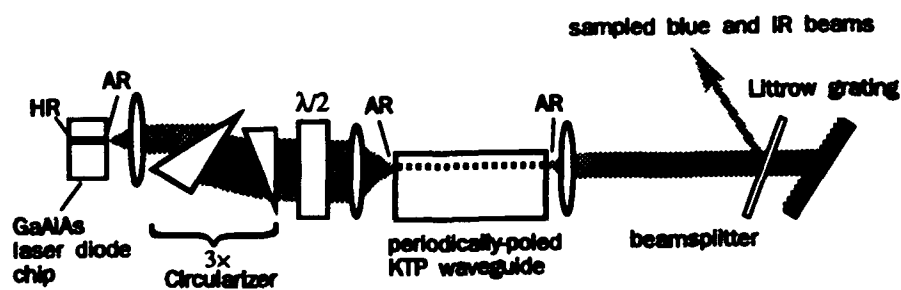


Figure 1

Characteristics of KTiOPO_4 Waveguides Up to High Power Densities

P. A. Morris, J. B. Brown, J. D. Bierlein

*DuPont, Central Research & Development, Experimental Station,
Wilmington, DE 19880-0356, (302)-695-2153*

KTiOPO_4 (KTP) possesses a unique combination of properties making it useful for a variety of bulk and waveguide nonlinear optical applications.¹ Spatially well-defined waveguide and domain structures are readily produced in crystals through ion exchange techniques.^{2,3} Highly efficient second harmonic generation into the blue wavelength range is achieved in KTP using quasi-phase matching in segmented/domain-inverted waveguides.⁴ Recently, results have been reported indicating that there are power limitations or instabilities which occur when quasi-phase matching into the blue using KTP.⁵ However, the transmission characteristics of conventional KTP waveguides have been reported to be stable at 514 and 488 nm to high powers.⁶

This study was undertaken to understand the propagation characteristics of KTP waveguides as a function of power and wavelength and their implications to various nonlinear optical processes using these waveguide structures. The transmission, input coupling and scattering were measured using both TE and TM polarized 458, 514 and 790 nm CW radiation at power densities of 5 kW/cm² to 1 MW/cm². Segmented and continuous waveguides produced with Ba/Rb-, Rb- and Ba/Rb/Tl-doping in flux and hydrothermally grown KTP substrates were examined.

The results of this work indicate that the propagation constant of the waveguide depends on the power density (5 kW/cm² to 1 MW/cm²) and on the wavelength. Effects on the propagation constant are quickly observed at high power levels and at short wavelengths. They are also observed at lower power levels in longer times. These changes are not due to nonlinear absorption or the formation of gray tracks (photochromic damage⁷), but are due to changes in the real part of the propagation constant and appear to be related to the linear absorption. These changes are observed in both segmented and continuous waveguides. The effects are observed to be more pronounced using TM polarized radiation and in waveguides fabricated in flux vs. hydrothermally grown KTP substrates.

Figures 1a and 1b show the characteristics of segmented waveguides produced in flux and hydrothermal substrates, respectively. The propagation characteristics are shown as a function of the laser power before and after exposure to 22 mW of 458 nm radiation for 30 minutes. The effects of the exposure on the waveguide fabricated in the flux grown substrate consist of a drop in the percent of guided light and an increase in the percent of uncoupled light. These changes in the amounts of guided and uncoupled light can be reduced by recoupling the laser to the waveguide after the exposure. No effects are observed in the waveguide produced in the hydrothermal substrate.

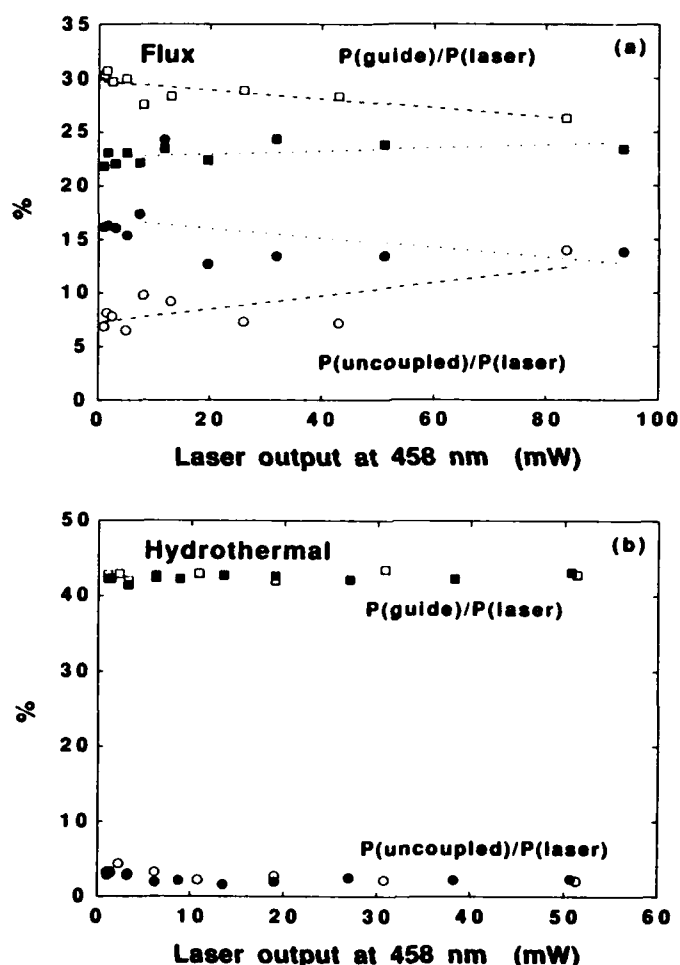


Figure 1. Characteristics of segmented, $4\mu\text{m}$ wide waveguides produced with a 5% Ba/95% Rb nitrate ion exchange in (a) flux and (b) hydrothermal KTP substrates. The open symbols represent the $P(\text{guide})/P(\text{laser})$: (\square) and $P(\text{uncoupled})/P(\text{laser})$: (\circ) before a 30 minute exposure of 22 mW of 458 nm radiation and the solid symbols (\blacksquare) and (\bullet), respectively, are the characteristics immediately after. The measurements and the exposure were made with TM polarized, CW radiation.

Although the specific origin of the observed changes in the propagation constant is not known, several possibilities exist. These include thermal rearrangement of the ions that form the waveguide and a photorefractive-like process caused by the pyroelectric effect (a temperature increase in the waveguide will generate an internal field across the guide which will alter the index through the electro-optic effect). Electronic photorefractive, which is observed in other materials (i.e. LiNbO_3), is also a possibility. However, this may not occur due to the relatively high ionic conductivity of the KTP substrates. The thermal refraction coefficients are known and cannot account for these effects.

Techniques to minimize or eliminate the observed effects on the propagation constant of KTP waveguides are currently being explored.

1. J. D. Bierlein, H. Vanherzeele, J. Opt. Soc. Am. B **6**, 622 (1989).
2. M. G. Roelofs, P. A. Morris, J.D. Bierlein, J. Appl. Phys. **70**, 720 (1991).
3. F. Laurell, M. G. Roelofs, W. Bindloss, H. Hsiung, A. Suna, J. D. Bierlein, J. Appl. Phys. **71**, 4664 (1992).
4. C. J. van der Poel, J. D. Bierlein, J. B. Brown, S. Colak, Appl. Phys. Lett. **57**, 2074 (1990).
5. M. J. Jongerius, R.R. Drenton, R. B. J. Droste, in *Conference on Laser and Electro-Optics* Vol. 12, 1992 OSA Technical Digest series. (Optical Society of America, Washington, DC, 1992), paper CTHA2.
6. K. S. Buritskii, E. M. Dianov, Y. M. Grjaznov, N. G. Dobryakova, V. A. Maslov, V.A. Chernykh, E. A. Shcherbakov, Sov. Lightwave Commun. **1**, 107 (1991).
7. P. A. Morris, M. K. Crawford, M. G. Roelofs, J. D. Bierlein, T. M. Baer, Proc. Soc. Photo-Opt. Instrum. Eng. **1561**, 104 (1991).

Thursday, February 4, 1993

Poster Session

CThC 1:30pm–3:00pm
La Salle Ballroom A

Cerenkov-type second harmonic generation in lossy slab waveguides

T.Kinoshita K.Sasaki

Department of Electrical Engineering, Keio University

3-14-1 Hiyoshi, Kohoku-ku, Yokohama, Kanagawa 223, Japan. TEL. +81-45-563-1141

Y.Yokoh H.Ashitaka

Ube Industries, LTD.

8-1 Goiminamikaigan, Ichihara, Chiba 290, Japan. TEL. +81-436-23-5157

N.Ogata

Department of Chemistry, Sophia University

7-1 Kioi-cho, Chiyoda-ku, Tokyo, 102, Japan. TEL. +81-3-3238-3447

Introduction

Poled polymer films have been extensively studied because of easy preparation and their potential for applications of nonlinear optical devices. In frequency doubling by optical waveguides Cerenkov-type phase matching is advantageous because it requires only loose specifications of film thickness and refractive indices in device designings.

In this paper further advantage of Cerenkov-type phase matching is presented as a useful conception to overcome absorption loss for efficient blue and green second harmonic generation in waveguide structures.

Theory

To estimate the loss influence on efficiency of SHG, a simple model slab waveguide is introduced (Fig.1) with refractive indices as in Table 1. The lossy film with thickness d has nonlinear quadratic coefficient d_{33} . Anisotropies of the film index and loss at fundamental wavelength are ignored. Expressions of a TM guided mode fundamental wave and a TM radiation mode by D.Marcuse are applied to this analysis[1]. The magnetic field of second harmonic wave is represented as

$$H_y = \int_0^{\rho_s} a(\rho, z) h_y(\rho, x) e^{j\omega t - j\beta z} d\rho \quad (1)$$

$a(\rho, z)$ is amplitude, β is the propagation constant and $\rho^2 = n_2^2 k^2 - \beta^2$ with $k = 2\pi/\lambda$. The range of ρ is

$$0 \leq \rho \leq \rho_s = k \sqrt{n_2^2 - n_3^2} \quad (2)$$

$h_y(\rho, x)$ is nonperturbated normalized magnetic field and it can be given by

$$\partial^2 h_y / \partial x^2 + (\mu_0 \epsilon_0 n^2 \omega^2 - \beta^2) h_y = 0 \quad (3)$$

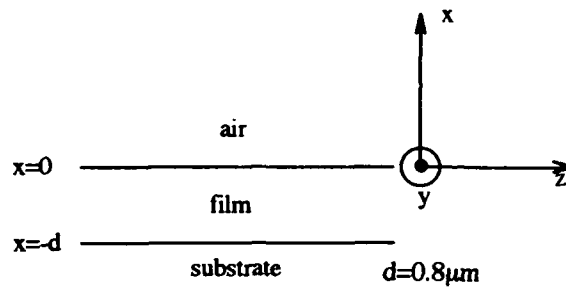


Table 1. Refractive indices

wavelength		1064 nm	532 nm
air	n3	1.0	1.0
film	n1	1.5	1.55
substrate	n2	1.4	1.45

Fig.1 A slab waveguide

The wave equation with loss (conductivity) σ and nonlinear polarization $P_{NL}(x)$ induced by a TM guided fundamental wave with the propagation constant β is represented as

$$\nabla^2 H_y - \mu_0 \epsilon_0 n^2 \frac{\partial^2 H_y}{\partial t^2} - \mu_0 \sigma \frac{\partial H_y}{\partial t} - \frac{\mu_0 \epsilon_0 n^2 \omega}{\beta} \frac{\partial^2 P_{NL}(x)}{\partial t^2} e^{j\omega t - j\beta z} = 0 \quad (4)$$

This analysis can be alternatively extended using a complex refractive index for the lossy film, however the loss is treated as a perturbation in this paper. Replaced H_y in eq.(4) by eq.(1) and ignored the pump depletion and slowly varying envelope approximation is assumed, then being multiplied by $h_y(\rho', x)$ and integrated by x , eq.(4) is transformed into

$$\frac{\partial a(\rho', z)}{\partial z} = -\frac{\mu_0}{4\epsilon_0 \beta'} \int_0^{\rho'} \int_{-\infty}^{\infty} \frac{\sigma}{n^2} a(\rho, z) h_y(\rho, x) h_y(\rho', x) \beta e^{j\beta' z - j\beta z} dx d\rho - j \frac{\mu_0 \omega^2}{4\beta'} \int_{-\infty}^{\infty} P_{NL}(x) h_y(\rho', x) e^{j\beta' z - j\beta z} dx \quad (5)$$

Note that the propagation constant β' corresponds to ρ' and mode orthogonality is used. Eq.(5) is numerically solved for the initial condition $a(\rho', z=0)=0$.

Fig.2 is dependence of second harmonic normalized efficiency (100% for the lossless case) on the propagation length l for various loss values. The efficiency is linearly proportional to the propagation length and the absolute efficiency of a lossless waveguides ($\alpha=0$) is 1.54% for $l=1\text{mm}$, fundamental power $p^*=1\text{W}$, $d33=5\text{pm/v}$, and waveguide width $w=10\mu\text{m}$. When the propagation loss is less than several tens of dB/cm^{-1} , which is required for practical waveguide devices, the reduction of efficiency is less than 1% and it is negligibly small. For further increment of loss 4340dBcm^{-1} , for which a guided mode wave hardly propagates, the efficiency is as much as 79% of the lossless case and it is equivalent to 10dBcm^{-1} propagation loss for a guided mode. The remarkable reduction of loss influence in Cerenkov-type SHG comes from immediate radiation of generated second harmonic wave to transparent substrate along the waveguide.

Experiment

The authors have reported Cerenkov-type blue and green SHG using a poled polymer containing an azo dye Disperse Red 1 (4-[N-ethyl-N-(2-hydroxyethyl)]-amino-4'-nitroazobenzene) as side chain [2]. In this work another poled polymer p-NAn-PVA was used in the experiments. Fig.3 is p-NAn-PVA co-polymer with unit fraction $x=0.82$ and its glass-rubber transition temperature is

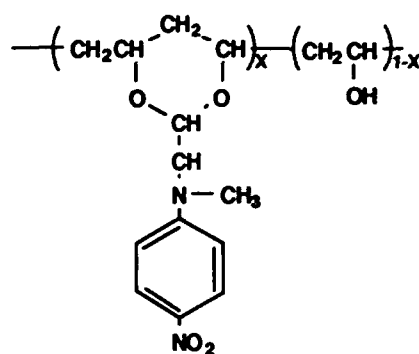
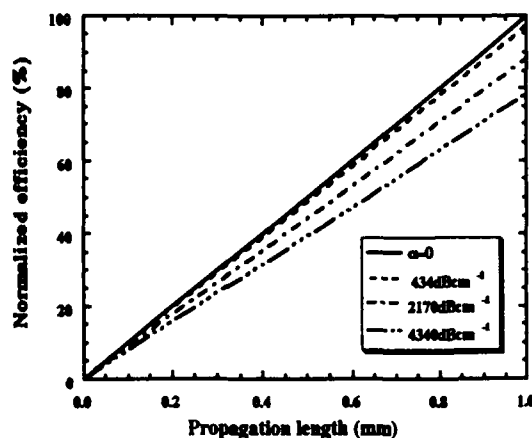


Fig.3 p-NAn-PVA

Fig.2 Dependence of SHG efficiency on propagation length.

120°C. First the polymer was dissolved in dimethyl sulfoxide and spincoated on a pyrex substrate. Then it was corona-poled at 150°C for 15 minutes with applied voltage, 6kV. The cut-off wavelength after poling was 480nm. Absorption at 532nm was 1500cm⁻¹, which corresponded to transmission of 15% for 1μm film thickness for normal incidence and it was as much as 6510dBcm⁻¹ propagation loss. Anisotropy of absorbance is ignored, however a poled polymer film is more lossy for a TM radiation mode than for normal incidence. The typical d33 value was 10pm/v.

Fundamental wave of 1064nm Q-switched Nd:YAG laser was coupled with a SF-11 glass prism and generated 532nm wave was filtered and detected by a Si photo diode power meter. The efficiency was 0.66% at 240kW fundamental input power. Even at lower fundamental power of 580W second harmonic radiation could be viewed. When fundamental wave at 1135nm of a LiF:F₂⁻ color center laser was used the efficiency was 0.04% at 20kW input. The decay of the d33 was slow and only little reduction was recognized 100 days after poling. The polymer can play as a negative photoresist for irradiation of uv light or electron beam. This property is applicable to corona poled channel waveguide structure.

Conclusion

Loss influence on Cerenkov-type second harmonic generation(SHG) was estimated and it was indicated that even 4340dBcm⁻¹ loss for guided mode is equivalent to 10dBcm⁻¹ loss for Cerenkov-type SHG. As an example SHG experiments using p-NAn-PVA poled film waveguides were demonstrated. This technique is advantageous for blue or green SHG.

Acknowledgements

It is a pleasure to thank M.Kikuchi, T.Sassa, and K.Tsuchiya for important roles in experiments. The authors wish to thank Dr.S.Yoshida(Hutech Inc.) for operating a LiF:F₂⁻ color center laser (MALSAN203) and Dr.S.Umegaki for encouragements and discussion.

References

- [1] D.Marcuse, Theory of dielectric waveguides, Academic press(1974).
- [2] T.Kinoshita, Y.Nonaka, E.Nihei, Y.Koike, and K.Sasaki, "Poled polymer Frequency Doubling Waveguide in Purple-blue wavelength Region", Proc.of 5th.Toyota conference on Nonlinear Optical Materials 479(Japan, 1991).

COMPACT RAMAN SHIFTER

D.E.Gakhovich, A.S.Grabchikov, V.A.Orlovich
 Institute of Physics, Belarus Academy of Sciences,
 Skarina avenue, 70, 220602 Minsk, Belarus.
 S.S.Dvornikov
 STC "Solar", Masherov avenue 5, 220600 Minsk Belarus

An opportunity to concentrate the energy of scattered light in the one Stokes component of the stimulated Raman scattering (SRS) exists both for the forward and backward scattering [1,2]. The regime of backward SRS (BSRS) has an advantage over the forward one due to the phase conjugation of the backward wave [3].

In this communication we address the problem of characterizing the effect of different parameters on the time and energy characteristics of such BSRS regime. BSRS regime can be realized with tightly focusing pump beams with high efficiency [2]. These conditions allows to design the small size Raman shifter with cell length shorter than 10cm. We discuss the comparison aspects of coherent and noncoherent pumping conditions. The opportunity of the influence on the asymmetry of SRS and the transition from the one Stokes component conversion to the multiple component one is shown. The data on the conversion efficiency with third and second YAG:Nd-laser output harmonics and their optimization are given.

REFERENCES

1. S.R.J.Brueck, H.Kildal IEEE J.of Quant. Electron., 8 (1982) 310.
2. D.E.Gakhovich, A.S.Grabchikov, Ju.E.Djakov et all., Soviet journal Izv. AN SSSR ser. fiz., 53, (1989) 1131.
3. A.I.Sokolovskaja, G.I.Brekhovskikh, A.D.Kudrjavitseva IEEE J. of Quant. Electron., 23 (1987) 1332.

GaN for short-wavelength light emitting devices: growth kinetics and techniques

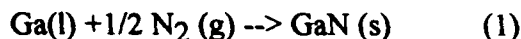
Jennifer Ross, Nathan Newman, and Mike Rubin

Lawrence Berkeley Laboratory, 1 Cyclotron Rd, MS 2-300, Berkeley, CA 94720, 510-486-4291

In the recent year, great steps have been achieved in the development of blue-green semiconductor diode lasers and LEDs, however material issues in the wide-bandgap semiconductors still limit practical device applications. The II-VI compounds ZnSe and ZnS and the III-V semiconductors GaN and AlN are the two material system being investigated for green to ultra- violet light emitting devices, with most research to date concentrating on the II-VI materials. Problems with electromigration, heating, and subsequent processing in early ZnSe/ZnS laser diodes has led many researchers to investigate the more robust material GaN for commercially viable short wavelength LEDs and laser diodes. GaN blue LEDs at room temperature have been demonstrated by Akasaki et al. [1], but p-type doping levels are not yet sufficiently high for laser diodes. The main obstacle in fabricating high quality GaN for device applications has been controlling background impurity and dopant concentrations during crystal growth and finding suitable substrates with closely matching lattice and thermal expansion coefficients. The dilemma in obtaining p-type conduction in GaN is hypothesized to be due to a large concentration of nitrogen vacancies[2] acting as shallow donors making compensation difficult. Aside from Akasaki's and Nakamura's work in Japan [1,13], all GaN material by any growth techniques has been n-type. Advances in the last few years, have produced undoped material with a reduced concentration using Metal Organic Chemical Vapor Deposition (MOCVD) ($4 \times 10^{16} \text{ cm}^{-3}$) [3] and plasma/ion-assisted Molecular Beam Epitaxy (MBE) ($8 \times 10^{13} \text{ cm}^{-3}$)[4].

We report the production of GaN epitaxial films with very low free electron concentrations ($8.4 \times 10^{14} \text{ cm}^{-3}$) using UHV reactive magnetron sputtering on R-plane sapphire substrates. Our data, when combined with earlier literature, is used to understand the thermodynamic and kinetic processes involved in GaN film growth and the limiting factors involved in nitrogen incorporation during the growth process. We show that our films are formed using a non-equilibrium kinetically-limited process which is controlled by a competition between the forward and reverse reaction. The forward reaction depends on the arrival of activated nitrogen species at the growing surface and the reverse reaction is rate limited by the unusually large kinetic barrier of decomposition of GaN. Hopefully, better understanding of this rather unique material system will lead to improved compensation techniques and high p-type concentrations.

The phase stability conditions of GaN for the following reactions will reveal that only chemical vapor deposition (CVD) with the reactant NH_3 utilizes growth conditions in the stable region of the GaN phase diagram



All other successful GaN thin-film growth techniques supplement the growth process with the introduction of activated nitrogen species using a plasma discharge[6], electron cyclotron resonance (ECR) plasma source,[5,7-11] or an ion gun[4] and operate in the unstable, kinetically limited region of the phase diagram. Although it is not clear if GaN films grown under a kinetically limited condition produce less nitrogen vacancies than equilibrium growth techniques, we observe that the lowest free electron concentrations measured in undoped GaN material have been obtained in our study and in the ion assisted MBE study of Powell [4]. Activated species (e.g. N_2^+ , excited N_2 and/or atomic nitrogen) are important in reducing both the free energy of reaction and overcoming the kinetic barriers of the growth process. The resulting growth depends on the competition between the decomposition reaction and the enhanced forward reaction. The details of this type of growth process are difficult to access, but we will try to elucidate the important rate controlling steps which are involved.

The GaN films were deposited by reactive magnetron sputtering using a 5 cm modular source produced by U.S. Inc. Film properties were then examined over a large range of substrate temperature (400-700 C), N_2 partial pressure (0-30 mTorr) and N_2 :Ar gas ratios (0-1) on both R-plane sapphire substrates and (111) GaAs. Details concerning the growth are published elsewhere [6,12]. X-ray diffraction was performed using $\text{Cu-K}\alpha$ ($\lambda=1.54 \text{ \AA}$) radiation from a commercial Siemens D5000 diffractometer. Films were also characterized by Rutherford back scattering (RBS), 4-point probe and Hall measurements.

The substrate temperature and N_2 :Ga arrival rates greatly affect the degree of crystallinity, nitrogen incorporation, growth rate, and resistivity of GaN films. For set arrival rates, only within a narrow temperature range could epitaxial GaN be grown (620-670 C for R-plane sapphire and 550-620 C for (111) GaAs). For temperatures above this range, a loss of epitaxy, a drop in the growth rate, and a decreased N/Ga concentration ratio in the films is observed. While temperatures below this range result in increasingly sub-stoichiometric films. Our data shows that even with the use of highly energetic N_2 species, thermal energy on the growing surface is still important for the uptake of both Ga and N. There are several possible mechanisms for the sudden

degradation in film properties for temperatures above the epitaxial range. Using our data and that from the literature [4] we will show that the thermal decomposition determines an upper bound to the growth temperature, not only for films grown by reactive sputter deposition but for the other techniques that operate in the kinetically-limited growth regime (plasma/ion-assisted MBE).

In sputtering experiments, independent control of the Ga and activated nitrogen flux to the substrate is difficult. Altering parameters such as the N_2 partial pressure, total pressure, or sputtering power directly affects the spatial extent and nature of the plasma. However, optical emission spectroscopy (OES) was used to determine the relative abundance of excited species in the plasma for different N_2 partial pressures. Shown in Figure 1, as the N_2 :Ar ratio is increased, the Ga arrival rate drops significantly. Although qualitative rates cannot be extracted from this measurement, if the concentration of excited species is assumed to be proportional to the total species concentration, the N/Ga arrival rate at N_2 :Ar = 9 is 5 times what it is at N_2 :Ar = 3. GaN film quality proved to be a sensitive function of N_2 :Ga arrival with the lowest free electron concentrations obtained with N_2 :Ar = 8-9.

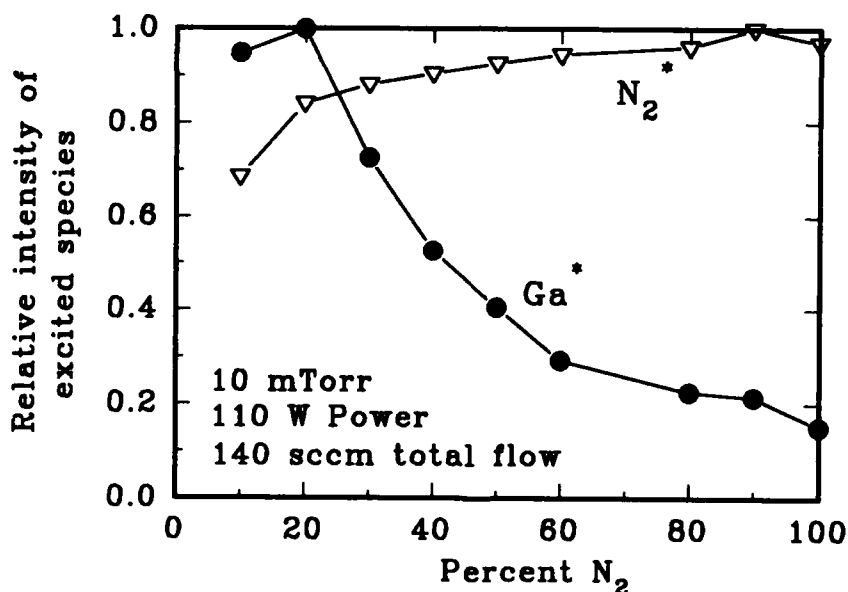


Figure 1. Optical emission intensity of the 417.4 nm Ga^* line and the 316.0 nm N_2^* line normalized to each species maximum.

Choosing our deposition conditions accordingly, high quality epitaxial GaN (11 $\bar{2}$ 0) layers were grown on R-plane (01 $\bar{1}$ 2) sapphire with room temperature free carrier concentrations as low as $8 \times 10^{14}/cm^3$ with Hall mobility's of $200 cm^2/(V sec)$. We have shown that GaN films fabricated

using reactive magnetron sputtering, plasma/ion-assisted MBE, and ECR-assisted MOCVD use a non-equilibrium kinetically-limited process. For these methods, we find that the growth process is controlled by a competition between the forward reaction which critically depends on the arrival of activated nitrogen species at the growing surface and the reverse reaction whose rate limiting step is the unusually large kinetic barrier of decomposition of GaN. When these processes are taken into account, very good quantitative agreement is found between the expected conditions for high quality GaN growth and the thermodynamic and kinetic data.

References

1. I Akasaki, H. Amano, Materials Research Society Fall Meeting, Boston, MA, 1991, vol. 242, p383.
2. H. P. Maruska and J. J. Tietjen, Appl. Phys. Lett. 15, 327 (1969).
3. Shuji, Nakamura, Jap. J. Appl. Phys. 30, L1705 (1991).
4. R. C. Powell, G. A. Tomasch, Y. -W. Kim, J. A. Thornton and J. E. Greene, Mat. Res. Soc. Symp. Proc. vol 162, 525 (1990).
5. T. Lei, T. D. Moustakas, R.J. Graham, Y. He and S. J. Berkowitz, J. Appl. Phys., 71, 4933 (1992).
6. J. Ross and M. Rubin, Materials Letters 12, 215 (1991).
7. M. J. Paisley, Z. Sitar, J. B. Posthill and R. F. Davis, J. Vac. Sci. Technol. A7, 701 (1989).
8. Z. Sitar, M. J. Paisley, B. Yan, J. Ruan, W. J. Choyke and R. F. Davis, J. Vac. Sci. Technol. B8, 316 (1990).
9. G. Martin, S. Strite, J. Thornton and H. Markoc, Appl. Phys. Lett. 58, 2375 (1991).
10. Hirotsgo Sato, Toru Sasaki, Takashi Matsuoka and Akinori Katsui, Jap. J. Appl. Phys. 29, 1654 (1990).
11. S. Strite, J. Ruan, Z. Li, A. Salvador, H. Chen, David J. Smith, W. J. Choyke, and H. Morkoc, J. Vac. Sci. Technol. B9, 1924 (1991).
12. J. Ross, M. Rubin, and T.K. Gustafson, Materials Research Society Fall Meeting, Boston, MA 1991, vol. 242, p 457.
13. S. Nakamura, M. Senoh, and T. Mukai, Jap. J. Appl. Phys. 30, L1708 (1991); *ibid.* 30, L1998 (1991).

Abdulsabirov, R. — ATuA6

Alzal, Robert S. — AMB9

Ahrenkeil, P. — CTuC5

Akimoto, K. — CTuC1

Al-Jassim, M. — CTuC5

Alfano, Robert R. — ATuD4, ATuE1

Allik, Toomas H. — ATuC4

Aminou, Donny — ATuB5

Andou, T. — JWB4

Ashitaka, H. — CThC1

Audouard, E. — AMD2

Azumai, Yuji — CWA1

Baer, Thomas M. — AMD1, JWD

Bair, C. H. — AWB6

Balembois, François — ATuF3, JWC10

Balmer, J. E. — ATuB1

Barnes, James C. — ATuF

Barnes, Norman P. — AMB3, AMB8, ATuB10, AWB2, AWB5, AWB6

Barnes, William L. — ATuA4

Barr, John R. M. — AMC3, ATuC1

Basiev, Tasoltan T. — AMF6

Bass, Michael — AMB11, AMC2, JWC1, JWC3, JWC11

Basun, S. A. — ATuE7

Beigang, Rene — AMF4, AMF5

Belt, Roger F. — ATuA2

Bendall, Charles — ATuE9

Berg, Jacqueline G. — AMA1

Bibeau, C. — AMC5

Bierlein, John D. — AMF3, CThB, CThB2, CThB4

Bindloss, W. — CThB2

Bleckmann, A. — ATuB1

Bona, G. L. — CThB3

Bonnin, C. — JWA2

Bordui, Peter F. — JWA

Bortz, Michael L. — CThA2

Bosenberg, Walter R. — AMB7, AMF3

Boulanger, B. — JWA2

Bourmes, P. — AMA3, AMA4

Bowers, John E. — ATuB3

Bowers, Mark S. — AMA5, AME7

Bowman, Steven R. — AWA5, AWB3

Braun, F. D. — AMB1

Breteau, Jean-Marc — AME9

Brockman, Philip — AWB6

Brown, Andrew J. W. — AMB7

Brown, J. B. — CThB4

Brun, Alain — ATuF3, JWC10

Brunel, L. — ATuD2

Buchal, Ch. — CThA3

Budni, Peter A. — AMF2

Burnham, Ralph L. — AMA3, AMA4, AMC, AMD6

Buschert, J. R. — CTuC5

Buser, Rudolf G. — AMA

Butashin, A. V. — ATuE8

Cabirol, X. — JWA2

Cai, Ying — AMB10

Callenäs, Anders — AWB12

Capps, David — AMC4

Cassanho, Arlette — AMB3, AMB6, ATuB2, ATuF4

Chai, Bruce H. T. — AMB11, AMC2, ATuA1, ATuB9, ATuC4, AWA2, JWC1, JWC3, JWC11, JWE

Chang, Robert S. F. — AWB8

Chartier, I. — JWD4

Chen, T. — AMA2

Cheng, H. — CTuC2

Cheng, Lapkin — AMF3

Chicklis, Evan P. — AMF2

Chiu, Pay Hung — ATuD1

Chuang, Ti — AMB4, ATuE5

Clausen, R. — AWA2

Creamer, John E. — ATuA2

Crofts, G. J. — AMD4

Damzen, Micheal J. — AMD4, AME1

Davis, John — ATuD1

Davydov, S. V. — JWC7

Dawes, Judith M. — AMB10

Debusschert, Thierry — AME5

Dekker, Peter — AMB10

DeLoach, L. D. — ATuA3, ATuB9, ATuF5

DePuydt, James M. — CTuC, CTuC2

Deyst, John P. — AWA4

DiBiase, D. — AMA3

Dinerman, Bradley J. — AWA1

Dinndorf, Kenneth M. — AMB3, ATuB2

Ditmire, Todd — ATuF1

Dixon, George J. — AME2, JWB2

Djeu, Nicholas — AWB7, AWB8

Dobrowolska, M. — CTuC5

Dowley, Mark W. — CTuA

Drenten, R. R. — CTuC3

Dubinskii, Mark A. — ATuA6, ATuB4

Durand, E. — AMD2

Dvorinkov, S. S. — CThC2

Ebihara, T. — JWC9

Effenberger, Frank J. — AME2

Eilers, Hergen — AWB10, AWB11

Estable, F. — ATuD2

Esterowitz, Leon — ATuA2

Eyres, L. A. — CThA1

Fallnich, C. — AMF4, AMF5

Fejer, Martin M. — CThA, CThA2

Feldman, Barry J. — AWA5, AWB3

Feofilov, S. P. — ATuE7

Ferrand, B. — JWD4

Feugnet, G. — AMC6

Fève, J. P. — JWA2

Fields, Renny A. — ATuB8

Filer, Elizabeth D. — ATuB10, AWB2

Fleuster, M. — CThA3

Fluck, Daniel — CThA3

Frel, B. — ATuB11

Freitag, I. — ATuB6

French, Paul M. W. — ATuD5, ATuF2

Frerichs, Christian — AWA3
Furdyna, J. K. — CTuC5

Gaines, J. — CTuC3
Gakhovich, D. E. — CThC2
Georges, Patrick — ATuF3, JWC10
Gharavi, Alireza — JWC2
Giordano, G. — AMF1
Glenn, William E. — CTuA2
Goto, Chiaki — CWA2
Grabchikov, A. S. — CThC2
Graf, T. — ATuB11
Green, R. P. M. — AMD4
Gregor, Eduard — AMA2, AME10
Grubb, S. G. — JWE1
Gruber, John B. — ATuB7, ATuC4
Guillot, Daniel — CTuB
Günter, Peter — CThA3
Gurskii, A. L. — JWC7
Guyot, Y. — ATuA5, JWC8

Haase, M. A. — CTuC2
Hale, Charley P. — AWB1
Hamilton, Charles E. — AMB1
Han, Gooywan — AWB6
Hanna, David C. — ATuA4, ATuC1, JWB, JWD4
Hanson, Frank E. — ATuE9
Hansson, Goran H. — AWB12
Harada, Akinori — CWA2
Hardy, Amos — JWD3
Haub, J. G. — AME11
Hauglie-Hanssen, Christian — AWB7
Hays, Alan D. — AMD6
Hays, John M. — JWE4
Heine, Frank — ATuB1, AWA6
Helmfrid, S. — JWB4
Henderson, Sammy W. — AWB1
Hess, Robert V. — AWB6
Heumann, Ernst — AWA6
Hiel, F. — CTuC1
Hills, Marian E. — ATuB7, ATuC4
Hilyard, Roger C. — AMA1
Hoefler, Carolyn S. — AMA1
Hömmrich, Uwe — AWB10, AWB11
Huber, Guenter — AMC1, ATuB1, ATuE6, ATuE7, AWA2, AWA6
Hughes, D. W. — ATuC1
Humphrey, Paul D. — ATuB3
Hunt, John T. — AME3
Hutchinson, J. Andrew — ATuC4
Hyuga, H. — CWA2

Injeyan, Hagop — AMA1
Isyanova, Yelena D. — AMB2
Ito, Hiromasa — JWA1
Ito, Kohei — CThA4
Izumitani, Tetsuro — ATuC5, AWB9, JWC4

Jackson, Stuart — AMB10
Jacobsen, Stuart M. — AWB10, AWB11
Jacquier, Bernard B. — JWE3

Jaeckel, H. — CThB3
Jani, Mahendra G. — AMB8, AWB5
Jansson, Mårten — CTuB2
Jensen, T. — AMC1
Jenssen, Hans P. — AMB3, AMB6, ATuB2, ATuF4
Jia, Weiyl — AWB11
Jiang, X. B. — AWB8
Johnson, M. J. — AME11
Joubert, M. F. — JWC8
Jourdain, C. — AME9

Kahan, Osher — AMA2
Kalina, C. — AMA2
Kaminskii, A. A. — ATuE8
Kamiyama, Koji — CWA2
Kannari, Fumihiko — ATuE10
Kaplyanski, A. A. — ATuE7
Kasinski, Jeff — AMA3, AMA4
Kato, M. — JWB3, CThA5
Kaz, Alex — AMD3
Keirstead, Mark S. — AMD1
Kinoshita, T. — CThC1
Kitaoka, Y. — JWB3, CThA5
Klimov, I. V. — ATuE4, AWB4
Kmetec, Jeffrey D. — ATuD1
Knights, Mark G. — AMF2
Knowles, David S. — AMB10
Koch, Grady J. — AWA4
Kokta, Milan R. — ATuE1, AWB2
Korableva, Stella L. — ATuA6
Koryagina, E. L. — ATuB4
Kozlovsky, William J. — CThB3
Kronick, Mel N. — CTuB1
Kröpke, Ingo — ATuB6
Krupke, William F. — ATuA3, ATuB9, ATuF5
Kubota, Shigeo — CTuA1
Kück, S. — ATuE6
Kulak, I. I. — JWC7
Kuleshov, Nikolai — ATuE3, ATuE11
Kway, W. L. — ATuA3, ATuB9, ATuF5

Lamb, R. A. — AME1
Lang, Robert J. — JWD3
Larat, Christian — AMC6
Large, Alan C. — JWD4
Lau, Suzanne D. — CThB3
Laurell, Fredrik — CTuB3
Le, K. — AMA3
Lee, Chang J. — AWB6
Lee, Ian — AME6
Lee, J. D. — CThB2
Lefaucheur, Jean Luc V. — AMC2, ATuA1
Lejus, A. M. — ATuC3
Lenth, Wilfried — CThB3
Lepine, T. — AME9
Li, C. — JWC6
Liang, G. Y. — AMC3
Lin, Liu — JWC9
Lin, Y. — JWC4

Linarès, C. — JWC8
 Liu, Lin — JWC9
 Lowenthal, Dennis D. — AME7, AMF1
 Luo, H. — CTuC5
 Lutsenko, E. V. — JWC7
 Lutta, G. B. — ATuA1
 Lynn, James G. — AWA5, AWB3

Machan, Jason P. — AMA1
 Mackechnie, C. J. — ATuA4
 Magana, Art — ATuD1
 Majidabudi, A. A. — ATuC1
 Makio, Satoshi — CThA4
 Maleki, Lute — JWC8
 Manaa, H. — ATuE8
 Manes, Kenneth R. — AME3
 Marnier, G. — JWA2
 Marquardt, Charles L. — AMF, AMF2, AWA5
 Marshall, Larry R. — AMD3
 Marshall, T. — CTuC3
 Maslov, Vladislav A. — CThB1
 Matone, G. — AMF1
 Matsuoka, Yoshihiko — JWC9
 Matthews, Steven C. — AMA2, AMC4
 McInnes, Alasdair — ATuB12
 McIntosh, Bruce — ATuD6
 McPherson, Gary L. — JWC2
 Mead, Roy D. — AMB7
 Mehuy, David G. — JWD3
 Mènaert, B. — JWA2
 Merkle, Larry D. — ATuC4, ATuD6
 Meyn, J. P. — AMC1, ATuB1
 Mikhailov, Victor P. — ATuE3, ATuE11
 Mill, B. — ATuE8
 Mitcovets, A. I. — JWC7
 Mito, K. — JWA3
 Mitsumoto, S. — CWA2
 Miyai, T. — JWB4
 Miyajima, T. — CTuC1
 Miyake, C. I. — AMB1
 Miyamoto, Akio — JWC5
 Mizuuchi, Kiminori — CThA5
 Moncorge, R. — ATuA5, ATuE8, JWC6
 Mordaunt, David W. — AME10
 Morinaga, Y. — CTuC1
 Morris, Patricia A. — CThB4
 Morrison, Clyde A. — ATuB7, ATuB10, ATuC4
 Mottay, Eric — AMD2, ATuD2
 Moulton, Peter F. — AWA1
 Muir, R. — AMA2
 Murray, James T. — AMF6
 Murray, Keith E. — AMB3, AWB5

Nada, N. — CThA1
 Nakai, S. — JWC5
 Nam, Derek W. — JWD3
 Naranjo, Felipe E. — AWB2
 Naumov, Alexander — ATuA6, ATuB4
 Nebel, A. K. — AMF4, AMF5
 Nelsson, C. — AWB12

Newman, Nathan — CThC3
 Nguyen, H. — ATuF1
 Nicholls, John — ATuA1
 Nielson, K. — AMA2
 Nightingale, John L. — JWD2
 Nitanda, Fumio — CThA4
 Noginov, Mikhail A. — ATuF4

Obara, Minoru — ATuE10
 O'Brien, Steve — JWD3
 Ogata, N. — CThC1
 Ohashi, Motoki — JWA1
 Ohmori, S. — JWB3
 Oka, Micha — CTuA1
 Okada, A. — JWA3
 Okazaki, Y. — CWA2
 Okuyama, H. — CTuC1
 Orlovich, V. A. — CThC2
 Orr, Brian J. — AME11
 Ortiz, J. — AMA2
 Ostroumov, Vasilij G. — AMC1
 Otsuka, Kenju — AMD5
 Ozawa, M. — CTuC1

Palombo, Katherine V. — AMC4, AME10
 Papuchon, Michel R. — AME5
 Pareek, A. — CTuC5
 Parke, Ross — JWD3
 Payne, Stephen A. — AMC5, ATuA3, ATuB9, ATuC,
 ATuF5
 Peale, R. E. — AMB11, JWC1, JWC11
 Peiris, F. C. — CTuC5
 Pelenc, D. — JWD4
 Peng, Bo — AWB9, JWC4
 Perry, Michael D. — ATuF1
 Petermann, Klaus — ATuB1, ATuE6, ATuE7
 Petricević, Vladimir — ATuD4, ATuE1
 Petruzzello, J. — CTuC3
 Pham, A. — AMC2, ATuA1
 Phillips, Mark W. — AMC3
 Piper, James A. — AMB10
 Pocholle, Jean-Paul — AMC6, AME5
 Pohlmann, U. — ATuE6
 Poignant, H. — JWE3
 Pollak, Thomas M. — AMF2
 Polumbo, M. — AMA2
 Powell, Howard T. — AMC5
 Powell, Richard C. — AMF6, ATuA
 Prokoshin, P. V. — ATuE11

Qiu, J. — CTuC2
 Quarles, Gregory J. — ATuA2, ATuB7, AWA5, AWB3

Raffy, Jean — AME5
 Randies, Mark H. — ATuA2, ATuE1
 Rapoport, William R. — ATuD, ATuF6
 Reeves, Roger J. — AMF6
 Remillieux, A. — JWE3
 Renard, P. A. — AME3

Richards, J. — ATuB12
 Rieger, Harry — AME8
 Rines, David M. — AWA1
 Risk, William P. — CThB3
 Rizvi, N. H. — ATuD5, ATuF2
 Roelofs, M. G. — CThB2
 Roeraade, Johan — CTuB2
 Roger, Gérard — ATuF3, JWC10
 Romero, R. — ATuC3
 Rose, Todd S. — ATuB8
 Rosenblatt, Gregg H. — ATuA2
 Ross, Jennifer T. — CThC3
 Roy, Rajarshi — JWD1
 Rubin, Michael D. — CThC3

Saber, D. — ATuC3
 Saitoh, M. — CThA1
 Salin, François — ATuD2, ATuF3, JWC10
 Samarth, N. — CTuC5
 Sandulenko, V. A. — ATuE11
 Sarukura, Nobuhiko — ATuD3
 Sasaki, K. — JWA3, CThC1
 Sasaki, Takatomo — JWB1, JWB3, JWC5
 Sato, Heihachi — CWA1
 Sato, Masayoshi — CThA4
 Schmaul, B. — AWA2
 Schönherr, T. — ATuE6
 Schunemann, P. G. — AMF2
 Schwarz, M. — AMC6
 Scifres, Donald R. — JWD3
 Scott, Andrew M. — AME4
 Seamans, J. F. — AMA5, AME7, AMF1
 Searles, Stuart K. — AWA5
 Seas, Antonios — ATuD4, ATuE1
 Segawa, Yusaburo — ATuD3
 Seidel, D. J. — JWC8
 Seltzer, Michael D. — ATuB7, ATuC4
 Semashko, Vadim V. — ATuA6, ATuB4
 Seo, Iwao — CWA1
 Serova, V. N. — ATuB4
 Shan, W. — JWE4
 Shaw, L. B. — AWB8
 Shcherbakov, Eugene A. — CThB1
 Shcherbakov, Ivan A. — AMC1, ATuC2, ATuE4, AWB4
 Sheldrake, Stephen J. — AMC4
 Shepherd, David P. — JWD4
 Shestakov, A. V. — ATuD5
 Shikida, A. — JWE2
 Short, S. — CTuC5
 Silfvast, William T. — CTuB2
 Simon, F. — AME9
 Sims, Newton L., Jr. — AMB8
 Smith, Donald J. — AWA
 Smith, Larry K. — ATuA3, ATuB9, ATuF5
 Song, Jin-Joo — JWE4
 Sorokin, E. — ATuC2
 Sorokina, I. T. — ATuC2
 Source, J. — AMA2
 Squier, Jeffrey A. — ATuB5
 St. Pierre, Randall J. — AMA1
 Storm, Mark E. — AWA4
 Suna, A. — CThB2
 Suni, Paul J. M. — AWB1

Takeda, H. — ATuE10
 Takyu, Choichi — JWA1
 Tapié, Jean Lue — ATuF3
 Tassano, J. B. — ATuA3, ATuF5
 Tatsuno, Kimio — JWB4
 Taylor, James R. — ATuD5, ATuF2
 Tidwell, Steve C. — AMA5, AME7, AMF1
 Tonelli, Mauro — ATuB2
 Toratani, H. — JWC9, JWE2
 Townsend, J. E. — ATuA4
 Tropper, Anne C. — JWD4
 Tsvetkov, V. B. — ATuE4, AWB4

Umegaki, Shinsuke — CWA, CWA2

Vasil'ev, A. A. — ATuB4
 Vemashko, V. V. — ATuB4
 Verdún, Horacio R. — AMB4, AMD3, ATuD6, ATuE2, ATuE5
 Viana, B. — ATuC3
 Villaverde, A. B. — AMC2
 Villeval, P. — JWA2
 Vivien, D. — ATuC3

Waarts, Robert G. — JWD3
 Walker, C. T. — CTuC2
 Wang, Y. — AWB11
 Watanabe, K. — CThA1
 Webb, D. J. — CThB3
 Weber, Mark E. — AMA1
 Weber, Rudolf — AMB5
 Weidner, H. — AMB11
 Welch, David F. — JWD3
 Welford, David — AMB2
 Welling, Herbert — ATuB6
 Whitney, W. T. — AME4
 Wickham, Michael G. — AMA1
 Williams, A. — JWC8
 Wintner, E. — ATuC2
 Worster, Bruce — CTuA3
 Wyon, Christophe — ATuC3

Yablonskii, Gennadii P. — JWC7
 Yamada, Masahiro — CThA1
 Yamagishi, Kiyoshi — ATuD3
 Yamaguchi, Yasuhide — AMB6, ATuB2
 Yamakawa, Koichi — ATuD1
 Yamamoto, K. — JWB3, CThA5
 Yanagita, H. — JWE2
 Yang, X. H. — JWE4
 Yen, William M. — AWB10, AWB11
 Yin, A. — CTuC5
 Yokoh, Y. — CThC1
 Yokotani, Atsushi — JWC5
 Yumashev, K. V. — ATuE11

Zagumennyi, A. I. — AMC1, ATuC2
 Zbinden, H. — AMB5
 Zhang, X. X. — AMB11, AMC2, JWC1, JWC3, JWC11
 Zharikov, Evgenii V. — AMD
 Zhavoronkov, N. I. — ATuE11
 Zou, X. — AWB9
 Zverev, P. G. — AMF6